

Redox-sensing mechanisms under hypochlorite stress in *Staphylococcus aureus*

Inaugural-Dissertation
to obtain the academic degree
Doctor rerum naturalium (Dr. rer. nat.)

submitted to the Department of Biology, Chemistry and Pharmacy
of the **Freie Universität Berlin**

by

VU VAN LOI

from Ninh Binh, Vietnam

Year of submission: 2018

1st. Reviewer: **Prof. Dr. Haike Antelmann**

Institut für Biologie – Mikrobiologie, Freie Universität Berlin

2nd. Reviewer: **Prof. Dr. Luise Krauth-Siegel**

Biochemie-Zentrum der Universität Heidelberg

Date of defence: 07.05.2018

In this PhD thesis the following manuscripts and reviews were published:

- (1) **Loi VV**, Rossius M, Antelmann H. Redox regulation by reversible protein S-thiolation in bacteria. *Front Microbiol.* 6:187. (2015)
- (2) Chandrangu P, **Loi VV**, Antelmann H, Helmann JD. The role of bacillithiol in Gram-positive Firmicutes. *Antioxid Redox Signal.* 28: 445-462. (2018)
- (3) Imber M*, Huyen NT*, Pietrzyk-Brzezinska AJ*, **Loi VV***, Hillion M, Bernhardt J, Thärichen L, Kolšek K, Saleh M, Hamilton CJ, Adrian L, Gräter F, Wahl MC, Antelmann H. Protein S-bacillithiolation functions in thiol protection and redox regulation of the glyceraldehyde-3-phosphate dehydrogenase Gap in *Staphylococcus aureus* under hypochlorite stress. *Antioxid Redox Signal.* 28: 410-430. (2018)
- (4) Imber M*, **Loi VV***, Reznikov S, Fritsch VN, Pietrzyk-Brzezinska AJ, Prehn J, Hamilton CJ, Wahl MC, Bronowska AK, Antelmann H. The aldehyde dehydrogenase AldA contributes to the hypochlorite defense and is redox-controlled by protein S-bacillithiolation in *Staphylococcus aureus*. *Redox Biol.* 15: 557-568. (2018)
- (5) Hillion M, Imber M, Pedre B, Bernhardt J, Saleh M, **Loi VV**, Maaß S, Becher D, Astolfi Rosado L, Adrian L, Weise C, Hell R, Wirtz M, Messens J, Antelmann H. The glyceraldehyde-3-phosphate dehydrogenase GapDH of *Corynebacterium diphtheriae* is redox-controlled by protein S-mycothiolation under oxidative stress. *Sci Rep* 7: 5020. (2017)
- (6) **Loi VV**, Busche T, Bernhardt J, Tedin K, Wollenhaupt J, Huyen NTT, Weise C, Kalinowski J, Wahl M, Fulde M, Antelmann H. Redox-sensing under hypochlorite stress and infection conditions by the Rrf2-family repressor HypR in *Staphylococcus aureus*. *Antioxid Redox Signal.* in press. doi: 10.1089/ars.2017.7354 (2018)
- (7) **Loi VV**, Harms M, Müller M, Huyen NT, Hamilton CJ, Hochgräfe F, Pané-Farré J, Antelmann H. Real-time imaging of the bacillithiol redox potential in the human pathogen *Staphylococcus aureus* using a genetically encoded bacilliredoxin-fused redox biosensor. *Antioxid Redox Signal.* 26: 835-848. (2017)
- (8) Tung QN, Linzner N, **Loi VV**, Antelmann H. Application of genetically encoded redox biosensors to measure dynamic changes in the glutathione, bacillithiol and mycothiol redox potentials in pathogenic bacteria. *Free Radic Biol Med.* in press. doi: 10.1016/j.freeradbiomed.2018.02.018 (2018)

*Shared first authorships.

Content

Zusammenfassung der Dissertation	5
Summary of the dissertation	8
Introduction and general conclusion	10
1. Introduction into <i>Staphylococcus aureus</i> as major human pathogen	10
1.1 The prevalence of multiple antibiotics resistant <i>S. aureus</i> isolates	10
1.2 The diversity of virulence factors of <i>S. aureus</i> contributing to pathogenesis	11
1.3 Regulatory mechanisms of <i>S. aureus</i> virulence factor expression	13
2. Adaptation of <i>S. aureus</i> to reactive oxygen and chlorine species (ROS and RCS) under infection conditions	14
2.1 Sources of ROS and RCS in bacteria	15
2.2 Post-translational thiol-modifications caused by ROS and RCS in bacteria	16
2.3 The low molecular weight thiols bacillithiol and mycothiol are bacterial defense mechanisms against ROS and RCS	17
2.3.1 Biosynthesis and functions of bacillithiol in <i>Firmicutes</i>	18
2.3.2 Functions of mycothiol and its role in protein S-mycothiolation	24
2.4 Thiol-based redox regulators as ROS and RCS defense mechanisms	27
2.4.1 The SarA-family of virulence, redox and antibiotic resistance regulators in <i>S. aureus</i>	27
2.4.2 QsrR as MarR/DUF24-family thiol-based redox sensor of quinones	30
2.4.3 The Rrf2-family redox sensors CymR, SaiR and HypR in <i>Firmicutes</i>	31
2.4.4 The Rrf2-family redox sensors IscR and NsrR	35
3. Genetically encoded redox biosensors to measure dynamic changes in the glutathione, mycothiol and bacillithiol redox potentials in human pathogens	37
3.1 Development of redox-sensitive GFPs (roGFP2) as dynamic biosensors to measure real-time changes in the GSH redox potential	37
3.2 Monitoring intrabacterial changes in the GSH, BSH and MSH redox potentials in Gram-negative and Gram-positive bacteria	38
3.2.1 Application of Grx1-roGFP2 biosensors in eukaryotic organisms	38
3.2.2 Application of the Mrx1-roGFP2 biosensor in <i>Mycobacterium tuberculosis</i>	39
3.2.3 Application of the Brx-roGFP2 biosensor in <i>Staphylococcus aureus</i>	41
4. Conclusion and future perspectives	43
References	44

Chapter 1: Redox regulation by reversible protein S-thiolation in bacteria

Chapter 2: The role of bacillithiol in Gram-positive *Firmicutes*

Chapter 3: Protein S-bacillithiolation functions in thiol-protection and redox regulation of the glyceraldehyde-3-phosphate dehydrogenase Gap in *Staphylococcus aureus* under hypochlorite stress

Chapter 4: The aldehyde dehydrogenase AldA contributes to the hypochlorite defense and is redox-controlled by protein S-bacillithiolation in *Staphylococcus aureus*

Chapter 5: The glyceraldehyde-3-phosphate dehydrogenase GapDH of *Corynebacterium diphtheriae* is redox-controlled by protein S-mycothioloation under oxidative stress

Chapter 6: Redox-sensing under hypochlorite stress and infection conditions by the Rrf2-family repressor HypR in *Staphylococcus aureus*

Chapter 7: Real-time imaging of the bacillithiol redox potential in the human pathogen *Staphylococcus aureus* using a genetically encoded bacilliredoxin-fused redox biosensor

Chapter 8: Application of genetically encoded redox biosensors to measure dynamic changes in the glutathione, bacillithiol and mycothiol redox potentials in pathogenic bacteria

Curriculum vitae

Acknowledgements

Declaration

Zusammenfassung der Dissertation

Glutathion (GSH) ist die wichtigste niedermolekulare Thiolverbindung in eukaryontischen Organismen und Gram-negativen Bakterien, um die Redoxbalance aufrechtzuerhalten (**Kapitel 1-2**). Gram-positive Bakterien produzieren kein GSH, sondern dafür alternative Thiolverbindungen. Bacillithiol (BSH) fungiert als alternative Thiolverbindung in *Firmicutes*, wie z.B. in *Bacillus subtilis* und *Staphylococcus aureus*. Mycothiol kommt dagegen als wichtigste Thiolverbindung in allen Actinomycetes vor, wie z.B. in Mycobakterien und Corynebakterien. Niedermolekulare Thiolverbindungen spielen eine wichtige Rolle bei post-translationalen Modifikationen nach oxidativem Stress, wobei Cysteine zu S-Thiolierungen oxidiert werden können. S-Thiolierungen schützen die Thiolgruppe vor irreversibler Oxidation zur Cystein-Sulfonsäure und fungieren als Redox-Schalter.

Das Hauptziel dieser Arbeit war es, neue Thiolschalter und S-Thiolierungen im Thiolredoxproteom in den pathogenen Bakterien *S. aureus* und *Corynebacterium diphtheriae* nach HOCl stress zu identifizieren. HOCl ist ein sehr reaktives Oxidant und wird von Neutrophilen während der Infektion produziert. HOCl ist deshalb für die Abwehr des angeborenen Immunsystems gegen Bakterien von großer Bedeutung. Im Thiolredoxproteom von *S. aureus* USA300 konnten mittels der OxICAT-Methode 58 NaOCl-sensitive Cysteine identifiziert werden, die >10% erhöhte Oxidation nach NaOCl-Stress aufwiesen (**Kapitel 3-4**). Dazu zählten fünf S-bacillithiolierte Proteine, wie z.B. die Aldehyd-Dehydrogenasen GapDH und AldA, die ca. 29 % stärker oxidiert waren in der OxICAT-Analyse. GapDH und AldA sind in ihrem katalytischen Zentrum S-bacillithioliert, am Cys151 von GapDH und am Cys279 von AldA. GapDH ist das am häufigsten vorkommende S-bacillithiolierte Protein, welches mit 4% zum Gesamt-Cystein-Proteom in *S. aureus* beiträgt. Die katalytischen aktiven Zentren von GapDH und AldA sind sehr sensitiv gegenüber Überoxidationen und irreversiblen Inaktivierungen durch ROS *in vitro*. In Gegenwart von BSH und ROS kommt es zur S-Bacillithiolierung der aktiven Zentren von GapDH und AldA. Die S-Bacillithiolierung dient als Schutz der Thiolgruppe vor Überoxidation und führt ebenfalls zur reversiblen Inaktivierung der Enzyme. Durch molekulares Docking konnte weiterhin gezeigt werden, dass die S-Bacillithiolierung der Cysteine in den aktiven Zentren von GapDH und AldA keine Konformationsänderungen erfordert.

In *C. diphtheriae* wurde die glykolytische GapDH als S-mycothioliert nach HOCl-Stress identifiziert (**Kapitel 5**). GapDH ist ebenfalls das am häufigsten vorkommende Protein im Cystein-Proteom von *C. diphtheriae*. Nach Exposition von gereinigtem GapDH mit H₂O₂ und NaOCl kam es zur Überoxidation des aktiven Zentrums zur Sulfonsäure, was zur irreversiblen Inaktivierung führte. Die Oxidation von GapDH durch H₂O₂ und NaOCl in Gegenwart von MSH führte zur S-mycothioliierung und reversiblen GapDH Inaktivierung *in vitro*. Kinetische Messungen zeigten

weiterhin, dass die S-Mycothiolyse schneller abläuft als die Überoxidation zur Sulfonsäure. Die Reaktivierung von S-mycothiolierten GapDH konnte sowohl durch den Trx-Pathway als auch durch Mrx1 katalysiert werden *in vitro*. Die Reduktion der Mycothiolierungen mittels Mrx1 verlief wesentlich schneller im Vergleich zur Reduktion durch Trx. Somit wurde hiermit die glykolytische Glycerinaldehyd-3-Phosphat-Dehydrogenase GapDH als ein wichtiges S-thioliertes metabolisches Enzym in verschiedenen Gram-positiven Bakterien identifiziert und charakterisiert.

Wir waren weiterhin interessiert, neue HOCl-spezifische redox-sensitive Regulatoren zu identifizieren. Dazu wurde eine RNA-seq Transkriptomanalyse nach NaOCl-Stress durchgeführt. Wir konnten einen neuen Regulator der Rrf2-Familie identifizieren, der sehr stark durch HOCl-Stress im Transkriptom induziert wurde (**Kapitel 6**). HypR wurde als neuer redox-sensitiver Repressor charakterisiert, der die Expression des *hypR-merA*-Operons negativ reguliert. HypR wird direkt nach NaOCl und Diamid-Stress über eine reversible Thioloxydation reguliert. Durch Mutagenese wurde gezeigt, dass Cys33 und das konservierte Cys99 essential für das Redox-sensing nach NaOCl-Stress sind. Cys99 ist ebenfalls wichtig für die Repressor-Aktivität von HypR *in vitro* und *in vivo*. HypR wird nach NaOCl-Stress durch eine intermolekulare Disulfidbrückenbildung zwischen Cys33 und Cys99 *in vitro* und *in vivo* reguliert. HypR reguliert die Flavin-Disulfid-Oxidoreduktase MerA. Es konnte gezeigt werden, dass MerA am Schutz von *S. aureus* gegenüber NaOCl-Stress beteiligt ist und zum Überleben in Infektionsassays mit Makrophagen beiträgt.

Unsere weiteren Untersuchungen zielten darauf ab, die Veränderungen im BSH-Redoxpotential in *S. aureus* nach oxidativen Stress zu messen. Dafür wurde ein genetisch-kodierter Bacilliredoxin-fusionierter Brx-roGFP2-Biosensor konstruiert für die Analyse des BSH-Redoxpotentials in *S. aureus* während des Wachstums, nach oxidativem Stress und nach Antibiotika-Behandlung (**Kapitel 7-8**). Der Brx-roGFP2-Biosensor zeigte eine spezifische und schnelle Oxidation nach Inkubation mit geringen Mengen BSSB *in vitro*, welche auf das aktive Zentrum von Brx zurückzuführen war. Keine Oxidation des Biosensors wurde nach Inkubation mit anderen niedermolekularen Thiolverbindungen gemessen. Biosensor-Messungen in zwei MRSA-Isolaten USA300 und COL zeigten eine schnelle und dynamische Oxidation des Brx-roGFP2 Biosensors nach NaOCl und H₂O₂-Stress. Der Biosensor war konstitutiv oxidiert in verschiedenen BSH-negativen *S. aureus* Mutanten. Durch konfokale Laser-Scanning-Mikroskopie konnten die Veränderungen im BSH-Redoxpotential in *S. aureus* auf Einzelzell-Ebene bestätigt werden. Nach Infektionsversuchen mit THP-1 Makrophagen wurde eine 87 %-ige Oxidation des Biosensors in *S. aureus* COL gemessen. Jedoch wurden keine Veränderungen des BSH-Redoxpotentials nach Behandlung mit verschiedenen Antibiotika nachgewiesen. Dies weist darauf hin, dass Antibiotika in *S. aureus* keinen oxidativen Stress verursachen.

Unsere Untersuchungen zeigten, dass der neue Brx-roGFP2 Biosensor eine spezifische Äquilibrierung zwischen den BSH und roGFP2 Redoxpaaren katalysiert. Deshalb kann der Biosensor weiterhin in *S. aureus* angewandt werden für dynamische Messungen des BSH-Redoxpotentials. In zukünftigen Studien soll der Brx-roGFP2 Biosensor für das Screening des BSH-Redoxpotentials in *S. aureus*-Isolaten verschiedener klonaler Komplexe eingesetzt werden. Somit könnten Unterschiede in der Fitness und Entgiftung von ROS zwischen verschiedenen *S. aureus*-Isolaten untersucht werden als Abwehrmechanismen gegen das Immunsystem des Wirts. Der Biosensor kann ebenfalls in der Antibiotika-Forschung eingesetzt werden, um nach neuen ROS-produzierenden Antibiotika zu screenen, die einen Einfluss auf das BSH-Redoxpotential von *S. aureus* haben.

Summary of the dissertation

Glutathione (GSH) is the major low molecular weight (LMW) thiol of eukaryotic organisms and Gram-negative bacteria to maintain the redox balance (**chapters 1-2**). However, Gram-positive bacteria do not produce GSH. Bacillithiol (BSH) is utilized as alternative LMW thiol in *Firmicutes*, such as *Bacillus subtilis* and *Staphylococcus aureus*. Mycothiol functions instead as major LMW thiol in all Actinomycetes, such as *Mycobacteria* and *Corynebacteria*. Under oxidative stress, LMW thiols form mixed disulfides with proteins thiols, termed as S-thiolations which function as thiol-protection and redox-control mechanism.

The main goal of this work was the identification of novel thiol-switches and S-thiolated proteins in the thiol-redox proteome of the human pathogens *S. aureus* and *Corynebacterium diphtheriae* under hypochlorous acid (HOCl) stress. HOCl is a highly reactive oxidant that is produced during neutrophil infections and is the major cause of bacterial killing. Using the thiol-redox proteomics approach OxICAT, 58 NaOCl-sensitive protein thiols with >10% increased oxidations could be identified in *S. aureus* USA300 (**chapters 3-4**). Among these are five S-bacillithiolated proteins, including the two aldehyde dehydrogenases GapDH and AldA which showed the highest oxidation increase of ~29 % in the OxICAT analysis. GapDH and AldA were S-bacillithiolated at their active site Cys residues, Cys151 in GapDH and Cys279 in AldA. GapDH represents the most abundant S-bacillithiolated protein contributing with 4% to the total Cys proteome of *S. aureus*. The catalytic active sites of GapDH and AldA are very sensitive to overoxidation and irreversible inactivation by ROS *in vitro*. In the presence of BSH, S-bacillithiolation protects the active sites against irreversible oxidation and functions in reversible inactivation. Using molecular docking it was further shown that BSH can undergo disulfide formation with the GapDH and AldA active site Cys residues without major conformational changes.

In *C. diphtheriae*, the glycolytic GapDH was identified as main target for S-mycothiolation under HOCl stress (**chapter 5**). In addition, GapDH is also the most abundant protein in the Cys proteome of *C. diphtheriae*. Exposure of purified GapDH to H₂O₂ and NaOCl resulted in irreversible inactivation due to overoxidation of the active site *in vitro*. Treatment of GapDH with H₂O₂ or NaOCl in the presence of MSH resulted in S-mycothiolation and reversible GapDH inactivation *in vitro*, which was faster compared to the overoxidation pathway. Reactivation of S-mycothiolated GapDH was catalyzed by the Trx and the Mrx1 pathways *in vitro*. De-mycothiolation by Mrx1 was faster compared to Trx. Thus, it is interesting to note that the glycolytic GapDH is a major target for S-thiolation by BSH and MSH across Gram-positive bacteria.

To identify novel redox-sensing regulators in *S. aureus* USA300 that could provide protection under HOCl stress, we used an RNA-seq transcriptomic approach. We identified the

novel Rrf2-family redox-sensing regulator HypR as most strongly induced under NaOCl stress in the transcriptome under NaOCl stress (**chapter 6**). HypR was characterized as redox-sensing repressor that negatively controls expression of the *hypR-merA* operon and directly senses and responds to NaOCl and diamide stress by a thiol-based redox switch. Mutational analysis identified Cys33 and the conserved Cys99 as essential for NaOCl-sensing while Cys99 is also important for repressor activity of HypR *in vitro* and *in vivo*. The redox-sensing mechanism of HypR involves Cys33-Cys99' intersubunit disulfide formation by NaOCl stress both *in vitro* and *in vivo*. Moreover, the HypR-controlled flavin disulfide reductase MerA was shown to protect *S. aureus* against NaOCl stress and increased survival in J774A.1 macrophage infection assays.

We were further interested to investigate the changes in the BSH redox potential under NaOCl stress in *S. aureus*. Thus, we constructed a genetically encoded bacilliredoxin-fused Brx-roGFP2 redox biosensor for dynamic live-imaging of BSH redox potential changes in *S. aureus* during the growth, oxidative stress and under antibiotics treatment (**chapter 7-8**). The Brx-roGFP2 biosensor showed a specific and rapid response to low levels BSSB *in vitro* which required the active-site Cys of Brx. However, the biosensor was unresponsive to other LMW thiol disulfides *in vitro*. Dynamic live-imaging in two MRSA isolates USA300 and COL revealed fast and dynamic responses of the Brx-roGFP2 biosensor under NaOCl and H₂O₂ stress and constitutive oxidation of the probe in different BSH-deficient mutants. Using confocal laser scanning microscopy, the changes in the BSH redox potential in *S. aureus* were confirmed at the single cell level. In phagocytosis assays with THP-1 macrophages, the biosensor was 87 % oxidized in *S. aureus* COL. However, no changes in the BSH redox potential were measured after treatment with different antibiotics classes indicating that antibiotics do not cause oxidative stress in *S. aureus*.

Our studies demonstrate that this novel Brx-roGFP2 biosensor catalyzes specific equilibration between the BSH and roGFP2 redox couples and can be used for dynamic live imaging of the BSH redox potential inside *S. aureus*. Future studies are directed to apply this Brx-roGFP2 biosensor for screening of the BSH redox potential across *S. aureus* isolates of different clonal complexes to reveal the differences in pathogen fitness and in their ROS detoxification capacities as defense mechanisms against the host immune system. In addition, this biosensor can be applied in drug research to screen for new ROS-generating antibiotics that affect the BSH redox potential in *S. aureus*.

Introduction and general conclusion

1. Introduction into *Staphylococcus aureus* as major human pathogen

Staphylococcus aureus is an opportunistic human pathogen that colonizes the anterior nares and the skin of one-quarter of the human population without symptoms of infections (49). However, *S. aureus* is also a serious human pathogen that can cause many infectious diseases ranging from local skin abscesses to life-threatening diseases, such as septicaemia, endocarditis and pneumonia (73,96).

The population structure of *S. aureus* is clonal with several genetic lineages defined as clonal complexes (CC) of sequence types (STs). These include ten dominant human lineages of *S. aureus* that are responsible for most infections (CC1, CC5, CC8, CC12, CC15, CC22, CC25, CC30, CC45 and CC51). Variation in the core genome is the result of single nucleotide polymorphisms (SNPs) which are either silent or result in a change in the amino acid sequence (50). The divergence can also occur by the difference in the lengths of repetitive sequences in the *S. aureus* genome (50,66). DNA transfer between lineages is controlled by restriction-modification systems that are partly encoded on mobile genetic elements (MGE) (50). Approximately 15-20% of the *S. aureus* genome consists of MGE, including bacteriophages, pathogenicity islands, plasmids, transposons, integrative conjugative elements (ICEs), integrons, and the staphylococcal cassette chromosome *mec* (SCC*mec*). These MGE encode many virulence factors, immune evasion clusters and antibiotic resistance determinants (50,66,92,134). The high variation of the MGE across *S. aureus* genetic lineages results in a high genome diversity and plasticity. Moreover, MGEs lead to spread of antibiotics resistance determinants resulting in the prevalence of multiple antibiotic resistant *S. aureus* isolates in hospitals and in the community.

1.1. The prevalence of multiple antibiotics resistant *S. aureus* isolates

Previously, β -lactam antibiotics were successful applied for the treatment of *S. aureus* infections. However, over the last years multiple antibiotic resistant strains, such as methicillin-resistant *S. aureus* (MRSA) isolates spread rapidly in hospitals and in the community (18,66). *S. aureus* with its extraordinary adaptive evolution quickly responds to each new challenge by the development of a new resistance mechanism (66). Nowadays, *S. aureus* strains are resistant to the last resort of antibiotics, such as vancomycin, daptomycin, and linezolid (94,107,137). Bacteria have evolved several antibiotics resistance mechanisms, including limiting uptake of the drug, modification of the drug or drug target, inactivation of the drug, and efflux pumps for elimination of the drug (117). For example, penicillin binds to the transpeptidases, termed as penicillin binding proteins (PBP),

and inhibits the formation of peptide cross-bridges in the peptidoglycan cell wall. As penicillin resistance mechanism, β -lactamases were acquired to hydrolyze the peptide bond of the β -lactam ring structure for drug inactivation (117). Ampicillin and oxacillin are β -lactamase stable β -lactam antibiotics that were later introduced to treat *S. aureus* infections. However, *S. aureus* acquired an alternative PBP2a encoded by *mecA* with lower affinity to β -lactam antibiotics that allowed continued cell wall biosynthesis. The *mecA* gene is located on the MGE SCC*mec* and is transferred through horizontal gene transfer (107,140,176). Moreover, another alternative PBP4 evolved as additional β -lactam resistance mechanism in MRSA strains (107).

The glycopeptide antibiotic vancomycin binds to the D-Ala-D-Ala moiety of the peptide side chain and blocks peptide crosslinks of the peptidoglycan (57,111). There are low and high level vancomycin resistant *S. aureus* strains, termed as vancomycin-intermediate *S. aureus* (VISA) and vancomycin-resistant *S. aureus* (VRSA) strains (57). VISA strains possess a thicker cell wall, which reduces the permeability for vancomycin uptake. VRSA strains have acquired the *vanA* operon, carried by the transposon Tn 1546 from vancomycin-resistant *Enterococci* (57,72). The *vanA* operon catalyzes the synthesis of the modified peptidoglycan precursors with the D-Ala-D-lactate peptide, which has lower affinity for vancomycin compared to the D-Ala-D-Ala moiety (17,72).

The epoxide antibiotic fosfomycin inhibits bacterial peptidoglycan biosynthesis by inactivation of the UDP-N-acetylglucosamine-3-enolpyruvyltransferase (MurA). In *S. aureus*, FosB functions as a BSH-S-transferase (Bst) to conjugate BSH to the epoxide forming an inactive BS-fosfomycin conjugate (136,141). Other fosfomycin resistance mechanisms involve the mutation of the *glpT* or *uhpT* transporters, which blocks the uptake of fosfomycin (39,136).

1.2. The diversity of virulence factors of *S. aureus* contributing to pathogenesis

S. aureus is an important human pathogen that can cause many life-threatening infections in humans, especially when it enters the bloodstream. *S. aureus* produces many different virulence factors that participate in pathogenesis, allowing this pathogen to adhere to surfaces and tissues, to evade from the innate immune system, and to cause toxic effects in the host (32,37,52,98). These virulence factors are often encoded on MGEs, such as prophages or pathogenicity islands that can spread resulting in new virulent strains (1,7,93). The virulence factors include cell surface-associated proteins, such as adhesins as well as secreted extracellular toxins and enzymes (**Fig. 1**) (32,63,91,183). In addition, immune evasion clusters often encode virulence factors that function in neutralization of the complement system, antibodies and other immune defense components that are implicated in immune evasion.

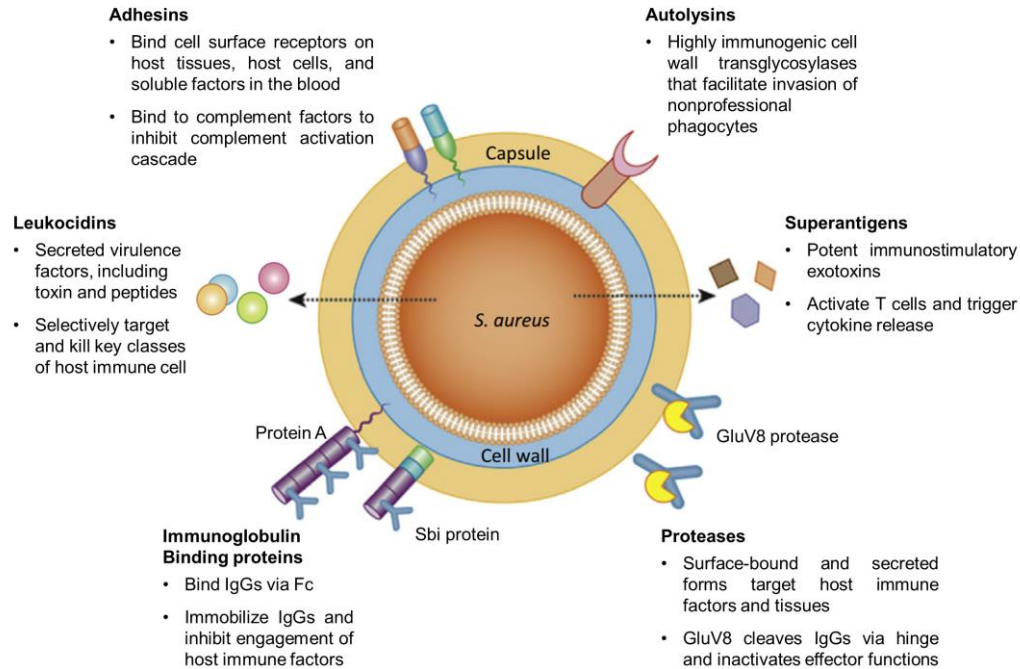


Figure 1. *Staphylococcus aureus* virulence factors. *S. aureus* produces different virulence factors that contribute to pathogenesis and immune evasion. The figure is from reference (147).

S. aureus produces several cell surface factors that have numerous functions, including adhesion to and invasion of host cells and tissues, evasion of immune responses and biofilm formation. The largest class of surface-associated virulence factors are “microbial surface components recognizing adhesive matrix molecules” (MSCRAMMs) (51). Fibronectin-binding proteins (FnBP), clumping factors (Clf), proteinA (Spa) and collagen-binding protein (Cna) are the major *S. aureus* MSCRAMMs. These proteins play important roles in microbial adhesion to host cells and establish the first steps of an infection. They also prevent *S. aureus* from recognition by the host immune system (51,63,183). Apart from MSCRAMMs, the capsular polysaccharides expressed by *S. aureus* are involved in the pathogenesis of staphylococcal infections. The main functions of the capsule are to impede phagocytosis by neutrophils, and to enhance bacterial colonization and persistence on mucosal surfaces (91,128). *S. aureus* produces also Staphyloxanthin which is the golden carotenoid pigment from which the species name “aureus” is derived (30). This yellow pigment has antioxidant functions to resist oxidative stress and killing by neutrophils after phagocytosis. Non-pigmented *S. aureus* mutants have increased sensitivity toward ROS, RNS and HOCl, and are more vulnerable to neutrophil killing (59,91).

S. aureus also secretes many virulence factors, such as extracellular enzymes and toxins, which play important roles in pathogenesis. They function in host cell lysis, tissue degradation and interfere with the host immune system (91). These secreted virulence factors include superantigens, cytolytic toxins and various extracellular enzymes. The enterotoxins are superantigens that stimulate 5–30% of all T-cells for enhanced cytokine secretion causing

immune-stimulatory host responses. This allows *S. aureus* to cause a variety of life-threatening systemic infections, such as toxic shock syndrome, atopic dermatitis, pneumonia and endocarditis (91,145,154). In addition, *S. aureus* secretes many cytolytic toxins, including pore-forming α -, β -, and γ -hemolysins, leukocidins, and phenol-soluble modulins (Psm). These toxins form barrel-like pores in the host cell membranes and cause cell lysis and inflammation (91). *S. aureus* also secretes extracellular enzymes, which function in host tissue degradation and inactivation of host antimicrobial components, such as lipids, defensins, antibodies and complement mediators. Host cell degradation is required for supply of nutrients for bacterial growth and dissemination (37,91). *S. aureus* encodes also several immune evasion factors, including staphylococcal complement inhibitor (SCIN), chemotaxis inhibitory protein of *S. aureus* (CHIPS), extracellular fibrinogen binding protein (Efb), and formyl peptide receptor-like-1 inhibitory protein (FLIPr). These proteins can have a profound impact on the innate and adaptive immune system (32).

1.3. Regulatory mechanisms of *S. aureus* virulence factor expression

The pathogenesis of *S. aureus* infection is a complex process involving a tight regulation of virulence factors during different stages of infections, such as colonization, internalization, intracellular growth and dissemination (3,157). *S. aureus* encodes several interlinked regulatory pathways for virulence factors expression, composed of two-component signal transduction systems (TCS), global transcriptional regulators, alternative sigma factors and small non-coding RNAs. Important virulence gene regulatory systems are the staphylococcal accessory gene regulator A (SarA) and other SarA-family proteins (SarA, SarZ, MgrA, SarR, SarS, SarT, SarU, Rot), the alternative stationary phase sigma factor SigB, the quorum sensing accessory gene regulator TCS (AgrABC) and the staphylococcal accessory element TCS (SaeRS) that are induced under infection conditions (32,50). These virulence gene regulators respond to different signals in the host, e.g. cell density, nutrient availability, temperature, pH, osmolarity, and oxygen tension to up-regulate different virulence factors (157).

The Agr TCS controls the expression of a large regulon, including many exotoxins and exoenzymes as well as surface-associated proteins that are essential for virulence. The Agr system is also important for biofilm formation since it responds to quorum sensing cell density signals produced in *S. aureus* after attachment on surfaces (15,83). The major effector of the Agr system is the small non-coding RNAIII which regulates post-transcriptionally the expression of virulence genes by enhancing mRNA stability of the *hla* transcript encoding α -toxin and by preventing translation of *spa* or *coa* transcripts (50,83). Thus, activation of the Agr TCS leads to induction of cytotoxins and exoenzymes as well as down-regulation of surface-associated proteins.

The SaeRS two-component system is crucial for the survival of *S. aureus in vivo* and regulates the expression of many virulence factors involved in bacterial adhesion, toxicity and immune evasion (32,142). The SaeRS regulon includes genes encoding hemolysins and leukocidins which promote the destruction of neutrophils by intracellular *S. aureus*. Other virulence factors up-regulated by SaeRS include nucleases, proteases, immune evasion factors and FnBPs. In addition, the SaeRS system contributes to virulence in animal models of necrotizing pneumonia and skin infection (15,50).

The regulation of virulence determinants also involves the alternative sigma factor SigB which controls a large general stress regulon and is induced under heat, salt, MnCl₂ and alkaline stress (12,130). SigB has been shown to play an important role under infection conditions and controls biofilm formation and several virulence factors, such as adhesins (113,114). SigB specifically protects *S. aureus* against superoxide stress released by neutrophils during the oxidative burst (15). The SigB regulon was induced after internalization of *S. aureus* by bronchial epithelial cells. SigB was required for intracellular growth as demonstrated by transcriptomics and proteomics (102,110,133). Moreover, SigB has been implicated as central regulator in long-term persistence in human osteoblasts and controls the small colony variant (SCV) phenotype of persistent *S. aureus* infections (161,162).

SCVs are characterized by small colonies of slow growing *S. aureus* cells with a reduced metabolism, resulting in a decreased susceptibility to antibiotics and oxidative stress. *S. aureus* SCVs are able to survive and persist for long time periods inside macrophages and neutrophils (87,163). SCVs express a changed pattern of virulence factors to allow intracellular persistence. Reduced levels of α -hemolysin are secreted to ensure intracellular survival and the level of fibronectin-binding proteins is increased to promote invasion of epithelial and endothelial cells. Furthermore, SCVs are frequently auxotrophic for menadione and heme, which are electron carriers of the respiratory chain and its defect leads to growth arrest (58,163). In conclusion, *S. aureus* encodes many virulence factors that are regulated by a complex network of virulence regulators and phenotypic switches to SCV allowing its adaptation to different stages of infections, such as colonization, internalization, dissemination and long-term persistence.

2. Adaptation of *S. aureus* to reactive oxygen and chlorine species (ROS and RCS) under infection conditions

In addition to these virulence factors, *S. aureus* has also efficient protection mechanisms against the host immune defense during invasion (94). During infections, *S. aureus* is exposed to the oxidative burst of activated macrophages and neutrophils, including reactive oxygen and nitrogen species (ROS, RNS) and the strong oxidant hypochlorous acid (HOCl) (178,179). As defense

mechanisms, *S. aureus* produces detoxification and antioxidant enzymes that are regulated by redox-sensing virulence regulators of the SarA/MarR family including SarZ and MgrA as well as the novel redox sensing HOCl-specific regulator HypR (59,95) that was discovered as part of this PhD thesis. In addition, *S. aureus* utilizes the low-molecular-weight (LMW) thiol bacillithiol (BSH, Cys-GlcNAc-Mal) as defense mechanism against the oxidative burst under infection conditions (97). Importantly, *S. aureus* BSH-deficient mutant showed an increased sensitivity in macrophage infection assays indicating the important role of BSH for *S. aureus* survival and in host-pathogen interactions (136,137). The generation of ROS and RCS in bacteria as well as the bacterial defense mechanisms against ROS and RCS are summarized in the following sections.

2.1. Sources of ROS and RCS in bacteria

Reactive Oxygen Species (ROS) are generated in bacteria during aerobic respiration, intracellular redox reactions, and redox-active antibiotics (59,169). Molecular oxygen (O_2) is the best terminal electron acceptor in aerobic bacteria and is reduced by four electrons to water during respiration. The incomplete stepwise electron transfer to O_2 leads to generation of ROS, including superoxide anion ($O_2^{\bullet-}$) hydrogen peroxide (H_2O_2) and the highly reactive hydroxyl radical ($HO\bullet$) (59,97). $O_2^{\bullet-}$ and H_2O_2 can be also generated by accidental autooxidation of flavoproteins (47,75). Superoxide dismutases are metalloenzymes that rapidly convert $O_2^{\bullet-}$ to H_2O_2 . In presence of Fe^{2+} , H_2O_2 is converted to the highly reactive $HO\bullet$ in the Fenton reaction (97).

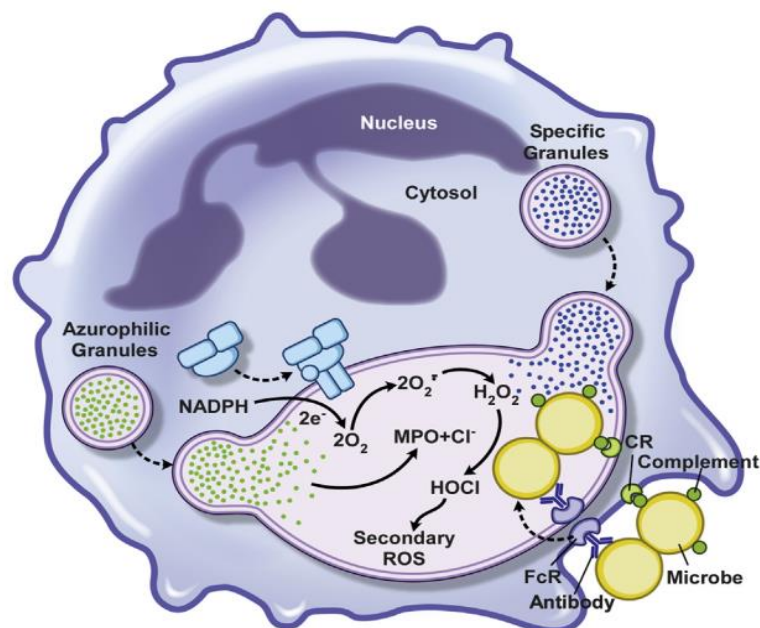


Figure 2. Neutrophils produce Reactive Oxygen Species (ROS) and HOCl to kill *S. aureus*. The enzyme NADPH-dependent oxidase (Nox, blue cluster) produces superoxide anion, which is converted to H_2O_2 by SOD. The myeloperoxidase MPO catalyzes the conversion of H_2O_2 and chloride to the strong oxidant HOCl. The figure is from reference (85).

Pathogenic bacteria are exposed to ROS and RCS during the oxidative burst of activated macrophages and neutrophils. The phagocyte NADPH-dependent oxidase (NOX) transfers electrons from cytosolic NADPH to intra-phagosomal molecular oxygen, to generate $O_2^{\bullet-}$. The superoxide anion is converted to H_2O_2 by the superoxide dismutase (105). Myeloperoxidase (MPO) is released during degranulocytosis producing the highly reactive HOCl from H_2O_2 and Cl^- (**Fig. 2**) (48,59,85,172). HOCl is a strong two-electron oxidant and the primary killing agent for bacteria as first line defense of the innate immune system. HOCl reacts with most cellular macromolecules leading to cell death and hence it is important to study the bacterial targets for oxidation by HOCl and bacterial defense mechanisms, which avoid pathogen destruction (99,178).

2.2. Post-translational thiol-modifications caused by ROS and RCS in bacteria

ROS and HOCl can damage all cellular macromolecules, including DNA, proteins and lipids. Therefore, bacteria are equipped with several defense mechanisms, such as ROS detoxification enzymes (catalases, peroxiredoxins and superoxide dismutases) and thiol-disulfide reducing systems to neutralize the reactive species or to repair the resulting damage (97,159).

The cysteine thiol group is the strongest nucleophile and susceptible for oxidation by ROS and HOCl. However, most Cys residues are present in its protonated form and have a neutral pK_a of 8.3–8.6, which are not susceptible for oxidation (41,156,177). In presence of positively charged residues surrounding the Cys thiol, the pK_a value can decrease leading to a more reactive Cys residue. An acidic Cys thiol is mostly present in its deprotonated form as thiolate anion at physiological pH values (41,177). Thiolates are highly reactive nucleophiles and can be reversibly and irreversibly post-translationally modified by ROS or HOCl (41,69,177). ROS lead first to oxidation of protein thiols to Cys sulfenic acids as unstable intermediates (SOH). Sulfenic acids react further to form a disulfide bond with another Cys residue or are irreversibly oxidized to sulfinic acid (SO_2H) and sulfonic acid (SO_3H). Among the disulfides, we can differ between intramolecular and intermolecular protein disulfides or mixed disulfides between protein thiols and LMW thiols, termed as S-thiolations (e.g. S-glutathionylations, S-mycothiolations, and S-bacillithiolations) (**Fig. 3**).

HOCl is a strong two-electron oxidant and chlorinating agent and reacts with Cys thiols seven orders of magnitudes faster compared to H_2O_2 (36,64). Cys residues are oxidized by HOCl to the unstable sulfenyl chloride intermediate (SCI), which reacts further to form protein disulfides or S-thiolations with LMW thiols. In the absence of proximal thiols, Cys-SCI is quickly overoxidized to Cys sulfinic or sulfonic acids (35). In addition, sulfenyl chlorides can react with amines to form irreversible sulfonamide linkages ($R-SO_2-NH-R'$) (64,69). Of note, reversible thiol-oxidations

including S-thiolations protect thiol groups against irreversible overoxidations and function as thiol-redox switches to regulate protein functions. Advances in thiol-redox proteomics methods and high-resolution mass spectrometers allow the proteome-wide detection and quantifications of redox modifications that are caused by different reactive species. Identification of the protein disulfides and protein S-thiolations in bacteria is the basis for the detailed characterization of their physiological roles in the adaptation of bacteria to oxidative stress (27-29,70,71,73).

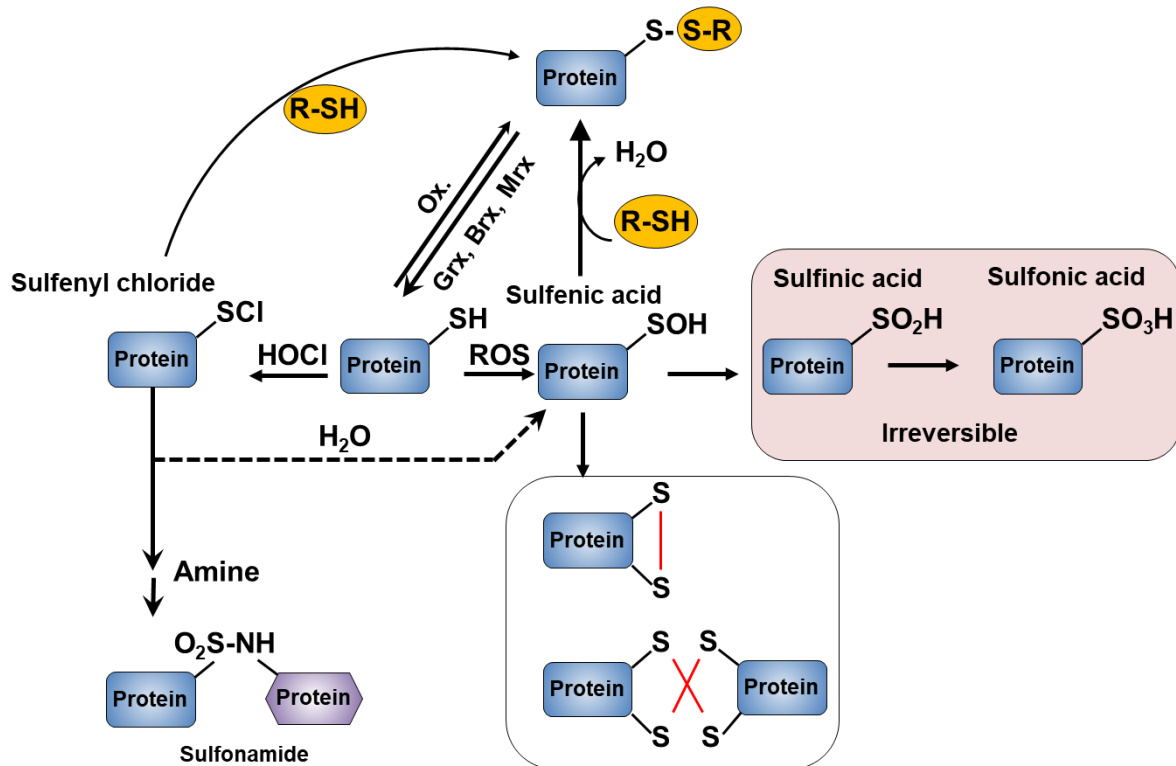


Figure 3. Post-translational thiol-modifications of cysteine residues. The Cys thiol group is oxidized by ROS to form an unstable Cys sulfenic acid intermediate (Cys-SOH) that reacts further with proximal thiols to form intramolecular and intermolecular disulfides. The Cys-SOH can also undergo mixed disulfide formation with LMW thiols (RSH), such as glutathione (GSH), bacillithiol (BSH) or cysteine, termed as S-thiolations. HOCl leads to chlorination of protein thiols to sulfenylchloride intermediates (Cys-SCI) that react further to form disulfides. In the absence of proximal thiols, the chlorinated Cys is overoxidized to Cys sulfinic and sulfonic acids. Sulfenyl chlorides can also react with amines to form irreversible sulfonamide linkages. Disulfides function as redox switches to control protein activity and to protect thiols against irreversible overoxidation. The figure is adapted from references (97,132).

2.3. The low molecular weight (LMW) thiols bacillithiol and mycothiol as bacterial defense mechanisms against ROS and RCS

All cells have to maintain their reduced state of the cytoplasm to ensure proper protein functions and cellular survival. To maintain the redox balance, eukaryotic and prokaryotic organisms utilize LMW thiols, which are small thiol-containing compounds that are often produced in millimolar concentrations (97). LMW thiols play an important role in the defense against ROS, RES,

antibiotics, heavy metals and other redox-active compounds (20,104,174). The best-studied LMW thiol is the tripeptide glutathione (GSH), that is produced in eukaryotic organisms, most Gram-negative bacteria and in some Gram-positive bacteria, including *Streptococcus agalactiae*, *Listeria monocytogenes*, and *Clostridium acetobutylicum* (42,97). However, Gram-positive bacteria do not produce GSH and instead utilize alternative LMW thiols. *Bacillus* and *Staphylococcus* species utilize bacillithiol (BSH) while Actinomycetes, such as *Streptomyces*, *Mycobacterium* and *Corynebacterium* species produce mycothiol (MSH) as their major LMW thiol (Fig. 4) (124,127).

2.3.1. Biosynthesis and functions of bacillithiol in *Firmicutes*

2.3.1.1. Biosynthesis of BSH in *B. subtilis* and *S. aureus*

In 2009, bacillithiol (BSH) was discovered as major LMW thiol in many *Firmicutes*, including *Bacillus* and *Staphylococcus* species, *Deinococcus radiodurans*, and *Streptococcus agalactiae* (97,149). BSH is composed of Cys-GlcN-malate and is synthesized in three steps. The glycosyltransferase BshA catalyzes the addition of UDP-N-acetylglucosamine (UDP-GlcNAc) to L-malate through a metal-independent SN1-like mechanism, forming N-acetylglucosaminyl-malate (GlcNAc-Mal). This is followed by the deacetylation of GlcNAc-Mal by the N-acetylhydrolase BshB to generate glucosamine malate (GlcN-Mal). The last step of BSH biosynthesis involves the putative cysteine ligase BshC that adds Cys to GlcN-Mal intermediate (55).

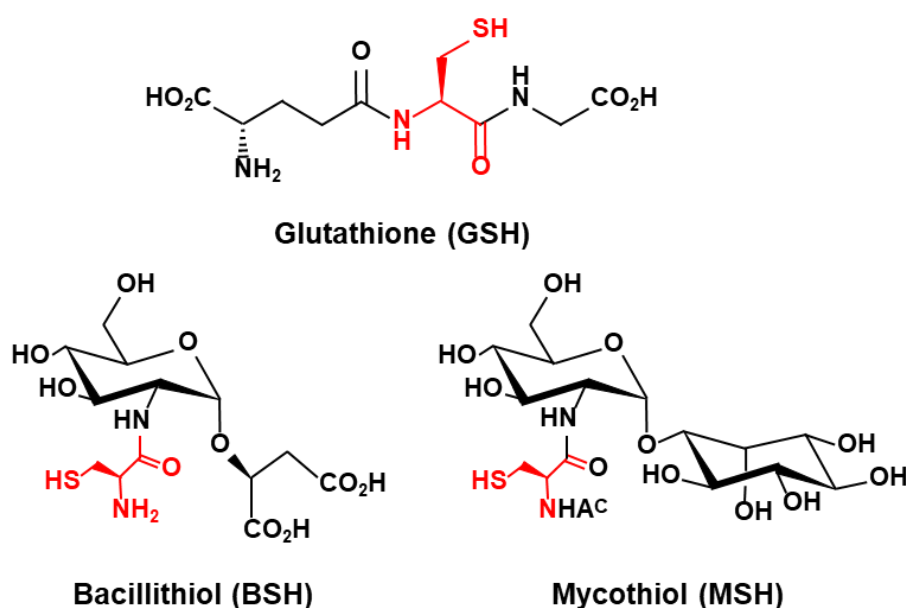


Figure 4. The main LMW thiols in bacteria. Glutathione (GSH) is utilized as major LMW thiols in eukaryotes and Gram-negative bacteria. Mycothiol (MSH) is the major LMW thiol in Actinomycetes and bacillithiol (BSH) is utilized by some *Firmicutes*. The figure is from reference (97).

B. subtilis encodes two deacetylases, BshB1 and BshB2. BSH levels can be still detected in the *bshB1* mutant, but not in *bshB1 bshB2* double mutant strain (55). This indicates that both BshB1 and BshB2 enzymes have overlapping roles for deacetylation to allow BSH synthesis, although BshB1 seems to play the major role. In contrast, *S. aureus* has only a single BshB deacetylase which is essential for BSH synthesis. BshB also functions as BSH conjugate amidase (Bca) in detoxification of toxic electrophiles analogous to the MSH-S-conjugate amidase Mca (20,55,97,138).

2.3.1.2. Functions of BSH in detoxification and metal homeostasis in *B. subtilis* and *S. aureus*

BSH plays an important role in detoxification of ROS, RNS, RCS, metal homeostasis and antibiotics. BSH deficient mutants are sensitive to various oxidants and electrophiles such as hypochlorite, diamide, H₂O₂, monobromobimane and methylglyoxal (**Fig. 5**) (20,97). Reactive electrophiles and xenobiotics are detoxified by direct conjugation to BSH or by conjugation reactions catalyzed by the DinB-family S-transferases. BSH participates in the detoxification of antibiotics such as rifamycin and fosfomycin (125,141). *B. subtilis* and *S. aureus* encode the BSH-S-transferase or epoxide hydrolase FosB, which inactivates fosfomycin by catalyzing the nucleophilic addition of BSH to the C₂ position of the epoxide ring forming an inactive BS-fosfomycin conjugate (136,141). BSH is involved in methylglyoxal detoxification and functions as a cofactor for BSH-dependent glyoxalases (GlxA and GlxB) in *B. subtilis* (68). Methylglyoxal reacts spontaneously with BSH to form BSH-hemithioacetal that is converted to S-lactosyl BSH by GlxA. GlxB catalyzes the hydrolysis of S-lactosyl-BSH to lactate as endproduct which is secreted (19,20).

In addition, the function of BSH in metal homeostasis (e.g. Zn, Fe) has been investigated recently (20). In *B. subtilis*, BSH is used as Zn buffer under conditions of Zn²⁺ excess, allowing the cells to avoid zinc intoxication (101). The thiolate and carboxylate groups of BSH can bind and store Zn²⁺ as BSH₂: Zn complex under conditions of Zn²⁺ stress (101). Treatment of BSH deficient mutants with Zn²⁺ resulted in a decreased accumulation of Zn²⁺ compared to the wild type due to increased expression of CadA and CzcD metal efflux systems. BSH also protects against Zn²⁺ toxicity in cells lacking Zn efflux pumps. Moreover, the Zn efflux system that is encoded by *cadA* is induced under thiol-stress conditions, such as diamide (20,97).

BSH also plays a role in Fe homeostasis and in the transport of FeS clusters to apo-proteins in *B. subtilis* and *S. aureus* (43,144). The BSH deficient mutant has a growth defect in media lacking leucine or isoleucine compared to the wild type. The growth defect could be compensated after addition of these amino acids or by exogenous Fe²⁺ (144). In *S. aureus*, FeS

clusters are synthesized by the gene products of the *suf* operon. The FeS cluster are then transferred via carrier proteins (Nfu or SufA) to the apo-proteins (103,144). The *bshA nfu* double mutant showed growth defects in defined medium lacking glutamate or glutamine. In addition, the enzyme activities of aconitase and glutamate synthase were lower in the double mutants compared to that in the single mutants (144). In addition, growth phenotypes and enzymatic defects of the *bshA* mutant were restored in strains overexpressing *nfu* or *sufA* (143,144). These results indicate that BSH participates in the biogenesis of FeS cluster proteins independently of the Suf and Nfu carrier proteins. However, the details have yet to be explored and may involve also bacilliredoxins for the transfer of the FeS clusters.

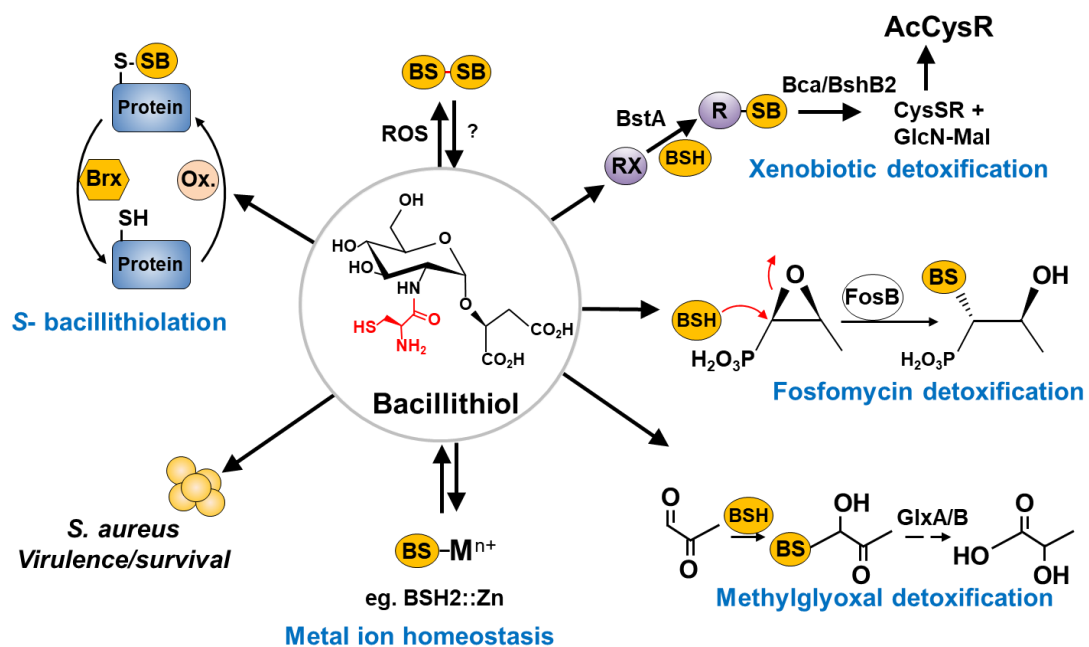


Figure 5. The main cellular functions of bacillithiol (BSH) in *B. subtilis* and *S. aureus*. Bacillithiol (BSH) functions in detoxification of ROS, RES, HOCl, and antibiotics (fosfomycin, rifampicin) in *B. subtilis* and *S. aureus*. BSH is oxidized by ROS to bacillithiol disulfide (BSSB). Electrophiles (RX) are conjugated to BSH by the BSH S-transferase BstA to form BS-electrophiles (BSR). BSH S-conjugate amidase Bca or BshB2 cleave BSR into CysSR and mercapturic acids (AcCysR) that are exported from the cell. BSH is cofactor for the epoxide hydrolase FosB which adds BSH to fosfomycin for its detoxification. BSH functions in methylglyoxal detoxification as a cofactor for the glyoxalases GlxA and GlxB in *B. subtilis*. GlxA converts BSH-hemithioacetal to S-lactoyl-BSH that is further detoxified by GlxB to D-lactate. BSH serves as Zn buffer under conditions of Zn excess in *B. subtilis*. In *S. aureus*, BSH is important under infection-related conditions and increased the survival of *S. aureus* in phagocytosis assays using murine macrophages. Under conditions of NaOCl stress, proteins are oxidized to mixed disulfides with BSH, termed as S-bacillithiolations which is reversed by bacilliredoxins. The figure is adapted from reference (97).

2.3.1.3. Functions of BSH in the virulence of *S. aureus*

The role of BSH in stress resistance and under infection conditions in *S. aureus* was investigated in phenotype analyses of *bshA* mutants. The survival of the *bshA* mutant was decreased in human whole blood phagocytosis assays with neutrophils and macrophages (136). Microarray analyses

of the *S. aureus* COL *bshA* mutant showed that staphyloxanthin biosynthetic genes (*crtMNQ*) are upregulated (2.08 to 2.63-fold) while the level of staphyloxanthin was strongly decreased in the *bshA* mutant. This suggests lower radical scavenging ability in the absence of BSH (20). Staphyloxanthin is an important virulence factor and protects *S. aureus* against the oxidative burst in neutrophil infection assays and enhances the fitness of *S. aureus* (30). Notably, strains of the *S. aureus* NCTC8325 lineage (e.g. *S. aureus* SH1000) do not produce BSH due to an 8 bp-duplication in the *bshC* gene that catalyzes the last step of the BSH biosynthesis (125,137). In phagocytosis assays using murine macrophages or human epithelial cell lines, the survival of SH1000 was impaired compared to the *bshC* complemented *S. aureus* SH1000 strain (137). Hence, BSH provides protection against the host-immune system under infection conditions and contributes to virulence and fitness of *S. aureus*.

2.3.1.4. Physiological role of protein S-bacillithiolations in *B. subtilis* and *S. aureus*

BSH plays an important role in post-translational modifications of proteins under oxidative stress in *B. subtilis* and *S. aureus*. In response to HOCl stress, protein thiols are oxidized to mixed disulfides with BSH, termed as protein S-bacillithiolation (69,97). Protein S-bacillithiolations have analogous functions compared to S-glutathionylations in eukaryotes to protect vulnerable Cys residues against irreversible overoxidation to Cys sulfinic and sulfonic acids (97). In addition, we have shown that protein S-bacillithiolation can regulate the activities of metabolic enzymes and redox-sensing regulators. S-bacillithiolation is a widespread redox-modification in *Bacillus* and *Staphylococcus* species. Eight conserved and 29 unique S-bacillithiolated proteins were identified using shotgun proteomics in *Bacillus subtilis*, *B. amyloliquefaciens*, *B. pumilus*, *B. megaterium*, *Staphylococcus carnosus* and *S. aureus* (28,29).

In general, the S-bacillithiolome contains mainly biosynthetic enzymes for amino acids (methionine, cysteine, branched chain and aromatic amino acids), cofactors (thiamine), nucleotides (GTP) as well as translation factors (Tuf), chaperones (DnaK, GrpE), redox and antioxidant proteins, such as peroxiredoxins (YkuU), thiol-disulfide oxidoreductases (YumC) and bacilliredoxins (BrxA, BrxB and BrxC) (29). Many conserved S-bacillithiolated proteins are also targets for S-mycothiolation in the MSH-producing *C. glutamicum*, such as TufA, the methionine synthase MetE, the inosine monophosphate dehydrogenase GuaB and the inorganic pyrophosphatase PpaC (27). The most abundant S-bacillithiolated protein in *Bacillus* species under NaOCl stress is the methionine synthase MetE. MetE is S-bacillithiolated at its Zn-binding active site Cys730 and at the surface exposed Cys719 (28). S-bacillithiolation of MetE inactivates the enzyme causing a methionine auxotrophy phenotype under NaOCl stress. Since formyl methionine is required for initiation of translation, MetE inactivation could stop translation during

the time of hypochlorite detoxification (97). The redox-regulatory mechanism of S-bacillithiolation in response to NaOCl stress was first studied in *B. subtilis* (28). S-bacillithiolation controls the activity of the redox-sensing OhrR repressor (28,88). The OhrR repressor is inactivated by S-bacillithiolation under NaOCl and cumene hydroperoxide (CHP) stress resulting in up-regulation of the thiol-dependent OhrA peroxiredoxin for detoxification of HOCl and organic peroxides (28,53).

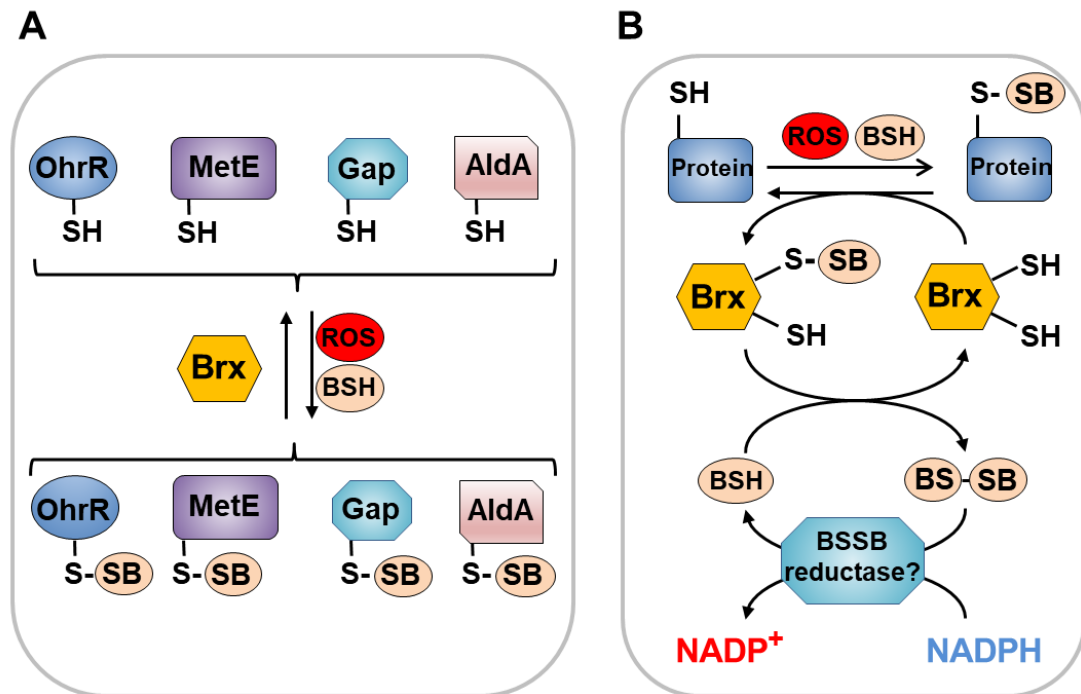


Figure 6. (A) Protein S-bacillithiolations function as both redox-regulatory device and in thiol protection under NaOCl treatment of *B. subtilis* and *S. aureus*. (B) Reduction of protein S-bacillithiolations by bacilliredoxin pathways. The S-bacillithiolated proteins are reduced by bacilliredoxins (Brx) leading to Brx-SSB formation. Brx-SSB is reduced by BSH with the generation of BSSB that likely requires the uncharacterized NADPH-dependent BSSB reductase for regeneration of BSH. The figure is adapted from (97).

As part of this PhD thesis, we were interested to identify S-bacillithiolated proteins in the human pathogen *S. aureus* under NaOCl stress (73). Using the thiol-redox proteomics method OxICAT, about 58 redox-sensitive proteins with >10% increased thiol-oxidation levels could be quantified under NaOCl stress (73). Among these are five S-bacillithiolated proteins which showed the highest oxidation increase of ~29% in the OxICAT analysis, including GapDH, AldA, GuaB, RpmJ, and PpaC (73).

The glycolytic glyceraldehyde-3-phosphate dehydrogenase (GapDH) represents the most abundant S-bacillithiolated protein in *S. aureus* contributing 4% to the total Cys proteome. GapDH is S-bacillithiolated at the conserved catalytic active site Cys151 resulting in reversible inhibition of Gap activity under NaOCl stress (**Fig. 6A**). The active site Cys of GapDH is highly reactive and susceptible for various post-translational thiol-modifications, including S-glutathionylation in many

eukaryotes and S-mycothiolation in *C. diphtheriae* (71). S-bacillithiolation protects the active site Cys against irreversible oxidation under both H₂O₂ and NaOCl treatments. This was shown in kinetic GapDH assays with increasing doses of the oxidants in the absence or presence of BSH. The S-bacillithiolation pathway was faster compared to the overoxidation pathway indicating that S-bacillithiolation can efficiently protect the active site against overoxidation (73). Molecular docking of BSH into the GapDH active site revealed that BSH can undergo disulfide formation with Cys151 without major conformational changes (73).

Apart from GapDH, the aldehyde dehydrogenase AldA was S-bacillithiolated under NaOCl stress and strongly oxidized at its conserved Cys279 in the OxICAT approach (74). Our recent results revealed that *aldA* is induced under NaOCl and aldehyde stress in a SigB-independent manner. Expression of *aldA* seems to be controlled by an unknown redox-sensing regulator under thiol-stress conditions (74). AldA showed broad substrate specificity *in vitro* for oxidation of various aldehyde substrates, including formaldehyde, methylglyoxal, acetaldehyde and glycolaldehyde. In survival phenotype assays, the *aldA* mutant was more sensitive to NaOCl stress, but not to aldehyde stress. This indicates that AldA could be involved in detoxification of unknown aldehydes that are elevated under HOCl stress. In addition, we could confirm that AldA is inactivated by S-bacillithiolation *in vitro*. Using molecular dynamic simulation, we could show that the BSH molecule occupies two different positions in the AldA active site, depending on the presence of the NAD⁺ cofactor. In the apoenzyme, Cys279 is modified in the “resting” state position, while the holoenzyme forms the covalent BSH complex with Cys279 in the “attacking” state position. The same location of BSH was found for the BSH mixed disulfide in the GapDH Cys151 active site, which also depends on the Cys activation state. Moreover, our computational chemistry studies revealed that formation of the BSH mixed disulfide does not require structural changes for both, GapDH and AldA.

2.3.1.5. Redox-regulation of protein S-bacillithiolation by bacilliredoxins

The pathways for reduction of disulfide bonds involve the thioredoxin (Trx)/ thioredoxin reductase (TrxR) system and the glutaredoxin (Grx)/ GSH/ glutathione reductase (Gor) system in *E. coli* (45). The Trx system is mainly involved in the reduction of inter- and intramolecular protein disulfides and the Grx proteins function in de-glutathionylation upon return to non-stress conditions (90). Grx proteins have a basic Trx-fold and are structurally classified into the di-thiol Grx with the CPTC active site and the monothiol Grx containing a CGPS active site (90). The N-terminal Cys has a lower pK_a value (~3.5) and is present as nucleophilic thiolate anion. The Grx thiolate anion attacks the S-glutathionylated protein, resulting in a reduction of the mixed GSH disulfide and the formation of a Grx-SSG intermediate. This Grx-SSG intermediate is reduced by

GSH, resulting in the formation of glutathione disulfide (GSSG) that is reduced by Gor on expense of NADPH (90).

In *Firmicutes*, three bacilliredoxins have been identified as glutaredoxin homologs that co-occur together with the BSH biosynthesis enzymes in BSH producing bacteria as revealed in the STRING search (55). The bacilliredoxins BrxA and BrxB are paralogs of the DUF1094 family with a conserved Trx-fold and an unusual CGC active site motif (54). The monothiol BrxC (YtxJ) has a conserved TCIPS active site motif, but its function is still unknown. Under NaOCl stress, these Brx proteins were identified as S-bacillithiolated at their active sites in *B. subtilis* and *S. carnosus* using mass spectrometry (28,29). The S-bacillithiolations of BrxA and BrxC during NaOCl stress could represent intermediates of the bacilliredoxin redox pathway. The function of BrxA and BrxB in the reduction of the S-bacillithiolated substrates MetE, OhrR and GapDH were demonstrated *in vitro* (**Fig. 6**) (54,73). S-bacillithiolated OhrR could be reduced by the BrxBCGA resolving Cys mutant to generate the DNA-binding activity of OhrR *in vitro*, but S-cysteinylated OhrR could not be reactivated (54). Both bacilliredoxins BrxA and BrxB can catalyze de-bacillithiolation of MetE-SSB, but the regeneration of MetE activity was not possible. Our kinetic assays have further shown that Brx of *S. aureus* was able to de-bacillithiolate and reactive GapDH (73). GapDH reactivation upon de-bacillithiolation was possible with the Brx resolving Cys mutant, but not with the Brx active site mutant. These results provide evidence for the function of bacilliredoxins in de-bacillithiolation in BSH-producing bacteria (20,73). However, all attempts to find phenotypes of *brx* single and double mutants failed thus far, indicating that the Brx enzymes are not essential. Thus, other thiol-disulfide oxidoreductases or the Trx pathway might be alternatively involved in reduction of S-bacillithiolated proteins *in vivo* which remains to be investigated in detailed future studies (97).

2.3.2. Functions of mycothiol and its role in protein S-mycothiolation

Mycothiol (MSH) consists of N-Acetyl-Cys-GlcN-myoinositol and serves as the major LMW thiol in most Actinomycetes, such as *Mycobacteria*, *Corynebacteria* and *Streptomyces* (79,124). MSH-deficient mutants are very sensitive to many thiol-reactive species and antibiotics that affect the redox balance (79,124). Thus, MSH functions in all Actinomycetes in detoxification of various redox-active compounds, including ROS, electrophiles, toxins, heavy metal stress and antibiotics (**Fig. 7**) (97). Under oxidative stress conditions, MSH is oxidized to MSH disulfide (MSSM), which is recycled back to MSH by the NADPH-dependent mycothiol disulfide reductase Mtr. The MSH/Mtr/NADPH electron pathway provides the reducing power for mycoredoxin-1 (Mrx1) to reduce mixed MSH-disulfides (2,173).

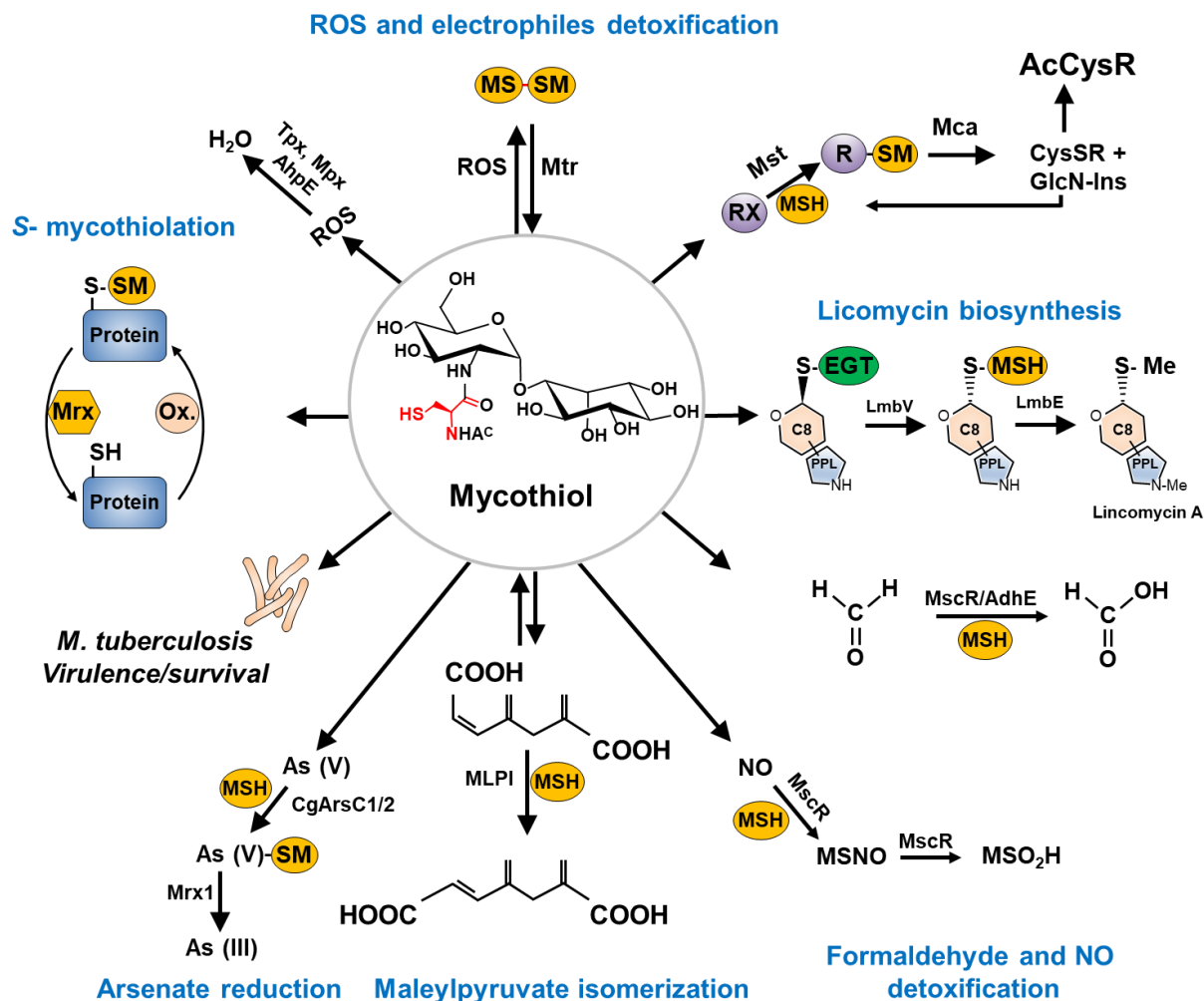


Figure 7. The functions of mycothiol (MSH) in *Mycobacteria* and *Corynebacteria*. Mycothiol (MSH) is oxidized by ROS to mycothiol disulfide (MSSM). MSSM is reduced back to MSH by the mycothiol disulfide reductase Mtr on expense of NADPH. MSH-dependent peroxidases, such as Mpx, Tpx, and AhpE function in peroxide detoxification. Electrophiles (RX) are conjugated to MSH by the MSH S-transferase Mst to form MS-electrophiles (MSR) which are cleaved by the MSH S-conjugate amidase Mca to mercapturic acids (AcCysR) that are exported from the cell. The Mca-homologs LmbT, LmbV, and LmbE function also in the assembly and biosynthesis of the sulfur-containing lincosamide antibiotic lincomycin in *Streptomyces lincolnensis*. MSH serves as a cofactor for the alcohol dehydrogenase AdhE/MscR in *Mycobacteria* and *Corynebacteria* for detoxification of formaldehyde to formate and MSNO to MSO₂H. MSH functions in detoxification of maleylpyruvate as a cofactor for maleylpyruvate isomerase (MLPI) in *C. glutamicum*. Arsenate reductases CgArsC1 and CgArsC2 conjugate MSH and arsenate As(V) to form As(V)-SM that is reduced to As(III) by Mrx1. In *M. tuberculosis*, MSH is important under infection conditions and for growth and survival. Under conditions of NaOCl stress, proteins are oxidized to mixed disulfides with MSH, termed as S-mycothiolations which is reversed by mycoredoxins. The figure is adapted from (97).

MSH is also a cofactor for MSH-dependent enzymes that are involved in various detoxification pathways (97). MSH forms conjugates with xenobiotics and antibiotics either spontaneously or by DinB family MSH-S-transferases Mst (126). MS-conjugates are further cleaved by the MSH S-conjugate amidase Mca to GlcN-Ins and mercapturic acids (AcCysR). GlcN-Ins is used to regenerate MSH. Mercapturic acids are exported from the cell (126). The alcohol dehydrogenase MscR (MSNO reductase/formaldehyde dehydrogenase) is another MSH-dependent enzyme required for detoxification of formaldehyde and S-nitrosyl-mycothiol (MSNO)

(124). Formaldehyde reacts with MSH generating MS-CH₂OH. MscR is able to convert MS-CH₂OH to formate and MSNO to MSH sulfinamide (MSONH₂). In *C. glutamicum*, MSH functions in degradation of maleylpyruvate and acts as a cofactor for maleylpyruvate isomerase in the isomerization of maleylpyruvate to fumaryl pyruvate (44). In addition, MSH contributes to the metal ion resistance. The detoxification of arsenate As(V) to arsenite As(III) depends on the MSH-dependent arsenate reductases ArsC1/C2. These enzymes catalyze the conjugation of MSH and arsenate As(V) to form As(V)-SM that is reduced to As(III) by Mrx1.

MSH functions also in post-translational thiol-modification of proteins by formation of MSH mixed disulfides, termed as protein S-mycothiolation (**Fig. 7**) (71,97). In *C. glutamicum*, 25 S-mycothiolated proteins were previously identified (27). These include conserved targets for S-thiolation across different Gram-positive bacteria, such as the thiol-peroxidase Tpx, the inosine monophosphate (IMP) dehydrogenase GuaB and ribosomal proteins. Tpx was S-mycothiolated at its active and resolving Cys residues (Cys60 and Cys94) *in vivo* under NaOCl stress (27). S-mycothiolation of Tpx inhibits the peroxidase activity, which was restored after its reduction by the Mrx1/MSH/Mtr pathway. Thus S-mycothiolation controls Tpx activity and protects the peroxidatic Cys against overoxidation (97). The putative MSH peroxidase Mpx and methionine sulfoxide reduction MsrA form intramolecular disulfides and S-mycothiolations under H₂O₂ treatment *in vitro* and require both the Trx and Mrx1 pathways for regeneration (151,158).

In *M. smegmatis*, protein S-mycothiolation was more abundant with 58 identified proteins that participate in many different metabolic pathways (70). In the pathogen *C. diphtheriae*, 26 S-mycothiolated proteins were identified (71). The glyceraldehyde dehydrogenase GapDH was discovered as the main target for S-mycothiolation in. GapDH was S-mycothiolated at the active site Cys153 under hypochlorite stress *in vivo*. Treatment of GapDH with increasing H₂O₂ and NaOCl concentrations in the presence of MSH resulted in S-mycothiolation and reversible inactivation of GapDH *in vitro*. In the absence of MSH, high concentration of H₂O₂ leads to irreversible inactivation of the Gap activity due to overoxidation of the active site. Detailed kinetic assays showed that S-mycothiolation occurred faster compared to overoxidation *in vitro*. The S-mycothiolated GapDH was re-activated using both, the Trx and the Mrx1 pathway *in vitro*, while the overoxidized GapDH remained inactive (71). However, de-mycothiolation of GapDH using Mrx1 occurred much faster compared to reduction by the Trx pathway indicating that Mrx1 is probably the major enzyme for de-mycothiolation *in vivo* (71).

Interestingly, the comparison of the kinetics for the dose-dependent GapDH inactivation suggests that the *C. diphtheriae* GapDH is more resistant to oxidative inactivation compared to *S. aureus* GapDH. Lower concentration of H₂O₂ and NaOCl significantly inhibited *S. aureus* GapDH activity, but not GapDH from *C. diphtheriae* (71). The resistance of *C. diphtheriae* GapDH

to oxidative inactivation may be due to the highly conserved C₁₅₃TTNC₁₅₇ motif that was shown to form in part intramolecular disulfides under H₂O₂ stress to prevent overoxidation (71,73). In conclusion, the results have shown that S-myoithiolation can function in redox-regulation and protection of the GapDH active site against overoxidation *in C. diphtheriae* and can be reversed by both, the Mrx1 and Trx pathway *in vitro*.

2.4. Thiol-based redox regulators as ROS and RCS defense mechanisms

Bacteria encode various defensive mechanisms to cope with ROS and HOCl, including detoxification and antioxidant enzymes to destroy the reactive compound and mechanisms to repair the subsequent damages (41,97). These defense mechanisms are often controlled by redox-sensing regulators that use conserved Cys residues to sense the redox-active compounds (59). Post-translational thiol modifications of conserved Cys residues often lead to conformational changes that activate or inactivate redox-sensing transcription factors. The best-studied example for a redox-sensitive regulator is the OxyR protein of *E. coli* that uses a thiol-disulfide switch model for redox-sensing of peroxide stress, to activate gene transcription for H₂O₂ detoxification and protein repair (115). Apart from reversible thiol-modifications, many other redox-regulatory mechanisms have been described, such as sulfenamide formation, histidine oxidation and overoxidation to sulfonic acids (84). In the following sections, the current knowledge of redox-regulatory mechanisms in *S. aureus* will be summarized.

2.4.1. The SarA-family of virulence, redox and antibiotic resistance regulators in *S. aureus*

S. aureus has multiple thiol-based redox sensors for oxidative stress and antibiotic resistance that are required for virulence and the defense against the host immune system (22). These include the staphylococcal accessory regulators SarA and SarZ as well as the multiple gene regulator MgrA (**Fig. 8**).

SarA is a global redox-sensing regulator of virulence gene expression in *S. aureus* exerting both positive and negative transcriptional control (24). The *sarA* locus positively controls genes encoding fibrinogen binding proteins, hemolysins, enterotoxins, TSST-1 toxin, and capsule biosynthesis (24). SarA negatively controls expression of proteases, proteinA, and a collagen binding protein (15,25). SarA also binds to several regulatory and target gene promoters (e.g., *agr*, *sarS*, *rot*, *sarV*, *sarT*, *hla*, *fnb*, *spa*, *cna*, *bap*, and *icaRA*) to modulate gene transcription, implicating both *agr*-dependent and *agr*-independent pathways in SarA-mediated regulation (4). Sequence alignment of several SarA homologs reveals that there is a unique cysteine residue in

SarA homologs (e.g. SarZ, MgrA). SarA contains a single Cys9 residue at the dimer interface required to sense oxidative stress (69). However, SarA seems to be more sensitive to thiol-alkylation than to oxidation (22).

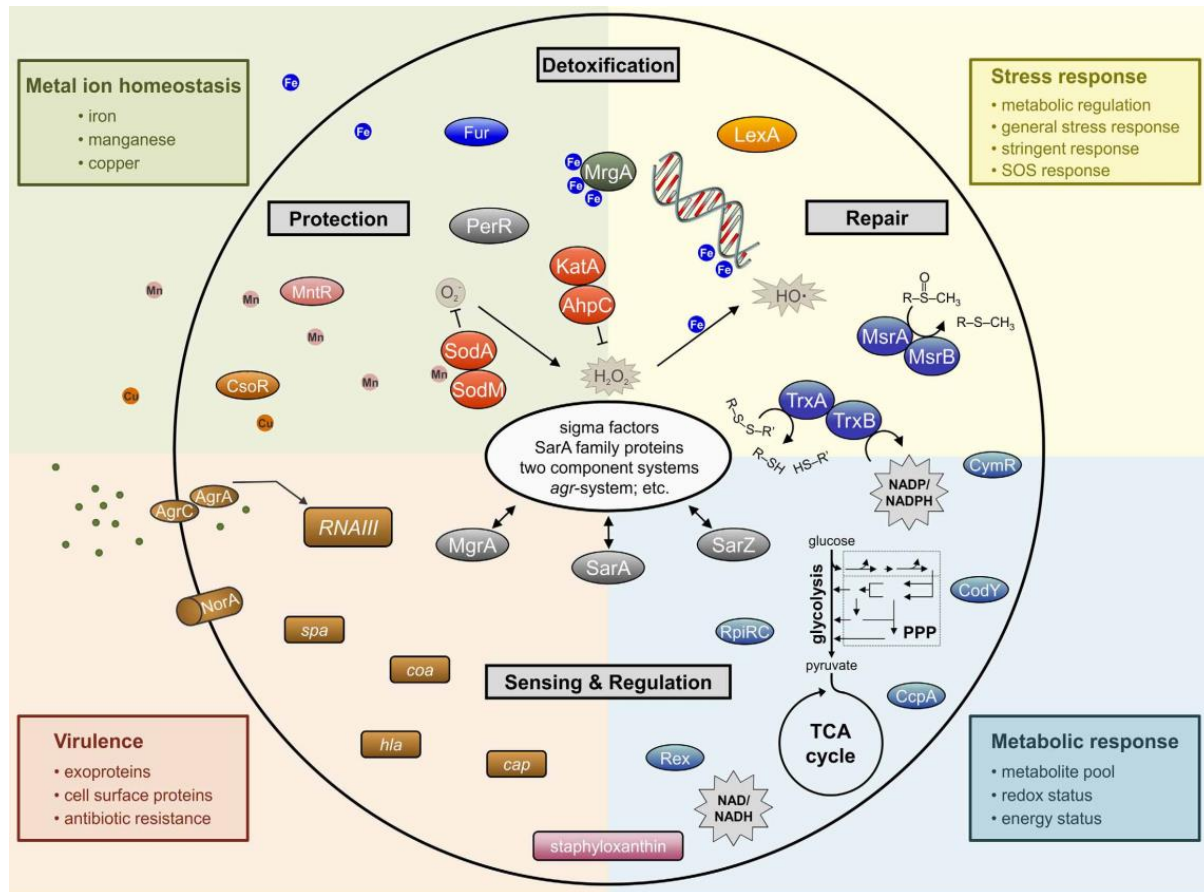


Figure 8. Schematic overview of regulatory mechanisms involved in the response of *S. aureus* to oxidative stress affecting whole cell physiology. This figure is from reference (59).

MgrA and SarZ are paralogs that belong to the MarR/OhrR family in *S. aureus* (22). Transcriptional profiling has revealed that MgrA regulates more than 300 genes including those encoding a variety of virulence factors, biofilm formation, cell wall biosynthesis, and genes involved in autolysis, antibiotic resistance as well as other global regulatory genes (22,100). MgrA controls resistance mechanisms to a broad spectrum of antibiotics, like fluoroquinolones, vancomycin, tetracycline, and penicillin by regulating transcription of several multidrug efflux pumps (e.g. NorA, NorB, NorC, and Tet38) (59). In addition, MgrA is required for virulence in murine abscess, septic arthritis and sepsis models (59).

The dimeric structure of MgrA contains a helix-turn-helix DNA binding domain and a dimerization domain in each subunit that are typical for MarR family regulators (21). MgrA has a single conserved Cys12 in the dimerization domain that is accessible to oxidizing agents and uses a thiol-based oxidation-sensing mechanism to control virulence and antibiotic resistance (21).

Thiol-oxidation by different peroxides (CHP, H₂O₂) leads to dissociation of MgrA from the operator DNA *in vitro* and derepression of antibiotic resistance genes in *S. aureus in vivo* (21,23).

S. aureus SarZ is a close homolog of MgrA and controls a variety of genes involved in virulence, peroxide and antibiotic resistance (23). Interestingly, SarZ is transcriptionally activated by MgrA (4) and may also control the metabolic shift to anaerobic growth conditions (23). SarZ regulates transcription of the *ohr* gene encoding an H₂O₂-inducible OhrA-like peroxiredoxin. The conserved Cys13 of SarZ is the redox-sensing Cys which is oxidized by peroxides to form the sulfenic acid that still retains DNA-binding activity. Further oxidation to the mixed disulfide with a synthetic benzene thiol leads to repressor inactivation resulting in derepression of transcription of the target genes (59,135). In addition, DNA-binding activity of SarZ and MgrA can be reversibly regulated by cysteine phosphorylation via the threonine kinase/phosphatase. The threonine kinase was required for full virulence and resistance to the antibiotic vancomycin by controlling Cys-phosphorylation of MgrA, SarZ and SarA (155). Our recent study showed that Cys12 of MgrA and Cys13 of SarZ have increased oxidation levels under NaOCl stress (73), indicating that both MgrA and SarZ could be redox controlled by S-bacillithiolation analogous to OhrR of *B. subtilis* (88).

In addition to these redox sensors, *S. aureus* has several antioxidant enzymes to cope with oxidative stress. These ROS detoxification systems include superoxide dismutases (SodA and SodM), the catalase KatA as well as the peroxiredoxins AhpC and Tpx which confer protection under infection conditions (**Fig. 8**) (13, 23,59,180). The superoxide dismutases SodA and SodM are Mn-dependent metalloenzymes that prevent the accumulation of O₂•⁻ by converting it to H₂O₂. Catalases and peroxidases are involved in H₂O₂ detoxification (56,59). Transcription of *sodA* and *sodM* is regulated by the SarA transcription factor. SodA is the major superoxide dismutase presents in all staphylococci whereas SodM is unique to *S. aureus* (59,168). SodA and SodM both contribute to virulence of *S. aureus* in a mouse abscess model (56,80). In addition, SodM is important for resistance of *S. aureus* to the immune effector Calprotectin which comprises 40–60% of the cytoplasmic proteins in neutrophils (46,56). Transcription of *sodM* is induced during long-term persistence of *S. aureus* in the airways of cystic fibrosis patients. This points to an important role of SodM under chronic *S. aureus* infections to protect the bacteria against neutrophil attack (160). The catalase KatA plays a major role in *S. aureus* resistance to high concentrations of H₂O₂ while AhpC confers resistance to lower levels of ROS (31,59). KatA and AhpC are regulated by the PerR repressor and play important roles in bacterial survival and persistence. The *ahpC katA* double mutant showed a reduced growth rate due to accumulation of H₂O₂ and probably HO• that is generated in the Fenton reaction (31).

2.4.2. QsrR as MarR/DUF24-family thiol-based redox sensor of quinones

S. aureus encodes a specific MarR/DUF24-family redox sensor for quinones, termed as QsrR (77). QsrR contains a conserved N-terminal Cys5 and two C-terminal Cys30 and Cys33 residues. QsrR shares 38% sequence identity with the 2-Cys-type YodB repressor of *B. subtilis*. Moreover, QsrR controls similar genes involved in quinone detoxification in *S. aureus* (26). The *qsrR* mutant was highly resistant to benzoquinone, indicating that QsrR is involved in quinone detoxification. The transcriptomic and qRT-PCR analysis identified QsrR regulon members to be up-regulated in the wild type during benzoquinone stress and derepressed in untreated cells of the *qsrR* mutant. The QsrR regulon includes genes encoding for FMN-dependent quinone reductases, nitroreductases, glyoxalases/dioxygenases, and riboflavin biosynthesis genes (77). In *S. aureus*, the QsrR regulon has a crucial role in virulence regulation since the *qsrR* mutant was much more resistant to killing by macrophages in a phagocytosis assay compared to the wild type. The QsrR regulator is postulated to sense quinones by thiol-S-alkylation at the conserved Cys5. The QsrR dimer has winged helix-turn-helix (wHTH) motifs, which bind to the major and minor grooves of the DNA double helix (Fig. 9).

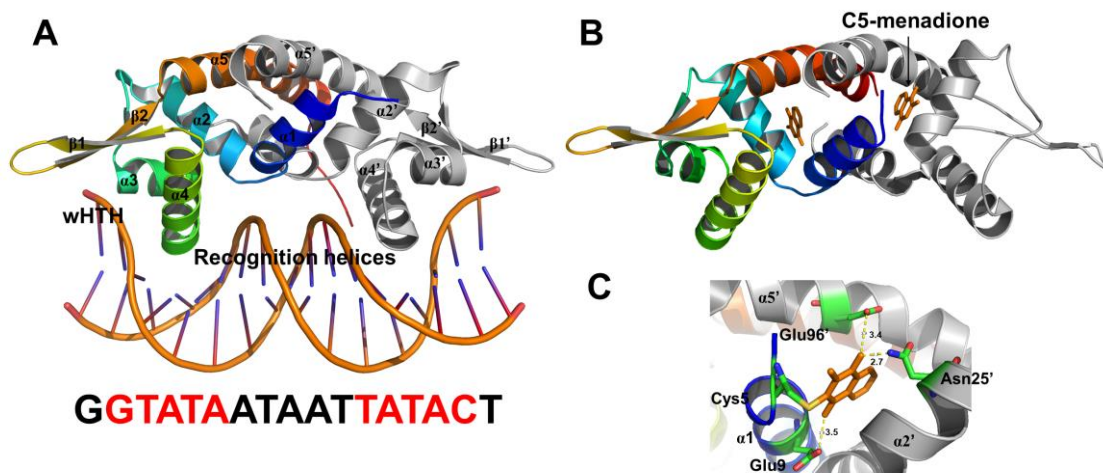


Figure 9. Crystal structure of the QsrR-DNA and QsrR-menadione complexes. One subunit of the QsrR dimer is colored in rainbow and the other subunit is colored in gray and the C5-menadione is colored in orange. (A) Structure of the QsrR–DNA complex depicting interactions between QsrR and the palindromic sequence. (B) Crystal structure of the QsrR–menadione complex. (C) Hydrogen bonds between menadione and QsrR. Distances of putative hydrogen bonds are labeled in angstrom units. The figure is adapted from (77).

The menadione-bound QsrR structure was resolved for the QsrRC30, QsrRC33S mutant to elucidate the structural changes upon quinone binding at Cys5. Menadione binding at Cys5 causes a shift in the distance and rotation between the $\alpha 4/\alpha 4'$ DNA recognition helices from 29.9 Å distance with 106° rotation in reduced QsrR to 39.1 Å distance and 117° rotation in the menadione-bound form. These structural changes lead to the dissociation of QsrR from the operator DNA (77). The YodB repressor resembles a typical 2-Cys-type regulator and senses

diamide and quinones by intermolecular disulfide bond formation. Thus, redox-sensing of QsrR under diamide stress in *S. aureus* could also involve disulfide formation (77).

2.4.3. The Rrf2-family redox sensors CymR, SaiR and HypR in *Firmicutes*

The Rrf2-family of transcription factors is widespread in bacteria and controls diverse functions, many of those contain FeS-clusters. Among the FeS-cluster containing Rrf2-redox sensors are best characterized IscR that controls FeS cluster biogenesis, NsrR as redox sensor for nitric oxide (NO) and RsrR (81,108,131,139). In addition, *Firmicutes* encode Rrf2 redox-regulators that do not contain FeS-clusters, such as CymR of *S. aureus* as central regulator of cysteine metabolism and SaiR of *Bacillus anthracis* as disulphide stress regulator (120,152,153).

CymR is the cysteine metabolism repressor, which represses transcription of genes involved in the uptake of cystine or other sulfur compounds and in the cysteine biosynthesis in *S. aureus*. It also plays an important role in the virulence and oxidative stress resistance of *S. aureus* (152,153). The CymR regulon includes genes and operons encoding for L-cystine transporters (*tcyP*, *tcyABC*), sulphonate ABC transporter (*ssu*), sulphate permeases and methionine ABC-transporters that are derepressed in the *cymR* mutant (153). Deletion of *cymR* increases sensitivity of *S. aureus* to oxidative stress, even though the genes for ROS detoxification are highly expressed (153). The *cymR* mutant shows increased transcription of multiple genes involved in the oxidative stress response (e.g., *ahpC*, *ahpF*, *dps*, *sodA*, *sodM* and *perR*). In addition, genes encoding virulence regulators (*sarA*, *saeR* and *mgrA*) were differentially expressed in *cymR* mutant. Furthermore, the *cymR* mutant was more resistant under infection assays with murine macrophage compared to the wild type. These results suggest that CymR inactivation may affect redox-mediated virulence control and adaptation of *S. aureus* for survival inside host cells (152,153).

CymR forms a homodimer in solution, which consists of a winged helix-turn-helix domain and a long dimerization domain in each subunit (78,150). The oxidation-sensing mechanism of CymR resembles that of the one-Cys type OhrR repressor. The non-conserved Cys25 of CymR is exposed and located in the N-terminal wHTH DNA-binding of CymR. Under H₂O₂ treatment, Cys25 forms a sulfenic acid intermediate which is not sufficient for repressor inactivation (**Fig. 10**). In the presence of Cys or CoenzymeA, mixed disulfide formation of CymR inactivates the protein resulting in transcriptional derepression of the CymR regulon (78). However, it remains to be investigated if CymR can be inactivated by S-bacillithiolation *in vivo* and *in vitro*.

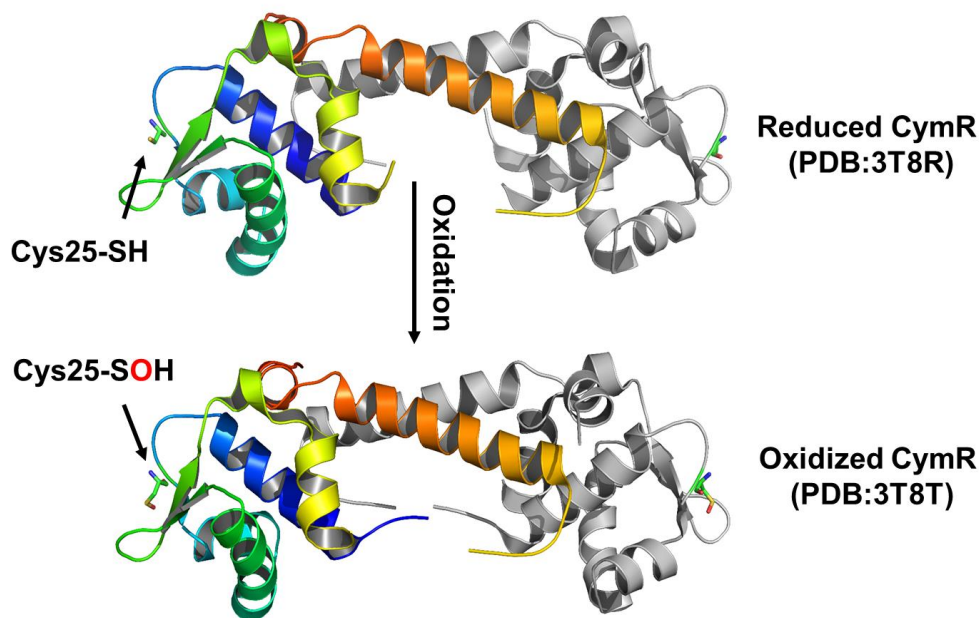


Figure 10. Crystal structures of the reduced and oxidized CymR at 1.7 Å resolution. The Cys-25 is shown in the reduced and oxidized sulfenic acid form. The atoms are colored in green (carbon), dark blue (nitrogen), red (oxygen) and yellow (sulfur). Figure is adapted from (78).

Among the Rrf2-family regulators, the SaiR repressor of *B. anthracis* (**Fig. 11**) was further shown to be involved in the disulphide stress response and virulence regulation. SaiR directly controls transcription of *spxA2* and three unknown function genes (120). SpxA2 is a member of the ArsC (arsenate reductase) family that responds to NaOCl, diamide and H₂O₂ stress by thiol-oxidation. Spx interacts with the α -C-terminal domain of the RNA polymerase to activate transcription of a large disulfide stress regulon (121,123,184). SpxA2 together with its paralogue SpxA1 were shown to be required for diamide resistance and the *saiR* mutant conferred a peroxide-resistant phenotype (6,120). Thus, SaiR of *B. anthracis* confers protection under oxidative stress conditions *via* control of SpxA2. In addition, *spxA2* is highly induced in *B. anthracis* in infection assays inside macrophages, which suggests an important role in virulence (8). Moreover, the SpxA2 paralog SpxA1 was also shown to be involved in the peroxide stress response in *B. anthracis* (5).

SaiR has two Cys residues in positions Cys89 and Cys96 (**Fig. 11**). The conserved Cys96 was shown to be required for SaiR repressor activity *in vitro* and *in vivo* (120). Moreover, mutational analysis of the *spxA2* promoter showed that the inverted repeat in the *spxA2* promoter is the operator site for SaiR.

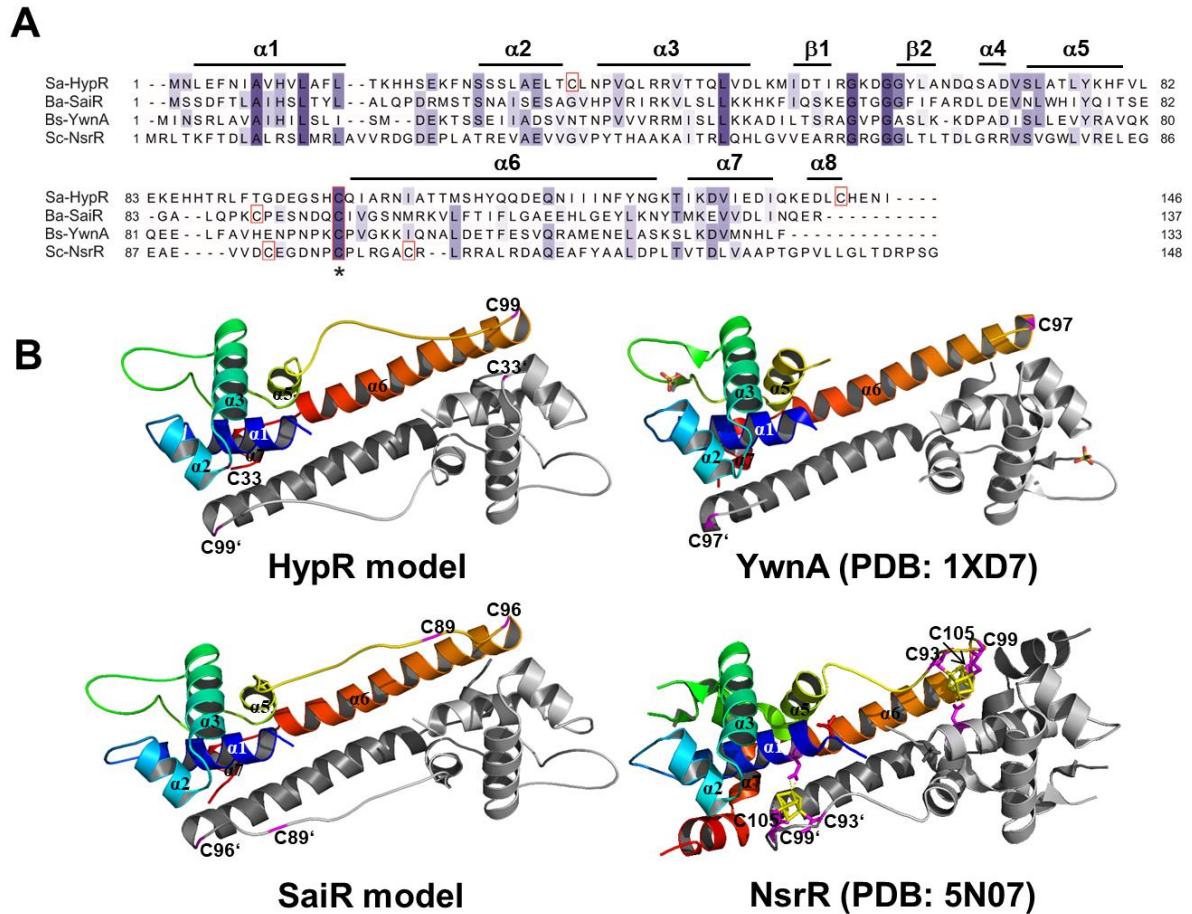


Figure 11. Multiple protein sequence alignments of the Rrf2 regulators HypR, SaiR, YwnA and NsrR (A) and structural modelling of HypR and SaiR in comparison to YwnA and NsrR (B). **A)** The protein sequence alignment was performed with Clustal Ω 2 and is presented in Jalview. The following protein sequences were aligned and the % identity to HypR is given in parenthesis: HypR (SACOL0641) of *S. aureus* COL, SaiR (BAS3200) of *Bacillus anthracis* (20.4 %), YwnA (P71036) of *Bacillus subtilis* (23.48%) and NsrR (Q9L132) of *Streptomyces coelicolor* (17.86%). Intensity of the blue color gradient is based on 50% sequence identity. The conserved Cys99 in HypR is labelled in red with an asterisk (*). **B)** The structural models of HypR and SaiR were generated using SWISS-MODEL (<https://swissmodel.expasy.org/>) (10) and visualized with PyMol using the template of *Bacillus subtilis* YwnA (1xd7) that showed 23.5 % and 25.78 % sequence identity to HypR and SaiR, respectively. For comparison, we show the structures of YwnA (1xd7) and NsrR (5no7) with labels for the conserved Cys97 in YwnA and the 3 Fe-S-cluster coordinating Cys residues (Cys93, Cys99 and Cys105) in NsrR. The FeS-cluster of NsrR is displayed in yellow.

In this PhD thesis, we used an RNA seq transcriptomics approach to identify HypR as close SaiR homolog of the Rrf2-family, which specifically senses and responds to NaOCl stress in *S. aureus* (**Fig. 11**) (95). The *hypR-merA* operon was most strongly (180-fold) up-regulated under NaOCl stress in the RNAseq transcriptome. Northern blot analysis confirmed that HypR is a redox-sensing repressor that controls transcription of the *hypR-merA* operon under NaOCl and diamide stress. MerA encodes for the NADPH-dependent flavin disulfide reductase MerA that protects *S. aureus* against NaOCl stress and under macrophage infections *in vivo*.

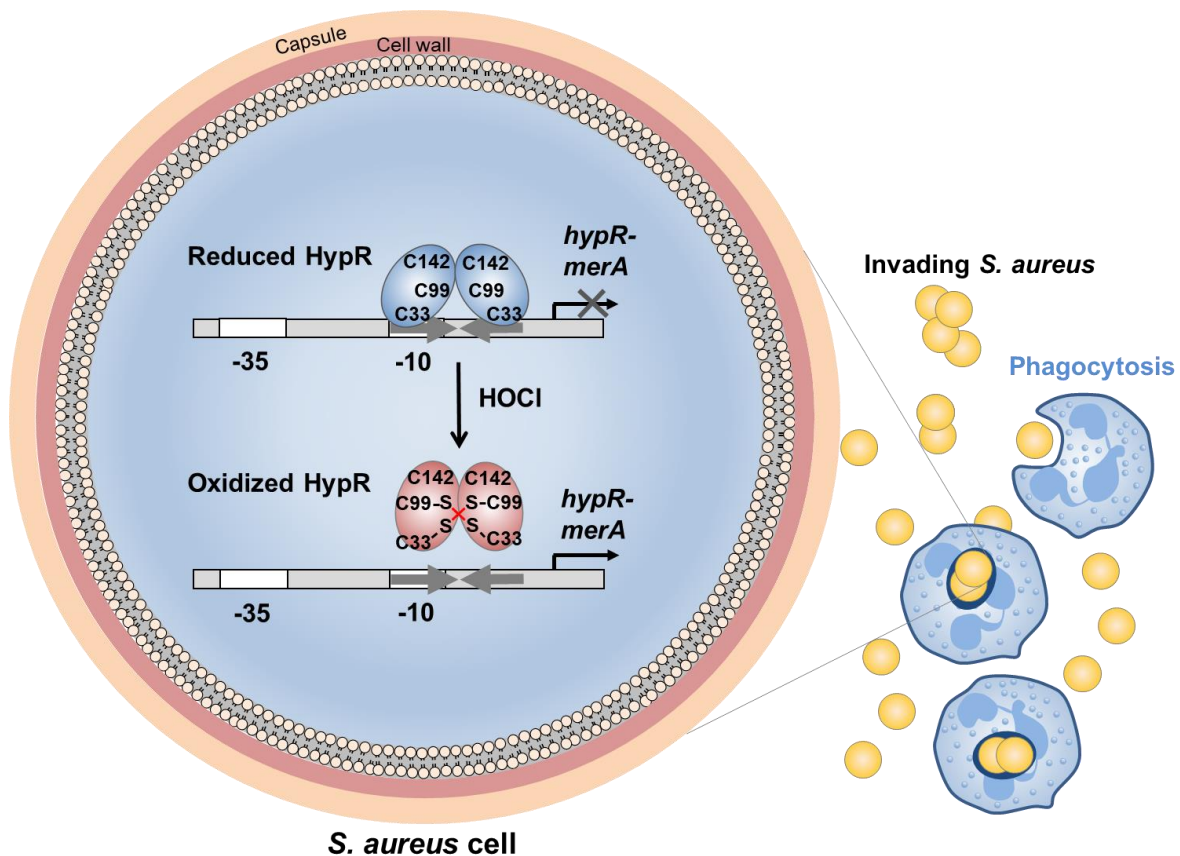


Figure 12. Redox-sensing mechanism of HypR in response to HOCl stress and during infection in *S. aureus*. HypR controls the NADPH-dependent thiol-disulfide oxidoreductase MerA that is required for growth and survival under hypochlorite stress and in macrophage infection assays in *S. aureus*. Cys33 of HypR is required for redox-sensing *in vivo*. Under NaOCl stress, HypR is oxidized to Cys33-Cys99' intersubunit disulfides leading to derepression of *hypR-merA* transcription.

HypR belongs to the 2-Cys-type redox regulators that directly senses and responds to NaOCl stress *via* a thiol-based mechanism in *S. aureus* (**Fig. 12**). HypR has a conserved Cys residue (Cys99) and two non-conserved Cys residues in positions 33 and 142 (**Fig. 11**). Mutational analysis identified Cys33 and Cys99 as essential for NaOCl-sensing while Cys99 is also important for repressor activity of HypR *in vivo*. The Cys99Ala mutant was unable to bind to the DNA *in vitro* and *in vivo* which might be caused by structural changes in the HTH DNA binding motifs. Using CD spectroscopy, we confirmed that the mutation of Cys99 did not caused conformational changes in the secondary structure elements in HypR. HypR was shown to bind specifically to a highly conserved 12-3-12 bp inverted repeat sequence in its upstream promoter region to inhibit *hypR-merA* transcription. Under NaOCl stress, HypR is oxidized to Cys33-Cys99' intersubunit disulfides resulting in dissociation of HypR from its operator and derepression of *hypR-merA* transcription. Of note, HypR responds only to NaOCl and diamide stress, conditions that cause disulfide stress in *S. aureus*, but not to peroxides and aldehydes. Thus, HypR can be

regarded as most HOCl-specific transcription factor of *S. aureus* that is important under infection conditions.

2.4.4. The Rrf2-family transcription factors IscR and NsrR.

Many previously described Rrf2 family regulators are known to contain FeS-clusters, such as IscR and NsrR (139). The IcsR repressor coordinates a [2Fe-2S] cluster. IscR is a sensor of the cellular FeS status and a global transcriptional regulator for FeS biogenesis (139). IscR controls the expression of the *isc* and *suf* operons that encode the machineries for FeS biogenesis (60,61). The Isc machinery is considered as housekeeping system for the maturation of a large variety of FeS proteins. The expression of the Suf machinery is induced under oxidative stress or iron starvation (60,146). IscR occurs as apo-IscR without the FeS cluster and as holo-IscR ligated to the FeS cluster. Under conditions unfavorable for FeS cluster formation, apo-IscR is formed resulting in derepression of the *isc* operon transcription. At the same time, apo-IscR activates the *suf* operon to further compensate for the loss of Fe-S clusters (89,181). Once sufficient FeS clusters are provided, holo-IscR binds to the *iscR* promoter leading to repression of the Isc pathway. In addition, the *sufA* operon is switched off in the presence of holo-IscR. The stability of the IscR [2Fe-2S] cluster is affected by ROS or under iron limitation resulting in increased expression of the *isc* and *suf* operons due to inactivation of IscR (108,146,181).

IscR also controls expression of several other FeS cluster containing anaerobic respiratory enzymes as well as the Mn²⁺-containing superoxide dismutase and ribonucleotide reductase (61,108). IscR recognizes two distinct DNA-binding motifs in the promoter regions of its target genes including a type-1 and a type-2 binding site. The promoter regions with type-1 sites are found in the promoters of the *iscR*, *yadR*, and *yhgl* genes, which are repressed by holo-IscR. The *sufA*, *hyaA* and *ydiU* promoter regions contain type-2 binding sites, which are bound by apo-IcsR. A molecular-level understanding of the complex processes of FeS cluster biosynthesis in several organisms is now emerging. However, these machineries have to be studied in more detail in Gram-positive bacteria (108,146,181).

Another transcriptional regulator of the Rrf2 family is NsrR which senses and responds to NO stress in many Gram-negative and Gram-positive bacteria (62,119,164). NsrR controls the expression of genes involved in NO detoxification and anaerobic respiration, such as *hmp*, *ytfE* and *nrf* in *E. coli*. The *hmp* gene encodes for a flavohemoglobin that converts NO to nitrate. The *ytfE* gene is implicated in FeS cluster repair. The *nrf* gene encodes a periplasmic respiratory nitrite reductase that catalyzes the reduction of nitrite to NO and further to NH₃ (34,81,86,108,131,165). NsrR also regulates genes important for diverse cellular processes, including motility, surface attachment, biofilm development, virulence, and symbiosis (81,108,131).

NsrR contains three conserved Cys residues that act as ligands for a [2Fe-2S] or [4Fe-4S] cluster (108). NsrR from *Streptomyces venezuelae* and *Neisseria gonorrhoeae* were shown to contain a [2Fe-2S] cluster whereas NsrR from *S. coelicolor* and *B. subtilis* accommodate a [4Fe-4S] cluster (76,164,182). A possible explanation for the different types of Fe-S clusters in NsrR could be aerobic or anaerobic purification methods or the spacing of the conserved Cys residues (108). The [4Fe-4S] cluster is usually O₂ labile and rapidly converted to the [2Fe-2S] cluster under aerobic conditions (34).

NsrR functions as a repressor and requires the FeS cluster for DNA-binding to its target promoters. The loss of the FeS cluster disrupts its DNA binding ability, resulting in derepression of the NsrR regulon (33,86,108,118,165,175). However, NsrR of *B. subtilis* can bind to the target DNA in its dimeric apo and holo forms (86). Recently, the crystal structure of holo-NsrR of *S. coelicolor* was reported (**Fig. 13**). The [4Fe-4S] cluster is coordinated by three conserved Cys residues in positions 93, 99 and 105. In addition, an aspartic acid (D8) serves as fourth ligand in the adjacent subunit (175). DNA-binding affinity of NsrR was either reduced or abolished when D8 was replaced by Cys or alanine residues (175). The crystal structure analyses suggest that disruption of the hydrogen bonds between Asp8 and the [4Fe-4S] cluster leads to cluster degradation and structural changes. Since Asp8 is connected to the HTH motif and the FeS-cluster, the Asp8 mutation causes a loss of the DNA binding ability of NsrR (175).

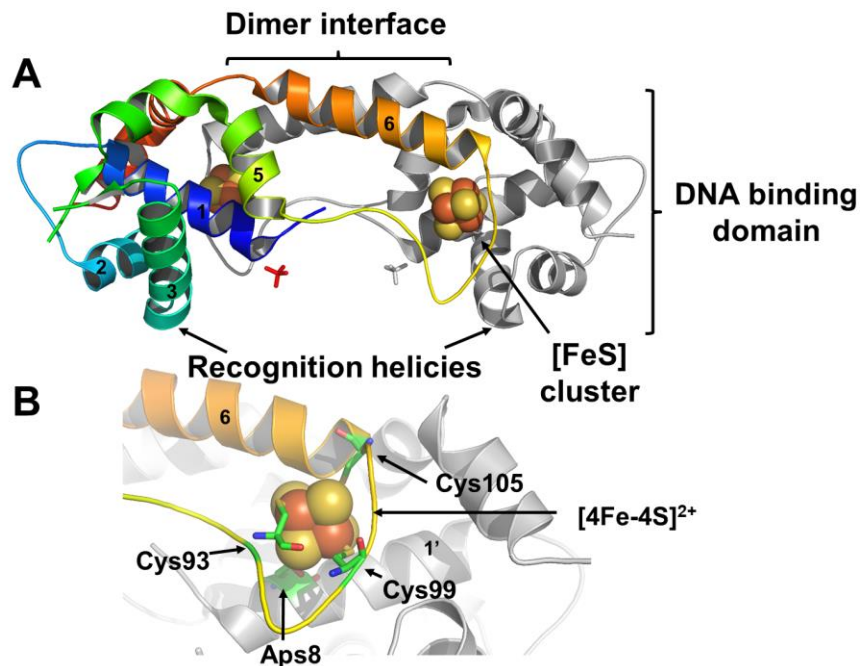


Figure 13. Crystal structure of holo- NsrR. A) *S. coelicolor* NsrR is a dimer with an elongated fold of the dimerization domains. Each subunit contains an N-terminal DNA binding domain (helices 1-3), a long dimerization helix, and a C-terminal loop that binds the [4Fe-4S] cluster. B) The [4Fe-4S] cluster binding loop is shown in more detail. The 3 Cys residues at positions 93, 99, and 105 are shown that coordinate the FeS-cluster together with Asp8 in the opposing subunit (PDB: 5N07). The figure is from reference (33).

3. Genetically encoded redox biosensor to measure dynamic changes in glutathione, mycothiol and bacillithiol redox potentials in the human pathogens

3. 1. Development of redox-sensitive GFPs (roGFP2) as dynamic biosensors to measure real-time changes in the GSH redox potential

Recent advances in the design of genetically encoded redox biosensors, such as redox-sensitive GFP (roGFP) have facilitated the real-time imaging of the cellular redox potential of living cells with high sensitivity and at spatiotemporal resolution (65,109,148). The chromophore of GFP is formed through intramolecular cyclization of the three amino acids S65, Y66 and G67 (109). These amino acids undergo a post-translational cyclization reaction, followed by dehydration and oxidation steps, leading to the mature chromophore formation.

Depending on the protonation state of the Y66, GFP has two different excitation maxima. The protonated neutral form of the chromophore shows a high excitation maximum at 395 nm while the de-protonated form has the highest excitation maximum at 475 nm (14,40,109). The proton is reversibly translocated between Y66 and E222 mediated by a structural water molecule and the hydroxyl group of S205. Small structural changes in the proximity of this proton lead to significant changes in the protonation of Y66. This causes opposing shifts in the relative intensities of the two excitation maxima (148).

Many redox-sensitive GFP (roGFP) derivatives with different midpoint potentials were constructed during the last years (38,67). In the roGFP biosensors, the amino acids S147 and Q204 were replaced by Cys residues, which are located on the surface of the β -barrel (38). The Cys residues are in close proximity to the chromophore and form a disulfide upon oxidation. Oxidation of the roGFP biosensors results in small conformational changes that influence the excitation spectrum (**Fig. 14A**) (38,148). The roGFP2 biosensor has two excitation maxima at 405 and 488 nm and the intensities of the excitation maxima depend on the redox state of the biosensor. In the reduced roGFP2 probe, the fluorescence intensity at the 405 nm excitation maximum is low while the intensity of the 488 nm maximum is very high (**Fig. 14B**). Oxidation of roGFP2 leads to an increase in the intensity at the 405 nm excitation maximum and a decrease at the 488 nm excitation maximum (38,109). The ratiometric changes in the intensities at both excitation maxima are used for calculation of the biosensor oxidation degree and the intracellular redox potential changes. The roGFP2 biosensor has a midpoint potential of -280 mV and is the most widely used biosensor that allows a ratiometric measurement of the redox changes independent of the biosensor concentration. roGFP2 is also brighter in fluorescence and has a 3-fold higher dynamic range of ~ 9 compared to roGFP1 (109). Moreover, roGFP2 measurements are not pH-sensitive making the biosensor well suited to study redox changes of intracellular pathogens that replicate inside the acidic phagosome.

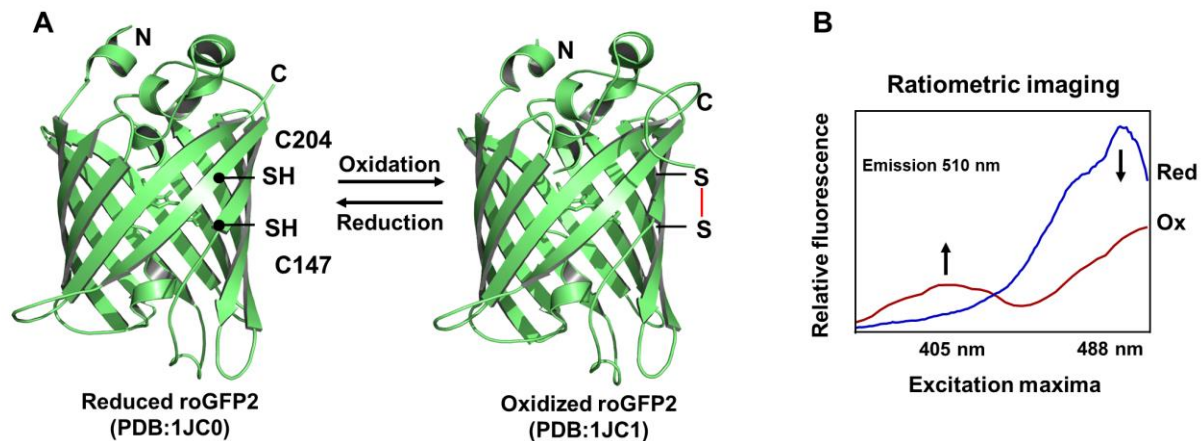


Figure 14. Redox-sensitive GFP2 (roGFP2) contains two Cys residues in the β -barrel structure that form a disulfide upon oxidation (A) resulting in a ratiometric change of the excitation maxima at 405 nm and 488nm (B) allowing the ratiometric measurements. The figure is adapted from (11,67).

3.2. Monitoring intrabacterial changes in the GSH, BSH and MSH redox potentials in Gram-negative and Gram-positive bacteria

3.2.1. Application of Grx1-roGFP2 biosensors in eukaryotic organisms

The roGFP2 biosensor was shown to equilibrate with the glutathione redox couple GSH/GSSG in eukaryotic cells, which depends on the level of endogenous glutaredoxins (Grx) (109). However, the reaction of endogenous Grx with roGFPs is very slow, to allow the detection of rapid cellular redox events under oxidative stress. In addition, availability of glutaredoxins varies in different tissues, cells and cellular compartments which can influence the kinetic properties of roGFP, making observations much less comparable and reliable (109). Moreover, in some measurements the endogenous signals and redox pairs of roGFP biosensors were unknown and the specificity of roGFP2 biosensors was questioned (116). Thus, unfused roGFP2 had some limitations for measurements of the GSH redox potential in eukaryotic cells.

To overcome these limitations, roGFP was fused to human Grx1 to construct a coupled Grx1-roGFP2 biosensor for dynamic and specific measurements of the GSH redox potential changes at high sensitivity (65,109). The Grx1-roGFP2 fusion facilitates rapid and specific equilibration with the GSH/GSSG redox couple and does not react with other redox pairs of the cell (65,109,148). Of note, the steady-state E_{GSH} from cells expressing Grx1-roGFP2 and roGFP2 does not differ significantly, indicating that the redox potential was not affected by the fused glutaredoxin (11). Today, Grx1-roGFP2 is the most widely used biosensor for *in vivo* imaging of GSH redox potential changes in eukaryotic cells and different compartments (148). The Grx1-roGFP2 biosensor detects nanomolar concentrations of GSSG against a backdrop of millimolar

GSH within seconds (11,65,109). The response properties of Grx1-roGFP2 are based on the well-established monothiol mechanism of glutaredoxins. Under oxidative stress conditions, GSSG specifically reacts with the nucleophilic Cys23 of Grx1 to form a Grx1-SSG intermediate, which is transferred to roGFP2 and subsequently rearranges to the roGFP2 disulfide (109).

Recently, roGFP-based biosensors were applied in pathogenic organisms to study E_{GSH} changes under infection conditions and antibiotic treatment, including the malaria parasite *Plasmodium falciparum* (82) and the Gram-negative bacterium *Salmonella Typhimurium* (170,171). In malaria parasites, several antimalarial drugs affected the cellular redox metabolism and showed differential responses of the Grx-roGFP2 biosensor under short- and long-term measurements *in vivo*. The Grx1-roGFP2 biosensor responds rapidly and strongly to methylene blue or pyocyanin in *P. falciparum*, that are used as antimalarial drugs (82). However, these antimalarial drugs showed direct interactions with the Grx1-roGFP2 probe. In contrast, the antimalarial compounds quinolone, chloroquine, amodiaquine, quinine, mefloquine and artemisinin caused strong effects on E_{GSH} after longer incubation times that were not caused by their direct interaction with the probe (82).

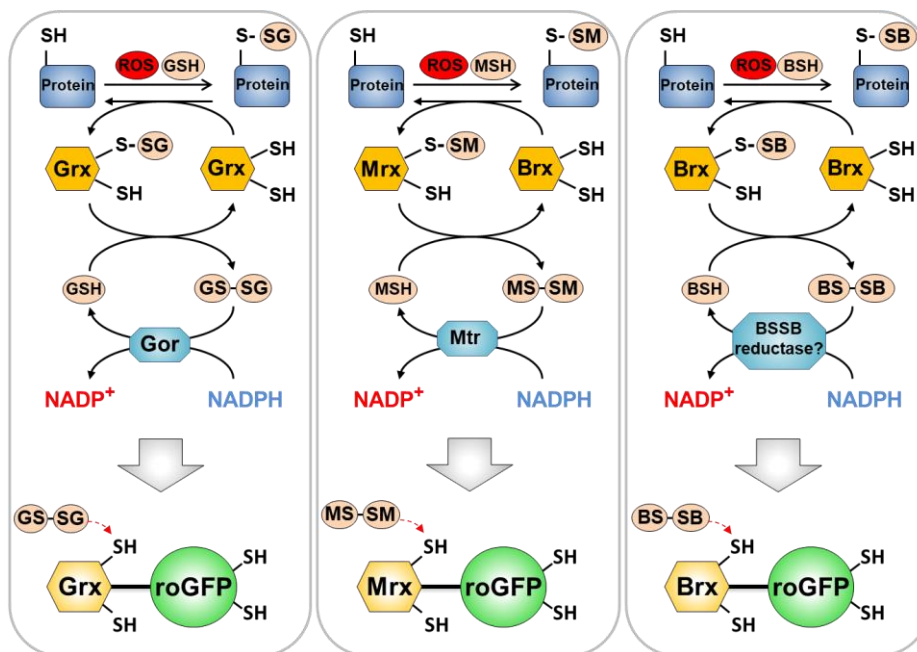


Figure 15. The roGFP2 biosensor was fused to glutaredoxin (Grx), mycoredoxin (Mrx) and bacilliredoxin (Brx) resulting in rapid equilibration with intracellular GSH/GSSG, MSH/MSSM and BSH/BSSB redox couples, respectively. This figure is adapted from (166).

3.2.2. Application of the Mrx1-roGFP2 biosensor in *Mycobacterium tuberculosis*

The roGFP2 and Grx1-roGFP2 biosensors were used to detect E_{GSH} changes in many eukaryotic organisms with high sensitivity and at spatiotemporal resolution (**Fig. 15**). In the intracellular

pathogen *Mycobacterium tuberculosis* (*Mtb*), an analogous Mrx1-roGFP2 biosensor was developed for dynamic measurements of the MSH redox potential (E_{MSH}) in drug-resistant and drug-sensitive *Mtb* isolates and inside the acidic phagosome of macrophages during infections (Fig. 16) (9). The increasing prevalence of persistent and chronic relapsing *Mtb* infections as well as multiple and extreme drug-resistant (MDR/XDR) *Mtb* isolates are a major health burden. Thus, the development of new drugs against severe tuberculosis infections is an urgent need. The Mrx1-roGFP2 biosensor was successfully applied to screen for ROS-generating anti-TB drugs and combination therapies (e.g. augmentin or isoniazid combinations) that affected E_{MSH} to study drug actions linked to the E_{MSH} to combat life-threatening TB infections (9,112,129,167). It was revealed that the E_{MSH} inside infected macrophages is heterogeneous with sub-populations that have reduced, oxidized and basal levels of E_{MSH} . This redox heterogeneity depends on sub-vacuolar compartments inside macrophages and the cytoplasmic acidification that requires WhiB3 as central redox regulator (9,106). The biosensor has further contributed to elucidate novel ROS defense mechanism in *Mtb*, such as the radical scavenging membrane MRC complex and the role of host GSH to regulate the MSH redox balance of *Mtb* inside macrophages (16,122). These results using the Mrx1-roGFP2 biosensor have advanced the understanding how this major pathogen copes with anti-TB drug and persists inside macrophages.

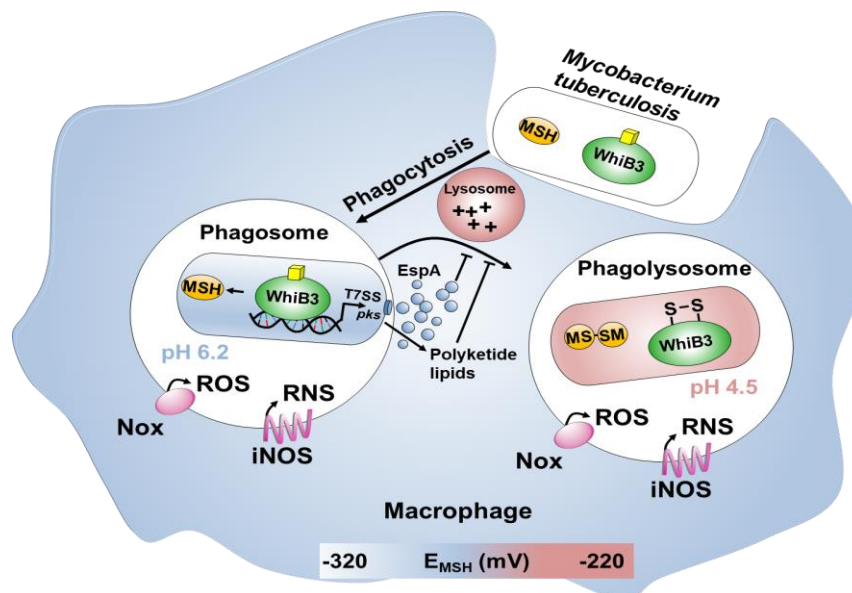


Figure 16: The role of E_{MSH} and the WhiB3 transcription factor in *M. tuberculosis* persistence under acidic conditions during infection of macrophages as shown by the Mrx1-roGFP2 biosensor. *M. tuberculosis* is an intracellular pathogen that replicates inside the acidic phagosome of macrophages (pH ~6.2) preventing phagosomal maturation to phagolysosomes as survival mechanism. During immune activation of macrophages, phagosomes are fused with lysosomes resulting in further pH decrease to pH 4.5. The mild acidification in phagosomes causes a highly reduced E_{MSH} inside *M. tuberculosis*, while strong acidification leads to oxidized E_{MSH} as measured in phagolysosomes. The WhiB3 transcription factor senses acidic conditions in the phagosome and activates transcription of WhiB3 regulon genes, such as type-VII-secretion system effectors (EspA) and polyketide lipids that inhibit phagosomal maturation. WhiB3 causes up-regulation of antioxidant systems (MSH, Trx) to restore the redox balance and to promote survival and persistence of *M. tuberculosis* inside the phagosome. The figure is adapted from (166).

3.2.3. Application of the Brx-roGFP2 biosensor in *Staphylococcus aureus*

In this PhD thesis, we have developed a novel genetically encoded Brx-roGFP2 biosensor to measure BSH redox potential changes in the human pathogen *S. aureus* (96). The bacilliredoxin (Brx) was fused to roGFP2 for construction of the Brx-roGFP2 biosensor (**Fig. 17**). This biosensor is able to follow the intracellular BSH redox potential changes in *S. aureus* with high sensitivity and specificity (**Fig. 18**).

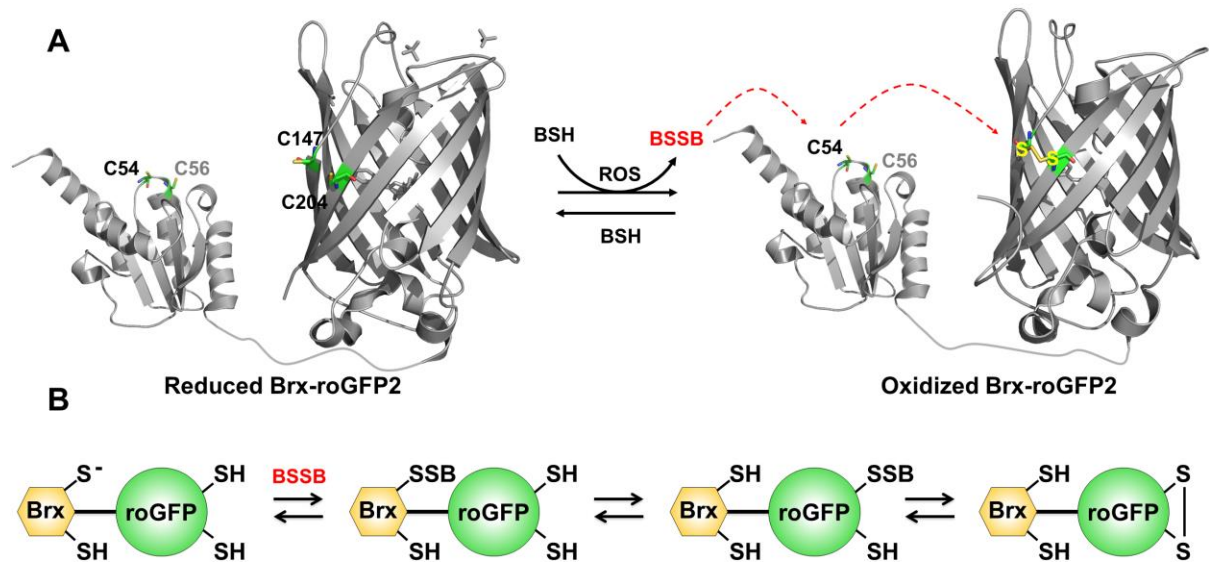


Figure 17. Principle of Brx-roGFP2 biosensor oxidation. (A, B) The Brx-roGFP2 biosensor reacts first with BSSB at the active site Cys (C54) of Brx leading to Brx-SSB intermediate formation. Brx-SSB interacts with one of the two proximal Cys thiols on roGFP2 and converts it into S-bacillithiolated roGFP2. In the final step, S-bacillithiolated roGFP2 rearranges to form intermolecular disulfide bridge leading to change of the 405/488 nm excitation ratio.

Brx-roGFP2 is highly specific and responds to physiological concentrations of BSSB *in vitro*. The response of the Brx-roGFP2 biosensor to BSSB required the Brx active site Cys. Brx-roGFP2 was expressed inside *S. aureus* cells to study the E_{BSH} changes during exposure of cells to H_2O_2 , NaOCl, antibiotics and under infections conditions (96). A fast and strong biosensor oxidation was measured in *S. aureus* after exposure to low doses of 100 μ M NaOCl. This confirms the high reactivity of NaOCl inside *S. aureus* that requires fast thiol-protection by S-bacillithiolation to avoid overoxidation of thiols. In contrast, exposure of *S. aureus* to high doses of 100mM H_2O_2 did not cause complete oxidation of the Brx-roGFP2 biosensor. This slow reaction of the biosensor to H_2O_2 stress might be caused by the high level of peroxide resistance in *S. aureus* (96). *S. aureus* BSH-deficient mutants expressing Brx-roGFP2 showed constitutive oxidation of the biosensor indicating an impaired redox balance in the absence of BSH (96).

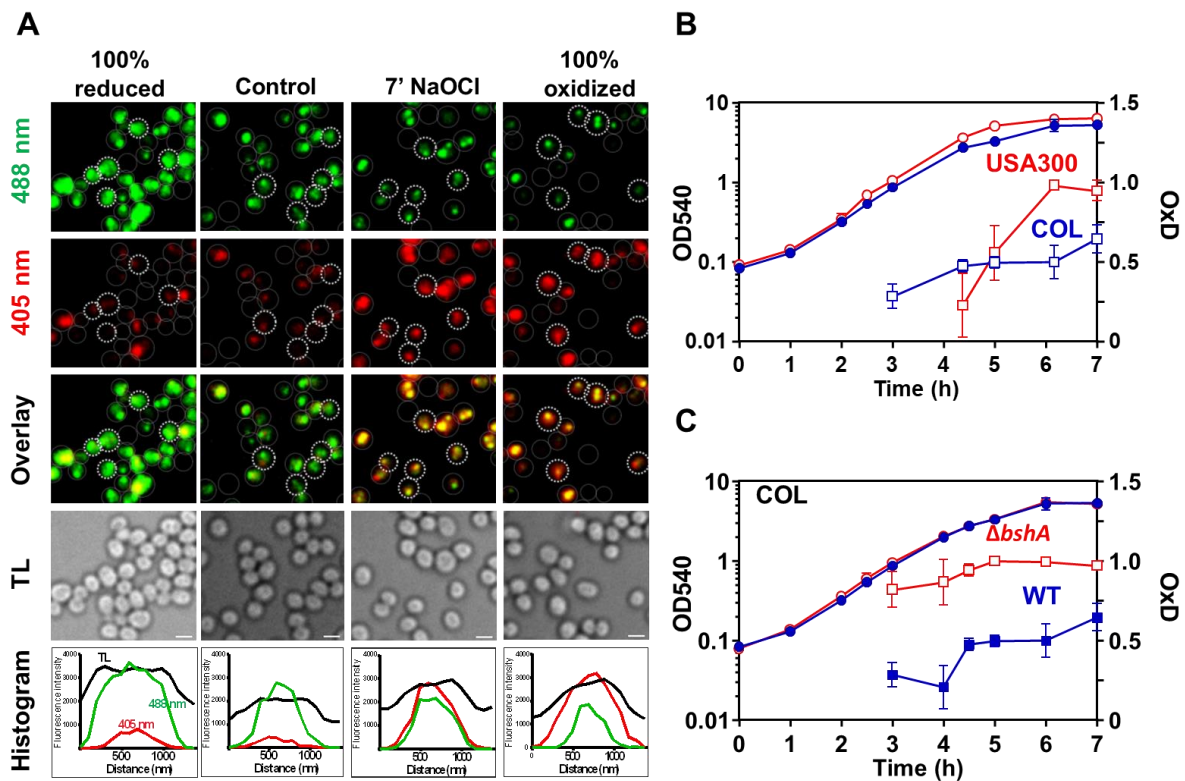


Figure 18. Dynamic changes in the BSH redox potential as monitored by the novel Brx-roGFP2 redox biosensor in *S. aureus*. **A)** Increased biosensor oxidation (OxD) was measured under NaOCl stress in *S. aureus* COL wild type by confocal microscopy. **(B)** The BSH redox potential is increased in *S. aureus* COL and USA300 during the growth in LB medium upon entry into the stationary phase and **(C)** the biosensor is fully oxidized in the BSH-deficient *bshA* mutant as measured using the microplate reader.

Due to the controversial debate about the involvement of ROS in the killing mode of antibiotics, the Brx-roGFP2 biosensor response was measured after treatment with different antibiotics classes in *S. aureus*, including rifampicin, fosfomycin, ampicillin, oxacillin, vancomycin, aminoglycosides and fluoroquinolones. However, exposure to sub-lethal doses of antibiotics did not lead to changes in the BSH redox potential inside *S. aureus* (96). This indicates that antibiotics do not cause oxidative stress in *S. aureus*. However, the Mrx1-roGFP2 biosensor measurements revealed an impact of ROS-generation by antibiotics under infection conditions inside the acidic phagosome. Moreover, a link between killing by isoniazid and augmentin and the E_{MSH} has been revealed in *Mtb* (129,166,167). Thus, future studies are required also in *S. aureus* to study the susceptibility to antibiotics and its effect on E_{BSH} during internalization in macrophages. Moreover, the Brx-roGFP2 biosensor can be further applied in drug-research to screen for novel ROS-generating antibiotics or combination therapies and their impact on E_{BSH} changes in *S. aureus* in shake-flasks and after internalization (96). Our current studies are further directed to apply this Brx-roGFP2 biosensor for screening of the BSH redox potential across *S. aureus* isolates of different clonal complexes to reveal the differences in pathogen fitness and in their ROS detoxification capacities as defense mechanisms against the host immune system.

4. Conclusion and future perspectives

In this PhD thesis, we have studied the physiological responses of the major human pathogen *S. aureus* under HOCl stress and identified novel thiol-based redox switches that were characterized in detail and are important for virulence. These novel thiol-switches include the glyceraldehyde dehydrogenases GapDH and AldA as main metabolic enzymes that are protected and redox-regulated by protein S-bacillithiolation in *S. aureus*. We have further identified the Rrf2-family regulator HypR as novel thiol-based redox-sensing regulator which senses and responds directly to HOCl stress in *S. aureus*. HypR is oxidized to a Cys33-Cys99' intersubunit disulfide resulting in derepression of *hypR-merA* operon transcription. HypR negatively controls the NADPH-dependent flavin enzyme MerA which provides protection under HOCl stress and macrophage infection conditions. Finally, we developed a novel redox Brx-roGFP2 biosensor, which catalyzes specific equilibration between the BSH and roGFP2 redox couples to monitor dynamic changes in the BSH redox potential in *S. aureus* under oxidative stress and antibiotics treatments. The overall results have been published in 6 original publications and 3 review articles that are included in the following chapters.

In conclusion, in this work important novel thiol-switches were characterized that contribute to a better understanding of the defense mechanisms of *S. aureus* against the host immune system. Since BSH, AldA and MerA are required for the survival under HOCl stress, these could be candidate drug targets for the development of new drugs to combat MRSA infections.

References

1. Amissah NA, Chlebowicz MA, Ablordey A, Tetteh CS, Prah I, van der Werf TS, Friedrich AW, van Dijk JM, Stienstra Y, Rossen JW. Virulence potential of *Staphylococcus aureus* isolates from Buruli ulcer patients. *Int J Med Microbiol.* 307: 223-232. (2017).
2. Antelmann H, Hamilton CJ. Bacterial mechanisms of reversible protein S-thiolation: structural and mechanistic insights into mycoredoxins. *Mol Microbiol.* 86(4):759-64. (2012).
3. Bacconi M, Haag AF, Chiarot E, Donato P, Bagnoli F, Delany I, Bensi G. In vivo analysis of *Staphylococcus aureus*-infected mice reveals differential temporal and spatial expression patterns of fhuD2. *Infect Immun.* 85 (10):1-15. (2017).
4. Ballal A, Ray B, Manna AC. sarZ, a sarA family gene, is transcriptionally activated by MgrA and is involved in the regulation of genes encoding exoproteins in *Staphylococcus aureus*. *J Bacteriol.* 191: 1656-65. (2009).
5. Barendt S, Birch C, Mbengi L, Zuber P. Evidence that Oxidative Stress Induces spxA2 Transcription in *Bacillus anthracis* Sterne through a mechanism requiring SpxA1 and positive autoregulation. *J Bacteriol.* 198: 2902-2913. (2016).
6. Barendt S, Lee H, Birch C, Nakano MM, Jones M, Zuber P. Transcriptomic and phenotypic analysis of paralogous spx gene function in *Bacillus anthracis* Sterne. *Microbiologyopen.* 2: 695-714. (2013).
7. Ben Zakour NL, Guinane CM, Fitzgerald JR. Pathogenomics of the staphylococci: insights into niche adaptation and the emergence of new virulent strains. *FEMS Microbiol Lett.* 289: 1-12. (2008).
8. Bergman NH, Anderson EC, Swenson EE, Janes BK, Fisher N, Niemeyer MM, Miyoshi AD, Hanna PC. Transcriptional profiling of *Bacillus anthracis* during infection of host macrophages. *Infect Immun.* 75: 3434-44. (2007).
9. Bhaskar A, Chawla M, Mehta M, Parikh P, Chandra P, Bhawe D, Kumar D, Carroll KS, Singh A. Reengineering redox sensitive GFP to measure mycothiol redox potential of *Mycobacterium tuberculosis* during infection. *PLoS Pathog.* 10: e1003902. (2014).
10. Biasini M, Bienert S, Waterhouse A, Arnold K, Studer G, Schmidt T, Kiefer F, Gallo Cassarino T, Bertoni M, Bordoli L, Schwede T. SWISS-MODEL: modelling protein tertiary and quaternary structure using evolutionary information. *Nucleic Acids Res.* 42: W252-8. (2014).
11. Bilan DS, Belousov VV. New tools for redox biology: From imaging to manipulation. *Free Radic Biol Med.* 109: 167-188. (2017).
12. Bischoff M, Dunman P, Kormanec J, Macapagal D, Murphy E, Mounts W, Berger-Bachi B, Projan S. Microarray-based analysis of the *Staphylococcus aureus* sigmaB regulon. *J Bacteriol.* 186: 4085-99. (2004).
13. Blaiotta G, Fusco V, Ercolini D, Pepe O, Coppola S. Diversity of *Staphylococcus* species strains based on partial kat (catalase) gene sequences and design of a PCR-restriction fragment length polymorphism assay for identification and differentiation of coagulase-positive species (*S. aureus*, *S. delphini*, *S. hyicus*, *S. intermedius*, *S. pseudintermedius*, and *S. schleiferi* subsp. coagulans). *J Clin Microbiol.* 48: 192-201. (2010).
14. Brejc K, Sixma TK, Kitts PA, Kain SR, Tsien RY, Ormo M, Remington SJ. Structural basis for dual excitation and photoisomerization of the *Aequorea victoria* green fluorescent protein. *Proc Natl Acad Sci U S A.* 94: 2306-11. (1997).
15. Bronner S, Monteil H, Prevost G. Regulation of virulence determinants in *Staphylococcus aureus*: complexity and applications. *FEMS Microbiol Rev.* 28: 183-200. (2004).
16. Cai Y, Yang Q, Liao M, Wang H, Zhang C, Nambi S, Wang W, Zhang M, Wu J, Deng G, Deng Q, Liu H, Zhou B, Jin Q, Feng CG, Sasseti CM, Wang F, Chen X. xCT increases tuberculosis susceptibility by regulating antimicrobial function and inflammation. *Oncotarget.* 7: 31001-13. (2016).

17. Cetinkaya Y, Falk P, Mayhall CG. Vancomycin-resistant *enterococci*. *Clinical Microbiology Reviews*. 13: 686-707. (2000).
18. Chambers HF, Deleo FR. Waves of resistance: *Staphylococcus aureus* in the antibiotic era. *Nat Rev Microbiol*. 7: 629-641. (2009).
19. Chandrangu P, Dusi R, Hamilton CJ, Helmann JD. Methylglyoxal resistance in *Bacillus subtilis*: contributions of bacillithiol-dependent and independent pathways. *Mol Microbiol*. 91: 706-715. (2014)
20. Chandrangu P, Loi VV, Antelmann H, Helmann JD. The role of bacillithiol in Gram-positive *Firmicutes*. *Antioxid Redox Signal*. 28(6): 445-462. (2017)
21. Chen PR, Bae T, Williams WA, Duguid EM, Rice PA, Schneewind O, He C. An oxidation-sensing mechanism is used by the global regulator MgrA in *Staphylococcus aureus*. *Nat Chem Biol*. 2: 591-595. (2006)
22. Chen PR, Brugarolas P, He C. Redox signaling in human pathogens. *Antioxid Redox Signal*. 14: 1107-1118. (2011)
23. Chen PR, Nishida S, Poor CB, Cheng A, Bae T, Kuechenmeister L, Dunman PM, Missiakas D, He C. A new oxidative sensing and regulation pathway mediated by the MgrA homologue SarZ in *Staphylococcus aureus*. *Mol Microbiol*. 71: 198-211. (2009)
24. Cheung AL, Bayer AS, Zhang G, Gresham H, Xiong YQ. Regulation of virulence determinants in vitro and in vivo in *Staphylococcus aureus*. *FEMS Immunol Med Microbiol*. 40: 1-9. (2004).
25. Cheung AL, Nishina KA, Trotonda MP, Tamber S. The SarA protein family of *Staphylococcus aureus*. *Int J Biochem Cell Biol*. 40: 355-361. (2008)
26. Chi BK, Albrecht D, Gronau K, Becher D, Hecker M, Antelmann H. The redox-sensing regulator YodB senses quinones and diamide via a thiol-disulfide switch in *Bacillus subtilis*. *Proteomics* 10: 3155-3164. (2010)
27. Chi BK, Busche T, Van Laer K, Basell K, Becher D, Clermont L, Seibold GM, Persicke M, Kalinowski J, Messens J, Antelmann H. Protein S-mycothiolation functions as redox-switch and thiol protection mechanism in *Corynebacterium glutamicum* under hypochlorite stress. *Antioxid Redox Signal*. 20: 589-605. (2014)
28. Chi BK, Gronau K, Mader U, Hessling B, Becher D, Antelmann H. S-bacillithiolation protects against hypochlorite stress in *Bacillus subtilis* as revealed by transcriptomics and redox proteomics. *Mol Cell Proteomics*. 10: M1111 009506. (2011)
29. Chi BK, Roberts AA, Huyen TT, Basell K, Becher D, Albrecht D, Hamilton CJ, Antelmann H. S-bacillithiolation protects conserved and essential proteins against hypochlorite stress in *firmicutes* bacteria. *Antioxid Redox Signal*. 18: 1273-1295. (2013)
30. Clauditz A, Resch A, Wieland KP, Peschel A, Gotz F. Staphyloxanthin plays a role in the fitness of *Staphylococcus aureus* and its ability to cope with oxidative stress. *Infect Immun*. 74: 4950-4953. (2006)
31. Cosgrove K, Coutts G, Jonsson IM, Tarkowski A, Kokai-Kun JF, Mond JJ, Foster SJ. Catalase (KatA) and alkyl hydroperoxide reductase (AhpC) have compensatory roles in peroxide stress resistance and are required for survival, persistence, and nasal colonization in *Staphylococcus aureus*. *J Bacteriol*. 189: 1025-1035. (2007)
32. Costa ARB, Batistão DWF, Ribas RM, Sousa AM, Pereira MO, Botelho CM. *Staphylococcus aureus* virulence factors and disease. In: *Microbial pathogens and strategies for combating them: science, technology and education*. Formatex research center. 702-710. (2013)
33. Crack JC, Le Brun NE. Redox-sensing iron-sulfur cluster regulators. *Antioxid Redox Signal*. doi: 10.1089/ars.2017.7361. (2017)
34. Crack JC, Munnoch J, Dodd EL, Knowles F, Al Bassam MM, Kamali S, Holland AA, Cramer SP, Hamilton CJ, Johnson MK, Thomson AJ, Hutchings MI, Le Brun NE. NsrR

- from *Streptomyces coelicolor* is a nitric oxide-sensing [4Fe-4S] cluster protein with a specialized regulatory function. *J Biol Chem.* 290: 12689-12704. (2015)
35. Davies MJ. Myeloperoxidase-derived oxidation: mechanisms of biological damage and its prevention. *J Clin Biochem Nutr.* 48: 8-19. (2011)
 36. Davies MJ. Protein oxidation and peroxidation. *Biochem J.* 473: 805-825. (2016)
 37. Dinges MM, Orwin PM, Schlievert PM. Exotoxins of *Staphylococcus aureus*. *Clin Microbiol Rev.* 13: 16-34. (2000)
 38. Dooley CT, Dore TM, Hanson GT, Jackson WC, Remington SJ, Tsien RY. Imaging dynamic redox changes in mammalian cells with green fluorescent protein indicators. *J Biol Chem.* 279: 22284-22293. (2004)
 39. Dorries K, Schlueter R, Lalk M. Impact of antibiotics with various target sites on the metabolome of *Staphylococcus aureus*. *Antimicrob Agents Chemother.* 58: 7151-7163. (2014)
 40. Elsliger MA, Wachter RM, Hanson GT, Kallio K, Remington SJ. Structural and spectral response of green fluorescent protein variants to changes in pH. *Biochemistry.* 38: 5296-5301. (1999)
 41. Ezraty B, Gennaris A, Barras F, Collet JF. Oxidative stress, protein damage and repair in bacteria. *Nat Rev Microbiol.* 15: 385-396. (2017)
 42. Fahey RC. Glutathione analogs in prokaryotes. *Biochim Biophys Acta.* 1830: 3182-3198. (2013)
 43. Fang Z, Dos Santos PC. Protective role of bacillithiol in superoxide stress and Fe-S metabolism in *Bacillus subtilis*. *Microbiologyopen.* 4: 616-31. (2015)
 44. Feng J, Che Y, Milse J, Yin YJ, Liu L, Ruckert C, Shen XH, Qi SW, Kalinowski J, Liu SJ. The gene ncgl2918 encodes a novel maleylpyruvate isomerase that needs mycothiol as cofactor and links mycothiol biosynthesis and gentisate assimilation in *Corynebacterium glutamicum*. *J Biol Chem.* 281: 10778-10785. (2006)
 45. Fernandes AP, Holmgren A. Glutaredoxins: glutathione-dependent redox enzymes with functions far beyond a simple thioredoxin backup system. *Antioxid Redox Signal.* 6: 63-74. (2004)
 46. Foell D, Wittkowski H, Vogl T, Roth J. S100 proteins expressed in phagocytes: a novel group of damage-associated molecular pattern molecules. *J Leukoc Biol.* 81: 28-37. (2007)
 47. Forman HJ, Torres M. Redox signaling in macrophages. *Mol Aspects Med.* 22: 189-216. (2001)
 48. Forman HJ, Torres M, Fukuto J. Redox signaling. *Mol Cell Biochem.* 234-235: 49-62. (2002)
 49. Foster TJ. The *Staphylococcus aureus* "superbug". *J Clin Invest.* 114: 1693-1696. (2004)
 50. Foster TJ, Geoghegan JA. Chapter 37 - *Staphylococcus aureus* A2 - Tang, Yi-Wei. In: *Molecular Medical Microbiology (Second Edition)*. Edited by Sussman M, Liu D, Poxton I, Schwartzman J. Boston: Academic Press. 655-674. (2015)
 51. Foster TJ, Geoghegan JA, Ganesh VK, Hook M. Adhesion, invasion and evasion: the many functions of the surface proteins of *Staphylococcus aureus*. *Nat Rev Microbiol.* 12: 49-62. (2014)
 52. Foster TJ, Hook M. Surface protein adhesins of *Staphylococcus aureus*. *Trends Microbiol.* 6: 484-488. (1998)
 53. Fuangthong M, Atichartpongkul S, Mongkolsuk S, Helmann JD. OhrR is a repressor of ohrA, a key organic hydroperoxide resistance determinant in *Bacillus subtilis*. *J Bacteriol.* 183: 4134-4141. (2001)
 54. Gaballa A, Chi BK, Roberts AA, Becher D, Hamilton CJ, Antelmann H, Helmann JD. Redox regulation in *Bacillus subtilis*: The bacilliredoxins BrxA(YphP) and BrxB(YqiW) function in de-bacillithiolation of S-bacillithiolated OhrR and MetE. *Antioxid Redox Signal.* 21: 357-367. (2014)

55. Gaballa A, Newton GL, Antelmann H, Parsonage D, Upton H, Rawat M, Claiborne A, Fahey RC, Helmann JD. Biosynthesis and functions of bacillithiol, a major low-molecular-weight thiol in Bacilli. *Proc Natl Acad Sci U S A*. 107: 6482-6486. (2010)
56. Garcia YM, Barwinska-Sendra A, Tarrant E, Skaar EP, Waldron KJ, Kehl-Fie TE. A superoxide dismutase capable of functioning with iron or manganese promotes the resistance of *Staphylococcus aureus* to calprotectin and nutritional immunity. *PLoS Pathog*. 13: e1006125. (2017)
57. Gardete S, Tomasz A. Mechanisms of vancomycin resistance in *Staphylococcus aureus*. *J Clin Invest*. 124: 2836-2840. (2014)
58. Garzoni C, Kelley WL. *Staphylococcus aureus*: new evidence for intracellular persistence. *Trends Microbiol*. 17: 59-65. (2009)
59. Gaupp R, Ledala N, Somerville GA. *Staphylococcal* response to oxidative stress. *Front Cell Infect Microbiol*. 2: 33. (2012)
60. Giel JL, Nesbit AD, Mettert EL, Fleischhacker AS, Wanta BT, Kiley PJ. Regulation of iron-sulphur cluster homeostasis through transcriptional control of the Isc pathway by [2Fe-2S]-IscR in *Escherichia coli*. *Mol Microbiol*. 87: 478-492. (2013)
61. Giel JL, Rodionov D, Liu M, Blattner FR, Kiley PJ. IscR-dependent gene expression links iron-sulphur cluster assembly to the control of O₂-regulated genes in *Escherichia coli*. *Mol Microbiol*. 60: 1058-1075. (2006)
62. Gilberthorpe NJ, Lee ME, Stevanin TM, Read RC, Poole RK. NsrR: a key regulator circumventing *Salmonella* enterica serovar Typhimurium oxidative and nitrosative stress in vitro and in IFN-gamma-stimulated J774.2 macrophages. *Microbiology*. 153: 1756-1771. (2007)
63. Gordon RJ, Lowy FD. Pathogenesis of methicillin-resistant *Staphylococcus aureus* infection. *Clin Infect Dis*. 46: S350-S359. (2008)
64. Gray MJ, Wholey WY, Jakob U. Bacterial responses to reactive chlorine species. *Annu Rev Microbiol*. 67: 141-160. (2013)
65. Gutscher M, Pauleau AL, Marty L, Brach T, Wabnitz GH, Samstag Y, Meyer AJ, Dick TP. Real-time imaging of the intracellular glutathione redox potential. *Nat Methods*. 5: 553-559. (2008)
66. Haaber J, Penades JR, Ingmer H. Transfer of antibiotic resistance in *Staphylococcus aureus*. *Trends Microbiol*. 25: 893-905. (2017)
67. Hanson GT, Aggeler R, Oglesbee D, Cannon M, Capaldi RA, Tsien RY, Remington SJ. Investigating mitochondrial redox potential with redox-sensitive green fluorescent protein indicators. *J Biol Chem*. 279: 13044-13053. (2004)
68. Helmann JD. Bacillithiol, a new player in bacterial redox homeostasis. *Antioxid Redox Signal*. 15: 123-133. (2011)
69. Hillion M, Antelmann H. Thiol-based redox switches in prokaryotes. *Biol Chem*. 396: 415-444. (2015)
70. Hillion M, Bernhardt J, Busche T, Rossius M, Maass S, Becher D, Rawat M, Wirtz M, Hell R, Ruckert C, Kalinowski J, Antelmann H. Monitoring global protein thiol-oxidation and protein S-mycothiolation in *Mycobacterium smegmatis* under hypochlorite stress. *Sci Rep*. 7: 1195. (2017)
71. Hillion M, Imber M, Pedre B, Bernhardt J, Saleh M, Loi VV, Maass S, Becher D, Astolfi Rosado L, Adrian L, Weise C, Hell R, Wirtz M, Messens J, Antelmann H. The glyceraldehyde-3-phosphate dehydrogenase GapDH of *Corynebacterium diphtheriae* is redox-controlled by protein S-mycothiolation under oxidative stress. *Sci Rep*. 7: 5020. (2017)
72. Howden BP, Davies JK, Johnson PDR, Stinear TP, Grayson ML. Reduced vancomycin susceptibility in *Staphylococcus aureus*, including vancomycin-intermediate and heterogeneous vancomycin-intermediate strains: resistance mechanisms, laboratory detection, and clinical implications. *Clin Microbiol Rev*. 23(1): 99-139. (2010)

73. Imber M, Huyen NTT, Pietrzyk-Brzezinska AJ, Loi VV, Hillion M, Bernhardt J, Tharichen L, Kolsek K, Saleh M, Hamilton CJ, Adrian L, Grater F, Wahl MC, Antelmann H. Protein S-bacillithiolation functions in thiol protection and redox regulation of the glyceraldehyde-3-phosphate dehydrogenase Gap in *Staphylococcus aureus* under hypochlorite stress. *Antioxid Redox Signal.* 28(6): 410–430. (2017)
74. Imber M, Loi VV, Reznikov S, Fritsch VN, Pietrzyk-Brzezinska AJ, Prehn J, Hamilton C, Wahl MC, Bronowska AK, Antelmann H. The aldehyde dehydrogenase AldA contributes to the hypochlorite defense and is redox-controlled by protein S-bacillithiolation in *Staphylococcus aureus*. *Redox Biol.* 15: 557-568. (2018)
75. Imlay JA. The molecular mechanisms and physiological consequences of oxidative stress: lessons from a model bacterium. *Nat Rev Microbiol.* 11: 443-454. (2013)
76. Isabella VM, Lapek JD, Jr., Kennedy EM, Clark VL. Functional analysis of NsrR, a nitric oxide-sensing Rrf2 repressor in *Neisseria gonorrhoeae*. *Mol Microbiol.* 71: 227-239. (2009)
77. Ji Q, Zhang L, Jones MB, Sun F, Deng X, Liang H, Cho H, Brugarolas P, Gao YN, Peterson SN, Lan L, Bae T, He C. Molecular mechanism of quinone signaling mediated through S-quinonization of a YodB family repressor QsrR. *Proc Natl Acad Sci U S A.* 110: 5010-5015. (2013)
78. Ji Q, Zhang L, Sun F, Deng X, Liang H, Bae T, He C. *Staphylococcus aureus* CymR is a new thiol-based oxidation-sensing regulator of stress resistance and oxidative response. *J Biol Chem.* 287: 21102-21109. (2012)
79. Jothivasan VK, Hamilton CJ. Mycothiol: synthesis, biosynthesis and biological functions of the major low molecular weight thiol in actinomycetes. *Nat Prod Rep.* 25: 1091-1117. (2008)
80. Karavolos MH, Horsburgh MJ, Ingham E, Foster SJ. Role and regulation of the superoxide dismutases of *Staphylococcus aureus*. *Microbiology.* 149: 2749-2758. (2003)
81. Karlinsey JE, Bang IS, Becker LA, Frawley ER, Porwollik S, Robbins HF, Thomas VC, Urbano R, McClelland M, Fang FC. The NsrR regulon in nitrosative stress resistance of *Salmonella enterica* serovar Typhimurium. *Mol Microbiol.* 85: 1179-1193. (2012)
82. Kasozi D, Mohring F, Rahlf S, Meyer AJ, Becker K. Real-time imaging of the intracellular glutathione redox potential in the malaria parasite *Plasmodium falciparum*. *PLoS Pathog.* 9: e1003782. (2013)
83. Kavanaugh JS, Horswill AR. Impact of environmental cues on staphylococcal quorum sensing and biofilm development. *J Biol Chem.* 291: 12556-12564. (2016)
84. Kiley PJ, Storz G. Exploiting thiol modifications. *PLoS Biol.* 2: e400. (2004)
85. Kobayashi SD, Malachowa N, DeLeo FR. Pathogenesis of *Staphylococcus aureus* abscesses. *Am J Pathol.* 185: 1518-1527. (2015)
86. Kommineni S, Lama A, Popescu B, Nakano MM. Global transcriptional control by NsrR in *Bacillus subtilis*. *J Bacteriol.* 194: 1679-1688. (2012)
87. Lacoma A, Cano V, Moranta D, Rigueiro V, Dominguez-Villanueva D, Laabei M, Gonzalez-Nicolau M, Ausina V, Prat C, Bengoechea JA. Investigating intracellular persistence of *Staphylococcus aureus* within a murine alveolar macrophage cell line. *Virulence.* 8(8): 1761–1775. (2017).
88. Lee JW, Soonsanga S, Helmann JD. A complex thiolate switch regulates the *Bacillus subtilis* organic peroxide sensor OhrR. *Proc Natl Acad Sci U S A.* 104: 8743-8748. (2007)
89. Lee KC, Yeo WS, Roe JH. Oxidant-responsive induction of the *suf* operon, encoding a Fe-S assembly system, through Fur and IscR in *Escherichia coli*. *J Bacteriol.* 190: 8244-8247. (2008)
90. Lillig CH, Berndt C, Holmgren A. Glutaredoxin systems. *Biochim Biophys Acta.* 1780: 1304-1317. (2008)
91. Lin Y-C, Peterson ML. New insights into the prevention of staphylococcal infections and toxic shock syndrome. *Expert Rev Clin Pharmacol.* 3: 753-767. (2010)

92. Lindsay JA. Genomic variation and evolution of *Staphylococcus aureus*. *Int J Med Microbiol.* 300: 98-103. (2010)
93. Lindsay JA, Moore CE, Day NP, Peacock SJ, Witney AA, Stabler RA, Husain SE, Butcher PD, Hinds J. Microarrays reveal that each of the ten dominant lineages of *Staphylococcus aureus* has a unique combination of surface-associated and regulatory genes. *J Bacteriol.* 188: 669-676. (2006)
94. Livermore DM. Antibiotic resistance in staphylococci. *Int J Antimicrob Agents.* 16: S3-S10. (2000).
95. Loi VV, Busche T, Bernhardt J, Tedin K, Wollenhaupt J, Huyen NTT, Weise C, Kalinowski J, Wahl M, Fulde M, Antelmann H. Redox-sensing under hypochlorite stress and infection conditions by the Rrf2-family repressor HypR in *Staphylococcus aureus*. *Antioxid Redox Signal.* doi: 10.1089/ars.2017.7354. (2017)
96. Loi VV, Harms M, Muller M, Huyen NTT, Hamilton CJ, Hochgrafe F, Pane-Farre J, Antelmann H. Real-time imaging of the bacillithiol redox potential in the human pathogen *Staphylococcus aureus* using a genetically encoded bacilliredoxin-fused redox biosensor. *Antioxid Redox Signal.* 26: 835-848. (2017).
97. Loi VV, Rossius M, Antelmann H. Redox regulation by reversible protein S-thiolation in bacteria. *Front Microbiol.* 6: 187. (2015)
98. Lowy FD. *Staphylococcus aureus* infections. *N Engl J Med.* 339: 520-532. (1998)
99. Luebke JL, Giedroc DP. Cysteine sulfur chemistry in transcriptional regulators at the host-bacterial pathogen interface. *Biochemistry.* 54: 3235-3249. (2015)
100. Luong TT, Dunman PM, Murphy E, Projan SJ, Lee CY. Transcription profiling of the *mgrA* regulon in *Staphylococcus aureus*. *J Bacteriol.* 188: 1899-1910. (2006)
101. Ma Z, Chandrangsu P, Helmann TC, Romsang A, Gaballa A, Helmann JD. Bacillithiol is a major buffer of the labile zinc pool in *Bacillus subtilis*. *Mol Microbiol.* 94: 756-770. (2014)
102. Mader U, Nicolas P, Depke M, Pane-Farre J, Debarbouille M, van der Kooi-Pol MM, Guerin C, Derozier S, Hiron A, Jarmer H, Leduc A, Michalik S, Reilman E, Schaffer M, Schmidt F, Bessieres P, Noirot P, Hecker M, Msadek T, Volker U, van Dijl JM. *Staphylococcus aureus* transcriptome architecture: from laboratory to infection-mimicking conditions. *PLoS Genet.* 12: e1005962. (2016)
103. Mashruwala AA, Pang YY, Rosario-Cruz Z, Chahal HK, Benson MA, Mike LA, Skaar EP, Torres VJ, Nauseef WM, Boyd JM. Nfu facilitates the maturation of iron-sulfur proteins and participates in virulence in *Staphylococcus aureus*. *Mol Microbiol.* 95: 383-409. (2015)
104. Masip L, Veeravalli K, Georgiou G. The many faces of glutathione in bacteria. *Antioxid Redox Signal.* 8: 753-762. (2006)
105. McGuinness WA, Kobayashi SD, DeLeo FR. Evasion of neutrophil killing by *Staphylococcus aureus*. *Pathogens.* 5: 32. (2016)
106. Mehta M, Rajmani RS, Singh A. *Mycobacterium tuberculosis* WhiB3 responds to vacuolar pH-induced changes in mycothiol redox potential to modulate phagosomal maturation and virulence. *J Biol Chem.* 291: 2888-2903. (2016)
107. Memmi G, Filipe SR, Pinho MG, Fu Z, Cheung A. *Staphylococcus aureus* PBP4 is essential for beta-lactam resistance in community-acquired methicillin-resistant strains. *Antimicrob Agents Chemother.* 52: 3955-3966. (2008)
108. Mettert EL, Kiley PJ. Fe-S proteins that regulate gene expression. *Biochim Biophys Acta.* 1853: 1284-1293. (2015)
109. Meyer AJ, Dick TP. Fluorescent protein-based redox probes. *Antioxid Redox Signal.* 13: 621-650. (2010)
110. Michalik S, Depke M, Murr A, Gesell Salazar M, Kusebauch U, Sun Z, Meyer TC, Surmann K, Pfortner H, Hildebrandt P, Weiss S, Palma Medina LM, Gutjahr M, Hammer E, Becher D, Pribyl T, Hammerschmidt S, Deutsch EW, Bader SL, Hecker M, Moritz RL, Mader U, Volker U, Schmidt F. A global *Staphylococcus aureus* proteome resource applied to the *in vivo* characterization of host-pathogen interactions. *Sci Rep.* 7: 9718. (2017)

111. Miller WR, Munita JM, Arias CA. Mechanisms of antibiotic resistance in enterococci. *Expert Rev Anti Infect Ther.* 12: 1221-1236. (2014)
112. Mishra S, Shukla P, Bhaskar A, Anand K, Baloni P, Jha RK, Mohan A, Rajmani RS, Nagaraja V, Chandra N, Singh A. Efficacy of beta-lactam/beta-lactamase inhibitor combination is linked to WhiB4-mediated changes in redox physiology of *Mycobacterium tuberculosis*. *Elife.* 6: e25624. (2017)
113. Mitchell G, Brouillette E, Seguin DL, Asselin AE, Jacob CL, Malouin F. A role for sigma factor B in the emergence of *Staphylococcus aureus* small-colony variants and elevated biofilm production resulting from an exposure to aminoglycosides. *Microb Pathog.* 48: 18-27. (2010)
114. Mitchell G, Seguin DL, Asselin AE, Deziel E, Cantin AM, Frost EH, Michaud S, Malouin F. *Staphylococcus aureus* sigma B-dependent emergence of small-colony variants and biofilm production following exposure to *Pseudomonas aeruginosa* 4-hydroxy-2-heptylquinoline-N-oxide. *BMC Microbiol.* 10: 33. (2010)
115. Mongkolsuk S, Helmann JD. Regulation of inducible peroxide stress responses. *Mol Microbiol.* 45: 9-15. (2002)
116. Morgan B, Sobotta MC, Dick TP. Measuring E_{GSH} and H_2O_2 with roGFP2-based redox probes. *Free Radic Biol Med.* 51: 1943-1951. (2011)
117. Munita JM, Arias CA. Mechanisms of antibiotic resistance. *Microbiol Spectr.* 4: 10. (2016)
118. Munnoch JT, Martinez MT, Svistunen DA, Crack JC, Le Brun NE, Hutchings MI. Characterization of a putative NsrR homologue in *Streptomyces venezuelae* reveals a new member of the Rf2 superfamily. *Sci Rep.* 6: 31597. (2016)
119. Nakano MM, Geng H, Nakano S, Kobayashi K. The nitric oxide-responsive regulator NsrR controls ResDE-dependent gene expression. *J Bacteriol.* 188: 5878-5887. (2006)
120. Nakano MM, Kominos-Marvell W, Sane B, Nader YM, Barendt SM, Jones MB, Zuber P. spxA2, encoding a regulator of stress resistance in *Bacillus anthracis*, is controlled by SaiR, a new member of the Rf2 protein family. *Mol Microbiol.* 94: 815-827. (2014)
121. Nakano S, Kuster-Schock E, Grossman AD, Zuber P. Spx-dependent global transcriptional control is induced by thiol-specific oxidative stress in *Bacillus subtilis*. *Proc Natl Acad Sci U S A.* 100: 13603-13608. (2003)
122. Nambi S, Long JE, Mishra BB, Baker R, Murphy KC, Olive AJ, Nguyen HP, Shaffer SA, Sasseti CM. The oxidative stress network of *Mycobacterium tuberculosis* reveals coordination between radical detoxification systems. *Cell Host Microbe.* 17: 829-837. (2015)
123. Newberry KJ, Nakano S, Zuber P, Brennan RG. Crystal structure of the *Bacillus subtilis* anti-alpha, global transcriptional regulator, Spx, in complex with the alpha C-terminal domain of RNA polymerase. *Proc Natl Acad Sci U S A.* 102: 15839-15844. (2005)
124. Newton GL, Buchmeier N, Fahey RC. Biosynthesis and functions of mycothiol, the unique protective thiol of *Actinobacteria*. *Microbiol Mol Biol Rev.* 72: 471-494. (2008)
125. Newton GL, Fahey RC, Rawat M. Detoxification of toxins by bacillithiol in *Staphylococcus aureus*. *Microbiology.* 158: 1117-1126. (2012)
126. Newton GL, Leung SS, Wakabayashi JI, Rawat M, Fahey RC. The DinB superfamily includes novel mycothiol, bacillithiol, and glutathione S-transferases. *Biochemistry.* 50: 10751-10760. (2011)
127. Newton GL, Rawat M, La Clair JJ, Jothivasan VK, Budiarto T, Hamilton CJ, Claiborne A, Helmann JD, Fahey RC. Bacillithiol is an antioxidant thiol produced in *Bacilli*. *Nat Chem Biol.* 5: 625-627. (2009)
128. O'Riordan K, Lee JC. *Staphylococcus aureus* capsular polysaccharides. *Clin Microbiol Rev.* 17: 218-234. (2004)
129. Padiadpu J, Baloni P, Anand K, Munshi M, Thakur C, Mohan A, Singh A, Chandra N. Identifying and tackling emergent vulnerability in drug-resistant *Mycobacteria*. *ACS Infect Dis.* 2: 592-607. (2016)

130. Pane-Farre J, Jonas B, Forstner K, Engelmann S, Hecker M. The *sigmaB* regulon in *Staphylococcus aureus* and its regulation. *Int J Med Microbiol.* 296: 237-258. (2006)
131. Partridge JD, Bodenmiller DM, Humphrys MS, Spiro S. NsrR targets in the *Escherichia coli* genome: new insights into DNA sequence requirements for binding and a role for NsrR in the regulation of motility. *Mol Microbiol.* 73: 680-694. (2009)
132. Paulsen CE, Carroll KS. Orchestrating redox signaling networks through regulatory cysteine switches. *ACS Chem Biol.* 5: 47-62. (2010)
133. Pfortner H, Wagner J, Surmann K, Hildebrandt P, Ernst S, Bernhardt J, Schurmann C, Gutjahr M, Depke M, Jehmlich U, Dhople V, Hammer E, Steil L, Volker U, Schmidt F. A proteomics workflow for quantitative and time-resolved analysis of adaptation reactions of internalized bacteria. *Methods.* 61: 244-250. (2013)
134. Planet PJ, Narechania A, Chen L, Mathema B, Boundy S, Archer G, Kreiswirth B. Architecture of a species: phylogenomics of *Staphylococcus aureus*. *Trends Microbiol.* 25: 153-166. (2017)
135. Poor CB, Chen PR, Duguid E, Rice PA, He C. Crystal structures of the reduced, sulfenic acid, and mixed disulfide forms of SarZ, a redox active global regulator in *Staphylococcus aureus*. *J Biol Chem.* 284: 23517-23524. (2009)
136. Posada AC, Kolar SL, Dusi RG, Francois P, Roberts AA, Hamilton CJ, Liu GY, Cheung A. Importance of bacillithiol in the oxidative stress response of *Staphylococcus aureus*. *Infect Immun.* 82: 316-332. (2014)
137. Pother DC, Gierok P, Harms M, Mostertz J, Hochgrafe F, Antelmann H, Hamilton CJ, Borovok I, Lalk M, Aharonowitz Y, Hecker M. Distribution and infection-related functions of bacillithiol in *Staphylococcus aureus*. *Int J Med Microbiol.* 303: 114-123. (2013)
138. Rajkarnikar A, Strankman A, Duran S, Vargas D, Roberts AA, Barretto K, Upton H, Hamilton CJ, Rawat M. Analysis of mutants disrupted in bacillithiol metabolism in *Staphylococcus aureus*. *Biochem Biophys Res Commun.* 436: 128-33. (2013)
139. Remes B, Eisenhardt BD, Srinivasan V, Klug G. IscR of *Rhodobacter sphaeroides* functions as repressor of genes for iron-sulfur metabolism and represents a new type of iron-sulfur-binding protein. *Microbiologyopen.* 4: 790-802. (2015)
140. Reygaert W. Methicillin-resistant *Staphylococcus aureus* (MRSA): molecular aspects of antimicrobial resistance and virulence. *Clin Lab Sci.* 22: 115-119. (2009)
141. Roberts AA, Sharma SV, Strankman AW, Duran SR, Rawat M, Hamilton CJ. Mechanistic studies of FosB: a divalent-metal-dependent bacillithiol-S-transferase that mediates fosfomycin resistance in *Staphylococcus aureus*. *Biochem J.* 451: 69-79. (2013)
142. Rogasch K, Ruhmling V, Pane-Farre J, Hoper D, Weinberg C, Fuchs S, Schmutde M, Broker BM, Wolz C, Hecker M, Engelmann S. Influence of the two-component system SaeRS on global gene expression in two different *Staphylococcus aureus* strains. *J Bacteriol.* 188: 7742-7758. (2006)
143. Rosario-Cruz Z, Boyd JM. Physiological roles of bacillithiol in intracellular metal processing. *Curr Genet.* 62: 59-65. (2016)
144. Rosario-Cruz Z, Chahal HK, Mike LA, Skaar EP, Boyd JM. Bacillithiol has a role in Fe-S cluster biogenesis in *Staphylococcus aureus*. *Mol Microbiol.* 98: 218-242. (2015)
145. Salgado-Pabon W, Breshears L, Spaulding AR, Merriman JA, Stach CS, Horswill AR, Peterson ML, Schlievert PM. Superantigens are critical for *Staphylococcus aureus* infective endocarditis, sepsis, and acute kidney injury. *MBio.* 4: e00494-13. (2013).
146. Santos JA, Alonso-Garcia N, Macedo-Ribeiro S, Pereira PJ. The unique regulation of iron-sulfur cluster biogenesis in a Gram-positive bacterium. *Proc Natl Acad Sci U S A.* 111: E2251-E2260. (2014)
147. Sause WE, Buckley PT, Strohl WR, Lynch AS, Torres VJ. Antibody-based biologics and their promise to combat *Staphylococcus aureus* infections. *Trends Pharmacol Sci.* 37: 231-241. (2016)

148. Schwarzlander M, Dick TP, Meye AJ, Morgan B. Dissecting redox biology using fluorescent protein sensors. *Antioxid Redox Signal*. 24: 680-712. (2016)
149. Sharma SV, Arbach M, Roberts AA, Macdonald CJ, Groom M, Hamilton CJ. Biophysical features of bacillithiol, the glutathione surrogate of *Bacillus subtilis* and other *firmicutes*. *Chembiochem*. 14: 2160-2168. (2013)
150. Shepard W, Soutourina O, Courtois E, England P, Haouz A, Martin-Verstraete I. Insights into the Rrf2 repressor family-the structure of CymR, the global cysteine regulator of *Bacillus subtilis*. *FEBS J*. 278: 2689-2701. (2011)
151. Si M, Zhang L, Chaudhry MT, Ding W, Xu Y, Chen C, Akbar A, Shen X, Liu SJ. *Corynebacterium glutamicum* methionine sulfoxide reductase A uses both mycoredoxin and thioredoxin for regeneration and oxidative stress resistance. *Appl Environ Microbiol*. 81: 2781-2796. (2015)
152. Soutourina O, Dubrac S, Poupel O, Msadek T, Martin-Verstraete I. The pleiotropic CymR regulator of *Staphylococcus aureus* plays an important role in virulence and stress response. *PLoS Pathog*. 6: e1000894. (2010)
153. Soutourina O, Poupel O, Coppee JY, Danchin A, Msadek T, Martin-Verstraete I. CymR, the master regulator of cysteine metabolism in *Staphylococcus aureus*, controls host sulphur source utilization and plays a role in biofilm formation. *Mol Microbiol*. 73: 194-211. (2009)
154. Spaulding AR, Salgado-Pabon W, Kohler PL, Horswill AR, Leung DY, Schlievert PM. Staphylococcal and streptococcal superantigen exotoxins. *Clin Microbiol Rev*. 26: 422-447. (2013)
155. Sun F, Ding Y, Ji Q, Liang Z, Deng X, Wong CC, Yi C, Zhang L, Xie S, Alvarez S, Hicks LM, Luo C, Jiang H, Lan L, He C. Protein cysteine phosphorylation of SarA/MgrA family transcriptional regulators mediates bacterial virulence and antibiotic resistance. *Proc Natl Acad Sci U S A*. 109: 15461-15466. (2012)
156. Thurlkill RL, Grimsley GR, Scholtz JM, Pace CN. pK values of the ionizable groups of proteins. *Protein Sci*. 15: 1214-1248. (2006)
157. Torres VJ, Attia AS, Mason WJ, Hood MI, Corbin BD, Beasley FC, Anderson KL, Stauff DL, McDonald WH, Zimmerman LJ, Friedman DB, Heinrichs DE, Dunman PM, Skaar EP. *Staphylococcus aureus* fur regulates the expression of virulence factors that contribute to the pathogenesis of pneumonia. *Infect Immun*. 78: 1618-1628. (2010)
158. Tossounian MA, Pedre B, Wahni K, Erdogan H, Vertommen D, Van Molle I, Messens J. *Corynebacterium diphtheriae* methionine sulfoxide reductase a exploits a unique mycothiol redox relay mechanism. *J Biol Chem*. 290: 11365-11375. (2015)
159. Trachootham D, Lu W, Ogasawara MA, Nilisa RD, Huang P. Redox regulation of cell survival. *Antioxid Redox Signal*. 10: 1343-1374. (2008)
160. Treffon J, Block D, Moche M, Reiss S, Fuchs S, Engelmann S, Becher D, Langhanki L, Mellmann A, Peters G, Kahl BC. Adaptation of *Staphylococcus aureus* to the airways of cystic fibrosis patients by the up-regulation of superoxide dismutase M and iron-scavenging proteins. *J Infect Dis*. doi: 10.1093/infdis/jiy012. (2018)
161. Tuchscher L, Bischoff M, Lattar SM, Noto Llana M, Pfortner H, Niemann S, Geraci J, Van de Vyver H, Fraunholz MJ, Cheung AL, Herrmann M, Volker U, Sordelli DO, Peters G, Loffler B. sigma factor SigB is crucial to mediate *Staphylococcus aureus* adaptation during chronic infections. *PLoS Pathog*. 11: e1004870. (2015)
162. Tuchscher L, Loffler B. *Staphylococcus aureus* dynamically adapts global regulators and virulence factor expression in the course from acute to chronic infection. *Curr Genet*. 62: 15-17. (2016)
163. Tuchscher L, Medina E, Hussain M, Volker W, Heitmann V, Niemann S, Holzinger D, Roth J, Proctor RA, Becker K, Peters G, Loffler B. *Staphylococcus aureus* phenotype switching: an effective bacterial strategy to escape host immune response and establish a chronic infection. *EMBO Mol Med*. 3: 129-141. (2011)

164. Tucker NP, Hicks MG, Clarke TA, Crack JC, Chandra G, Le Brun NE, Dixon R, Hutchings MI. The transcriptional repressor protein NsrR senses nitric oxide directly via a [2Fe-2S] cluster. *PLoS One*. 3: e3623. (2008)
165. Tucker NP, Le Brun NE, Dixon R, Hutchings MI. There's NO stopping NsrR, a global regulator of the bacterial NO stress response. *Trends Microbiol*. 18: 149-156. (2010)
166. Tung QN, Linzner N, Loi VV, Antelmann H. Application of genetically encoded redox biosensors to measure dynamic changes in the glutathione, bacillithiol and mycothiol redox potentials in pathogenic bacteria. *Free Radic Biol Med*. doi: 10.1016/j.freeradbiomed.2018.02.018 (2018)
167. Tyagi P, Dharmaraja AT, Bhaskar A, Chakrapani H, Singh A. *Mycobacterium tuberculosis* has diminished capacity to counteract redox stress induced by elevated levels of endogenous superoxide. *Free Radic Biol Med*. 84: 344-354. (2015)
168. Valderas MW, Gatson JW, Wreyford N, Hart ME. The superoxide dismutase gene *sodM* is unique to *Staphylococcus aureus*: absence of *sodM* in coagulase-negative staphylococci. *J Bacteriol*. 184: 2465-2472. (2002)
169. Van Acker H, Coenye T. The role of reactive oxygen species in antibiotic-mediated killing of bacteria. *Trends Microbiol*. 25: 456-466. (2017)
170. van der Heijden J, Bosman ES, Reynolds LA, Finlay BB. Direct measurement of oxidative and nitrosative stress dynamics in *Salmonella* inside macrophages. *Proc Natl Acad Sci U S A*. 112: 560-565. (2015)
171. van der Heijden J, Vogt SL, Reynolds LA, Pena-Diaz J, Tupin A, Aussel L, Finlay BB. Exploring the redox balance inside gram-negative bacteria with redox-sensitive GFP. *Free Radic Biol Med*. 91: 34-44. (2015)
172. van der Veen BS, de Winther MP, Heeringa P. Myeloperoxidase: molecular mechanisms of action and their relevance to human health and disease. *Antioxid Redox Signal*. 11: 2899-2937. (2009)
173. Van Laer K, Buts L, Foloppe N, Vertommen D, Van Belle K, Wahni K, Roos G, Nilsson L, Mateos LM, Rawat M, van Nuland NA, Messens J. Mycoredoxin-1 is one of the missing links in the oxidative stress defence mechanism of *Mycobacteria*. *Mol Microbiol*. 86: 787-804. (2012)
174. Van Laer K, Hamilton CJ, Messens J. Low-molecular-weight thiols in thiol-disulfide exchange. *Antioxid Redox Signal*. 18: 1642-1653. (2013)
175. Volbeda A, Dodd EL, Darnault C, Crack JC, Renoux O, Hutchings MI, Le Brun NE, Fontecilla-Camps JC. Crystal structures of the NO sensor NsrR reveal how its iron-sulfur cluster modulates DNA binding. *Nat Commun*. 8: 15052. (2017)
176. Vuong C, Yeh AJ, Cheung GY, Otto M. Investigational drugs to treat methicillin-resistant *Staphylococcus aureus*. *Expert Opin Investig Drugs*. 25: 73-93. (2016)
177. Winterbourn CC, Hampton MB. Thiol chemistry and specificity in redox signaling. *Free Radic Biol Med*. 45: 549-561. (2008)
178. Winterbourn CC, Kettle AJ. Redox reactions and microbial killing in the neutrophil phagosome. *Antioxid Redox Signal*. 18: 642-660. (2013)
179. Winterbourn CC, Kettle AJ, Hampton MB. Reactive oxygen species and neutrophil function. *Annu Rev Biochem*. 85: 765-792. (2016)
180. Wolf C, Hochgrafe F, Kusch H, Albrecht D, Hecker M, Engelmann S. Proteomic analysis of antioxidant strategies of *Staphylococcus aureus*: diverse responses to different oxidants. *Proteomics*. 8: 3139-3153. (2008)
181. Yeo WS, Lee JH, Lee KC, Roe JH. IscR acts as an activator in response to oxidative stress for the suf operon encoding Fe-S assembly proteins. *Mol Microbiol*. 61: 206-218. (2006)
182. Yukl ET, Elbaz MA, Nakano MM, Moenne-Loccoz P. Transcription factor NsrR from *Bacillus subtilis* senses nitric oxide with a 4Fe-4S cluster (dagger). *Biochemistry*. 47: 13084-13092. (2008)

183. Zecconi A, Scali F. *Staphylococcus aureus* virulence factors in evasion from innate immune defenses in human and animal diseases. *Immunol Lett.* 150: 12-22. (2013)
184. Zuber P. Spx-RNA polymerase interaction and global transcriptional control during oxidative stress. *J Bacteriol.* 186: 1911-1918. (2004)

Chapter 1

Redox regulation by reversible protein S-thiolation in bacteria

Vu Van Loi¹, Martina Rossius¹ and Haike Antelmann[#]

¹Freie Universität Berlin, Institute for Biology-Microbiology, D-14195 Berlin, Germany

Published in: Frontiers in Microbiology. 6: 187. (2015)

<https://doi.org/10.3389/fmicb.2015.00187>

#Corresponding author: haike.antelmann@fu-berlin.de

Authors contributions

Haike Antelmann wrote the main part of the review and prepared most figures. **Vu Van Loi** and Martina Rossius contributed with writing the parts about bacillithiol and mycothiol, respectively and the preparation of the corresponding figures.

Redox regulation by reversible protein S-thiolation in bacteria

Vu Van Loi, Martina Rossius and Haike Antelmann*

Institute of Microbiology, Ernst-Moritz-Armdt-University of Greifswald, Greifswald, Germany

OPEN ACCESS

Edited by:

Jörg Stülke,
Georg-August-Universität Göttingen,
Germany

Reviewed by:

Ulrike Kappler,
University of Queensland, Australia
Jan Maarten Van Dijk,
University of Groningen and University
Medical Center Groningen,
Netherlands

*Correspondence:

Haike Antelmann,
Institute of Microbiology,
Ernst-Moritz-Armdt-University of
Greifswald,
Friedrich-Ludwig-Jahnstr. 15,
Greifswald, Germany
antelman@uni-greifswald.de

Specialty section:

This article was submitted to *Microbial Physiology and Metabolism*, a section of the journal *Frontiers in Microbiology*

Received: 25 November 2014

Accepted: 20 February 2015

Published: 16 March 2015

Citation:

Loi VV, Rossius M and Antelmann H (2015) Redox regulation by reversible protein S-thiolation in bacteria. *Front. Microbiol.* 6:187. doi: 10.3389/fmicb.2015.00187

Low molecular weight (LMW) thiols function as thiol-redox buffers to maintain the reduced state of the cytoplasm. The best studied LMW thiol is the tripeptide glutathione (GSH) present in all eukaryotes and Gram-negative bacteria. Firmicutes bacteria, including *Bacillus* and *Staphylococcus* species utilize the redox buffer bacillithiol (BSH) while Actinomycetes produce the related redox buffer mycothiol (MSH). In eukaryotes, proteins are post-translationally modified to S-glutathionylated proteins under conditions of oxidative stress. S-glutathionylation has emerged as major redox-regulatory mechanism in eukaryotes and protects active site cysteine residues against overoxidation to sulfonic acids. First studies identified S-glutathionylated proteins also in Gram-negative bacteria. Advances in mass spectrometry have further facilitated the identification of protein S-bacillithiolations and S-mycothiolation as BSH- and MSH-mixed protein disulfides formed under oxidative stress in Firmicutes and Actinomycetes, respectively. In *Bacillus subtilis*, protein S-bacillithiolation controls the activities of the redox-sensing OhrR repressor and the methionine synthase MetE *in vivo*. In *Corynebacterium glutamicum*, protein S-mycothiolation was more widespread and affected the functions of the maltodextrin phosphorylase MalP and thiol peroxidase (Tpx). In addition, novel bacilliredoxins (Brx) and mycoredoxins (Mrx1) were shown to function similar to glutaredoxins in the reduction of BSH- and MSH-mixed protein disulfides. Here we review the current knowledge about the functions of the bacterial thiol-redox buffers glutathione, bacillithiol, and mycothiol and the role of protein S-thiolation in redox regulation and thiol protection in model and pathogenic bacteria.

Keywords: oxidative stress, protein S-thiolation, thiol-redox buffer, glutathione, bacillithiol, mycothiol

Introduction

The cytoplasm is a reducing environment and protein thiols are maintained in their reduced state by low molecular weight (LMW) thiol-redox buffers and enzymatic thiol-disulfide oxidoreductases, including the thioredoxin and glutaredoxin systems (Fahey, 2013; Van Laer et al., 2013). In their natural environment or during infections, bacteria encounter different reactive species, such as reactive oxygen, nitrogen, chlorine, and electrophilic species (ROS, RNS, RCS, RES) (Antelmann and Helmann, 2011; Gray et al., 2013a). These reactive species cause different post-translational thiol-modifications in proteins and activate or inactivate specific transcription factors resulting in expression of detoxification pathways. LMW thiol-redox buffers function in detoxification of different reactive species and are often present in millimolar concentrations in the cytoplasm.

The best studied LMW thiol is glutathione (GSH) present in eukaryotes and Gram-negative bacteria (Fahey, 2013). Most Gram-positive bacteria do not produce GSH. Instead, the Actinomycetes

utilize mycothiol (MSH) as thiol-redox buffer (Jothivasan and Hamilton, 2008; Newton et al., 2008). In *Bacillus megaterium*, *Bacillus cereus*, and *Staphylococcus aureus*, coenzyme A (CoASH) serves as an abundant LMW thiol (Newton et al., 1996). Many Firmicutes bacteria, including *Bacillus* and *Staphylococcus* species utilize bacillithiol (BSH) and cysteine as major thiol-redox buffers (Newton et al., 2009). Alternative LMW thiols include also the betaine-histidine derivative ergothioneine that compensates for the absence of MSH in *Mycobacterium smegmatis mshA* mutants (Ta et al., 2011). Cysteine is used for alternative S-thiolations in the absence of BSH and MSH in *Bacillus subtilis* and *Corynebacterium glutamicum* since S-cysteinylated proteins were identified in *bsh* and *msh* mutants (Chi et al., 2011, 2014).

The protozoa *Leishmania* and *Trypanosoma* produce the glutathione-derivative trypanothione (bis-glutathionylspermidine or TSH₂). In *Escherichia coli*, glutathionylspermidine (GSP) was detected during the stationary phase (Fahey, 2013). Some microaerophilic γ -proteobacteria utilize glutathione amide (GASH) which forms a persulfide (GASSH) during photoautotrophic growth on high concentrations of sulfide (Bartsch et al., 1996).

Under conditions of oxidative stress, LMW thiols form mixed disulfides with protein thiols which is termed protein S-thiolation. In eukaryotes, protein S-glutathionylation has emerged as major redox-regulatory mechanism that controls the activity of redox sensing transcription factors and protects active site Cys residues against irreversible oxidation to sulfonic acids (Dalle-Donne et al., 2009). S-glutathionylation controls numerous physiological processes, such as cellular growth and differentiation, cell cycle progression, transcriptional activity, cytoskeletal function, cellular metabolism, and apoptosis (Klatt and Lamas, 2000; Ghezzi, 2005, 2013; Dalle-Donne et al., 2007, 2009). S-glutathionylation must meet several criteria to function as redox-control mechanism: (1) reversibility, (2) specificity to active site Cys, (3) change in protein function/activity, and (4) induction by ROS or RNS. S-glutathionylation serves as a form of GSH storage to prevent the export of GSSG under oxidative stress (Dalle-Donne et al., 2009). Many eukaryotic proteins, like α -ketoglutarate dehydrogenase, glyceraldehyde 3-phosphate dehydrogenase, ornithine δ -aminotransferase, pyruvate kinase, heat specific chaperones, and regulatory proteins (c-Jun, NF- κ B) are reversibly inactivated or activated by S-glutathionylation (Dalle-Donne et al., 2009; Kehr et al., 2011). However, the regulatory role of protein S-thiolation for bacterial physiology has only recently been investigated. Here we review the current knowledge about the functions of the bacterial redox buffers GSH, MSH, and BSH and their roles for protein S-thiolations in GSH-, MSH- and BSH-producing bacteria.

Sources of Reactive Oxygen, Electrophile, and Chlorine Species (ROS, RES, RCS)

Bacteria encounter ROS during respiration or by the oxidative burst of activated neutrophils during infections (Imlay, 2003, 2008, 2013). The incomplete stepwise reduction of molecular oxygen (O₂) leads to generation of superoxide anions (O₂^{•-}),

hydrogen peroxide (H₂O₂) and the highly reactive hydroxyl radical (OH[•]) (Figure 1). Superoxide anion and H₂O₂ are also produced by autoxidation of flavoenzymes (Mishra and Imlay, 2012; Imlay, 2013). Superoxide dismutases (SOD) convert O₂^{•-} to H₂O₂. Several peroxide scavenging enzymes, such as catalases and peroxidases catalyze the detoxification of H₂O₂. H₂O₂ reacts with ferrous iron (Fe²⁺) in the Fenton reaction generating the highly toxic hydroxyl radical (OH[•]) which can damage all cellular macromolecules (Imlay, 2003, 2008). H₂O₂ destroys the Fe-S-cluster of dehydratases and inactivates single ferrous iron-centers of redox enzymes (Mishra and Imlay, 2012; Imlay, 2013).

During the oxidative burst, activated neutrophils release O₂^{•-}, H₂O₂, nitric oxide (NO), and hypochlorous acid (HOCl) with the aim to kill invading pathogenic bacteria (Forman and Torres, 2001; Winterbourn and Kettle, 2013). The neutrophil NADPH oxidase (NOX) shuttles electrons from NADPH to O₂ in the phagosomal lumen and generates around 20 μ M superoxide anion. Myeloperoxidase (MPO) is released upon degranulation in millimolar concentrations. MPO catalyzes the dismutation of O₂^{•-} to H₂O₂ and subsequent conversion of H₂O₂ and chloride to HOCl (Figure 1) (Winterbourn and Kettle, 2013). NO is generated in neutrophils by the inducible nitric oxide synthase (iNOS) catalyzing the oxidation of L-arginine to L-citrulline. The reaction of NO with O₂^{•-} leads to formation of peroxynitrite (ONOO⁻). Thus, neutrophils release ROS, RNS, and the highly reactive HOCl as antimicrobial defense mechanism.

Reactive electrophilic species (RES) have electron-deficient centers and can react with the nucleophilic Cys thiol group via the thiol-S-alkylation chemistry (Figure 2) (Antelmann and Helmann, 2011). RES include quinones, aldehydes, epoxides, diamide and α,β -unsaturated dicarbonyl compounds. RES are often generated as secondary reactive intermediates from oxidation products of amino acids, lipids or carbohydrates (Marnett et al., 2003; Rudolph and Freeman, 2009). Quinones are lipid-electron carriers of the respiratory chain, including

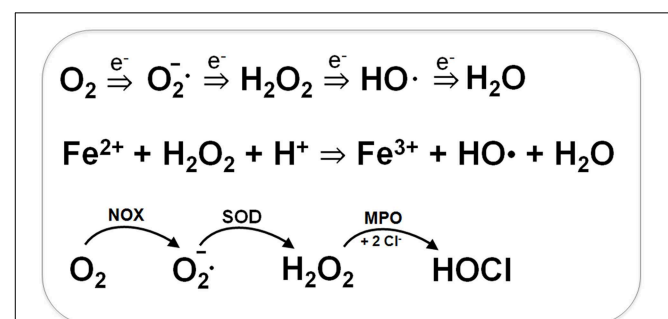
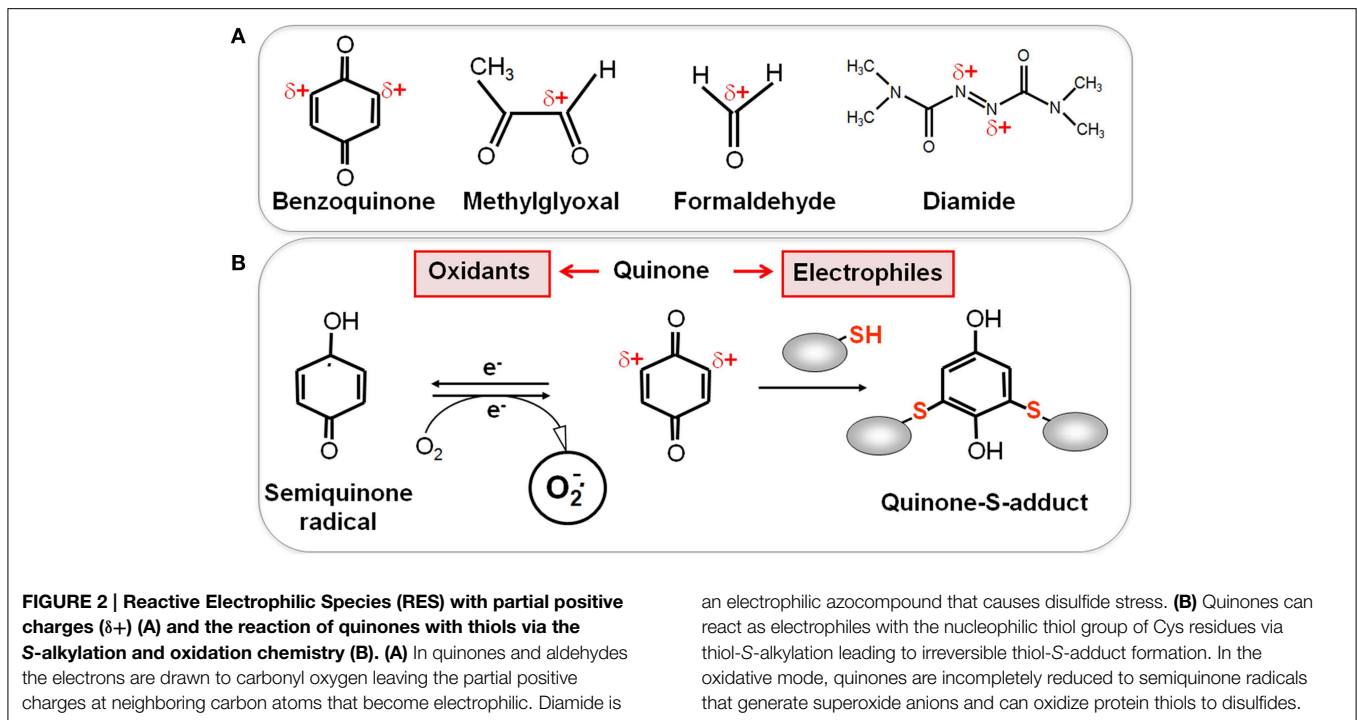


FIGURE 1 | Generation of Reactive Oxygen Species (ROS) during respiration and HOCl production by activated neutrophils during infections. ROS are generated in bacteria during respiration by stepwise one-electron transfer to O₂ producing superoxide anion, hydrogen peroxide and hydroxyl radical. The highly reactive hydroxyl radical is also produced from H₂O₂ and Fe²⁺ in the Fenton reaction. During infections, activated neutrophils generate superoxide anion by the NADPH oxidase (NOX) that is converted to H₂O₂ by the superoxide dismutase (SOD). Myeloperoxidase (MPO) is released upon degranulocytosis producing the highly reactive hypochlorous acids (HOCl) from H₂O₂ and Cl⁻ as potent killing agent for pathogenic bacteria.



an electrophilic azocompound that causes disulfide stress. (B) Quinones can react as electrophiles with the nucleophilic thiol group of Cys residues via thiol-S-alkylation leading to irreversible thiol-S-adduct formation. In the oxidative mode, quinones are incompletely reduced to semiquinone radicals that generate superoxide anions and can oxidize protein thiols to disulfides.

ubiquinone and menaquinone (Farrand and Taber, 1974). Soil bacteria encounter quinones as redox active components of humic substances and in dissolved organic matter (Ratasuk and Nanny, 2007). The toxic dicarbonyl compound methylglyoxal is produced in all organisms from triose-phosphate intermediates as byproduct of the glycolysis and can be generated also from amino acids metabolism (Ferguson et al., 1998; Booth et al., 2003; Kalapos, 2008). Bacteria also have to cope with the carbonyl compound formaldehyde. Formaldehyde is an intermediate in the C_1 -metabolism of methanotrophic and methylotrophic bacteria and is ubiquitously distributed in the environment. Thus, bacteria have evolved conserved pathways for detoxification of formaldehyde and methylglyoxal that involve LMW thiols.

In eukaryotic cells, RES are implicated in many pathophysiological processes and modulate signaling pathways (Mackay and Knock, 2015). Eukaryotic cells produce lipid-derived RES, such as malondialdehyde (MDA) and 4-hydroxy-2-nonenal (HNE) (Rudolph and Freeman, 2009). HNE is generated from polyunsaturated fatty acids in biological membranes by a radical-based peroxidation chain reaction (Jacobs and Marnett, 2010). Furthermore, 15-deoxy- Δ 12,14-prostaglandin J2 (15d-PGJ2) is generated from arachidonic acid during inflammation and 2-trans-hexadecenal (2-HD) is produced during sphingolipid metabolism which promotes apoptosis (Wang et al., 2014). Bacterial membrane lipids also contain unsaturated fatty acids which are synthesized at higher levels during adaptation to cold shock to maintain the fluidity of the membrane (De Mendoza, 2014). These unsaturated fatty acids in bacterial membrane lipids could be the target for ROS leading to lipid peroxidation products in bacteria. Lipid hydroperoxides, such as linoleic acid hydroperoxide are sensed by the redox-sensing MarR-type repressor OhrR.

OhrR regulates the peroxiredoxin OhrA that functions in detoxification of organic hydroperoxides (Atichartpongkul et al., 2001; Fuangthong et al., 2001). However, the fatty acid-derived peroxidation product which is sensed by OhrR *in vivo* remains to be identified.

Post-Translational Thiol-Modifications of Proteins by ROS, RES, and RCS in Bacteria

ROS, RES, and RCS can damage all cellular macromolecules including proteins, nucleic acids or carbohydrates (Imlay, 2008, 2013; Jacobs and Marnett, 2010; Gray et al., 2013a). However, in eukaryotes low levels of ROS and RES act also as second messengers to modulate signal transduction pathways (Rudolph and Freeman, 2009; Mackay and Knock, 2015). Bacterial transcription factors often use redox-sensitive Cys residues for sensing of ROS, RES, and RCS to control the expression of specific detoxification pathways (Antelmann and Helmann, 2011; Gray et al., 2013a). The thiol group of cysteine is subject to reversible and irreversible post-translational thiol-modifications that lead to inactivation or activation of the transcription factor. Protein thiols can be reversibly oxidized to protein disulfides and irreversibly overoxidized to sulfinic or sulfonic acids by ROS (Antelmann and Helmann, 2011). ROS lead first to oxidation of protein thiols to Cys sulfenic acids as unstable intermediates (R-SOH) (Figure 3). Cys sulfenic acid rapidly reacts further with other thiols to form intramolecular and intermolecular protein disulfides or mixed disulfides with LMW thiols, collectively termed as S-thiolations (e.g., S-cysteinylations, S-glutathionylations, S-mycothiolations, and S-bacillithiolations). Protein S-thiolations protect the thiol groups against the irreversible overoxidation to

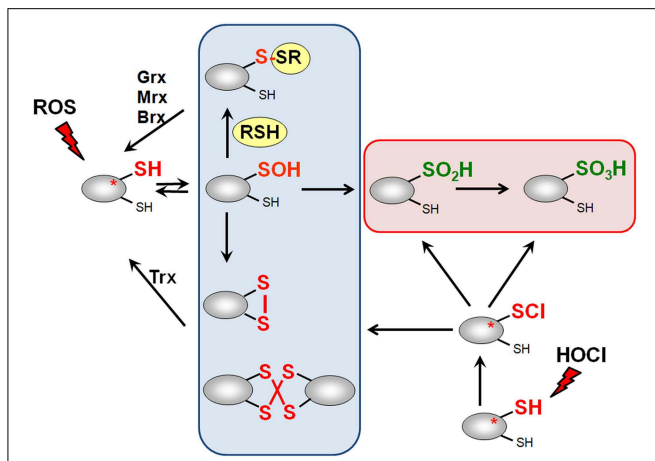


FIGURE 3 | Thiol-chemistry of ROS and HOCl with thiol-containing proteins. The Cys thiol group is oxidized by ROS to an unstable Cys sulfenic acid intermediate (Cys-SOH) that reacts further with proximal thiols to form intramolecular and intermolecular disulfides or mixed disulfides with LMW thiols (RSH), such as glutathione, bacillithiol or cysteine, termed as S-thiolations. HOCl leads to chlorination of protein thiols to sulfenylchloride intermediates (Cys-SCI) that react further to form disulfides. In the absence of proximal thiols, the chlorinated Cys is overoxidized to Cys sulfinic and sulfonic acids. Disulfides function as redox switches to control protein activity and protect thiol groups against overoxidation to Cys sulfinic and sulfonic acids.

Cys sulfinic (R-SO₂H) and sulfonic acid (R-SO₃H). This is particularly important for essential and abundant proteins whose overoxidation would lead to loss of cell viability and requires new protein synthesis to replace inactivated proteins. However, eukaryotic sulfiredoxins are able to reduce sulfinic acids in 2-Cys peroxiredoxins, but sulfiredoxins are not present in bacteria (Lowther and Haynes, 2011).

Hypochlorous acid (HOCl) is a strong two-electron oxidant and chlorinating agent with a high redox potential [E^0 (HOCl/Cl⁻) = 1.28 mV] (Davies, 2011). HOCl targets most strongly the sulfur-containing amino acids cysteine and methionine with the second-order rate constant of $k = 3 \times 10^7 \text{ M}^{-1} \text{ s}^{-1}$ (Hawkins et al., 2003). HOCl first chlorinates the thiol group to form the unstable sulfenylchloride intermediate that reacts further with another thiol group to disulfides. In the absence of another thiol, the chlorinated thiol group is overoxidized very rapidly to sulfinic or sulfonic acids (Hawkins et al., 2003) (Figure 3). We confirmed that strong disulfide stress responses are caused by HOCl in different Gram-positive bacteria *in vivo* and detected mixed protein disulfides with Cys, BSH, and MSH as major oxidation products (Chi et al., 2011, 2013, 2014).

RNS cause reversible thiol-modifications: nitric oxide (NO) leads to S-nitrosothiol formation (RS-NO) and peroxynitrite (ONOO⁻) causes S-nitrothiol (RS-NO₂) formation. Alternatively, S-nitrosothiol (e.g., GSNO or MSNO) can be formed by direct reaction of NO with LMW thiols (Antelmann and Helmann, 2011).

RES can react via the thiol-S-alkylation chemistry with Cys thiols. However, quinones have two modes of action, an oxidation and an alkylation mode. In the oxidation mode, the

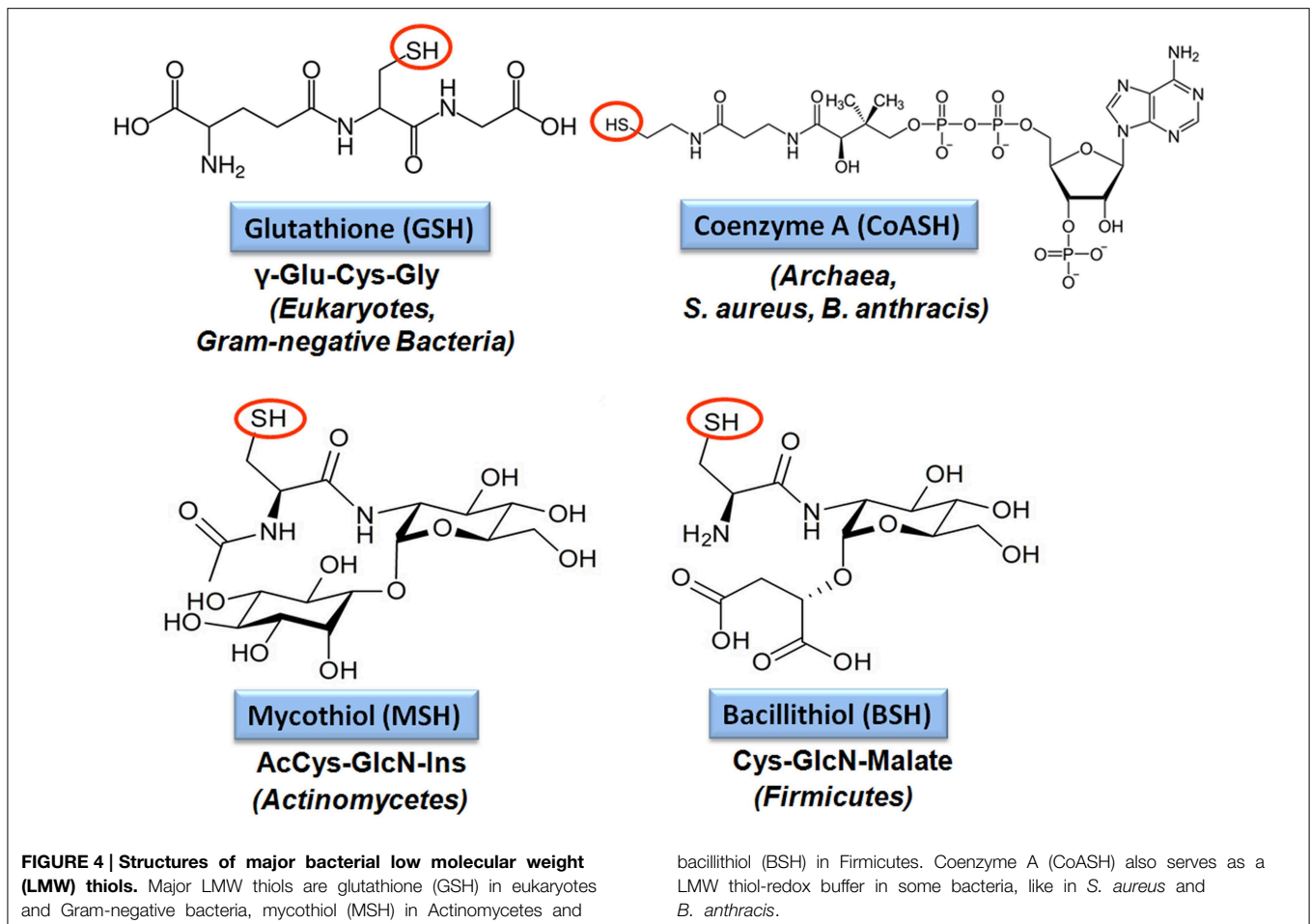
one-electron reduction of quinones generates the highly reactive semiquinone radical leading to generation of superoxide anions (Figure 2). The electrophilic reaction of quinones involves the 1,4-reductive Michael-type addition of thiols to quinones (Marrett et al., 2003). Quinones lead to irreversible thiol-S-alkylation and protein aggregation to deplete protein thiols in the proteome *in vivo* (Liebeke et al., 2008). However, non-toxic quinone concentrations resulted in reversible thiol-disulfide switches in RES-sensing redox regulators (e.g., YodB, CatR, QsrR, NemR) to activate the expression of specific quinone detoxification pathways (Antelmann and Helmann, 2011; Gray et al., 2013a; Lee et al., 2013). Methylglyoxal reacts with nucleophilic centers of the DNA and with the amino acids arginine, lysine and cysteine causing advanced glycation end-products (Bourajaj et al., 2003). The lipid-derived electrophiles MDA and HNE were shown to alkylate DNA bases and protein thiols leading to DNA and membrane damages in eukaryotes (Rudolph and Freeman, 2009).

Biosynthesis and Functions of Major LMW Thiol-Redox Buffers in Bacteria

Biosynthesis, Uptake, and Functions of Glutathione in Bacteria

The tripeptide glutathione (γ -glutamylcysteinyl-glycine; GSH) is utilized as major LMW thiol-redox buffer in Gram-negative bacteria and in some Gram-positive Firmicutes bacteria, including *Streptococcus agalactiae*, *Listeria monocytogenes*, and *Clostridium acetobutylicum* (Figure 4). In *E. coli*, GSH biosynthesis occurs in two steps: The γ -glutamylcysteine ligase (GshA) catalyzes the formation of γ -glutamylcysteine (γ -Glu-Cys) from glutamate and cysteine. In the second step, ligation of glycine to γ -Glu-Cys is catalyzed by glutathione synthase (GshB) (Meister, 1995; Anderson, 1998). In *S. agalactiae* and *L. monocytogenes*, a bifunctional fusion protein GshF is present that exhibits both GshA and GshB activities (Gopal et al., 2005; Janowiak and Griffith, 2005). Interestingly, *Lactococcus lactis*, *Streptococcus pneumoniae* and *Haemophilus influenzae* do not synthesize GSH, but encode GSH-uptake mechanisms. In *S. pneumoniae*, the GSH-uptake from the host is mediated by the ABC transporter binding protein GshT (Potter et al., 2012; Vergauwen et al., 2013). In addition, the cystine importer TcyBC was shown to be primed for GSH import by GshT. In *H. influenzae*, GSH import is mediated by the ABC-transporter DppBCDF and requires the periplasmic GSH-binding protein GbpA (Vergauwen et al., 2010). Strikingly, these pathogens utilize host-derived GSH as protection mechanism against the host immune defense.

GSH is present in millimolar concentrations in the cytoplasm of *E. coli* (Masip et al., 2006; Fahey, 2013). GSH maintains protein thiols in the reduced state and serves as a storage form of cysteine. In contrast to cysteine, GSH is resistant to metal-catalyzed autooxidation because of its bound Cys amino and carboxyl groups that prevent ligation of heavy metal ions (Fahey, 2013). During the bacterial growth and under oxidative stress, GSH is oxidized to glutathione disulfide (GSSG). The NADPH-dependent glutathione reductase (Gor) keeps GSH in its reduced state to maintain a high GSH/GSSG ratio ranging



from 30:1 to 100:1 in the cytoplasm. The standard thiol-disulfide redox potential of the GSH redox couple was calculated as $E^{0'}(\text{GSSG}/\text{GSH}) = -240 \text{ mV}$ at physiological pH values (Hwang et al., 1995; Van Laer et al., 2013).

The various detoxification functions of GSH have been extensively studied in *E. coli gsh* mutants. In *E. coli*, GSH functions in detoxification of ROS, RES, RCS, RNS, xenobiotics, antibiotics, toxic metals, and metalloids (Masip et al., 2006) (Table 1). Detoxification of xenobiotics, electrophiles and antibiotics by GSH occurs either spontaneously by S-conjugation or by the catalytic activity of GSH-S-transferases (Fahey, 2013). The GSH-S-conjugates are usually excreted from the cell as non-toxic mercapturic acid derivatives. GSH was shown to function as a cofactor in methylglyoxal detoxification in *E. coli*. The major pathway for methylglyoxal detoxification in *E. coli* is the GSH-dependent glyoxalase pathway. The glyoxalase-I (GloA) catalyzes formation of S-lactoyl-GSH from GSH-hemithioacetal and glyoxalase-II (GloB) converts S-lactoyl-GSH to D-lactate (Ferguson et al., 1998; Booth et al., 2003). In addition, glyoxalase-III operates GSH-independently to convert methylglyoxal to lactate. The glyoxalase-I encoding *gloA* gene and the *nemRA* operon are redox-regulated by the NemR repressor under methylglyoxal, quinone and HOCl stress (Gray et al., 2013b; Lee et al.,

2013; Ozyamak et al., 2013). The glyoxalase GloA and the oxidoreductase NemA are important for methylglyoxal survival and confer resistance to methylglyoxal in *E. coli* (Ozyamak et al., 2013). The resistance to methylglyoxal is also linked to the activation of potassium efflux by the S-lactoyl-GSH intermediate leading to cytoplasmic acidification (Ferguson et al., 1998; Booth et al., 2003). The cytoplasmic acidification limits the interaction of methylglyoxal with DNA bases. Thus, potassium efflux and detoxification by GloA protect against methylglyoxal toxicity in *E. coli*.

Interestingly, expression of the *E. coli gshAB* genes in the industrial important *Clostridium acetobutylicum* enhances robustness and alcohol production as a promising strategy for engineering industrial production strains. Thus, GSH protects also against large-scale ethanol and butanol production in *C. acetobutylicum* during fermentation (Hou et al., 2013).

Functions of Glutathione in the Virulence of Pathogenic Bacteria

GSH has many detoxification functions to maintain the redox balance of the cytoplasm, but only recently the role of GSH for the control of virulence functions has been explored in the pathogenic bacteria *S. pneumoniae*, *L. monocytogenes*, and

TABLE 1 | Functions of the bacterial redox buffers glutathione, bacillithiol, and mycothiol.

Redox buffer	Organism	Functions of thiol-redox buffers and thiol-dependent enzymes	References
Glutathione	<i>Escherichia coli</i>	GSH functions in detoxification of ROS, RES, RCS, RNS, xenobiotics, antibiotics, toxic metals, metalloids	Masip et al., 2006 Potter et al., 2012
	<i>Salmonella Typhimurium</i>	Gor: GSSG reductase Gpx: GSH-dependent peroxidase Gst: GSH S-transferases required for conjugation of alkylating agents and antibiotics Grx: Glutaredoxins for reduction of S-glutathionylated proteins GloA/GloB: glyoxalase-I/II for GSH-dependent conversion of methylglyoxal to lactate	
Bacillithiol	<i>Bacillus subtilis</i>	BSH involved in detoxification of hypochlorite, diamide, methylglyoxal, ROS (paraquat, H ₂ O ₂), alkylating agents and fosfomycin	Gaballa et al., 2010 Chi et al., 2011
	<i>Staphylococcus aureus</i>	BSH provides a Zn buffer for labile Zn pool YpdA: possible BSSB reductase FosB: BSH-dependent epoxide hydrolase for fosfomycin detoxification YfiT/BstA: DinB-family BSH S-transferases required for conjugation of alkylating agents (monochlorobimane, 1-chloro-2,4-dinitrobenzene and cerulenin) BrxA/BrxB: Bacilliredoxins for reduction of S-bacillithiolated proteins GlxA/GlxB: glyoxalase-I/II for BSH-dependent conversion of methylglyoxal to lactate	Ma et al., 2014 Gaballa et al., 2010 Lamers et al., 2012 Roberts et al., 2013 Thompson et al., 2013, 2014 Newton et al., 2011 Perera et al., 2014 Gaballa et al., 2014 Chandrangu et al., 2014
Mycothiol	<i>Streptomyces coelicolor</i>	MSH protects against ROS, RES, NO, toxins, antibiotics (erythromycin, vancomycin, rifampicin), heavy metals, maleylpyruvate, ethanol, gentisate, glyphosate, arsenate in Actinomycetes	Newton et al., 2008 Fahey, 2013 Liu et al., 2013
	<i>Mycobacterium tuberculosis</i>	Mtr: MSSM reductase Tpx, AhpE, Mpx: MSH-dependent peroxidases	Chi et al., 2014 Hugo et al., 2014 Newton et al., 2012
	<i>Corynebacterium glutamicum</i>	Mst: DinB-family MSH S-transferases required for conjugation of alkylating agents and antibiotics (monochlorobimane, DTNB, rifampicin, cerulenin) LmbT, LmbV and LmbE: MSH S-transferases for biosynthesis of the lincosamide antibiotic lincosmycin in <i>S. lincolnensis</i> Mca: S-conjugate amidase cleaves MSH-S-conjugates to mercapturic acids Mrx1: Mycoredoxin-1 for reduction of S-mycothiolations MscR/AdhE/Fadh: MSNO reductase/ formaldehyde dehydrogenase Cg3349: maleylpyruvate isomerase for maleylpyruvate detoxification in <i>C. glutamicum</i> ArsC1/C2: MSH-dependent arsenate reductases	Zhao et al., 2015 Newton et al., 2008, 2011 Van Laer et al., 2012 Newton et al., 2008 Lessmeier et al., 2013 Witthoff et al., 2013 Feng et al., 2006 Ordonez et al., 2009

Salmonella Typhimurium (Potter et al., 2012; Song et al., 2013; Reniere et al., 2015) (Table 2). In *S. pneumoniae*, the glutathione reductase Gor and the GSH-importer GshT were required for oxidative stress protection and metal ion resistance. Moreover, the *gshT* mutant was attenuated in colonization and invasion in a mouse model of pneumococcal infection (Potter et al., 2012). Thus, GSH protects against the host immune defense and contributes to fitness of *S. pneumoniae*.

The intracellular pathogen *L. monocytogenes* is able to synthesize GSH via the *gshF* fusion protein, but GSH can be also imported from the host (Reniere et al., 2015). The *L. monocytogenes gshF* mutant was two-fold less virulent compared to the wild type in a mice model. In addition, the *gshF* mutant was sensitive to oxidative stress, contains lower levels of ActA and formed small plaques in tissue culture assays that measure cell-to-cell spread (Reniere et al., 2015). The Actin assembly-inducing protein ActA is controlled by the virulence regulator PrfA and used by *L. monocytogenes* to move through the host cells (Freitag et al., 2009). It was shown that the virulence phenotype of the *gshF* mutant is caused by the lack of PrfA activation by bacterial and

host-derived GSH (Reniere et al., 2015). Interestingly, activation of PrfA is mediated by an allosteric binding of GSH to PrfA, but not by S-glutathionylation. Thus, GSH plays a role as signaling molecule to activate virulence gene expression in an intracellular pathogen.

In *S. Typhimurium*, GSH antagonizes the bacteriostatic effects of RNS *in vivo* and *gshA* mutants were sensitive to ROS and RNS (Song et al., 2013). Thus, GSH presents a first line defense against ROS and RNS produced by the host immune system. This was shown in an acute model of salmonellosis in mice expressing the wild-type NRAMP1^R allele (natural resistance-associated macrophage protein 1) which is linked to high NO production of the macrophages. The *gshA* and *gshB* mutants were attenuated in this acute model of salmonellosis. It was further shown that GSH protects against ROS and RNS produced by the NADPH phagocyte oxidase and inducible nitric oxide synthase (iNOS) in this mice model (Song et al., 2013). These recent studies highlight the important roles of GSH in the control of virulence functions, expression of virulence factors and pathogen fitness under infection conditions in *S. pneumoniae*, *L. monocytogenes*, and

TABLE 2 | The role of thiol-redox buffers for virulence in pathogenic bacteria.

Redox buffer	Organism	Genes for biosynthesis or uptake	Virulence phenotypes of mutants	References
Glutathione (uptake)	<i>Streptococcus pneumoniae</i>	<i>gshT</i> (GSH importer)	<i>gshT</i> mutant attenuated in colonization and invasion in a mouse model of pneumococcal infection	Potter et al., 2012
Glutathione (biosynthesis and uptake)	<i>Listeria monocytogenes</i>	<i>gshF</i> (γ -Glu-Cys ligase/GSH synthase)	Virulence defect of the <i>gshF</i> mutant caused the lack of PrfA activation and lower <i>actA</i> expression by bacterial and host GSH	Reniere et al., 2015
Glutathione (biosynthesis)	<i>Salmonella Typhimurium</i>	<i>gshA</i> (γ -Glu-Cys ligase) <i>gshB</i> (GSH synthase)	<i>gshA</i> and <i>gshB</i> mutants attenuated in acute model of salmonellosis in NRAMP1 ^R mice; GSH protects against ROS and RNS produced by NOX in mice	Song et al., 2013
Bacillithiol (biosynthesis)	<i>Staphylococcus aureus</i>	<i>bshA</i> (glycosyltransferase) <i>bshB</i> (deacetylase) <i>bshC</i> (Cys ligase)	COL and USA300 <i>bshA</i> mutants impaired in human whole-blood survival assays; SH1000 natural <i>bshC</i> mutant survival defect in macrophage phagocytosis assays	Posada et al., 2014 Pöther et al., 2013
Mycothioliol (biosynthesis)	<i>Mycobacterium tuberculosis</i>	<i>mshA1</i> (glycosyltransferase) <i>mshA2</i> (phosphatase) <i>mshB</i> (deacetylase) <i>mshC</i> (Cys ligase) <i>mshD</i> (acetyltransferase)	<i>mshC</i> mutant impaired in growth and survival in mouse model of infection	Sareen et al., 2003; Sasseti and Rubin, 2003

S. Typhimurium. As shown for *L. monocytogenes*, GSH might play similar roles to activate virulence gene expression by redox control of virulence gene regulators in other pathogens which remains to be elucidated.

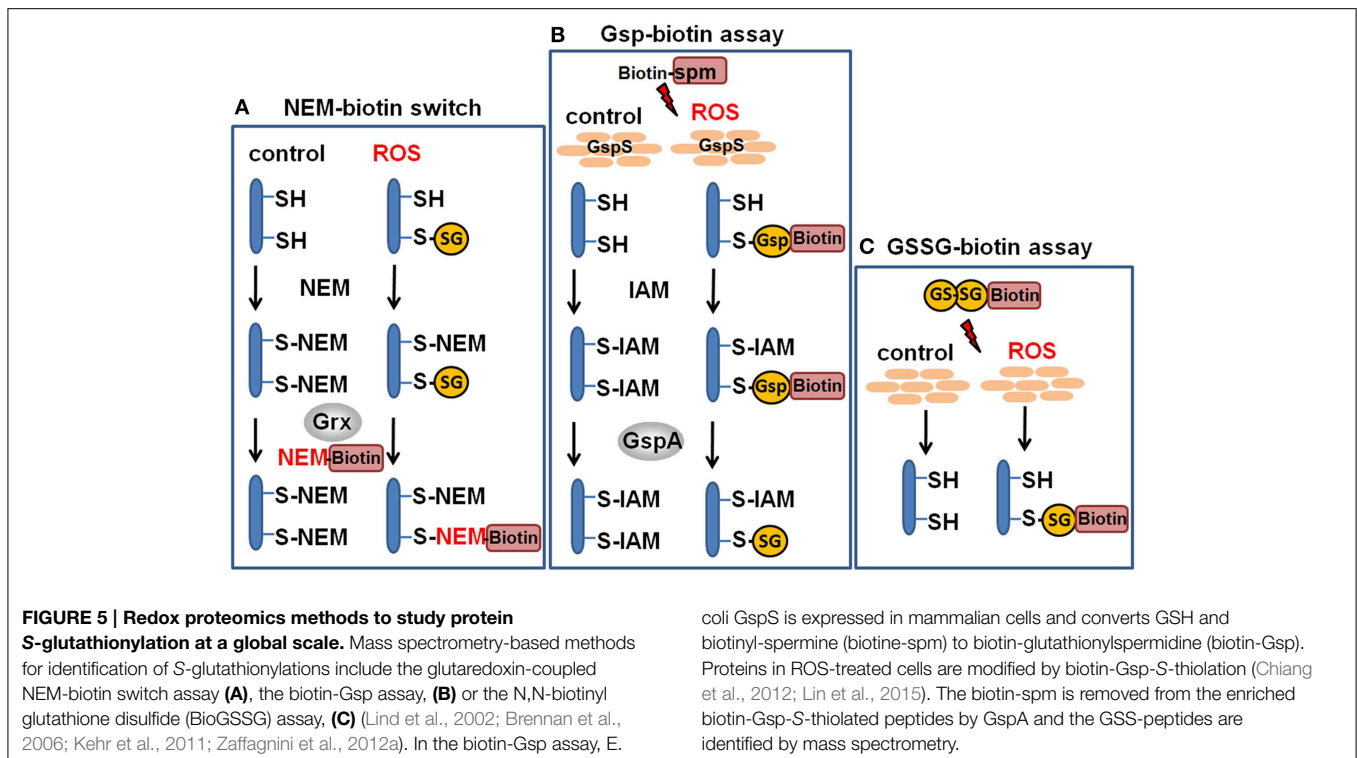
Redox Proteomic Methods to Study Protein S-Glutathionylation at a Global Scale

Advances in probe design and mass spectrometry-based thiol-trapping approaches have facilitated the detection of specific reversible thiol-modifications, including sulfenylation, nitrosylation, glutathionylation, and sulphydrations of proteins at a global scale (Leonard and Carroll, 2011; Pan and Carroll, 2013; Paulsen and Carroll, 2013; Gupta and Carroll, 2014; Zhang et al., 2014). Different methods have been applied for specific detection of S-glutathionylations in eukaryotic cells, including the use of GSH-specific antibodies and the labeling of S-thiolations with ³⁵S-cysteine followed by 2D gel electrophoresis and phosphoimaging (Fratelli et al., 2002, 2003, 2004). However, the specificity of the GSH antibodies is questionable and the gel-based detection of S-thiolations using ³⁵S-cysteine does not distinguish between S-cysteinylations and S-glutathionylations or other forms of S-thiolations. Hence, more sensitive mass spectrometry-based redox proteomics methods have been developed, including the glutaredoxin-coupled NEM-biotin switch assay and the treatment of cell extracts with N,N-biotinyl glutathione disulfide (BioGSSG) (Lind et al., 2002; Brennan et al., 2006; Kehr et al., 2011; Zaffagnini et al., 2012a) (Figure 5). Both methods make use of the specific streptavidin enrichment of biotinylated peptides that improve the identification of S-glutathionylated peptides using mass spectrometry. The NEM biotin-switch assay was successfully applied to detect protein S-glutathionylation in eukaryotic endothelial cells and

malaria parasites which applies glutaredoxin for reduction of protein-SSG followed by NEM-biotin alkylation and enrichment using streptavidin columns (Lind et al., 2002; Kehr et al., 2011). The biotin-GSSG approach has been applied to identify S-glutathionylated proteins in the green algae *Chlamydomonas reinhardtii* (Zaffagnini et al., 2012a) and in the photosynthetic cyanobacterium *Synechocystis* sp. PCC6803 (Chardonnet et al., 2015). In total, 383 S-glutathionylated proteins were identified in *Synechocystis* sp. PCC6803 and 125 glutathionylation sites were mapped by mass spectrometry. In addition, the peroxiredoxin PrxII (S11621) and the 3-phosphoglycerate dehydrogenase PGDH (S11908) could be S-glutathionylated by BioGSSG *in vitro* (Chardonnet et al., 2015).

In another approach, biotinyl-spermine (biotine-spm) and *in vivo* expressed *E. coli* GspS have been applied for mammalian cells to convert GSH to biotin-glutathionylspermidine (biotin-Gsp) which subsequently modified proteins by Biotin-Gsp-S-thiolation (Chiang et al., 2012; Lin et al., 2015). The biotine-spm is removed enzymatically by GspA from the enriched biotin-Gsp-S-thiolated peptides and the GSS-peptides are identified by mass spectrometry. This approach allows the identification of S-glutathionylation sites without the biotin-tag and enhances the coverage for S-glutathionylated proteins. In mammalian cells, 1409 S-glutathionylated cysteines in 913 proteins were identified using the Gsp-biotin approach (Chiang et al., 2012; Lin et al., 2015). This makes the application of this chemoenzymatic approach using the GspS enzyme attractive for global and specific studies of S-glutathionylated proteins.

In *S. Typhimurium*, protein S-glutathionylation has been studied at a global scale by top-down and bottom-up proteomic approaches (Ansong et al., 2013). Top-down proteomics uses whole proteins for separation and fragmentation directly



in the mass spectrometer. In bottom-up proteomics approaches proteins are digested by a protease and the peptide mixtures are analyzed by mass spectrometry to identify proteins at the peptide level. The top-down proteomic approach identified 563 proteins with 1665 post-translational modifications in *S. Typhimurium*. The authors identify 25 S-thiolated proteins in cells grown in complete LB medium including 16 S-glutathionylated proteins and nine S-cysteinylation proteins. Interestingly, a subset of nine S-glutathionylated are modified by S-cysteinylation in infection-like minimal LPM medium (Table 3). This could indicate a shift from S-glutathionylation to S-cysteinylation under infection-like conditions in *S. Typhimurium*. These S-thiolated proteins include phosphoglycerate kinase (Pgk), elongation factor (Tuf) and enolase (Eno) that are also targets for S-glutathionylations in endothelial cells (Fratelli et al., 2002). The top-down proteomics results were verified by bottom-up proteomics approaches to identify the specific S-thiolated Cys peptides (Ansong et al., 2013). Structural analysis revealed that S-glutathionylation occurred mostly at buried Cys residues and not at surface-exposed Cys. S-glutathionylation on buried Cys was also shown for the enolase whose activity is known to be modified by S-thiolation in human cells (Fratelli et al., 2002). It is postulated that *S. Typhimurium* switches from S-glutathionylation to S-cysteinylation during infection conditions as novel redox-control mechanism. In agreement with the proteome data, transcriptome results point to an up-regulation of Cys biosynthesis and down-regulation of GSH biosynthesis under infection-like conditions. However, the physiological role of this S-thiolation switch for redox control of the identified protein targets under ROS stress remains to be elucidated.

Furthermore, no blocking of reduced thiols with NEM or IAM was performed to avoid artificial disulfide formation. Thus, it remains to be verified that the observed S-thiolations are not caused by artificial thiol-disulfide exchange. Previous studies have also shown that *L. monocytogenes* is able to both import and synthesize GSH (Reniere et al., 2015). Furthermore, the non-GSH-utilizing *S. aureus* was shown to import GSH during growth in LB medium (Pöthner et al., 2013). Thus, the possible uptake of GSH in *S. Typhimurium* from LB-medium could contribute to the observed S-glutathionylations which needs to be investigated.

The Regulatory Potential of Protein S-Glutathionylation in Gram-negative Bacteria

The role of protein S-glutathionylation for redox control has been studied in few Gram-negative bacteria, including *E. coli*, *S. Typhimurium*, *Neisseria meningitidis*, *Pseudoalteromonas haloplanktis*, and *Synechocystis* sp. PCC6803 (Table 3). In *E. coli*, the peroxide-sensing regulator OxyR is activated by S-glutathionylation at its redox-sensing Cys199 *in vitro* (Kim et al., 2002). In addition, the activities of glyceraldehyde-3-phosphate dehydrogenase, methionine synthase and the PAPS reductase are inhibited by S-glutathionylation in *E. coli* (Lillig et al., 2003; Hondorp and Matthews, 2004; Brandes et al., 2009). A recent study provides a model for the S-glutathionylation of the conserved active site Cys in GapDH and explains the reactivity of the active site toward H₂O₂ (Peralta et al., 2015). Reaction of the active site Cys with H₂O₂ is catalyzed by a mechanism which stabilizes the transition state and promotes leaving group departure by providing a proton relay. This model suggests the conserved

TABLE 3 | Targets for protein S-thiolation by bacterial thiol-redox buffers.

Redox buffer	Organism	Functions of S-thiolated proteins	S-thiolated Cys	References
Glutathione	<i>Salmonella</i> Typhimurium	16 protein-SSG and nine protein-SSCys identified in LB medium cultures nine protein-SSG in LB switch to protein-SSCys in minimal medium: DnaK (chaperone) CspD (cold shock protein) HNS (transcription regulator) MinE (cell division factor) Ndk (nucleoside diphosphate kinase) GrxC (glutaredoxin) RplC (50S ribosomal protein) YifE (unknown function) YjgF (translation inhibitor)	Cys15 Cys19 Cys21 Cys16 Cys139 Cys66 Cys199 Cys64 Cys107	Ansong et al., 2013
Glutathione	<i>Escherichia coli</i>	OxyR (peroxide sensor) Gap (glyceraldehyde-3-phosphate DH) MetE (methionine synthase) PpaC (PAPS reductase)	Cys199 redox-sensing Cys152 active site Cys645 not conserved Cys239 active site	Kim et al., 2002 Brandes et al., 2009 Hondorp and Matthews, 2004 Lillig et al., 2003
Glutathione	<i>Neisseria meningitidis</i>	EstD (esterase)	Cys54 substrate binding	Chen et al., 2013
Glutathione	<i>Pseudo-alteromonas haloplanktis</i>	PhSOD (iron-superoxide dismutase)	Cys57 conserved	Castellano et al., 2008
Glutathione	<i>Synechocystis</i> sp. PCC6803	383 total protein-SSG 125 S-glutathionylation sites: Inorganic pyrophosphatase Phosphoribulokinase PAPS reductase Triose phosphate isomerase IMP dehydrogenase ADP-glucose pyrophosphorylase RubisCo MerA (mercury reductase) AbrB (repressor of hydrogenase operon)	Cys164 Cys19 Cys230 Cys127 Cys222 Cys55 Cys422, Cys242 Cys78 active site Cys34 redox-sensing	Chardonnet et al., 2015 Marteyn et al., 2013 Cassier-Chauvat et al., 2014
Bacillithiol	<i>Bacillus subtilis</i> <i>Bacillus pumilus</i> <i>Bacillus amyloliquefaciens</i> <i>Staphylococcus carnosus</i>	54 total protein-SSB including eight conserved protein-SSB: MetE (methionine synthase) PpaC (Mn-dependent inorganic pyrophosphatase) SerA (D-3-phosphoglycerate DH) AroA (chorismate mutase) TufA (Elongation factor Tu) GuaB (IMP dehydrogenase) YphP/BrxA (bacilliredoxin) YumC (Ferrodoxin-NADP reductase2)	Cys730 active site Cys158 active site Cys410 conserved Cys126 conserved Cys83 GTP-binding site Cys308 active site Cys53 active site Cys85 active site	Chi et al., 2011 Chi et al., 2013
Mycothioliol	<i>Corynebacterium glutamicum</i>	25 total protein-SSM identified: MalP (Maltodextrin phosphorylase) MetE (Methionine synthase) Hom (Homoserine DH) Ino-1 (Myo-inositol-1-P-synthase) Fba (Fructose-bisphosphate aldolase) SerA (Phosphoglycerate DH) Pta (Phosphate acetyltransferase) XylB (pentulose/hexulose kinase) GuaB1/2 (IMP dehydrogenase) NadC (Nicotinate-nucleotide pyrophosphorylase)	Cys180 conserved Cys713 active site Cys239 Cys79 Cys332 Cys266 Cys367 Cys338 Cys302/Cys317 active site Cys114	

(Continued)

TABLE 3 | Continued

Redox buffer	Organism	Functions of S-thiolated proteins	S-thiolated Cys	References
Mycothioli	<i>Corynebacterium glutamicum</i>	PurL (Phosphoribosyl formylglycinamide synthase) TheD/ThiD2 (Thiamine biosynthesis) Tpx (Thiol peroxidase) Mpx (Mycothioli peroxidase) MsrA (Met-SO reductase) HmuO (Heme oxygenase) RpsC/F/M, RplM (ribosomal proteins) Tuf (translation elongation factor) PheT (Phe-tRNA synthetase)	Cys716 Cys451 active site/Cys111 Cys60 active site/Cys94 resolving Cys36 active site Cys91 conserved Cys165 Cys153/67/50/86 Cys277 conserved Cys89 tRNA binding	Chi et al., 2014

redox-regulation of GapDH by S-thiolation of its active site Cys across all domains of life.

In *Neisseria meningitidis*, an esterase EstD acts together with the GSH-dependent alcohol dehydrogenase AdhC in formaldehyde detoxification. EstD is inactivated via S-glutathionylation at its conserved Cys54 by its substrate S-formyl-GSH during formaldehyde detoxification *in vitro* (Chen et al., 2013). In the psychrophilic bacterium *Pseudoalteromonas haloplanktis*, S-glutathionylation of the iron-superoxide dismutase PhSOD at the single Cys57 protected the enzyme from tyrosine nitration and peroxynitrite inactivation *in vitro* and *in vivo* (Castellano et al., 2008).

In *Synechocystis* sp. PCC6803, a MerA-like enzyme that functions in mercury and uranium reduction was shown to be redox-controlled by S-glutathionylation (Marteyn et al., 2013). MerA was S-glutathionylated at Cys78 that is required for mercury reduction resulting in inhibition of MerA activity. MerA redox regulation and reactivation required reduction by glutaredoxin-1 (Grx1). The active site Cys31 and Cys86 of Grx-1 operate in MerA interactions and both Cys are required for MerA reactivation. Furthermore, S-glutathionylation was shown to control the activity of the transcription factor AbrB2 in *Synechocystis* sp. PCC6803 (Cassier-Chauvat et al., 2014). AbrB2 is a repressor of the hydrogenase-encoding *hoxEFUYH* operon and also down-regulates antioxidant genes, such as *cydAB* encoding the cytochrome bd-quinol oxidase and *norB* encoding the nitric oxide reductase. The production of hydrogen is thought to be an antioxidant mechanism to eliminate electrons for oxygen reduction and ROS generation. AbrB2 contains a conserved single cysteine that is essential for redox-regulation and oligomerisation of AbrB2 as shown in C34S mutants. S-glutathionylation of Cys34 affected the binding of AbrB2 to the *hox* promoter and the stability of AbrB2 *in vitro*. In conclusion, S-glutathionylation has been shown to function in the redox-control of two transcriptional regulators, OxyR and AbrB2 in Gram-negative bacteria *in vitro*. However, compared to the many targets for S-glutathionylation that have been studied in eukaryotic organisms, there is much to be discovered about the regulatory potential of S-glutathionylation in bacteria.

Protein S-glutathionylation is a reversible redox switch mechanism. The glutaredoxin (Grx)/GSH/GSH reductase (Gor) system catalyzes specific de-glutathionylation of S-glutathionylated proteins (Fernandes and Holmgren, 2004; Inaba, 2009). Grx

were first discovered in *E. coli* (Holmgren, 1976) where they have important functions as electron donors for ribonucleotide reductase (RNR), adenosine-5'-phosphosulfate (APS) reductase, 3'-phosphoadenosine-5'-phosphosulfate (PAPS) reductase and arsenate reductases (Holmgren, 1981; Aslund et al., 1994). Grx are structurally classified into the classical di-thiol Grxs with a CPTC redox active site and the monothiol Grx containing a CGPS redox active site (Lillig et al., 2008). In *E. coli*, three di-thiol Grx proteins (Grx1, Grx2, and Grx3) and one monothiol protein (Grx4) have been characterized.

The de-glutathionylation by Grx enzymes involves thiol-disulfide exchange reactions with GSH via nucleophilic double displacement (ping-pong) mechanisms and occurs via mono- or di-thiol mechanisms. Most di-thiol Grx use monothiol mechanisms that take place in two steps: In the first step, the nucleophilic thiolate anion attacks the S-glutathionylated substrate protein, resulting in reduction of the mixed disulfide and the S-glutathionylated Grx (Grx-SSG) intermediate. This Grx-SSG intermediate is regenerated by GSH and Gor at expense of NADPH (Allen and Mieyal, 2012). The di-thiol mechanism involves a second active site Cys that forms an intramolecular disulfide to resolve the Grx-SSG intermediate that has been shown for some plant Grx enzymes (Zaffagnini et al., 2012b). However, this di-thiol mechanism of Grx is less efficient for protein de-glutathionylation and more involved in the reduction of intermolecular protein disulfides (Lillig et al., 2008; Allen and Mieyal, 2012). Thus far, the knowledge about Grx functions and substrates in most GSH-producing bacteria is scarce and remains an important subject for future studies.

Biosynthesis and Regulation of Bacillithiol in Gram-Positive Firmicutes Bacteria

Bacillithiol (BSH) is composed of Cys-GlcN-malate and serves as major LMW thiol in many Firmicutes bacteria, including *Bacillus* and *Staphylococcus* species, *Deinococcus radiodurans*, and *Streptococcus agalactiae* (Newton et al., 2009) (Figure 4). The BSH biosynthesis pathway was first identified in *B. subtilis*. In the first step, the glycosyltransferase BshA couples UDP-GlcNAc to L-malic acid for generation GlcNAc-Mal (Ruane et al., 2008; Gaballa et al., 2010; Parsonage et al., 2010). The deacetylase BshB1 catalyzes deacetylation of GlcNAc-Mal to GlcN-Mal. The last step involves the putative cysteine ligase YIIA (BshC) that presumably adds Cys to GlcN-Mal (Gaballa et al., 2010). BshB1 has a

paralog BshB2 and both enzymes have deacetylase activity. The functional redundancy of BshB1 and BshB2 in *B. subtilis* suggests that BshB2 might function as BSH-S-conjugate amidase Bca in detoxification of RES similar to the MSH-S-conjugate amidase Mca (Parsonage et al., 2010). The functions of the BshB1/2 homologs of *B. anthracis* (BA1557 and BA3888) and *B. cereus* (BC1534 and BC3461) in the deacetylation of GlcNAc-Mal have been demonstrated *in vitro*. In addition, BA3888 was shown to function as BSH-S-conjugate amidase (Bca) (Fang et al., 2013). In contrast to BshA and BshB, the activity of the putative cysteine ligase BshC has never been demonstrated biochemically *in vitro*. The structure of BshC was resolved revealing a core Rossmann fold with connecting peptide motifs (CP1 and CP2) and an α -helical coiled-coil domain required for dimerization (Vanduinen et al., 2015). BshC was crystallized with citrate and glycerol in the canonical active site and ADP bound in a second binding pocket that is different from the ADP-binding pocket in the related MshC structure. The active sites are solvent exposed and open for possible interactions with a protein, substrate or cofactor that remain to be elucidated to understand the catalytic mechanism of BshC (Vanduinen et al., 2015).

The regulation of the BSH biosynthesis genes has been studied in *B. subtilis*. The *bshA* and *bshB1* genes belong to a large operon of seven genes including *mgsA* which encodes a methylglyoxal synthase. The *bshB2* and *bshC* genes are encoded by two different operons. The *bshA*, *bshB*, and *bshC* genes are induced under conditions of disulfide stress provoked by diamide or NaOCl and positively controlled by the disulfide stress regulator Spx (Chi et al., 2011; Rochat et al., 2012; Gaballa et al., 2013). Consistent with the Spx-dependent control of the BSH biosynthesis genes, lower BSH levels were detected in the *spx* mutant using thiol-metabolomics (Chi et al., 2011; Rochat et al., 2012; Gaballa et al., 2013). It is interesting to note, that the Trx pathway and BSH biosynthesis genes are both regulated by the major disulfide stress regulator Spx in *B. subtilis* (Zuber, 2004, 2009; Chi et al., 2011; Rochat et al., 2012; Gaballa et al., 2013).

Functions of Bacillithiol and BSH-Dependent Detoxification Enzymes

BSH is predominantly present in its reduced form in the cytoplasm with BSH/BSSB ratios ranging from 100:1 to 400:1 in *B. subtilis* indicating the presence of an efficient bacillithiol disulfide reductase (Sharma et al., 2013). The FAD-dependent pyridine nucleotide disulfide oxidoreductase YpdA (IPR023856) was suggested to function as BSSB reductase because of its phylogenetic relationship to the BSH biosynthesis enzymes as revealed by a STRING search (Gaballa et al., 2010). However, the function of YpdA has not yet been demonstrated.

The standard thiol-redox potential of BSH was calculated as E° (BSSB/BSH) = -221 mV which is higher than the GSH redox potential [E° (GSSG/GSH) = -240 mV] (Sharma et al., 2013). The microscopic pK_a values of the thiol group of BSH were determined as $pK_a = 7.97$ when the amino group of the Cys is protonated and as $pK_a = 9.55$ in the presence of the deprotonated amino group of Cys (Sharma et al., 2013). Thus, the thiol group in BSH is more acidic compared to the thiol group in Cys suggesting an enhanced level and reactivity of the BSH thiolate anions

to detoxify reactive species. The BSH concentrations in *B. subtilis* vary during the growth in LB medium and increase strongly during the stationary phase to 3.5–5.2 mM. In contrast, the cellular Cys concentration is kept at a relatively low level (0.13–0.28 mM). Thus, BSH concentrations are ~ 17 -fold higher compared to the level of Cys (Sharma et al., 2013). Similar concentrations of BSH (2 mM) were measured in *Bacillus pumilus* during growth. In *B. pumilus*, BSH levels increased under peroxide stress to 6 mM which is caused by an increased *bshB* expression (Handtke et al., 2014). BSH levels are also two-fold increased under diamide and NaOCl stress in *B. subtilis* due to Spx-dependent induction of *bshA*, *bshB*, and *bshC* (Chi et al., 2013; Gaballa et al., 2013). In *S. aureus*, the BSH levels are lower (0.3–1 mM) in the different clinical isolates (COL, USA300, Mu50, or N315) and BSH levels are not up-regulated during the stationary phase (Posada et al., 2014).

The physiological functions of BSH were studied in *bsh* mutants of *B. subtilis* and *S. aureus* (Table 1). Phenotype analyses showed increased sensitivities of *bsh* mutants toward hypochlorite, diamide, methylglyoxal, ROS (paraquat, H_2O_2), osmotic, and acidic stress, alkylating agents and fosfomycin in *B. subtilis* (Gaballa et al., 2010; Chi et al., 2011). The fosfomycin-sensitive phenotype of *bsh* mutants depends on the epoxide hydrolase FosB that requires BSH as a cofactor to open the ring structure for fosfomycin detoxification (Lamers et al., 2012; Roberts et al., 2013; Thompson et al., 2013) (Figure 6). FosB shows a preference for BSH as thiol cofactor and does only work poorly with Cys. The biochemical activity has been demonstrated for various *Bacillus* and *Staphylococcus* FosB homologs (Lamers et al., 2012; Roberts et al., 2013; Thompson et al., 2013). In *B. subtilis* and *S. aureus*, both FosB and BSH confer resistance to fosfomycin treatment in survival assays *in vivo* (Gaballa et al., 2010; Thompson et al., 2014). Co-crystallization of *S. aureus* FosB with L-Cys or BSH revealed a mixed disulfide at the active site Cys9 of FosB which is unique in FosB from *S. aureus* (Thompson et al., 2014).

Reactive electrophiles, such as monobromobimane are detoxified by direct conjugation to BSH or by conjugation reactions catalyzed by BSH S-transferases. BSH functions as a cofactor for DinB-family S-transferases that are widely distributed among GSH-, BSH-, and MSH-producing bacteria (Newton et al., 2011; Perera et al., 2014). The *B. subtilis* DinB-family YfiT protein was active as S-transferase with BSH to conjugate monochlorobimane, but inactive with MSH or GSH (Newton et al., 2011). The *yfiT* gene is flanked by *yfiS* and *yfiU* encoding putative efflux transporters for mercapturic acids produced during electrophile detoxification. The YfiT-homolog of *S. aureus* BstA catalyzed the conjugation of BSH to monochlorobimane, 1-chloro-2,4-dinitrobenzene and cerulenin, while rifampicin was BstA-independently conjugated to BSH (Perera et al., 2014).

BSH is involved in methylglyoxal detoxification and functions as a cofactor for BSH-dependent glyoxalases in *B. subtilis* (Chandrangsu et al., 2014). Methylglyoxal rapidly depletes BSH leading to BSH-hemithioacetal formation that is converted to S-lactoyl BSH by the glyoxalase-I (GlxA). The glyoxalase-II (GlxB) catalyzes conversion of S-lactoyl-BSH to lactate (Figure 6). Phenotype studies further indicated that BSH can detoxify heavy metal ions, such as tellurite and selenite in *B. subtilis* (Helmman, 2011).

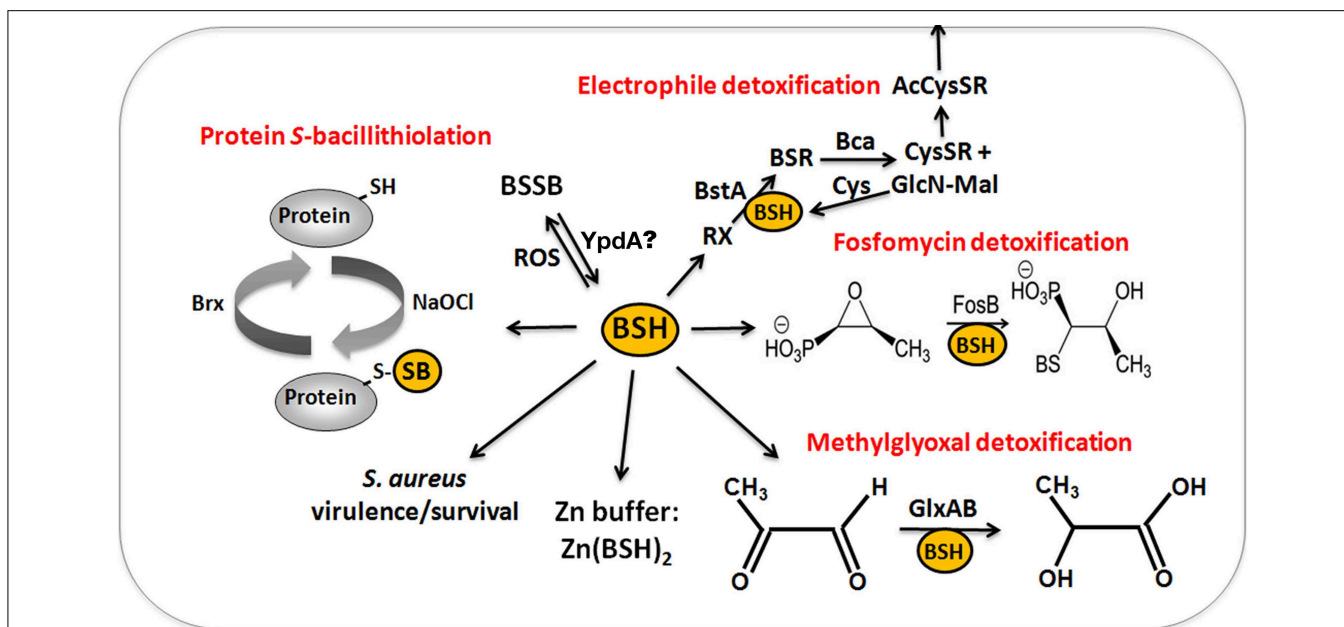


FIGURE 6 | The functions of bacillithiol (BSH) in *B. subtilis* and *S. aureus*. Bacillithiol functions in detoxification of ROS, RES, HOCl, and antibiotics (fosfomycin, rifampicin) in *B. subtilis* and *S. aureus*. BSH is oxidized by ROS to bacillithiol disulfide (BSSB). Electrophiles (RX) are conjugated to BSH by the BSH S-transferase BstA to form BS-electrophiles (BSR) which are cleaved by the BSH S-conjugate amidase Bca to CysSR and mercapturic acids (AcCysSR) that are exported from the cell. BSH serves as a cofactor for the epoxide hydrolase FosB which adds BSH to fosfomycin to open the ring structure

for its detoxification. BSH functions in methylglyoxal detoxification as a cofactor for the glyoxalases I/II (GlxA and GlxB) in *B. subtilis*. GlxA converts BSH-hemithioacetal to S-lactoyl-BSH that is further converted by GlxB to D-lactate. BSH serves as Zn buffer under conditions of Zn excess in *B. subtilis*. In *S. aureus*, BSH is important under infection-related conditions and increased the survival of *S. aureus* in phagocytosis assays using murine macrophages. Under conditions of NaOCl stress, proteins are oxidized to mixed disulfides with BSH, termed as S-bacillithiolations which is reversed by bacilliredoxins.

In addition, BSH functions as Zn buffer in metal ion homeostasis (Ma et al., 2014). The Cys thiol and carboxylate moieties of BSH can bind and store Zn(II) as $\text{BSH}_2\text{:Zn}$ complex under conditions of Zn(II) stress (Ma et al., 2014). BSH binding to Zn(II) occurred at much higher affinity compared to GSH. Mutants lacking BSH are more sensitive to Zn(II) stress and induced the Zn efflux CadA system at lower Zn levels compared to the wild type. BSH also protected against Zn(II) toxicity in cells lacking Zn efflux pumps. In addition, Zn efflux is elevated under conditions of diamide stress when the pool of reduced BSH is depleted. These results establish a new role of BSH as buffer for the labile Zn pool that are likely important for related pathogens under infection conditions.

In conclusion, functional analyses of *bsh* mutants established important roles of BSH as GSH surrogate in Firmicutes bacteria, including similar detoxification functions and BSH-dependent enzymes, such as DinB-family S-transferases and glyoxalases that are widely conserved across bacteria. However, the conserved role of FosB as BSH-dependent fosfomycin hydrolase and the function of BSH as Zn buffer have been described only in BSH-producing bacteria.

Functions of Bacillithiol in the Virulence of *Staphylococcus aureus*

Phenotype analyses of *S. aureus* *bsh* mutants were conducted for different clinical isolates of methicillin-resistant *S. aureus*

strains (MRSA) that revealed a role of BSH for stress resistance and under infection conditions (Pöther et al., 2013; Posada et al., 2014) (Table 2). In survival assays, *S. aureus* USA300 LAC transposon *bsh* mutants were more sensitive to alkylating agents (iodoacetamide and CDNB), methylglyoxal, peroxide and superoxide stress, diamide, fosfomycin, cerulenin, rifampicin and metals ions, like copper and cadmium (Rajkarnikar et al., 2013). In *S. aureus* COL and USA300 backgrounds, *bshA* and *fosB* mutants with clean deletions showed increased sensitivities to fosfomycin, diamide and H_2O_2 and the levels of NADPH and BSH were decreased in *fosB* mutants suggesting a function of FosB as S-transferase in the oxidative stress resistance (Posada et al., 2014). The *S. aureus* COL and USA300 *bshA* mutants showed a decreased survival in human whole-blood survival assays (Posada et al., 2014). Microarray analyses of the *bshA* mutant further revealed that staphyloxanthin biosynthetic genes are induced while the level of staphyloxanthin was strongly decreased in the *S. aureus* *bshA* mutant. Interestingly, the widely used strains of the *S. aureus* NCTC8325 lineage including SH1000 harbor natural *yllA* (*bshC*) null mutations that are caused by a 8 bp duplication in the *bshC* gene and these strains do not produce BSH (Gaballa et al., 2010; Newton et al., 2012; Posada et al., 2014). In contrast, *S. aureus* Newman encodes a functional *bshC* gene and produces BSH as revealed by thiol metabolomics (Newton et al., 2012; Pöther et al., 2013). BSH biosynthesis in *S. aureus* SH1000 could be restored by plasmid-encoded expression of the

bshC gene (Pöther et al., 2013; Posada et al., 2014). In phagocytosis assays using murine macrophages and human epithelial cell lines the survival of the SH1000 strain was decreased compared to the *bshC* complemented *S. aureus* strain (Pöther et al., 2013; Posada et al., 2014). Thus, BSH is involved in the defense against the host-immune system and contributes to pathogen fitness in *S. aureus* clinical MRSA isolates under infection-related conditions. It will be exciting to unravel the regulatory mechanisms that contribute to virulence control by BSH in *S. aureus*.

The Role of Protein S-Bacillithiolation in Gram-Positive Firmicutes Bacteria

Protein S-bacillithiolation was recently discovered as a widespread thiol protection and redox-regulatory mechanism in different Firmicutes bacteria (Chi et al., 2011, 2013) (Figure 7). S-bacillithiolation functions as a redox-switch mechanism to control the activity of redox-sensing transcription factors and metabolic enzymes, including OhrR and MetE (Lee et al., 2007; Chi et al., 2011) (Table 3). S-bacillithiolation of the OhrR repressor occurs at its lone Cys15 residue leading to inactivation of OhrR and expression of the thiol-dependent OhrA peroxiredoxin for detoxification of organic hydroperoxides and NaOCl (Fuangthong et al., 2001; Chi et al., 2011). S-bacillithiolation is also widespread among other Firmicutes

with eight common and 29 unique S-bacillithiolated proteins identified in *B. subtilis*, *Bacillus amyloliquefaciens*, *Bacillus pumilus*, *B. megaterium*, and *Staphylococcus carnosus* (Chi et al., 2011, 2013). The S-bacillithiolome contains mainly biosynthetic enzymes for amino acids (methionine, cysteine, branched chain and aromatic amino acids), cofactors (thiamine), nucleotides (GTP), as well as translation factors, chaperones, redox, and antioxidant proteins. Among the most conserved protein-SSB were abundant and essential proteins like TufA, MetE, GuaB that are targets for S-thiolation also in MSH-producing bacteria (Chi et al., 2014).

The methionine synthase MetE is the most abundant S-bacillithiolated protein in *Bacillus* species after NaOCl exposure. S-bacillithiolation of MetE occurs at its Zn-binding active site Cys730 and at the non-essential surface-exposed Cys719, leading to methionine starvation in NaOCl-treated cells (Chi et al., 2011). Similarly, methionine auxotrophy is caused by S-glutathionylation of MetE in *E. coli* after diamide stress (Hondorp and Matthews, 2004). The active site Zn center of MetE is also S-mycothiolated in *C. glutamicum* (Chi et al., 2014). Since formyl methionine is required for initiation of translation, MetE inactivation could stop translation during the time of hypochlorite detoxification. This translation arrest caused by S-bacillithiolation is supported by the strong repression of the

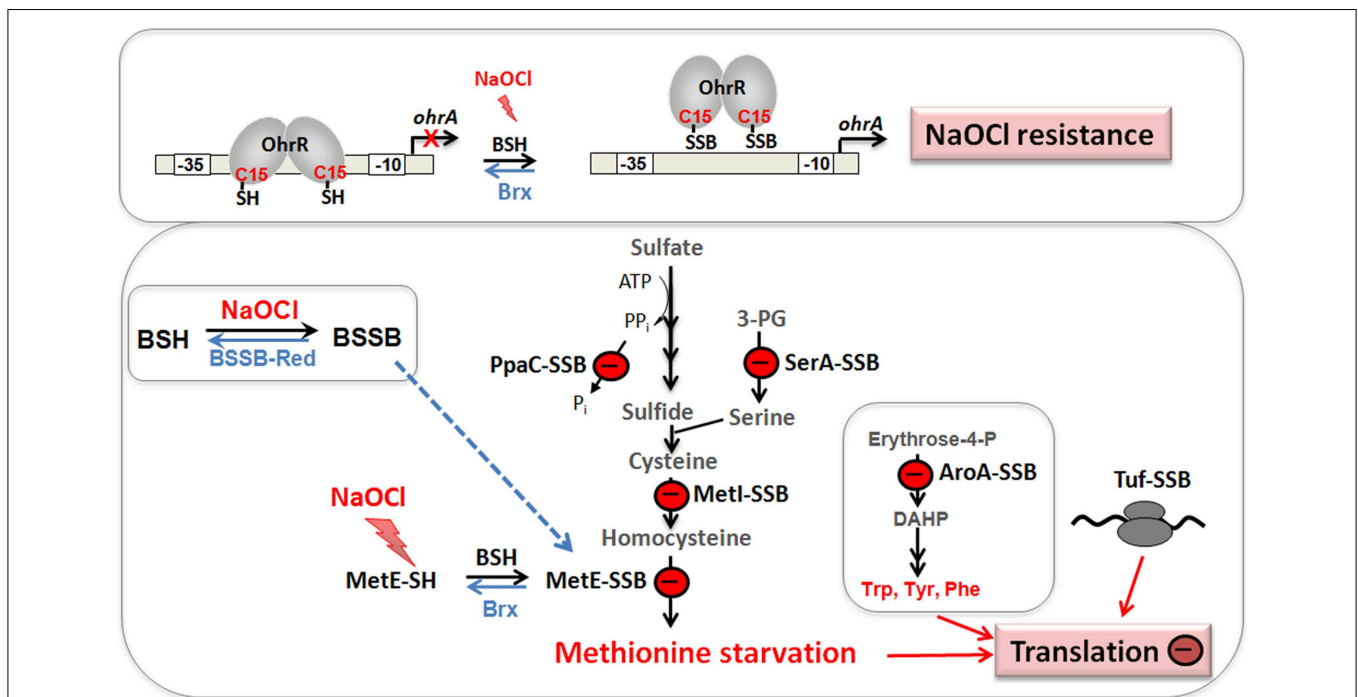


FIGURE 7 | Physiological roles of S-bacillithiolations in *B. subtilis* and other Firmicutes. NaOCl leads to S-bacillithiolation of OhrR, MetE, YxjG, PpaC, SerA, AroA, GuaB, YumC, TufA, and YphP in *B. subtilis* (Chi et al., 2011). S-bacillithiolation of OhrR inactivates the repressor and causes induction of the OhrA peroxiredoxin that confers NaOCl resistance. S-bacillithiolation of the methionine synthase MetE at its active site Cys730 and other enzymes of the Cys and Met biosynthesis pathway (YxjG, PpaC, SerA, MetI) leads to methionine auxotrophy (Chi et al., 2011, 2013). In

addition, other amino acids biosynthesis enzymes, translation factors and ribosomal proteins are S-bacillithiolated in Firmicutes bacteria. Thus, we hypothesize that S-bacillithiolation leads to a transient translation stop during the time of NaOCl detoxification to prevent further protein damage. NaOCl stress causes oxidation of BSH to BSSB and a two-fold decreased BSH/BSSB redox ratio that possibly contributes to S-bacillithiolation. The reduction of MetE-SSB and OhrR-SSB is catalyzed by bacilliredoxins (BrxA/B) in *B. subtilis*.

stringent response RelA regulon under NaOCl stress, which includes genes for ribosomal proteins and translation factors (Chi et al., 2011).

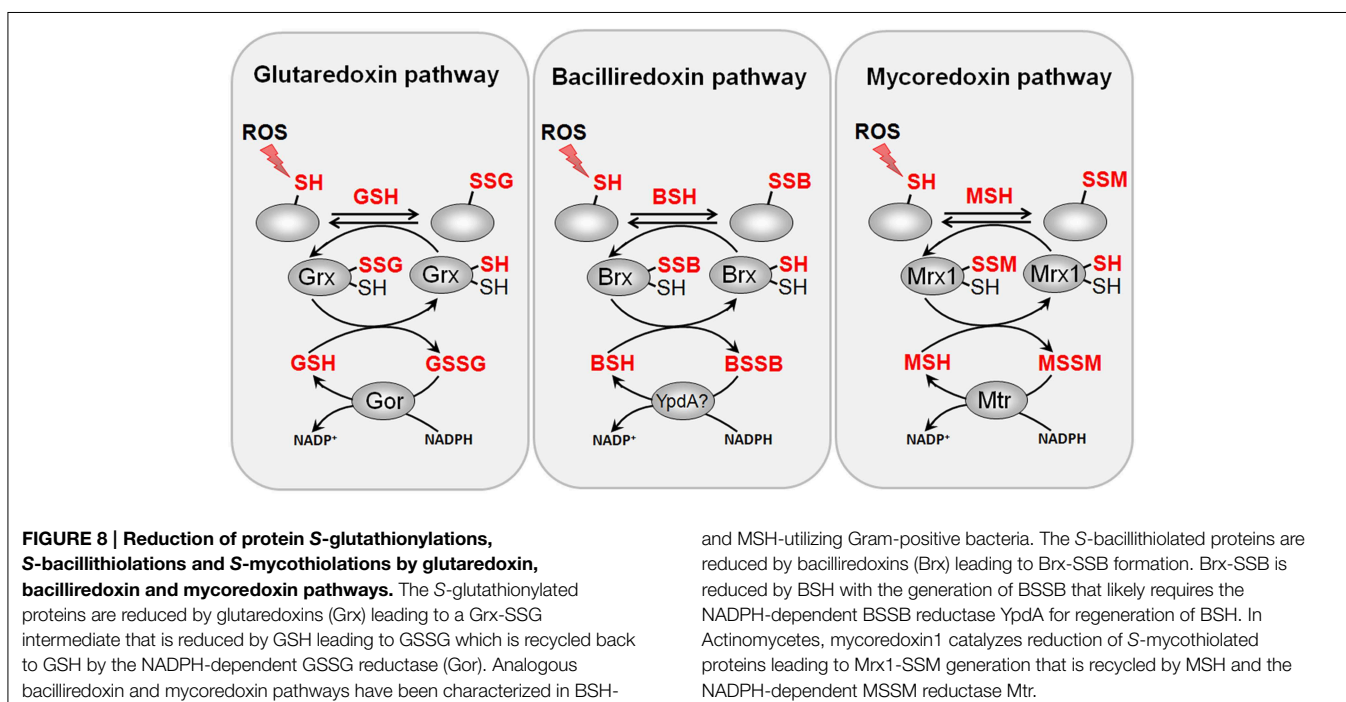
Our studies revealed that S-bacillithiolations were observed under diamide and NaOCl stress, but not under control conditions. This confirms previous results about the mechanisms of S-glutathionylations which requires activation of protein thiols by ROS. S-glutathionylation can be caused via thiol-disulfide exchange with GSSG and by activation of thiols to sulfenic acid, sulfenylamides, thiyl radicals, thiosulfinate or S-nitrosyl intermediates (Gallogly and Mieyal, 2007; Mieyal et al., 2008; Allen and Mieyal, 2012; Mieyal and Chock, 2012). Hypochlorite leads to chlorination of the thiol group to form sulfenylchloride that is unstable and rapidly reacts further to form mixed BSH protein disulfides (Hawkins et al., 2003; Davies, 2011). The increased BSSB level under NaOCl-stress might also contribute to S-bacillithiolation via thiol-disulfide exchange.

Among the S-bacillithiolated proteins, the thioredoxin-like proteins YtxJ, YphP, and YqiW were identified in *B. subtilis* and *Staphylococcus* that occur only in BSH-producing bacteria (Chi et al., 2013). These Trx-like enzymes were suggested to function as bacilliredoxins (Brx) in the de-bacillithiolation process. YtxJ could function as monothiol Brx and contains a single Cys in the conserved TCPIS motif. YphP (BrxA) and YqiW (BrxB) are paralogs of the uncharacterized DUF1094 family (53% identity) with unusual CGC active sites (Gaballa et al., 2010). YphP has also weak thiol-disulfide isomerase activity and a relatively high standard redox potential of $E^0 = -130$ mV (Derewenda et al., 2009). It was demonstrated that BrxA and BrxB function in the reduction of the S-bacillithiolated substrates MetE and OhrR *in vitro* (Gaballa et al., 2014) (Figure 8). The BrxBCxA resolving Cys mutant protein was able to reduce

S-bacillithiolated OhrR to restore the DNA-binding activity of OhrR. However, the BrxBCxA mutant was unable to reduce S-cysteinylated OhrR. These results provide first evidence for the function of glutaredoxin-like enzymes in BSH-producing bacteria. However, phenotype analyses revealed that both, BrxA and BrxB are not essential and rather dispensable for oxidative stress resistance under conditions of S-bacillithiolations in *B. subtilis* (Gaballa et al., 2014). Thus, the bacilliredoxin pathway is redundant with other thiol-disulfide oxidoreductases or the thioredoxin pathway *in vivo* for reduction of BSH mixed disulfides. In conclusion, the redox regulation of enzymes and transcription regulators by S-bacillithiolation and bacilliredoxins has been studied in detail in the model bacterium *B. subtilis*. Future studies should be directed to elucidate if S-bacillithiolation and bacilliredoxins control virulence functions and pathogen fitness in the major pathogen *S. aureus*.

Biosynthesis and Regulation of Mycothiol in Actinomycetes

Mycothiol (MSH) is composed of N-Acetyl-Cys-GlcN-myooinositol (Figure 4) and is present in high-GC Gram-positive Actinomycetes, such as Streptomycetes, Mycobacteria and Corynebacteria (Jothivasan and Hamilton, 2008; Newton et al., 2008). The biosynthesis of MSH proceeds from myo-inositol-1-phosphate, UDP-GlcNAc and cysteine and occurs in five steps (Jothivasan and Hamilton, 2008; Newton et al., 2008). The glycosyltransferase MshA conjugates myo-inositol-1-P to UDP-GlcNAc and produces GlcNAc-Ins-P. Dephosphorylation of GlcNAc-Ins-P by the phosphatase MshA2 generates GlcNAc-Ins which is the substrate for the deacetylase MshB. The MshB enzyme is homologous to the MSH S-conjugate amidase (Mca), and has both deacetylase and amidase activities. The cysteine



ligase MshC adds Cys to GlcN-Ins to generate Cys-GlcN-Ins. The final acetylation of the Cys is catalyzed by the acetyltransferase MshD to produce MSH (Jothivasan and Hamilton, 2008; Newton et al., 2008). The structure of MSH is similar to that of BSH and the glycosyltransferase BshA and deacetylase BshB of *B. subtilis* are homologs of the MshA and MshB enzymes of Mycobacteria.

MSH biosynthesis enzymes in *Streptomyces* are redox-controlled under diamide stress by the disulfide stress specific σ^R ECF sigma factor/RsrA anti sigma factor system (Kim et al., 2012). σ^R is sequestered by its redox-sensitive anti sigma factor RsrA in non-stressed cells. RsrA is oxidized at redox-sensing Cys residues in the Zn-binding site under disulfide stress that leads to relief of σ^R . Free σ^R transcribes genes required to maintain the thiol-redox homeostasis, including the genes for TrxAB and MSH biosynthesis, such as *mshA*, *mshB*, *mshC*, *mshD*, *mca* (Bae et al., 2004; Newton and Fahey, 2008; Park and Roe, 2008). In *C. glutamicum*, the homologous ECF sigma factor σ^H /RshA system controls the disulfide stress response genes for the Trx/TrxR system (*trxB*, *trxB1*, *trxC*) and for MSH biosynthesis and recycling (*mshC*, *mca*, *mtr*) (Ehira et al., 2009; Busche et al., 2012). The regulation of the Trx and MSH pathways by σ^R /RsrA or σ^H /RshA is conserved among Actinomycetes (Park and Roe, 2008; Antelmann and Helmann, 2011; Kim et al., 2012). Thus, it is common in Gram-positive bacteria that the genes for BSH and MSH biosynthesis pathways are under redox-control of the major disulfide stress regulators, Spx in Firmicutes bacteria and RsrA/RshA in Actinomycetes, respectively.

Functions of Mycothiol and MSH-Dependent Enzymes in Actinomycetes

MSH serves as the major thiol-redox buffer in Actinomycetes. MSH is oxidized to MSH disulfide (MSSM) under oxidative stress conditions. The mycothiol disulfide reductase Mtr maintains MSH in its reduced state at the expense of NADPH. MSH is involved in protection against oxidative and electrophile stress, alkylating agents, toxins, antibiotics (erythromycin, vancomycin, rifampin, azithromycin), heavy metal stress, aromatic compounds, ethanol and glyphosate in Streptomycetes, Mycobacteria and Corynebacteria (Buchmeier et al., 2003, 2006; Rawat et al., 2007; Newton et al., 2008; Liu et al., 2013) (Table 1). MSH is used as a cofactor for MSH-dependent enzymes during detoxification of toxins, electrophiles and antibiotics in Actinomycetes (Figure 9, Table 1). MSH forms conjugates with xenobiotics and antibiotics either spontaneously or by the DinB-family MSH S-transferases (Newton et al., 2011). The MSH S-transferase Mst of *M. smegmatis* was shown to catalyze the conjugation of monochlorobimane and DTNB to MSH but its natural substrate is not known (Newton et al., 2011). MSH-S-conjugates are rapidly cleaved by the MSH-S-conjugate amidase (Mca) to glucoseamine-myoinositol (GlcN-Ins) and mercapturic acid derivatives (AcCysSR) that are excreted from the cell. Mca is the major detoxification enzyme for MSH S-conjugates with antibiotics, including cerulenin and rifamycin in *Mycobacteria* (Newton et al., 2008, 2011). Interestingly, MSH and the Mca-homologs LmbT, LmbV and LmbE play also a direct role in the biosynthesis of the sulfur-containing lincosamide antibiotic

lincomycin in *Streptomyces lincolnensis* (Zhao et al., 2015). MSH functions as the sulfur donor for incorporation of the methylmercapto group into lincomycin after thiol exchange. In addition, ergothioneine (EGT), that is utilized as another thiol by Actinomycetes, acts as a carrier for the assembly of the N-methylated 4-propyl-L-proline (PPL) and lincosamide moieties to form lincomycin. EGT and MSH were shown to function in lincomycin biosynthesis through unusual S-glycosylations documenting a first biochemical role of LMW thiols in bacteria. Since the biosynthetic pathways for many sulfur-containing natural compounds include Mca homologs, the involvement of LMW thiols in natural product biosynthesis might be a common mechanism (Zhao et al., 2015).

MSH functions as a cofactor for many redox enzymes that are involved in the detoxification of peroxides, electrophiles (formaldehyde), NO, aromatic compounds (maleylpyruvate) and arsenate (Fahey, 2013) (Table 1). There is evidence for a MSH-peroxidase Mpx involved in peroxide detoxification that was identified as S-mycothiolated Gpx-homolog under oxidative stress in *C. glutamicum* (Chi et al., 2014). The MSH-dependent alcohol dehydrogenase MscR (MSNO reductase/formaldehyde dehydrogenase) catalyzes the detoxification of formaldehyde and S-nitrosyl-mycothiol (MSNO) (Newton et al., 2008). MSH reacts with formaldehyde to MS-CH₂OH that is converted to formate by MscR. MscR also converts MSNO to MSH sulfenamide (MSONH₂). In *C. glutamicum*, a similar MSH-dependent pathway for formaldehyde oxidation by the MSH-dependent formaldehyde dehydrogenase AdhE/FadH has been characterized (Lessmeier et al., 2013; Witthoff et al., 2013). In *C. glutamicum*, MSH is further involved in degradation of aromatic compounds, including gentisate, 3-hydroxybenzoate, maleylpyruvate, resorcinol, and naphthalene and *msh* mutants were unable to grow on these substrates (Liu et al., 2013). MSH functions as a cofactor for the maleylpyruvate isomerase in the gentisate ring-cleavage pathway to catalyze the isomerization of maleylpyruvate to fumaryl pyruvate in *C. glutamicum* (Feng et al., 2006). Similarly, MSH was suggested as a cofactor for enzymes of the naphthalene and resorcinol degradation pathway (Liu et al., 2013).

MSH confers resistance to metal ions, such as Cr(VI), Zn(II), Cd(II), Co(II), and Mn(II) in *C. glutamicum* (Liu et al., 2013). The detoxification of arsenate [As(V)] to arsenite [As(III)] depends on the MSH-dependent arsenate reductases ArsC1/C2 (Ordonez et al., 2009). ArsC1/C2 function similar to S-transferases in arsenate detoxification by formation of an arseno-MSH conjugate that requires the mycoredoxin-1/MSH/Mtr electron pathway for reduction. In contrast, another arsenate reductase Cg_ArsC1' detoxifies arsenate with electrons from the Trx pathway (Viladangos et al., 2011).

MSH enhanced also the robustness of *C. glutamicum* during industrial production of glutamate and L-lysine (Liu et al., 2014). The overexpression of *mshA* resulted in increased MSH biosynthesis and higher resistance of *C. glutamicum* to peroxides, methylglyoxal, antibiotics (erythromycin and streptomycin), metal ions, organic acids, furfural and ethanol (Liu et al., 2014). Thus, the increased biosynthesis of LMW thiol redox buffers, as shown for GSH in *C. acetobutylicum* and MSH in

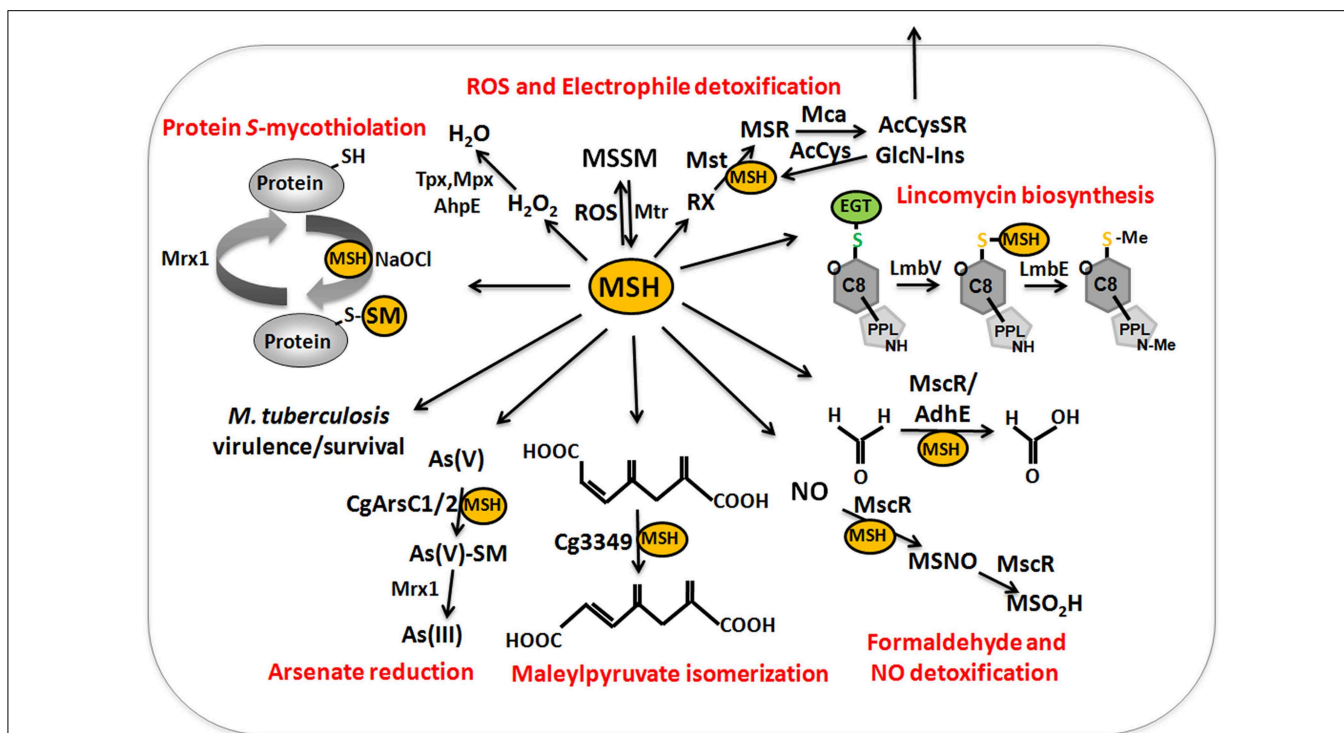


FIGURE 9 | The functions of mycothiol (MSH) in Mycobacteria and Corynebacteria. Mycothiol (MSH) is oxidized by ROS to mycothiol disulfide (MSSM). MSSM is reduced back to MSH by the mycothiol disulfide reductase Mtr on expense of NADPH. MSH-dependent peroxidases, such as Mpx, Tpx, and AhpE function in peroxide detoxification. Electrophiles (RX) are conjugated to MSH by the MSH S-transferase Mst to form MS-electrophiles (MSR) which are cleaved by the MSH S-conjugate amidase Mca to mercapturic acids (AcCysSR) that are exported from the cell. The Mca-homologs LmbT, LmbV, and LmbE function also in the assembly and biosynthesis of the sulfur-containing lincosamide antibiotic lincomycin in

Streptomyces lincolnensis (Zhao et al., 2015). MSH serves as a cofactor for the alcohol dehydrogenase AdhE/MscR in Mycobacteria and Corynebacteria for detoxification of formaldehyde to formate and MSNO to MSO₂H. MSH functions in detoxification of maleylpyruvate as a cofactor for maleylpyruvate isomerase in *C. glutamicum*. Arsenate reductases CgArsC1 and CgArsC2 conjugate MSH and arsenate As(V) to form As(V)-SM that is reduced to As(III) by Mrx1. In *M. tuberculosis*, MSH is important under infection conditions and for growth and survival. Under conditions of NaOCl stress, proteins are oxidized to mixed disulfides with MSH, termed as S-mycothiolations which is reversed by mycothiolase.

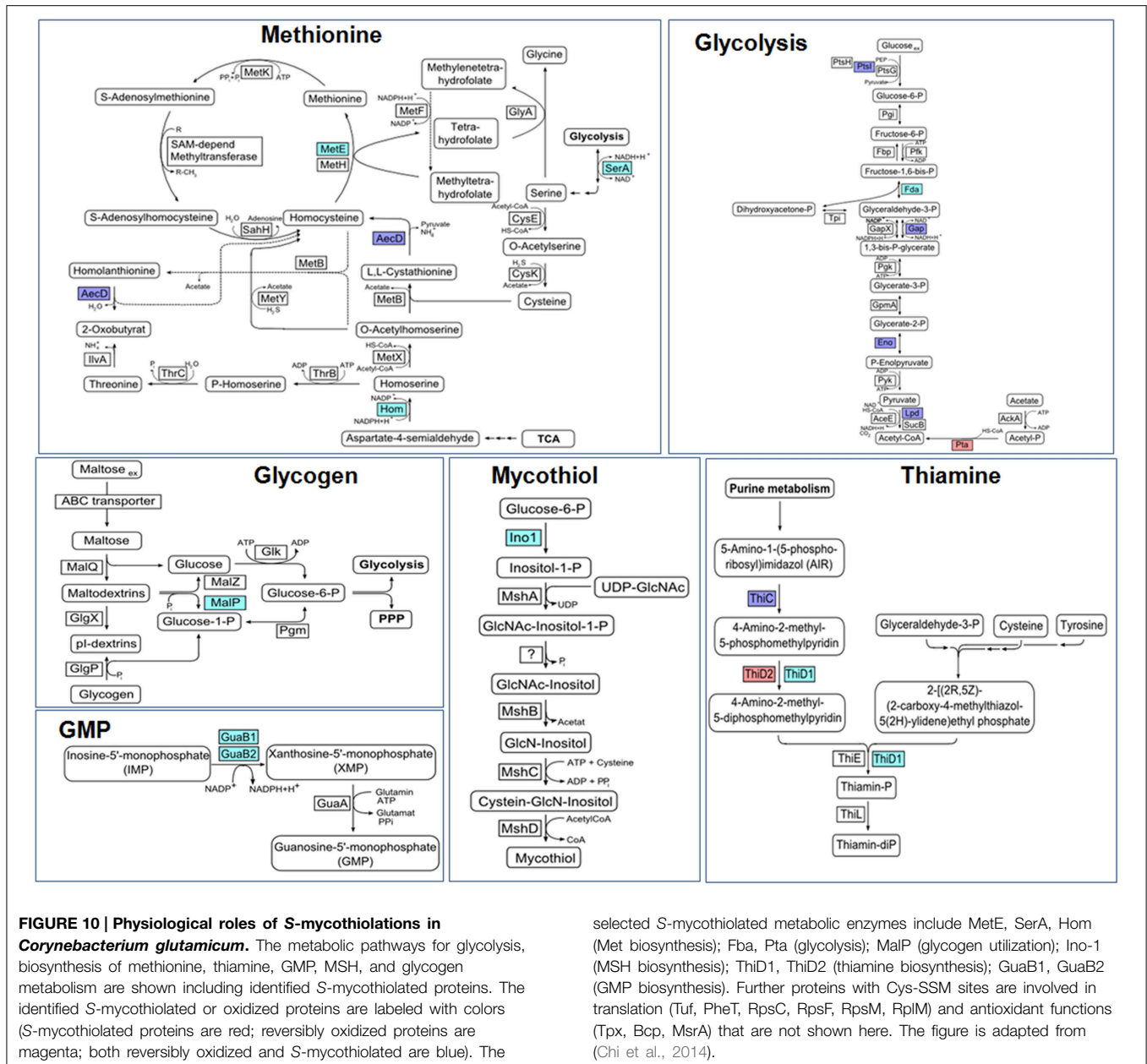
C. glutamicum, might be a promising strategy to engineer robust industrial production strains.

In *Mycobacterium tuberculosis*, MSH is essential for growth and survival of *M. tuberculosis* under infection conditions (Sareen et al., 2003; Sassetti and Rubin, 2003). In addition, MSH is required to activate the antituberculosis prodrug isoniazid and hence *M. tuberculosis mshA* mutants are resistant to isoniazid (Buchmeier et al., 2003). Tuberculosis (TB) causes still nearly 2 million death each year and multiple and extensive drug resistant strains occur that require new targets for antituberculosis drugs. Thus, inhibitors of MSH biosynthesis enzymes are promising candidates for antituberculosis drug developments. Several MSH biosynthesis inhibitors have been applied that target the MSH-S-conjugate amidase Mca, the deacetylase MshB, the cysteine ligase MshC and the MSSM reductase Mtr that are attractive antituberculosis drug targets (Nilewar and Kathiravan, 2014).

The Role of Protein S-Mycothiolation in Gram-Positive Actinomycetes

Protein S-mycothiolation was first studied in *C. glutamicum* and 25 S-mycothiolated proteins could be identified under NaOCl

stress by mass spectrometry (Chi et al., 2014) (Table 3). The thiol-peroxidase Tpx and the putative MSH peroxidase Mpx were S-mycothiolated under control and NaOCl stress conditions at their active site Cys residues. The fragment ion spectra of the S-mycothiolated Cys-peptides are characterized by diagnostic myoinositol-loss precursor ions (−180 Da) that serve as markers for identification. The 25 S-mycothiolated proteins overlap with 16 NaOCl-sensitive proteins identified in the fluorescent-label thiol-redox proteome. These include Tuf, GuaB1, GuaB2, SerA, and MetE as conserved abundant targets for S-thiolations across Gram-positive bacteria (Chi et al., 2013). The S-mycothiolated proteins are involved in the metabolism of carbohydrates, such as glycolysis (Fba, Pta, XylB), glycogen and maltodextrin degradation (MalP) and several biosynthesis pathways for serine, cysteine, methionine (SerA, Hom, MetE), nucleotides and thiamine (GuaB1, GuaB2, PurL, NadC, ThiD1, and ThiD2) and myo-inositol-1-phosphate (Ino-1 or Cg3323) (Figure 10). Further protein-SSM function in peroxide detoxification (Tpx, Gpx), methionine sulfoxide reduction (MsrA), heme degradation for iron mobilization (HmuO) and protein translation (RpsF, RpsC, RpsM, RplM, Tuf). The glycogen phosphorylase MalP is one of



selected S-mycothioliated metabolic enzymes include MetE, SerA, Hom (Met biosynthesis); Fba, Pta (glycolysis); MalP (glycogen utilization); Ino-1 (MSH biosynthesis); ThiD1, ThiD2 (thiamine biosynthesis); GuaB1, GuaB2 (GMP biosynthesis). Further proteins with Cys-SSM sites are involved in translation (Tuf, PheT, RpsC, RpsF, RpsM, RplM) and antioxidant functions (Tpx, Bcp, MsrA) that are not shown here. The figure is adapted from (Chi et al., 2014).

the most abundantly S-mycothioliated proteins in NaOCl-treated cells (Chi et al., 2014). S-mycothioliation of MalP is important for oxidative stress resistance in *C. glutamicum* since the *malP* deletion mutant is NaOCl-sensitive in growth assays. MalP functions in glycogen degradation during the stationary phase. S-mycothioliation of MalP may prevent glycogen degradation under NaOCl stress since the glycogen content remained stable despite a strongly decreased glucose uptake rate.

The mycoredoxin-1 (Mrx1) has been characterized as glutaredoxin-homolog of Actinomycetes in reduction of MSH mixed disulfides (Van Laer et al., 2012) (Figure 8). Mrx-1 has a typical Trx-like fold with a CGYC motif and a *cis*-Pro57 in a groove that presumable binds MSH. The redox potential of

Mrx-1 was calculated as $E^0 = -218 \text{ mV}$ and the pK_a of the active site Cys17 was 5.1–5.6. Mrx-1 catalyzed de-mycothioliation in a hydroxyethyl disulfide (HED) assay and is coupled to the MSH/Mtr/NADPH pathway. Mrx-1 operates via a monothiol reaction mechanism in the de-mycothioliation reaction analogous to most glutaredoxins that are involved in de-glutathionylation. The first Mrx1 substrate was identified as the thiol-peroxidase Tpx that was S-mycothioliated at its active site Cys60 and resolving site Cys94 in *C. glutamicum* *in vivo* under hypochlorite stress (Chi et al., 2014). Tpx showed NADPH-linked peroxidase activity and reduced H_2O_2 in a Trx/TrxR-coupled electron assay. S-mycothioliation of Tpx inhibits the peroxidase activity which was restored after reduction by the Mrx1/MSH/Mtr pathway. Thus,

S-mycothiolation controls Tpx activity and protects the peroxidic Cys against overoxidation. In *M. tuberculosis*, Mrx1 has been shown to reduce the one-Cys peroxidase AhpE (Hugo et al., 2014). AhpE is a membrane-associated peroxidase that detoxifies peroxynitrite and fatty acid hydroperoxides as preferred substrates (Hugo et al., 2009; Reyes et al., 2011). AhpE is oxidized by peroxides to form a sulfenic acid intermediate (AhpE-SOH) that can be reduced directly by Mrx1. Alternatively, AhpE-SOH can react with MSH to S-mycothiolated AhpE-SSM which is reduced by the Mrx1/MSH/Mtr electron pathway (Hugo et al., 2014). The direct AhpE-SOH reduction may occur in the membrane when MSH is not available and the formation of AhpE-SSM and subsequent Mrx1-reduction was suggested to predominate in the cytosol. Interestingly, the reducing mechanism of AhpE-SSM is similar to the detoxification of arsenate by CgArsC1 and CgArsC2. Arsenate reacts with MSH to an arseno-(V)-MSH complex that is reduced by Mrx1 releasing As(III) and Mrx1-SSM that is recycled by the MSH/Mtr/NADPH electron pathway (Ordonez et al., 2009; Villadangos et al., 2011). It remains to be shown if AhpE is mycothiolated under oxidative stress in *M. tuberculosis* cells *in vivo*. These results show that Mrx1 functions as glutaredoxin homolog in *C. glutamicum* and *M. tuberculosis* in the reduction of S-mycothiolated peroxidases (Tpx and AhpE), when coupled to the MSH/Mtr/NADPH electron pathway and as electron donor for arsenate reductase in arsenate detoxification.

Recently, Mrx1 has been coupled to redox sensitive GFP (roGFP2) to construct a new genetically encoded biosensor for dynamic measurements of the MSH redox potential in different *M. tuberculosis* strains (Bhaskar et al., 2014). This study revealed phenotypic redox heterogeneity of E^0 (MSSM/MSH) within Mycobacteria inside infected macrophages that are caused by sub-vacuolar compartments. Those sub-populations with higher E^0 (MSSM/MSH) were more susceptible to clinical relevant antibiotics whereas populations with lower MSH redox potentials were resistant to antibiotics. The results further show that several anti-TB drugs induce oxidative stress in *M. tuberculosis* during infections. In conclusion, this Mrx1-roGFP2 biosensor is a promising tool to study MSH redox potential changes of *M. tuberculosis* under infections and antibiotic treatments. This is the first example for a genetically encoded redox biosensor that measures dynamic changes of the mycothiol redox potential in bacteria. Future studies should be directed to apply similar biosensors in other pathogenic bacteria to study the dynamics of redox potential changes during infections.

Conclusion and Perspectives for Future Research

In this review, we provide an overview about the biosynthesis pathways and functions of the bacterial redox buffers glutathione, bacillithiol and mycothiol and their regulatory roles for protein S-thiolations. Bacterial redox buffers maintain the reduced state of the cytoplasm and function as cofactors of conserved enzymes for detoxification of ROS, RES, chlorines, antibiotics and xenobiotics. These thiol-dependent enzymes include

NADPH-dependent disulfide reductases (Gor, Mtr, YpdA) and related glutaredoxin-like enzymes (Grx, Mrx, Brx), DinB-family S-transferases (Gst, Mst, BstA), S-conjugate amidases (Mca, Bca) and glyoxalases (GloAB, GlxAB). However, some detoxification enzymes still need to be characterized in BSH-utilizing bacteria, including the BSH-dependent formaldehyde reductase (AdhA), the putative BSH peroxidase (Bpx) or thiol-dependent dioxygenases (MhqA, MhqE and MhqO) (Antelmann et al., 2008). The discovery of the biochemical functions of MSH, EGT and S-transferases in the lincomycin antibiotic biosynthesis opens perspectives to characterize the roles of thiol-redox buffers in the biosynthesis of sulfur-containing co-factors, natural compounds and antibiotics in other bacteria.

The structures of BSH and MSH are similar and the BSH biosynthesis enzymes BshA, BshB and BshC are homologous to the MSH biosynthesis enzymes MshA, MshB, and MshC. However, the crystal structure of BshC has revealed significant differences compared to MshC which requires further studies to understand the still unknown cysteine ligation mechanism of BshC (Vanduinen et al., 2015). It is further interesting, that the levels of BSH and MSH vary strongly between Firmicutes and Actinomycetes and also during growth and stress conditions. While Mycobacteria produce up to 20 mM MSH, the levels of BSH are much lower reaching 1–6 mM in Firmicutes bacteria. The differences in BSH and MSH levels during growth and under stress can be explained by the redox control of the BSH and MSH biosynthesis enzymes by the major thiol-based redox sensors (Spx and RsrA/RshA), presumably to enhance the redox buffer capacity under certain conditions to keep the reduced state of the cytoplasm. In contrast, redox regulation of GSH biosynthesis genes has not been shown. However, the pathogen *L. monocytogenes* is able to synthesize GSH and to import host-derived GSH as adaptation strategy under infection conditions (Reniere et al., 2015). Importantly, synthesized and host-derived GSH both contribute to virulence factor regulation in *L. monocytogenes*, while GSH-import was required for full virulence in *S. pneumoniae* (Potter et al., 2012; Reniere et al., 2015). Overall, the roles of GSH, BSH and MSH for virulence and pathogen fitness have been shown for many important human pathogens, including *L. monocytogenes*, *S. pneumoniae*, *S. Typhimurium*, *S. aureus*, and *M. tuberculosis*. Future studies in the field of infection biology should be directed to understand the molecular mechanisms of virulence factor regulation by thiol-redox buffers that might involve also protein S-thiolation mechanisms. The GSH, BSH and MSH biosynthesis enzymes, GSH uptake systems as well as S-thiolated proteins could be promising drug targets for the development of novel anti-infectives against emerging drug resistant strains of *S. pneumoniae*, *S. aureus* and *M. tuberculosis*. Thus, the large scale identification and quantification of S-thiolated proteins in pathogens is an important topic for future research.

Advances in mass spectrometry and chemical probe design have facilitated the development of more sensitive redox proteomics methods, such as the NEM-biotin switch assay or the Gsp-biotin assay to study targets for protein S-glutathionylation at a global scale (Lind et al., 2002; Kehr et al., 2011; Lin et al.,

2015). In addition, numerous BSH- and MSH-mixed protein disulfides have been identified recently under disulfide stress conditions, such as NaOCl and diamide. However, more quantitative MS-based redox proteomics approaches are required to determine the level of mixed BSH- and MSH-protein disulfides by combining the direct shotgun approach with OxICAT or the NEM-biotin switch assay coupled to Brx or Mrx1 (Leichert et al., 2008; Kehr et al., 2011). In addition, the regulatory roles for only few S-bacillithiolated and S-mycothioloated proteins have been studied thus far, including the redox regulator OhrR and the methionine synthase MetE (Lee et al., 2007; Chi et al., 2011). However, many interesting metabolic enzymes, redox-sensing transcription factors or virulence factors might be controlled by

protein S-thiolations in the pathogenic bacteria *S. aureus* and *M. tuberculosis* that remain to be elucidated in future research. Thus, it is an exciting field for new frontiers of science to unravel the regulatory potential of emerging protein S-thiolations in bacteria.

Acknowledgments

This work was supported by grants from the Deutsche Forschungsgemeinschaft (DFG) AN746/3-1 and AN746/4-1 within the DFG priority program SPP1710, by the DFG Research Training Group GRK1947, project [C1] and by an ERC Consolidator Grant (GA 615585) MYCOTHIOLOME to H.A.

References

- Allen, E. M., and Mielay, J. J. (2012). Protein-thiol oxidation and cell death: regulatory role of glutaredoxins. *Antioxid. Redox Signal.* 17, 1748–1763. doi: 10.1089/ars.2012.4644
- Anderson, M. E. (1998). Glutathione: an overview of biosynthesis and modulation. *Chem. Biol. Interact.* 111–112, 1–14. doi: 10.1016/S0009-2797(97)00146-4
- Ansong, C., Wu, S., Meng, D., Liu, X., Brewer, H. M., Deatherage Kaiser, B. L., et al. (2013). Top-down proteomics reveals a unique protein S-thiolation switch in *Salmonella* Typhimurium in response to infection-like conditions. *Proc. Natl. Acad. Sci. U.S.A.* 110, 10153–10158. doi: 10.1073/pnas.1221210110
- Antelmann, H., Hecker, M., and Zuber, P. (2008). Proteomic signatures uncover thiol-specific electrophile resistance mechanisms in *Bacillus subtilis*. *Expert Rev. Proteomics* 5, 77–90. doi: 10.1586/14789450.5.1.77
- Antelmann, H., and Helmman, J. D. (2011). Thiol-based redox switches and gene regulation. *Antioxid. Redox Signal.* 14, 1049–1063. doi: 10.1089/ars.2010.3400
- Aslund, F., Ehn, B., Miranda-Vizuete, A., Pueyo, C., and Holmgren, A. (1994). Two additional glutaredoxins exist in *Escherichia coli*: glutaredoxin 3 is a hydrogen donor for ribonucleotide reductase in a thioredoxin/glutaredoxin 1 double mutant. *Proc. Natl. Acad. Sci. U.S.A.* 91, 9813–9817. doi: 10.1073/pnas.91.21.9813
- Atichartpongkul, S., Loprasert, S., Vattanaviboon, P., Whangsuk, W., Helmman, J. D., and Mongkolsuk, S. (2001). Bacterial Ohr and OsmC paralogues define two protein families with distinct functions and patterns of expression. *Microbiology* 147, 1775–1782.
- Bae, J. B., Park, J. H., Hahn, M. Y., Kim, M. S., and Roe, J. H. (2004). Redox-dependent changes in RsrA, an anti-sigma factor in *Streptomyces coelicolor*: zinc release and disulfide bond formation. *J. Mol. Biol.* 335, 425–435. doi: 10.1016/j.jmb.2003.10.065
- Bartsch, R. G., Newton, G. L., Sherrill, C., and Fahey, R. C. (1996). Glutathione amide and its perthiol in anaerobic sulfur bacteria. *J. Bacteriol.* 178, 4742–4746.
- Bhaskar, A., Chawla, M., Mehta, M., Parikh, P., Chandra, P., Bhawe, D., et al. (2014). Reengineering redox sensitive GFP to measure mycothiol redox potential of *Mycobacterium tuberculosis* during infection. *PLoS Pathog.* 10:e1003902. doi: 10.1371/journal.ppat.1003902
- Booth, I. R., Ferguson, G. P., Miller, S., Li, C., Gunasekera, B., and Kinghorn, S. (2003). Bacterial production of methylglyoxal: a survival strategy or death by misadventure? *Biochem. Soc. Trans.* 31, 1406–1408.
- Bourajjaj, M., Stehouwer, C. D., Van Hinsbergh, V. W., and Schalkwijk, C. G. (2003). Role of methylglyoxal adducts in the development of vascular complications in diabetes mellitus. *Biochem. Soc. Trans.* 31, 1400–1402. doi: 10.1042/BST0311400
- Brandes, N., Schmitt, S., and Jakob, U. (2009). Thiol-based redox switches in eukaryotic proteins. *Antioxid. Redox Signal.* 11, 997–1014. doi: 10.1089/ars.2008.2285
- Brennan, J. P., Miller, J. I., Fuller, W., Wait, R., Begum, S., Dunn, M. J., et al. (2006). The utility of N,N-biotinyl glutathione disulfide in the study of protein S-glutathiolation. *Mol. Cell. Proteomics* 5, 215–225. doi: 10.1074/mcp.M500212-MCP200
- Buchmeier, N. A., Newton, G. L., and Fahey, R. C. (2006). A mycothiol synthase mutant of *Mycobacterium tuberculosis* has an altered thiol-disulfide content and limited tolerance to stress. *J. Bacteriol.* 188, 6245–6252. doi: 10.1128/JB.00393-06
- Buchmeier, N. A., Newton, G. L., Koledin, T., and Fahey, R. C. (2003). Association of mycothiol with protection of *Mycobacterium tuberculosis* from toxic oxidants and antibiotics. *Mol. Microbiol.* 47, 1723–1732. doi: 10.1046/j.1365-2958.2003.03416.x
- Busche, T., Silar, R., Picmanova, M., Patek, M., and Kalinowski, J. (2012). Transcriptional regulation of the operon encoding stress-responsive ECF sigma factor SigH and its anti-sigma factor RshA, and control of its regulatory network in *Corynebacterium glutamicum*. *BMC Genomics* 13:445. doi: 10.1186/1471-2164-13-445
- Cassier-Chauvat, C., Veaudor, T., and Chauvat, F. (2014). Advances in the function and regulation of hydrogenase in the cyanobacterium *Synechocystis* PCC6803. *Int. J. Mol. Sci.* 15, 19938–19951. doi: 10.3390/ijms151119938
- Castellano, I., Ruocco, M. R., Cecere, F., Di Maro, A., Chambéry, A., Michniewicz, A., et al. (2008). Glutathionylation of the iron superoxide dismutase from the psychrophilic eubacterium *Pseudoalteromonas haloplanktis*. *Biochim. Biophys. Acta* 1784, 816–826. doi: 10.1016/j.bbapap.2008.02.003
- Chandrangsu, P., Dusi, R., Hamilton, C. J., and Helmman, J. D. (2014). Methylglyoxal resistance in *Bacillus subtilis*: contributions of bacillithiol-dependent and independent pathways. *Mol. Microbiol.* 91, 706–715. doi: 10.1111/mmi.12489
- Chardonnet, S., Sakr, S., Cassier-Chauvat, C., Le Marechal, P., Chauvat, F., Lemaire, S. D., et al. (2015). First proteomic study of S-glutathionylation in cyanobacteria. *J. Proteome Res.* 14, 59–71. doi: 10.1021/pr500625a
- Chen, N. H., Counago, R. M., Djoko, K. Y., Jennings, M. P., Apicella, M. A., Kobe, B., et al. (2013). A glutathione-dependent detoxification system is required for formaldehyde resistance and optimal survival of *Neisseria meningitidis* in biofilms. *Antioxid. Redox Signal.* 18, 743–755. doi: 10.1089/ars.2012.4749
- Chi, B. K., Busche, T., Van Laer, K., Basell, K., Becher, D., Clermont, L., et al. (2014). Protein S-mycothioloation functions as redox-switch and thiol protection mechanism in *Corynebacterium glutamicum* under hypochlorite stress. *Antioxid. Redox Signal.* 20, 589–605. doi: 10.1089/ars.2013.5423
- Chi, B. K., Gronau, K., Mader, U., Hessling, B., Becher, D., and Antelmann, H. (2011). S-bacillithiolation protects against hypochlorite stress in *Bacillus subtilis* as revealed by transcriptomics and redox proteomics. *Mol. Cell. Proteomics* 10, M111.009506. doi: 10.1074/mcp.M111.009506
- Chi, B. K., Roberts, A. A., Huyen, T. T., Basell, K., Becher, D., Albrecht, D., et al. (2013). S-bacillithiolation protects conserved and essential proteins against hypochlorite stress in firmicutes bacteria. *Antioxid. Redox Signal.* 18, 1273–1295. doi: 10.1089/ars.2012.4686
- Chiang, B. Y., Chou, C. C., Hsieh, F. T., Gao, S., Lin, J. C., Lin, S. H., et al. (2012). *In vivo* tagging and characterization of S-glutathionylated proteins by a chemoenzymatic method. *Angew. Chem. Int. Ed Engl.* 51, 5871–5875. doi: 10.1002/anie.201200321
- Dalle-Donne, I., Rossi, R., Colombo, G., Giustarini, D., and Milzani, A. (2009). Protein S-glutathionylation: a regulatory device from bacteria to humans. *Trends Biochem. Sci.* 34, 85–96. doi: 10.1016/j.tibs.2008.11.002

- Dalle-Donne, I., Rossi, R., Giustarini, D., Colombo, R., and Milzani, A. (2007). S-glutathionylation in protein redox regulation. *Free Radic. Biol. Med.* 43, 883–898. doi: 10.1016/j.freeradbiomed.2007.06.014
- Davies, M. J. (2011). Myeloperoxidase-derived oxidation: mechanisms of biological damage and its prevention. *J. Clin. Biochem. Nutr.* 48, 8–19. doi: 10.3164/jcfn.11-006FR
- De Mendoza, D. (2014). Temperature sensing by membranes. *Annu. Rev. Microbiol.* 68, 101–116. doi: 10.1146/annurev-micro-091313-103612
- Derewenda, U., Boczek, T., Gorres, K. L., Yu, M., Hung, L. W., Cooper, D., et al. (2009). Structure and function of *Bacillus subtilis* YphP, a prokaryotic disulfide isomerase with a CXC catalytic motif. *Biochemistry* 48, 8664–8671. doi: 10.1021/bi900437z
- Ehira, S., Teramoto, H., Inui, M., and Yukawa, H. (2009). Regulation of *Corynebacterium glutamicum* heat shock response by the extracytoplasmic-function sigma factor SigH and transcriptional regulators HspR and HrcA. *J. Bacteriol.* 191, 2964–2972. doi: 10.1128/JB.00112-09
- Fahey, R. C. (2013). Glutathione analogs in prokaryotes. *Biochim. Biophys. Acta* 1830, 3182–3198. doi: 10.1016/j.bbagen.2012.10.006
- Fang, Z., Roberts, A. A., Weidman, K., Sharma, S. V., Claiborne, A., Hamilton, C. J., et al. (2013). Cross functionalities of *Bacillus deacetylases* involved in bacillithiol biosynthesis and bacillithiol-S-conjugate detoxification pathways. *Biochem. J.* doi: 10.1042/BJ20130415
- Farrand, S. K., and Taber, H. W. (1974). Changes in menaquinone concentration during growth and early sporulation in *Bacillus subtilis*. *J. Bacteriol.* 117, 324–326.
- Feng, J., Che, Y., Milse, J., Yin, Y. J., Liu, L., Ruckert, C., et al. (2006). The gene ncg12918 encodes a novel maleylpyruvate isomerase that needs mycothiol as cofactor and links mycothiol biosynthesis and gentisate assimilation in *Corynebacterium glutamicum*. *J. Biol. Chem.* 281, 10778–10785. doi: 10.1074/jbc.M513192200
- Ferguson, G. P., Totemeyer, S., Maclean, M. J., and Booth, I. R. (1998). Methylglyoxal production in bacteria: suicide or survival? *Arch. Microbiol.* 170, 209–218.
- Fernandes, A. P., and Holmgren, A. (2004). Glutaredoxins: glutathione-dependent redox enzymes with functions far beyond a simple thioredoxin backup system. *Antioxid. Redox Signal.* 6, 63–74. doi: 10.1089/152308604771978354
- Forman, H. J., and Torres, M. (2001). Redox signaling in macrophages. *Mol. Aspects Med.* 22, 189–216. doi: 10.1016/S0098-2997(01)00010-3
- Fratelli, M., Demol, H., Puype, M., Casagrande, S., Eberini, I., Salmons, M., et al. (2002). Identification by redox proteomics of glutathionylated proteins in oxidatively stressed human T lymphocytes. *Proc. Natl. Acad. Sci. U.S.A.* 99, 3505–3510. doi: 10.1073/pnas.052592699
- Fratelli, M., Demol, H., Puype, M., Casagrande, S., Villa, P., Eberini, I., et al. (2003). Identification of proteins undergoing glutathionylation in oxidatively stressed hepatocytes and hepatoma cells. *Proteomics* 3, 1154–1161. doi: 10.1002/pmic.200300436
- Fratelli, M., Gianazza, E., and Ghezzi, P. (2004). Redox proteomics: identification and functional role of glutathionylated proteins. *Expert Rev. Proteomics* 1, 365–376. doi: 10.1586/14789450.1.3.365
- Freitag, N. E., Port, G. C., and Miner, M. D. (2009). *Listeria monocytogenes* – from saprophyte to intracellular pathogen. *Nat. Rev. Microbiol.* 7, 623–628. doi: 10.1038/nrmicro2171
- Fuangthong, M., Atichartpongkul, S., Mongkolsuk, S., and Helmann, J. D. (2001). OhrR is a repressor of ohrA, a key organic hydroperoxide resistance determinant in *Bacillus subtilis*. *J. Bacteriol.* 183, 4134–4141. doi: 10.1128/JB.183.14.4134-4141.2001
- Gaballa, A., Antelmann, H., Hamilton, C. J., and Helmann, J. D. (2013). Regulation of *Bacillus subtilis* bacillithiol biosynthesis operons by SpX. *Microbiology* 159, 2025–2035. doi: 10.1099/mic.0.070482-0
- Gaballa, A., Chi, B. K., Roberts, A. A., Becher, D., Hamilton, C. J., Antelmann, H., et al. (2014). Redox regulation in *Bacillus subtilis*: the bacilliredoxins BrxA(YphP) and BrxB(YqiW) function in de-bacillithiolation of S-bacillithiolated OhrR and MetE. *Antioxid. Redox Signal.* 21, 357–367. doi: 10.1089/ars.2013.5327
- Gaballa, A., Newton, G. L., Antelmann, H., Parsonage, D., Upton, H., Rawat, M., et al. (2010). Biosynthesis and functions of bacillithiol, a major low-molecular-weight thiol in Bacilli. *Proc. Natl. Acad. Sci. U.S.A.* 107, 6482–6486. doi: 10.1073/pnas.1000928107
- Gallogly, M. M., and Mieyal, J. J. (2007). Mechanisms of reversible protein glutathionylation in redox signaling and oxidative stress. *Curr. Opin. Pharmacol.* 7, 381–391. doi: 10.1016/j.coph.2007.06.003
- Ghezzi, P. (2005). Regulation of protein function by glutathionylation. *Free Radic. Res.* 39, 573–580. doi: 10.1080/10715760500072172
- Ghezzi, P. (2013). Protein glutathionylation in health and disease. *Biochim. Biophys. Acta* 1830, 3165–3172. doi: 10.1016/j.bbagen.2013.02.009
- Gopal, S., Borovok, I., Ofer, A., Yanku, M., Cohen, G., Goebel, W., et al. (2005). A multidomain fusion protein in *Listeria monocytogenes* catalyzes the two primary activities for glutathione biosynthesis. *J. Bacteriol.* 187, 3839–3847. doi: 10.1128/JB.187.11.3839-3847.2005
- Gray, M. J., Wholey, W. Y., and Jakob, U. (2013a). Bacterial responses to reactive chlorine species. *Annu. Rev. Microbiol.* 67, 141–160. doi: 10.1146/annurev-micro-102912-142520
- Gray, M. J., Wholey, W. Y., Parker, B. W., Kim, M., and Jakob, U. (2013b). NemR is a bleach-sensing transcription factor. *J. Biol. Chem.* 288, 13789–13798. doi: 10.1074/jbc.M113.454421
- Gupta, V., and Carroll, K. S. (2014). Sulfenic acid chemistry, detection and cellular lifetime. *Biochim. Biophys. Acta* 1840, 847–875. doi: 10.1016/j.bbagen.2013.05.040
- Handtke, S., Schroeter, R., Jurgen, B., Methling, K., Schluter, R., Albrecht, D., et al. (2014). *Bacillus pumilus* reveals a remarkably high resistance to hydrogen peroxide provoked oxidative stress. *PLoS ONE* 9:e85625. doi: 10.1371/journal.pone.0085625
- Hawkins, C. L., Pattison, D. I., and Davies, M. J. (2003). Hypochlorite-induced oxidation of amino acids, peptides and proteins. *Amino Acids* 25, 259–274. doi: 10.1007/s00726-003-0016-x
- Helmann, J. D. (2011). Bacillithiol, a new player in bacterial redox homeostasis. *Antioxid. Redox Signal.* 15, 123–133. doi: 10.1089/ars.2010.3562
- Holmgren, A. (1976). Hydrogen donor system for *Escherichia coli* ribonucleoside-diphosphate reductase dependent upon glutathione. *Proc. Natl. Acad. Sci. U.S.A.* 73, 2275–2279. doi: 10.1073/pnas.73.7.2275
- Holmgren, A. (1981). Regulation of ribonucleotide reductase. *Curr. Top. Cell. Regul.* 19, 47–76. doi: 10.1016/B978-0-12-152819-5.50019-1
- Hondorp, E. R., and Matthews, R. G. (2004). Oxidative stress inactivates cobalamin-independent methionine synthase (MetE) in *Escherichia coli*. *PLoS Biol.* 2:e336. doi: 10.1371/journal.pbio.0020336
- Hou, X., Peng, W., Xiong, L., Huang, C., Chen, X., and Zhang, W. (2013). Engineering *Clostridium acetobutylicum* for alcohol production. *J. Biotechnol.* 166, 25–33. doi: 10.1016/j.jbiotec.2013.04.013
- Hugo, M., Turell, L., Manta, B., Botti, H., Monteiro, G., Netto, L. E., et al. (2009). Thiol and sulfenic acid oxidation of AhpE, the one-cysteine peroxiredoxin from *Mycobacterium tuberculosis*: kinetics, acidity constants, and conformational dynamics. *Biochemistry* 48, 9416–9426. doi: 10.1021/bi901221s
- Hugo, M., Van Laer, K., Reyes, A. M., Vertommen, D., Messens, J., Radi, R., et al. (2014). Mycothiol/mycoredoxin 1-dependent reduction of the peroxiredoxin AhpE from *Mycobacterium tuberculosis*. *J. Biol. Chem.* 289, 5228–5239. doi: 10.1074/jbc.M113.510248
- Hwang, C., Lodish, H. F., and Sinskey, A. J. (1995). Measurement of glutathione redox state in cytosol and secretory pathway of cultured cells. *Meth. Enzymol.* 251, 212–221. doi: 10.1016/0076-6879(95)51123-7
- Imlay, J. A. (2003). Pathways of oxidative damage. *Annu. Rev. Microbiol.* 57, 395–418. doi: 10.1146/annurev.micro.57.030502.090938
- Imlay, J. A. (2008). Cellular defenses against superoxide and hydrogen peroxide. *Annu. Rev. Biochem.* 77, 755–776. doi: 10.1146/annurev.biochem.77.061606.161055
- Imlay, J. A. (2013). The molecular mechanisms and physiological consequences of oxidative stress: lessons from a model bacterium. *Nat. Rev. Microbiol.* 11, 443–454. doi: 10.1038/nrmicro3032
- Inaba, K. (2009). Disulfide bond formation system in *Escherichia coli*. *J. Biochem.* 146, 591–597. doi: 10.1093/jb/mvp102
- Jacobs, A. T., and Marnett, L. J. (2010). Systems analysis of protein modification and cellular responses induced by electrophile stress. *Acc. Chem. Res.* 43, 673–683. doi: 10.1021/ar900286y
- Janowiak, B. E., and Griffith, O. W. (2005). Glutathione synthesis in *Streptococcus agalactiae*. One protein accounts for gamma-glutamylcysteine synthetase and glutathione synthetase activities. *J. Biol. Chem.* 280, 11829–11839. doi: 10.1074/jbc.M414326200

- Jothivasan, V. K., and Hamilton, C. J. (2008). Mycothiol: synthesis, biosynthesis and biological functions of the major low molecular weight thiol in actinomycetes. *Nat. Prod. Rep.* 25, 1091–1117. doi: 10.1039/b616489g
- Kalapos, M. P. (2008). The tandem of free radicals and methylglyoxal. *Chem. Biol. Interact.* 171, 251–271. doi: 10.1016/j.cbi.2007.11.009
- Kehr, S., Jortzik, E., Delahunty, C., Yates, J. R. III, Rahlfs, S., and Becker, K. (2011). Protein S-glutathionylation in malaria parasites. *Antioxid. Redox Signal.* 15, 2855–2865. doi: 10.1089/ars.2011.4029
- Kim, M. S., Dufour, Y. S., Yoo, J. S., Cho, Y. B., Park, J. H., Nam, G. B., et al. (2012). Conservation of thiol-oxidative stress responses regulated by SigR orthologues in actinomycetes. *Mol. Microbiol.* 85, 326–344. doi: 10.1111/j.1365-2958.2012.08115.x
- Kim, S. O., Merchant, K., Nudelman, R., Beyer, W. F. Jr., Keng, T., Deangelo, J., et al. (2002). OxyR: a molecular code for redox-related signaling. *Cell* 109, 383–396. doi: 10.1016/S0092-8674(02)00723-7
- Klatt, P., and Lamas, S. (2000). Regulation of protein function by S-glutathiolation in response to oxidative and nitrosative stress. *Eur. J. Biochem.* 267, 4928–4944. doi: 10.1046/j.1432-1327.2000.01601.x
- Lamers, A. P., Keithly, M. E., Kim, K., Cook, P. D., Stec, D. F., Hines, K. M., et al. (2012). Synthesis of bacillithiol and the catalytic selectivity of FosB-type fosfomycin resistance proteins. *Org. Lett.* 14, 5207–5209. doi: 10.1021/ol302327t
- Lee, C., Shin, J., and Park, C. (2013). Novel regulatory system nemRA-gloA for electrophile reduction in *Escherichia coli* K-12. *Mol. Microbiol.* 88, 395–412. doi: 10.1111/mmi.12192
- Lee, J. W., Soonsanga, S., and Helmann, J. D. (2007). A complex thiolate switch regulates the *Bacillus subtilis* organic peroxide sensor OhrR. *Proc. Natl. Acad. Sci. U.S.A.* 104, 8743–8748. doi: 10.1073/pnas.0702081104
- Leichert, L. I., Gehrke, F., Gudiseva, H. V., Blackwell, T., Ilbert, M., Walker, A. K., et al. (2008). Quantifying changes in the thiol redox proteome upon oxidative stress *in vivo*. *Proc. Natl. Acad. Sci. U.S.A.* 105, 8197–8202. doi: 10.1073/pnas.0707723105
- Leonard, S. E., and Carroll, K. S. (2011). Chemical ‘omics’ approaches for understanding protein cysteine oxidation in biology. *Curr. Opin. Chem. Biol.* 15, 88–102. doi: 10.1016/j.cbpa.2010.11.012
- Lessmeier, L., Hoefener, M., and Wendisch, V. F. (2013). Formaldehyde degradation in *Corynebacterium glutamicum* involves acetaldehyde dehydrogenase and mycothiol-dependent formaldehyde dehydrogenase. *Microbiology* 159, 2651–2662. doi: 10.1099/mic.0.072413-0
- Liebeke, M., Pother, D. C., Van Duy, N., Albrecht, D., Becher, D., Hochgrafe, F., et al. (2008). Depletion of thiol-containing proteins in response to quinones in *Bacillus subtilis*. *Mol. Microbiol.* 69, 1513–1529. doi: 10.1111/j.1365-2958.2008.06382.x
- Lillig, C. H., Berndt, C., and Holmgren, A. (2008). Glutaredoxin systems. *Biochim. Biophys. Acta* 1780, 1304–1317. doi: 10.1016/j.bbagen.2008.06.003
- Lillig, C. H., Potamitou, A., Schwenn, J. D., Vlamis-Gardikas, A., and Holmgren, A. (2003). Redox regulation of 3'-phosphoadenylylsulfate reductase from *Escherichia coli* by glutathione and glutaredoxins. *J. Biol. Chem.* 278, 22325–22330. doi: 10.1074/jbc.M302304200
- Lin, J. C., Chiang, B. Y., Chou, C. C., Chen, T. C., Chen, Y. J., and Lin, C. H. (2015). Glutathionylspermidine in the modification of protein SH groups: the enzymology and its application to study protein glutathionylation. *Molecules* 20, 1452–1474. doi: 10.3390/molecules20011452
- Lind, C., Gerdes, R., Hammell, Y., Schuppe-Koistinen, I., Von Lowenhielm, H. B., Holmgren, A., et al. (2002). Identification of S-glutathionylated cellular proteins during oxidative stress and constitutive metabolism by affinity purification and proteomic analysis. *Arch. Biochem. Biophys.* 406, 229–240. doi: 10.1016/S0003-9861(02)00468-X
- Liu, Y. B., Chen, C., Chaudhry, M. T., Si, M. R., Zhang, L., Wang, Y., et al. (2014). Enhancing *Corynebacterium glutamicum* robustness by over-expressing a gene, mshA, for mycothiol glycosyltransferase. *Biotechnol. Lett.* 36, 1453–1459. doi: 10.1007/s10529-014-1501-x
- Liu, Y. B., Long, M. X., Yin, Y. J., Si, M. R., Zhang, L., Lu, Z. Q., et al. (2013). Physiological roles of mycothiol in detoxification and tolerance to multiple poisonous chemicals in *Corynebacterium glutamicum*. *Arch. Microbiol.* 195, 419–429. doi: 10.1007/s00203-013-0889-3
- Lowther, W. T., and Haynes, A. C. (2011). Reduction of cysteine sulfenic acid in eukaryotic, typical 2-Cys peroxidoredoxins by sulfiredoxin. *Antioxid. Redox Signal.* 15, 99–109. doi: 10.1089/ars.2010.3564
- Ma, Z., Chandransu, P., Helmann, T. C., Romsang, A., Gaballa, A., and Helmann, J. D. (2014). Bacillithiol is a major buffer of the labile zinc pool in *Bacillus subtilis*. *Mol. Microbiol.* 94, 756–770. doi: 10.1111/mmi.12794
- Mackay, C. E., and Knock, G. A. (2015). Control of vascular smooth muscle function by Src-family kinases and reactive oxygen species in health and disease. *J. Physiol. (Lond)*. doi: 10.1113/jphysiol.2014.285304
- Marnett, L. J., Riggins, J. N., and West, J. D. (2003). Endogenous generation of reactive oxidants and electrophiles and their reactions with DNA and protein. *J. Clin. Invest.* 111, 583–593. doi: 10.1172/JCI200318022
- Marteyn, B., Sakr, S., Farci, S., Bedhomme, M., Chardonnet, S., Decottignies, P., et al. (2013). The *Synechocystis* PCC6803 MerA-like enzyme operates in the reduction of both mercury and uranium under the control of the glutaredoxin 1 enzyme. *J. Bacteriol.* 195, 4138–4145. doi: 10.1128/JB.00272-13
- Masip, L., Veeravalli, K., and Georgiou, G. (2006). The many faces of glutathione in bacteria. *Antioxid. Redox Signal.* 8, 753–762. doi: 10.1089/ars.2006.8.753
- Meister, A. (1995). Glutathione biosynthesis and its inhibition. *Meth. Enzymol.* 252, 26–30. doi: 10.1016/0076-6879(95)52005-8
- Mieyal, J. J., and Chock, P. B. (2012). Posttranslational modification of cysteine in redox signaling and oxidative stress: focus on s-glutathionylation. *Antioxid. Redox Signal.* 16, 471–475. doi: 10.1089/ars.2011.4454
- Mieyal, J. J., Gallogly, M. M., Qanungo, S., Sabens, E. A., and Shelton, M. D. (2008). Molecular mechanisms and clinical implications of reversible protein S-glutathionylation. *Antioxid. Redox Signal.* 10, 1941–1988. doi: 10.1089/ars.2008.2089
- Mishra, S., and Imlay, J. (2012). Why do bacteria use so many enzymes to scavenge hydrogen peroxide? *Arch. Biochem. Biophys.* 525, 145–160. doi: 10.1016/j.abb.2012.04.014
- Newton, G. L., Arnold, K., Price, M. S., Sherrill, C., Delcardayre, S. B., Aharonowitz, Y., et al. (1996). Distribution of thiols in microorganisms: mycothiol is a major thiol in most actinomycetes. *J. Bacteriol.* 178, 1990–1995.
- Newton, G. L., Buchmeier, N., and Fahey, R. C. (2008). Biosynthesis and functions of mycothiol, the unique protective thiol of Actinobacteria. *Microbiol. Mol. Biol. Rev.* 72, 471–494. doi: 10.1128/MMBR.00008-08
- Newton, G. L., and Fahey, R. C. (2008). Regulation of mycothiol metabolism by sigma(R) and the thiol redox sensor anti-sigma factor RsrA. *Mol. Microbiol.* 68, 805–809. doi: 10.1111/j.1365-2958.2008.06222.x
- Newton, G. L., Fahey, R. C., and Rawat, M. (2012). Detoxification of toxins by bacillithiol in *Staphylococcus aureus*. *Microbiology* 158, 1117–1126. doi: 10.1099/mic.0.055715-0
- Newton, G. L., Leung, S. S., Wakabayashi, J. I., Rawat, M., and Fahey, R. C. (2011). The DinB superfamily includes novel mycothiol, bacillithiol, and glutathione S-transferases. *Biochemistry* 50, 10751–10760. doi: 10.1021/bi201460j
- Newton, G. L., Rawat, M., La Clair, J. J., Jothivasan, V. K., Budiarto, T., Hamilton, C. J., et al. (2009). Bacillithiol is an antioxidant thiol produced in Bacilli. *Nat. Chem. Biol.* 5, 625–627. doi: 10.1038/nchembio.189
- Nilewar, S. S., and Kathiravan, M. K. (2014). Mycothiol: a promising antitubercular target. *Bioorg. Chem.* 52, 62–68. doi: 10.1016/j.bioorg.2013.11.004
- Ordonez, E., Van Belle, K., Roos, G., De Galan, S., Letek, M., Gil, J. A., et al. (2009). Arsenate reductase, mycothiol, and mycoredoxin concert thiol/disulfide exchange. *J. Biol. Chem.* 284, 15107–15116. doi: 10.1074/jbc.M900877200
- Ozyamak, E., De Almeida, C., De Moura, A. P., Miller, S., and Booth, I. R. (2013). Integrated stress response of *Escherichia coli* to methylglyoxal: transcriptional readthrough from the nemRA operon enhances protection through increased expression of glyoxalase I. *Mol. Microbiol.* 88, 936–950. doi: 10.1111/mmi.12234
- Pan, J., and Carroll, K. S. (2013). Persulfide reactivity in the detection of protein s-sulfhydration. *ACS Chem. Biol.* 8, 1110–1116. doi: 10.1021/cb4001052
- Park, J. H., and Roe, J. H. (2008). Mycothiol regulates and is regulated by a thiol-specific antisigma factor RsrA and sigma(R) in *Streptomyces coelicolor*. *Mol. Microbiol.* 68, 861–870. doi: 10.1111/j.1365-2958.2008.06191.x
- Parsonage, D., Newton, G. L., Holder, R. C., Wallace, B. D., Paige, C., Hamilton, C. J., et al. (2010). Characterization of the N-acetyl-alpha-D-glucosaminyl l-malate synthase and deacetylase functions for bacillithiol biosynthesis in *Bacillus anthracis*. *Biochemistry* 49, 8398–8414. doi: 10.1021/bi100698n
- Paulsen, C. E., and Carroll, K. S. (2013). Cysteine-mediated redox signaling: chemistry, biology, and tools for discovery. *Chem. Rev.* 113, 4633–4679. doi: 10.1021/cr300163e
- Peralta, D., Bronowska, A. K., Morgan, B., Doka, E., Van Laer, K., Nagy, P., et al. (2015). A proton relay enhances H2O2 sensitivity of GAPDH to facilitate

- metabolic adaptation. *Nat. Chem. Biol.* 11, 156–163. doi: 10.1038/nchem-bio.1720
- Perera, V. R., Newton, G. L., Parnell, J. M., Komives, E. A., and Pogliano, K. (2014). Purification and characterization of the *Staphylococcus aureus* bacillithiol transferase BstA. *Biochim. Biophys. Acta* 1840, 2851–2861. doi: 10.1016/j.bbagen.2014.05.001
- Posada, A. C., Kolar, S. L., Dusi, R. G., Francois, P., Roberts, A. A., Hamilton, C. J., et al. (2014). Importance of bacillithiol in the oxidative stress response of *Staphylococcus aureus*. *Infect. Immun.* 82, 316–332. doi: 10.1128/IAI.01074-13
- Pöther, D. C., Gierok, P., Harms, M., Mostertz, J., Hochgrafe, F., Antelmann, H., et al. (2013). Distribution and infection-related functions of bacillithiol in *Staphylococcus aureus*. *Int. J. Med. Microbiol.* 303, 114–123. doi: 10.1016/j.ijmm.2013.01.003
- Potter, A. J., Trappetti, C., and Paton, J. C. (2012). *Streptococcus pneumoniae* uses glutathione to defend against oxidative stress and metal ion toxicity. *J. Bacteriol.* 194, 6248–6254. doi: 10.1128/JB.01393-12
- Rajkarnikar, A., Strankman, A., Duran, S., Vargas, D., Roberts, A. A., Barretto, K., et al. (2013). Analysis of mutants disrupted in bacillithiol metabolism in *Staphylococcus aureus*. *Biochem. Biophys. Res. Commun.* 436, 128–133. doi: 10.1016/j.bbrc.2013.04.027
- Ratasuk, N., and Nanny, M. A. (2007). Characterization and quantification of reversible redox sites in humic substances. *Environ. Sci. Technol.* 41, 7844–7850. doi: 10.1021/es071389u
- Rawat, M., Johnson, C., Cadiz, V., and Av-Gay, Y. (2007). Comparative analysis of mutants in the mycothiol biosynthesis pathway in *Mycobacterium smegmatis*. *Biochem. Biophys. Res. Commun.* 363, 71–76. doi: 10.1016/j.bbrc.2007.08.142
- Reniere, M. L., Whiteley, A. T., Hamilton, K. L., John, S. M., Lauer, P., Brennan, R. G., et al. (2015). Glutathione activates virulence gene expression of an intracellular pathogen. *Nature* 517, 170–173. doi: 10.1038/nature14029
- Reyes, A. M., Hugo, M., Trostchansky, A., Capece, L., Radi, R., and Trujillo, M. (2011). Oxidizing substrate specificity of *Mycobacterium tuberculosis* alkyl hydroperoxide reductase E: kinetics and mechanisms of oxidation and overoxidation. *Free Radic. Biol. Med.* 51, 464–473. doi: 10.1016/j.freeradbiomed.2011.04.023
- Roberts, A. A., Sharma, S. V., Strankman, A. W., Duran, S. R., Rawat, M., and Hamilton, C. J. (2013). Mechanistic studies of FosB: a divalent-metal-dependent bacillithiol-S-transferase that mediates fosfomycin resistance in *Staphylococcus aureus*. *Biochem. J.* 451, 69–79. doi: 10.1042/BJ20121541
- Rochat, T., Nicolas, P., Delumeau, O., Rabatnova, A., Korelusova, J., Leduc, A., et al. (2012). Genome-wide identification of genes directly regulated by the pleiotropic transcription factor Spx in *Bacillus subtilis*. *Nucleic Acids Res.* 40, 9571–9583. doi: 10.1093/nar/gks755
- Ruane, K. M., Davies, G. J., and Martinez-Fleites, C. (2008). Crystal structure of a family GT4 glycosyltransferase from *Bacillus anthracis* ORF BA1558. *Proteins* 73, 784–787. doi: 10.1002/prot.22171
- Rudolph, T. K., and Freeman, B. A. (2009). Transduction of redox signaling by electrophile-protein reactions. *Sci Signal* 2:re7. doi: 10.1126/scisignal.290re7
- Sareen, D., Newton, G. L., Fahey, R. C., and Buchmeier, N. A. (2003). Mycothiol is essential for growth of *Mycobacterium tuberculosis* Erdman. *J. Bacteriol.* 185, 6736–6740. doi: 10.1128/JB.185.22.6736-6740.2003
- Sasseti, C. M., and Rubin, E. J. (2003). Genetic requirements for mycobacterial survival during infection. *Proc. Natl. Acad. Sci. U.S.A.* 100, 12989–12994. doi: 10.1073/pnas.2134250100
- Sharma, S. V., Arbach, M., Roberts, A. A., Macdonald, C. J., Groom, M., and Hamilton, C. J. (2013). Biophysical features of bacillithiol, the glutathione surrogate of *Bacillus subtilis* and other firmicutes. *ChemBiochem* 14, 2160–2168. doi: 10.1002/cbic.201300404
- Song, M., Husain, M., Jones-Carson, J., Liu, L., Henard, C. A., and Vazquez-Torres, A. (2013). Low-molecular-weight thiol-dependent antioxidant and anti-invasive defences in *Salmonella pathogenesis*. *Mol. Microbiol.* 87, 609–622. doi: 10.1111/mmi.12119
- Ta, P., Buchmeier, N., Newton, G. L., Rawat, M., and Fahey, R. C. (2011). Organic hydroperoxide resistance protein and ergothioneine compensate for loss of mycothiol in *Mycobacterium smegmatis* mutants. *J. Bacteriol.* 193, 1981–1990. doi: 10.1128/JB.01402-10
- Thompson, M. K., Keithly, M. E., Goodman, M. C., Hammer, N. D., Cook, P. D., Jagessar, K. L., et al. (2014). Structure and function of the genomically encoded fosfomycin resistance enzyme, FosB, from *Staphylococcus aureus*. *Biochemistry* 53, 755–765. doi: 10.1021/bi4015852
- Thompson, M. K., Keithly, M. E., Harp, J., Cook, P. D., Jagessar, K. L., Sulikowski, G. A., et al. (2013). Structural and chemical aspects of resistance to the antibiotic fosfomycin conferred by FosB from *Bacillus cereus*. *Biochemistry* 52, 7350–7362. doi: 10.1021/bi4009648
- Van Laer, K., Buts, L., Foloppe, N., Vertommen, D., Van Belle, K., Wahni, K., et al. (2012). Mycoredoxin-1 is one of the missing links in the oxidative stress defence mechanism of Mycobacteria. *Mol. Microbiol.* 86, 787–804. doi: 10.1111/mmi.12030
- Van Laer, K., Hamilton, C. J., and Messens, J. (2013). Low-molecular-weight thiols in thiol-disulfide exchange. *Antioxid. Redox Signal.* 18, 1642–1653. doi: 10.1089/ars.2012.4964
- Vanduinen, A. J., Winchell, K. R., Keithly, M. E., and Cook, P. D. (2015). X-ray crystallographic structure of BshC, a unique enzyme involved in bacillithiol biosynthesis. *Biochemistry* 54, 100–103. doi: 10.1021/bi501394q
- Vergauwen, B., Eleghert, J., Dansercoer, A., Devreese, B., and Savvides, S. N. (2010). Glutathione import in *Haemophilus influenzae* Rd is primed by the periplasmic heme-binding protein HbpA. *Proc. Natl. Acad. Sci. U.S.A.* 107, 13270–13275. doi: 10.1073/pnas.1005198107
- Vergauwen, B., Verstraete, K., Senadheera, D. B., Dansercoer, A., Cvitkovitch, D. G., Guedon, E., et al. (2013). Molecular and structural basis of glutathione import in Gram-positive bacteria via GshT and the cystine ABC importer TcyBC of *Streptococcus mutans*. *Mol. Microbiol.* 89, 288–303. doi: 10.1111/mmi.12274
- Villadangos, A. F., Van Belle, K., Wahni, K., Dufe, V. T., Freitas, S., Nur, H., et al. (2011). *Corynebacterium glutamicum* survives arsenic stress with arsenate reductases coupled to two distinct redox mechanisms. *Mol. Microbiol.* 82, 998–1014. doi: 10.1111/j.1365-2958.2011.07882.x
- Wang, C., Weerapana, E., Blewett, M. M., and Cravatt, B. F. (2014). A chemoproteomic platform to quantitatively map targets of lipid-derived electrophiles. *Nat. Methods* 11, 79–85. doi: 10.1038/nmeth.2759
- Winterbourn, C. C., and Kettle, A. J. (2013). Redox reactions and microbial killing in the neutrophil phagosome. *Antioxid. Redox Signal.* 18, 642–660. doi: 10.1089/ars.2012.4827
- Withhoff, S., Muhlroth, A., Marienhagen, J., and Bott, M. (2013). C1 metabolism in *Corynebacterium glutamicum*: an endogenous pathway for oxidation of methanol to carbon dioxide. *Appl. Environ. Microbiol.* 79, 6974–6983. doi: 10.1128/AEM.02705-13
- Zaffagnini, M., Bedhomme, M., Groni, H., Marchand, C. H., Puppo, C., Gontero, B., et al. (2012a). Glutathionylation in the photosynthetic model organism *Chlamydomonas reinhardtii*: a proteomic survey. *Mol. Cell. Proteomics* 11:M111.014142. doi: 10.1074/mcp.M111.014142
- Zaffagnini, M., Bedhomme, M., Lemaire, S. D., and Trost, P. (2012b). The emerging roles of protein glutathionylation in chloroplasts. *Plant Sci.* 185–186, 86–96. doi: 10.1016/j.plantsci.2012.01.005
- Zhang, D., Macinkovic, I., Devarie-Baez, N. O., Pan, J., Park, C. M., Carroll, K. S., et al. (2014). Detection of protein S-sulfhydration by a tag-switch technique. *Angew. Chem. Int. Ed Engl.* 53, 575–581. doi: 10.1002/anie.201305876
- Zhao, Q., Wang, M., Xu, D., Zhang, Q., and Liu, W. (2015). Metabolic coupling of two small-molecule thiols programs the biosynthesis of lincomycin A. *Nature* 518, 115–119. doi: 10.1038/nature14137
- Zuber, P. (2004). Spx-RNA polymerase interaction and global transcriptional control during oxidative stress. *J. Bacteriol.* 186, 1911–1918. doi: 10.1128/JB.186.7.1911-1918.2004
- Zuber, P. (2009). Management of oxidative stress in *Bacillus*. *Annu. Rev. Microbiol.* 63, 575–597. doi: 10.1146/annurev.micro.091208.073241

Conflict of Interest Statement: The authors declare that the research was conducted in the absence of any commercial or financial relationships that could be construed as a potential conflict of interest.

Copyright © 2015 Loi, Rossius and Antelmann. This is an open-access article distributed under the terms of the Creative Commons Attribution License (CC BY). The use, distribution or reproduction in other forums is permitted, provided the original author(s) or licensor are credited and that the original publication in this journal is cited, in accordance with accepted academic practice. No use, distribution or reproduction is permitted which does not comply with these terms.

Chapter 2

The role of bacillithiol in Gram-positive *Firmicutes*

Pete Chandrangsu¹, Vu Van Loi², Haike Antelmann^{2#}, and John D. Helmann^{2#}

¹*Department of Microbiology, Cornell University, Ithaca, New York*

²*Freie Universität Berlin, Institute for Biology-Microbiology, D-14195 Berlin, Germany*

Published in: Antioxidants & Redox Signaling. 28: 445-462. (2018)

<https://doi.org/10.1089/ars.2017.7057>

#Corresponding authors: haike.antelmann@fu-berlin.de

jdh9@cornell.edu

Authors contributions

Haike Antelmann, Pete Chandrangsu and John D. Helmann wrote the main part of the review and prepared most of the figures. Vu Van Loi wrote the Brx-roGFP2 biosensor part and prepared the figure about Brx-roGFP2.



The Role of Bacillithiol in Gram-Positive *Firmicutes*

Pete Chandrangu, ¹ Vu Van Loi, ² Haike Antelmann, ² and John D. Helmann ¹

Abstract

Significance: Since the discovery and structural characterization of bacillithiol (BSH), the biochemical functions of BSH-biosynthesis enzymes (BshA/B/C) and BSH-dependent detoxification enzymes (FosB, Bst, GlxA/B) have been explored in *Bacillus* and *Staphylococcus* species. It was shown that BSH plays an important role in detoxification of reactive oxygen and electrophilic species, alkylating agents, toxins, and antibiotics.

Recent Advances: More recently, new functions of BSH were discovered in metal homeostasis (Zn buffering, Fe-sulfur cluster, and copper homeostasis) and virulence control in *Staphylococcus aureus*. Unexpectedly, strains of the *S. aureus* NCTC8325 lineage were identified as natural BSH-deficient mutants. Modern mass spectrometry-based approaches have revealed the global reach of protein *S*-bacillithiolation in *Firmicutes* as an important regulatory redox modification under hypochlorite stress. *S*-bacillithiolation of OhrR, MetE, and glyceraldehyde-3-phosphate dehydrogenase (Gap) functions, analogous to *S*-glutathionylation, as both a redox-regulatory device and in thiol protection under oxidative stress.

Critical Issues: Although the functions of the bacilliredoxin (Brx) pathways in the reversal of *S*-bacillithiolations have been recently addressed, significantly more work is needed to establish the complete Brx reduction pathway, including the major enzyme(s), for reduction of oxidized BSH (BSSB) and the targets of Brx action *in vivo*.

Future Directions: Despite the large number of identified *S*-bacillithiolated proteins, the physiological relevance of this redox modification was shown for only selected targets and should be a subject of future studies. In addition, many more BSH-dependent detoxification enzymes are evident from previous studies, although their roles and biochemical mechanisms require further study. This review of BSH research also pin-points these missing gaps for future research. *Antioxid. Redox Signal.* 28, 445–462.

Keywords: *Bacillus subtilis*, *Staphylococcus aureus*, bacillithiol, BSH biosynthesis, metal homeostasis, methylglyoxal, *S*-bacillithiolation, bacilliredoxin

Historical Context: Glutathione and the Discovery of Alternative Low-Molecular-Weight Thiols

LOW-MOLECULAR-WEIGHT (LMW) thiols serve a critical protective role in cells by helping maintain cytosolic proteins in their reduced state and as protection against reactive oxygen species (ROS) and reactive electrophilic species, antibiotics, as well as heavy metals. Glutathione (GSH), a tripeptide with composition γ -L-glutamyl-L-cysteinylglycine (Fig. 1), is, by far, the best studied member from this class of compounds.

Although thiols were detected in tissues in the late 19th century, the discovery of GSH is appropriately attributed to the

celebrated biochemist Sir Fredrick Hopkins in 1921, co-winner (with Christiaan Eijkman) of the 1929 Nobel Prize in Physiology or Medicine for his discovery of vitamins. In his seminal paper on GSH (53), Hopkins begins by giving credit to the studies of Joseph de Rey-Pailhade (20), several decades prior (1888), that led to the description of “philothion” as a cellular reductant. Despite uncertainty regarding the precise chemical composition, Hopkins proposed the name glutathione for what he surmised was a dipeptide containing Glu and Cys:

Provisionally, for easy reference, the name Glutathione will perhaps be admissible. It leaves a link with the historic Phi-

¹Department of Microbiology, Cornell University, Ithaca, New York.

²Institute for Biology-Microbiology, Freie Universität Berlin, Berlin, Germany.

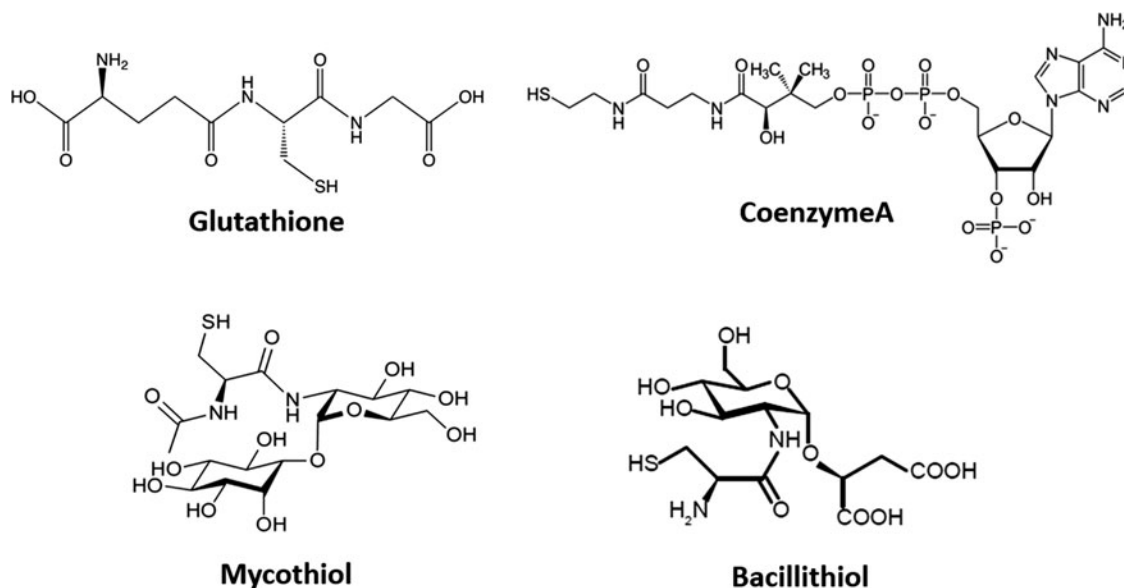


FIG. 1. Structures of major LMW thiols in bacteria. Glutathione is utilized as the major LMW thiol in eukaryotes and Gram-negative bacteria, mycothiol in Actinomycetes, and BSH in *Firmicutes*. Coenzyme A (CoASH) also serves as an LMW thiol in *Staphylococcus aureus* and *Bacillus anthracis*. BSH, bacillithiol; LMW, low molecular weight.

lothion, has the same termination as Peptone, which has long served as a name for the simpler peptides, and is a sufficient reminder that the dipeptide contains glutamic acid linked to a sulphur compound (53).

Doubts about the proposed chemical composition soon emerged. Hopkins acknowledged this, and in 1929 published evidence of the general tripeptide composition of GSH as well as methods for its large-scale purification (54). These studies revealed that GSH does not contain a thione (C=S) moiety, but instead has a thiol (C-SH) (Fig. 1), but the name glutathione has since been retained.

By the 1950s, the chemistry of thiols had been thoroughly investigated, and Barron (6) could conclude that GSH, as the major LMW thiol in cells, "...protects essential -SH groups from oxidation, and it protects the tissues from the toxic effects of heavy metals." By this time, the impression had emerged that GSH was a universal constituent of cells (6). Despite the proclaimed ubiquity of GSH, by the mid-1970s, Robert Fahy's group had developed evidence pointing to the absence of GSH in several species of bacteria (28).

Following up on this insight, the alternative thiol designated mycothiol (MSH) was purified and structurally characterized from *Streptomyces* sp. AJ 9463 in the disulfide form (119), from *Mycobacterium bovis* (125) and from *Streptomyces clavuligerus* (94), and shown to be the major LMW thiol in most actinomycetes (Fig. 1) (92). As discussed later, the biosynthetic pathways leading to MSH and to bacillithiol (BSH) are closely related. The discovery and properties of MSH have been recently reviewed (27, 59).

In addition to MSH, some mycobacteria also produce another LMW thiol, ergothioneine (EGT; 2-mercaptohistidine trimethylbetaine), originally discovered in the ergot fungus as reviewed in (26). Chemically, EGT is distinct from other LMW thiols in that a major fraction exists as the thione tautomer. In addition to MSH, other alternative thiols have also become appreciated for their roles as alternative LMW thiols. One of the first to be described, trypanothione [T(SH)₂; Bis-

glutathionylspermidine], is found in trypanosomatid parasites and consists of two GSH molecules linked by spermidine (29). Trypanosomes also contain ovoidthiol A (N1-methyl-4-mercaptohistidine).

Bacillithiol: Discovery, Structure Determination, and Biosynthetic Pathway

Although the absence of GSH in many bacteria was appreciated by 1978 (28), nearly 20 years would elapse before bacillithiol (BSH) would be identified as the major LMW thiol in many *Firmicutes* (low GC, Gram-positive bacteria). This phylum is represented by the model organism *Bacillus subtilis* and includes several important human pathogens. BSH has, to date, been documented in *Bacillus* and *Staphylococcus* spp., *Streptococcus agalactiae*, and *Deinococcus radiodurans* (97). In the interim, it was speculated that the function of GSH in these organisms might have been subsumed by Cys (10) or coenzyme A (CoASH) (21). The presence of a specific CoA-disulfide reductase in *Staphylococcus aureus* and *Bacillus anthracis* supports the notion that CoASH is reversibly oxidized *in vivo* and may serve as an LMW thiol (21).

BSH was initially detected by HPLC analysis, together with CoASH, as an abundant 398 Da LMW thiol during studies of thiol-dependent enzymes in *B. anthracis* (99). Independently, a thiol of this same mass was detected by mass spectrometry as the major adduct for *in vivo* oxidized OhrR protein in *B. subtilis* (64). OhrR is a DNA-binding protein with a single redox-active Cys residue in each monomer and responds to thiol oxidants by formation of mixed disulfides, including, as a dominant product, the S-bacillithiolated protein.

Following up on this initial discovery, rapid progress was made in a coordinated multi-laboratory effort that led to the determination of the chemical structure for BSH, and insights into its distribution (97) and biosynthetic pathway (40). The identification of the biosynthetic pathway enabled the generation of mutant strains lacking BSH, and initial insights into

its physiological role. Working on the general assumption that BSH has likely supplanted GSH as an enzyme cofactor in these organisms, it was also possible to predict the presence of various different types of BSH-dependent enzymes (*e.g.*, bacillithiol-*S*-transferases [BST], analogous to glutathionyl-*S*-transferases) and redox partners (*e.g.*, bacilliredoxins [Brx], analogous to glutaredoxins). Even at this early stage (only two prior research papers on BSH had appeared), this enabled the presentation of an early preview of how the BSH field might evolve, and readers are referred to this prior review for a more detailed discussion of these early steps, which provides a context for the present review (50).

The structure of BSH was determined, after purification of the *S*-bimane derivative from *D. radiodurans*, to be the α -anomeric glycoside of L-cysteinyl-D-glucosamine with L-malic acid (97). Based on the chemical similarities between MSH and BSH, it was possible to identify candidate genes for the first two steps in BSH biosynthesis by homology (40). This led to the identification of a cluster of co-transcribed genes in *B. subtilis* that includes *bshA* (encoding a L-malic acid glycosyltransferase) and *bshB1* (one of two partially redundant deacetylases for conversion of GlcNAc-Mal to GlcN-Mal). This same operon also includes *mgsA* (a methylglyoxal synthase), which is of interest since (as discussed below) BSH plays a major role in methylglyoxal (MG) detoxification (11). This gene cluster is immediately upstream of and co-directional with the *panBCD* operon encoding enzymes in the CoASH biosynthetic pathway.

The *bshC* gene could not be identified by homology-based searches, but was revealed by phylogenomic comparisons (using the EMBL STRINGS web-based tool) as a gene with a high co-occurrence (and occasional co-localization) with *bshA* in bacterial genomes (40). The *bshC* gene is transcribed both from its own promoter and also as part of a two-gene operon with another predicted pantothenate biosynthesis gene, *panE* (*ylbQ*) (37).

The significance of this gene clustering and possible coordinate regulation is not yet understood, but an obvious suggestion is that the synthesis of CoASH and BSH may be positively correlated (50). Indeed, in *B. subtilis*, all of the genes required for BSH synthesis are upregulated in response to disulfide stress (*e.g.*, diamide) through the action of the Spx transcription factor (37). A similar induction has also been documented in *S. aureus* (111). More broadly, genes for both BSH synthesis and BSH-dependent detoxification reactions are upregulated by several reactive oxidants and reactive electrophiles, as noted in several studies in *B. subtilis*, *B. anthracis*, and *S. aureus* [reviewed in Perera et al. (107)].

In addition to providing a candidate gene for the last and missing step in BSH biosynthesis (*bshC*), phylogenomic profiling also provided an intriguing list of genes encoding proteins that are likely to function in core BSH metabolism. These included several genes of previously unassigned function (so-called γ -genes). The *ypdA* gene encodes a putative thioredoxin reductase (TrxR) homolog and is postulated to function as a bacillithiol disulfide (BSSB) reductase, although experimental evidence is still lacking. Two others (*yqiW* and *yphP*) encode proteins with DUF1094 domains (domain of unknown function containing a conserved Cys-x-Cys motif), and YphP was shown to be active as a disulfide isomerase (22). This led to the prediction that these proteins might function as Brx for the reduction of *S*-bacillithiolated

proteins, as described later. Finally, *ytxJ* was found to encode another putative redox-active protein related to Trx that also presumably functions in BSH metabolism.

Identification of the biosynthetic genes for BSH enabled the generation of mutants lacking this thiol, confirming that BSH is non-essential. Mutants lacking the ability to synthesize BSH are sensitive to a variety of oxidative and electrophilic stress conditions in *B. subtilis* and *S. aureus* (14, 15, 40, 111, 114). Moreover, it quickly became apparent that a previous suggestion that the *B. subtilis* FosB fosfomycin resistance protein might utilize Cys as a cofactor (10) was incorrect. FosB (as described in more detail later) is a BSH-dependent enzyme, and cells lacking either *fosB* or BSH biosynthesis are equally sensitive to fosfomycin in *B. subtilis* and *S. aureus* (40, 111). In practice, this provides a very convenient (although indirect) assay for BSH levels in *B. subtilis* (40).

Chemical Properties of BSH

A key challenge for the further investigation of BSH was the need to obtain quantities that are sufficient for chemical and biochemical characterization. The development of methods for the chemical synthesis of BSH ultimately met this need. Chris Hamilton reported both a complete chemical synthesis and a hybrid chemoenzymatic route taking advantage of the ability of purified BshA to provide the D-GlcNAc-L-Mal precursor (121). These approaches provided access to not only BSH but also BSSB and to the biosynthetic intermediates GlcNAc-Mal and GlcN-Mal (Fig. 2). A complete chemical synthesis was also reported by Richard Armstrong's laboratory in which BSH could be obtained in 8–9% yield after 11 chemical steps (62). Purified BSH has facilitated the development of a detailed understanding of the redox chemistry and ionization behavior of BSH (120), the generation of specific BSH antibodies (an important tool for the study of *S*-bacillithiolation) (15), and provides a necessary cofactor for the study of BSH-dependent enzymes.

A detailed chemical study of BSH redox and ionization properties indicates that the BSH thiol is more acidic than Cys or GSH, with a higher fraction in the reactive thiolate state at physiological pH (120). For example, at pH 7.7, an estimated 22% of BSH is in the bacillithiolate (BS[−]) form compared with 14.5% for Cys. The standard thiol redox potential for the BSH, BSSB couple (−221 mV) is much closer to that of free Cys (−223 mV) compared with GSH (−240 mV). Considering the relative abundance of Cys, CoASH, and BSH in the cell, it was concluded that BSH (which is present at levels near 1 mM during growth in *B. subtilis* and *S. aureus*) is the dominant LMW thiol, with levels of the BSH thiolate exceeding those of CoASH and Cys thiolates by ~10–100-fold (111, 120).

The chemistry of LMW thiol redox buffers is dominated by the interconversion of the reduced (thiol) and oxidized (disulfide) forms, and this chemistry accounts for their role in maintaining proteins in their reduced states in the cytosol. However, the thiolate anion can also serve as a nucleophile in conjugate addition reactions as commonly employed in detoxification pathways. For BSH, these reactions are mediated by BST enzymes, analogous to the well-characterized GST enzymes (Fig. 3A, B). The best characterized representative for this type of enzyme to date is FosB, as noted earlier.

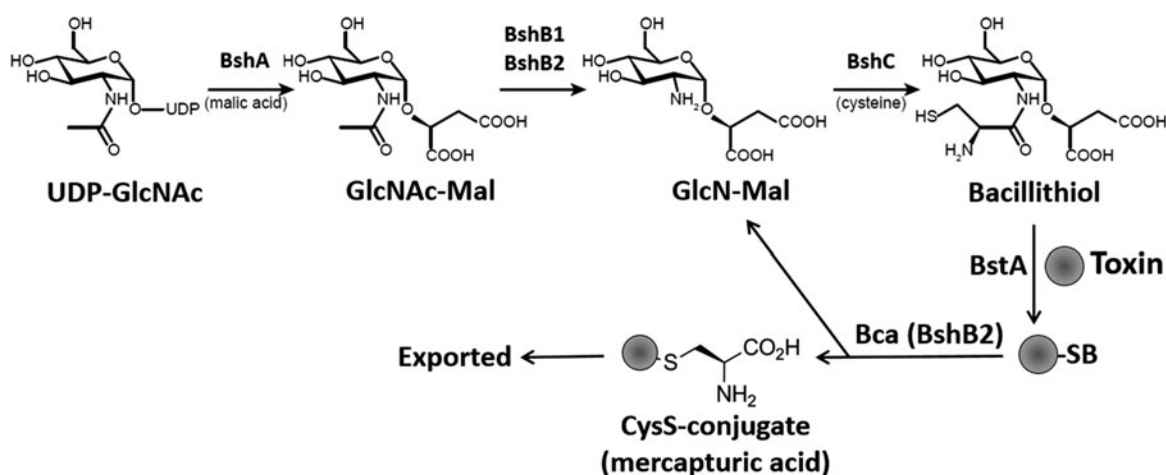


FIG. 2. Biosynthesis pathway of BSH and BSH-dependent detoxification. In the BSH synthesis pathway of *Bacillus subtilis*, the glycosyltransferase BshA first adds GlcNAc to malate-producing GlcNAc-Mal. Then, the paralog *N*-deacetylases BshB1 and BshB2 catalyze deacetylation of GlcNAc-Mal, and BshC adds cysteine (presumably in an unidentified activated form) to GlcN-Mal, producing BSH. Detoxification of toxins, xenobiotics, or electrophiles involves their conjugation with BSH by the BSH-*S*-transferase BstA, generating BS-conjugates that are cleaved by the deacetylase BshB2 (Bca) to CysS-conjugates and GlcN-Mal used for BSH recycling. The CysS-conjugates are exported from the cells as mercapturic acid derivatives. In *S. aureus*, only one BshB-like enzyme is present that functions both as deacetylase and amidase and is essential for BSH biosynthesis.

Oxidized disulfides can also react with hydrogen sulfide (H_2S), a metabolite produced by sulfate-reducing bacteria and also serving as a secondary messenger in mammalian systems (7). H_2S exists predominantly as the hydrosulfide anion (HS^-), which reacts with BSSB to generate BSH and BSSH (bacillithiol persulfide). *S. aureus* was recently shown to contain an inducible system that functions to detoxify reactive persulfides. The CstB protein, a persulfide dioxygenase sulfurtransferase, oxidizes BSSH (as well as other LMW thiol persulfides) in the presence of sulfite to generate reduced thiols (BSH) and thiosulfate (122). These authors also suggest that previously noted enzymes with a homology to CoASH disulfide reductases (CoA disulfide reductase-rhodanese homology domain protein; CoADR-RHD) may actually function as reductases for the CoASSH persulfide. The general prevalence of persulfides in bacterial physiology, and the various means for their detoxification, is not yet fully understood.

Biochemical Mechanism of BSH Biosynthesis

Since BSH plays a critical role in antibiotic detoxification and oxidative stress responses, the enzymes involved in BSH biosynthesis are attractive targets for novel antibiotic development. In fact, *S. aureus* strains unable to produce BSH are compromised for survival in the presence of macrophages and neutrophils (111). BshA, BshB, and BshC catalyze the enzymatic synthesis of BSH (Fig. 2). BshA is homologous to *Mycobacterium tuberculosis* MshA and is a GT-4 class glycosyltransferase that is required for the first committed step in BSH biosynthesis. BshA catalyzes the addition of UDP-*N*-acetylglucosamine (UDP-GlcNAc) to L-malate through a metal-independent $\text{S}_{\text{N}}1$ -like mechanism, forming *N*-acetylglucosaminyl-malate (GlcNAc-Mal) and free UDP (130, 133). Structural and functional studies suggest that the release of the UDP-leaving group and nucleophilic attack by L-malate occur on the same face of the

hexose sugar and are asynchronous, resulting in the formation of a short-lived oxocarbenium intermediate (133).

The second step of BSH biosynthesis is catalyzed by BshB, an *N*-acetylhydrolase, that generates glucosamine malate (GlcN-Mal) from GlcNAc-Mal. Genetic studies indicate the presence of one or more functionally redundant proteins in *B. subtilis*, *B. anthracis*, and *B. cereus* (31, 40). In *B. subtilis*, strains lacking BshB1 still produced detectable levels of BSH (40). However, BSH is completely absent on inactivation of both BshB1 and a second deacetylase BshB2, encoded by *bshB2* (40). The same overlapping roles in BSH synthesis were observed for the two BshB-paralogs BA1557 and BA3888 in *B. anthracis* as well as for BC1534 and BC3461 in *B. cereus* (31). Biochemical evidence was provided that both BshB-paralogs (BA1557 and BA3888) and the orthologs in *B. cereus* have BshB activity and catalyze the *N*-deacetylation of GlcNAc-Mal (31). In contrast, *S. aureus* only encodes a single BshB-like protein that is essential for BSH synthesis and has a dual function as BSH conjugate amidase (Bca) (114).

Redundancy has been observed also for MSH biosynthesis, where the deacetylation can be carried out by either the BshB-like enzyme MshB or the “moonlighting” enzyme Mca (mycothiol-*S*-conjugate amidase). The primary role of Mca is in detoxification of xenobiotic compounds through the cleavage of MSH conjugates, resulting in GlcN-myoinositol and the Cys-*S*-conjugate (mercapturic acid) that is exported from the cell (93).

Biochemical studies of the BshB-paralogs of *B. anthracis* and *B. cereus* identified only BA3888 as a bacillithiol-*S*-conjugate amidase (Bca) able to hydrolyze the amide linkage of bacillithiol-*S*-bimane (BSmB) to liberate GlcNAc-Mal (31). The reaction proceeds *via* a Zn^{2+} dependent acid-base catalysis. The active site is highly conserved, the Zn^{2+} is coordinated by two histidine residues and one aspartate (His12, His113, and Asp15), and the residues involved in catalysis await identification. Bca activity is highly specific to

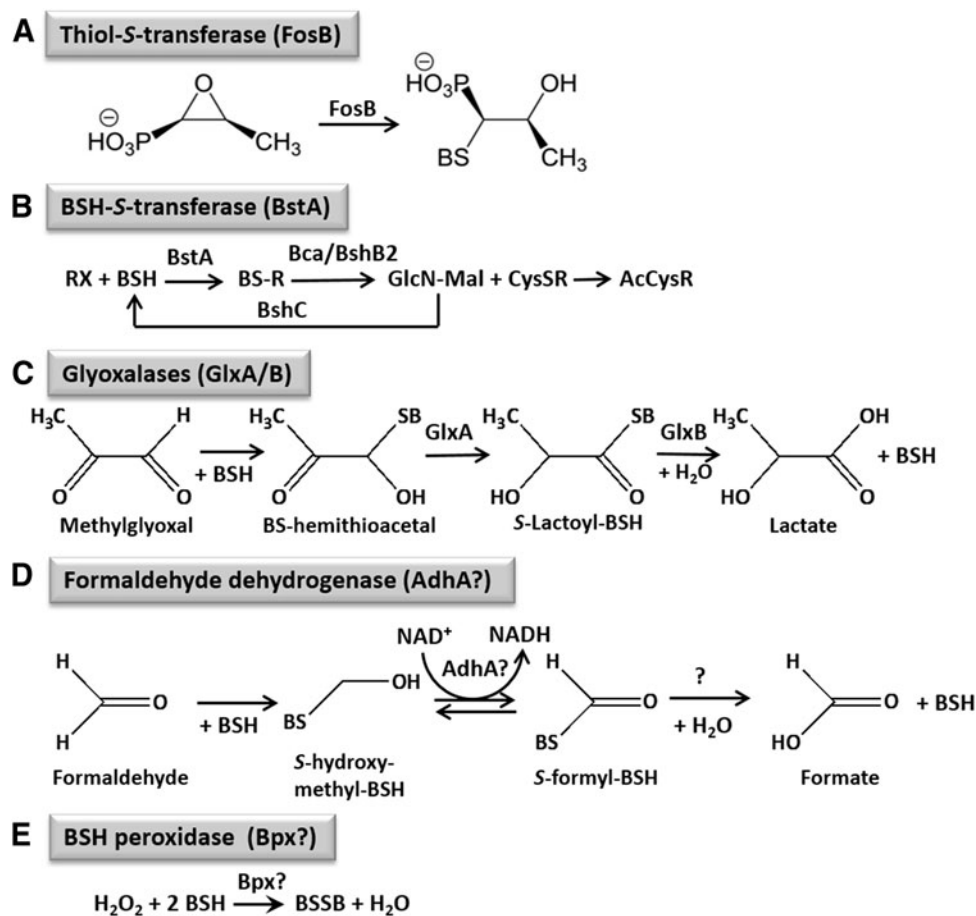


FIG. 3. The functions of BSH-dependent detoxification enzymes in *B. subtilis* and *S. aureus*. BSH functions in detoxification of reactive oxygen and electrophilic species, HOCl, and antibiotics, such as fosfomycin in *B. subtilis* and *S. aureus*. (A) BSH is a cofactor for the thiol *S*-transferase FosB that adds BSH to fosfomycin for its detoxification. (B) Electrophiles, xenobiotics, and toxins (RX) are conjugated to BSH by the BSH *S*-transferase BstA to form BS-conjugates (BSR), which are cleaved by the BSH *S*-conjugate amidase BshB2 (Bca) to CysSR and a mercapturic acid (AcCysR) that is exported from the cell. (C) BSH functions in methylglyoxal detoxification as a cofactor for the glyoxalases I/II (GlxA/B) in *B. subtilis*. GlxA converts BS-hemithioacetal to *S*-lactoyl-BSH that is hydrolyzed by GlxB to D-lactate. (D) AdhA is a thiol-dependent formaldehyde dehydrogenase that is induced under FA stress (98), likely converting *S*-hydroxymethyl-BSH to *S*-formyl-BSH. In the final step, BSH and formate are released by an unidentified *S*-formyl-BSH hydrolase. (E) Unknown thiol-dependent peroxidases or peroxiredoxins (Bpx) might function in peroxide detoxification. Question marks indicate uncharacterized reactions.

the methyl aglycone, as suggested by its low enzymatic activity when tested with BSH analogs where the methyl aglycone was replaced with an uncharged methyl or benzyl group. The *in vivo* contribution of Bca to BSH biosynthesis and the physiological substrates of Bca remain to be identified.

The addition of Cys to GlcN-Mal, the final step in BSH biosynthesis, is catalyzed by the putative cysteine ligase, BshC. BshC was identified by a phylogenomic analysis for genes whose presence was correlated with the presence of BshA and BshB utilizing the STRING protein interaction network tool (40). Strains lacking BshC are unable to produce BSH and accumulate elevated levels of the BSH precursor GlcN-Mal (40). Interestingly, the reaction catalyzed by BshC is unknown and has yet to be reconstituted *in vitro*, possibly due to the absence of a required cofactor, substrate, or protein. Structural and functional studies suggest that BshC forms a dimer in solution through interactions between an extended coiled-coil domain from each subunit and that the BshC active sites are solvent exposed, which may allow for access by an additional protein involved in catalysis (132).

BSH and Detoxification

Fosfomycin and other antibiotics

LMW thiols play an important role in the detoxification of xenobiotic compounds and antibiotics. The most well understood LMW-based detoxification mechanism involves thiol-*S*-transferases, which catalyze the reaction of LMW thiols to a variety of substrates. The first characterized BST was FosB, involved in the detoxification of fosfomycin (Fig. 3A) (62, 115, 128). Fosfomycin is a broad-spectrum antibiotic that is also used in clinical practice to treat methicillin-resistant *S. aureus* (MRSA) infections (84, 127). Fosfomycin inhibits the first step in cell wall synthesis through covalent modification of the active site cysteine of the MurA enzyme.

To counter the action of this antibiotic, bacteria have evolved fosfomycin detoxification enzymes. *B. subtilis* and *S. aureus* encode FosB, an Mn²⁺-dependent BST. FosB inactivates fosfomycin by catalyzing the nucleophilic addition of BSH to the C2 position of the fosfomycin epoxide ring,

resulting in an inactive BS-fosfomycin complex (115). Strains lacking FosB or BSH are hypersensitive to fosfomycin and the increase in sensitivity is comparable to strains lacking both FosB and BSH, indicating that FosB utilizes BSH as a thiol substrate (40). In support of this hypothesis, biochemical studies demonstrated that *S. aureus* FosB is significantly more active in the presence of BSH than other LMW thiols (115).

A second class of BSTs comprised members of the DinB/YfiT superfamily of thiol transferases, which utilize a thiol cofactor to detoxify reactive electrophiles and xenobiotics (Fig. 3B). *B. subtilis* YfiT was identified as a putative BST by structural homology to the mycothiol-S-transferase (RV0443) found in *M. tuberculosis* (96). *In vitro* studies monitoring the reaction of the electrophilic compound monochlorobimane with BSH demonstrated that YfiT (96) and BstA (106), a structural homolog found in *S. aureus*, indeed, function as BSTs and are highly specific for BSH as a thiol substrate. The relevant compounds detoxified by BSTs *in vivo* are currently unknown. The only DinB/YfiT family protein with an identified function *in vivo* is the MSH-dependent maleylpyruvate isomerase (*ngcl2918*) from *Corynebacterium glutamicum*, which is essential for growth on aromatic compounds as a carbon source (32).

BSTs may also be involved in the detoxification of endogenously produced toxins that are byproducts or intermediates during secondary metabolite biosynthesis. In fact, toxic metabolites that are produced during actinorhodin biosynthesis by *Streptomyces coelicolor* appear to be detoxified by formation of an MSH-S-conjugate (126). The formation of this conjugate may be dependent on a DinB/YfiT-like protein.

Toxic electrophiles

The discovery of BSH as the major LMW thiol in *B. subtilis* led us to postulate that BSH may serve a protective function against the toxic dicarbonyl compound MG in a manner that is functionally analogous to GSH (Fig. 3C). The first hint came from the observation that the gene encoding MGS, *mgxA*, is co-transcribed with the genes encoding the first two enzymes

in the BSH biosynthetic pathway, *bshA* and *bshB1*. In fact, strains lacking BSH are more sensitive to added MG (40).

MG, an α,β unsaturated aldehyde, is a toxic, endogenous byproduct of glycolysis, synthesized by MGS under conditions of excess carbon or phosphate limitation due to an imbalance between the rate of carbon acquisition and the lower segment of glycolysis (129). The main role of MGS is to restore inorganic phosphate levels. As an electrophile, MG can modify guanine bases in DNA, leading to DNA damage and an increased rate of mutation in surviving cells (33). Furthermore, MG can react with arginine, lysine, and cysteine residues in proteins, resulting in protein inactivation (72).

The major mechanism of protection from MG in *Escherichia coli* is the GSH-dependent acidification of the cytoplasm mediated by the KefGB and KefFC K⁺ efflux systems (34). Exposure to MG leads to the spontaneous formation of the GSH adduct hemithioacetal (HTA). Glyoxalase I (GlxI) catalyzes the formation of S-lactoylglutathione (SLG) from HTA (77). Subsequently, glyoxalase II converts SLG to D-lactate and regenerates GSH (102). KefGB and KefFC K⁺ efflux systems are directly inhibited by GSH and activated by GSH adducts. Thus, the SLG intermediate is critical for protection from MG stress as it is required for the full activation of the KefGB and KefFC K⁺ efflux pumps (77, 87). The H⁺ influx that accompanies the KefGB and KefFC-mediated K⁺ efflux leads to the cytoplasmic acidification that is sufficient to confer resistance to MG (34). Interestingly, protection from MG by cytoplasmic acidification does not increase the rate of MG detoxification (33, 34). Rather, cytoplasmic acidification likely protects cells from MG and other electrophiles by protonating nucleophilic residues on DNA, thereby preventing alkylation of DNA by electrophiles (33).

B. subtilis encodes a BSH-dependent MG-detoxification pathway (Figs. 3C and 4) (11). Null mutants of the glyoxalase I and II homologs, GlxA (formerly YwbC) and GlxB (formerly YurT), respectively, are more sensitive to MG and function in the same genetic pathway as BSH and a putative BSH-gated K⁺/H⁺ antiporter, KhtSTU (formerly YhaSTU). Upon MG stress, intracellular pH decreases ~ 0.4 U, as

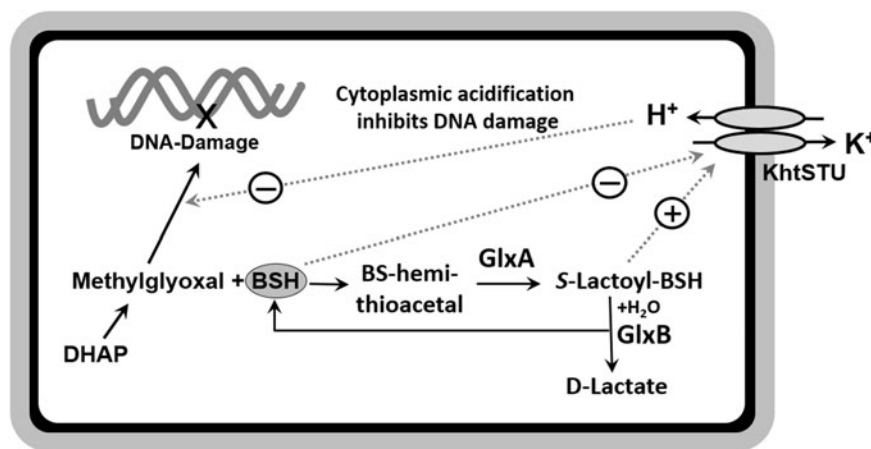


FIG. 4. BSH-dependent detoxification of methylglyoxal, leading to cytoplasmic acidification. Methylglyoxal can be produced as a byproduct of the glycolysis from DHAP. Methylglyoxal reacts spontaneously with BSH, forming BS-hemithioacetal, which is converted to S-lactoyl-BSH by the glyoxalase-I (GlxA) and to lactate by the glyoxalase-II (GlxB). S-lactoyl-BSH activates the potassium proton antiporter KhtSTU for K⁺-efflux and proton import, leading to cytoplasmic acidification that likely inhibits interaction of methylglyoxal with the DNA to prevent DNA damage. BSH inhibits the antiporter KhtSTU. DHAP, dihydroxyacetone phosphate.

measured by an intracellular GFP-based pH reporter (Fig. 4). This cytoplasmic acidification is sufficient for protection against MG, since cells treated with the weak membrane-permeant acid sodium acetate before MG exposure are less sensitive to MG.

A GSH-independent MG detoxification pathway is also present in *E. coli*, in which MG is converted directly to D-lactate by the glyoxalase III enzyme, HchA. Using the Phyre2 structural homology search tool, a glyoxalase III homolog, GlxC (formerly YdeA) in *B. subtilis* was identified (11). GlxC null mutants are more sensitive to MG than wild-type cells, although to a lesser extent than a BSH null mutant. The MG sensitivity of the *glcX bshC* double mutant was additive when compared with the *glcX* and *bshC* single mutants, which suggests that GlxC is a BSH-independent glyoxalase III enzyme and that the major detoxification pathway is BSH dependent (11).

Methanotrophic and methylotrophic bacteria generate formaldehyde (FA) as an intermediate during the oxidation of methane to carbon dioxide. FA is a toxic carbonyl compound that, similar to MG, is a reactive electrophile and can react with nucleophilic groups in proteins and DNA, leading to protein-protein and protein-DNA crosslinking. In these bacteria, FA is either assimilated by the serine or ribose monophosphate pathway (RuMP) to be used as a major source of cellular carbon or oxidized to generate NADH and formate by LMW thiol-dependent formaldehyde dehydrogenases (Fdh).

Recently, a metabolomics approach identified a role for BSH in FA detoxification in *Bacillus methanolicus* (90) (Fig. 3D). *B. methanolicus* is a thermotolerant, facultative methylotroph, making it a useful strain for the large-scale production of amino acids from methanol. When grown in the presence of methanol, an *S*-formyl-BSH intermediate was detected in cell lysates by LC-MS. The hydrolysis of related *S*-formyl-GSH is usually catalyzed by *S*-formyl-GSH-hydrolases that are homologs of human esterases and participate in FA oxidation in GSH-producing bacteria (46). The putative esterase that is specific for hydrolysis of *S*-formyl-BSH is unknown in *B. subtilis*. The BSH-dependent FA oxidation pathway appears to be the most important under conditions where the RuMP and THF pathways are overwhelmed, such as on a rapid shift in carbon source from mannitol to methanol. Non-methanotrophs, such as *B. subtilis*, also use the RuMP pathway to detoxify FA. In addition, transcriptomic and proteomic characterization of the *B. subtilis* response to FA stress led to the identification of AdhA as a putative LMW thiol-dependent Fdh that is induced under FA and MG stress, although its precise role has not been confirmed (Fig. 3D) (98).

BSH and Metal Homeostasis

Metal ions are essential for life, yet many fundamental questions regarding the size of the cellular metal quota, how it varies with growth conditions, and how it is modulated in response to stress still remain. Metal deficiency leads to a genome-wide response that serves to increase metal import, decrease metal demand, mobilize stored metals, redistribute metals from lower-priority enzymes to support higher-priority needs, and replace metal-dependent enzymes with pathways that are dependent on other cofactors (82). Conversely, metal excess induces the expression of metal efflux systems to

prevent the mismetallation of essential enzymes and the production of ROS (100). Both metal deficiency and excess are utilized by the host immune system in response to pathogens (23, 103).

The chemical speciation of metals within cells is largely unexplored. Metallation of metalloenzymes, and detection of cellular metal status by metalloregulatory proteins, is governed by the labile metal pool, which is defined as those metal ions that are hydrated or otherwise in a rapidly exchanging form. LWM thiols in eukaryotic and GSH-producing bacteria are known to participate in buffering the labile pool and in detoxifying metal ions. GSH was shown to function together with glutaredoxins in iron-sulfur (FeS)-cluster trafficking since an FeS cluster could be assembled and bridged between the active site Cys of monothiol Grx3/4 and GSH, as demonstrated both *in vitro* and *in vivo* in yeast cells (67, 89, 108).

In plants and fungi, GSH is necessary for heavy-metal sequestration as it is the major substrate for the synthesis of the heavy metal-binding peptide phytochelatin (44). In yeast, resistance to cadmium requires GSH (69). In contrast, the contribution of LWM thiols to metal ion homeostasis is poorly understood in non-GSH-producing bacteria (45, 48, 49). In the next section, we discuss the emerging role of BSH as a key player in metal homeostasis.

Zinc buffering

Between 5% and 10% of proteins require Zn^{2+} as either a structural or catalytic cofactor (3). Unlike Fe^{2+} , which generates cell-damaging hydroxyl radicals in the presence of hydrogen peroxide (H_2O_2), Zn^{2+} is not redox reactive, allowing it to be adopted as a structural cofactor in a number of proteins. Zn^{2+} must be kept at a high enough concentration to ensure that the Zn^{2+} quota is sufficient for Zn^{2+} to perform its essential roles. However, since Zn^{2+} , in general, binds with higher avidity than most other metals (except for Cu^{2+}), Zn^{2+} must not be present in excess so that proteins utilizing other metals are not mismetallated (58). Thus, the free steady-state Zn^{2+} levels are highly regulated at multiple levels such that they are buffered in with a total intracellular concentration of ~ 1 mM and a free Zn^{2+} concentration in the $\sim pM$ range (101).

The narrow range of intracellular free Zn^{2+} is set by Zn^{2+} sensing transcription factors (101). In *B. subtilis*, Zur acts as a sensor of Zn^{2+} limitation and CzrA is a sensor of Zn^{2+} excess (39, 88). These metalloregulators sense the labile Zn(II) pool, consisting of Zn(II) bound reversibly to small molecules, nucleotides, and proteins in a rapidly exchanging form. Under conditions of Zn^{2+} sufficiency, the Zn^{2+} -sensing transcription factor Zur represses transcription of the Zn^{2+} uptake systems. When Zn^{2+} is in excess, CzrA is inactivated, leading to derepression of transcription of the *cadA* and *czcD* efflux pumps and Zn^{2+} efflux. Organisms have also evolved Zn^{2+} -independent paralogs that can functionally replace Zn^{2+} -requiring proteins under Zn^{2+} starvation conditions (1, 91). In addition, Zn^{2+} may be mobilized from a labile Zn^{2+} pool in response to stress under non-steady state conditions. Work from the Maret lab demonstrated that metallothionein (MT), a cysteine-rich, Zn^{2+} -binding LMW protein, serves as a zinc "sink" in eukaryotes and is able to control the availability of kinetically available Zn^{2+} in response to oxidative stress (80).

Since *B. subtilis* utilizes BSH as the major LMW thiol and does not produce MT or GSH, BSH could serve a similar

function in metal buffering. BSH has several potential metal coordinating ligands, including a sulfur-containing thiolate, a primary amine, and two carboxylates (97). Genetic, physiological and biochemical evidence suggests that, in *B. subtilis* and related low G+C *Firmicutes*, BSH serves as the major buffer of the labile Zn^{2+} pool (Fig. 5) (75). BSH binds Zn^{2+} as a $(BSH)_2:Zn^{2+}$ complex with an affinity (K_a) of $1.9 \times 10^{12} M^{-2}$ (75). Given that the intracellular concentration of BSH can range from 1 to 5 mM (120), depending on the growth phase, it is reasonable to suggest that BSH can account for $\sim 1/3$ of the total Zn^{2+} pool under Zn^{2+} excess conditions (75).

BSH may also have direct effects on Zn^{2+} sensing by Zur and CzrA. *In vitro* experiments monitoring the binding of CzrA to its operator site as a proxy for CzrA metallation status demonstrated that Zn^{2+} dissociation from holo-CzrA was much faster in the presence of BSH. This suggests that BSH can facilitate Zn^{2+} loading and removal into CzrA, presumably through a ligand-exchange mechanism that was analogous to that described for Cu^+ chaperones (116). This may provide a mechanism for rapid re-repression of Zn^{2+} efflux if cells experience a sudden shift from Zn^{2+} excess to starvation. Thus, BSH influences Zn^{2+} homeostasis at multiple levels as a significant intracellular Zn^{2+} buffer under conditions of Zn^{2+} excess to prevent intoxication, and as a facilitator of transcription regulation in response to fluctuations in Zn^{2+} levels.

Iron-sulfur cluster assembly

The major cytosolic requirements for Fe^{2+} are for utilization in heme-containing enzymes and the assembly of FeS clusters. FeS cluster-containing proteins are involved in a wide range of cellular functions (83). Many key enzymes in amino acid biosynthesis, carbon metabolism, cofactor biosynthesis, and antibiotic resistance are dependent on FeS

cluster-containing enzymes. Thus, inactivation of these enzymes under conditions of Fe^{2+} starvation or oxidative stress is detrimental for proliferation (57).

A broad phenotypic survey of a *S. aureus* strain lacking BSH revealed many phenotypes that are consistent with defects in FeS biogenesis (Fig. 5) (30, 118). *S. aureus* strains lacking BSH are severely impaired for growth in media lacking leucine (Leu) or isoleucine (Ile). This growth defect could be suppressed by supplementation with either amino acid or Fe^{2+} . The activity of key FeS requiring dehydratase enzymes in Leu or Ile biosynthesis is decreased in a BSH null mutant strain. In addition, aconitase activity, an unrelated FeS-dependent enzyme that catalyzes the conversion of citrate to isocitrate, also decreased, suggestive of an overall defect in cellular FeS cluster biogenesis.

The FeS biosynthetic machinery in *S. aureus* is encoded by the *suf* operon, which utilizes cysteine as a sulfur source and an unidentified Fe^{2+} source. On assembly, the FeS clusters are transferred to FeS carrier proteins (Nfu and/or SufA) for delivery to FeS-containing proteins (81). Genetic analysis suggests that the role of BSH in FeS biogenesis is independent of Nfu and SufA (118). Thus BSH, Nfu and SufA perform independent, yet overlapping roles in FeS biogenesis.

In yeast, monothiol glutaredoxins together with GSH play a key role in FeS cluster biogenesis and trafficking (17, 67, 68, 89, 108). Grx3/4 were shown to bind a bridging $[2Fe-2S]$ cluster *in vitro* that is coordinated by the active-site Cys residue of the Grx domain and GSH as ligands (67, 108). The deficiency of Grx affected the synthesis of Fe/S clusters, heme, and di-iron centers and thus, this Grx FeS center has a crucial role in iron trafficking and sensing in yeast cells. It remains an interesting question for future studies to unravel whether BSH chelates Fe^{2+} directly or is involved in FeS cluster assembly *via* a BSH-containing Brx FeS center that perhaps could function in iron trafficking and sensing.

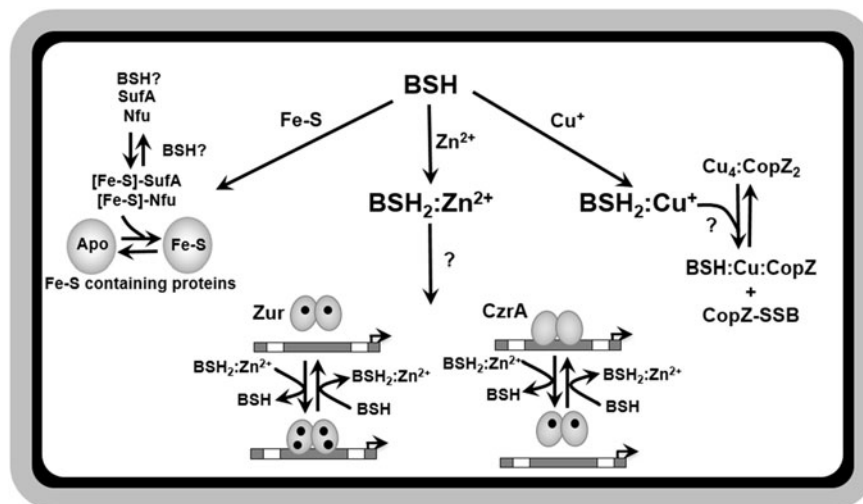


FIG. 5. The functions of BSH in metal homeostasis. A role for BSH in metal homeostasis has been identified for iron, zinc, and copper. BSH is required for the full activity of FeS requiring proteins in *S. aureus*, possibly as a key component in the assembly and delivery of FeS clusters. BSH is believed to function in an independent, yet overlapping role with the FeS carrier proteins, SufA and Nfu. BSH can also bind zinc with a high affinity and serves as a major cytosolic zinc buffer as demonstrated in *B. subtilis*, allowing the cell to avoid zinc intoxication under conditions of excess. Biochemical evidence also suggests a role for BSH in facilitating the delivery and removal of zinc from the zinc-sensing metalloregulators, Zur and CzrA. Lastly, BSH may also work in concert with CopZ in intercellular copper buffering and delivery to metallo-proteins and may protect CopZ from overoxidation through *S*-bacilliothiolation. FeS, iron-sulfur.

BSH may also have a role in maintaining the labile Fe^{2+} pool. In bacteria, Fe^{2+} sufficiency is sensed by the Fe^{2+} -specific metalloregulator, Fur (63). On Fe^{2+} sufficiency, *B. subtilis* Fur binds Fe^{2+} at two different sensing sites, leading to DNA binding and repression of its regulon (76). Fur controls a large and complex regulon, including many iron uptake systems and an iron efflux pump (PfeT) (4). In addition, Fur indirectly regulates many more genes by repression of a small noncoding RNA (FsrA) and putative RNA chaperones (FbpABC) that are analogous in function to Hfq from enterobacteria, which together mediate an Fe^{2+} -sparing response (36, 123, 124). A *S. aureus* BSH null strain contains lower levels of Fur-accessible Fe^{2+} , as judged by slower transcriptional repression on Fe^{2+} sufficiency of the Fur-regulated *isdB* promoter, which is involved in Fe^{2+} acquisition from heme (118).

Copper trafficking

Copper plays a critical role in many cellular processes, yet Cu^+ is highly toxic in excess due to enzyme mismetallation (78, 79). Thus, bacteria have evolved mechanisms to limit intracellular Cu^+ toxicity by keeping it tightly bound to proteins, thereby limiting deleterious side reactions. Delivery of Cu^+ into Cu^+ -containing proteins is often mediated by Cu^+ chaperones, such as Atx1 in yeast (70) or possibly CopZ in *B. subtilis* (5). CopZ is a Atx1-like protein that may sequester excess intracellular Cu^+ and deliver Cu^+ to the CopA CPx-type ATP-ase for efflux. Recent *in vitro* studies identified S-bacillithiolated forms of apo-CopZ as well as CopZ loaded with BSH: Cu^+ adducts (Fig. 5) (60). Further biochemical analysis revealed that BSH binds Cu^+ with a relatively high affinity of $\beta_2(\text{BSH}) = 4 \times 10^{17} \text{ M}^{-2}$ and a stoichiometry of 2 BSH to 1 Cu^+ , indicating a possible role for BSH in intracellular Cu^+ buffering. Cells lacking BSH are no more sensitive to Cu^+ than wild-type cells. Interestingly, expression of the CsoR-regulated, Cu^+ -responsive *copZA* operon is induced in the absence of BSH, suggesting elevated levels of labile Cu^+ and a role for BSH in Cu^+ buffering (75). However, the precise *in vivo* role of BSH in Cu^+ homeostasis remains to be determined.

Functions of BSH in *S. aureus* Virulence

BSH also plays an important role under infection-like conditions in the *S. aureus* clinical isolates, as shown in two phenotype studies using macrophage infection assays (111, 112). BSH-deficient mutants in clinical MRSA strains COL and USA300 showed a decreased survival in human whole-blood survival assays (111). In microarray analyses, the biosynthetic operon for staphyloxanthin was upregulated and the staphyloxanthin level was strongly decreased in the *bshA* mutant, suggesting lower radical scavenging ability in the absence of BSH. Staphyloxanthin is a carotenoid pigment that is produced by some *S. aureus* strains and is responsible for the yellow color from which the species name is derived. Staphyloxanthin provides protection against oxidative stress in neutrophil-infection assays and enhances the fitness of *S. aureus* (16).

Among the various *S. aureus* clonal complexes, it was found that natural BSH-deficient *S. aureus* strains have evolved that belong to the *S. aureus* NCTC8325 lineage (e.g., strain SH1000). They carry a *bshC* null mutation due to an 8 bp duplication in the *bshC* gene as a possible remnant of a transposon insertion (95, 111, 112). The natural *S. aureus*

SH1000 *bshC* mutant was compromised in survival during infection assays using murine macrophages and human epithelial cell lines in comparison to the repaired and *bshC*-complemented *S. aureus* SH1000 strain (111, 112). Thus, BSH is an important virulence factor contributing to pathogen fitness and provides protection against the host-immune system in *S. aureus* clinical MRSA isolates under infection-related conditions.

This makes the BSH biosynthesis enzymes attractive drug targets for the treatment of emerging MRSA infections. In particular, BshB inhibitors would be good candidates for anti-infectives that block biosynthesis and salvage of BSH. Future studies should be directed toward unraveling the mechanisms of virulence control by BSH in *S. aureus*, which could involve S-bacillithiolation of key enzymes or regulators.

Protein S-Bacillithiolation and Its Reversal by Brx

Targets of protein S-bacillithiolation in *B. subtilis* and *S. aureus*

In eukaryotes, protein S-glutathionylation functions as an important thiol-protection and redox-regulatory mechanism and is implicated in many physiological and pathophysiological processes, such as neurodegenerative and cardiovascular diseases, cancer, and diabetes (18, 42, 43). In *Firmicutes*, BSH plays a related role in a redox modification termed protein S-bacillithiolation (Fig. 6) (74). Protein S-bacillithiolation was first discovered as redox modification of the organic hydroperoxide repressor OhrR under cumene hydroperoxide (CHP) stress (Fig. 7). OhrR is inactivated due to S-bacillithiolation at its lone Cys15 residue under CHP stress, leading to upregulation of the OhrA peroxiredoxin that is involved in CHP detoxification (35, 64). However, OhrR is also involved in redox sensing of hypochloric acid and is inactivated by S-bacillithiolation under NaOCl stress, leading to *ohrA* derepression that confers resistance against NaOCl stress in *B. subtilis* (14). Thus, S-bacillithiolation functions as a redox-switch mechanism to control the activity of the redox-sensing transcription factor OhrR in *B. subtilis* in response to both CHP and NaOCl treatment.

Although the role of the OhrA peroxiredoxin in the detoxification of organic hydroperoxides to their corresponding alcohols is well known in several bacteria (24), the function of OhrA in NaOCl detoxification has still to be demonstrated *in vitro*. Moreover, there are two OhrR homologs encoded in the genomes of *S. aureus*, SarZ and MgrA, controlling *ohrA* homologs and large regulons for antibiotics resistance determinants and virulence factors (12). Evidence for the redox control and structural changes of SarZ and MgrA at the conserved single Cys by S-thiolation was demonstrated by using a synthetic thiol, benzene thiol *in vitro* (110). Recently, the quantitative redox proteomics approach OxICAT revealed increased oxidation of both SarZ and MgrA under NaOCl stress in *S. aureus* USA300, suggesting their redox regulation by S-bacillithiolation *in vivo* (56).

Apart from OhrR, the methionine synthase MetE was identified as the most abundant S-bacillithiolated protein in *Bacillus* species under NaOCl stress (Fig. 7). S-bacillithiolation of MetE was observed when cells were grown in minimal medium under NaOCl stress and MetE-SSB could be visualized as a major band in BSH-specific Western blots under NaOCl and diamide stress. MetE was S-bacillithiolated at its Zn-binding active site Cys730 and at the non-essential surface-

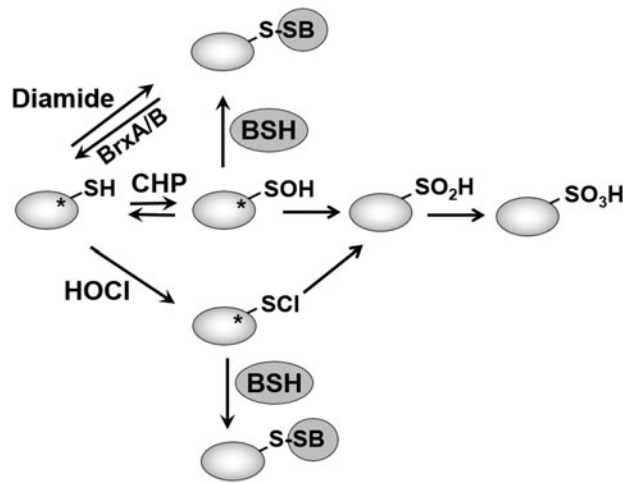


FIG. 6. Mechanisms of S-bacillithiolation and its reversal. Proteins are S-bacillithiolated under CHP, HOCl, and diamide stress in *Bacillus* and *Staphylococcus* species. Diamide is a reactive electrophile species leading directly to the formation of mixed BSH disulfides. CHP and HOCl activate thiols to a sulfenic acid (-SOH) and sulfenylchloride (-SCI) intermediates, respectively, that react further with BSH to form S-bacillithiolated proteins. In the absence of proximal thiols, -SOH and -SCI are overoxidized to sulfinic or sulfonic acids. Thus, S-bacillithiolation serves to protect vulnerable thiols against irreversible overoxidation. The asterisk indicates that often active site Cys residues are targets for S-bacillithiolation. The reversal of S-bacillithiolation is catalyzed by the BrxA/B. Brx, bacilliredoxin; CHP, cumene hydroperoxide.

exposed Cys719, causing a methionine auxotrophy phenotype under NaOCl stress (12). MetE is also a main target for S-glutathionylation and the most susceptible protein for thiol-oxidation in *E. coli* under diamide treatment (52, 66). S-glutathionylation of MetE occurs at a non-conserved Cys645 that is located at the entrance to the active site, also leading to methionine auxotrophy in *E. coli* (52).

We have shown that the conserved Zn-binding active site forms the mixed disulfide with BSH in *B. subtilis*, which is also target for S-mycothiolation in *C. glutamicum* under NaOCl stress (13). Inactivation of MetE under NaOCl stress in *B. subtilis* is accompanied by an increased transcription of the S-box regulon controlling genes for methionine biosynthesis. It is hypothesized that MetE inactivation could lead to a translation arrest to enable detoxification of hypochlorite and to avoid further protein damage. Further support for this postulated translation stop is provided by the observation that other amino acid biosynthesis enzymes (AroA), protein translation factors (Tuf), and ribosomal proteins (RpsM) are also targets for S-thiolation across Gram-positive bacteria (14).

In *S. aureus*, S-bacillithiolation was recently shown to control the activity of the glycolytic enzyme glyceraldehyde-3-phosphate dehydrogenase (Gap) of *S. aureus* under NaOCl stress (Fig. 7) (56). Gap is S-bacillithiolated at the conserved active site Cys151, which is a well-known target for various post-translational thiol-modifications, also including S-glutathionylation in eukaryotes. The reactivity of the Gap active site was shown to depend on a specific H₂O₂-binding pocket, transition state stabilization, and a proton relay mechanism promoting leaving-group departure (51, 105).

In *S. aureus*, Gap contributes as the most abundant Cys protein in the proteome, with 4% to the total Cys proteome of *S. aureus* and the S-bacillithiolated Gap was observed as a major band in NaOCl-treated cells using BSH-specific Western blots (56). Using OxICAT, Gap showed the highest oxidation increase of 29% at the S-bacillithiolated active site Cys151 under NaOCl stress. Detailed Gap activity assays in the presence of H₂O₂ and NaOCl with or without BSH revealed that Gap inactivation is faster due to S-bacillithiolation compared with overoxidation. These results lead to the conclusion that S-bacillithiolation of the Gap active site can efficiently prevent its irreversible overoxidation under both H₂O₂ and NaOCl treatments. Molecular docking of BSH into the Gap active site was used to model the structure of the S-bacillithiolated active site. The model of the Gap-SSB structure suggests that BSH can undergo disulfide formation with Cys151 without major conformational changes. This may explain why the most abundant Cys-protein Gap is the preferred and dominant target for S-bacillithiolation inside *S. aureus* cells (56).

Protein S-bacillithiolation is a widespread thiol-protection and redox-regulatory mechanism in different *Firmicutes* under hypochlorite stress, including industrially important *Bacillus* and *Staphylococcus* species, such as *B. subtilis*, *Bacillus amyloliquefaciens*, *Bacillus megaterium*, *Bacillus pumilus*, and the meat-starter culture *Staphylococcus carnosus* (8, 14, 74). Eight common and 29 unique S-bacillithiolated proteins were identified in the different *Firmicutes* using shotgun proteomics based on the mass increase of 396 Da at Cys residues (14, 15). The complete set of S-bacillithiolated proteins (the S-bacillithiolome) includes antioxidant function proteins, such as peroxiredoxins (YkuU), thiol-disulfide oxidoreductases (YumC) and Brx (YphP YqiW, YtxJ), translation factors (Tuf), chaperones (DnaK, GrpE), and several metabolic enzymes involved in the biosynthesis of amino acids, cofactors, and nucleotides. The translation elongation factor TufA, the methionine synthase MetE and its homolog YxjG, the inosine monophosphate dehydrogenase GuaB, and the inorganic pyrophosphatase PpaC belong to the conserved targets for S-bacillithiolation across *Firmicutes* bacteria that are also modified by S-mycothiolation in Actinomycetes (13).

Surprisingly, the glycolytic Gap is the major target for S-bacillithiolation in *S. aureus* (56), but Gap is not S-bacillithiolated in *Bacillus* species. Instead, the Gap enzyme of *B. subtilis* is oxidized to an intramolecular disulfide in its highly conserved CTTNC motif under NaOCl stress, as confirmed by mass spectrometry (14). This intracellular disulfide was also shown for the *E. coli* Gap homolog under NaOCl stress, since both Cys residues showed increased oxidations in the OxICAT analysis (65). However, in *S. aureus* Gap, the second Cys in this CTTNC motif is replaced by a serine explaining the preference of Cys151 for S-bacillithiolation under NaOCl stress.

All global S-bacillithiolome studies to date identified S-bacillithiolated proteins in *Firmicutes* bacteria by mass spectrometry and non-reducing BSH-Western blot analyses under NaOCl and diamide stress, but not under H₂O₂ stress *in vivo* (15). Previously, strongly increased S-thiolations were also observed at the global level under diamide stress in *B. subtilis* and *S. aureus* (113). S-glutathionylation requires activation of thiols to sulfenic acid, sulfenylamides, thiyl radicals, thio-sulfinate, or S-nitrosyl intermediates that, subsequently, react

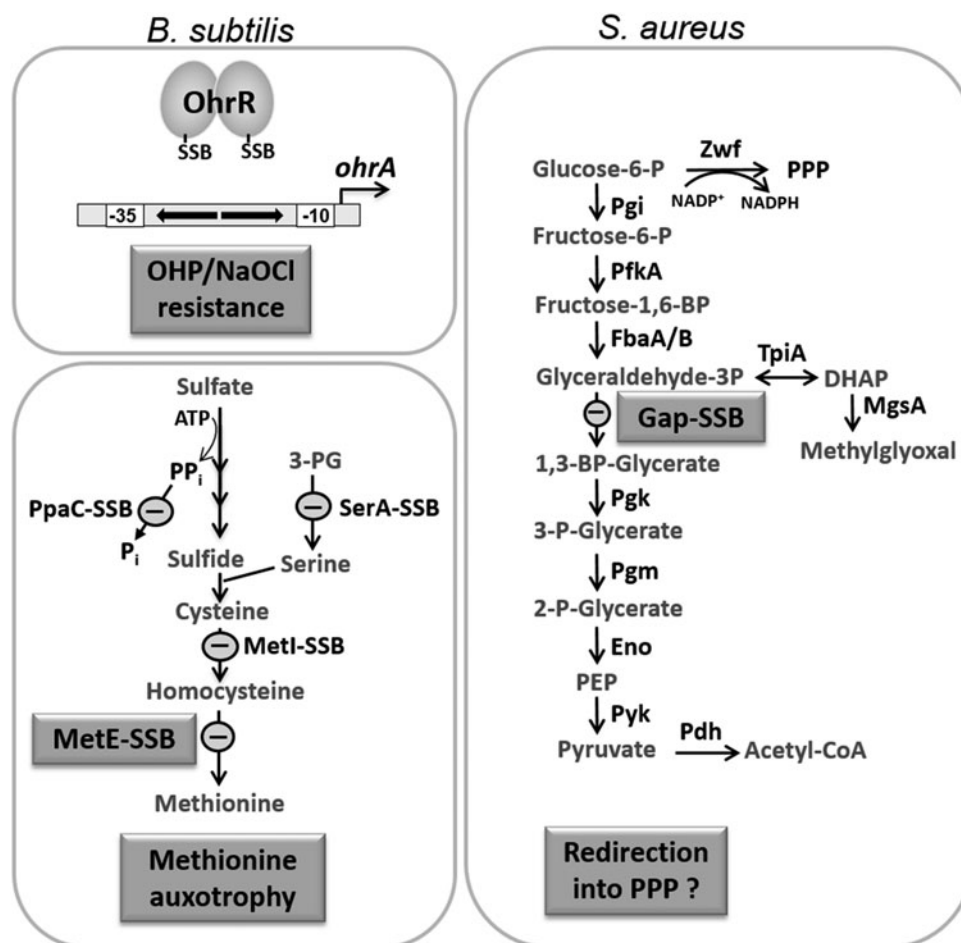


FIG. 7. Physiological roles of *S*-bacillithiolations for OhrR and MetE in *B. subtilis* and for Gap of *S. aureus*. NaOCl leads to *S*-bacillithiolation of OhrR and MetE as main targets in *B. subtilis* that have regulatory roles under NaOCl stress. *S*-bacillithiolation inactivates the OhrR repressor, leading to induction of the OhrA peroxiredoxin that confers resistance to NaOCl and OHP. *S*-bacillithiolation of the methionine synthase MetE at its active site Cys730 and of other enzymes of the Cys and Met biosynthesis pathway (YxjG, PpaC, SerA, MetI) leads to methionine auxotrophy. In *S. aureus*, the glycolytic Gap is the main target for *S*-bacillithiolation under NaOCl stress. *S*-bacillithiolation of the Gap active site Cys151 leads to reversible Gap inactivation and prevents its overoxidation to Cys sulfonic acid. Gap inactivation under oxidative stress might redirect the glycolytic flux into the PPP for NADPH regeneration, as shown in yeast cells. Gap, glyceraldehyde-3-phosphate dehydrogenase; OHP, organic hydroperoxide; PPP, pentose phosphate pathway.

further with GSH to the mixed disulfide (2, 41, 85, 86). Hypochlorite activates the thiol group *via* chlorination, leading to an unstable sulphenylchloride intermediate that quickly reacts further to generate *S*-bacillithiolations (Fig. 6) (19, 47). Diamide is a reactive electrophile known to form mixed disulfides, including *S*-thiolations in several organisms (113). The second-order rate constant of the reaction of HOCl with thiols is seven orders of magnitude higher compared with H₂O₂ (19, 104), explaining why *S*-bacillithiolation was not observed under H₂O₂ stress *in vivo*. Moreover, the pathogen *S. aureus* exhibits a remarkable resistance to 200 mM H₂O₂ due to efficient detoxification mechanisms that allow the survival under infection conditions (55, 73).

Apart from H₂O₂, *S. aureus* encounters HOCl during infections by activated neutrophils that is produced by myeloperoxidase (134), and hence, *S*-bacillithiolation serves as a major thiol-protection mechanism of essential enzymes, such as Gap under infection-related HOCl stress conditions. It will be interesting to uncover the targets for *S*-bacillithiolation

during infections, or in the anterior nares as the natural niche of *S. aureus* in future studies.

The BrxA and BrxB function in protein de-bacillithiolation

The Trx-fold proteins YtxJ, BrxA (YphP), and BrxB (YqiW) were identified as *S*-bacillithiolated in *B. subtilis* and *S. carnosus* that co-occur with the BSH biosynthesis enzymes (BshA, BshB, BshC) only in BSH-producing *Firmicutes* bacteria and were suggested to function as Brx in the reversal of *S*-bacillithiolations (Fig. 8A, B) (15). YtxJ is suggested as a monothiol Brx with the active site Cys located in a conserved TCPIS motif.

BrxA (YphP) and BrxB (YqiW) are DUF1094-family proteins with unusual CGC active site motifs, rather than the more common CxxC spacing seen in glutaredoxin (38, 40). BrxA was originally suggested to function as a thiol-disulfide isomerase based on its high standard redox potential of

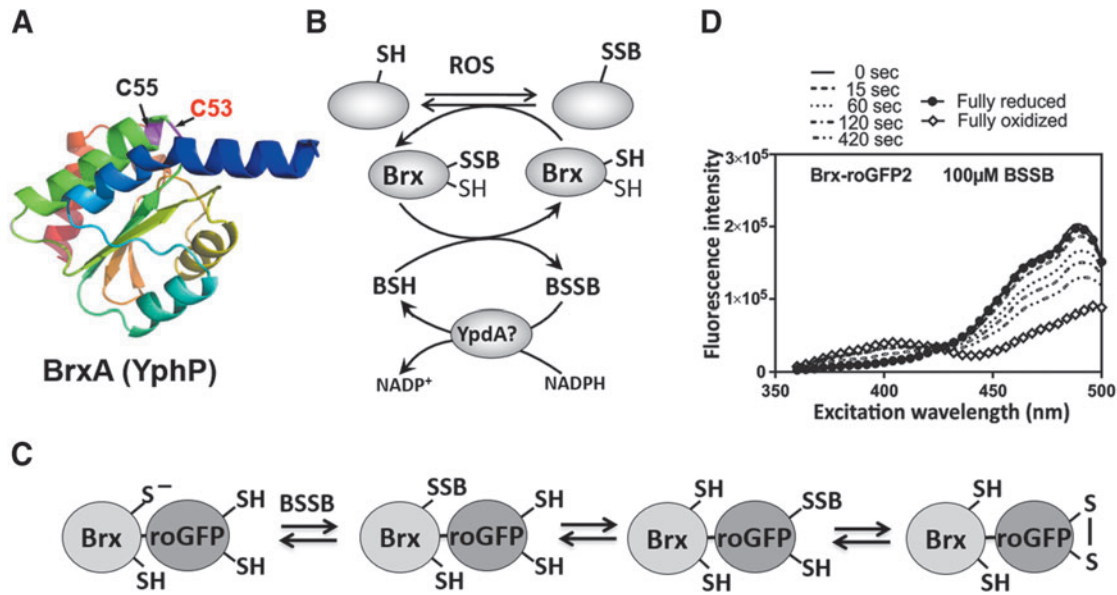


FIG. 8. Structure of the BrxA (YphP) of *B. subtilis* (A), Brx redox pathway (B), principle of Brx-roGFP2 biosensor oxidation (C), and ratiometric change of excitation spectra of Brx-roGFP2 by BSSB *in vitro* (D). (A) The structure of the BrxA (YphP) with the CGC active site motif was generated by using the software Phyre2 and PyMol. (B) BrxA reduces *S*-bacillithiolated proteins, resulting in Brx-SSB formation. Recycling of BrxA may require BSH and an NADPH-dependent BSSB reductase that could be YpdA. (C) The Brx-roGFP2 biosensor reacts first with BSSB at the active site Cys of Brx, leading to Brx-SSB formation, subsequent transfer of the BSH moiety to the coupled roGFP2, and re-arrangement to the roGFP2 disulfide. The roGFP2 disulfide causes a change of the 405/488 nm excitation ratio. (D) Brx-roGFP2 reacts very fast with purified 100 μM BSSB, as shown by the ratiometric change in the excitation maxima at 405 and 488 nm. For fully oxidized and reduced probes, Brx-roGFP2 was treated with 5 mM diamide and 10 mM DTT, respectively. The Brx-roGFP2 fluorescence excitation spectra were monitored by using the Clariostar microplate reader. Adapted from a previous publication (73). BSSB, oxidized bacillithiol disulfide.

$E^0 = -130$ mV (22). However, both BrxA and BrxB function in the reduction of the *S*-bacillithiolated MetE and OhrR *in vitro*, thereby demonstrating Brx activity (38). The BrxBCGA-resolving Cys mutant could regenerate DNA-binding activity of *S*-bacillithiolated OhrR *in vitro*, but *S*-cysteinylated OhrR could not be reactivated. MetE de-bacillithiolation was catalyzed by the BrxBCGA mutant as revealed by non-reducing BSH-specific Western blot analysis and mass spectrometry, but MetE reactivation could not be demonstrated *in vitro*. In *S. aureus*, Gap is the major *S*-bacillithiolated protein under NaOCl stress and Gap activity could be fully restored by using the BrxA (YphP) homolog SAUSA300_1321 (Brx) and the BrxCGA-resolving Cys mutant *in vitro* (56).

In conclusion, the BrxA and BrxB have been characterized to catalyze the de-bacillithiolation of two essential metabolic enzymes (MetE and Gap) and of the redox-sensing regulator OhrR in *B. subtilis* or *S. aureus*. These results provide evidence for the function of glutaredoxin-like Brx in industrially and medically important BSH-producing bacteria. However, phenotypic analyses of *brxA* and *brxB* single and double mutants revealed no significant growth phenotypes under NaOCl stress in *B. subtilis* (38). Thus, the Brx pathway is not essential and the Trx pathway might be alternatively involved in the de-bacillithiolation in *B. subtilis*.

A Brx-roGFP2 biosensor monitors dynamic changes in the BSH redox potential in *S. aureus*

Recently, Brx (YphP) was fused to redox-sensitive GFP (roGFP2) to construct a genetically encoded Brx-roGFP2

biosensor to monitor dynamic changes in the BSH redox potential in *S. aureus* (Fig. 8C, D) (73). Brx-roGFP2 responds specifically only to physiological concentrations of BSSB *in vitro*, but it does not react with other thiol disulfides (cysteine, GSSG, MSSM, CoASH disulfides). This further confirms the specificity of Brx for the reduction of BSH mixed disulfides in *S. aureus*.

The specificity of the Brx-roGFP2 biosensor to low doses of BSSB was shown to depend on the Brx active site *in vitro*, whereas direct responses of the roGFP2 to the oxidants *in vivo* could not be excluded. Brx-roGFP2 was shown to react very fast in *S. aureus* COL to low doses of 20–100 μM NaOCl *in vivo*, but high doses of a maximum of 100 mM H₂O₂ did not lead to complete biosensor oxidation. This confirms the high reactivity of NaOCl inside *S. aureus* that requires fast thiol protection by *S*-bacillithiolation to avoid the overoxidation of thiols. The weak biosensor response to H₂O₂ can be explained by the high level of peroxide resistance in *S. aureus*.

This Brx-roGFP2 biosensor was further applied to investigate the involvement of oxidative stress in the killing mode of antibiotics in *S. aureus* (73). The role of ROS in the mechanism of action of bactericidal antibiotics has been a subject of controversy (61, 71). Antibiotics that are commonly used to treat *S. aureus* infections were selected that target the RNA polymerase (rifampicin), cell-wall biosynthesis (fosfomycin, ampicillin, oxacillin, and vancomycin), protein biosynthesis (gentamycin, lincomycin, erythromycin, and linezolid), and DNA replication (ciprofloxacin). These different antibiotic classes did not lead to changes in the BSH redox potential at

sub-lethal concentrations, indicating that these antibiotics do not impose strong oxidative stress in *S. aureus*.

These results are consistent with roGFP2 biosensor results obtained in *Salmonella* under antibiotic treatment (131). However, due to its high peroxide resistance, *S. aureus* might be able to quickly detoxify ROS generated during antibiotic treatment. In the case of fosfomycin, BSH is directly required as a cofactor for FosB for detoxification in *S. aureus* (111). However, previous studies found no correlation between the level of fosfomycin resistance and BSH levels in different *S. aureus* clinical isolates, and no increased BSH redox potential was measured under fosfomycin treatment in *S. aureus* COL.

The Brx-roGFP2 biosensor was further expressed in two MRSA isolates, *S. aureus* COL and USA300, and the latter is highly virulent community-acquired MRSA. An increased BSH redox potential was measured during the entry into stationary phase in both strains, ranging from -300 to -270 mV in COL and from -300 to -235 mV in USA300 along the growth curve. Our future studies are directed to apply this Brx-roGFP2 biosensor for screening of the BSH redox potential across *S. aureus* isolates of different clonal complexes to reveal the differences in pathogen fitness and in their ROS detoxification capacities as defense mechanisms against the host immune system.

Concluding Remarks

In a previous review in this journal (50), written soon after the discovery of BSH, readers were introduced to this novel thiol and given a preview of how the field might develop, guided by analogy with the prior extensive work on GSH and, to a lesser extent, MSH. Many of the predictions made at that time have held true, but there have also been many surprises as well as frustrations. Here, we briefly highlight some of the pressing questions in the field that have not yet been resolved, although ongoing efforts will surely work to address these challenges.

Although the biosynthetic pathway of BSH is now well established, and extensive structural and biochemical studies have led to a detailed understanding of this process, the actual reaction catalyzed by BshC is still undetermined. The analogous enzyme for MSH synthesis uses aminoacylated tRNA^{Cys} as an activated form of Cys. We assume that BshC also requires an activated form of Cys, but the identity of this last substrate is unknown. Another key “missing” activity for our understanding of BSH biology is the BSSB reductase. Certainly, the *B. subtilis* YpdA protein (a TrxR homolog) is an attractive candidate, but attempts to demonstrate BSSB activity biochemically have been unsuccessful.

Although many of the proteins involved in the core metabolism of BSH are, by now, known, including the biosynthesis pathway and Brx, many BSH-utilizing enzymes and accessory functions are yet to be discovered. There are several peroxidases annotated as Gpx, thiol-peroxidase, or thiol-dependent peroxiredoxin in *Bacillus* and *Staphylococcus* species that could use BSH as a thiol cofactor for peroxide detoxification (Fig. 3E). It is also unclear as to whether BSH (or perhaps BSSB) is imported or exported from cells. In *E. coli*, GSH is exported to the periplasm (109), but an analogous process for BSH is not established. It is worth noting that *B. subtilis* has multiple importers assigned as having a role in cystine uptake (9), but it is not known as to whether one or more may, in addition, or instead, use BSSB as a substrate.

Although the role of BSH in thiol redox chemistry is well established, there are also other aspects that are still largely unexplored. As noted earlier, in some cases, BSH may play a key role in protecting cells against H₂S stress (122), and by analogy with GSH a role in protection against reactive nitrogen species can be predicted. Although BSH has already been investigated for its role in buffering of Zn²⁺ (25, 75) and in the assembly of FeS clusters (30, 117, 118), many details remain to be discovered, such as the possible roles of BSH and other thiols together with Brx (glutaredoxin-like enzymes) in bridging FeS clusters, analogous to the role of GSH and Grx proteins in iron trafficking and sensing in GSH-producing eukaryotic organisms.

Similarly, proteomics studies have documented an abundance of protein S-bacillithiolation as a major post-translational modification under oxidative stress conditions (14, 15, 56, 64, 74, 107), but the pathways that reverse this modification (Brx) and the consequences for enzyme activity are still only now emerging. On a broader level, a clear picture has not yet emerged as to which bacteria synthesize BSH instead of GSH (or MSH), and whether one offers specific advantages over the other. We look forward to the continued rapid progress in this area and the resolution of these questions, and others not yet even imagined.

Acknowledgments

This work was supported by grants from the National Institutes of Health (NIGMS) under award numbers GM059323 and GM109993 (J.D.H.) and from the Deutsche Forschungsgemeinschaft (DFG) AN746/3-1 and AN746/4-1 within the DFG priority program SPP1710 (H.A.), by the DFG Research Training Group GRK1947, project (C1) (H.A.), and by an ERC Consolidator grant (GA 615585) MYCOTHILOME (H.A.).

References

1. Akanuma G, Nanamiya H, Natori Y, Nomura N, and Kawamura F. Liberation of zinc-containing L31 (RpmE) from ribosomes by its paralogous gene product, YtiA, in *Bacillus subtilis*. *J Bacteriol* 188: 2715–2720, 2006.
2. Allen EM and Mieyal JJ. Protein-thiol oxidation and cell death: regulatory role of glutaredoxins. *Antioxid Redox Signal* 17: 1748–1763, 2012.
3. Andreini C, Banci L, Bertini I, and Rosato A. Zinc through the three domains of life. *J Proteome Res* 5: 3173–3178, 2006.
4. Baichoo N, Wang T, Ye R, and Helmann JD. Global analysis of the *Bacillus subtilis* Fur regulon and the iron starvation stimulon. *Mol Microbiol* 45: 1613–1629, 2002.
5. Banci L, Bertini I, Del Conte R, Markey J, and Ruiz-Duenas FJ. Copper trafficking: the solution structure of *Bacillus subtilis* CopZ. *Biochemistry* 40: 15660–15668, 2001.
6. Barron ES. Thiol groups of biological importance. *Adv Enzymol Relat Subj Biochem* 11: 201–266, 1951.
7. Barton LL, Fardeau ML, and Fauque GD. Hydrogen sulfide: a toxic gas produced by dissimilatory sulfate and sulfur reduction and consumed by microbial oxidation. *Met Ions Life Sci* 14: 237–277, 2014.
8. Berney M, Weimar MR, Heikal A, and Cook GM. Regulation of proline metabolism in mycobacteria and its role in carbon metabolism under hypoxia. *Mol Microbiol* 84: 664–681, 2012.

9. Burguiere P, Auger S, Hullo MF, Danchin A, and Martin-Verstraete I. Three different systems participate in L-cystine uptake in *Bacillus subtilis*. *J Bacteriol* 186: 4875–4884, 2004.
10. Cao M, Bernat BA, Wang Z, Armstrong RN, and Helmann JD. FosB, a cysteine-dependent fosfomycin resistance protein under the control of sigma(W), an extracytoplasmic-function sigma factor in *Bacillus subtilis*. *J Bacteriol* 183: 2380–2383, 2001.
11. Chandrangsou P, Dusi R, Hamilton CJ, and Helmann JD. Methylglyoxal resistance in *Bacillus subtilis*: contributions of bacillithiol-dependent and independent pathways. *Mol Microbiol* 91: 706–715, 2014.
12. Chen PR, Brugarolas P, and He C. Redox signaling in human pathogens. *Antioxid Redox Signal* 14: 1107–1118, 2011.
13. Chi BK, Busche T, Van Laer K, Basell K, Becher D, Clermont L, Seibold GM, Persicke M, Kalinowski J, Messens J, and Antelmann H. Protein S-mycothiolation functions as redox-switch and thiol protection mechanism in *Corynebacterium glutamicum* under hypochlorite stress. *Antioxid Redox Signal* 20: 589–605, 2014.
14. Chi BK, Gronau K, Mader U, Hessling B, Becher D, and Antelmann H. S-bacillithiolation protects against hypochlorite stress in *Bacillus subtilis* as revealed by transcriptomics and redox proteomics. *Mol Cell Proteomics* 10: M111 009506, 2011.
15. Chi BK, Roberts AA, Huyen TT, Basell K, Becher D, Albrecht D, Hamilton CJ, and Antelmann H. S-bacillithiolation protects conserved and essential proteins against hypochlorite stress in firmicutes bacteria. *Antioxid Redox Signal* 18: 1273–1295, 2013.
16. Clauditz A, Resch A, Wieland KP, Peschel A, and Gotz F. Staphyloxanthin plays a role in the fitness of *Staphylococcus aureus* and its ability to cope with oxidative stress. *Infect Immun* 74: 4950–4953, 2006.
17. Couturier J, Przybyla-Toscano J, Roret T, Didierjean C, and Rouhier N. The roles of glutaredoxins ligating Fe-S clusters: sensing, transfer or repair functions? *Biochim Biophys Acta* 1853: 1513–1527, 2015.
18. Dalle-Donne I, Rossi R, Colombo G, Giustarini D, and Milzani A. Protein S-glutathionylation: a regulatory device from bacteria to humans. *Trends Biochem Sci* 34: 85–96, 2009.
19. Davies MJ. Myeloperoxidase-derived oxidation: mechanisms of biological damage and its prevention. *J Clin Biochem Nutr* 48: 8–19, 2011.
20. de Rey Pailhade J. Sur un corps d'origine organique hydrogénéant le soufre à froid. *Compt Rend* 106: 1683, 1888.
21. delCardayre SB, Stock KP, Newton GL, Fahey RC, and Davies JE. Coenzyme A disulfide reductase, the primary low molecular weight disulfide reductase from *Staphylococcus aureus*. Purification and characterization of the native enzyme. *J Biol Chem* 273: 5744–5751, 1998.
22. Derewenda U, Boczek T, Gorres KL, Yu M, Hung LW, Cooper D, Joachimiak A, Raines RT, and Derewenda ZS. Structure and function of *Bacillus subtilis* YphP, a prokaryotic disulfide isomerase with a CXC catalytic motif. *Biochemistry* 48: 8664–8671, 2009.
23. Djoko KY, Ong CL, Walker MJ, and McEwan AG. The role of copper and zinc toxicity in innate immune defense against bacterial pathogens. *J Biol Chem* 290: 18954–18961, 2015.
24. Dubbs JM and Mongkolsuk S. Peroxiredoxins in bacterial antioxidant defense. *Subcell Biochem* 44: 143–193, 2007.
25. Eide DJ. Bacillithiol, a new role in buffering intracellular zinc. *Mol Microbiol* 94: 743–746, 2014.
26. Fahey RC. Novel thiols of prokaryotes. *Annu Rev Microbiol* 55: 333–356, 2001.
27. Fahey RC. Glutathione analogs in prokaryotes. *Biochim Biophys Acta* 1830: 3182–3198, 2013.
28. Fahey RC, Brown WC, Adams WB, and Worsham MB. Occurrence of glutathione in bacteria. *J Bacteriol* 133: 1126–1129, 1978.
29. Fairlamb AH, Blackburn P, Ulrich P, Chait BT, and Cerami A. Trypanothione: a novel bis(glutathionyl)-spermidine cofactor for glutathione reductase in trypanosomatids. *Science* 227: 1485–1487, 1985.
30. Fang Z and Dos Santos PC. Protective role of bacillithiol in superoxide stress and Fe-S metabolism in *Bacillus subtilis*. *Microbiologyopen* 4: 616–631, 2015.
31. Fang Z, Roberts AA, Weidman K, Sharma SV, Claiborne A, Hamilton CJ, and Dos Santos PC. Cross-functionalities of *Bacillus* deacetylases involved in bacillithiol biosynthesis and bacillithiol-S-conjugate detoxification pathways. *Biochem J* 454: 239–247, 2013.
32. Feng J, Che Y, Milse J, Yin YJ, Liu L, Ruckert C, Shen XH, Qi SW, Kalinowski J, and Liu SJ. The gene ncg12918 encodes a novel maleylpyruvate isomerase that needs mycothiol as cofactor and links mycothiol biosynthesis and gentisate assimilation in *Corynebacterium glutamicum*. *J Biol Chem* 281: 10778–10785, 2006.
33. Ferguson GP, Battista JR, Lee AT, and Booth IR. Protection of the DNA during the exposure of *Escherichia coli* cells to a toxic metabolite: the role of the KefB and KefC potassium channels. *Mol Microbiol* 35: 113–122, 2000.
34. Ferguson GP, McLaggan D, and Booth IR. Potassium channel activation by glutathione-S-conjugates in *Escherichia coli*: protection against methylglyoxal is mediated by cytoplasmic acidification. *Mol Microbiol* 17: 1025–1033, 1995.
35. Fuangthong M, Atichartpongkul S, Mongkolsuk S, and Helmann JD. OhrR is a repressor of *ohrA*, a key organic hydroperoxide resistance determinant in *Bacillus subtilis*. *J Bacteriol* 183: 4134–4141, 2001.
36. Gaballa A, Antelmann H, Aguilar C, Khakh SK, Song KB, Smaldone GT, and Helmann JD. The *Bacillus subtilis* iron-sparing response is mediated by a Fur-regulated small RNA and three small, basic proteins. *Proc Natl Acad Sci U S A* 105: 11927–11932, 2008.
37. Gaballa A, Antelmann H, Hamilton CJ, and Helmann JD. Regulation of *Bacillus subtilis* bacillithiol biosynthesis operons by Spx. *Microbiology* 159: 2025–2035, 2013.
38. Gaballa A, Chi BK, Roberts AA, Becher D, Hamilton CJ, Antelmann H, and Helmann JD. Redox regulation in *Bacillus subtilis*: the bacilliredoxins BrxA(YphP) and BrxB(YqiW) function in de-bacillithiolation of S-bacillithiolated OhrR and MetE. *Antioxid Redox Signal* 21: 357–367, 2014.
39. Gaballa A and Helmann JD. Identification of a zinc-specific metalloregulatory protein, Zur, controlling zinc transport operons in *Bacillus subtilis*. *J Bacteriol* 180: 5815–5821, 1998.
40. Gaballa A, Newton GL, Antelmann H, Parsonage D, Upton H, Rawat M, Claiborne A, Fahey RC, and Helmann JD. Biosynthesis and functions of bacillithiol, a major low-molecular-weight thiol in Bacilli. *Proc Natl Acad Sci U S A* 107: 6482–6486, 2010.

41. Gallogly MM and Mieyal JJ. Mechanisms of reversible protein glutathionylation in redox signaling and oxidative stress. *Curr Opin Pharmacol* 7: 381–391, 2007.
42. Ghezzi P. Regulation of protein function by glutathionylation. *Free Radic Res* 39: 573–580, 2005.
43. Ghezzi P. Protein glutathionylation in health and disease. *Biochim Biophys Acta* 1830: 3165–3172, 2013.
44. Grill E, Löffler S, Winnacker EL, and Zenk MH. Phytochelatins, the heavy-metal-binding peptides of plants, are synthesized from glutathione by a specific gamma-glutamylcysteine dipeptidyl transpeptidase (phytochelatin synthase). *Proc Natl Acad Sci U S A* 86: 6838–6842, 1989.
45. Grosse C, Schleuder G, Schmöle C, and Nies DH. Survival of *Escherichia coli* cells on solid copper surfaces is increased by glutathione. *Appl Environ Microbiol* 80: 7071–7078, 2014.
46. Harms N, Ras J, Reijnders WN, van Spanning RJ, and Stouthamer AH. S-formylglutathione hydrolase of *Paracoccus denitrificans* is homologous to human esterase D: a universal pathway for formaldehyde detoxification? *J Bacteriol* 178: 6296–6299, 1996.
47. Hawkins CL, Pattison DI, and Davies MJ. Hypochlorite-induced oxidation of amino acids, peptides and proteins. *Amino Acids* 25: 259–274, 2003.
48. Helbig K, Bleuel C, Krauss GJ, and Nies DH. Glutathione and transition-metal homeostasis in *Escherichia coli*. *J Bacteriol* 190: 5431–5438, 2008.
49. Helbig K, Grosse C, and Nies DH. Cadmium toxicity in glutathione mutants of *Escherichia coli*. *J Bacteriol* 190: 5439–5454, 2008.
50. Helmann JD. Bacillithiol, a new player in bacterial redox homeostasis. *Antioxid Redox Signal* 15: 123–133, 2011.
51. Hildebrandt T, Knesting J, Berndt C, Morgan B, and Scheibe R. Cytosolic thiol switches regulating basic cellular functions: GAPDH as an information hub? *Biol Chem* 396: 523–537, 2015.
52. Hondorp ER and Matthews RG. Oxidative stress inactivates cobalamin-independent methionine synthase (MetE) in *Escherichia coli*. *PLoS Biol* 2: e336, 2004.
53. Hopkins FG. On an autoxidisable constituent of the cell. *Biochem J* 15: 286–305, 1921.
54. Hopkins FG. On glutathione: a reinvestigation. *J Biol Chem* 84: 269–320, 1929.
55. Horsburgh MJ, Clements MO, Crossley H, Ingham E, and Foster SJ. PerR controls oxidative stress resistance and iron storage proteins and is required for virulence in *Staphylococcus aureus*. *Infect Immun* 69: 3744–3754, 2001.
56. Imber M, Huyen NT, Pietrzyk-Brzezinska AJ, Loi VV, Hillion M, Bernhardt J, Tharichen L, Kolsek K, Saleh M, Hamilton CJ, Adrian L, Grater F, Wahl M, and Antelmann H. Protein S-bacillithiolation functions in thiol-protection and redox regulation of the glyceraldehyde-3-phosphate dehydrogenase Gap in *Staphylococcus aureus* under hypochlorite stress. *Antioxid Redox Signal* 2016 [Epub ahead of print]; DOI: 10.1089/ars.2016.6897.
57. Imlay JA. Iron-sulphur clusters and the problem with oxygen. *Mol Microbiol* 59: 1073–1082, 2006.
58. Irving H and Williams RJP. 637. The stability of transition-metal complexes. *J Chem Soc (Resumed)* 1953: 3192–3210, 1953.
59. Jothivasan VK and Hamilton CJ. Mycothiol: synthesis, biosynthesis and biological functions of the major low molecular weight thiol in actinomycetes. *Nat Prod Rep* 25: 1091–1117, 2008.
60. Kay KL, Hamilton CJ, and Le Brun NE. Mass spectrometry of *B. subtilis* CopZ: Cu(i)-binding and interactions with bacillithiol. *Metallomics* 8: 709–719, 2016.
61. Kohanski MA, Dwyer DJ, Hayete B, Lawrence CA, and Collins JJ. A common mechanism of cellular death induced by bactericidal antibiotics. *Cell* 130: 797–810, 2007.
62. Lamers AP, Keithly ME, Kim K, Cook PD, Stec DF, Hines KM, Sulikowski GA, and Armstrong RN. Synthesis of bacillithiol and the catalytic selectivity of FosB-type fosfomycin resistance proteins. *Org Lett* 14: 5207–5209, 2012.
63. Lee JW and Helmann JD. Functional specialization within the Fur family of metalloregulators. *Biometals* 20: 485–499, 2007.
64. Lee JW, Soonsanga S, and Helmann JD. A complex thiolate switch regulates the *Bacillus subtilis* organic peroxide sensor OhrR. *Proc Natl Acad Sci U S A* 104: 8743–8748, 2007.
65. Leichert LI, Gehrke F, Gudiseva HV, Blackwell T, Ilbert M, Walker AK, Strahler JR, Andrews PC, and Jakob U. Quantifying changes in the thiol redox proteome upon oxidative stress in vivo. *Proc Natl Acad Sci U S A* 105: 8197–8202, 2008.
66. Leichert LI and Jakob U. Protein thiol modifications visualized in vivo. *PLoS Biol* 2: e333, 2004.
67. Li H, Mapolelo DT, Dingra NN, Naik SG, Lees NS, Hoffman BM, Riggs-Gelasco PJ, Huynh BH, Johnson MK, and Outten CE. The yeast iron regulatory proteins Grx3/4 and Fra2 form heterodimeric complexes containing a [2Fe-2S] cluster with cysteinyl and histidyl ligation. *Biochemistry* 48: 9569–9581, 2009.
68. Li H and Outten CE. Monothiol CGFS glutaredoxins and BolA-like proteins: [2Fe-2S] binding partners in iron homeostasis. *Biochemistry* 51: 4377–4389, 2012.
69. Li ZS, Szczypka M, Lu YP, Thiele DJ, and Rea PA. The yeast cadmium factor protein (YCF1) is a vacuolar glutathione S-conjugate pump. *J Biol Chem* 271: 6509–6517, 1996.
70. Lin SJ, Pufahl RA, Dancis A, O'Halloran TV, and Culotta VC. A role for the *Saccharomyces cerevisiae* ATX1 gene in copper trafficking and iron transport. *J Biol Chem* 272: 9215–9220, 1997.
71. Liu Y and Imlay JA. Cell death from antibiotics without the involvement of reactive oxygen species. *Science* 339: 1210–1213, 2013.
72. Lo TW, Westwood ME, McLellan AC, Selwood T, and Thornalley PJ. Binding and modification of proteins by methylglyoxal under physiological conditions. A kinetic and mechanistic study with N alpha-acetylglycine, N alpha-acetylcysteine, and N alpha-acetyllysine, and bovine serum albumin. *J Biol Chem* 269: 32299–32305, 1994.
73. Loi VV, Harms M, Müller M, Huyen NT, Hamilton CJ, Hochgrafe F, Pane-Farre J, and Antelmann H. Real-time imaging of the bacillithiol redox potential in the human pathogen *Staphylococcus aureus* using a genetically encoded bacilliredoxin-fused redox biosensor. *Antioxid Redox Signal* 2016 [Epub ahead of print]; DOI:10.1089/ars.2016.6733.
74. Loi VV, Rossius M, and Antelmann H. Redox regulation by reversible protein S-thiolation in bacteria. *Front Microbiol* 6: 187, 2015.
75. Ma Z, Chandransu P, Helmann TC, Romsang A, Gaballa A, and Helmann JD. Bacillithiol is a major buffer of the labile zinc pool in *Bacillus subtilis*. *Mol Microbiol* 94: 756–770, 2014.

76. Ma Z, Faulkner MJ, and Helmann JD. Origins of specificity and cross-talk in metal ion sensing by *Bacillus subtilis* Fur. *Mol Microbiol* 86: 1144–1155, 2012.
77. MacLean MJ, Ness LS, Ferguson GP, and Booth IR. The role of glyoxalase I in the detoxification of methylglyoxal and in the activation of the KefB K⁺ efflux system in *Escherichia coli*. *Mol Microbiol* 27: 563–571, 1998.
78. Macomber L and Imlay JA. The iron-sulfur clusters of dehydratases are primary intracellular targets of copper toxicity. *Proc Natl Acad Sci U S A* 106: 8344–8349, 2009.
79. Macomber L, Rensing C, and Imlay JA. Intracellular copper does not catalyze the formation of oxidative DNA damage in *Escherichia coli*. *J Bacteriol* 189: 1616–1626, 2007.
80. Maret W. Oxidative metal release from metallothionein via zinc-thiol/disulfide interchange. *Proc Natl Acad Sci U S A* 91: 237–241, 1994.
81. Mashruwala AA, Pang YY, Rosario-Cruz Z, Chahal HK, Benson MA, Mike LA, Skaar EP, Torres VJ, Nauseef WM, and Boyd JM. Nfu facilitates the maturation of iron-sulfur proteins and participates in virulence in *Staphylococcus aureus*. *Mol Microbiol* 95: 383–409, 2015.
82. Merchant SS and Helmann JD. Elemental economy: microbial strategies for optimizing growth in the face of nutrient limitation. *Adv Microb Physiol* 60: 91–210, 2012.
83. Mettert EL and Kiley PJ. How is Fe-S cluster formation regulated? *Annu Rev Microbiol* 69: 505–526, 2015.
84. Michalopoulos AS, Livaditis IG, and Gougoutas V. The revival of fosfomycin. *Int J Infect Dis* 15: e732–e739, 2011.
85. Mieyal JJ and Chock PB. Posttranslational modification of cysteine in redox signaling and oxidative stress: focus on S-glutathionylation. *Antioxid Redox Signal* 16: 471–475, 2012.
86. Mieyal JJ, Gallogly MM, Qanungo S, Sabens EA, and Shelton MD. Molecular mechanisms and clinical implications of reversible protein S-glutathionylation. *Antioxid Redox Signal* 10: 1941–1988, 2008.
87. Miller S, Douglas RM, Carter P, and Booth IR. Mutations in the glutathione-gated KefC K⁺ efflux system of *Escherichia coli* that cause constitutive activation. *J Biol Chem* 272: 24942–24947, 1997.
88. Moore CM, Gaballa A, Hui M, Ye RW, and Helmann JD. Genetic and physiological responses of *Bacillus subtilis* to metal ion stress. *Mol Microbiol* 57: 27–40, 2005.
89. Muhlenhoff U, Molik S, Godoy JR, Uzarska MA, Richter N, Seubert A, Zhang Y, Stubbe J, Pierrel F, Herrero E, Lillig CH, and Lill R. Cytosolic monothiol glutaredoxins function in intracellular iron sensing and trafficking via their bound iron-sulfur cluster. *Cell Metab* 12: 373–385, 2010.
90. Muller JE, Meyer F, Litsanov B, Kiefer P, and Vorholt JA. Core pathways operating during methylotrophy of *Bacillus methanolicus* MGA3 and induction of a bacillithiol-dependent detoxification pathway upon formaldehyde stress. *Mol Microbiol* 98: 1089–1100, 2015.
91. Natori Y, Nanamiya H, Akanuma G, Kosono S, Kudo T, Ochi K, and Kawamura F. A fail-safe system for the ribosome under zinc-limiting conditions in *Bacillus subtilis*. *Mol Microbiol* 63: 294–307, 2007.
92. Newton GL, Arnold K, Price MS, Sherrill C, Delcardayre SB, Aharonowitz Y, Cohen G, Davies J, Fahey RC, and Davis C. Distribution of thiols in microorganisms: mycothiol is a major thiol in most actinomycetes. *J Bacteriol* 178: 1990–1995, 1996.
93. Newton GL, Av-Gay Y, and Fahey RC. A novel mycothiol-dependent detoxification pathway in mycobacteria involving mycothiol S-conjugate amidase. *Biochemistry* 39: 10739–10746, 2000.
94. Newton GL, Bewley CA, Dwyer TJ, Horn R, Aharonowitz Y, Cohen G, Davies J, Faulkner DJ, and Fahey RC. The structure of U17 isolated from *Streptomyces clavuligerus* and its properties as an antioxidant thiol. *Eur J Biochem* 230: 821–825, 1995.
95. Newton GL, Fahey RC, and Rawat M. Detoxification of toxins by bacillithiol in *Staphylococcus aureus*. *Microbiology* 158: 1117–1126, 2012.
96. Newton GL, Leung SS, Wakabayashi JI, Rawat M, and Fahey RC. The DinB superfamily includes novel mycothiol, bacillithiol, and glutathione S-transferases. *Biochemistry* 50: 10751–10760, 2011.
97. Newton GL, Rawat M, La Clair JJ, Jothivasan VK, Budiarto T, Hamilton CJ, Claiborne A, Helmann JD, and Fahey RC. Bacillithiol is an antioxidant thiol produced in Bacilli. *Nat Chem Biol* 5: 625–627, 2009.
98. Nguyen TT, Eiamphungporn W, Mader U, Liebeke M, Lalk M, Hecker M, Helmann JD, and Antelmann H. Genome-wide responses to carbonyl electrophiles in *Bacillus subtilis*: control of the thiol-dependent formaldehyde dehydrogenase AdhA and cysteine proteinase YraA by the MerR-family regulator YraB (AdhR). *Mol Microbiol* 71: 876–894, 2009.
99. Nicely NI, Parsonage D, Paige C, Newton GL, Fahey RC, Leonardi R, Jackowski S, Mallett TC, and Claiborne A. Structure of the type III pantothenate kinase from *Bacillus anthracis* at 2.0 Å resolution: implications for coenzyme A-dependent redox biology. *Biochemistry* 46: 3234–3245, 2007.
100. Nies DH. Efflux-mediated heavy metal resistance in prokaryotes. *FEMS Microbiol Rev* 27: 313–339, 2003.
101. Outten CE and O'Halloran TV. Femtomolar sensitivity of metalloregulatory proteins controlling zinc homeostasis. *Science* 292: 2488–2492, 2001.
102. Ozyamak E, Black SS, Walker CA, Maclean MJ, Bartlett W, Miller S, and Booth IR. The critical role of S-lactoylglutathione formation during methylglyoxal detoxification in *Escherichia coli*. *Mol Microbiol* 78: 1577–1590, 2010.
103. Palmer LD and Skaar EP. Transition metals and virulence in bacteria. *Annu Rev Genet* 50: 67–91, 2016.
104. Pattison DI and Davies MJ. Absolute rate constants for the reaction of hypochlorous acid with protein side chains and peptide bonds. *Chem Res Toxicol* 14: 1453–1464, 2001.
105. Peralta D, Bronowska AK, Morgan B, Doka E, Van Laer K, Nagy P, Grater F, and Dick TP. A proton relay enhances H₂O₂ sensitivity of GAPDH to facilitate metabolic adaptation. *Nat Chem Biol* 11: 156–163, 2015.
106. Perera VR, Newton GL, Parnell JM, Komives EA, and Pogliano K. Purification and characterization of the *Staphylococcus aureus* bacillithiol transferase BstA. *Biochim Biophys Acta* 1840: 2851–2861, 2014.
107. Perera VR, Newton GL, and Pogliano K. Bacillithiol: a key protective thiol in *Staphylococcus aureus*. *Expert Rev Anti Infect Ther* 13: 1089–1107, 2015.
108. Picciocchi A, Saguez C, Boussac A, Cassier-Chauvat C, and Chauvat F. CGFS-type monothiol glutaredoxins from the cyanobacterium *Synechocystis* PCC6803 and other evolutionary distant model organisms possess a glutathione-ligated [2Fe-2S] cluster. *Biochemistry* 46: 15018–15026, 2007.
109. Pittman MS, Robinson HC, and Poole RK. A bacterial glutathione transporter (*Escherichia coli* CytDC) exports

- reductant to the periplasm. *J Biol Chem* 280: 32254–32261, 2005.
110. Poor CB, Chen PR, Duguid E, Rice PA, and He C. Crystal structures of the reduced, sulfenic acid, and mixed disulfide forms of SarZ, a redox active global regulator in *Staphylococcus aureus*. *J Biol Chem* 284: 23517–23524, 2009.
 111. Posada AC, Kolar SL, Dusi RG, Francois P, Roberts AA, Hamilton CJ, Liu GY, and Cheung A. Importance of bacillithiol in the oxidative stress response of *Staphylococcus aureus*. *Infect Immun* 82: 316–332, 2014.
 112. Pother DC, Gierok P, Harms M, Mostertz J, Hochgrafe F, Antelmann H, Hamilton CJ, Borovok I, Lalk M, Aharonowitz Y, and Hecker M. Distribution and infection-related functions of bacillithiol in *Staphylococcus aureus*. *Int J Med Microbiol* 303: 114–123, 2013.
 113. Pother DC, Liebeke M, Hochgrafe F, Antelmann H, Becher D, Lalk M, Lindequist U, Borovok I, Cohen G, Aharonowitz Y, and Hecker M. Diamide triggers mainly S Thiolations in the cytoplasmic proteomes of *Bacillus subtilis* and *Staphylococcus aureus*. *J Bacteriol* 191: 7520–7530, 2009.
 114. Rajkarnikar A, Strankman A, Duran S, Vargas D, Roberts AA, Barretto K, Upton H, Hamilton CJ, and Rawat M. Analysis of mutants disrupted in bacillithiol metabolism in *Staphylococcus aureus*. *Biochem Biophys Res Commun* 436: 128–133, 2013.
 115. Roberts AA, Sharma SV, Strankman AW, Duran SR, Rawat M, and Hamilton CJ. Mechanistic studies of FosB: a divalent-metal-dependent bacillithiol-S-transferase that mediates fosfomycin resistance in *Staphylococcus aureus*. *Biochem J* 451: 69–79, 2013.
 116. Robinson NJ and Winge DR. Copper metallochaperones. *Annu Rev Biochem* 79: 537–562, 2010.
 117. Rosario-Cruz Z and Boyd JM. Physiological roles of bacillithiol in intracellular metal processing. *Curr Genet* 62: 59–65, 2016.
 118. Rosario-Cruz Z, Chahal HK, Mike LA, Skaar EP, and Boyd JM. Bacillithiol has a role in Fe-S cluster biogenesis in *Staphylococcus aureus*. *Mol Microbiol* 98: 218–242, 2015.
 119. Sakuda S, Zhou ZY, and Yamada Y. Structure of a novel disulfide of 2-(N-acetylcysteinyl)amido-2-deoxy- α -D-glucopyranosyl-myo-inositol produced by *Streptomyces* sp. *Biosci Biotechnol Biochem* 58: 1347–1348, 1994.
 120. Sharma SV, Arbach M, Roberts AA, Macdonald CJ, Groom M, and Hamilton CJ. Biophysical features of bacillithiol, the glutathione surrogate of *Bacillus subtilis* and other firmicutes. *Chembiochem* 14: 2160–2168, 2013.
 121. Sharma SV, Jothivasan VK, Newton GL, Upton H, Wakabayashi JI, Kane MG, Roberts AA, Rawat M, La Clair JJ, and Hamilton CJ. Chemical and chemoenzymatic syntheses of bacillithiol: a unique low-molecular-weight thiol amongst low G+C gram-positive bacteria. *Angew Chem Int Ed Engl* 50: 7101–7104, 2011.
 122. Shen J, Keithly ME, Armstrong RN, Higgins KA, Edmonds KA, and Giedroc DP. *Staphylococcus aureus* CstB is a novel multidomain persulfide dioxygenase-sulfurtransferase involved in hydrogen sulfide detoxification. *Biochemistry* 54: 4542–4554, 2015.
 123. Smaldone GT, Antelmann H, Gaballa A, and Helmann JD. The FsrA sRNA and FbpB protein mediate the iron-dependent induction of the *Bacillus subtilis* lutABC iron-sulfur-containing oxidases. *J Bacteriol* 194: 2586–2593, 2012.
 124. Smaldone GT, Revelles O, Gaballa A, Sauer U, Antelmann H, and Helmann JD. A global investigation of the *Bacillus subtilis* iron-sparing response identifies major changes in metabolism. *J Bacteriol* 194: 2594–2605, 2012.
 125. Spies HS and Steenkamp DJ. Thiols of intracellular pathogens. Identification of ovothiol A in *Leishmania donovani* and structural analysis of a novel thiol from *Mycobacterium bovis*. *Eur J Biochem* 224: 203–213, 1994.
 126. Taguchi T, Yabe M, Odaki H, Shinozaki M, Metsa-Ketela M, Arai T, Okamoto S, and Ichinose K. Biosynthetic conclusions from the functional dissection of oxygenases for biosynthesis of actinorhodin and related *Streptomyces* antibiotics. *Chem Biol* 20: 510–520, 2013.
 127. Tang HJ, Chen CC, Cheng KC, Toh HS, Su BA, Chiang SR, Ko WC, and Chuang YC. In vitro efficacy of fosfomycin-containing regimens against methicillin-resistant *Staphylococcus aureus* in biofilms. *J Antimicrob Chemother* 67: 944–950, 2012.
 128. Thompson MK, Keithly ME, Harp J, Cook PD, Jagessar KL, Sulikowski GA, and Armstrong RN. Structural and chemical aspects of resistance to the antibiotic fosfomycin conferred by FosB from *Bacillus cereus*. *Biochemistry* 52: 7350–7362, 2013.
 129. Totemeyer S, Booth NA, Nichols WW, Dunbar B, and Booth IR. From famine to feast: the role of methylglyoxal production in *Escherichia coli*. *Mol Microbiol* 27: 553–562, 1998.
 130. Upton H, Newton GL, Gushiken M, Lo K, Holden D, Fahey RC, and Rawat M. Characterization of BshA, bacillithiol glycosyltransferase from *Staphylococcus aureus* and *Bacillus subtilis*. *FEBS Lett* 586: 1004–1008, 2012.
 131. van der Heijden J, Vogt SL, Reynolds LA, Pena-Diaz J, Tupin A, Aussel L, and Finlay BB. Exploring the redox balance inside gram-negative bacteria with redox-sensitive GFP. *Free Radic Biol Med* 91: 34–44, 2015.
 132. VanDuinen AJ, Winchell KR, Keithly ME, and Cook PD. X-ray crystallographic structure of BshC, a unique enzyme involved in bacillithiol biosynthesis. *Biochemistry* 54: 100–103, 2015.
 133. Winchell KR, Egeler PW, VanDuinen AJ, Jackson LB, Karpen ME, and Cook PD. A structural, functional, and computational analysis of BshA, the first enzyme in the bacillithiol biosynthesis pathway. *Biochemistry* 55: 4654–4665, 2016.
 134. Winterbourn CC, Kettle AJ, and Hampton MB. Reactive oxygen species and neutrophil function. *Annu Rev Biochem* 85: 765–792, 2016.

Address correspondence to:
 Dr. John D. Helmann
 Department of Microbiology
 Cornell University
 Ithaca, NY 14853-8101

E-mail: jdh9@cornell.edu

Prof. Haike Antelmann
 Institute for Biology-Microbiology
 Freie Universität Berlin
 Berlin D-14195
 Germany

E-mail: haike.antelmann@fu-berlin.de

Date of first submission to ARS Central, March 8, 2017; date of acceptance, March 15, 2017.

Abbreviations Used

Bca = BSH S-conjugate amidase
 Brx = bacilliredoxin
 BSH = bacillithiol
 BshA = glycosyltransferase for GlcNAc-Mal biosynthesis
 BshB = deacetylase-producing GlcN-Mal
 BshC = cysteine ligase for BSH biosynthesis
 BSSB = oxidized bacillithiol disulfide
 Bst = BSH-S-transferases
 CA-MRSA = community-acquired MRSA
 CHP = cumene hydroperoxide
 CoASH = coenzymeA
 Cys = cysteine
 DHAP = dihydroxyacetone phosphate
 EGT = ergothioneine
 FA = formaldehyde
 Fdh = formaldehyde dehydrogenases
 FeS = iron-sulfur
 Gap = glycolytic glyceraldehyde -3-phosphate dehydrogenase
 GlcNAc = N-acetyl glucoseamine
 GlxA/B = glyoxalases A and B
 Grx = glutaredoxin
 GSH = glutathione
 GSSG = oxidized glutathione disulfide
 Gst = GSH-S-transferases
 H₂O₂ = hydrogen peroxide
 H₂S = hydrogen sulfide

HTA = hemithioacetal
 LC-MS/MS = liquid chromatography tandem mass spectrometry
 LMW = low molecular weight
 Mal = malate
 Met = methionine
 MG = methylglyoxal
 MgsA = methylglyoxal synthase
 MRSA = methicillin-resistant *Staphylococcus aureus*
 Mrx1 = mycoredoxin1
 MSH = mycothiol
 MT = metallothionein
 NADH = nicotinamide adenine dinucleotide
 NADPH = nicotinamide adenine dinucleotide phosphate
 NaOCl = sodium hypochlorite
 OHP = organic hydroperoxide
 OhrR = organic hydroperoxide repressor
 PPP = pentose phosphate pathway
 protein-SSB = BSH protein mixed disulfide
 roGFP2 = redox-sensitive green fluorescent protein
 ROH = organic alcohol
 ROS = reactive oxygen species
 RuMP = ribose monophosphate pathway
 SLG = S-lactoylglutathione
 T(SH)₂ = trypanothione
 Trx = thioredoxin
 TrxR = thioredoxin reductase

Chapter 3

Protein S-bacillithiolation functions in thiol-protection and redox regulation of the glyceraldehyde-3-phosphate dehydrogenase Gap in *Staphylococcus aureus* under hypochlorite stress

Marcel Imber^{1*}, Nguyen Thi Thu Huyen^{1*}, Agnieszka J. Pietrzyk-Brzezinska^{2*}, **Vu Van Loi**^{1*}, Melanie Hillion¹, Jörg Bernhardt³, Lena Thärichen^{4,5}, Katra Kolsek⁵, Malek Saleh¹, Chris J. Hamilton⁶, Lorenz Adrian⁷, Frauke Gräter^{4,5}, Markus C. Wahl, and Haike Antelmann^{1#}

¹*Institute for Biology-Microbiology and* ²*Laboratory of Structural Biochemistry, Freie Universität Berlin, Berlin, Germany.*

³*Institute for Microbiology, Ernst-Moritz-Arndt-Universität of Greifswald, Greifswald, Germany.*

⁴*Molecular Biomechanics, Interdisciplinary Center for Scientific Computing (IWR), Heidelberg University, Heidelberg, Germany.*

⁵*Heidelberg Institute of Theoretical Studies, Heidelberg, Germany.*

⁶*School of Pharmacy, University of East Anglia, Norwich Research Park, Norwich, United Kingdom.*

⁷*Department Isotope Biogeochemistry, Helmholtz Centre for Environmental Research-UFZ, Leipzig, Germany*

Published in: Antioxidants & Redox Signaling. 28: 410-430. (2018)

<https://doi.org/10.1089/ars.2016.6897>

#Corresponding author: haike.antelmann@fu-berlin.de

Authors contributions

Vu Van Loi was involved in cloning of *gap*, Western blot experiments and tryptic digestions of the Gap proteins for Orbitrap LC-MS/MS analysis. Marcel Imber performed the biochemical experiments and GapDH enzyme assays. Nguyen Thi Thu Huyen and Melanie Hillion contributed with the proteomics analysis. Pietrzyk-Brzezinska, Markus C. Wahl, Lena Thärichen and Frauke Gräter were involved in structural analysis and molecular docking. Haike Antelmann wrote the manuscript. Marcel Imber, Agnieszka J. Pietrzyk-Brzezinska, **Vu Van Loi**, Melanie Hillion and Lena Thärichen prepared the figures.

* Shared first authorships



Protein S-Bacillithiolation Functions in Thiol Protection and Redox Regulation of the Glyceraldehyde-3-Phosphate Dehydrogenase Gap in *Staphylococcus aureus* Under Hypochlorite Stress

Marcel Imber,^{1,*} Nguyen Thi Thu Huyen,^{1,*} Agnieszka J. Pietrzyk-Brzezinska,^{2,*} Vu Van Loi,^{1,*} Melanie Hillion,¹ Jörg Bernhardt,³ Lena Thärichen,^{4,5} Katra Kolšek,⁵ Malek Saleh,¹ Chris J. Hamilton,⁶ Lorenz Adrian,⁷ Frauke Gräter,^{4,5} Markus C. Wahl,² and Haike Antelmann¹

Abstract

Aims: Bacillithiol (BSH) is the major low-molecular-weight thiol of the human pathogen *Staphylococcus aureus*. In this study, we used OxICAT and Voronoi redox treemaps to quantify hypochlorite-sensitive protein thiols in *S. aureus* USA300 and analyzed the role of BSH in protein S-bacillithiolation.

Results: The OxICAT analyses enabled the quantification of 228 Cys residues in the redox proteome of *S. aureus* USA300. Hypochlorite stress resulted in >10% increased oxidation of 58 Cys residues (25.4%) in the thiol redox proteome. Among the highly oxidized sodium hypochlorite (NaOCl)-sensitive proteins are five S-bacillithiolated proteins (Gap, AldA, GuaB, RpmJ, and PpaC). The glyceraldehyde-3-phosphate (G3P) dehydrogenase Gap represents the most abundant S-bacillithiolated protein contributing 4% to the total Cys proteome. The active site Cys151 of Gap was very sensitive to overoxidation and irreversible inactivation by hydrogen peroxide (H₂O₂) or NaOCl *in vitro*. Treatment with H₂O₂ or NaOCl in the presence of BSH resulted in reversible Gap inactivation due to S-bacillithiolation, which could be regenerated by the bacilliredoxin Brx (SAUSA300_1321) *in vitro*. Molecular docking was used to model the S-bacillithiolated Gap active site, suggesting that formation of the BSH mixed disulfide does not require major structural changes.

Conclusion and Innovation: Using OxICAT analyses, we identified 58 novel NaOCl-sensitive proteins in the pathogen *S. aureus* that could play protective roles against the host immune defense and include the glycolytic Gap as major target for S-bacillithiolation. S-bacillithiolation of Gap did not require structural changes, but efficiently functions in redox regulation and protection of the active site against irreversible overoxidation in *S. aureus*. *Antioxid. Redox Signal.* 28, 410–430.

Keywords: *Staphylococcus aureus*, S-bacillithiolation, thiol-redox proteomics, Gap, bacilliredoxin

¹Institute for Biology-Microbiology and ²Laboratory of Structural Biochemistry, Freie Universität Berlin, Berlin, Germany.

³Institute for Microbiology, Ernst-Moritz-Arndt-Universität of Greifswald, Greifswald, Germany.

⁴Molecular Biomechanics, Interdisciplinary Center for Scientific Computing (IWR), Heidelberg University, Heidelberg, Germany.

⁵Heidelberg Institute of Theoretical Studies, Heidelberg, Germany.

⁶School of Pharmacy, University of East Anglia, Norwich Research Park, Norwich, United Kingdom.

⁷Department Isotope Biogeochemistry, Helmholtz Centre for Environmental Research-UFZ, Leipzig, Germany.

*These authors contributed equally to this work.

Innovation

Using quantitative redox proteomics, 58 redox-sensitive protein thiols were identified in the methicillin-resistant *Staphylococcus aureus* strain USA300 that showed >10% increased oxidation under NaOCl stress. The glyceraldehyde-3-phosphate dehydrogenase Gap was identified as most abundant target for thiol oxidation and represents the major S-bacillithiolated protein in *S. aureus* cells. Molecular docking of bacillithiol (BSH) into the active site suggests that S-bacillithiolation does not require major structural changes. Finally, our biochemical assays confirm that S-bacillithiolation efficiently protects the Gap active site against overoxidation by H₂O₂ and NaOCl and inhibits Gap activity, which can be reversed by the bacilliredoxin Brx *in vitro*.

Introduction

STAPHYLOCOCCUS AUREUS IS a common commensal bacterium that colonizes the anterior nares and the skin of one quarter of the human population without causing symptoms of infections (22). However, *S. aureus* can also cause infections ranging from local skin or soft tissue infections to life-threatening diseases, such as septicemia, endocarditis, and necrotizing pneumonia, when the pathogen enters the bloodstream (2, 8, 53). Many nosocomial infections are caused by multiple antibiotic-resistant strains, such as methicillin-resistant *S. aureus* (MRSA) isolates (50). Moreover, new community-acquired MRSA strains are emerging quickly with other strains that are resistant to the last resort of antibiotics, such as vancomycin (22). Thus, to understand the adaptation of the pathogen to the host defense, it is of utmost importance to identify new drug targets for the treatment of MRSA infections.

The success of *S. aureus* as a leading pathogen is caused by high diversity of different virulence factors, such as toxins, proteases, lipases, and superantigens, as well as efficient protection mechanisms against the host immune defense during invasion. During infections, *S. aureus* has to cope with the oxidative burst of activated macrophages and neutrophils, including reactive oxygen and nitrogen species (ROS, RNS) and the strong oxidant hypochlorous acid (HOCl) (75, 76). HOCl is produced in neutrophils by the enzyme myeloperoxidase (MPO) from hydrogen peroxide (H₂O₂) and chloride (44). The involvement of HOCl as prime mechanism for oxidative killing of *S. aureus* by neutrophils has been shown using MPO inhibitors (29). Moreover, killing of many bacteria by isolated neutrophils is strongly inhibited in the absence of MPO (44).

S. aureus uses several redox-sensing virulence regulators, such as SarA and the MarR/OhrR-type regulators, MgrA and SarZ, for defense against oxidative stress. These control large regions of virulence factors, antibiotic resistance determinants, and ROS detoxification enzymes (11–13, 35). MgrA and SarZ are both single Cys MarR/OhrR-type repressors that sense and respond to ROS *via* thiol-based redox switches and by Cys phosphorylation (63, 70). In addition, *S. aureus* uses the low-molecular-weight (LMW) thiol bacillithiol (BSH, Cys-GlcNAc-Mal) to maintain the reduced state of the cytoplasm. BSH plays an important role in detoxification of redox-active compounds in *S. aureus* since *bshA* mutants displayed increased sensitivities to ROS, hypochlorite,

electrophiles, and the antibiotic fosfomycin (52, 64, 65). Moreover, BSH mediates protection under infection-like conditions as shown in phagocytosis assays using human macrophages (64, 65). Apart from BSH, also CoenzymeA (CoASH) and cysteine are found as abundant alternative LMW thiols in *S. aureus* cells (58).

Under hypochlorite stress, we have shown that BSH is also used for S-thiolation of redox-sensitive Cys residues and forms mixed disulfides with proteins that are termed as S-bacillithiolation. S-bacillithiolation protects protein thiols against overoxidation to sulfonic acids and is an important redox regulatory device in Firmicutes analogous to S-glutathionylation in eukaryotes (15, 16, 47, 52). The presence of CoASH and cysteine as LMW thiols suggests that alternative S-thiolations are also possible in *S. aureus*, such as S-cysteinylation or CoASH mixed disulfides. In support of this notion, *S. aureus* encodes a CoASH disulfide reductase (Cdr) that functions in reduction of CoASH mixed protein disulfides (55).

Using shotgun proteomics, we have previously identified 54 S-bacillithiolated proteins in different *Bacillus species* and *Staphylococcus carnosus* (16). Among these are eight conserved S-bacillithiolated proteins, such as the methionine synthase MetE, the inorganic pyrophosphatase PpaC, and the inosine-5'-monophosphate (IMP) dehydrogenase GuaB. The glutaredoxin-like YphP protein of the UPF0403 family was also S-bacillithiolated in *Bacillus subtilis in vivo* at its CGC active site motif (15). YphP and its paralog YqiW were renamed as BrxA and BrxB based on their function as bacilliredoxins in the reduction of S-bacillithiolated OhrR and MetE *in vitro* (24). Reduction of S-bacillithiolated proteins leads to Brx-SSB formation, which requires BSH and a still unknown BSSB reductase for recycling (24, 25, 31, 52). We have recently fused the YphP homolog (Brx) of *S. aureus* USA300 (SAUSA300_1321) to roGFP2 to construct a dynamic biosensor to monitor BSH redox potential changes *in vivo* (51). Brx-roGFP2 was highly specific to recognize BSSB, which confirms the role of Brx as bacilliredoxin also in *S. aureus*.

The physiological role of S-bacillithiolation in redox regulation has been demonstrated for the redox-sensing OhrR repressor and the methionine synthase MetE under hypochlorite stress in *B. subtilis*. S-bacillithiolation of MetE in its active site Zn center leads to its inactivation and subsequent methionine auxotrophy (15). The DNA-binding activity of the organic hydroperoxide repressor, OhrR, is inhibited by S-bacillithiolation under sodium hypochlorite (NaOCl) and cumene hydroperoxide stress, which results in the expression of the OhrA peroxiredoxin as ROS protection mechanism (15, 47).

However, the targets for S-bacillithiolation or reversible thiol oxidation under hypochlorite stress are unknown in the major pathogen *S. aureus*, which could provide leads in drug design to treat MRSA infections. In this study, we have combined the quantitative redox proteomic approach OxICAT (9, 48, 49) and shotgun proteomics to quantify NaOCl-sensitive proteins and to identify S-bacillithiolated proteins in *S. aureus* USA300. We found that 25% protein thiols showed >10% increased oxidation under NaOCl stress. The glycolytic Gap was identified as the most abundant S-bacillithiolated protein in *S. aureus*. Our results document that S-bacillithiolation protects the active site against overoxidation and inhibits Gap activity *in vitro*.

Results

Identification of 58 NaOCl-sensitive proteins using the quantitative redox proteomic approach OxICAT in *S. aureus* USA300

We were interested to study the role of BSH for *S.* bacillithiolation and the global thiol oxidation state under hypochlorite stress in the major pathogen *S. aureus*. Thus, we performed a quantitative thiol redox proteomic approach based on OxICAT (48, 49) and analyzed the percentages of thiol oxidation levels in *S. aureus* USA300 in response to 150 μ M NaOCl stress, as determined previously (51). OxICAT is based on the differential thiol labeling of reduced Cys residues with light isotope-coded affinity tag (12 C-ICAT), followed by reduction of reversible thiol oxidation (e.g., protein disulfides and *S*-thiolation) with Tris (2-carboxyethyl) phosphine (TCEP) and subsequent labeling of previously oxidized thiols with heavy 13 C-ICAT reagent (48). Light and heavy ICAT-labeled peptide pairs show a mass difference of 9 Da

after separation using mass spectrometry (MS). The quantification of the percentage of thiol oxidation for each Cys peptide is based on the calculation of the intensity of the heavy ICAT-labeled Cys peptide in relation to the total intensity of the light and heavy ICAT-labeled Cys peptides.

The OxICAT analysis enabled the quantification of the percentages of reversible thiol oxidation for 228 Cys peptides in the thiol redox proteome of *S. aureus* USA300 (Supplementary Table S1; Supplementary Data; Supplementary Data are available online at www.liebertpub.com/ars). The percentages of thiol oxidation were color coded and visualized in *Voronoi redox treemaps* according to the TIGRfam classification of *S. aureus* USA300 (Fig. 1).

In untreated *S. aureus* cells, we identified 193 Cys residues (84.6%) with a thiol oxidation level of <25%, including 107 Cys residues (46.9%) with <10% oxidation, indicating that the majority of thiols are in a reduced state (Tables 1 and 2; Supplementary Table S1). Only 35 Cys residues (15.3%) showed basal-level oxidation of >25% in the control. These

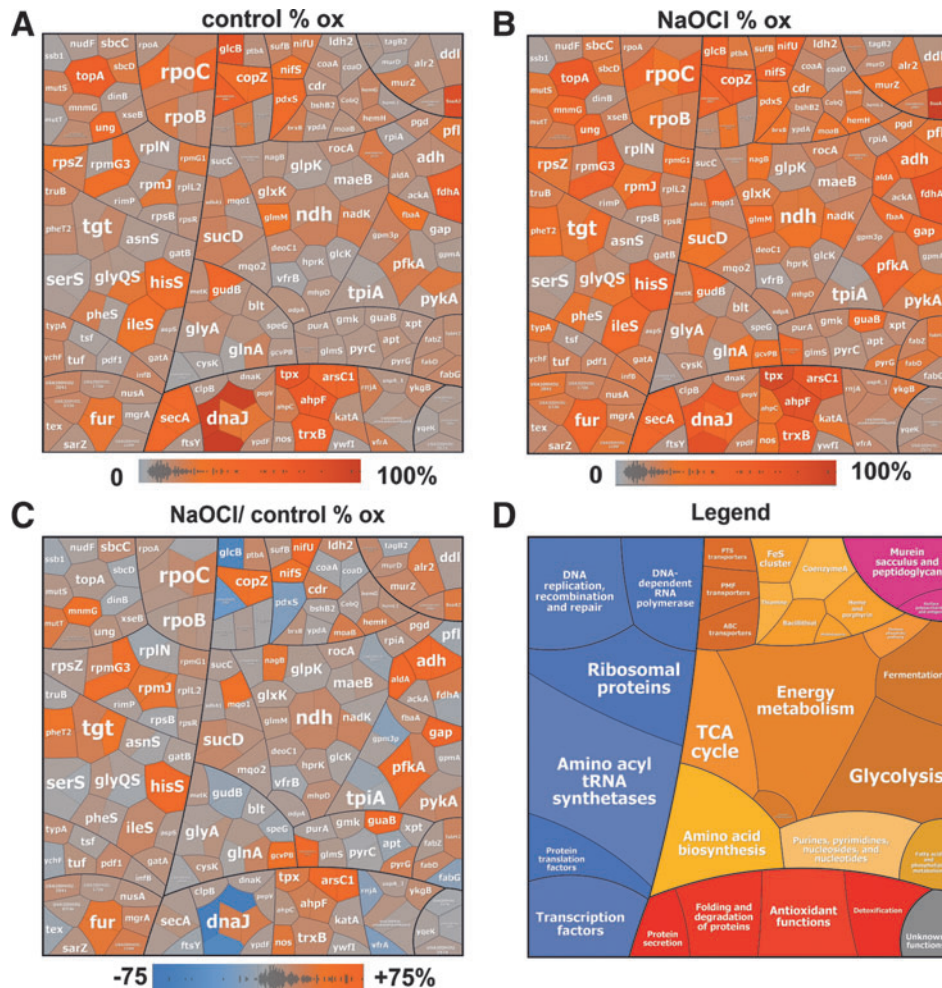


FIG. 1. Percentages of thiol oxidation for 228 Cys peptides that are identified in *Staphylococcus aureus* USA300 and visualized using *Voronoi redox treemaps*. The percentages of thiol oxidation of 228 Cys residues that are identified using OxICAT in *S. aureus* USA300 in the control (A) and 30 min after exposure to 150 μ M NaOCl stress (B) are visualized using *Voronoi redox treemaps*. The gray–red color gradient denotes 0–100% oxidation. The *Voronoi redox treemap* in (C) shows the percentages of oxidation changes under NaOCl stress using a blue–red color gradient ranging from –75% to +75% oxidation. The treemap in (D) serves as the legend showing the functional classifications of proteins. The treemaps are generated using the Paver software (Decodon) based on the OxICAT data presented in Supplementary Tables S1 and proteins were classified according to the *S. aureus* USA300 TIGRfam annotation. NaOCl, sodium hypochlorite.

TABLE 1. OVERVIEW OF % THIOL OXIDATION OF 228 CYS RESIDUES IN THE REDOX PROTEOME OF *STAPHYLOCOCCUS AUREUS*

228 Cys residues	<25% (<10%)	>25% (>40%)
% Thiol oxidation Control	193 (107) 84.6% (46.9%)	35 (15) 15.3% (6.6%)
% Thiol oxidation NaOCl	159 (35) 69.7% (15.3%)	69 (27) 30.2% (11.8%)
	<10%	>10% (20–30%)
% Thiol oxidation increase (NaOCl/Control)	170 74.6%	58 (19) 25.4% (8.3%)

Overview of % thiol oxidation of 228 Cys peptides identified in the redox proteome of the *S. aureus* USA300 under control and NaOCl stress, as revealed by OxICAT. All reduced Cys peptides have an oxidation degree of <25% that include those with <10% oxidation, shown in parenthesis. Oxidized Cys peptides have an oxidation degree of >25%. The % thiol oxidation increase includes Cys peptides with no significant increased oxidation (<10%) and those with >10% increased oxidation in response to NaOCl stress compared with the control. The % thiol-oxidation and % thiol-oxidation increase and related Cys numbers are shown in *bold-faced*. The percentage of Cys numbers in relation to all Cys residues is shown in *non-bold faced*.

NaOCl, sodium hypochlorite.

basal-level oxidized proteins include predicted redox-sensitive proteins (21), such as the thiol peroxidase Tpx, the alkyl hydroperoxide reductase large subunit AhpF, the arsenate reductase ArsC1, and the thioredoxin reductase TrxB1. Tpx and AhpCF were previously found as basal-level oxidized in the redox proteomes of *Escherichia coli* and *Bacillus* species (16, 48). Tpx was also S-mycothiolated in *Corynebacterium glutamicum* at the conserved active site Cys60 (14). In addition, the topoisomerase TopA and the DnaJ chaperone are basal-level oxidized at their Zn-binding Cys residues.

To discover novel NaOCl-sensitive proteins, we analyzed the percentages of thiol oxidation levels under NaOCl stress and its oxidation increase using OxICAT (Fig. 1 and Tables 2; Supplementary Table S1). The OxICAT approach enabled the identification of 58 NaOCl-sensitive Cys residues (25.4%) with >10% increased oxidation, including 19 Cys residues with 20–30% oxidation change under NaOCl stress (Tables 1 and 2 and Supplementary Table S1). Several NaOCl-sensitive proteins have antioxidant functions, such as the AhpCF peroxiredoxins, the thioredoxin reductase TrxB1, and the arsenate reductase ArsC. Furthermore, interesting proteins are the nitric oxide synthase (USA300HOU_1916) and the CoASH disulfide reductase Cdr (USA300HOU_0929), the latter is oxidized at the conserved Cys16. Apart from Cdr, the putative BSH disulfide reductase YpdA (USA300GOU_1417) was oxidized at the same conserved Cys14, but its oxidation is not increased under NaOCl stress (Supplementary Table S1). Moreover, we observed a slightly increased oxidation of the deacetylase BshB2 involved BSH biosynthesis and of the bacilliredoxin YqiW (BrxB) under NaOCl stress. The oxidation of Cdr, YpdA, BshB2, and BrxB could indicate increased S-bacillithiolation and CoASH mixed protein disulfides under NaOCl stress.

NaOCl-sensitive proteins are often oxidized in CxxC motifs and at conserved Zn-binding sites. Examples for Zn redox switches are the Zn-containing alcohol dehydrogenase Adh (USA300HOU_0610), the ribosomal proteins RpmG3

(USA300HOU_1553), and RpmJ (USA300HOU_2218). Zn-containing ribosomal proteins share three to four Cys residues that are suggested to serve as reservoir for Zn storage (54). As another Zn redox switch, we identified the ferric uptake repressor Fur that showed 16.6% increased oxidation at its Zn-binding site at Cys 140 and Cys143 under NaOCl stress (Tables 2; Supplementary Table S1; Figs. 1–2). Fur contains two CxxC motifs that form a structural Cys4:Zn site and are required for stability. In addition, two regulatory iron-binding sites are present in Fur (32). FurA of *Anabaena* was described as redox switch under oxidative stress and Cys101 in the CxxC motif is essential for iron-sensing and DNA-binding activity (7).

The copper chaperone CopZ was 19.8% oxidized in its CxxC motif that is required for Cu binding (67). The interaction of the *B. subtilis* CopZ homolog with BSH has been recently studied leading to the formation of S-bacillithiolated apo-CopZ and Cu(i)-bound forms of CopZ (42). In addition, NaOCl-sensitive Cys residues often coordinate FeS clusters or function in FeS cluster biogenesis. The FeS cluster scaffold protein NifU showed 26% increased oxidation at Cys41 that binds the FeS cluster during the assembly. The cysteine desulfurase NifS exhibits 20.6% higher oxidation levels at the catalytic Cys371 that forms the persulfide with the sulfur released during cysteine desulfuration (5). In addition, the FeS cluster assembly protein SufB is oxidized in its FeS cluster binding Cys302. It is interesting to note that the *nifS-nifU-sufB* genes are cotranscribed in an operon.

As NaOCl-sensing redox regulators, the MarR/OhrR family repressors, MgrA and SarZ (USA300HOU_0709 and USA300HOU_2368), were identified that showed 10.5% and 6.5% increased oxidation levels under NaOCl stress at their redox-sensing single Cys (Fig. 2). The DNA-binding activity of MgrA and SarZ was inhibited by S-thiolation using a synthetic thiol *in vitro* (11, 13, 35). In this study, increased oxidation of MgrA and SarZ was found in *S. aureus* under NaOCl stress, indicating that both could be redox controlled by S-bacillithiolation analogous to OhrR of *B. subtilis* (47). OhrR and SarZ both control a homologous *ohrA* peroxiredoxin gene that confers resistance to organic hydroperoxides and NaOCl in *B. subtilis* (13). Northern blot analyses revealed increased transcription of *ohrA* under NaOCl stress, indicating that SarZ oxidation leads to its inactivation and derepression of *ohrA* transcription (Fig. 3). We further noted the 15% increased oxidation of the virulence factor and secretory antigen SsaA2 at its conserved single Cys171 under NaOCl stress. The homologous SceB precursor (Sca_1790) of *S. carnosus* was previously S-bacillithiolated at the conserved Cys in NaOCl-treated cells (16). Thus, SsaA2 is most likely also S-bacillithiolated in *S. aureus*.

The NaOCl-sensitive proteins of *S. aureus* include many metabolic enzymes that function in energy metabolism and in different biosynthesis pathways for amino acids, fatty acids, nucleotides, and cofactors. NaOCl-sensitive enzymes involved in energy metabolism include the glycolytic glyceraldehyde-3-phosphate (G3P) dehydrogenase Gap and phosphofructokinase PfkA (USA300HOU_1685), the alcohol dehydrogenase Adh, the aldehyde dehydrogenase AldA (USA300HOU_2110), the formate dehydrogenase FdhA (USA300HOU_2291), and the malate dehydrogenase Mqo (USA300HOU_2348). Gap and AldA both showed the highest oxidation increase of 29% and 26% under NaOCl stress at their

TABLE 2. QUANTIFICATION OF 58 CYS PEPTIDES WITH REVERSIBLE THIOL OXIDATION THAT SHOWED >10% INCREASED OXIDATION IN *STAPHYLOCOCCUS AUREUS* USA300 UNDER NaOCl STRESS USING THE OXICAT APPROACH

<i>Locus tag</i>	<i>Gene name</i>	<i>Protein function</i>	<i>Cys</i>	<i>Buried/ Exposed</i>	<i>RSA (%)</i>	<i>% Diff NaOCl/Co</i>	<i>Mean % oxidation control</i>	<i>CV</i>	<i>Mean % oxidation NaOCl</i>	<i>CV</i>
Cell envelope function										
USA300HOU_2065	alr2	Alanine racemase	Cys311 ^a	B	3.7	14.56	8.22	0.16	22.79	0.14
USA300HOU_2065	alr2	Alanine racemase	Cys304	B	8.7	13.89	9.86	0.11	23.75	0.08
USA300HOU_2112	murZ	UDP-N-acetylglucosamine 1-carboxyvinyltransferase	Cys110	B	7.7	10.03	16.57	0.10	26.60	0.16
USA300HOU_2112	murZ	UDP-N-acetylglucosamine 1-carboxyvinyltransferase	Cys118 ^a	E	56.2	10.03	16.57	0.10	26.60	0.16
USA300HOU_2280	SsaA2	Secretory antigen SsaA2	Cys171 ^a	B	1.3	14.94	71.35	0.14	86.29	0.02
Protein quality control (Chaperones and proteases)										
USA300HOU_1580	dnaJ	Chaperone DnaJ	Cys149 ^a	B	8.3	13.44	21.81	0.43	35.24	0.10
USA300HOU_1580	dnaJ	Chaperone DnaJ	Cys152 ^a	B	24.7	13.44	21.81	0.43	35.24	0.10
Detoxification and adaptation to atypical environments										
USA300HOU_1700	tpx [#]	Thiol peroxidase	Cys60 ^a	B	2.6	14.48	62.73	0.05	77.21	0.02
USA300HOU_0403	ahpF [#]	Peroxiredoxin subunit F	Cys335 ^a	B	3.3	12.54	56.65	0.08	69.19	0.05
USA300HOU_0403	ahpF [#]	Peroxiredoxin subunit F	Cys338 ^a	B	7.5	12.54	56.65	0.08	69.19	0.05
USA300HOU_0839	arsC1 [#]	Arsenate reductase	Cys10 ^a	B	10.1	24.59	38.55	0.11	63.14	0.12
USA300HOU_0839	arsC1 [#]	Arsenate reductase	Cys13 ^a	B	8.9	24.59	38.55	0.11	63.14	0.12
USA300HOU_1916	nos	Nitric oxide synthase	Cys131	B	10.9	15.52	9.34	0.03	24.85	0.53
DNA replication, recombination, and repair										
USA300HOU_2714	mnmG	Glucose-inhibited division protein A	Cys274 ^a	B	13.4	20.86	13.36	0.41	34.22	0.18
USA300HOU_2481	mutT	Mutator protein mutT	Cys87	B	1.5	14.82	4.45	0.25	19.26	0.19
Transcription and transcriptional regulators										
USA300HOU_1499	fur	Fur repressor	Cys140 ^a	B	3.1	16.63	22.73	0.51	39.36	0.30
USA300HOU_1499	fur	Fur repressor	Cys143 ^a	B	7.5	16.63	22.73	0.51	39.36	0.30
USA300HOU_0709	mgrA	MarR/OhrR transcriptional regulator MgrA	Cys12	B	5.0	10.46	6.62	0.11	17.08	0.02
USA300HOU_2368	sarZ	MarR/OhrR transcriptional regulator SarZ	Cys13	B	4.2	6.31	8.43	0.29	14.73	0.07
USA300HOU_1199	USA300HOU_1199	Nucleic acid-binding, transcription termination	Cys11 ^a	B	2.8	13.33	8.21	0.35	21.54	0.38
USA300HOU_0537	rpoC	RNA polymerase subunit beta'	Cys75 ^a	B	4.3	13.00	37.68	0.11	50.69	0.08

(continued)

TABLE 2. (CONTINUED)

<i>Locus tag</i>	<i>Gene name</i>	<i>Protein function</i>	<i>Cys</i>	<i>Buried/ Exposed</i>	<i>RSA (%)</i>	<i>% Diff NaOCl/Co</i>	<i>Mean % oxidation control</i>	<i>CV</i>	<i>Mean % oxidation NaOCl</i>	<i>CV</i>
Translation (Aminacyl tRNA synthetases, translation factors, and ribosomal proteins)										
Amino acyl tRNA synthetases										
USA300HOU_1629	hisS	Histidine-tRNA ligase	Cys191	B	8.5	24.59	29.40	0.25	53.99	0.10
USA300HOU_1629	hisS	Histidine-tRNA ligase	Cys194	B	4.3	24.59	29.40	0.25	53.99	0.10
USA300HOU_1130	ileS	Isoleucine-tRNA ligase	Cys124 ^a	B	0.9	10.77	23.74	0.18	34.51	0.03
USA300HOU_1732	pheT2	Phenylalanine-tRNA ligase beta subunit	Cys126 ^a	B	4.0	18.48	11.13	0.74	29.61	0.01
USA300HOU_1732	pheT2	Phenylalanine-tRNA ligase beta subunit	Cys167 ^a	B	2.0	13.79	12.38	0.29	26.17	0.05
USA300HOU_1638	tgt	Queuine tRNA-ribosyltransferase	Cys12 ^a	B	15.2	12.73	9.32	0.07	22.04	0.42
USA300HOU_1638	tgt	Queuine tRNA-ribosyltransferase	Cys281 ^a	B	2.5	18.74	13.36	0.25	32.10	0.14
USA300HOU_1638	tgt	Queuine tRNA-ribosyltransferase	Cys174 ^a	B	1.5	11.40	8.79	0.00	20.19	0.34
Ribosomal proteins: synthesis and modification										
USA300HOU_1553	rpmG3	Ribosomal protein L33	Cys9 ^a	B	3.9	21.76	29.30	0.02	51.06	0.04
USA300HOU_1553	rpmG3	Ribosomal protein L33	Cys12 ^a	B	25.6	21.76	29.30	0.02	51.06	0.04
USA300HOU_1553	rpmG3	Ribosomal protein L33	Cys36 ^a	B	6.6	9.46	5.76	0.10	15.22	0.12
USA300HOU_2218	rpmJ	Ribosomal protein L36	Cys11^a (-SSB)	B	4.5	16.93	21.38	0.17	38.32	0.11
USA300HOU_2218	rpmJ	Ribosomal protein L36	Cys27 ^a	B	3.1	16.52	6.69	0.43	23.21	0.10
Transport and binding proteins										
USA300HOU_2553	copZ [#]	Copper chaperone	Cys13 ^a	B	6.2	19.85	30.60	0.28	50.45	0.13
USA300HOU_2553	copZ [#]	Copper chaperone	Cys16 ^a	B	3.3	19.85	30.60	0.28	50.45	0.13
Energy metabolism (ATP synthesis, central carbon metabolism)										
Glycolysis										
USA300HOU_0802	gap	Glyceraldehyde-3-phosphate DH	Cys151^a (-SSB)	B	10.5	29.46	8.28	0.13	37.74	0.04
USA300HOU_1685	pfkA	6-phosphofructokinase	Cys73 ^a	B	24.1	10.90	7.00	0.52	17.90	0.04
USA300HOU_1685	pfkA	6-phosphofructokinase	Cys226	B	17.4	23.24	18.46	0.11	41.70	0.18
USA300HOU_1685	pfkA	6-phosphofructokinase	Cys232	B	2.8	23.24	18.46	0.11	41.70	0.18
USA300HOU_1684	pykA	Pyruvate kinase	Cys266 ^a	B	1.7	10.52	11.24	0.31	21.76	0.11
Fermentation										
USA300HOU_0610	adh	Alcohol DH	Cys34	B	4.1	25.18	11.02	0.35	36.20	0.28
USA300HOU_0610	adh	Alcohol DH	Cys37 ^a	B	2.3	25.18	11.02	0.35	36.20	0.28
USA300HOU_2110	aldA	Aldehyde DH	Cys279^a (-SSB)	B	1.4	26.29	11.14	0.14	37.43	0.06
USA300HOU_2291	fdhA	Formate DH alpha subunit	Cys386 ^a	B	15.8	13.68	47.82	0.07	61.50	0.09
Tricarboxylic acid cycle										
USA300HOU_2348	mqo1	Malate:quinone oxidoreductase	Cys97	B	7.6	20.95	18.56	0.51	39.50	0.12

(continued)

TABLE 2. (CONTINUED)

Locus tag	Gene name	Protein function	Cys	Buried/ Exposed	RSA (%)	% Diff NaOCl/Co	Mean % oxidation control	CV	Mean % oxidation NaOCl	CV
Other energy metabolism										
USA300HOU_0964	nadK	NAD(+) kinase	Cys208 ^a	B	1.8	11.00	18.36	0.17	29.35	0.15
USA300HOU_0563	nagB	Glucosamine-6-phosphate deaminase	Cys239	B	3.9	16.40	9.49	0.07	25.89	0.11
USA300HOU_0902	ndh	NADH dehydrogenase	Cys199	B	2.6	10.23	15.39	0.19	25.62	0.08
Amino acid biosynthesis										
USA300HOU_1536	gcvPB	Glycine DH (decarboxylating) subunit 2	Cys80 ^a	B	4.0	20.24	7.86	0.81	28.10	0.48
USA300HOU_1240	glnA	Glutamate—ammonia ligase	Cys291	B	4.1	10.52	14.77	0.05	25.29	0.33
Fatty acid, phospholipid and sterol metabolism										
USA300HOU_0942	fabH2	3-oxoacyl-[acyl-carrier-protein] synthase	Cys220	B	7.2	11.15	11.09	0.35	22.24	0.06
Nucleotide biosynthesis										
USA300HOU_0413	guaB	Inosine-5'-monophosphate DH	Cys326	B	1.4	25.09	7.49	0.28	32.58	0.06
USA300HOU_2115	pyrG	CTP synthase	Cys439 ^a	B	2.1	12.29	8.25	0.47	20.54	0.09
USA300HOU_2265	USA300HOU_2265	Inosine-adenosine-guanosine-nucleoside hydrolase	Cys284	B	10.8	24.99	8.80	0.43	33.79	0.14
Biosynthesis of cofactors, prosthetic groups, and carriers										
USA300HOU_0929	cdr	Coenzyme A disulfide reductase	Cys16 ^a	B	2.1	12.44	9.59	0.26	22.03	0.79
USA300HOU_0561	bshB2	Bacillithiol biosynthesis deacetylase	Cys72 ^a	B	7.3	3.39	10.81	0.02	14.19	0.14
USA300HOU_1417	ypdA	Putative bacillithiol disulfide reductase	Cys14 ^a	B	5.9	3.20	8.39	0.58	11.59	0.08
USA300HOU_1365	brxB	Bacilliredoxin, YphP/YqiW family	Cys144 ^a	B	14.7	7.39	17.90	0.32	25.29	0.28
USA300HOU_1824	hemH	Ferrochelatase	Cys276	B	2.9	12.51	14.25	0.38	26.76	0.05
USA300HOU_0873	nifS	SufS subfamily cysteine desulfurase	Cys371 ^a	B	3.4	20.64	26.61	0.31	47.25	0.15
USA300HOU_0874	nifU	Iron-sulfur (Fe-S) cluster formation protein IscU	Cys41 ^a	B	11.1	26.30	17.85	0.09	44.15	0.15
USA300HOU_0875	sufB	Iron-sulfur (Fe-S) cluster formation protein SufB	Cys302	B	3.7	6.48	13.74	0.19	20.22	0.08
USA300HOU_2257	moaB	Molybdopterin cofactor biosynthesis protein MoaB	Cys34	B	20.8	13.81	9.42	0.06	23.23	0.13

Quantification of 58 Cys peptides with reversible thiol-oxidations in *S. aureus* USA300 that showed >10% increased oxidation under NaOCl stress using the OxICAT method. *S. aureus* USA300 was harvested before (control) and 30 min after exposure to 150 μ M NaOCl. Reduced and reversibly oxidized Cys residues were labeled with light and heavy ICAT reagents, respectively, using the OxICAT method. Quantification of % thiol oxidation was performed using the MaxQuant software (http://141.61.102.17/maxquant_doku/doku.php?id=start&#maxquant). The table includes locus tags, protein names, functions, Cys peptide sequences, surface access abilities, and % oxidation of the Cys residues under control and NaOCl stress conditions. Conserved Cys and their functions were marked with ^a and identified by searching the Conserved Domain Database (CDD) (www.ncbi.nlm.nih.gov/Structure/cdd/wrpsb.cgi). *S*-bacillithiolated Cys residues are marked with (+BSH) that are listed in Supplementary Figure S1. Cys functions were identified from the CDD and UniprotKB database and predicted proteins with redox-sensitive Cys residues are marked with # that were identified using the THIOREDOXOME database (<http://gladyshevlab.org/THIOREDOXOME/tdb.html>). The relative surface accessibility (RSA) for buried (B) or exposed (E) Cys residues was calculated using the NetSurfP ver. 1.1 (www.cbs.dtu.dk/services/NetSurfP/). The % thiol oxidation of each identified Cys peptide was calculated using the intensity values provided by MaxQuant software. Based on the % thiol oxidation of each Cys under control and NaOCl stress conditions, the % oxidation increase under NaOCl treatment was then calculated for each experiment. The CV is calculated as relative variability that equals the standard deviation divided by the mean of biological replicates for control and NaOCl stress samples, respectively. NaOCl-sensitive peptides with >10% increased thiol oxidation under NaOCl stress are highlighted using a gray shading gradient.

BSH, bacillithiol; CV, coefficient of variation; NADH, nicotinamide adenine dinucleotide; ICAT, isotope-coded affinity tag; RSA, relative surface accessibility; DH, dehydrogenase.

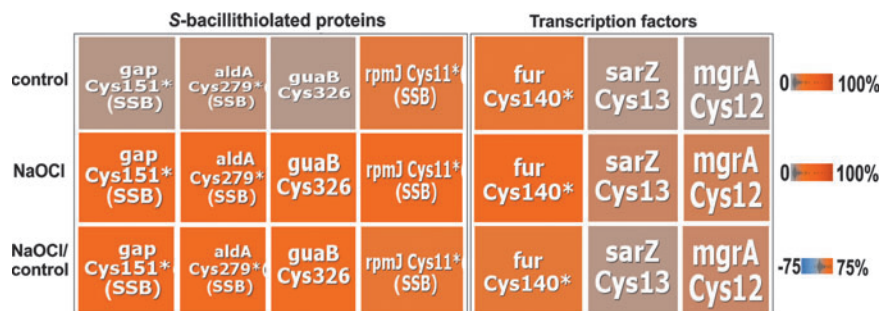


FIG. 2. Close-ups of the redox treemaps of *S. aureus* USA300 showing S-bacillithiolated enzymes and redox regulators (SarZ, MgrA, and Fur). Enlarged sections of the redox treemaps are shown that include the identified S-bacillithiolated proteins (Gap, AldA, GuaB, RpmJ) and NaOCl-sensitive redox-sensing regulators (MgrA, SarZ, and Fur). The close-ups show the percentages of thiol oxidation under control, NaOCl stress, and the percentage of oxidation change under NaOCl stress versus control as revealed in Figure 1 using the same color gradient. The symbol * denotes conserved Cys.

catalytic active sites at Cys151 and Cys279, respectively. Furthermore, the IMP dehydrogenase GuaB and the purine nucleosidase USA300HOU_2265 both displayed 25% increased oxidation under NaOCl stress (Tables 2; Supplementary Table S1).

Among the cell wall biosynthesis enzymes, the alanine racemase Alr2 (USA300HOU_2065) and the UDP-N-acetylglucosamine 1-carboxyvinyltransferase MurZ (USA300HOU_2112) were identified as NaOCl-sensitive proteins. The glucose-inhibited division protein MnmG showed 20.8% increased oxidation under NaOCl stress. Many aminoacyl-tRNA synthetases were strongly oxidized under NaOCl stress. We detected 18–24% higher oxidation levels for the histidine- and phenylalanine tRNA ligases (HisS and PheT2) and for the queuine tRNA ribosyltransferase (Tgt) under NaOCl stress.

Five S-bacillithiolated proteins were identified using shotgun proteomics in S. aureus, including the glycolytic Gap as major target

We used the previously applied shotgun proteomic approach for identification of S-bacillithiolated proteins under nonreducing conditions based on the 396 Da mass increase at Cys residues (16). Five S-bacillithiolated proteins were identified in NaOCl-treated cells of *S. aureus* USA300, including Gap, AldA, GuaB, RpmJ, and the manganese-dependent inorganic pyrophosphatase PpaC (Table 3; Supplementary Fig. S1). GuaB was S-bacillithiolated at its active

site Cys307, which forms the thioimidate intermediate with the substrate and is S-thiolated also in other gram-positive bacteria (Table 3; Supplementary Fig. S1).

Gap and AldA were S-bacillithiolated at their catalytic active sites at Cys151 and Cys279, respectively (Fig. 2 and Table 3; Supplementary Fig. S1). The AldA homolog of *S. carnosus* was previously found S-bacillithiolated at Cys279 (16). The active site Cys of Gap is a conserved target for S-glutathionylation in eukaryotic Gap homologs. Cys151 of Gap showed 29.5% oxidation increase under NaOCl stress in the OxICAT analysis, which is reflected also by the mass spectra of the ICAT-labeled Cys151-peptides (Fig. 4A). Nonreducing BSH-specific Western blots further identified that Gap is the most abundant S-bacillithiolated protein under hypochlorite stress based on the size and supported by the MS results (Fig. 4B; Supplementary Fig. S1). Gap-SSB was detected in the *S. aureus* USA300 and COL strains, but is absent in the *bshA* mutant as expected.

Gap contributes as most abundant Cys protein with 4% to the total Cys proteome

We were further interested in the contribution of Gap and other S-bacillithiolated proteins to the total Cys proteome of *S. aureus*. *S. aureus* USA300 encodes for 2694 proteins. These include 1864 proteins with 4935 Cys residues, indicating that the Cys content is 0.64% in the theoretical proteome (Supplementary Fig. S2A, B). Using shotgun proteomics, the spectral protein abundance for 600 proteins,

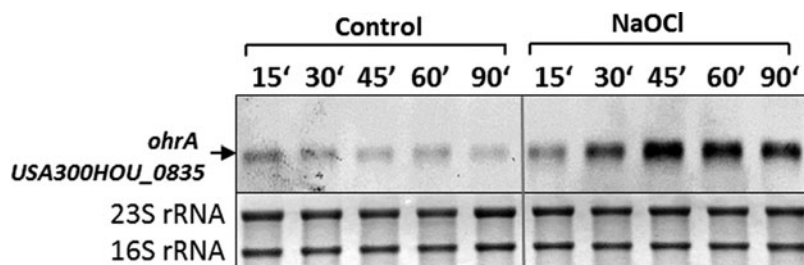


FIG. 3. Northern blot analysis showing transcriptional induction of the SarZ-regulated *ohrA* gene (USA300HOU_0835) under NaOCl stress. RNA was isolated from *S. aureus* USA300 grown in Belitsky minimal medium under control and NaOCl stress conditions and subjected to Northern blot analysis for *ohrA* (USA300HOU_0835) transcription. Transcription of *ohrA* is upregulated due to SarZ thiol oxidation and inactivation under NaOCl stress as revealed by OxICAT analysis *in vivo*.

TABLE 3. IDENTIFICATION OF THE S-BACILLITHIOLATED GAP, ALDA, PPAc, RpmJ, AND GUA_B IN STAPHYLOCOCCUS AUREUS USA300 USING SHOTGUN LC-MS/MS ANALYSIS

Protein	Accession	Function	Cys-SSB peptides	Prob (%)	SEQUEST X _{Corr}	SEQUEST ΔCn	Cys-Mod.	Observed mass	Actual mass	Charge	ΔDa	ΔPPM
Gap	A8Z1A0_ STAAT	Glyceraldehyde-3-phosphate dehydrogenase	(K)TIVENTNHQELDQ SETVVS ⁺ GASCI151 (+BSH)ITNSLAP VAK(V)	99	4.8813	0.7119	(+396)	1,262.92	3,785.73	3	0.00989	2.6
AldA	A8YY87_ STAAT	Aldehyde dehydrogenase	(K)VVNNITGQVC279 (+BSH)TAGTR(V)	99	2.9038	0.7827	(+396)	605.9328	1,814.78	3	-0.00041	-0.2
PpaC	PPAC_ STAAT	Mn-dependent inorganic pyrophosphatase	(R)JANFETAGPLC 110(+BSH)YR(A)	99	3.2907	0.6747	(+396)	925.9006	1,849.79	2	0.00081	0.4
RpmJ	RL36_ STAAT	50S ribosomal protein L36	(K)VRPSVKPIC11 (+BSH)EK(C)	99	2.0458	0.5926	(+396)	826.4047	1,650.79	2	-0.00051	-0.3
GuaB	A8Z0R0_ STAAT	Inosine-5'-monophosphate dehydrogenase	(K)VGIGPGSIC307 (+BSH)ITTR(V)	99	2.2835	0.6759	(+396)	778.8504	1,555.69	2	0.00077	0.5

Identification of S-bacillithiolated peptides in the *S. aureus* USA300 wild type using shotgun LC-MS/MS analysis and their Sequest X_{corr}s, ΔCn scores, and mass deviations. The *S. aureus* USA300 wild type was exposed to 150 μM NaOCl for 30 min and S-bacillithiolated proteins were identified using shotgun LC-MS/MS analysis and the Scaffold proteome software based on the mass increase of 396 Da (+BSH) at Cys peptides. The table lists the Uniprot accession number, protein name, function and molecular weight, the S-bacillithiolated Cys peptide sequence, and the quality control criteria for the peptide-SSB as obtained from the LC-MS/MS analysis and the Scaffold software (X_{corr}, ΔCn scores, mass deviations Δppm, and ΔDa, observed and theoretical peptide masses, and charges of the modified peptide).

The S-bacillithiolated Cys is shown in bold-faced. LC-MS/MS, liquid chromatography tandem mass spectrometry.

including 398 Cys-containing proteins, was determined in the proteome of *S. aureus* USA300 (Supplementary Table S2 and Supplementary Fig. S2C). The protein abundance in the proteome is visualized using Voronoi treemaps (Fig. 5). The cell size corresponds to the spectral protein abundance and the color code denotes the numbers of Cys residues. The majority of 226 Cys proteins identified in the proteome possess only 1–2 Cys residues. However, there are also six proteins with >10 Cys residues. The most Cys-rich protein was identified as the formate dehydrogenase FdhA that contains 26 Cys residues coordinating several FeS clusters. Based on their spectral abundance, we identified 50 abundant Cys-containing proteins that contribute to 60% of the total *S. aureus* Cys proteome (Supplementary Fig. S2C). The redox state for the majority of these Cys peptides was quantified using the OxICAT approach (Supplementary Table S1). The Cys abundance treemap also shows that many ribosomal proteins and the pyruvate dehydrogenase do not possess Cys residues (Fig. 5).

The S-bacillithiolated Gap was identified among the most abundant Cys-containing proteins and contributes with 4% of the total Cys proteome (Supplementary Fig. S2C). This indicates that Gap makes the major contribution to the S-bacillithiolome of *S. aureus* as visualized also by the BSH Western blots. The other S-bacillithiolated proteins, AldA, RpmJ, GuaB, and PpaC, are less abundant and make with 0.1–0.7% of Cys abundance only a minor contribution to the total Cys proteome (Supplementary Table S2).

H₂O₂ and NaOCl-induced inactivation pathways of Gap in *S. aureus* due to overoxidation and S-bacillithiolation in vitro

The active site of Gap is usually present in a highly conserved CTTNC motif in different organisms (Supplementary Fig. S3). However, in the *S. aureus* Gap, the second cysteine is replaced by a serine. The identification of S-bacillithiolated Gap under hypochlorite stress was intriguing since a previous proteomic study has shown that Gap of *S. aureus* is very sensitive to overoxidation to the sulfonic acid form in the presence of 100 mM H₂O₂ *in vivo* (73). In another proteomic study, Gap was identified as reversibly oxidized by 10 mM H₂O₂ in *S. aureus* (19). Thus, we were interested to study the inhibition of Gap activity *in vitro* due to overoxidation and S-bacillithiolation under both H₂O₂ and NaOCl stresses.

Gap of *S. aureus* was purified as His-tagged protein from *E. coli*. The inhibition of Gap activity by increasing H₂O₂ concentrations was monitored spectrophotometrically with G3P as substrate in the presence of NAD⁺. The remaining Gap activity was determined by nicotinamide adenine dinucleotide (NADH) generation as absorbance change at 340 nm during the slope in the reaction, as described previously (61). Treatment of Gap with 100 μM H₂O₂ leads to a 50% decrease in Gap activity, while exposure to 1–10 mM H₂O₂ resulted in complete enzyme inactivation (Fig. 6A). Inactivation of Gap with 1–10 mM H₂O₂ alone was irreversible due to overoxidation since Gap activity could be not restored with 10 mM dithiothreitol (DTT) (Fig. 6C). To investigate whether S-bacillithiolation can protect the enzyme against irreversible overoxidation, Gap was pretreated with 10-fold molar excess of BSH before H₂O₂ exposure. Gap activity was already 90% inhibited after oxidation with 100 μM H₂O₂ in the presence of

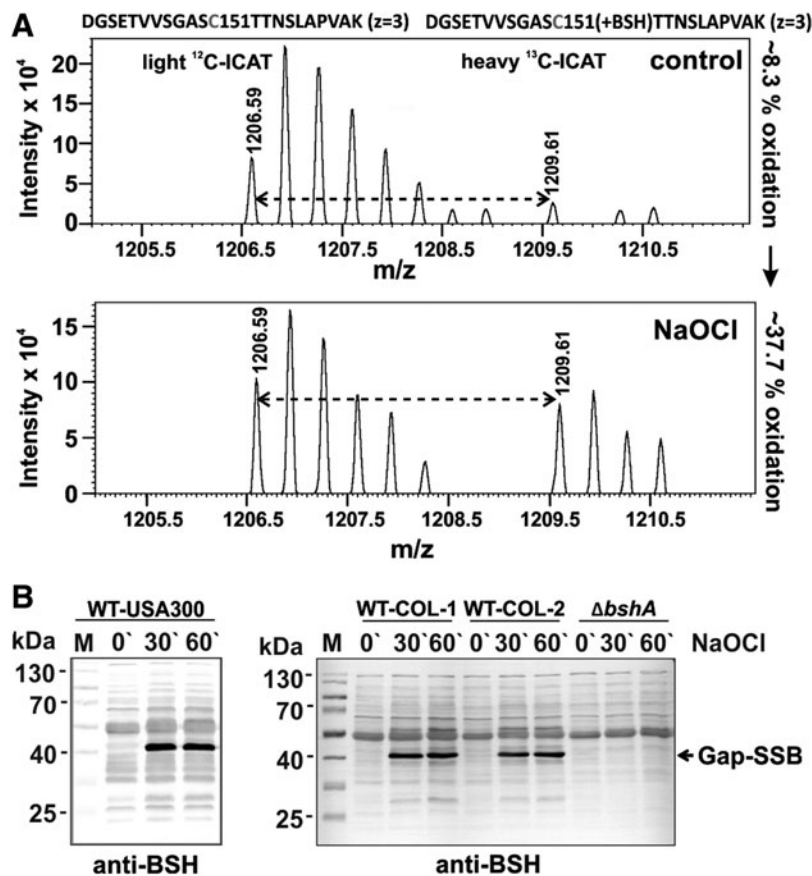


FIG. 4. OxICAT analysis revealed a 29% increased oxidation of the Gap Cys151 peptide (A) and Gap was identified as most abundant *S*-bacillithiolated protein in *S. aureus* under NaOCl stress as shown by BSH-specific Western blot analysis (B). (A) The OxICAT mass spectrometry results are shown for the Gap Cys151 peptide in *S. aureus* USA300 under control and 30 min after NaOCl stress. The reduced Gap Cys151 peptides in the cell extract are labeled with light ¹²C-ICAT, followed by reduction of all reversible thiol oxidation, including the *S*-bacillithiolated Cys151 peptides and subsequent labeling of previously oxidized Cys151 peptide by heavy ¹³C-ICAT reagent. According to the quantification by the MaxQuant software, the Cys151 peptide was 8.3% oxidized in the control and its oxidation level increased to 37.7% under NaOCl stress. (B) Nonreducing BSH-specific Western blot analysis identified Gap as most abundant *S*-bacillithiolated protein in *S. aureus* USA300 and COL strains under NaOCl stress. Two independent biological replicates are shown for *S. aureus* COL denoted as COL-1 and COL-2. Gap is *S*-bacillithiolated at the active site Cys151 under NaOCl stress as revealed by subsequent LC-MS/MS analysis (Supplementary Fig. S1A). BSH, bacillithiol; LC-MS/MS, liquid chromatography tandem mass spectry.

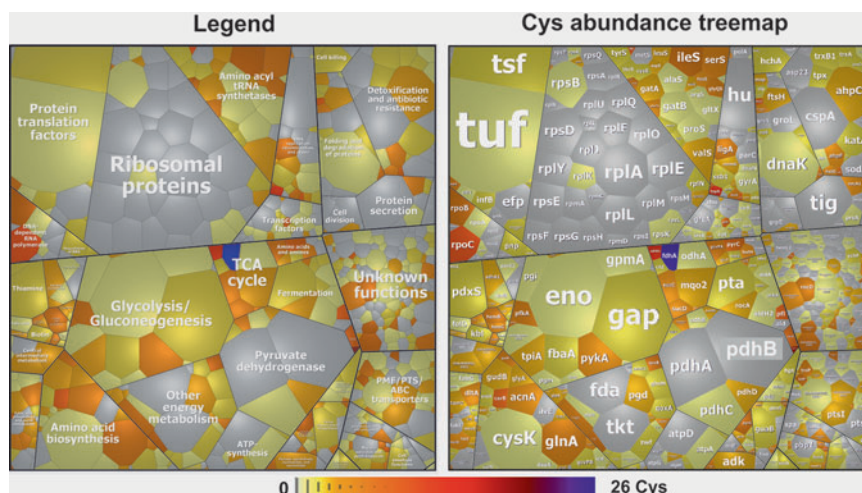


FIG. 5. Voronoi treemaps visualize Gap as the most abundant Cys protein in the total Cys proteome of *S. aureus* USA300. The treemap legend (left) indicates the classification of the *S. aureus* USA300 proteome into functional categories according to TIGRfam annotations. The cell size corresponds to the spectral counts of each protein identified in the proteome of *S. aureus* USA300 and classified according to TIGRfam. The Cys-containing proteins are color coded using a yellow–red color gradient based on their numbers of Cys residues (Supplementary Table S2). Proteins without Cys residues are displayed in gray.

BSH, while treatment with 100 μM H_2O_2 alone only led to 50% decreased activity (Fig. 6A, B). Gap inactivation with H_2O_2 and BSH was caused by reversible *S*-bacillithiolation since DTT reduction resulted in recovery of Gap activity (Fig. 6C–E; Supplementary Fig. S9). These results support that the Gap active site is highly sensitive to overoxidation, which can be prevented by *S*-bacillithiolation in the presence of H_2O_2 and BSH.

Next, we determined the time-dependent Gap inactivation by both H_2O_2 -dependent oxidation pathways (Supplementary

Fig. S4). Gap was treated with 1 mM H_2O_2 on ice with or without BSH and the remaining Gap activity was determined after different times of H_2O_2 -dependent overoxidation and *S*-bacillithiolation. The Gap activity assays revealed that both *S*-bacillithiolation and overoxidation lead to 80% enzyme inhibition after 7.5 min of H_2O_2 treatment (Supplementary Fig. S4A). In addition, we analyzed the time course for the detection of Gap-SSB or the overoxidized Cys151 under H_2O_2 treatment with or without BSH using BSH-specific Western

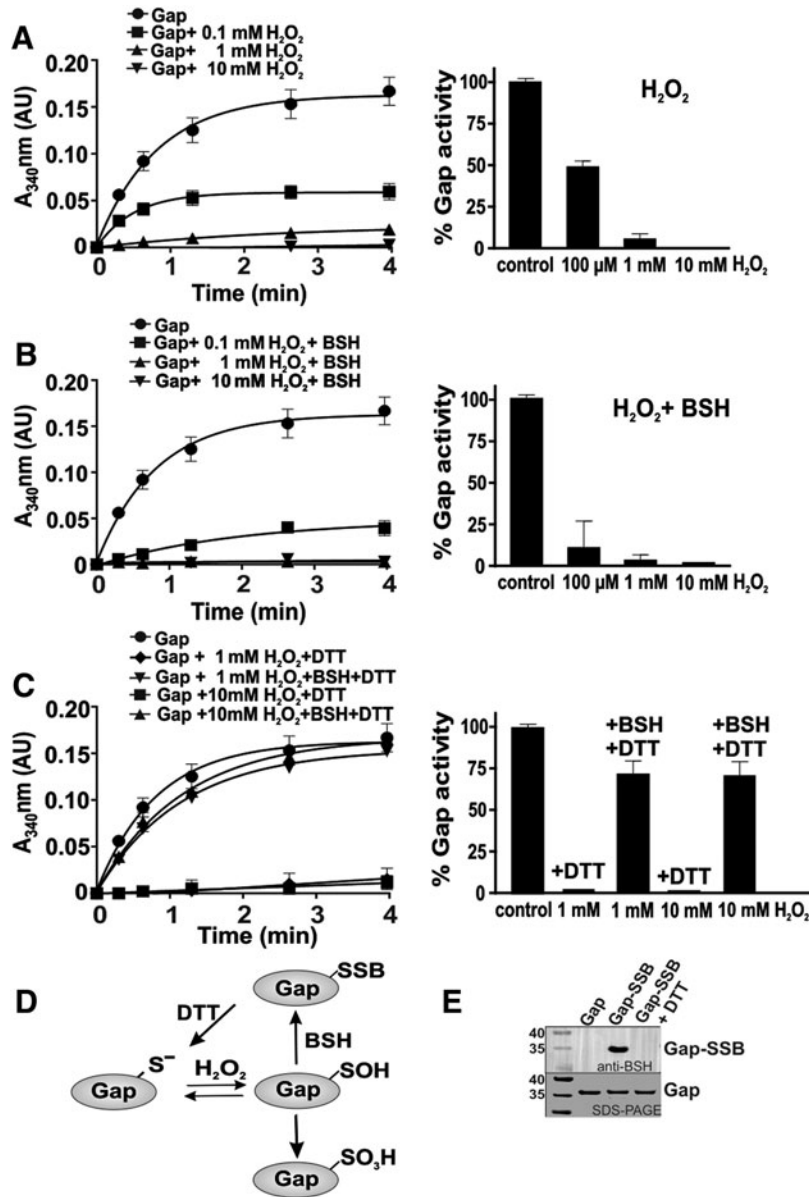


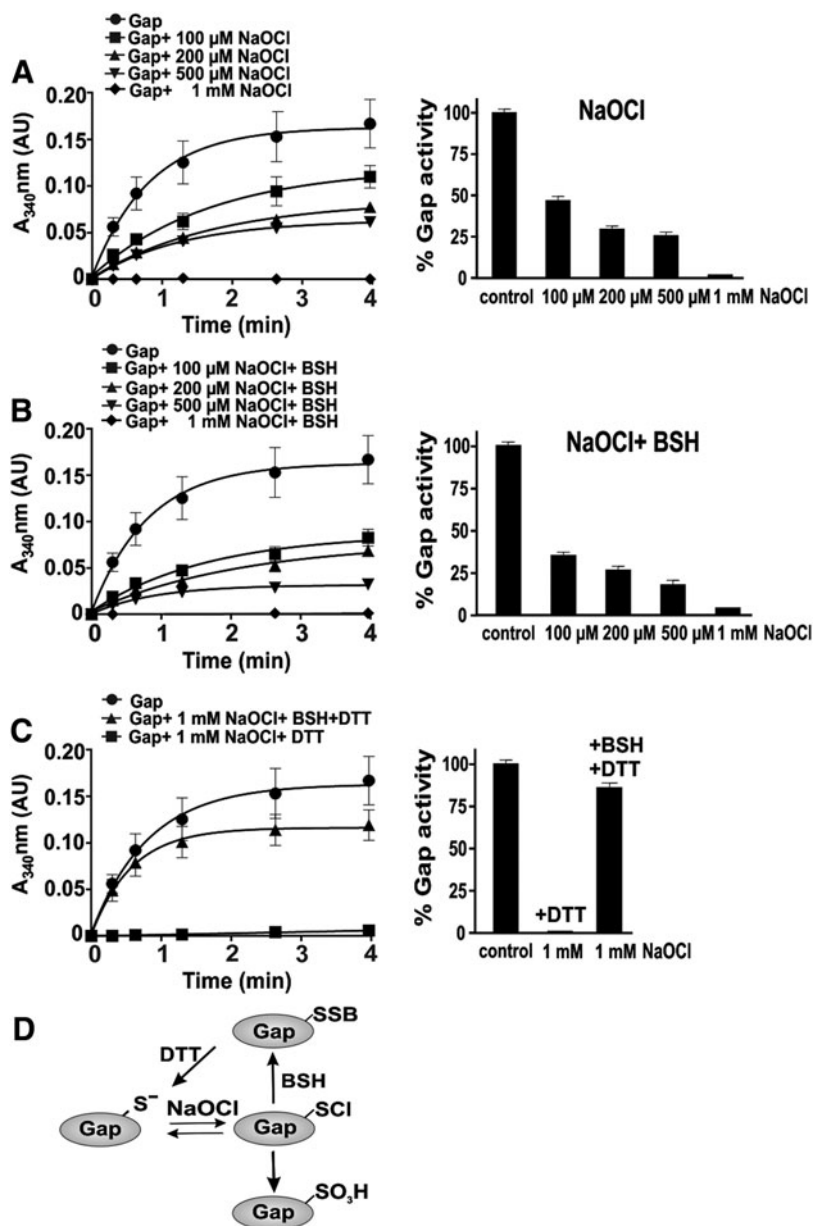
FIG. 6. Inactivation of Gap of *S. aureus* in response to H_2O_2 *in vitro*. (A, B) Reduced Gap (40 μM) was oxidized with 100 μM , 1, and 10 mM H_2O_2 for 5 min in the absence (A) or presence of 10-molar excess of BSH (400 μM) (B) in reaction buffer (100 mM Tris HCl, 1.35 mM EDTA, pH 8.0). The remaining Gap activity was measured in the presence of G3P and NAD^+ spectrophotometrically, following NADH production at 340 nm. The Gap activity was calculated as absorbance change from the slope of the reaction in the first 80 s, as described in the Materials and Methods section. (C) To assess the reversibility of Gap inactivation by H_2O_2 , Gap was treated with 1 and 10 mM H_2O_2 alone or with H_2O_2 and BSH, followed by reduction with 10 mM DTT. (D) Schematic showing the irreversible inhibition of Gap activity due to overoxidation of the active site Cys with H_2O_2 alone, while Gap activity was reversibly inhibited with H_2O_2 and BSH due to *S*-bacillithiolation. (E) *S*-bacillithiolation of Gap in the presence of 10 mM H_2O_2 and BSH was confirmed using a BSH-specific Western blot analysis before and after subsequent DTT reduction. DTT, dithiothreitol; EDTA, ethylenediaminetetraacetic acid; G3P, glyceraldehyde-3-phosphate; H_2O_2 , hydrogen peroxide.

blots or MS, respectively. The MS results identified the overoxidized Cys151 sulfonic acid (Cys151-SO₃H) after 1 min of H₂O₂ treatment (Supplementary Fig. S5). The S-bacillithiolated Gap could be also detected after 1 min of treatment with BSH and H₂O₂ (Supplementary Figs. S4B and S9). These results suggest that overoxidation and S-bacillithiolation occur at similar rates under H₂O₂ treatment *in vitro*. However, the Gap activity assays after treatment with different H₂O₂ concentrations indicate that Gap inhibition is faster with 100 μM H₂O₂ in the presence of BSH compared with 100 μM H₂O₂ alone, which only leads to 50% enzyme inhibition (Fig. 6A, B). Thus, S-bacillithiolation of Cys151 by H₂O₂ in the presence of BSH serves to protect the active site against overoxidation.

Since S-bacillithiolation of Gap was observed under NaOCl stress *in vivo*, we studied the dose-dependent Gap inactivation by NaOCl with or without prior exposure to BSH (Fig. 7). Treatment of Gap with 100–500 μM NaOCl led to

50–75% inhibition of Gap activity. Pretreatment of Gap with BSH before exposure to 100 μM NaOCl resulted in 70% activity decrease. Gap was fully inactivated with 1 mM NaOCl in the absence or presence of BSH. Treatment of Gap with 1 mM NaOCl alone resulted in irreversible inactivation due to overoxidation since Gap activity could be not restored using DTT. In the presence of BSH, Gap inactivation by NaOCl was caused by reversible S-bacillithiolation since 85% Gap activity could be restored by DTT reduction (Fig. 7C, D). Next, we studied the time course for NaOCl-induced overoxidation and S-bacillithiolation pathways in the presence of 1 mM NaOCl. The Gap activity assays with or without BSH showed that Gap inhibition is faster with BSH and NaOCl compared with NaOCl alone (Supplementary Fig. S6). These results indicate that S-bacillithiolation can efficiently prevent overoxidation of the Gap active site under NaOCl *in vitro*, supporting our *in vivo* finding.

FIG. 7. Inactivation of Gap of *S. aureus* in response to NaOCl *in vitro*. (A, B) Reduced Gap was treated with 0.1–1 mM NaOCl for 5 min without (A) or with 10-molar excess of BSH (B) in reaction buffer (100 mM Tris HCl, 1.35 mM EDTA, pH 8.0). The remaining Gap activity was measured spectrophotometrically, following NADH production at 340 nm. The Gap activity was calculated as absorbance change from the slope of the reaction in the first 80 s, as described in the Materials and Methods section. (C) To analyze the reversibility of Gap inactivation by NaOCl, Gap was inactivated with 1 mM NaOCl in the absence or presence of BSH, followed by DTT reduction. Gap activity was irreversibly inhibited after treatment with NaOCl due to overoxidation since Gap activity could be not restored by DTT. In the presence of NaOCl and BSH, Gap was reversibly inactivated due to S-bacillithiolation since DTT reduction resulted in 85% recovery of Gap activity. (D) Schematic showing that NaOCl leads to the transient sulfonylchloride formation as unstable intermediate that reacts further with BSH to form S-bacillithiolated Gap. In the absence of BSH, Gap-S-Cl is quickly overoxidized resulting in irreversible inhibition of Gap activity *in vitro*.



Regeneration of *S*-bacillithiolated Gap using the bacilliredoxin Brx (SAUSA300_1321) *in vitro*

The reversal of *S*-bacillithiolation was shown to require the glutaredoxin-like bacilliredoxins, YphP (BrxA) and YqiW (BrxB), in *B. subtilis* (24). Using a Brx-roGFP2 biosensor, we demonstrated recently that the YphP homolog of *S. aureus* (SAUSA300_1321 or Brx) is highly specific as bacilliredoxin to recognize BSSB (51). Thus, Gap activity was measured after debacillithiolation of Gap-SSB with Brx and Brx Cys mutant proteins (BrxCGA, BrxAGC) and G3P oxidation was followed by NADH production as absorbance change at 340 nm (Fig. 8A). Gap activity could be restored to 70% and 60% during debacillithiolation with Brx and the BrxCGA resolving Cys mutant *in vitro*, respectively. However, Gap activity was only 25% recovered with the BrxAGC active site mutant protein supporting the specificity of the Brx active site for the attack of BSH mixed disulfide. Debacillithiolation of

Gap-SSB by Brx and the BrxCGA mutant was verified in BSH-specific Western blots (Fig. 8B; Supplementary Fig. S9). These results indicate that *S*-bacillithiolation of Gap functions in protection and redox regulation of the active site Cys and can be reversed by the bacilliredoxin Brx *in vitro* (Fig. 8C).

Structural features of the Gap active site during overoxidation and *S*-bacillithiolation

We were interested in structural changes of Gap after overoxidation and *S*-bacillithiolation. The crystals of H₂O₂-treated overoxidized Gap diffracted X-rays to 2.6 Å resolution and belonged to the *P*₂₁₂₁₂₁ space group. Previously, several crystal structures of the Gap holo- and apoenzyme have been reported with the protein always crystallized in the *P*₂₁ space group (57). The structure of the overoxidized Gap contains four monomers in an asymmetric unit, each consisting of the NAD⁺-binding domain (residues 1–150) and the

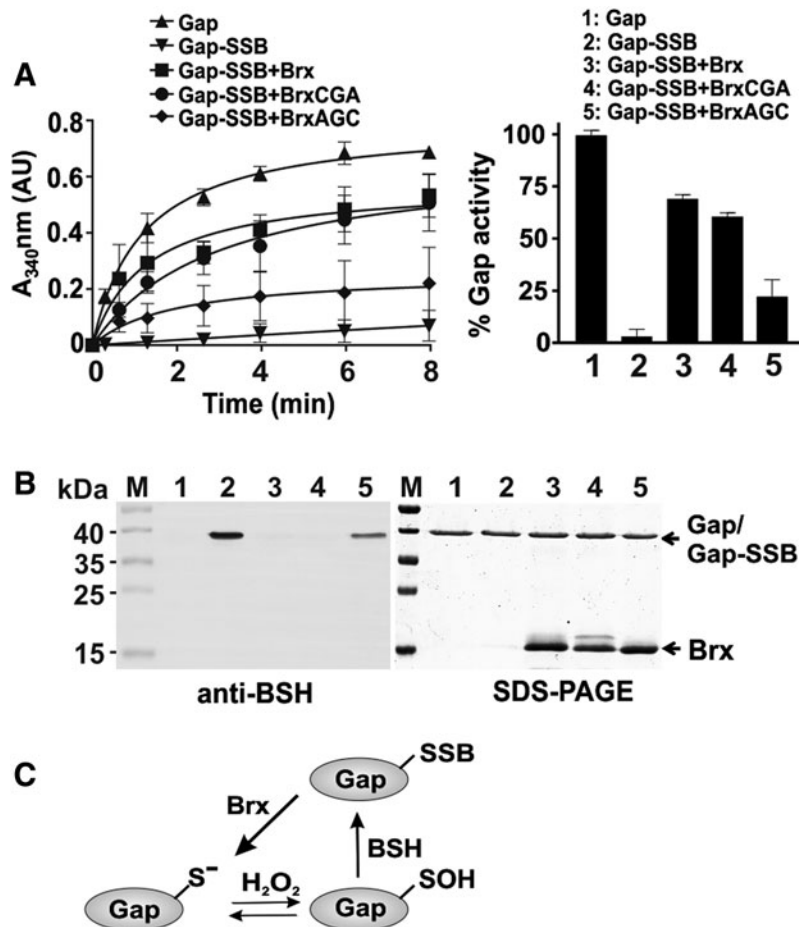


FIG. 8. Recycling of *S*-bacillithiolated Gap requires the bacilliredoxin Brx *in vitro*. (A) Gap activity is reversibly inhibited by *S*-bacillithiolation *in vitro* and can be restored by reduction using the bacilliredoxin Brx (SAUSA300_1321). Debacillithiolation required the Brx active site Cys. The BrxAGC mutant showed weak activity to reduce Gap-SSB, while the Brx resolving Cys mutant (BrxCGA) could restore Gap activity similar to the wild-type Brx protein. *S*-bacillithiolated Gap was generated *in vitro* by treatment of 25 μ M Gap with 2.5 mM H₂O₂ in the presence of 250 μ M BSH. For debacillithiolation, 2.5 μ M Gap-SSB was incubated with 12.5 μ M Brx, BrxAGC, and BrxCGA proteins for 30 min. Gap activity was measured after addition of G3P and NAD⁺ by spectrophotometric monitoring of NADH generation at 340 nm. (B) The level of debacillithiolation of Gap-SSB *in vitro* by Brx and BrxCys mutant proteins was monitored using nonreducing BSH-specific Western blot analysis. The SDS-PAGE is shown as loading control (*right*). The numbers 1–5 shown in the BSH Western blot and in the SDS-PAGE refer to the legend shown in (A). (C) Schematic for the reduction of *S*-bacillithiolated Gap using the bacilliredoxin Brx. SDS-PAGE, sodium dodecyl sulfate–polyacrylamide gel electrophoresis.

catalytic domain (residues 151–336) (57) (Supplementary Fig. S7A). The overall fold of overoxidized Gap is almost identical to previously reported reduced Gap structures, with only slight conformational differences observed in the loop regions comprising residues 59–72, 75–90, and 111–118. The root-mean square deviation after global superposition of overoxidized Gap with the holo- (PDB code: 3LVF) or apoenzyme (PDB code: 3LC7) was 1.01 and 1.11 Å, respectively. Interestingly, during previous structural analyses, Gap always copurified with NAD⁺, which had to be removed *via* activated charcoal to obtain the apoenzyme (57). In contrast, the present Gap structure does not contain NAD⁺, thus representing an apo form of the enzyme. Thus, H₂O₂ treatment seems to have led to loss of the coenzyme.

According to our MS results and previous publications (73), the Gap sulfonic acid was identified by MS as overoxidized form. In the structure of overoxidized Gap, the sulfonic acid form could be modeled into the electron density of the active

site Cys151 in each monomer (Supplementary Fig. S7B, C). Overoxidation of Cys151 results in enzyme inhibition as supported by our activity assays. During catalysis, the sulfhydryl group of Cys151 attacks the nucleophilic carbon of the G3P substrate to form a covalent intermediate, thiohemiacetal (72). In the active enzyme, His178 forms an ion pair with Cys151, which increases the acidity and nucleophilicity of the thiol group. During G3P oxidation, His178 hydrogen bonds with the acyl carbonyl of the substrate and stabilizes the hemithioacetal intermediate (57). Apart from interfering with the function of Cys151, the sulfonyl moiety of the hyperoxidized Cys151 also interacts with the main chain carbonyl of Asn316 and the imidazole ring of His178 (Fig. 9A; Supplementary Fig. S7D). Thus, hyperoxidation of Cys151 affects the function of two key catalytic residues of Gap, Cys151, and His178, leading to irreversible inactivation of the enzyme.

To obtain insights into the structural changes upon S-bacillithiolation, BSH was modeled into the active site of the

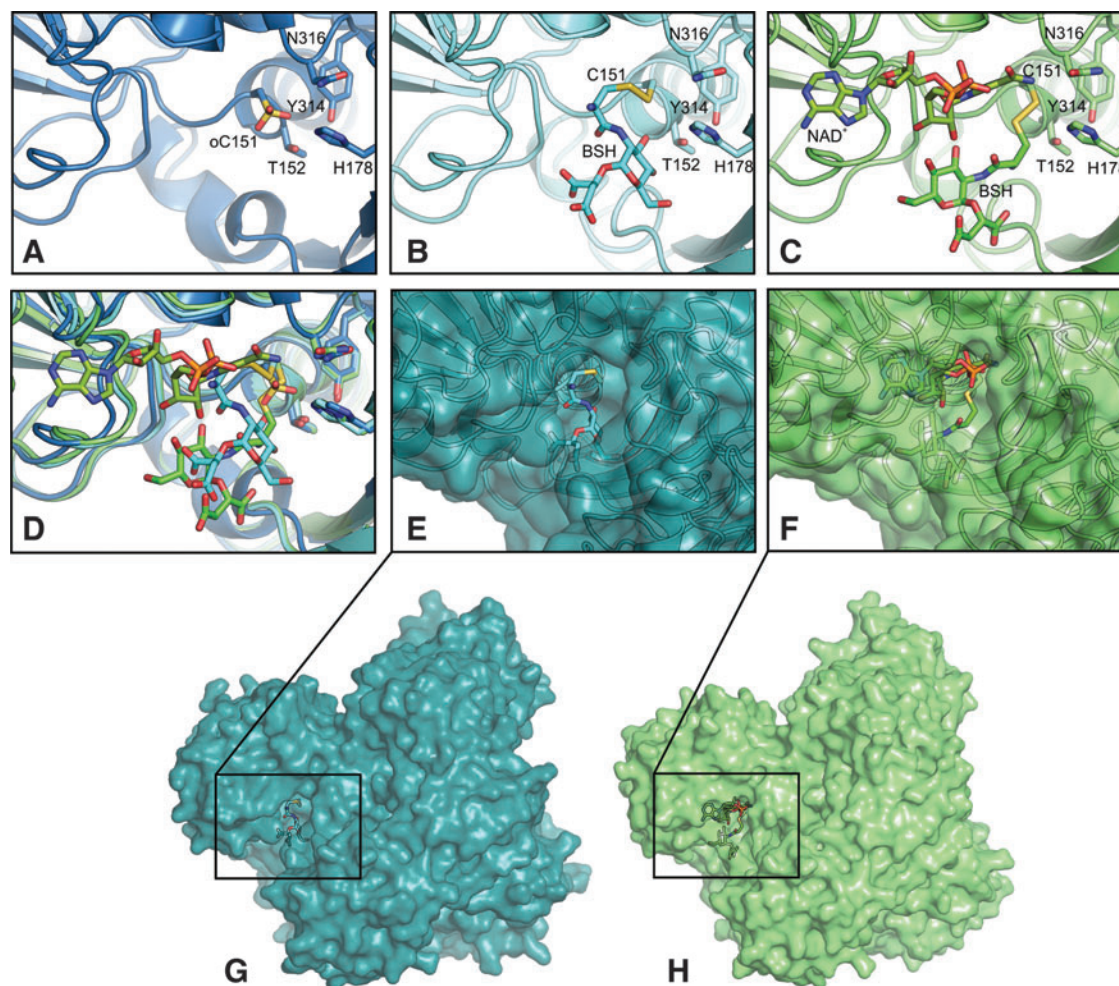


FIG. 9. Structural insights into the Gap active site after overoxidation and S-bacillithiolation. (A) Crystal structure of the overoxidized active site Cys151 (Cys-SO₃H, oC151) of Gap. (B, C) Computational model of BSH docked into the active site of the Gap apoenzyme (B) and holoenzyme with the NAD⁺ coenzyme (C) using a covalent docking algorithm that takes into account the possibility of bond formation between ligand and receptor. Shown is the best pose of 10 best poses of the S-bacillithiolated active site. (D) Superposition of Gap-SO₃H with the S-bacillithiolated apo- and holoenzyme active sites. (E, F) The S-bacillithiolated active site pocket of the apoenzyme (E) and holoenzyme (F) structures rotated by 25° over y axis in respect to (B, C). (G, H) Surface representation of apoenzyme (G) and holoenzyme (H) with docked BSH.

apo- and holoenzyme structures using molecular docking (Fig. 9B, C). We used a covalent docking algorithm that takes into account the possibility of bond formation between ligand and receptor. Docking of BSH into the apo- or holoenzyme structure resulted in a set of covalent complexes (10 best poses), in which the disulfide bond can readily form and which are structurally very similar at least in the vicinity of the disulfide bond, suggesting a high confidence in the docking pose (Supplementary Fig. S8). In the holoenzyme structure, the NAD⁺ cofactor partially occludes the binding pocket and narrows the space available for BSH binding. As a result, in the holo-Gap active site, where NAD⁺ is present, BSH takes up conformations, which differ significantly less compared with the ones in the apoenzyme. When superimposing the two best binding poses, BSH in the apoenzyme structure partially occupies the part of the pocket where NAD⁺ would be present (Fig. 9D). However, in both cases, *S*-bacillithiolation of the active site does not require major conformational changes of the protein (Fig. 9E–H). In addition, previous molecular dynamic simulations of human GAPDH (61) suggested little fluctuations of the protein. Taken together, we suggest that BSH can undergo disulfide formation with the active site at little energetic or entropic costs. This may further explain why Gap as the most abundant redox-sensitive protein in the proteome of *S. aureus* is also the most abundant *S*-bacillithiolated protein under NaOCl stress.

Discussion

Dynamic thiol redox switches are the hallmarks of oxidative stress response and the major principle of redox signaling mechanism in prokaryotes and eukaryotes (33). Quantitative redox proteomic methods such as OxICAT allow to determine the redox state of proteins thiols and to dissect redox-sensitive thiols at high resolution (9, 48). To date, global thiol redox proteomics in the major pathogen *S. aureus* identified only few targets for oxidation under H₂O₂ stress (19, 77). However, *S. aureus* shows remarkable resistance to 100 mM H₂O₂, which is attributed to the constitutive expression of the catalase KatA indicating that *S. aureus* is well adapted to peroxide stress during infections (36).

In this study, we used OxICAT to monitor the redox state of 228 Cys residues in *S. aureus* USA300 under more severe infection-like conditions as provoked by hypochlorite. In untreated cells, the majority of thiols (84.6%) are reduced with an oxidation degree <25%, which is in agreement with previous studies in *E. coli* and yeast cells (9, 48). Under NaOCl stress, 58 NaOCl-sensitive proteins showed >10% increased oxidation, indicating that 25% of all identified protein thiols are redox sensitive in *S. aureus*. To analyze whether these NaOCl-sensitive Cys residues are buried or surface exposed, we calculated their relative surface accessibilities (RSAs) using NetSurfP (www.cbs.dtu.dk/services/NetSurfP/). However, only 9 of 228 Cys residues have RSA values of >30% and are predicted as solvent exposed (Table 2 and Supplementary Table S1). The RSA calculations clearly indicate that NaOCl-sensitive Cys residues are often the active site centers that are not surface exposed and buried in the predicted secondary protein structure.

Among the NaOCl-sensitive proteins with the highest oxidation increase of 20–30%, we identified Gap, AldA, and GuaB as *S*-bacillithiolated at their conserved substrate-

binding active sites. Only a few *S*-bacillithiolated proteins were found by the shotgun proteomic approach due to the instability and low abundance of the BSH-modified peptides. Thus, we assume that many more NaOCl-sensitive proteins of our OxICAT dataset are modified by *S*-bacillithiolation, but failed to be identified using the shotgun method.

Apart from *S*-bacillithiolation, also alternative *S*-thiolations are possible in *S. aureus* under NaOCl stress such as *S*-cysteinylation or CoASH mixed disulfides since cysteine and CoASH are also present in the thiol metabolome of *S. aureus* (58, 64). Moreover, the Cdr displayed an increased oxidation level under NaOCl stress at its conserved Cys16 in our OxICAT analyses and was previously shown to function in reduction of CoASH disulfides in *S. aureus* (18, 55). However, *S*-cysteinylation and CoASH mixed disulfides were not detected by MS due to their low abundance or instability.

Many Zn-containing NaOCl-sensitive proteins were identified, such as the Fur repressor, which is oxidized in its Zn-binding site. Zn-binding sites are common redox switch motifs (37). The best-studied example is the oxidation-sensitive Hsp33 chaperone that responds to hypochlorite by a redox switch in its Zn motif and protects *E. coli* proteins against oxidative aggregation (26, 38, 46). NaOCl-sensitive Zn-containing proteins include the alcohol dehydrogenase Adh and the ribosomal proteins, RpmG3 and RpmJ. Several previously predicted redox-sensitive Cys residues are found in CxxC motifs, such as the copper chaperone, CopZ, and the antioxidant proteins, AhpC, TrxB, and ArsC (21). These results are in agreement with previous redox proteomic results in *E. coli* under NaOCl stress (48). Increased oxidation levels were detected for both MarR/OhrR family regulators MgrA and SarZ that are oxidized at their single Cys residues. Using Northern blot analyses, we confirmed that SarZ oxidation leads to derepression of transcription of the *ohrA* gene (*USA300-HOU_0835*) in *S. aureus*. Thus, the OxICAT approach identified increased oxidation of both major thiol redox regulators under NaOCl stress in *S. aureus*.

The most abundant *S*-bacillithiolated protein was the glycolytic Gap enzyme in *S. aureus* under NaOCl stress, which was *S*-bacillithiolated at the active site Cys151. Gap is the most abundant Cys-containing protein contributing 4% to the total Cys proteome. The active site Cys is used for the nucleophilic attack at the aldehyde group of the G3P substrate to catalyze the substrate-level phosphorylation of G3P to 1,3-bisphosphoglycerate with production of NADH (34). Gap homologs are common targets for oxidation in eukaryotes and prokaryotes and subject of different post-translational thiol modifications, including *S*-sulfenylation, *S*-glutathionylation, *S*-nitrosylation, and *S*-sulfhydration, resulting in reversible enzyme inactivation (10, 34). Inactivation of Gap has been shown to redirect the glycolytic flux into the pentose phosphate pathway to supply nicotinamide adenine dinucleotide phosphate (NADPH) as reducing power under oxidative stress (10, 66).

Gap of *S. aureus* was previously identified as oxidation-sensitive target for reversible thiol modification (19) and was also found to be overoxidized at its active site Cys151 under H₂O₂ stress (73). Using biochemistry, MS, and X-ray crystallography, we confirmed previous findings that the glycolytic Gap enzyme from *S. aureus* is highly sensitive to overoxidation to Cys sulfonic acid *in vitro* in the presence of H₂O₂ alone. In this work, we found that Gap is the most abundant *S*-bacillithiolated protein under NaOCl stress

in vivo. We further demonstrate that *S*-bacillithiolation functions in reversible inhibition of Gap activity under H₂O₂ and NaOCl treatment *in vitro* and protects the active site Cys against overoxidation to ensure fast regeneration of this essential glycolytic enzyme during recovery of cells. Our Gap activity assays suggest that both pathways, the overoxidation and *S*-bacillithiolation, operate at similar kinetics under H₂O₂ treatment, while inactivation due to *S*-bacillithiolation was faster under NaOCl stress. Together, our results confirm the preference for formation of *S*-thiolation in the presence of LMW thiols as observed in many eukaryotic Gap homologs (34, 43, 78).

The reactivity of the active site cysteine toward H₂O₂ and the substrate G3P was recently shown to depend on two different mechanisms (34, 61). The catalytic Cys is in close proximity with His178 in the structure of Gap of *S. aureus* that attracts the thiol proton, leading to deprotonation and increased acidity of the catalytic Cys. The acidic nature explains the reactivity of catalytic Cys toward the substrate G3P that covalently reacts with the nucleophilic thiolate during the catalytic cycle (34, 62). However, the increased acidity of Cys151 does not explain its strong reactivity toward H₂O₂. Instead, the reactivity of the active site thiolate depends on a specific H₂O₂-binding pocket, transition state stabilization, and a proton relay mechanism promoting leaving group departure (34, 61).

This proton relay mechanism also determines the preferred modification by *S*-bacillithiolation of Gap in *S. aureus* under H₂O₂ *in vitro*, which requires the initial formation of a sulfenic acid, followed by reaction to the BSH mixed disulfide. HOCl shows very fast reaction rates with thiols ($3 \times 10^7 \text{ M}^{-1} \text{ s}^{-1}$) that are several orders of magnitude higher compared with H₂O₂ (17, 27, 30, 60, 74). HOCl first leads to chlorination of thiols resulting in an unstable sulfenylchloride intermediate that reacts further to form disulfides in the presence of another thiol. In the absence of proximal thiols, the sulfenylchloride quickly leads to irreversible oxidation stages (17, 30, 52). We have shown in *S. aureus* that *S*-bacillithiolation functions in protection and redox regulation of the Gap active site against overoxidation under NaOCl stress *in vitro* and *in vivo*. Molecular docking of BSH into the active site of the Gap apo- and holoenzyme was used to model the *S*-bacillithiolated active site at high confidence. The model of Gap-SSB structure suggests that BSH can undergo disulfide formation with Cys151 without major conformational changes. This may explain why the most abundant Cys protein Gap is the preferred and dominant target for *S*-bacillithiolation inside *S. aureus* cells.

S-glutathionylation of the active site Cys of Gap was found in many eukaryotic organisms, such as *Arabidopsis thaliana*, the malaria parasite *Plasmodium falciparum*, or in human endothelial cells, leading to reversible inhibition of Gap activity (3, 43, 69). Reactivation of Gap was catalyzed by glutaredoxins and thioredoxins in plants and malaria parasites (3, 43). In *B. subtilis*, the bacilliredoxins, BrxA and BrxB, were shown to catalyze the reduction of *S*-bacillithiolated OhrR and MetE *in vitro* (24). In this study, we showed that *S*-bacillithiolated Gap is also a substrate for the bacilliredoxin Brx (SAUSA300_1321) in *S. aureus*, which requires the active site Cys for debacillithiolation *in vitro*. Thus, the bacilliredoxin pathway is also involved in regeneration of Gap activity in *S. aureus*.

Materials and Methods

Bacterial strains and growth conditions

Bacterial strains used were *S. aureus* COL and USA300 and its isogenic *bshA* mutants as described previously (64). For cloning and genetic manipulation, *E. coli* DH5a and BL21 (DE3) *plysS* were cultivated in Luria Bertani (LB) medium. For NaOCl stress experiments, *S. aureus* USA300 and COL strains were cultivated in LB medium until an optical density at 540 nm (OD₅₄₀) of 2.0, transferred to Belitsky minimal medium, and treated with 150 μM NaOCl stress as described (51). NaOCl, diamide, DTT, N-ethylmaleimide (NEM), and H₂O₂ (35% w/v) were purchased from Sigma-Aldrich.

MS-based thiol redox proteomics using the OxICAT approach

S. aureus USA300 was harvested before and after exposure to 150 μM NaOCl for 30 min, respectively. The OxICAT method was performed according to the protocol of Lindemann and Leichert (49) with the modification that cells were disrupted using a ribolyzer. The ICAT-labeled peptides were dissolved in 0.1% (v/v) acetic acid and loaded onto self-packed LC columns with 10 μl of buffer A (0.1% (v/v) acetic acid) at a constant pressure of 220 bar without trapping. Peptides were eluted using a nonlinear 85-min gradient from 1% to 99% buffer B (0.1% (v/v) acetic acid in acetonitrile) with a constant flow rate of 300 nl/min and measured using Orbitrap MS as described (6). The *S. aureus* USA300 sequence database was extracted from Uniprot and used by the search engine Andromeda and the MaxQuant software (version 1.5.1.2) to quantify the ICAT-labeled Cys peptides. Two miscleavages were allowed, the parent ion mass tolerance was 10 ppm and the fragment ion mass tolerance was 1.00 Da. The average percentage of oxidation of each Cys peptide and the percentage change under NaOCl stress were calculated from 2 to 3 biological replicates using the intensity values provided by MaxQuant. Voronoi treemaps were generated using the Paver software to visualize the percentage oxidation of all identified ICAT-labeled peptide pairs. The OxICAT proteomic data have been deposited to the ProteomeXchange Consortium *via* the PRIDE partner repository with the dataset identifier PXD004918.

Identification of *S*-bacillithiolated and overoxidized Cys peptides using LTQ-Orbitrap MS

For identification of *S*-bacillithiolated peptides, NEM-alkylated protein extracts were prepared from *S. aureus* USA300 cells after exposure to 150 μM NaOCl for 30 min as described (15). The protein extracts were separated by 15% nonreducing sodium dodecyl sulfate–polyacrylamide gel electrophoresis (SDS-PAGE), followed by tryptic in-gel digestion and LTQ-Orbitrap-Velos MS, as described (15). Post-translational thiol modifications of proteins were identified by searching all tandem mass spectrometry (MS/MS) spectra in dta format against the *S. aureus* USA300 target–decoy protein sequence database extracted from UniprotKB release 12.7 (UniProt Consortium, Nucleic acids research 2007, 35, D193-197) using Sorcerer™-SEQUEST® (Sequest v. 2.7 rev. 11, Thermo Electron, including Scaffold 4.0; Proteome Software, Inc., Portland, OR). The SEQUEST search parameters and thiol modifications were used as described (15).

The scores and mass deviations of the *S*-bacillithiolated peptides are shown in detail in Supplementary Figure S1, including their fragmentation spectrum and ion tables.

MS of the H₂O₂-treated overoxidized Gap was performed after in-gel tryptic digestion using nLC-MS/MS by Orbitrap fusion, as described previously (45). For Cys151-SO₃H peptide identification and quantification, MS1 data were filtered to the precursor target masses applying an *m/z* window of 3 ppm. Isotopic distribution and fragmentation spectra were inspected manually in different charge states in successive MS2 scans in different overoxidized Gap samples.

Cloning, expression, and purification of the *S. aureus* Gap, Brx, and Brx Cys-Ala mutant proteins in *E. coli*

The previously constructed plasmids, pET11b-Brx-roGFP2, pET11b-BrxAGC-roGFP2, and pET11b-BrxCGA-roGFP2 (51), were used as template to amplify *S. aureus brx* (SAUSA300_1321), *brxAGC*, and *brxCGA* by PCR using primer pairs 1321-roGFP2-For-NheI (5'-CTAGCTAGCATGAATGCATATGATGCTTATATGAAAG-3') and roGFP2-1321-Rev-BamHI (5'-CGCGGATCCTTAGTGATGGTGATGGTGATGTTTACAA TTT TCGTCAAAGGC-3'). The reverse primer also encodes the C-terminal His₆-tag. The PCR products were digested with *NheI* and *Bam*HI and inserted into plasmid pET11b (Novagen) that was digested using the same restriction enzymes to generate plasmids pET11b-*brx*, pET11b-*brxAGC*, and pET11b-*brxCGA*. The primer pairs *gap*-For-NdeI (5'-GGAATTCATATGGCA GTAAAAGTAGCAATTAATG-3') and *gap*-Rev-BamHI (5'-CGCGGATCCTTAGTGATGGTGATGGTGATGTTTAGAA AGTTCAGCTAAGTATGC-3') were used to amplify the *S. aureus gap* gene (SAUSA300_0756) by PCR. Chromosomal DNA of *S. aureus* USA300 was used as template. The PCR products were digested with the restriction enzymes, *NdeI* and *Bam*HI, and inserted into plasmid pET11b that was digested with the same enzymes to generate plasmids pET11b-*gap*. The correct sequences of the cloned genes were confirmed by sequencing. The plasmids were transformed into *E. coli* BL21 (DE3) *plysS* (Novagen).

For protein expression, *E. coli* BL21(DE3) *plysS* strains with the plasmids, pET11b-*gap*, pET11b-*brx*, pET11b-*brxAGC*, and pET11b-*brxCGA*, were grown in 1 liter LB medium and 1 mM isopropyl-β-D-thiogalactopyranoside (IPTG) was added at the exponential phase (OD₆₀₀ of 0.8) for 3 h at 37°C. His-tagged proteins were purified using His Trap™ HP Ni-NTA columns and the ÄKTA purifier liquid chromatography system (Amersham Bioscience). The proteins were further concentrated to 2–6 mg/ml using Amicon Ultra concentrators (Millipore). Before the activity assays, Gap and Brx proteins were reduced with 10 mM DTT for 30 min, followed by DTT removal using Micro Biospin 6 columns (Biorad).

Gap activity assay

Gap activity was monitored spectrophotometrically at 340 nm and 25°C by the production of NADH. The oxidation of G3P to 1,3-bisphosphoglycerate (1,3-BPG) was measured in an assay mixture containing 1.25 mM NAD⁺ and 0.25 μM Gap in argon-flushed 20 mM Tris-HCl, pH 8.7, with 1.25 mM ethylenediaminetetraacetic acid and 15 mM sodium arsenate. After preincubation, the reaction was started by addition of 0.25 mM D,L-G3P. Sodium arsenate was used as a cosubstrate to form unstable 1-arseno-3-phosphoglycerate, as de-

scribed previously (61). Degradation of the product allows a favorable equilibrium for measuring the rate of Gap activity in the glycolytic forward reaction. Initial rates were determined by calculation of the slope in the linear part of the curve during the first 80 seconds at the beginning of the reaction (linear regression function, GraphPad) as described previously (61). Percentage of Gap activity was calculated as (Rate_{inactivated}/Rate_{untreated} × 100%). The results are presented as mean ± SEM from at least three separate experiments.

S-bacillithiolation of Gap in vitro and reduction by the bacilliredoxin Brx

About 25 μM of purified Gap was *S*-bacillithiolated with 250 μM BSH in the presence of 2.5 mM H₂O₂ for 5 min. Excess of BSH and H₂O₂ was removed with Micro Biospin 6 columns (Biorad). For the Brx debacillithiolation assay, Gap-SSB was incubated with Brx, BrxCGA, and BrxAGC at 37°C for 30 min, followed by Gap activity assays and nonreducing BSH-specific Western blot analysis, as described (16).

Western blot analysis

The *S*-bacillithiolated proteins were harvested from *S. aureus* USA300 wild-type and *bshA* mutant cells after exposure to 150 μM NaOCl, separated by nonreducing SDS-PAGE, and subjected to BSH-specific Western blot analysis using the polyclonal rabbit anti-BSH antiserum, as described previously (16).

Northern blot experiments

Northern blot analyses were performed as described before (15) using RNA isolated from *S. aureus* USA300 wild type under control conditions and after treatment with 150 μM NaOCl. Hybridization specific for *ohrA* (USA300HOU_0835) was performed with the digoxigenin-labeled RNA probe synthesized *in vitro* using T7 RNA polymerase from T7 promoter containing internal PCR products using the primer pairs *ohrA*-for, 5' TGGCAATACATTATGAACTAAAGC 3', and *ohrA*-T7-rev, 5' CTAATACGACTCACTATAGGGAGA TTTAAATCGACATTAATATTTTCCTTGA 3'.

Crystallographic procedures

Before crystallization, H₂O₂-treated overoxidized Gap was concentrated to 11 mg/ml. Crystals of overoxidized Gap were grown at 18°C using the hanging drop vapor diffusion technique and 30% (w/v) PEG 3350, 0.1 M Tris, pH 8.5, as the reservoir solution. Crystals were cryoprotected by transfer into mother liquor mixed with 50% (v/v) PEG 400 in a 1:1 ratio and flash-cooled in liquid nitrogen. X-ray diffraction data were collected from a single crystal at 100 K on beamline 14.1 of the BESSY II storage ring (Berlin, Germany) (56) equipped with a PILATUS 6M detector (Company-REF), with a 0.1° oscillation and exposure time of 0.3 s per frame. Diffraction images were processed using XDS (41). Crystal parameters and data collection statistics are given in Supplementary Table S3. The Gap-SO₃H structure was solved by molecular replacement with Molrep (71) using the structure of the Gap apoenzyme (PDB entry 3LC7; [57]) as a model. The final model of the Gap-SO₃H was generated by iterative rounds of manual model building using Coot (20)

and automated refinement using the phenix.refine package in PHENIX (1) with the inclusion of TLS parameters generated by the TLSMD server (59). Coordinates and structure factor amplitudes have been deposited in the Protein Data Bank (4) under the accession code 5T73 and will be released upon publication.

Molecular docking of BSH into the Gap active site

To model a covalent complex between BSH and the *S. aureus* Gap active site Cys151, docking experiments were performed with the holo form containing NAD [PDB code: 3LVF chain R, (57)] as well as the apo form [PDB code: 3LC7 chain O, (57)] of the enzyme. Before molecular docking, both protein structures were prepared using the protein preparation wizard (68) in the Schrodinger software (Release 2016–1) graphical user interface Maestro. Hydrogen was added according to the protonation states at pH of 7.0 as predicted by PROPKA, bond orders were assigned, and disulfide bonds were allocated. Water with less than three hydrogen bonds to nonwater residues was removed and minimization of heavy atoms was performed using OPLS3. The BSH structure was obtained from Pubchem (ID: CID 42614123) and processed with the ligand preparation wizard. The ligand was protonated at pH of 7.0 ± 2.0 using Epik (28). Covalent molecular docking was performed using CovDock (79), which combines the two programs Glide (23) for docking and Prime (39, 40) for minimization. Cysteine 151 was set as reactive residue, and the reaction type was disulfide formation. All atom positions were fixed, except for the targeted residue and the ligand. Covalent docking was performed with default options and the poses were ranked according to the Prime energy.

Acknowledgments

This work was supported by a grant from the Deutsche Forschungsgemeinschaft (AN746/4-1) within the SPP1710 on Thiol-based Redox switches, by the DFG grants AN746/3-1 and project C1 of the Research Training Group GRK1947, and by the ERC Consolidator Grant (GA 615585) MYCOTHIOLOME to H.A. Protein crystal structure analysis was supported by an Alexander von Humboldt postdoc fellowship to A.J.P.-B. Molecular docking was supported by the Klaus Tschira Foundation to L.T., K.K., and F.G. The authors would like to thank Sandra Maaß and Dörte Becher (University of Greifswald) for MS of the ICAT-labeled peptides. MS of the over-oxidized Gap was performed at the Centre for Chemical Microscopy (ProVIS) at the Helmholtz Centre for Environmental Research, which is supported by European regional development funds (EFRE-Europe Funds Saxony) and the Helmholtz Association. The authors are grateful to Ambrose Cheung for the kind gift of *S. aureus* USA300 *bshA* mutant.

Author Disclosure Statement

No competing financial interests exist.

References

- Adams PD, Afonine PV, Bunkoczi G, Chen VB, Davis IW, Echols N, Headd JJ, Hung LW, Kapral GJ, Grosse-Kunstleve RW, McCoy AJ, Moriarty NW, Oeffner R, Read RJ, Richardson DC, Richardson JS, Terwilliger TC, and Zwart PH. PHENIX: a comprehensive Python-based system for macromolecular structure solution. *Acta Crystallogr D Biol Crystallogr* 66: 213–221, 2010.
- Archer GL. *Staphylococcus aureus*: a well-armed pathogen. *Clin Infect Dis* 26: 1179–1181, 1998.
- Bedhomme M, Adamo M, Marchand CH, Couturier J, Rouhier N, Lemaire SD, Zaffagnini M, and Trost P. Glutathionylation of cytosolic glyceraldehyde-3-phosphate dehydrogenase from the model plant *Arabidopsis thaliana* is reversed by both glutaredoxins and thioredoxins in vitro. *Biochem J* 445: 337–347, 2012.
- Berman HM, Westbrook J, Feng Z, Gilliland G, Bhat TN, Weissig H, Shindyalov IN, and Bourne PE. The Protein Data Bank. *Nucleic Acids Res* 28: 235–242, 2000.
- Blanc B, Gerez C, and Ollagnier de Choudens S. Assembly of Fe/S proteins in bacterial systems: biochemistry of the bacterial ISC system. *Biochim Biophys Acta* 1853: 1436–1447, 2015.
- Bonn F, Bartel J, Büttner K, Hecker M, Otto A, and Becher D. Picking vanished proteins from the void: how to collect and ship/share extremely dilute proteins in a reproducible and highly efficient manner. *Anal Chem* 86: 7421–7427, 2014.
- Botello-Morte L, Pellicer S, Sein-Echaluce VC, Contreras LM, Neira JL, Abian O, Velazquez-Campoy A, Peleato ML, Fillat MF, and Bes MT. Cysteine mutational studies provide insight into a thiol-based redox switch mechanism of metal and DNA binding in FurA from *Anabaena* sp. *PCC* 7120. *Antioxid Redox Signal* 24: 173–185, 2016.
- Boucher HW and Corey GR. Epidemiology of methicillin-resistant *Staphylococcus aureus*. *Clin Infect Dis* 46 Suppl 5: S344–S349, 2008.
- Brandes N, Reichmann D, Tienson H, Leichert LI, and Jakob U. Using quantitative redox proteomics to dissect the yeast redoxome. *J Biol Chem* 286: 41893–41903, 2011.
- Brandes N, Schmitt S, and Jakob U. Thiol-based redox switches in eukaryotic proteins. *Antioxid Redox Signal* 11: 997–1014, 2009.
- Chen PR, Bae T, Williams WA, Duguid EM, Rice PA, Schneewind O, and He C. An oxidation-sensing mechanism is used by the global regulator MgrA in *Staphylococcus aureus*. *Nat Chem Biol* 2: 591–595, 2006.
- Chen PR, Brugarolas P, and He C. Redox signaling in human pathogens. *Antioxid Redox Signal* 14: 1107–1118, 2011.
- Chen PR, Nishida S, Poor CB, Cheng A, Bae T, Kuechenmeister L, Dunman PM, Missiakas D, and He C. A new oxidative sensing and regulation pathway mediated by the MgrA homologue SarZ in *Staphylococcus aureus*. *Mol Microbiol* 71: 198–211, 2009.
- Chi BK, Busche T, Van Laer K, Bäsell K, Becher D, Clermont L, Seibold GM, Persicke M, Kalinowski J, Messens J, and Antelmann H. Protein S-mycothiolation functions as redox-switch and thiol protection mechanism in *Corynebacterium glutamicum* under hypochlorite stress. *Antioxid Redox Signal* 20: 589–605, 2014.
- Chi BK, Gronau K, Mäder U, Hessling B, Becher D, and Antelmann H. S-bacillithiolation protects against hypochlorite stress in *Bacillus subtilis* as revealed by transcriptomics and redox proteomics. *Mol Cell Proteomics* 10: M111.009506, 2011.
- Chi BK, Roberts AA, Huyen TT, Bäsell K, Becher D, Albrecht D, Hamilton CJ, and Antelmann H. S-bacillithiolation protects conserved and essential proteins against hypochlorite stress in firmicutes bacteria. *Antioxid Redox Signal* 18: 1273–1295, 2013.

17. Davies MJ. Myeloperoxidase-derived oxidation: mechanisms of biological damage and its prevention. *J Clin Biochem Nutr* 48: 8–19, 2011.
18. delCardayre SB, Stock KP, Newton GL, Fahey RC, and Davies JE. Coenzyme A disulfide reductase, the primary low molecular weight disulfide reductase from *Staphylococcus aureus*. Purification and characterization of the native enzyme. *J Biol Chem* 273: 5744–5751, 1998.
19. Deng X, Weerapana E, Ulanovskaya O, Sun F, Liang H, Ji Q, Ye Y, Fu Y, Zhou L, Li J, Zhang H, Wang C, Alvarez S, Hicks LM, Lan L, Wu M, Cravatt BF, and He C. Proteome-wide quantification and characterization of oxidation-sensitive cysteines in pathogenic bacteria. *Cell Host Microbe* 13: 358–370, 2013.
20. Emsley P, Lohkamp B, Scott WG, and Cowtan K. Features and development of Coot. *Acta Crystallogr D Biol Crystallogr* 66: 486–501, 2010.
21. Fomenko DE and Gladyshev VN. Comparative genomics of thiol oxidoreductases reveals widespread and essential functions of thiol-based redox control of cellular processes. *Antioxid Redox Signal* 16: 193–201, 2012.
22. Foster TJ. The *Staphylococcus aureus* “superbug”. *J Clin Invest* 114: 1693–1696, 2004.
23. Friesner RA, Murphy RB, Repasky MP, Frye LL, Greenwood JR, Halgren TA, Sanschagrin PC, and Mainz DT. Extra precision glide: docking and scoring incorporating a model of hydrophobic enclosure for protein-ligand complexes. *J Med Chem* 49: 6177–6196, 2006.
24. Gaballa A, Chi BK, Roberts AA, Becher D, Hamilton CJ, Antelmann H, and Helmann JD. Redox regulation in *Bacillus subtilis*: the bacilliredoxins BrxA(YphP) and BrxB(YqiW) function in de-bacillithiolation of S-bacillithiolated OhrR and MetE. *Antioxid Redox Signal* 21: 357–367, 2014.
25. Gaballa A, Newton GL, Antelmann H, Parsonage D, Upton H, Rawat M, Claiborne A, Fahey RC, and Helmann JD. Biosynthesis and functions of bacillithiol, a major low-molecular-weight thiol in Bacilli. *Proc Natl Acad Sci U S A* 107: 6482–6486, 2010.
26. Graumann J, Lilie H, Tang X, Tucker KA, Hoffmann JH, Vijayalakshmi J, Saper M, Bardwell JC, and Jakob U. Activation of the redox-regulated molecular chaperone Hsp33—a two-step mechanism. *Structure* 9: 377–387, 2001.
27. Gray MJ, Wholey WY, and Jakob U. Bacterial responses to reactive chlorine species. *Annu Rev Microbiol* 67: 141–160, 2013.
28. Greenwood JR, Calkins D, Sullivan AP, and Shelley JC. Towards the comprehensive, rapid, and accurate prediction of the favorable tautomeric states of drug-like molecules in aqueous solution. *J Comput Aided Mol Des* 24: 591–604, 2010.
29. Hampton MB, Kettle AJ, and Winterbourn CC. Involvement of superoxide and myeloperoxidase in oxygen-dependent killing of *Staphylococcus aureus* by neutrophils. *Infect Immun* 64: 3512–3517, 1996.
30. Hawkins CL, Pattison DI, and Davies MJ. Hypochlorite-induced oxidation of amino acids, peptides and proteins. *Amino Acids* 25: 259–274, 2003.
31. Helmann JD. Bacillithiol, a new player in bacterial redox homeostasis. *Antioxid Redox Signal* 15: 123–133, 2011.
32. Helmann JD. Specificity of metal sensing: iron and manganese homeostasis in *Bacillus subtilis*. *J Biol Chem* 289: 28112–28120, 2014.
33. Herrmann JM, Becker K, and Dick TP. Highlight: dynamics of thiol-based redox switches. *Biol Chem* 396: 385–387, 2015.
34. Hildebrandt T, Knuesting J, Berndt C, Morgan B, and Scheibe R. Cytosolic thiol switches regulating basic cellular functions: GAPDH as an information hub? *Biol Chem* 396: 523–537, 2015.
35. Hillion M and Antelmann H. Thiol-based redox switches in prokaryotes. *Biol Chem* 396: 415–444, 2015.
36. Horsburgh MJ, Clements MO, Crossley H, Ingham E, and Foster SJ. PerR controls oxidative stress resistance and iron storage proteins and is required for virulence in *Staphylococcus aureus*. *Infect Immun* 69: 3744–3754, 2001.
37. Ilbert M, Graf PC, and Jakob U. Zinc center as redox switch—new function for an old motif. *Antioxid Redox Signal* 8: 835–846, 2006.
38. Ilbert M, Horst J, Ahrens S, Winter J, Graf PC, Lilie H, and Jakob U. The redox-switch domain of Hsp33 functions as dual stress sensor. *Nat Struct Mol Biol* 14: 556–563, 2007.
39. Jacobson MP, Friesner RA, Xiang Z, and Honig B. On the role of the crystal environment in determining protein side-chain conformations. *J Mol Biol* 320: 597–608, 2002.
40. Jacobson MP, Pincus DL, Rapp CS, Day TJ, Honig B, Shaw DE, and Friesner RA. A hierarchical approach to all-atom protein loop prediction. *Proteins* 55: 351–367, 2004.
41. Kabsch W. Xds. *Acta Crystallogr D Biol Crystallogr* 66: 125–132, 2010.
42. Kay KL, Hamilton CJ, and Le Brun NE. Mass spectrometry of *B. subtilis* CopZ: Cu(i)-binding and interactions with bacillithiol. *Metallomics* 8: 709–719, 2016.
43. Kehr S, Jortzik E, Delahunty C, Yates JR, 3rd, Rahlfs S, and Becker K. Protein S-glutathionylation in malaria parasites. *Antioxid Redox Signal* 15: 2855–2865, 2011.
44. Klebanoff SJ, Kettle AJ, Rosen H, Winterbourn CC, and Nauseef WM. Myeloperoxidase: a front-line defender against phagocytosed microorganisms. *J Leukoc Biol* 93: 185–198, 2013.
45. Kublik A, Deobald D, Hartwig S, Schiffmann CL, Andrades A, von Bergen M, Sawers RG, and Adrian L. Identification of a multi-protein reductive dehalogenase complex in *Dehalococcoides mccartyi* strain CBDB1 suggests a protein-dependent respiratory electron transport chain obviating quinone involvement. *Environ Microbiol* 18: 3044–3056, 2016.
46. Kumsta C and Jakob U. Redox-regulated chaperones. *Biochemistry* 48: 4666–4676, 2009.
47. Lee JW, Soonsanga S, and Helmann JD. A complex thiolate switch regulates the *Bacillus subtilis* organic peroxide sensor OhrR. *Proc Natl Acad Sci U S A* 104: 8743–8748, 2007.
48. Leichert LI, Gehrke F, Gudiseva HV, Blackwell T, Ilbert M, Walker AK, Strahler JR, Andrews PC, and Jakob U. Quantifying changes in the thiol redox proteome upon oxidative stress in vivo. *Proc Natl Acad Sci U S A* 105: 8197–8202, 2008.
49. Lindemann C and Leichert LI. Quantitative redox proteomics: the NOxICAT method. *Methods Mol Biol* 893: 387–403, 2012.
50. Livermore DM. Antibiotic resistance in staphylococci. *Int J Antimicrob Agents* 16 Suppl 1: S3–S10, 2000.
51. Loi VV, Harms M, Müller M, Huyen NT, Hamilton CJ, Hochgräfe F, Pané-Farré J, and Antelmann H. Real-time imaging of the bacillithiol redox potential in the human pathogen *Staphylococcus aureus* using a genetically encoded

- bacilliredoxin-fused redox biosensor. *Antioxid Redox Signal* 2016 [Epub ahead of print]; DOI: 10/1089.ars.2016.6733.
52. Loi VV, Rossius M, and Antelmann H. Redox regulation by reversible protein S-thiolation in bacteria. *Front Microbiol* 6: 187, 2015.
 53. Lowy FD. *Staphylococcus aureus* infections. *N Engl J Med* 339: 520–532, 1998.
 54. Makarova KS, Ponomarev VA, and Koonin EV. Two C or not two C: recurrent disruption of Zn-ribbons, gene duplication, lineage-specific gene loss, and horizontal gene transfer in evolution of bacterial ribosomal proteins. *Genome Biol* 2: 14, 2001.
 55. Mallett TC, Wallen JR, Karplus PA, Sakai H, Tsukihara T, and Claiborne A. Structure of coenzyme A-disulfide reductase from *Staphylococcus aureus* at 1.54 Å resolution. *Biochemistry* 45: 11278–11289, 2006.
 56. Mueller U, Forster R, Hellmig M, Huschmann FU, Kastner A, Malecki P, Puhlinger S, Rower M, Sparta K, and Steffien M. The macromolecular crystallography beamlines at BESSY II of the Helmholtz-Zentrum Berlin: current status and perspectives. *Eur Phys J Plus* 130: 141, 2015.
 57. Mukherjee S, Dutta D, Saha B, and Das AK. Crystal structure of glyceraldehyde-3-phosphate dehydrogenase 1 from methicillin-resistant *Staphylococcus aureus* MRSA252 provides novel insights into substrate binding and catalytic mechanism. *J Mol Biol* 401: 949–968, 2010.
 58. Newton GL, Rawat M, La Clair JJ, Jothivasan VK, Budiarto T, Hamilton CJ, Claiborne A, Helmann JD, and Fahey RC. Bacillithiol is an antioxidant thiol produced in Bacilli. *Nat Chem Biol* 5: 625–627, 2009.
 59. Painter J and Merritt EA. LSMD web server for the generation of multi-group TLS models. *J Appl Crystallogr* 39: 109–111, 2006.
 60. Pattison DI and Davies MJ. Absolute rate constants for the reaction of hypochlorous acid with protein side chains and peptide bonds. *Chem Res Toxicol* 14: 1453–1464, 2001.
 61. Peralta D, Bronowska AK, Morgan B, Doka E, Van Laer K, Nagy P, Grater F, and Dick TP. A proton relay enhances H₂O₂ sensitivity of GAPDH to facilitate metabolic adaptation. *Nat Chem Biol* 11: 156–163, 2015.
 62. Polgar L. Ion-pair formation as a source of enhanced reactivity of the essential thiol group of D-glyceraldehyde-3-phosphate dehydrogenase. *Eur J Biochem* 51: 63–71, 1975.
 63. Poor CB, Chen PR, Duguid E, Rice PA, and He C. Crystal structures of the reduced, sulfenic acid, and mixed disulfide forms of SarZ, a redox active global regulator in *Staphylococcus aureus*. *J Biol Chem* 284: 23517–23524, 2009.
 64. Posada AC, Kolar SL, Dusi RG, Francois P, Roberts AA, Hamilton CJ, Liu GY, and Cheung A. Importance of bacillithiol in the oxidative stress response of *Staphylococcus aureus*. *Infect Immun* 82: 316–332, 2014.
 65. Pother DC, Gierok P, Harms M, Mostertz J, Hochgrafe F, Antelmann H, Hamilton CJ, Borovok I, Lalk M, Aharonowitz Y, and Hecker M. Distribution and infection-related functions of bacillithiol in *Staphylococcus aureus*. *Int J Med Microbiol* 303: 114–123, 2013.
 66. Ralser M, Wamelink MM, Kowald A, Gerisch B, Heeren G, Struys EA, Klipp E, Jakobs C, Breitenbach M, Lehrach H, and Krobitsch S. Dynamic rerouting of the carbohydrate flux is key to counteracting oxidative stress. *J Biol* 6: 10, 2007.
 67. Rodriguez-Granillo A and Wittung-Stafshede P. Tuning of copper-loop flexibility in *Bacillus subtilis* CopZ copper chaperone: role of conserved residues. *J Phys Chem B* 113: 1919–1932, 2009.
 68. Sastry GM, Adzhigirey M, Day T, Annabhimoju R, and Sherman W. Protein and ligand preparation: parameters, protocols, and influence on virtual screening enrichments. *J Comput Aided Mol Des* 27: 221–234, 2013.
 69. Schuppe-Koistinen I, Moldeus P, Bergman T, and Cotgreave IA. S-thiolation of human endothelial cell glyceraldehyde-3-phosphate dehydrogenase after hydrogen peroxide treatment. *Eur J Biochem* 221: 1033–1037, 1994.
 70. Sun F, Ding Y, Ji Q, Liang Z, Deng X, Wong CC, Yi C, Zhang L, Xie S, Alvarez S, Hicks LM, Luo C, Jiang H, Lan L, and He C. Protein cysteine phosphorylation of SarA/MgrA family transcriptional regulators mediates bacterial virulence and antibiotic resistance. *Proc Natl Acad Sci U S A* 109: 15461–15466, 2012.
 71. Vagin A and Teplyakov A. Molecular replacement with MOLREP. *Acta Crystallogr D Biol Crystallogr* 66: 22–25, 2010.
 72. Vospelnikova ND, Safronova MI, Shuvalova ER, Baratova LA, Kniazev SP, and Nagradova NK. Identification of an arginine residue important for catalytic activity in the primary structure of D-glyceraldehyde 3-phosphate dehydrogenase. Studies with the rat skeletal-muscle enzyme. *Biochem J* 199: 757–765, 1981.
 73. Weber H, Engelmann S, Becher D, and Hecker M. Oxidative stress triggers thiol oxidation in the glyceraldehyde-3-phosphate dehydrogenase of *Staphylococcus aureus*. *Mol Microbiol* 52: 133–140, 2004.
 74. Winterbourn CC and Hampton MB. Thiol chemistry and specificity in redox signaling. *Free Radic Biol Med* 45: 549–561, 2008.
 75. Winterbourn CC and Kettle AJ. Redox reactions and microbial killing in the neutrophil phagosome. *Antioxid Redox Signal* 18: 642–660, 2013.
 76. Winterbourn CC, Kettle AJ, and Hampton MB. Reactive oxygen species and neutrophil function. *Annu Rev Biochem* 85: 765–792, 2016.
 77. Wolf C, Hochgräfe F, Kusch H, Albrecht D, Hecker M, and Engelmann S. Proteomic analysis of antioxidant strategies of *Staphylococcus aureus*: diverse responses to different oxidants. *Proteomics* 8: 3139–3153, 2008.
 78. Zaffagnini M, Bedhomme M, Groni H, Marchand CH, Puppo C, Gontero B, Cassier-Chauvat C, Decottignies P, and Lemaire SD. Glutathionylation in the photosynthetic model organism *Chlamydomonas reinhardtii*: a proteomic survey. *Mol Cell Proteomics* 11: M111 014142, 2012.
 79. Zhu K, Borrelli KW, Greenwood JR, Day T, Abel R, Farid RS, and Harder E. Docking covalent inhibitors: a parameter free approach to pose prediction and scoring. *J Chem Inf Model* 54: 1932–1940, 2014.

Address correspondence to:

Prof. Haike Antelmann
 Institute for Biology-Microbiology
 Freie Universität Berlin
 Berlin D-14195
 Germany

E-mail: haike.antelmann@fu-berlin.de

Date of first submission to ARS Central, September 14, 2016;
 date of final revised submission, December 6, 2016; date of
 acceptance, December 7, 2016.

Abbreviations Used

1,3-BPG = 1,3-bis-phosphoglycerate
 BrxAGC = bacilliredoxin active site mutant
 BrxCGA = bacilliredoxin resolving Cys mutant
 BSH = bacillithiol
bshA = gene for BSH glycosyltransferase
 BSSB = oxidized bacillithiol disulfide
 Cdr = CoASH disulfide reductase
 CoASH = coenzyme A
 CV = coefficient of variation
 Cys = cysteine
 DTT = dithiothreitol
 EDTA = ethylenediaminetetraacetic acid
 G3P = glyceraldehyde-3-phosphate
 Gap = glyceraldehyde-3-phosphate dehydrogenase
 Gap-SO₃H = Gap sulfonic acid
 Gap-SSB = *S*-bacillithiolated Gap
 GlcNAc = N-acetyl glucoseamine
 H₂O₂ = hydrogen peroxide
 HOCl = hypochlorous acid
 ICAT = isotope-coded affinity tag
 IMP = inosine 5'-monophosphate
 IPTG = isopropyl-β-D-thiogalactopyranoside
 LB = Luria bertani
 LC = liquid chromatography
 LMW = low-molecular-weight
 LTQ = linear trap quadrupole
 Mal = malate

Met = methionine
 MPO = myeloperoxidase
 MRSA = methicillin-resistant *Staphylococcus aureus*
 Mrx1 = mycoredoxin1
 MS = mass spectrometry
 MS/MS = tandem mass spectrometry
 NADH = nicotinamide adenine dinucleotide
 NADPH = nicotinamide adenine dinucleotide phosphate
 NaOCl = sodium hypochlorite
 NEM = N-ethylmaleimide
 OxICAT = thiol redox proteomic methods based on the differential labeling of reduced Cys residues with light ICAT and of reversibly oxidized Cys residues with heavy ICAT after reduction using TCEP
 protein-SSB = BSH protein mixed disulfide
 RNS = reactive nitrogen species
 roGFP2 = redox-sensitive green fluorescent protein
 ROS = reactive oxygen species
 RSA = relative surface accessibility
 SDS-PAGE = sodium dodecyl sulfate-polyacrylamide gel electrophoresis
 TCEP = Tris (2-carboxyethyl) phosphine
 Trx = thioredoxin
 TrxR = thioredoxin reductase

Chapter 4

The aldehyde dehydrogenase AldA contributes to the hypochlorite defense and is redox-controlled by protein S-bacillithiolation in *Staphylococcus aureus*

Marcel Imber^{1*}, **Vu Van Loi**^{1*}, Sylvia Reznikov², Verena Nadin Fritsch¹, Agnieszka J. Pietrzyk-Brzezinska^{3,4}, Janek Prehn¹, Chris Hamilton⁵, Markus C. Wahl^{3,6}, Agnieszka K. Bronowska², Haike Antelmann^{1#}

¹Freie Universität Berlin, Institute for Biology-Microbiology, Königin-Luise-Strasse 12-16, D-14195 Berlin, Germany

²School of Chemistry, Bedson Building, Newcastle University, NE1 7RU Newcastle upon Tyne, UK

³Freie Universität Berlin, Laboratory of Structural Biochemistry, D-14195 Berlin, Germany

⁴Institute of Technical Biochemistry, Faculty of Biotechnology and Food Sciences, Lodz University of Technology, Lodz 90-924, Poland

⁵School of Pharmacy, University of East Anglia, Norwich Research Park, Norwich NR4 7TJ, UK

⁶Helmholtz-Zentrum Berlin für Materialien und Energie, Macromolecular Crystallography, D-12489 Berlin, Germany

Published in: Redox Biology. 15: 557-568. (2018)

<https://doi.org/10.1016/j.redox.2018.02.001>

#Corresponding author: haike.antelmann@fu-berlin.de

Authors contributions

Vu Van Loi contributed with *aldA* cloning and mutant constructions. Marcel Imber was involved in biochemical experiments, enzyme activity assays and Western blot analysis. **Vu Van Loi**, Verena Nadin Fritsch and Janek Prehn contributed with the Northern blot experiments, growth and survival assays. Haike Antelmann wrote the manuscript. Haike Antelmann, Marcel Imber, **Vu Van Loi**, and Verena Nadin Fritsch prepared the figures.

* Shared first authorships



Research Paper

The aldehyde dehydrogenase AldA contributes to the hypochlorite defense and is redox-controlled by protein S-bacillithiolation in *Staphylococcus aureus*



Marcel Imber^{a,1}, Vu Van Loi^{a,1}, Sylvia Reznikov^b, Verena Nadin Fritsch^a, Agnieszka J. Pietrzyk-Brzezinska^{c,d}, Janek Prehn^a, Chris Hamilton^e, Markus C. Wahl^{c,f}, Agnieszka K. Bronowska^b, Haike Antelmann^{a,*}

^a Freie Universität Berlin, Institute for Biology-Microbiology, Königin-Luise-Strasse 12-16, D-14195 Berlin, Germany

^b School of Chemistry, Bedson Building, Newcastle University, NE1 7RU Newcastle upon Tyne, UK

^c Freie Universität Berlin, Laboratory of Structural Biochemistry, D-14195 Berlin, Germany

^d Institute of Technical Biochemistry, Faculty of Biotechnology and Food Sciences, Lodz University of Technology, Lodz 90-924, Poland

^e School of Pharmacy, University of East Anglia, Norwich Research Park, Norwich NR4 7TJ, UK

^f Helmholtz-Zentrum Berlin für Materialien und Energie, Macromolecular Crystallography, D-12489 Berlin, Germany

ARTICLE INFO

Keywords:

Staphylococcus aureus

AldA

Bacillithiol

Hypochlorite stress

MD simulations

ABSTRACT

Staphylococcus aureus produces bacillithiol (BSH) as major low molecular weight (LMW) thiol which functions in thiol-protection and redox-regulation by protein S-bacillithiolation under hypochlorite stress. The aldehyde dehydrogenase AldA was identified as S-bacillithiolated at its active site Cys279 under NaOCl stress in *S. aureus*. Here, we have studied the expression, function, redox regulation and structural changes of AldA of *S. aureus*. Transcription of *aldA* was previously shown to be regulated by the alternative sigma factor SigmaB. Northern blot analysis revealed SigmaB-independent induction of *aldA* transcription under formaldehyde, methylglyoxal, diamide and NaOCl stress. Deletion of *aldA* resulted in a NaOCl-sensitive phenotype in survival assays, suggesting an important role of AldA in the NaOCl stress defense. Purified AldA showed broad substrate specificity for oxidation of several aldehydes, including formaldehyde, methylglyoxal, acetaldehyde and glycol aldehyde. Thus, AldA could be involved in detoxification of aldehyde substrates that are elevated under NaOCl stress. Kinetic activity assays revealed that AldA is irreversibly inhibited under H₂O₂ treatment *in vitro* due to over-oxidation of Cys279 in the absence of BSH. Pre-treatment of AldA with BSH prior to H₂O₂ exposure resulted in reversible AldA inactivation due to S-bacillithiolation as revealed by activity assays and BSH-specific Western blot analysis. Using molecular docking and molecular dynamic simulation, we further show that BSH occupies two different positions in the AldA active site depending on the AldA activation state. In conclusion, we show here that AldA is an important target for S-bacillithiolation in *S. aureus* that is up-regulated under NaOCl stress and functions in protection under hypochlorite stress.

1. Introduction

Staphylococcus aureus is a major human pathogen that causes local wound infections, but also life-threatening systemic and chronic

infections, such as septicemia, endocarditis, necrotizing pneumonia and osteomyelitis [1–3]. Moreover, there is an increasing prevalence of hospital- and community-acquired methicillin-resistant *S. aureus* (MRSA) isolates that are often resistant to multiple antibiotics [4]. *S.*

Abbreviations: ADH, aldehyde dehydrogenase; BSH, bacillithiol; BSSB, oxidized bacillithiol disulfide; CFU, colony-forming unit; CD, catalytic domain; Co-BD, coenzyme-binding domain; DTT, dithiothreitol; EDTA, ethylenediaminetetraacetic acid; FA, formaldehyde; H₂O₂, hydrogen peroxide; HOCl, hypochloric acid; IPTG, isopropyl-β-D-thiogalactopyranoside; LB, Luria Bertani; LMW thiol, low molecular weight thiol; MD, molecular dynamics; MG, methylglyoxal; MHQ, 2-methylhydroquinone; MPO, myeloperoxidase; MRSA, methicillin-resistant *Staphylococcus aureus*; NADH, nicotinamide adenine dinucleotide; NADPH, nicotinamide adenine dinucleotide phosphate; NaOCl, sodium hypochlorite; NEM, N-ethylmaleimide; OD₅₀₀, optical density at 500 nm; RCS, reactive chlorine species; RES, reactive electrophilic species; ROS, reactive oxygen species; SCV, small colony variant; SID, subunit interaction domain; X-gal, 5-bromo-4-chloro-3-indolyl-β-D-galactopyranoside

* Corresponding author.

E-mail address: haike.antelmann@fu-berlin.de (H. Antelmann).

¹ Both authors contributed equally to this work.

<https://doi.org/10.1016/j.redox.2018.02.001>

Received 22 November 2017; Received in revised form 1 February 2018; Accepted 2 February 2018

Available online 05 February 2018

2213-2317/ © 2018 The Authors. Published by Elsevier B.V. This is an open access article under the CC BY-NC-ND license (<http://creativecommons.org/licenses/by-nc-nd/4.0/>).

aureus quickly escapes to bactericidal action of new antibiotics and is therefore classified as ESKAPE pathogen by the “European Center of Disease Prevention and Control” [5]. The successful infection of *S. aureus* is mediated by a high diversity of virulence factors, such as toxins, proteases, lipases, superantigens, as well as efficient protection mechanisms against the host immune defense during invasion [6,7]. During infections, *S. aureus* has to cope with the oxidative burst of activated macrophages and neutrophils, including reactive oxygen and chlorine species (ROS, RCS), such as hydrogen peroxide (H₂O₂) and the strong oxidant hypochlorous acid (HOCl) [8–11]. HOCl is generated in neutrophils from H₂O₂ and chloride by the myeloperoxidase (MPO) which is the main cause of bacterial killing [12,13].

Apart from ROS and RCS, *S. aureus* is frequently exposed to reactive electrophile species (RES), such as quinones and aldehydes that originate from cellular metabolism, as secondary oxidation products from ROS and RCS as well as from external sources, such as antibiotics and host-defense components [11,14–17]. RES are α,β -unsaturated dicarbonyl compounds that have electron-deficient centers and can react with protein thiols via oxidation or thiol-S-alkylation chemistries [16,17]. Methylglyoxal is an example for a highly toxic and reactive aldehyde produced as by-product from triose-phosphate intermediates during glycolysis [14,15]. Methylglyoxal detoxification pathways and their regulatory mechanisms have been widely studied in *E. coli* and *B. subtilis*. *E. coli* utilizes a glutathione (GSH)-dependent glyoxalase pathway and a GSH-independent pathway for methylglyoxal detoxification. In the glyoxalase pathway, methylglyoxal reacts spontaneously with GSH to form hemithioacetal which is converted by glyoxalase-I to S-lactoylglutathione. S-lactoylglutathione is the substrate for glyoxalase-II leading to lactate production [14,18]. The glyoxalase *gloA* and the *nemRA* operon are induced by quinones, aldehydes and HOCl and regulated by the TetR-family NemR repressor in *E. coli* [19–22]. GloA functions as glyoxalase in methylglyoxal detoxification and NemA is an FMN-dependent oxidoreductase involved in detoxification of quinones and aldehydes. Moreover, it was shown that methylglyoxal is produced as consequence of hypochlorite stress and that NemR confers protection to methylglyoxal and HOCl via control of the *gloA-nemRA* operon [20].

Gram-positive Firmicutes, such as *Bacillus subtilis* and *S. aureus* produce bacillithiol (BSH) as GSH surrogate which functions as protection mechanism against redox-active compounds and co-factor for thiol-dependent enzymes [23,24]. Methylglyoxal detoxification in *B. subtilis* involves BSH-dependent and BSH-independent pathways [23,25]. In the BSH-dependent glyoxalase pathway, BSH reacts with methylglyoxal to form BS-hemithioacetal which is converted to S-lactoyl-BSH by Glx-I and further by Glx-II to lactate [23,25]. In addition, the thiol-dependent formaldehyde dehydrogenase AdhA confers protection under formaldehyde and methylglyoxal stress in *B. subtilis* which is controlled by the MerR/NmlR-like regulator AdhR [35]. However, the enzymatic pathways involved in detoxification of reactive aldehydes are unknown in *S. aureus*.

Recently, we identified the glycolytic glyceraldehyde-3-phosphate dehydrogenase GapDH as major S-bacillithiolated protein in *S. aureus* under NaOCl stress [26]. Apart from GapDH, the aldehyde dehydrogenase AldA was S-bacillithiolated at its active site Cys279 under NaOCl stress, which could function in detoxification of methylglyoxal or other aldehyde substrates. Here, we have studied the expression and function of AldA of *S. aureus* under formaldehyde, methylglyoxal and NaOCl stress. Transcriptional studies revealed an increased *aldA* transcription under aldehyde, NaOCl and diamide stress in *S. aureus*. In survival phenotype assays, the *aldA* mutant was more sensitive to NaOCl stress. Using biochemical activity assays, we provide evidence that S-bacillithiolation functions in redox-regulation of AldA activity. All-atom molecular dynamics (MD) simulations suggest that the location of BSH in the AldA active site depends on the Cys activation state in the apo- and holoenzyme structures. In conclusion, our results indicate that AldA plays an important role in the NaOCl stress defense and is

redox-regulated by S-bacillithiolation in *S. aureus*.

2. Materials and methods

2.1. Bacterial strains, growth and survival assays

Bacterial strains, plasmids and primers are listed in Tables S1 and S2. For cloning and genetic manipulation, *E. coli* was cultivated in Luria Bertani (LB) medium. *S. aureus* COL was cultivated either in LB or RPMI medium as described previously [26]. For survival phenotype assays, *S. aureus* COL was grown in RPMI medium until an OD₅₀₀ of 0.5, exposed to 2 mM formaldehyde, 4 mM methylglyoxal and 3.5 mM NaOCl stress and 10 μ l of serial dilutions were spotted onto LB agar plates for 24 h to observe colonies. All complemented *aldA* deletion mutants with plasmid pRB473 were grown in the presence of 1% xylose and 10 μ g/ml chloramphenicol. Sodium hypochlorite, diamide, dithiothreitol (DTT), hydrogen peroxide (H₂O₂, 35% w/v), formaldehyde, methylglyoxal and 2-methylhydroquinone (MHQ) were purchased from Sigma Aldrich.

2.2. RNA isolation and Northern blot analysis

For RNA isolation, *S. aureus* COL was cultivated in RPMI medium and treated with sub-lethal doses of 1 mM NaOCl, 0.75 mM formaldehyde (FA), 0.5 mM methylglyoxal (MG), 10 mM H₂O₂ and 50 μ M MHQ for different times as described previously [26]. *S. aureus* COL cells were harvested before and after stress exposure and disrupted in lysis buffer [10 mM Tris-HCl, pH 8.0; 200 mM sodium chloride (NaCl); 3 mM ethylene diamine tetra acetic acid (EDTA)] with a Precellys24 ribolyzer. RNA was isolated using acid phenol extraction as described [26] and RNA quality was assessed using the Nanodrop. Northern blot hybridizations were performed with the digoxigenin-labelled *aldA*-specific antisense RNA probe synthesized *in vitro* using T7 RNA polymerase and the primer pairs *aldA*-for and *aldA*-rev (Table S2) as described [26,27].

2.3. Cloning, expression and purification of His-tagged AldA and AldAC279S mutant proteins in *E. coli*

The *aldA* gene was amplified from chromosomal DNA of *S. aureus* COL by PCR using primers *aldA*-for-*NheI* and *aldA*-rev-*BamHI* (Table S2), digested with *NheI* and *BamHI* and inserted into plasmid pET11b (Novagen) that was digested using the same enzymes to generate plasmid pET11b-*aldA*. For construction of pET11b expressing AldAC279S mutant protein, Cys279 was replaced by serine using PCR mutagenesis. Two first-round PCR reactions were performed using primer pairs *aldA*-for-*NheI* and *aldA*-C279S-Rev as well as primer pairs *aldA*-C279S-for and *aldA*-rev-*BamHI* (Table S2). The two first round PCR products were hybridized and subsequently amplified by a second round of PCR using primers *aldA*-for-*NheI* and *aldA*-rev-*BamHI*. The second-round PCR products were digested with *NheI* and *BamHI* and inserted into plasmid pET11b digested with the same enzymes to generate plasmid pET11b-*aldAC279S*. The correct *aldA* and *aldAC279S* sequences of the plasmids were confirmed by DNA sequencing. Plasmid pET11b-*aldAC279S* was also used for construction of the *aldAC279S* mutant *in vivo* and subcloned into the *E. coli*/*S. aureus* shuttle vector pRB473 as described below.

For expression and purification of His-tagged AldA and AldAC279S mutant protein, *E. coli* BL21(DE3) *plysS* was used expressing plasmids pET11b-*aldA* and pET11b-*aldAC279S*, respectively. Cultivation was performed in 1 l LB medium until the exponential growth phase at OD₆₀₀ of 0.8 followed by addition of 1 mM isopropyl- β -D-thiogalactopyranoside (IPTG) for 3.5 h at 37 °C. Recombinant His-AldA and His-AldAC279S mutant proteins were purified after sonication of the *E. coli* cells in binding buffer (20 mM NaH₂PO₄, 500 mM NaCl, 20 mM imidazole, pH 7.4). Lysates were cleared from cell debris by repeated centrifugation and purification of the His-AldA and His-AldAC279S

mutant proteins was performed by application of an imidazole gradient (0–500 mM) using His Trap™ HP Ni-NTA columns (5 ml; GE Healthcare, Chalfont St. Giles, UK) and the ÄKTA purifier liquid chromatography system (GE Healthcare) according to the instructions of the manufacturer. Purified proteins were extensively dialyzed against 10 mM Tris-HCl (pH 8.0), 100 mM NaCl, and stored on ice until usage.

2.4. Construction of the *S. aureus* COL *aldA* deletion mutant and the complemented *aldA* and *aldAC279S* mutant strains

The *S. aureus* COL *aldA* deletion mutant was constructed by allelic replacement via the temperature-sensitive shuttle vector pMAD as described [28]. Briefly, for construction of the plasmids pMAD- Δ *aldA*, the 500 bp up- and downstream flanking gene regions of *aldA* were amplified using the primers *aldA*-pMAD-up-for/rev and *aldA*-pMAD-down-for/rev from *S. aureus* COL genomic DNA (Table S2). The *aldA* up- and downstream flanking regions were fused by overlap extension PCR and ligated into the *Bgl*II and *Sal*I sites of plasmid pMAD. The pMAD constructs were electroporated into the restriction-negative and methylation-positive intermediate *S. aureus* RN4220 strain and further transferred to *S. aureus* COL by phage transduction using phage 80 [29]. Transductants were streaked out on LB agar with 10 μ g/ml erythromycin and 40 μ g/ml 5-bromo-4-chloro-3-indolyl- β -D-galactopyranoside (X-gal) at 30 °C. Blue transductants with pMAD integrations were selected for plasmid excision by a heat shock as described [30]. Erythromycin-sensitive white colonies were selected on X-gal plates and screened for *aldA* deletions by PCR and DNA sequencing.

The complemented *aldA* and *aldAC279S* mutant strains were constructed using the pRB473 plasmid as described [31]. Briefly, *aldA* and *aldAC279S* sequences were amplified from plasmids pET11b-*aldA* and pET11b-*aldAC279S* using the primers *aldA*-pRB-for-*Bam*HI and *aldA*-pRB-rev-*Kpn*I. The PCR products were digested with *Bam*HI and *Kpn*I and inserted into the pRB473 plasmid that was digested using the same enzymes resulting in plasmids pRB473-*aldA* and pRB473-*aldAC279S*. The plasmids were transferred to the Δ *aldA* mutant via phage transduction as described [31].

2.5. AldA activity assays

AldA activity was monitored spectrophotometrically at 340 nm and 30 °C with the substrate and NAD⁺ as cofactor by the production of NADH using a CLARIOstar (BMG Labtech) spectrophotometer. The oxidation of different aldehyde substrates (formaldehyde, methylglyoxal, acetaldehyde and glycol aldehyde) was measured in an assay mixture containing 1.25 mM NAD⁺ and 2.5 μ M AldA in reaction buffer (100 mM Tris-HCl, 1.25 mM EDTA, pH 7.5). After pre-incubation, the reaction was started by addition of the aldehyde substrates and NADH production was measured at 340 nm. The kinetic curves are presented as mean \pm SEM from at least three independent experiments.

2.6. Western blot analysis

The purified His-AldA protein was separated using 12% SDS-PAGE and subjected to BSH-specific Western blot analysis using the polyclonal rabbit anti-BSH antiserum as described previously [32].

2.7. Molecular docking of the *S. bacillithiolated* AldA Cys279 active site

To model a covalent complex between BSH and the AldA Cys279 active site by molecular docking, the crystal structure of AldA from *S. aureus* was used as a receptor (PDB code 3TY7). The missing loop (residues 438–459) was modelled and fitted using MODELLER [33]. To identify the potential BSH binding site, FTMap solvent mapping calculations were performed [34] and two highest-occupancy binding sites were considered in the further calculations (Fig. 7EF). In the Q1 site, the NAD⁺ molecule has been fitted using crystal structures of the

Pseudomonas fluorescens pfAMSDH co-crystallised with NAD⁺ (PDB code 4I1W). Then, the hydrogen atoms were added, and the charges for NAD⁺ molecule were assigned using AM1-BCC method [35]. The Cys279 thiol group was considered deprotonated. The BSH molecule was built, energy minimised (5000 cycles of steepest-descent minimisation), and the partial atomic charges were generated using AM1-BCC [35].

Molecular docking was performed using the University of California, San Francisco DOCK 6.8 suite [36] with grid scoring in an implicit solvent. The grid spacing was 0.25 Å, and the grid included 12 Å beyond the NAD⁺ modelled, which was subsequently removed for the pose Q2. The energy score was the sum of electrostatic and van der Waals contributions. To check the suitability of the methodology, the NAD⁺ was removed from the binding site, its translational and rotational degrees of freedom were altered and the molecule has been redocked to the protein, in order to check whether the docking procedure was able to reproduce the native binding mode, as observed in related crystal structures. After the positive verification, the BSH molecule was docked to both Q1 (holo-enzyme with NAD⁺) and Q2 (apo-enzyme without NAD⁺) sites detected by FTMap [34].

During the docking calculations, the BSH molecule was subjected to 5000 cycles of molecular-mechanical energy minimisation at the protein-binding site. The number of maximum ligand orientations was 50,000. The constraint was the distance between sulfur atoms from the Cys279 thiol and the sulfur of BSH. The 25 best-scoring poses (BSH-protein complexes) were further analyzed by means of secondary rescoring using SeeSAR <https://www.biosolveit.de/SeeSAR/> package with more accurate HYDE scoring function [37]. The best-scoring poses in Q1 and Q2 putative binding sites were subjected to all-atom MD simulations.

2.8. Molecular dynamics (MD) simulation of *S. bacillithiolation*

All simulations for the 5 studied systems: apo-enzyme, holo-enzyme (protein-NAD⁺), BSH-holo-enzyme (Q1), BSH-apo-enzyme (Q1), and BSH-apo-enzyme (Q2) were carried out using GROMACS2016.2 code [38], with Amber99SB-ILDN [39] force field for the duplexes and the TIP3P water model. Parameters for NAD⁺ and BSH were assigned by ACPYPE [40]. Obtained partial atomic charges were derived using the RESP methodology [41] and validated with the Gaussian09 programme [42] using HF/6-31G* basis set.

The temperature was kept constant at T = 300 K by using velocity rescaling with a coupling time of 0.1 ps. The pressure was kept constant at 1 bar using an isotropic coupling to Parrinello-Rahman barostat with a coupling time of 0.1 ps [43]. A cut-off of 1 nm was used for all non-bonded interactions. Long-range electrostatic interactions were treated with the particle-mesh Ewald [44] method using a grid spacing of 0.1 nm with cubic interpolation. All bonds between hydrogens and heavy atoms were constrained using the LINCS algorithm [45]. Each of the systems were immersed in a cubic TIP3P water box containing ~ 115,000 atoms. Simulation units were maintained neutral by adding sodium and chloride counter ions (0.1 M concentration).

Prior to MD simulations, the systems undergone 50,000 steps of molecular mechanical energy minimisation. This was followed by 100 ps MD simulations, during which position constraints were used on all backbone atoms, heavy atoms of BSH and NAD⁺. After the following unrestrained equilibration phase (10 ns) the production runs were carried out for 50 ns, with an integration time step of 2 fs. The cut-off for non-bonded interactions was 0.1 nm. The atomic coordinates were saved every 100 ps. For the visual inspection of the results we used xmgrace [46] and UCSF Chimera [47] packages. Free binding energy calculations have been performed using the MMPBSA.py program from AmberTools package [48]. Binding energies have been calculated between BSH and the protein at the two different binding sites, as in Q1 and Q2, for the last 25 ns of the simulation.

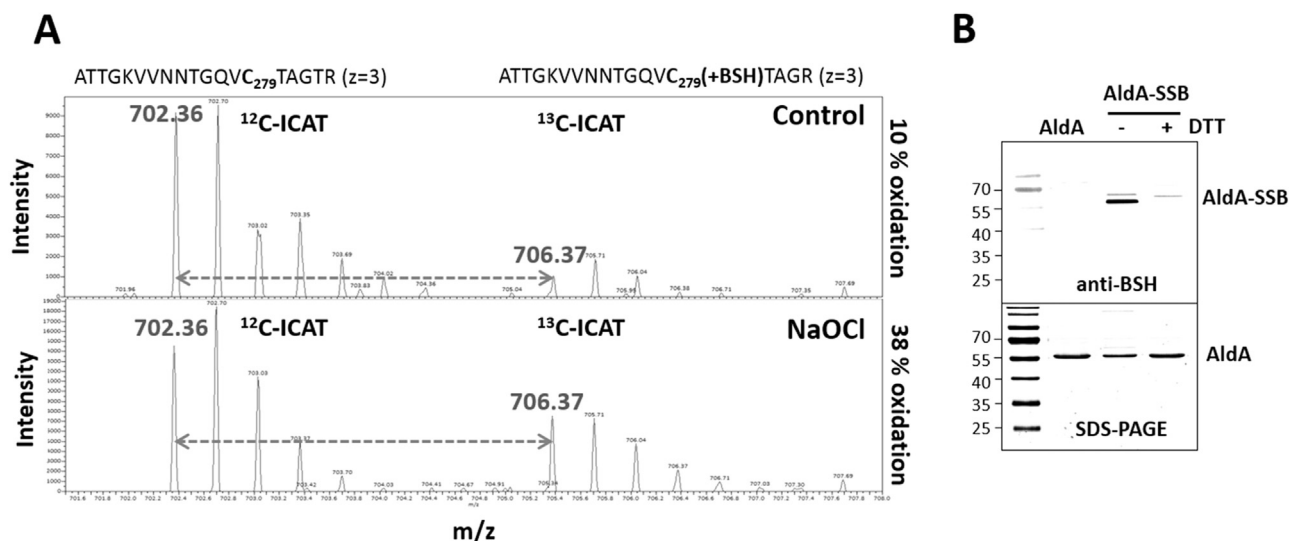


Fig. 1. OxICAT analysis revealed a 29% increased oxidation of the AldA Cys279-peptide (A) and *S*-bacillithiolation of the AldA protein *in vitro* is shown by BSH-specific Western blot analysis (B). (A) The OxICAT mass spectrometry results from the previous study [26] are shown for the AldA-Cys279-peptide in *S. aureus* under control and 30 min after NaOCl stress. The reduced Cys279-peptides is labelled with light ¹²C-ICAT, followed by reduction of the *S*-bacillithiolated Cys279-peptide and labelling with heavy ¹³C-ICAT reagent. The Cys279-peptide was 10% oxidized in the control and 38% oxidized in the NaOCl stress sample indicating a 29% oxidation increase. (B) AldA is *S*-bacillithiolated *in vitro* by H₂O₂ in the presence of BSH as revealed by BSH-specific Western blots. Reduced purified AldA (40 μM) is pretreated with 10-fold molar excess of BSH (400 μM) and incubated with 10 mM H₂O₂ for 5 min. The *S*-bacillithiolated AldA was detected using non-reducing BSH-specific Western blot analysis. The loading control of AldA and *S*-bacillithiolated AldA (AldA-SSB) is shown as SDS-PAGE stained with Coomassie below the anti-BSH blot.

3. Results

3.1. The aldehyde dehydrogenase AldA is strongly oxidized at its active site Cys279 due to *S*-bacillithiolation under NaOCl stress in *S. aureus*

The aldehyde dehydrogenase AldA was previously identified as *S*-bacillithiolated at its catalytic active site Cys279 in *S. aureus* and *Staphylococcus carnosus* [26,32]. In addition, both aldehyde dehydrogenases, GapDH and AldA displayed the highest oxidation increase of 29% under NaOCl stress in *S. aureus* using the thiol-redox proteomics approach OxICAT [26]. The OxICAT method is based on thiol-labelling of the reduced AldA Cys279 peptide with light ¹²C-ICAT reagent, followed by reduction of the Cys279-SSB peptide and its labelling with heavy ¹³C-ICAT reagent [49]. The percentage oxidation of the Cys279 peptide of AldA under control and NaOCl stress is reflected by the mass spectra of the ICAT-labelled peptide pair as quantified in the previous study [26] (Fig. 1A). The strong 29% oxidation increase of the active site Cys279 is shown here again which is caused by *S*-bacillithiolation [26]. To confirm that AldA can be *S*-bacillithiolated also *in vitro*, we expressed and purified His-tagged AldA from *E. coli* extracts. Purified AldA was treated with H₂O₂ after pre-exposure to 10-fold excess of BSH and the reversible *S*-bacillithiolation of AldA was verified using BSH-specific Western blot analyses in the absence and presence of DTT (Fig. 1B). The *S*-bacillithiolated AldA band is denoted with AldA-SSB. Next, we were interested to study the expression, function, redox-regulation and structural changes of AldA under NaOCl and aldehyde stress.

3.2. Transcription of *aldA* is induced SigmaB-independently under thiol-specific stress conditions by formaldehyde, NaOCl and diamide in *S. aureus* COL

We used Northern blot analysis to study *aldA* transcription in *S. aureus* COL under different thiol-specific stress conditions, including sub-lethal doses of 1 mM NaOCl, 2 mM diamide, 0.75 mM formaldehyde, 0.5 mM methylglyoxal, 50 μM methylhydroquinone (MHQ) and 10 mM H₂O₂ (Fig. 2A). The Northern blot results revealed that *aldA* transcription is strongly induced in *S. aureus* COL wild type after exposure to formaldehyde, diamide and NaOCl stress, but less strongly

under methylglyoxal stress (Fig. 2A). No significant induction of *aldA* was detected under MHQ and H₂O₂ treatment. These transcriptional results indicate that AldA could be involved in the hypochlorite stress defense or in detoxification of aldehydes. In previous microarray experiments, *aldA* was identified as member of the SigmaB general stress regulon, which responds to heat and salt stress (NaCl), MnCl₂ and alkaline stress conditions in *S. aureus* [50,51]. The *sigB*-dependent promoter sequence was mapped in the *aldA* regulatory upstream region (GTTTAT-N14-GGATAA) as promoter U1137.SigB.M2 previously (Fig. 2B) [52]. In the condition-dependent transcriptome of *S. aureus* NCTC8325-4 [53], the strongest *aldA* transcription was monitored during the stationary phase in rich LB and TSB medium as well as during plasma stress as visualized by the Aureowiki Expression data browser (http://genome.jouy.inra.fr/cgi-bin/aeb/viewdetail.py?id=NA_2184537_2185964_-1) [52].

To investigate whether the thiol-specific induction of *aldA* transcription by formaldehyde, diamide and NaOCl requires SigmaB, we performed Northern blot analysis with RNA isolated from a *sigB* deletion mutant in comparison to the wild type (Fig. 2B). The Northern blot results showed similar *aldA* transcriptional induction in the *sigB* mutant under NaOCl, diamide and formaldehyde stress compared to the wild type. Even a higher *aldA* transcription occurred under methylglyoxal stress in the *sigB* mutant. These results indicate that *aldA* transcription is subject to SigmaB-independent control mechanisms under thiol-specific stress conditions by an unknown thiol-specific transcription factor that remains to be elucidated. No additional SigA promoter was identified upstream of *aldA* previously [52], presumably because the conditions were different compared to our thiol-stress conditions. In previous studies, a refined consensus for SigA- and SigB-dependent promoter sequences was revealed based on 93% of *S. aureus* transcriptional units [52]. In the *aldA* regulatory region, a putative SigA-dependent promoter was identified upstream of the SigB promoter, which could drive the thiol-specific expression of *aldA* (Fig. 2B).

3.3. AldA plays important roles in the defense against NaOCl stress in *S. aureus* COL

Next, we analyzed the role of AldA in protection under NaOCl and aldehyde stress in *S. aureus*. It was previously shown that methylglyoxal

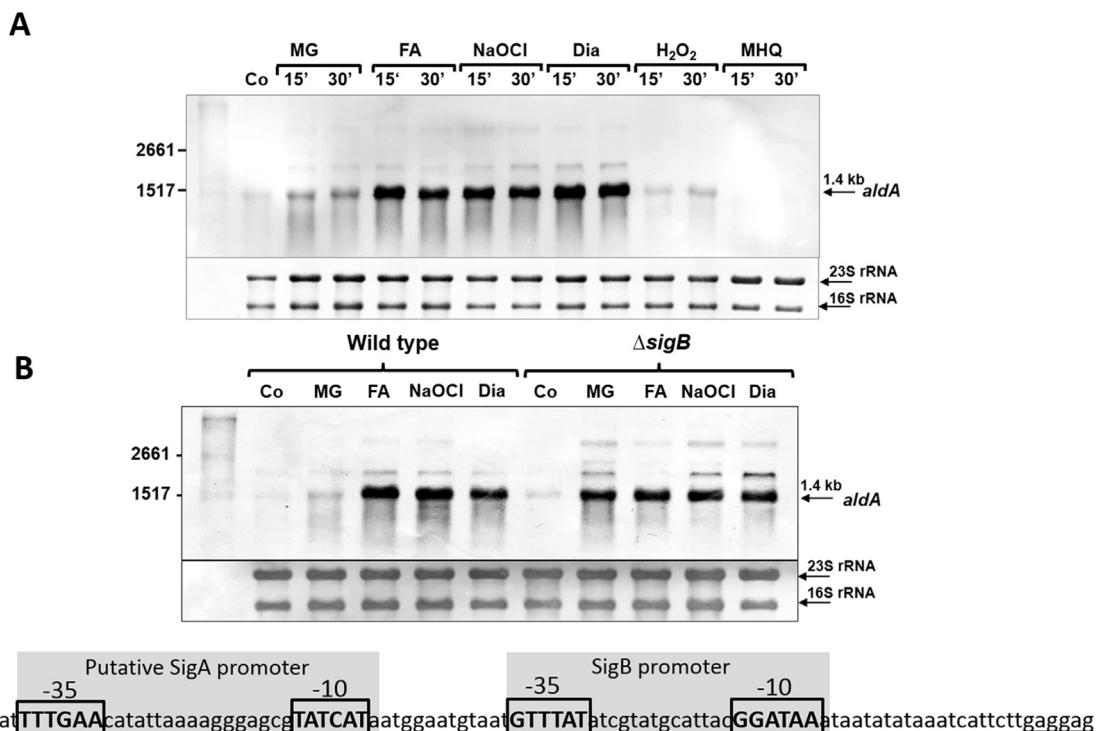


Fig. 2. Transcriptional induction of *aldA* under formaldehyde, methylglyoxal, NaOCl and diamide stress in *S. aureus* COL wild type (A) and in the *sigB* mutant (B). (A) RNA was isolated from *S. aureus* COL wild type under control conditions as well as after treatment with sub-lethal doses of 0.75 mM formaldehyde, 0.5 mM methylglyoxal, 1 mM NaOCl, 2 mM diamide, 10 mM H₂O₂ and 50 μM methylhydroquinone (MHQ) for 15 and 30 min and subjected to Northern blot analysis for *aldA* (SACOL2114) transcription. (B) For comparison of Northern blot analysis of *aldA* transcription between the wild type and the *sigB* mutant, RNA was isolated from *S. aureus* COL wild type and the *sigB* mutant after exposure to 0.75 mM formaldehyde, 0.5 mM methylglyoxal, 1 mM NaOCl and 2 mM diamide for 15 min. Transcription of *aldA* is similarly up-regulated under formaldehyde, NaOCl and diamide stress in the wild type (A) and in the *sigB* mutant (B) indicating a SigmaB-independent thiol-stress regulatory mechanism of *aldA* transcription. The known SigmaB-dependent promoter sequence and a putative SigA-dependent promoter in the *aldA* upstream regulatory region are shown below the Northern blot in (B). The methylene blue stain is the RNA loading control showing the abundant 16S and 23S rRNAs. The experiments were performed in 3 biological replicates.

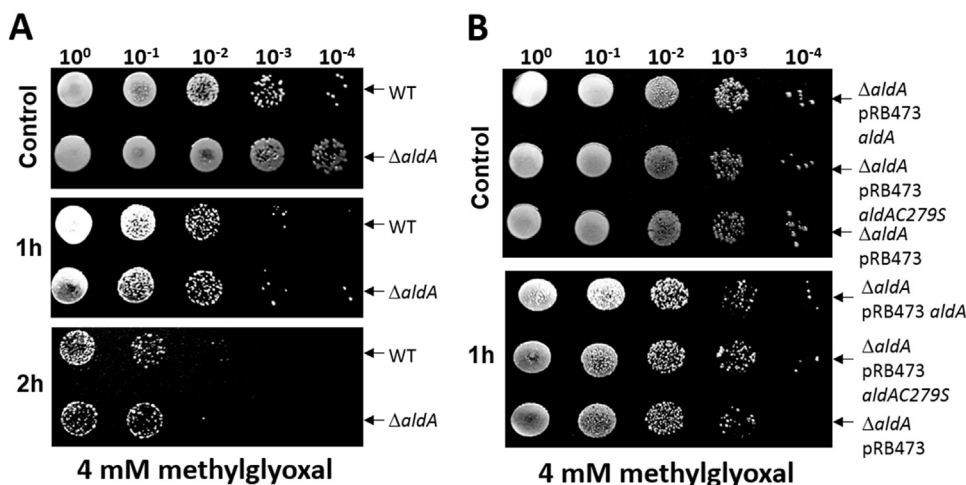


Fig. 3. AldA is not essential for the survival of *S. aureus* under methylglyoxal stress. For the survival phenotype assays, *S. aureus* COL wild-type (WT), the Δ *aldA* deletion mutant (A) and the *aldA* and *aldAC279S* complemented Δ *aldA* mutants (Δ *aldA* pRB473-*aldA* and Δ *aldA* pRB473-*aldAC279S*) (B) were grown in RPMI until an OD₅₀₀ of 0.5 and treated with 4 mM methylglyoxal. Survival assays were performed by spotting 10 μl of serial dilutions after 1–3 h of NaOCl exposure onto LB agar plates. The experiments were performed in 3 biological replicates.

is produced in *E. coli* cells treated with HOCl [20]. Thus, AldA could function in methylglyoxal detoxification under HOCl stress also in *S. aureus*. AldA harbors a conserved active site Cys279 which is essential for its catalytic activity [54–56]. The function of AldA and the conserved Cys279 under methylglyoxal, formaldehyde and HOCl stress was analyzed in growth and survival assays of an *aldA* deletion mutant and its *aldA* and *aldAC279S* complemented strains (Figs. 3, 4, S1 and S2). The growth of the *aldA* mutant was not affected under sub-lethal formaldehyde and methylglyoxal stress in comparison to the wild type (Fig. S1). In addition, no significant phenotypes of the *aldA* mutant and the *aldA* complemented strains were detected in survival assays after exposure to 4 mM methylglyoxal (Fig. 3AB) and 2 mM formaldehyde

stress (Fig. S2). However, the *aldA* mutant was significantly impaired in growth after exposure to sub-lethal concentrations of 1.5 mM NaOCl stress (Fig. 4A). In survival assays, the *aldA* mutant showed also a strongly decreased survival after treatment with 3.5 mM NaOCl (Fig. 4C). This survival defect of the Δ *aldA* mutant could be restored back to wild type level in the *aldA* complemented strain, but not in the *aldAC279S* mutant (Fig. 4D). This indicates that AldA is involved in protection of *S. aureus* against NaOCl stress and that Cys279 is essential for AldA activity *in vivo*.

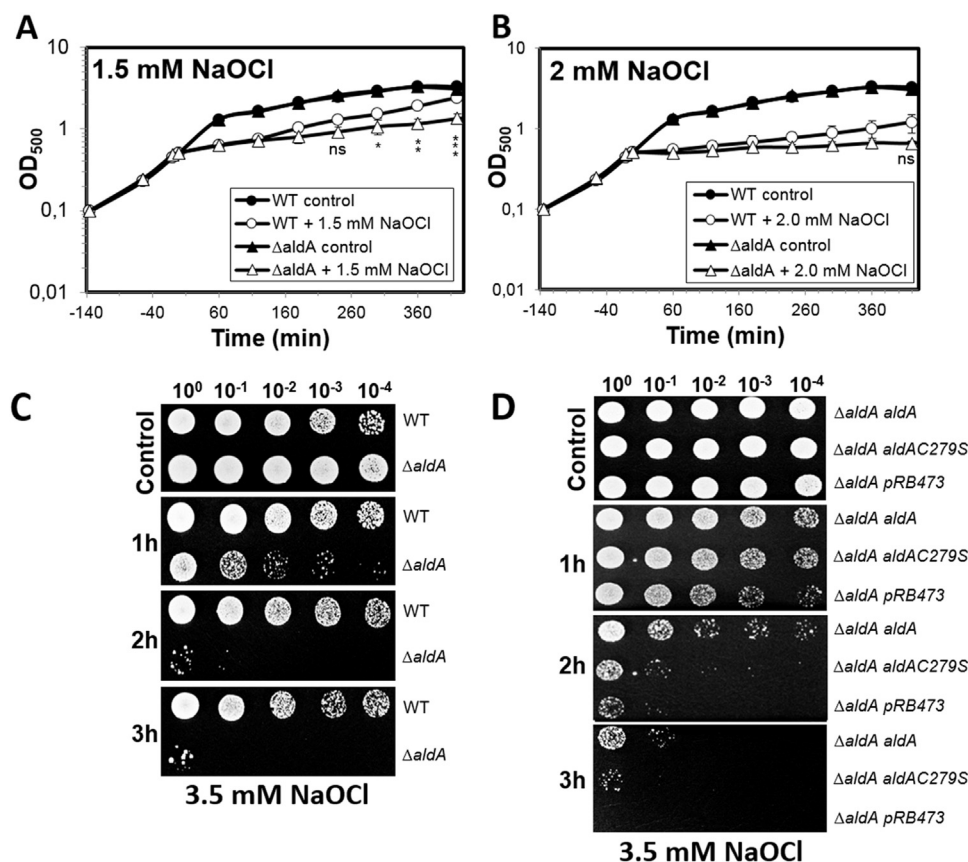


Fig. 4. AldA is required for growth and survival under NaOCl stress in *S. aureus*. (A, B) Growth curves of *S. aureus* COL wild type and the *aldA* deletion mutant in RPMI medium after exposure to sublethal concentrations of 1.5 mM and 2 mM NaOCl stress at an OD₅₄₀ of 0.5. The growth differences of the *aldA* mutant are significantly different compared to the wild type at 1.5 mM NaOCl. (C, D) For the survival phenotype assays, *S. aureus* COL wild-type (WT), the Δ aldA deletion mutant (C) and the *aldA* and *aldAC279S* complemented Δ aldA mutants (Δ aldApRB473-*aldA* and Δ aldA pRB473-*aldAC279S*) (D) were grown in RPMI until an OD₅₀₀ of 0.5 and treated with 3.5 mM NaOCl. Survival assays were performed by spotting 10 μ l of serial dilutions after 1–3 h of NaOCl exposure onto LB agar plates. Colonies were observed after overnight incubation of the LB plates at 37 °C. The active site Cys279 of AldA is required for NaOCl stress survival. The results for the growth curves and survival assays are from 5 biological replicate experiments. For the growth curves in Fig. 4AB, error bars represent the SEM and the statistics was calculated using a Student's unpaired two-tailed *t*-test by the graph prism software. Symbols are defined as follows: ns *p* > 0.05; **p* ≤ 0.05; ***p* ≤ 0.01 and ****p* ≤ 0.001.

3.4. AldA shows broad substrate specificity for oxidation of various aldehyde substrates, including formaldehyde and methylglyoxal *in vitro*

To study the function and substrate specificity of AldA *in vitro*, the catalytic activity was measured using different aldehyde substrates, including formaldehyde, methylglyoxal, glycol aldehyde and acetaldehyde in concentrations ranging from 0.5 to 100 mM. AldA activity was measured in a spectrophotometric assay in the presence of NAD⁺ as a cofactor with the different aldehyde substrates by monitoring the NADH production as absorbance increase at 340 nm. The AldA activity assays revealed increasing NADH production with increasing concentrations of all aldehyde substrates indicating that AldA has broad substrate specificities (Fig. 5). AldA showed the highest activities with 55 mM formaldehyde and 20 mM methylglyoxal, which could be possible substrates of AldA. Formaldehyde and methylglyoxal are oxidized to formate and lactate by AldA, resulting in NADH generation.

To further confirm that Cys279 is the active site residue and essential for AldA activity, we used the purified AldAC279S mutant protein which was analyzed for formaldehyde and methylglyoxal oxidation in the AldA activity assays. However, the AldAC279S mutant protein did not show significant activity for formaldehyde and methylglyoxal oxidation in our activity assays (Fig. S4). This indicates that the conserved Cys279 is the active site residue and required for AldA activity as shown also for other homologs previously [54,55,57].

3.5. AldA is redox-regulated and protected by protein S-bacillithiolation under H₂O₂ stress *in vitro*

We were interested whether S-bacillithiolation inhibits AldA activity and protects the active site Cys279 against overoxidation *in vitro*. Using the spectrophotometric assay, AldA activity was measured after oxidative stress with 15 mM methylglyoxal as substrate and NAD⁺ as coenzyme by monitoring NADH generation at 340 nm. Treatment of

AldA with 0.5–1 mM H₂O₂ resulted in a strong inactivation of its enzymatic activity (Fig. 6A). Inactivation of AldA with H₂O₂ alone was irreversible since AldA activity could not be restored after treatment with 10 mM DTT (Fig. 6B). These results indicate that the active site Cys279 of AldA is very sensitive to overoxidation by H₂O₂ in the absence of BSH. To assess the effect of S-bacillithiolation on AldA activity, the enzyme was pre-exposed to 0.3–0.5 mM BSH prior to oxidation with 0.3–1 mM H₂O₂ and the remaining AldA activity was measured in the spectrophotometric assay with 15 mM methylglyoxal as substrate. AldA activity was inhibited with 0.3–1 mM H₂O₂ after pre-treatment with 0.3–0.5 mM BSH (Fig. 6C). In this case, however, the activity of the oxidized AldA protein could be restored to 66% by DTT reduction indicating that AldA is subject to reversible S-bacillithiolation in the presence of BSH and H₂O₂ (Fig. 6D). S-bacillithiolation of AldA and its reversibility with DTT was further confirmed in BSH-specific Western blots (Fig. 1B). These results suggest that S-bacillithiolation protects the AldA active site Cys279 against overoxidation and functions in redox-regulation of AldA activity *in vitro*.

3.6. Structural comparison of AldA with other aldehyde dehydrogenases

We were further interested in the structure and the structural changes of AldA upon S-bacillithiolation. A crystal structure of *S. aureus* AldA (denoted as saAldA) has been determined by the Midwest Center for Structural Genomics (PDB 3TY7). For understanding the enzyme's catalytic mechanism, we performed structural homology searches for saAldA with the DALI server [58] (http://ekhidna.biocenter.helsinki.fi/dali_server/) and the PDBeFold (SSM) server (<http://www.ebi.ac.uk/msd-srv/ssm/>). SaAldA shows high homology to many other aldehyde dehydrogenases (ADHs) from bacteria, plants and humans. The root-mean-square deviations (r.m.s.d.'s) and sequence similarities of AldA's closest homologs are listed in Table S3.

In contrast to the tetrameric bacterial ADHs (*pf*AMSDH, *sa*BADH,

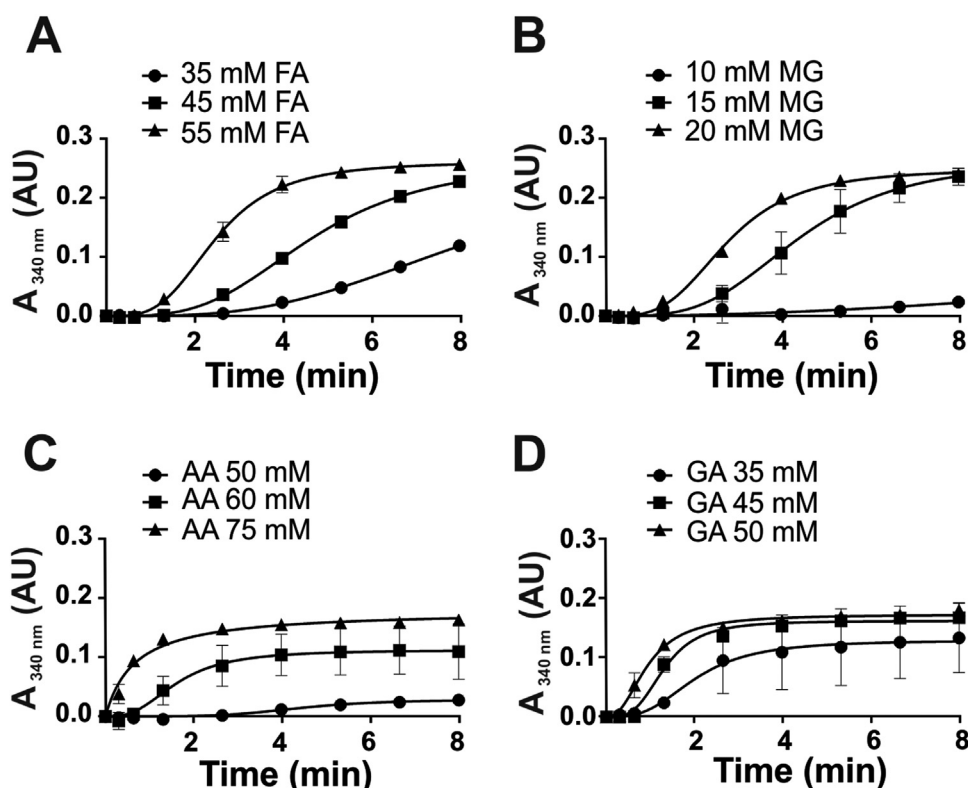


Fig. 5. Purified AldA shows broad substrate specificity towards various aldehydes *in vitro*. The catalytic activity of the aldehyde dehydrogenase AldA was analyzed with increasing concentrations of different aldehyde substrates, including (A) formaldehyde (FA), (B) methylglyoxal (MG), (C) acetaldehyde (AA) and (D) glycol aldehyde (GA). Reduced AldA (2.5 μ M) was incubated with different concentrations of aldehyde substrates ranging from 10 to 100 μ M in reaction buffer (100 mM Tris HCl, 1.25 mM EDTA, pH 7.5). The oxidation of the aldehydes was measured in the presence of NAD^+ as coenzyme and NADH generation was monitored at 340 nm using a spectrophotometer. The results are from 3 replicate experiments. Error bars represent the SEM.

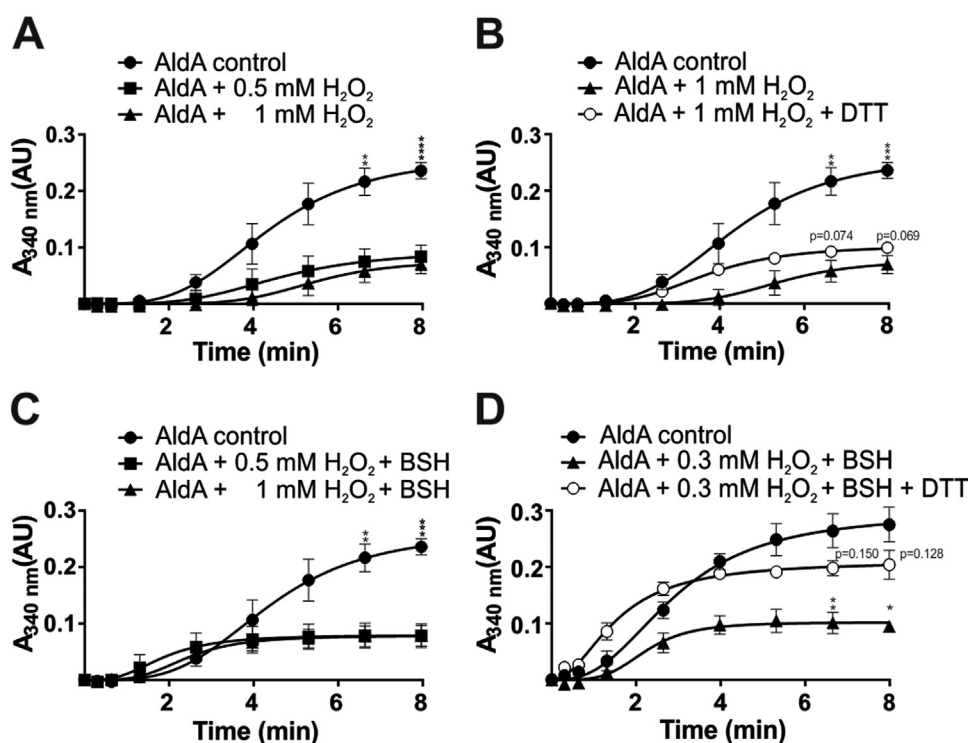


Fig. 6. Inactivation of AldA of *S. aureus* in response to H_2O_2 in the absence and presence of BSH *in vitro*. Reduced AldA (30 μ M) was oxidized with 0.3–1 mM H_2O_2 for 5 min in the absence (A, B) or presence of BSH (C, D) in reaction buffer (100 mM Tris HCl, 1.25 mM EDTA, pH 7.5). The AldA activities were measured with 15 mM methylglyoxal as substrate and NAD^+ as coenzyme by monitoring NADH production at 340 nm using a spectrophotometer. To analyze the irreversible inactivation of AldA by H_2O_2 alone, AldA was treated with 1 mM H_2O_2 without BSH followed by reduction with 10 mM DTT (C). The reversibility of AldA S-bacillithiolation with 0.3 mM H_2O_2 and 0.3 mM BSH is shown after DTT-reduction resulting in 66% of regeneration of AldA activity (D). The S-bacillithiolation of AldA and its reduction using DTT was further confirmed in BSH-specific Western blot analysis as shown in Fig. 1B. P-values were calculated as follows: $p = 0.0012$, $p = 0.0001$ for AldA control/0.5 mM H_2O_2 at 6.63 and 8 min, respectively (Fig. 6A); $p = 0.0012$, $p = 0.0002$ for AldA control/1 mM H_2O_2 at 6.63 and 8 min and $p = 0.074$, $p = 0.069$ for 1 mM H_2O_2 /1 mM H_2O_2 + DTT at 6.63 and 8 min, respectively (Fig. 6B); $p = 0.0021$, $p = 0.0008$ for AldA control/0.5 mM H_2O_2 + BSH at 6.63 and 8 min, respectively (Fig. 6C); $p = 0.003$, $p = 0.011$ for 0.3 mM H_2O_2 + BSH/0.3 mM H_2O_2 + BSH + DTT at 6.63 and 8 min; $p = 0.150$, $p = 0.128$ for AldA control/0.3 mM H_2O_2 + BSH + DTT at 6.63 and 8 min, respectively (Fig. 6D). Symbols are defined as follows: $^ns p > 0.05$; $^* p \leq 0.05$;

$^{**} p \leq 0.01$; $^{***} p \leq 0.001$; and $^{****} p \leq 0.0001$. The results are from 3 replicate experiments. In all graphs, mean values are shown, error bars represent the SEM and p-values are calculated using a Student's unpaired two-tailed t-test by the graph prism software.

ecADH, *paBADH*), *saAldA* is a dimeric enzyme and thus more similar to plant ADHs that are also active as dimer (Fig. 7A). Regardless of the oligomerization state, the overall fold of a subunit is highly conserved among all ADH enzymes. Similarly as in other ADHs, a *saAldA* subunit is composed of a coenzyme (NAD^+)-binding domain (Co-BD; residues

1-122, 137-244 and 439-464), a catalytic domain (CD; residues 245-438) and a subunit interaction domain (SID; residues 123-136 and 465-475; Fig. 7A).

In all ADHs, the active site harbors conserved Cys (C279 in *saAldA*) and glutamate (E245 in *saAldA*) residues (Fig. S5). The Cys residue can

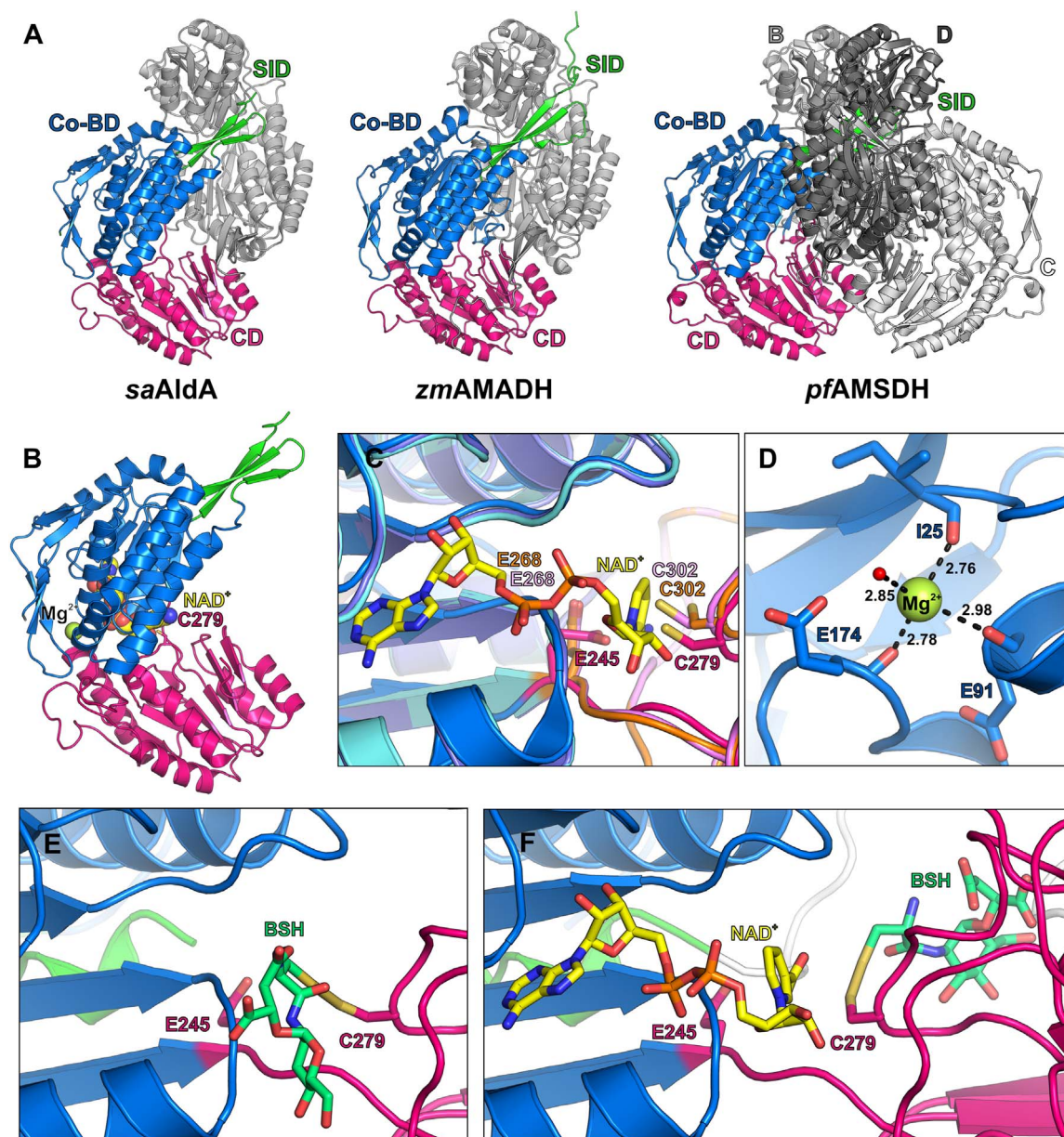


Fig. 7. Structural insights into the *S*-bacillithiolated *saAldA* active site. (A) Structural overviews of dimeric *saAldA* (PDB ID: 3TY7), dimeric *zmAMADH* (PDB ID: 4I8P) and tetrameric *pfAMSDH* (PDB ID: 4I26). Dimers formed by chains A (colored by domain; coenzyme-binding domain [Co-BD] – blue; subunit interaction domain [SID] – green; catalytic domain [CD] – magenta) and B (grey) are oriented in the same way. The other dimer of the *pfAMSDH* tetramer (chains C and D) is shown in different shades of grey. (B) Model for NAD⁺ binding by *saAldA* obtained by superimposing a subunit of NAD⁺-bound *pfAMSDH* (PDB ID: 4I1W) on apo-*saAldA*. The modelled NAD⁺ (colored by atom type; carbon – yellow; oxygen – red; nitrogen – blue; phosphorus – orange) and a bound Mg²⁺ ion (lime green) are shown as spheres, the active site cysteine (C279) is shown as sticks (carbon – magenta; sulfur – yellow). (C) Active sites and NAD⁺-binding cavities of ADHs. A subunit of *saAldA* (colored as in A) was structurally aligned with subunits of apo-*pfAMSDH* (Co-BD – violet; CD – light pink) and of NAD⁺-bound *pfAMSDH* (Co-BD – cyan; CD – orange). NAD⁺ is shown as sticks (colored by atom type as in B). The catalytic cysteine residue is in the resting state in the apo-structures and in the attacking state in NAD⁺-bound *pfAMSDH*. (D) Interactions at the cation-binding site of *saAldA*. Red sphere – water oxygen. (E, F) The *S*-bacillithiolated active site pocket of the apo-*saAldA* (E) and holo-*saAldA* (F). A subunit of *saAldA* colored as in A, view as in C, NAD⁺ and BSH are shown as sticks, NAD⁺ is colored as in B, BSH colored by atom type (carbon – aquamarine; oxygen – red; nitrogen – blue; sulfur – yellow). The loop composed of residues 438–459 that is not present in *saAldA* structure (PDB ID: 3TY7) was modelled and is shown in white.

adopt two alternative conformations, a “resting” and “attacking” (Fig. 7C), depending on the enzyme activation state. In the apo-enzyme structure, the Cys residue is in the resting conformation, whereas upon NAD⁺ binding the Cys thiol moiety rotates away from the nicotinamide part of NAD⁺ and is closer to the substrate-binding pocket [54–56]. The Cys residue serves as a nucleophile during catalysis, leading to a covalent thioester-enzyme adduct with the substrate *via* a nucleophilic addition [54,55,57]. The conserved glutamate residue then serves as a base to activate a water molecule for hydrolysis of the thioester-enzyme intermediate [55,59]. In addition to the Cys and glutamate residues,

there are two other conserved residues, a lysine (K156 in *saAldA*) and a glutamate (E455 in *saAldA*), that are involved in a proton relay that allows the deprotonation of E245, and, as a consequence, proton abstraction from the hydrolytic water [56].

Another common feature of the ADHs is the presence of a cation-binding site located in the Co-BD (Fig. 7B, D). Co-BD is formed by the three main chain carbonyl groups of an isoleucine/valine (I25 in *saAldA*), a glutamate/aspartate (E91 in *saAldA*) and a glutamate residue (E173 in *saAldA*) [60–62]. The cation bound at this site is usually sodium or potassium, and it was reported that the enzyme activity is

slightly higher in the presence of sodium [60]. In the *saAldA* structure, a magnesium ion is present at this site, most likely because magnesium was the only cation present in the crystallization solution. The role of the cation-binding site is to maintain the structural integrity of the protein and to stabilize a loop involved in binding of NAD^+ [60–62].

The available *saAldA* structure represents the apo-enzyme. In contrast, the structures of plant ADHs and of *paBADH* contain the coenzyme NAD^+ . In the case of *pfAMSDH*, the structures of *pfAMSDH*/ NAD^+ /intermediate complexes are also available [55]. Comparison of the apo, NAD^+ , NAD^+ /intermediate states shows that binding of the coenzyme or the formation of the intermediate does not influence the secondary structure elements within the enzyme, while rearrangements are observed in the side chains of residues involved in catalysis [54,55]. In the ADHs, the NAD^+ is bound in the hydrophobic pocket of the CoBD. Only the nicotinamide nucleotide moiety is turned towards a negatively charged pocket, in which the catalytic cysteine residue is located (Fig. 7B). NAD^+ is engaged in only few polar contacts with the enzyme [54,62].

Although the overall structure, the active site and the cation-binding site are highly conserved among the ADHs, these enzymes show broad substrate specificities and the amino acid residues involved in substrate binding are different among the ADHs. Nevertheless, even a single ADH is able to use many different aldehydes as substrates. For example, *slAMADH* can oxidize many different aminoaldehydes [62]. Thus, differences in the substrate-binding residues determine differences in the still comparatively broad substrate spectra of the enzymes.

3.7. S-bacillithiolation of the AldA active site depends on the Cys activation state as revealed by molecular dynamics simulation

Next, we analyzed the structural changes of AldA upon S-bacillithiolation and used molecular docking and molecular dynamics simulations to model BSH into the active site of the apo- and holoenzyme structures (Fig. 7EF). The structure of *saAldA* apo-enzyme (PDB 3TY7) was superimposed with the NAD^+ binding structure from *Pseudomonas fluorescens pfAMSDH* (PDB 4I1W) to model the NAD^+ cofactor into the AldA active site pocket (Fig. 7C). We further noticed that in the *saAldA* dimeric structure, the loop composed of residues 438–459 is not present which was modelled into the *saAldA* holo-enzyme structure based on the structure of *pfAMSDH* (Fig. 7F). This loop in the *saAldA* holo-enzyme structure may interfere with the location of BSH at the active site. To model the S-bacillithiolated active site Cys279 in the *saAldA* apo- and holoenzyme structures, we applied an adapted molecular docking algorithm based on Steric Clashes-Alleviated Receptor (SCAR) approaches [63], which takes into account the possibility of bond formation between ligand and receptor. Molecular docking and atomistic molecular dynamics simulation of the covalent BSH enzyme complex resulted in two best-scoring poses for BSH in the apo-enzyme (Q2) or holo-enzyme complex (Q1) (Fig. 7EF). However, no overlap between BSH and the loop (aa438–459) in the holo-enzyme structure was found and there was still room for an aldehyde substrate. Interestingly, these two different BSH positions in the AldA active site depend on the Cys279 activation state in the presence or absence of the NAD^+ cofactor (Fig. 7EF). In the apo-enzyme structure, Cys279 bound to BSH is still in "resting" position (Q2), while Cys279 is in the "attacking" position in the holo-enzyme (Q1). Thus, the location of BSH in the active site pocket depends on the Cys279 activation state in the presence or absence of NAD^+ . The Q2 pose of BSH at the apo-enzyme without NAD^+ seems to be energetically more favorable since Q2 had much better energy score (-50.2 kJ/mol), while the Q1 position of the holo-enzyme had a lower energy score (-38.1 kJ/mol). This results were quantitatively supported by our all-atom MD simulation of the complexes and the follow-up MM-PBSA calculations: the interaction energy in the apo-enzyme complex with BSH in Q2 position was -24.8 +/- 15.4 kJ/mol, while the holo-enzyme complex with BSH in Q1 position had interaction energy of -19.7 +/- 10.0 kJ/mol.

We have further plotted the dihedral distribution of N-CA-CB-SG dihedral (rotation around the CA-CB bond) of Cys279 and the dihedral angle at the function of simulation time (Fig. S6). The results showed that Cys279 in the apo-enzyme has very different dihedral propensity than in the holo-enzyme in complex with NAD^+ . These data support that the apo-enzyme prefers the resting state position of Cys279 with BSH while the holo-enzyme favors the BSH complex with the thiol in the attacking state position.

In agreement with our previous GapDH results [26], S-bacillithiolation of the AldA apo- and holoenzyme active site does not require major structural changes. After 50 ns of MD simulations there was very little change in the backbone flexibility of the protein between different binding positions of BSH in the apo-enzyme (Q2) or the holo-enzyme (Q1) compared to the apo-enzyme without BSH (Fig. S7). This further confirms that BSH can undergo disulfide formation with the active site Cys279 at different positions without major conformational changes.

4. Discussion

S. aureus is a major human pathogen of hospital and community-acquired infections, ranging from local skin infections to life-threatening systemic and chronic infections. During infections, *S. aureus* is exposed to ROS, RCS and RES that are produced as first line of defense by activated macrophages and neutrophils or can be also encountered as consequence of antibiotics treatment [10,11,64]. Thus, the understanding of the adaptation mechanisms of *S. aureus* to infection conditions to avoid killing by ROS, RCS and RES is important for the discovery of new drug targets to combat multi-resistant *S. aureus* infections.

In our previous work, we have identified the aldehyde dehydrogenase AldA as one of the most strongly oxidized proteins in the thiol-redox proteome in *S. aureus*, which showed a 29% oxidation increase under NaOCl stress using the OxICAT analysis [26]. AldA uses a conserved active site Cys279 that was modified by S-bacillithiolation under NaOCl stress. Apart from AldA, the glyceraldehyde-3-phosphate dehydrogenase Gap was identified as S-bacillithiolated at its active site Cys151 under NaOCl stress. Thus, it is interesting to note that two functionally related aldehyde dehydrogenases are targets for oxidation at their active site Cys residues that both function in aldehyde oxidation. In this study, we demonstrated that AldA is specifically induced under thiol-specific stress conditions, such as NaOCl, diamide and formaldehyde stress. Expression of *aldA* was previously shown to be regulated by the alternative sigma factor SigmaB in response to heat shock, salt stress caused by NaCl and Mn_2Cl as well as alkaline shock [50,51]. Here, we have shown that the thiol-specific expression of *aldA* occurs SigmaB-independently. Thus, *aldA* seems to be double-controlled by SigmaB and another thiol-stress sensing regulator to allow adaptation to general stress and starvation as well as thiol-stress conditions.

SigmaB has been previously shown to play an important role under infection conditions and controls biofilm formation and several virulence factors, such as adhesins [65,66]. The SigmaB regulon was induced after internalization of *S. aureus* by bronchial epithelial cells and required for intracellular growth as demonstrated by transcriptomics and proteomics [53,67,68]. Moreover, SigmaB has been implicated as central regulator in long-term persistence in human osteoblasts and controls the small colony variant (SCV) phenotype of persistent *S. aureus* infections [69,70]. Thus, it might be possible that adaptation of *S. aureus* from acute to chronic and persistent infections requires SigmaB and AldA to cope and adapt to the stationary phase and thiol-specific stress conditions inside macrophages and neutrophils. This adaptation to thiol-stress conditions is particularly important for *S. aureus* to survive under conditions of long-term persistent and chronic infections.

In this work, we have shown that AldA is an important member of the SigmaB regulon that provides protection under NaOCl stress

conditions as shown in survival assays. However, the thiol-specific induction of *aldA* transcription seems to be SigA-dependently since the same induction level was observed in the *sigB* mutant under thiol-stress. A putative SigA-promoter was observed upstream of the SigB-promoter indicating that *aldA* transcription might be controlled by SigB and SigA containing RNA polymerase (RNAP) from adjacent promoters. The stronger *aldA* induction in the *sigB* mutant under methylglyoxal stress could be explained by a higher affinity of SigA for the RNAP core enzyme compared to SigB and the lack of sigma factor competition in the *sigB* mutant [71]. Moreover, the thiol-stress-specific induction of *aldA* transcription might require additional transcriptional regulators that remain to be elucidated. In future studies, we also aim to investigate if AldA plays a role for the intracellular growth as well as persistence or chronic infections in *S. aureus*, which could require detoxification of toxic aldehydes to allow long-term survival.

To study the function of AldA and its redox-regulation under NaOCl stress *in vitro*, we purified the enzyme and determined its catalytic activities towards oxidation of various aldehydes. We could show that AldA has broad substrate specificities to oxidize formaldehyde, methylglyoxal, glycol aldehyde and acetaldehyde to their respective acids. The question arises about the physiological aldehyde substrate for AldA under *in vivo* conditions that are produced under infection conditions, such as under hypochlorite stress. Methylglyoxal was previously shown to be produced at higher levels under HOCl stress in *E. coli* [20]. Moreover, the *gloA-nemRA* operon was induced under methylglyoxal and HOCl stress, which functions as important HOCl and methylglyoxal defense mechanism [19–22]. The FMN-dependent oxidoreductase Nema functions in detoxification of various electrophiles, such as aldehydes, N-ethylmaleimide and quinones and its up-regulation under HOCl stress indicates the link between HOCl and aldehyde stress. In our work, we could also show that AldA responds to aldehydes, diamide and NaOCl and hence could be involved in methylglyoxal detoxification in *S. aureus* as well. However, in growth and survival assays, no phenotypes of the *aldA* mutant were detected under formaldehyde and methylglyoxal stress. Since AldA showed broad substrate specificity towards various aldehydes *in vitro*, its natural substrates could be different aldehydes that remain to be elucidated.

Of note, AldA shares strong 57% sequence similarity to betaine aldehyde dehydrogenases from *S. aureus*, *Pseudomonas aeruginosa* and *Spinacia oleracea*. These enzymes function in oxidation of the toxic betaine aldehyde to glycine betaine which is a well-known compatible solute and accumulates in bacteria under osmotic stress conditions as osmoprotectant [72,73]. Glycine betaine can be either taken up upon osmotic stress or synthesized from exogenously provided choline in a two oxidation steps *via* choline dehydrogenase (BetA) and betaine dehydrogenase (BetB) which are conserved in *B. subtilis* [72,73] and *S. aureus* [54]. The human tissues are rich sources of choline and betaine and thus, *S. aureus* encounters toxic aldehydes produced from choline during colonization and internalization. For some bacteria, the importance of the choline oxidation pathway for survival and virulence has been already demonstrated [73,74]. Of note, AldA is also induced under high osmolarity conditions provoked by NaCl stress in a SigmaB-dependent manner [50]. This could point to a possible function in the osmotic stress and thiol-stress response in *S. aureus* which remains to be elucidated. However, we could not detect AldA activity for oxidation of betaine aldehyde as substrate *in vitro*, indicating a different function of AldA in *S. aureus* (data not shown).

The catalytic activity of AldA depends on a highly conserved Cys279 active site which we identified as S-bacillithiolated under NaOCl stress in *S. aureus* [26]. Interestingly, this nucleophilic active site Cys residue was previously found oxidized to a mixed disulfide with beta-mercaptoethanol during protein crystallization of related betaine aldehyde dehydrogenases [54,74]. These results confirm the redox-sensitivity of the active site Cys of AldA as shown in this work. Our results have further demonstrated that S-bacillithiolation functions in redox-regulation and inactivation of AldA activity under H₂O₂ stress. In the

absence of BSH, the active site Cys279 was very sensitive to over-oxidation as shown by its irreversible inactivation. In the presence of BSH, Cys279 was protected against overoxidation by the S-bacillithiolation as shown for the glyceraldehyde-3-phosphate dehydrogenase GapDH in *S. aureus* [26]. Both enzymes use a similar catalytic mechanism for the NAD⁺-dependent oxidation of the aldehyde substrate to generate the acid product [54,55,57]. In the catalytic mechanism of aldehyde dehydrogenase, the active site Cys was shown to adopt two conformations: the “attacking” or “resting” conformation depending on the presence or absence of the NAD⁺ cofactor. We used molecular docking and molecular dynamic simulations to model the S-bacillithiolated active site in the presence and absence of NAD⁺. In the apo-enzyme structure, BSH was bound to Cys279 in the resting state (Q2) position and occupied the cofactor-binding pocket. In the presence of NAD⁺, Cys279 was modified in the attacking state position (Q1) and BSH was repositioned close to the substrate-binding site.

In our previous docking approach with BSH at the Cys151 active site of GapDH, we found similar locations of BSH in the apo-enzyme and holo-enzyme structures related to the resting and attacking state. Thus, the highly flexible active site and the redox-sensitivity of the nucleophilic Cys residues facilitate their fast oxidation to the mixed disulfides with BSH. In both structural models, S-bacillithiolation of GapDH and AldA did not require major structural changes, which further explains their preferred formation of the BSH mixed disulfides. This flexible BSH position may ensure that catalytic active and resting AldA and GapDH enzymes can both be protected against overoxidation under NaOCl stress to ensure fast regeneration and reactivation of the enzymes.

Acknowledgements

This work was supported by an ERC Consolidator Grant (GA 615585) MYCOTHILOME and grants from the Deutsche Forschungsgemeinschaft (AN746/4-1 and AN746/4-2) within the SPP1710 on “Thiol-based Redox switches”, by the Research Training Group GRK1947 (Project C01) and by the SFB973 Project C08 to H.A. Protein crystal structure analysis was supported by an Alexander von Humboldt Post-doc Fellowship to A.P.-B.

Author disclosure statement

No competing financial interests exist.

Appendix A. Supplementary material

Supplementary data associated with this article can be found in the online version at <http://dx.doi.org/10.1016/j.redox.2018.02.001>.

References

- [1] F.D. Lowy, *Staphylococcus aureus* infections, *New Engl. J. Med.* 339 (1998) 520–532.
- [2] H.W. Boucher, G.R. Corey, Epidemiology of methicillin-resistant *Staphylococcus aureus*, *Clin. Infect. Dis.: Off. Publ. Infect. Dis. Soc. Am.* 46 (Suppl. 5) (2008) S344–S349.
- [3] G.L. Archer, *Staphylococcus aureus*: a well-armed pathogen, *Clin. Infect. Dis.: Off. Publ. Infect. Dis. Soc. Am.* 26 (1998) 1179–1181.
- [4] D.M. Livermore, Antibiotic resistance in staphylococci, *Intern. J. Antimicrob. Agents* 16 (Suppl. 1) (2000) S3–S10.
- [5] J.N. Pendleton, S.P. Gorman, B.F. Gilmore, Clinical relevance of the ESKAPE pathogens, *Expert Rev. Anti-Infect. Ther.* 11 (2013) 297–308.
- [6] A.N. Spaan, J.A.G. van Strijp, V.J. Torres, Leukocidins: staphylococcal bi-component pore-forming toxins find their receptors, *Nat. Rev. Microbiol.* (2017).
- [7] M. Dal Peraro, F.G. van der Goot, Pore-forming toxins: ancient, but never really out of fashion, *Nat. Rev. Microbiol.* 14 (2016) 77–92.
- [8] C.C. Winterbourn, A.J. Kettle, Redox reactions and microbial killing in the neutrophil phagosome, *Antioxid. Redox Signal.* 18 (2013) 642–660.
- [9] C.C. Winterbourn, A.J. Kettle, M.B. Hampton, Reactive oxygen species and neutrophil function, *Annu. Rev. Biochem.* 85 (2016) 765–792.
- [10] W.N. Beavers, E.P. Skaar, Neutrophil-generated oxidative stress and protein damage in *Staphylococcus aureus*, *Pathog. Dis.* 74 (2016).
- [11] M. Hillion, H. Antelmann, Thiol-based redox switches in prokaryotes, *Biol. Chem.* 396 (2015) 415–444.

- [12] M.B. Hampton, A.J. Kettle, C.C. Winterbourn, Involvement of superoxide and myeloperoxidase in oxygen-dependent killing of *Staphylococcus aureus* by neutrophils, *Infect. Immun.* 64 (1996) 3512–3517.
- [13] S.J. Klebanoff, A.J. Kettle, H. Rosen, C.C. Winterbourn, W.M. Nauseef, Myeloperoxidase: a front-line defender against phagocytosed microorganisms, *J. Leukoc. Biol.* 93 (2013) 185–198.
- [14] I.R. Booth, G.P. Ferguson, S. Miller, C. Li, B. Gunasekera, S. Kinghorn, Bacterial production of methylglyoxal: a survival strategy or death by misadventure? *Biochem. Soc. Trans.* 31 (2003) 1406–1408.
- [15] G.P. Ferguson, S. Totemeyer, M.J. MacLean, I.R. Booth, Methylglyoxal production in bacteria: suicide or survival? *Arch. Microbiol.* 170 (1998) 209–218.
- [16] E.E. Farmer, C. Davoine, Reactive electrophile species, *Curr. Opin. Plant Biol.* 10 (2007) 380–386.
- [17] L.J. Marnett, J.N. Riggins, J.D. West, Endogenous generation of reactive oxidants and electrophiles and their reactions with DNA and protein, *J. Clin. Invest.* 111 (2003) 583–593.
- [18] G.P. Ferguson, I.R. Booth, Importance of glutathione for growth and survival of *Escherichia coli* cells: detoxification of methylglyoxal and maintenance of intracellular K⁺, *J. Bact.* 180 (1998) 4314–4318.
- [19] M.J. Gray, Y. Li, L.I. Leichert, Z. Xu, U. Jakob, Does the transcription factor NemR use a regulatory sulfenamide bond to sense bleach? *Antioxid. Redox Signal.* 23 (2015) 747–754.
- [20] M.J. Gray, W.Y. Wholey, B.W. Parker, M. Kim, U. Jakob, NemR is a bleach-sensing transcription factor, *J. Biol. Chem.* 288 (2013) 13789–13798.
- [21] C. Lee, J. Shin, C. Park, Novel regulatory system *nemRA-gloA* for electrophile reduction in *Escherichia coli* K-12, *Mol. Microbiol.* 88 (2013) 395–412.
- [22] E. Ozyamak, C. de Almeida, A.P. de Moura, S. Miller, I.R. Booth, Integrated stress response of *Escherichia coli* to methylglyoxal: transcriptional readthrough from the *nemRA* operon enhances protection through increased expression of glyoxalase I, *Mol. Microbiol.* 88 (2013) 936–950.
- [23] P. Chandrangsu, V.V. Loi, H. Antelmann, J.D. Helmann, The role of bacillithiol in gram-positive *Firmicutes*, *Antioxid. Redox Signal.* (2017).
- [24] G.L. Newton, M. Rawat, J.J. La Clair, V.K. Jothivasan, T. Budiarto, C.J. Hamilton, A. Claiborne, J.D. Helmann, R.C. Fahey, Bacillithiol is an antioxidant thiol produced in Bacilli, *Nat. Chem. Biol.* 5 (2009) 625–627.
- [25] P. Chandrangsu, R. Dusi, C.J. Hamilton, J.D. Helmann, Methylglyoxal resistance in *Bacillus subtilis*: contributions of bacillithiol-dependent and independent pathways, *Mol. Microbiol.* 91 (2014) 706–715.
- [26] M. Imber, N.T.T. Huyen, A.J. Pietrzyk-Brzezinska, V.V. Loi, M. Hillion, J. Bernhardt, T. Thärichen, K. Kosek, M. Saleh, C.J. Hamilton, L. Adrian, F. Gräter, M.C. Wahl, H. Antelmann, Protein S-Bacillithiolation functions in thiol protection and redox regulation of the glyceraldehyde-3-phosphate dehydrogenase gap in *Staphylococcus aureus* under hypochlorite stress, *Antioxid. Redox Signal.* (2017).
- [27] M. Wetstein, U. Völker, J. Dedio, S. Lobau, U. Zuber, M. Schiesswohl, C. Herget, M. Hecker, W. Schumann, Cloning, sequencing, and molecular analysis of the *dnkA* locus from *Bacillus subtilis*, *J. Bact.* 174 (1992) 3300–3310.
- [28] M. Arnaud, A. Chastanet, M. Debarbouille, New vector for efficient allelic replacement in naturally nontransformable, low-GC-content, gram-positive bacteria, *Appl. Environ. Microbiol.* 70 (2004) 6887–6891.
- [29] E.D. Rosenblum, S. Tyrone, Serology, density, and morphology of Staphylococcal phages, *J. Bact.* 88 (1964) 1737–1742.
- [30] M. Müller, S. Reiss, R. Schlüter, U. Mäder, A. Beyer, W. Reiss, J. Marles-Wright, R.J. Lewis, H. Pfortner, U. Völker, K. Riedel, M. Hecker, S. Engelmann, J. Pane-Farre, Deletion of membrane-associated Asp23 leads to upregulation of cell wall stress genes in *Staphylococcus aureus*, *Mol. Microbiol.* 93 (2014) 1259–1268.
- [31] V.V. Loi, M. Harms, M. Müller, N.T.T. Huyen, C.J. Hamilton, F. Hochgräfe, J. Pane-Farre, H. Antelmann, Real-time imaging of the bacillithiol redox potential in the human pathogen *Staphylococcus aureus* using a genetically encoded bacilliredoxin-fused redox biosensor, *Antioxid. Redox Signal.* 26 (2017) 835–848.
- [32] B.K. Chi, A.A. Roberts, T.T. Huyen, K. Baisel, D. Becher, D. Albrecht, C.J. Hamilton, H. Antelmann, S-bacillithiolation protects conserved and essential proteins against hypochlorite stress in firmicutes bacteria, *Antioxid. Redox Signal.* 18 (2013) 1273–1295.
- [33] B. Webb, A. Sali, Protein structure modeling with MODELLER, *Methods Mol. Biol.* 1654 (2017) 39–54.
- [34] D. Kozakov, L.E. Grove, D.R. Hall, T. Bohnuud, S.E. Mottarella, L. Luo, B. Xia, D. Beglov, S. Vajda, The FTMap family of web servers for determining and characterizing ligand-binding hot spots of proteins, *Nat. Prot.* 10 (2015) 733–755.
- [35] G.S. Couch, D.K. Hendrix, T.E. Ferrin, Nucleic acid visualization with UCSF Chimera, *Nucleic Acids Res.* 34 (2006) e29.
- [36] W.J. Allen, T.E. Balias, S. Mukherjee, S.R. Brozell, D.T. Moustakas, P.T. Lang, D.A. Case, I.D. Kuntz, R.C. Rizzo, DOCK 6: impact of new features and current docking performance, *J. Comput. Chem.* 36 (2015) 1132–1156.
- [37] N. Schneider, G. Lange, S. Hindle, R. Klein, M. Rarey, A consistent description of Hydrogen bond and Dehydration energies in protein-ligand complexes: methods behind the HYDE scoring function, *J. Comput. Mol. Des.* 27 (2013) 15–29.
- [38] D. Van Der Spoel, E. Lindahl, B. Hess, G. Groenhof, A.E. Mark, H.J. Berendsen, GROMACS: fast, flexible, and free, *J. Comput. Chem.* 26 (2005) 1701–1718.
- [39] K. Lindorff-Larsen, S. Piana, K. Palmo, P. Maragakis, J.L. Klepeis, R.O. Dror, D.E. Shaw, Improved side-chain torsion potentials for the Amber ff99SB protein force field, *Proteins* 78 (2010) 1950–1958.
- [40] A.W. Sousa da Silva, W.F. Vranken, ACPYPE – AnteChamber PYthon Parser interface, *BMC Res. Notes* 5 (2012) 367.
- [41] F.Y. Dupradeau, A. Pigache, T. Zaffran, C. Savinaud, R. Lelong, N. Grivel, D. Lelong, W. Rosanski, P. Cieplak, The R.E.D. tools: advances in RESP and ESP charge derivation and force field library building, *Phys. Chem. Chem. Phys.* 12 (2010) 7821–7839.
- [42] M.J. Frisch, G. T. H.B. Schlegel, G.E. Scuseria, M.A. Robb, J.R. Cheeseman, et al., Gaussian 09, Revision A.02, 34 Gaussian Inc., Wallingford, CT, 2009.
- [43] M. Parrinello, A. Rahman, Polymorphic transitions in single crystals: a new molecular dynamics method, *J. Appl. Phys.* 52 (1981) 7182–7190.
- [44] T. Darden, D. York, L., J. Pedersen, Particle mesh Ewald: an N-log(N) method for Ewald sums in large systems, *J. Chem. Phys.* 98 (1993) 10089–10092.
- [45] B. Hess, H. Bekker, H.J.C. Berendsen, J.G.E.M. Fraaije, LINCS: a linear constraint solver for molecular simulations, *J. Comput. Chem.* 18 (1997) 1463–1472.
- [46] C.C. Huang, E.C. Meng, J.H. Morris, E.F. Pettersen, T.E. Ferrin, Enhancing UCSF Chimera through web services, *Nucleic Acids Res.* 42 (2014) W478–484.
- [47] E.F. Pettersen, T.D. Goddard, C.C. Huang, G.S. Couch, D.M. Greenblatt, E.C. Meng, T.E. Ferrin, UCSF Chimera—a visualization system for exploratory research and analysis, *J. Comput. Chem.* 25 (2004) 1605–1612.
- [48] B.R. Miller 3rd, T.D. McGee Jr., J.M. Swails, N. Homeyer, H. Gohlke, A.E. Roitberg, MMPBSA.py: an efficient program for end-state free energy calculations, *J. Chem. Theory Comput.* 8 (2012) 3314–3321.
- [49] L.I. Leichert, F. Gehrke, H.V. Gudiseva, T. Blackwell, M. Ilbert, A.K. Walker, J.R. Strahler, P.C. Andrews, U. Jakob, Quantifying changes in the thiol redox pro- teom on oxidative stress in vivo, *Proc. Natl. Acad. Sci. USA* 105 (2008) 8197–8202.
- [50] J. Pane-Farre, B. Jonas, K. Förstner, S. Engelmann, M. Hecker, The sigmaB regulon in *Staphylococcus aureus* and its regulation, *Int. J. Med. Microbiol.* 296 (2006) 237–258.
- [51] M. Bischoff, P. Dunman, J. Kormanec, D. Macapagal, E. Murphy, W. Mounts, B. Berger-Bachi, S. Projan, Microarray-based analysis of the *Staphylococcus aureus* sigmaB regulon, *J. Bact.* 186 (2004) 4085–4099.
- [52] S. Fuchs, H. Mehlan, J. Bernhardt, A. Hennig, S. Michalik, K. Surmann, J. Pane-Farre, A. Giese, S. Weiss, L. Backert, A. Herbig, K. Niesel, M. Hecker, U. Völker, U. Mäder, AureoWiki the repository of the *Staphylococcus aureus* research and annotation community, *Int. J. Med. Microbiol.* (2017).
- [53] U. Mäder, P. Nicolas, M. Depke, J. Pane-Farre, M. Debarbouille, M.M. van der Kooi- Pol, C. Guerin, S. Derozier, A. Hiron, H. Jarmer, A. Leduc, S. Michalik, E. Reilman, M. Schaffer, F. Schmidt, P. Bessieres, P. Noirot, M. Hecker, T. Msadek, U. Völker, J.M. van Dijl, *Staphylococcus aureus* transcriptome architecture: from laboratory to infection-mimicking conditions, *PLoS Genet.* 12 (2016) e1005962.
- [54] A.S. Halavaty, R.L. Rich, C. Chen, J.C. Joo, G. Minasov, I. Dubrovskaya, J.R. Winsor, D.G. Myszkka, M. Duban, L. Shuvalova, A.F. Yakunin, W.F. Anderson, Structural and functional analysis of betaine aldehyde dehydrogenase from *Staphylococcus aureus*, *Act. Cryst. Sect. D. Biol. Cryst.* 71 (2015) 1159–1175.
- [55] L. Huo, I. Davis, F. Liu, B. Andi, S. Esaki, H. Iwaki, Y. Hasegawa, A.M. Orville, A. Liu, Crystallographic and spectroscopic snapshots reveal a dehydrogenase in action, *Nat. Commun.* 6 (2015) 5935.
- [56] L. Gonzalez-Segura, E. Rudino-Pinera, R.A. Munoz-Clares, E. Horjales, The crystal structure of a ternary complex of betaine aldehyde dehydrogenase from *Pseudomonas aeruginosa* provides new insight into the reaction mechanism and shows a novel binding mode of the 2'-phosphate of NADP⁺ and a novel cation binding site, *J. Mol. Biol.* 385 (2009) 542–557.
- [57] D.P. Abriola, R. Fields, S. Stein, A.D. MacKerell Jr, R. Pietruszko, Active site of human liver aldehyde dehydrogenase, *Biochemistry* 26 (1987) 5679–5684.
- [58] L. Holm, P. Rosenstrom, Dali server: conservation mapping in 3D, *Nucleic Acids Res.* 38 (2010) W545–549.
- [59] K. D'Ambrosio, A. Pailot, F. Talfournier, C. Didierjean, E. Benedetti, A. Aubry, G. Branlant, C. Corbier, The first crystal structure of a thioacylenzyme intermediate in the ALDH family: new coenzyme conformation and relevance to catalysis, *Biochemistry* 45 (2006) 2978–2986.
- [60] A. Gruez, V. Roig-Zamboni, S. Grisel, A. Salomoni, C. Valencia, V. Campanacci, M. Tegoni, C. Cambillau, Crystal structure and kinetics identify *Escherichia coli* ydcW gene product as a medium-chain aldehyde dehydrogenase, *J. Mol. Biol.* 343 (2004) 29–41.
- [61] T.D. Hurley, S. Perez-Miller, H. Breen, Order and disorder in mitochondrial aldehyde dehydrogenase, *Chem.-Biol. Interact.* 130–132 (2001) 3–14.
- [62] D. Koceny, R. Koncickova, M. Tylichova, A. Vigouroux, H. Moskalikova, M. Soural, M. Sebela, S. Morera, Plant ALDH10 family: identifying critical residues for substrate specificity and trapping a thiohemiacetal intermediate, *J. Biol. Chem.* 288 (2013) 9491–9507.
- [63] Y. Ai, L. Yu, X. Tan, X. Chai, S. Liu, Discovery of covalent ligands via noncovalent docking by dissecting covalent docking based on a "Steric-Clashes Alleviating Receptor (SCAR)" strategy, *J. Chem. Inform. Model.* 56 (2016) 1563–1575.
- [64] A.L. Cheung, K.A. Nishina, M.P. Trottonda, S. Tamber, The SarA protein family of *Staphylococcus aureus*, *Int. J. Biochem. Cell Biol.* 40 (2008) 355–361.
- [65] G. Mitchell, E. Brouillette, D.L. Seguin, A.E. Asselin, C.L. Jacob, F. Malouin, A role for sigma factor B in the emergence of *Staphylococcus aureus* small-colony variants and elevated biofilm production resulting from an exposure to aminoglycosides, *Microb. Pathog.* 48 (2010) 18–27.
- [66] G. Mitchell, D.L. Seguin, A.E. Asselin, E. Deziel, A.M. Cantin, E.H. Frost, S. Michaud, F. Malouin, *Staphylococcus aureus* sigma B-dependent emergence of small-colony variants and biofilm production following exposure to *Pseudomonas aeruginosa* 4-hydroxy-2-heptylquinoline-N-oxide, *BMC Microbiol.* 10 (2010) 33.
- [67] H. Pfortner, J. Wagner, K. Surmann, P. Hildebrandt, S. Ernst, J. Bernhardt, C. Schurmann, M. Gutjahr, M. Depke, U. Jehmlich, V. Dhole, E. Hammer, L. Steil, U. Völker, F. Schmidt, A proteomics workflow for quantitative and time-resolved analysis of adaptation reactions of internalized bacteria, *Methods* 61 (2013) 244–250.
- [68] S. Michalik, M. Depke, A. Murr, M. Gesell Salazar, U. Kusebauch, Z. Sun, T.C. Meyer, K. Surmann, H. Pfortner, P. Hildebrandt, S. Weiss, L.M. Palma Medina,

- M. Gutjahr, E. Hammer, D. Becher, T. Pribyl, S. Hammerschmidt, E.W. Deutsch, S.L. Bader, M. Hecker, R.L. Moritz, U. Mäder, U. Völker, F. Schmidt, A global *Staphylococcus aureus* proteome resource applied to the *in vivo* characterization of host-pathogen interactions, *Sci. Rep.* 7 (2017) 9718.
- [69] L. Tuchscher, M. Bischoff, S.M. Lattar, M. Noto Llana, H. Pfortner, S. Niemann, J. Geraci, H. Van de Vyver, M.J. Fraunholz, A.L. Cheung, M. Herrmann, U. Völker, D.O. Sordelli, G. Peters, B. Löffler, Sigma factor SigB is crucial to mediate *Staphylococcus aureus* adaptation during chronic infections, *PLoS Pathog.* 11 (2015) e1004870.
- [70] L. Tuchscher, B. Löffler, *Staphylococcus aureus* dynamically adapts global regulators and virulence factor expression in the course from acute to chronic infection, *Curr. Genet.* 62 (2016) 15–17.
- [71] C. Rollenhagen, H. Antelmann, J. Kirstein, O. Delumeau, M. Hecker, M.D. Yudkin, Binding of sigma(A) and sigma(B) to core RNA polymerase after environmental stress in *Bacillus subtilis*, *J. Bact.* 185 (2003) 35–40.
- [72] J. Boch, B. Kempf, E. Bremer, Osmoregulation in *Bacillus subtilis*: synthesis of the osmoprotectant glycine betaine from exogenously provided choline, *J. Bact.* 176 (1994) 5364–5371.
- [73] J. Boch, G. Nau-Wagner, S. Kneip, E. Bremer, Glycine betaine aldehyde dehydrogenase from *Bacillus subtilis*: characterization of an enzyme required for the synthesis of the osmoprotectant glycine betaine, *Arch. Microbiol.* 168 (1997) 282–289.
- [74] J.J. Lee, J.H. Kim, D.G. Kim, D.H. Kim, H.L. Simborio, W.G. Min, M.H. Rhee, J.H. Lim, H.H. Chang, S. Kim, Characterization of betaine aldehyde dehydrogenase (BetB) as an essential virulence factor of *Brucella abortus*, *Vet. Microbiol.* 168 (2014) 131–140.

Chapter 5

The glyceraldehyde-3-phosphate dehydrogenase GapDH of *Corynebacterium diphtheriae* is redox-controlled by protein S-mycothiolation under oxidative stress

Melanie Hillion^{1*}, Marcel Imber^{1*}, Brandán Pedre^{2,3,4*}, Jörg Bernhardt^{5*}, Malek Saleh¹, **Vu Van Loi**¹, Sandra Maaß⁵, Dörte Becher⁵, Leonardo Astolfi Rosado^{2,3,4}, Lorenz Adrian⁶, Chris Weise⁷, Markus Wirtz⁸, Rüdiger Hell⁸, Joris Messens^{2,3,4} and Haike Antelmann^{1#}

¹*Institute for Biology-Microbiology, Freie Universität Berlin, D-14195 Berlin, Germany*

²*Center for Structural Biology, VIB, B-1050 Brussels, Belgium*

³*Brussels Center for Redox Biology, B-1050 Brussels, Belgium*

⁴*Structural Biology Brussels, Vrije Universiteit Brussel, B-1050 Brussels, Belgium*

⁵*Institute for Microbiology, Ernst-Moritz-Arndt-University of Greifswald, D-17487 Greifswald, Germany*

⁶*Department Isotope Biogeochemistry, Helmholtz Centre for Environmental Research-UFZ, Leipzig, Germany*

⁷*Institute for Chemistry and Biochemistry, Freie Universität Berlin, D-14195 Berlin, Germany*

⁸*Plant Molecular Biology, Centre for Organismal Studies Heidelberg, University of Heidelberg, Heidelberg, Germany*

Published in: Scientific Reports. 7: 5020. (2017)

<https://doi.org/10.1038/s41598-017-05206-2>

#Corresponding author: haike.antelmann@fu-berlin.de

Authors contributions

Melanie Hillion, Brandán Pedre, Malek Saleh, Marcel Imber, **Vu Van Loi**, Leonardo Astolfi Rosado, Joris Messens and Haike Antelmann conceived the ideas and hypotheses, designed and performed the GapDH experiments and analyzed the data. **Vu Van Loi** was involved in the mass spectrometry of S-mycothiolated GapDH. Haike Antelmann, Melanie Hillion, Brandán Pedre and Joris Messens wrote the manuscript and prepared the figures.

* Shared first authorships

SCIENTIFIC REPORTS



OPEN

The glyceraldehyde-3-phosphate dehydrogenase GapDH of *Corynebacterium diphtheriae* is redox-controlled by protein S-mycothiolation under oxidative stress

Melanie Hillion¹ , Marcel Imber¹, Brandán Pedre^{2,3,4}, Jörg Bernhardt⁵, Malek Saleh¹, Vu Van Loi¹, Sandra Maaß⁵, Dörte Becher⁵, Leonardo Astolfi Rosado^{2,3,4}, Lorenz Adrian⁶, Christoph Weise⁷, Rüdiger Hell⁸, Markus Wirtz⁸ , Joris Messens^{2,3,4} & Haike Antelmann¹

Mycothiols (MSH) is the major low molecular weight (LMW) thiol in Actinomycetes and functions in post-translational thiol-modification by protein S-mycothiolation as emerging thiol-protection and redox-regulatory mechanism. Here, we have used shotgun-proteomics to identify 26 S-mycothiolated proteins in the pathogen *Corynebacterium diphtheriae* DSM43989 under hypochlorite stress that are involved in energy metabolism, amino acid and nucleotide biosynthesis, antioxidant functions and translation. The glyceraldehyde-3-phosphate dehydrogenase (GapDH) represents the most abundant S-mycothiolated protein that was modified at its active site Cys153 *in vivo*. Exposure of purified GapDH to H₂O₂ and NaOCl resulted in irreversible inactivation due to overoxidation of the active site *in vitro*. Treatment of GapDH with H₂O₂ or NaOCl in the presence of MSH resulted in S-mycothiolation and reversible GapDH inactivation *in vitro* which was faster compared to the overoxidation pathway. Reactivation of S-mycothiolated GapDH could be catalyzed by both, the Trx and the Mrx1 pathways *in vitro*, but demycothiolsation by Mrx1 was faster compared to Trx. In summary, we show here that S-mycothiolation can function in redox-regulation and protection of the GapDH active site against overoxidation in *C. diphtheriae* which can be reversed by both, the Mrx1 and Trx pathways.

Bacteria are exposed to various redox-active compounds, such as reactive oxygen species (ROS) in their natural habitat or during infections and are equipped with specific protection mechanisms¹. To cope with ROS, bacteria use different antioxidant enzymes, such as catalases, peroxidases, superoxide dismutase and low molecular weight (LMW) thiols to maintain the reduced state of the cytoplasm and to survive oxidative stress²⁻⁴. Gram-negative bacteria utilize glutathione (GSH) as their major LMW thiol, but GSH is absent in most Gram-positive bacteria. Instead, the Actinomycetes that include streptomycetes, corynebacteria and mycobacteria produce mycothiol (MSH) as their major LMW thiol⁵. MSH functions in detoxification of various redox-active compounds, including ROS, electrophiles and antibiotics in all Actinomycetes⁶⁻⁸. Apart from its

¹Institute for Biology-Microbiology, Freie Universität Berlin, D-14195, Berlin, Germany. ²Center for Structural Biology, VIB, B-1050, Brussels, Belgium. ³Brussels Center for Redox Biology, B-1050, Brussels, Belgium. ⁴Structural Biology Brussels, Vrije Universiteit Brussel, B-1050, Brussels, Belgium. ⁵Institute for Microbiology, Ernst-Moritz-Arndt-University of Greifswald, D-17487, Greifswald, Germany. ⁶Department Isotope Biogeochemistry, Helmholtz Centre for Environmental Research-UFZ, Leipzig, Germany. ⁷Institute for Chemistry and Biochemistry, Freie Universität Berlin, D-14195, Berlin, Germany. ⁸Plant Molecular Biology, Centre for Organismal Studies Heidelberg, University of Heidelberg, Heidelberg, Germany. Melanie Hillion, Marcel Imber, Brandán Pedre and Jörg Bernhardt contributed equally to this work. Correspondence and requests for materials should be addressed to H.A. (email: haike.antelmann@fu-berlin.de)

detoxification functions, MSH is also involved in post-translational thiol-modification and forms mixed disulfides with protein thiols under hypochlorite stress^{9,10}. Protein S-mycothiolation is an emerging thiol-protection and redox-regulatory mechanism in Actinomycetes. In *Corynebacterium glutamicum*, we identified 25 S-mycothiolated proteins using shotgun LC-MS/MS analysis¹⁰. These include conserved targets for S-thiolation across different Gram-positive bacteria, such as the thiol-peroxidase Tpx, the inosine monophosphate (IMP) dehydrogenase GuaB and ribosomal proteins^{10,11}. In *Mycobacterium smegmatis*, protein S-mycothiolation was more abundant with 58 identified proteins, which correlates with the 20-fold higher MSH content in mycobacteria compared to corynebacteria⁹.

The redox-regulatory mechanisms of S-mycothiolated proteins have been studied thus far for several antioxidant enzymes, such as thiol peroxidases (Tpx, Mpx, AhpE) and methionine sulfoxide reductases (MsrA)^{10,12–15}. Moreover, Tpx has been shown to function as a peroxidase and as oligomeric chaperone in response to different levels of H₂O₂¹⁵. Regeneration of peroxidase and methionine sulfoxide reductase activities requires both the mycoredoxin (Mrx1) and thioredoxin pathways *in vitro*^{10,12,13,16,17}. Apart from its redox-regulatory role for antioxidant enzymes, MSH also functions in thiol-protection of the methionine synthase MetE by protein S-mycothiolation under acid stress conditions¹⁸.

In this work, we have used shotgun proteomics to identify 26 S-mycothiolated proteins in the pathogen *Corynebacterium diphtheriae*. As major redox-controlled metabolic enzyme, the glycolytic glyceraldehyde-3-phosphate dehydrogenase DIP1310 (GapDH) was S-mycothiolated under NaOCl stress at the active site Cys in *C. diphtheriae in vivo*. GapDH is a conserved target for redox-regulation and post-translational thiol-modifications including S-glutathionylations across all domains of life^{19,20}. In *Staphylococcus aureus*, the glycolytic GapDH was recently shown as major target for S-bacillithiolation which contributes with 4% to the total Cys proteome²¹. GapDH uses the active site Cys for the nucleophilic attack at the aldehyde group of glyceraldehyde-3-phosphate (G3P) to catalyze its phosphorylation to 1,3-bisphosphoglycerate, generating NADH in this process²⁰. The relatively high reactivity of the active site thiolate towards H₂O₂ depends on the stabilization of the transition state and a dedicated proton relay mechanism that promotes leaving group departure^{20,22}. S-glutathionylation of GapDH from the plant *Arabidopsis thaliana* resulted in enzyme inactivation which could be faster regenerated by glutaredoxins compared to thioredoxins²³. Here, we studied the redox-regulation of GapDH of *C. diphtheriae* in response to oxidative stress by protein S-mycothiolation *in vitro*. We show that S-mycothiolation functions in redox regulation and efficiently protects the active site against overoxidation by H₂O₂ and NaOCl which can be reversed by both, the Mrx1 and Trx pathways. Thus, striking similarities exist in the redox-control mechanisms of GapDH homologs from prokaryotic and eukaryotic organisms that involve protein S-thiolations using different thiol-redox systems for recycling, and as such for controlling central glycolytic activities.

Results

Identification of 26 S-mycothiolated proteins in *C. diphtheriae* under NaOCl stress using shotgun LC-MS/MS analysis. The role of protein S-mycothiolation in thiol-protection and redox regulation has been studied previously in *C. glutamicum*¹⁰ and *M. smegmatis*⁹. In this study, we were interested to identify the targets for protein S-mycothiolation in the pathogen *C. diphtheriae* under NaOCl stress. Cells of *C. diphtheriae* DSM43989 were grown in heart-infusion broth (HIB) and transferred at an OD₅₈₀ of 0.8 into a minimal medium (BMM) for NaOCl stress exposure to avoid the quenching of NaOCl by the rich HIB medium. Treatment of cells with 300 μM and 400 μM NaOCl resulted in a delay of growth with slow recovery after overnight growth (Fig. 1A). Using MSH-specific non-reducing Western blots, a strongly increased protein S-mycothiolation pattern could be detected after 30 min of 300–400 μM NaOCl stress (Fig. 1B). We further analysed the MSH level in *C. diphtheriae* under NaOCl stress using thiol-metabolomics. The MSH level was determined as 0.3 ± 0.03 μmol/g raw dry weight (rdw) under control conditions which decreased 4-fold after 30 min of NaOCl treatment (Fig. 1C). Thus, the depletion of MSH correlates with increased protein S-mycothiolation under NaOCl stress. This confirms our previous results in *M. smegmatis* where strong MSH depletion was also observed under NaOCl stress⁹.

Using LTQ-Orbitrap LC-MS/MS analysis, we identified 26 S-mycothiolated proteins in *C. diphtheriae* in NaOCl-treated cells based on the 484 Da mass increase of MSH at cysteine residues (Tables 1, S1 and S2). These S-mycothiolated proteins are displayed in a Voronoi treemap where the spectral protein abundance determines the cell size of each protein that is present in the proteome and the S-mycothiolated proteins are marked in red (Fig. 2). The 26 S-mycothiolated proteins of *C. diphtheriae* include only 5 conserved targets for S-thiolation, such as the peroxiredoxin AhpC, the ribosomal proteins RplC and RpsM, the glycolytic enzyme glyceraldehyde-3-phosphate dehydrogenase (GapDH) and the IMP dehydrogenase GuaB (Tables 1, S1 and S2). The ribose 5-phosphate isomerase DIP1796 was identified as S-mycothiolated in *C. diphtheriae* which functions in the pentose phosphate pathway and was previously found S-glutathionylated in the photosynthetic organism *Chlamydomonas reinhardtii*²⁴. In *Leishmania*, this enzyme is essential for replication of the intracellular form of the parasite, and in *Trypanosoma brucei* the knockout mutant has a reduced infectivity in mice²⁵. Other S-mycothiolated proteins are involved in energy metabolism (Ndh, GlpD, DIP1726), amino acid biosynthesis pathways (ThrA, LeuB, DapA, GlnA), purine biosynthesis (PurA), iron sulfur cluster biosynthesis (DIP1631) and cell wall biosynthesis (GlmS). The NADH dehydrogenase (Ndh) is an abundant enzyme that plays a role in the respiratory chain. S-mycothiolation of Ndh was found at the non-conserved Cys159. Some S-mycothiolated proteins are Cys-rich proteins including the glutamine synthetase GlnA1, the 4- α -glucanotransferase MalQ (DIP1726), and PurA, which possess 4 to 8 Cys residues. GlnA1 catalyzes the condensation of glutamate and ammonia to form glutamine and plays a major role in the survival of *Mycobacterium tuberculosis* under infection inside macrophages²⁶. In conclusion, the identified S-mycothiolated proteins are mainly involved in cellular metabolism, and share as main and conserved targets for S-thiolations: GapDH, GuaB, AhpC and the ribosomal proteins RplC and RpsM.

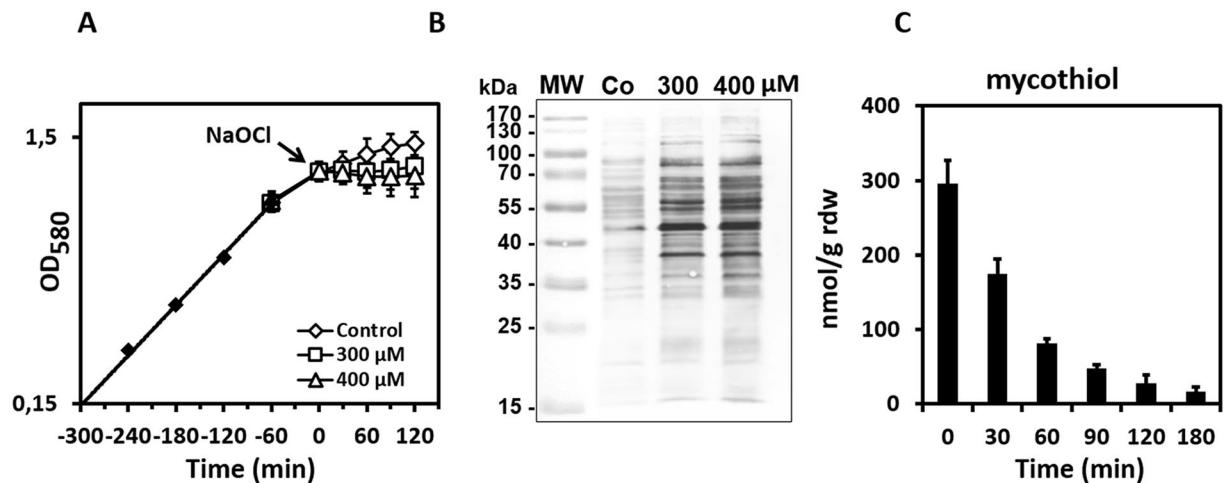


Figure 1. Protein S-mycothiolation pattern and MSH depletion in *C. diphtheriae* under NaOCl stress. *C. diphtheriae* was grown in HIB medium to an OD_{580} of 0.75–0.8, transferred to BMM and treated with 300 and 400 μM NaOCl which resulted in growth delay (A) and strongly increased protein S-mycothiolation as revealed by non-reducing MSH-specific Western blots (B). The level of reduced MSH was 0.3 $\mu\text{mol/g}$ rdw in the control and strongly depleted under NaOCl stress in the thiol-metabolome indicating that MSH is used for protein S-mycothiolation (C). All data represent mean values of three independent biological replicates and the error bars given were calculated as standard error of the mean (SEM).

Contribution of S-mycothiolated proteins to the total Cys proteome. It was interesting to note that GapDH was S-mycothiolated at the active site Cys153 in *C. diphtheriae*. Previously, we found that GapDH is the major target for S-bacillithiolation in *S. aureus* contributing with 4% Cys abundance to the total Cys proteome²¹. Thus, we calculated the percentages of Cys contributions of GapDH and other S-mycothiolated proteins to the total Cys proteome in *C. diphtheriae* (Figs 3 and S1, Table S4). In total, 2266 proteins are encoded in the genome of *C. diphtheriae* DSM43989 that include 1847 Cys proteins with 6156 Cys residues. The theoretical Cys content in the proteome of *C. diphtheriae* is 0.85% confirming that Cys is the rarest amino acid in the *C. diphtheriae* proteome (Figure S1). Next, we calculated the percentages of Cys abundances of all Cys proteins expressed in the proteome based on their spectral counts that are multiplied by the numbers of Cys residues. The spectral counts of the 1030 expressed proteins are visualized in a Cys proteome treemap including 805 Cys proteins (Fig. 3, Tables S3 and S4). The cell size indicates the spectral protein abundance and the color-code denotes the Cys content. About 395 Cys proteins contain only 1–2 Cys residues while the remaining 410 proteins have 3 or more Cys residues. These include 11 proteins with more than 10 Cys residues and the FeS-cluster oxidoreductase DIP2133 was identified as the most Cys-rich protein with 18 Cys residues. Of note, 83 Cys proteins were found to contribute to 60% of the total Cys abundances in the proteome including 55 Cys-rich proteins with more than 3 Cys residues (Figure S1). The RNA polymerase subunit beta' (RpoC) and two translation elongation factors (Tuf and FusA) account for 2.5–4.5% of the total Cys abundance in the proteome. Furthermore, the Cys abundance treemap also visualizes that many ribosomal proteins and abundant chaperones and proteases (GroES, GroL1, GroL2, DnaK and ClpB) are devoid of Cys residues (Fig. 3).

Of the 26 S-mycothiolated proteins, 24 proteins were quantified based on their total spectral counts (Tables S3 and S4). Eleven S-mycothiolated proteins were found to contribute with 0.2–0.75% to the total Cys abundance, including the glycolytic GapDH on the top with 0.75%. Thus, in *C. diphtheriae*, GapDH is also the most abundant target for S-mycothiolation in comparison to all other identified S-mycothiolated proteins. Apart from GapDH, the AhpC homolog DirA, the IMP dehydrogenase GuaB, the glucanotransferase MalQ (DIP1726) and the glutamine synthetase GlnA1 contributed with 0.4–0.6% to the total Cys abundance in the proteome (Fig. 3; Table S4). As noted already, many S-mycothiolated proteins are Cys-rich proteins with more than 4 Cys residues which might explain why they are susceptible to S-mycothiolation under NaOCl stress. In conclusion, the comparison of the S-mycothiolated proteins with their Cys abundances in the total Cys proteome indicates that GapDH makes a major contribution to the S-mycothiolome in *C. diphtheriae* under NaOCl stress.

GapDH is reversibly inhibited and protected against overoxidation by S-mycothiolation under H_2O_2 and NaOCl stress *in vitro*. GapDH was identified as S-mycothiolated at its active site Cys153 that is highly sensitive to oxidation by H_2O_2 and located in a conserved $\text{C}_{153}\text{TTNC}_{157}$ motif present in prokaryotic and eukaryotic GapDH homologs (Figure S2). Under peroxide stress, the active site Cys is initially oxidized to a sulfenic acid that reacts further with LMW thiols, such as GSH, leading to S-glutathionylation^{22,27}. In the absence of thiol-redox systems or adjacent thiols, Cys-SOH can react further to irreversible oxidation forms, such as sulfinic or sulfonic acids^{1,28}. S-glutathionylation functions in redox control and protects catalytic and vulnerable Cys residues against overoxidation^{22,29–31}.

We were interested to investigate if S-mycothiolation controls GapDH activity and functions in thiol-protection against overoxidation *in vitro*. The His-tagged enzyme was cloned in *Escherichia coli*, purified

Protein	Locus Tag	Function	Cys-SSM	Cys-SSM peptide sequence	Ortholog and conservation* of Cys with -SSM in <i>Mtb</i>
Antioxidant enzymes					
DirA (AhpC)	DIP1420	2-Cys peroxiredoxin	Cys61** active site	(K)DFTFVC ₆₁ PTEIAAFGK(L)	Rv2428*
Protein synthesis					
RplC	DIP0473	50S ribosomal protein L3	Cys154**	(R)VGGIGAC ₁₅₄ ATPGR(V)	Rv0701*
RpsM	DIP0546	30S ribosomal protein S13	Cys86**	(K)IEIGC ₈₆ YQGLR(H)	Rv3460c*
Pth	DIP0897	Peptidyl-tRNA hydrolase	Cys49	(K)ASGAVIEVGGC ₄₉ R(V)	Rv1014c
DIP1398	DIP1398	RNA methyltransferase	Cys376* nucleophile	(R)AIAQSGPQAAIHIGC ₃₇₆ DPATFAR(D)	Rv2689c*
Energy metabolism					
DIP1726	DIP1726	Putative glucanotransferase	Cys45	(R)SLGVC ₄₅ FGNEDEPATDHEPLTGPMPSEDQIR(Y)	Rv1781c
Gap	DIP1310	Glyceraldehyde 3-phosphate DH	Cys153** active site	(K)HNIISNASC ₁₅₃ TTNCLAPMAK(V)	Rv1436*
DIP1796	DIP1796	Putative ribose/galactose isomerase	Cys143	(R)RIDILC ₁₄₃ EYER(T)	Rv2465c
DIP0655	DIP0655	Putative ribokinase	Cys171	(R)GTVVVNLPVIDVDRDC ₁₇₁ LLR(A)	—
GlpD	DIP2237	Putative glycerol-3-phosphate DH	Cys10	(K)SHC ₁₀ TFNPDYQDVWQR(F)	Rv2249c
Ndh	DIP1217	NADH dehydrogenase	Cys159	(R)AEmC ₁₅₉ EDPKER(E)	Rv1854c
Biosynthesis of amino acids					
ThrA	DIP1036	Homoserine dehydrogenase	Cys243	(R)VTYADVYC ₂₄₃ EGISK(I)	Rv1294
DIP0511	DIP0511	4-hydroxy-tetrahydrodipicolinate synthase	Cys141	(R)AVAAATSLPVIAYDIPVC ₁₄₁ VHTK(L)	—
DapA	DIP1464	4-hydroxy-tetrahydrodipicolinate synthase	Cys161	(R)SVVPIAPDTLC ₁₆₁ R(L)	Rv2753c
DIP0974	DIP0974	Putative aminotransferase	Cys138	(R)C ₁₃₈ DAPHELPNDIDLVFINSNPTGR(V)	Rv1178
GlnA1	DIP1644	Glutamine synthetase	Cys220	(R)QHPEC ₂₂₀ GTGSQEQINR(F)	—
LeuB	DIP1105	3-isopropylmalate dehydrogenase	Cys130	(R)EGTEGLYC ₁₃₀ GNGGTLR(E)	Rv2995c
Biosynthesis of nucleotides					
DIP1631	DIP1631	Uncharacterized protein	Cys43*	(R)IAVQPGGC ₄₃ SGLR(Y)	Rv2204c*
GuaB	DIP0580	Inosine-5'-monophosphate DH	Cys317** active site	(K)VIGIGPGSIC ₃₁₇ TTR(V)	Rv3410c*
PurA	DIP2063	Adenylosuccinate synthetase	Cys423	(R)DQTIVC ₄₂₃ HDVMEA(-)	Rv0357c
Other functions					
DIP0913	DIP0913	Uncharacterized protein	Cys22	(K)ERPTAGPQLYPVTC ₂₂ EAVVSAIR(A)	—
DIP1026	DIP1026	Conserved ATP-binding protein	Cys75	(R)IC ₇₅ LEADLGPVR(F)	Rv1278
DIP1102	DIP1102	Putative uncharacterized protein	Cys441	(R)LLSAC ₄₄₁ PESGLYK(G)	—
DIP1250	DIP1250	M18 family aminopeptidase	Cys401*	(K)AGSSHQVFVGNNSVPC ₄₀₁ GSTIGPITATR(L)	Rv0800*
DIP1287	DIP1287	UPF0210 protein DIP1287	Cys324	(K)GGMMAC ₃₂₄ SR(V)	—
GlmS	DIP1700	Glutamine-fructose-6-P aminotransferase	Cys74	(K)VQALEQELETSPMPQSC ₇₄ LGIGHTR(W)	Rv3436c

Table 1. Identification of 26 S-mycothiolated proteins in *C. diphtheriae* DSM43989 using shotgun LC-MS/MS analysis after exposure to 400 μ M NaOCl for 30 min. The S-mycothiolated proteins were identified using shotgun LC-MS/MS analysis and the Scaffold proteome software based on the mass increase of 484 Da (for -SSM) at Cys peptides. The table lists the Uniprot-accession number, protein name, conservation of the protein and the S-mycothiolated Cys residue in *M. tuberculosis* (*Mtb*) and the Cys-SSM peptide sequence. Conserved Cys residues are indicated with (*) and are shown in bold-face. Cys residues that were previously identified S-mycothiolated or S-bacillithiolated in *C. glutamicum*, *M. smegmatis* or *S. aureus* are indicated with (#).

and subjected to GapDH activity assays after exposure to H₂O₂ and NaOCl in the absence and presence of MSH *in vitro*. The inhibition of glycolytic GapDH activity by H₂O₂ and NaOCl was measured spectrophotometrically with G3P as substrate in the presence of NAD⁺ as coenzyme. NADH production was monitored in function of time as an absorbance increase at 340 nm¹⁰. The remaining GapDH activity was calculated from the slope in the kinetic curves as described previously²². Treatment with 200 μ M H₂O₂ alone did not affect GapDH activity, but 500 μ M H₂O₂ resulted in a 60% GapDH activity decrease. The enzyme was fully inactivated with 1 mM H₂O₂ (Fig. 4A). GapDH inactivation with 1 mM H₂O₂ was 65% irreversible while 35% activity could be recovered with 10 mM DTT (Fig. 4C). This suggests that the GapDH active site was rapidly overoxidized to Cys sulfonic acid by H₂O₂, but part of the enzyme was also reversible inactivated perhaps due to an intramolecular disulfide between Cys153 and Cys157 (Fig. 4D). This intramolecular disulfide has been detected also in other GapDH homologs of *E. coli* and *Bacillus subtilis* under oxidative stress^{32,33}. Using Orbitrap mass spectrometry, we could confirm the formation of the Cys153-sulfonic acid and of the intramolecular disulfide between Cys153 and Cys157 after exposure to 1 mM H₂O₂ (Figure S3A). In agreement with the activity assays, the overoxidized Cys153-peptide was detected at higher abundance compared to the intramolecular disulfide peptide.

Next, we analyzed whether S-mycothiolation can prevent overoxidation of the GapDH active site. Thus, the inhibition of GapDH activity and its reversibility was analyzed in the presence of H₂O₂ and MSH. GapDH was

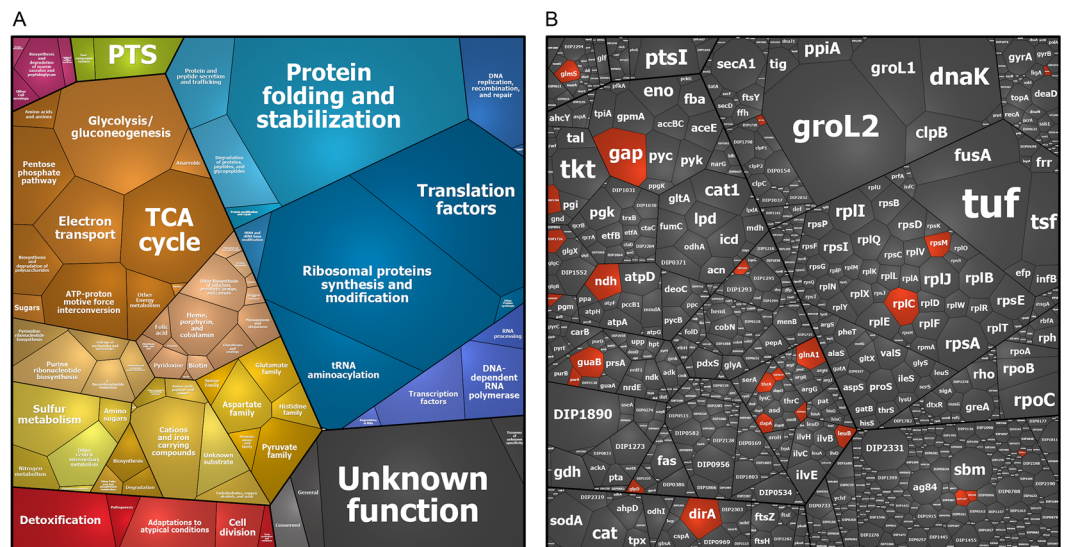


Figure 2. Voronoi treemaps show total protein abundance and 26 S-mycothiolated proteins identified in *C. diphtheriae* under NaOCl stress using shotgun LC-MS/MS analysis. **(A)** The treemap legend shows the classification of the *C. diphtheriae* proteome into functional categories as revealed by TIGRfam annotations. **(B)** The spectral protein abundance determines the cell size of each protein identified in the total proteome (Table S3). The 26 identified S-mycothiolated proteins under NaOCl stress are red-colored in the proteome treemap. The protein abundance treemap indicates that Gap, DirA (AhpC), Ndh and GuaB belong to the most abundant S-mycothiolated proteins in the total proteome.

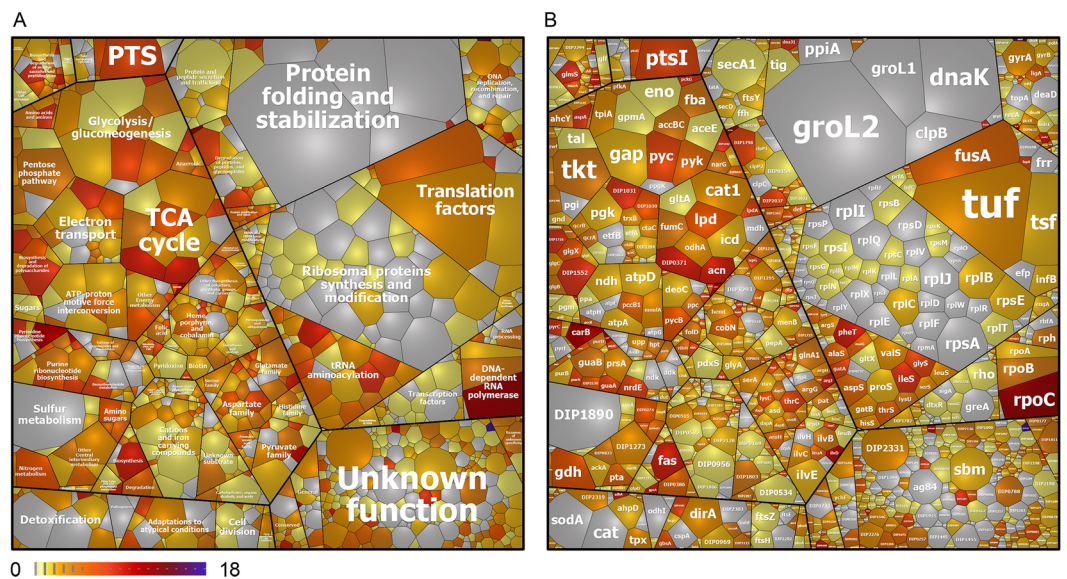


Figure 3. The total Cys abundance treemap of *C. diphtheriae* with proteins color-coded according to their number of Cys residues. **(A)** The treemap legend shows the functional classification of 1030 proteins detected in the proteome of *C. diphtheriae* as revealed by their TIGRfam annotations. **(B)** The spectral protein abundance determines the cell size of each protein identified in the total proteome (Table S3). The 805 Cys proteins were color-coded using a yellow-red color gradient based on their numbers of Cys residues. Non-Cys proteins are displayed in grey. The Cys abundance treemap visualizes that *C. diphtheriae* contains many Cys-rich proteins with >4 Cys residues in the proteome. The most abundant S-mycothiolated proteins Gap, DirA (AhpC), Ndh and GuaB contribute with 0.4–0.8% to the total Cys proteome. The values of calculated Cys abundances are shown in Table S4.

pre-treated with a 10-molar excess of MSH before it was subjected to 200 μ M, 500 μ M and 1 mM H_2O_2 . Of note, GapDH inactivation by H_2O_2 and MSH was faster compared to H_2O_2 alone since 200–500 μ M H_2O_2 resulted in a 40–75% GapDH activity decrease in the presence of MSH (Fig. 4B). The treatment with 1 mM H_2O_2 and MSH lead to a complete enzyme inactivation which was comparable to the inactivation by H_2O_2 alone. However,

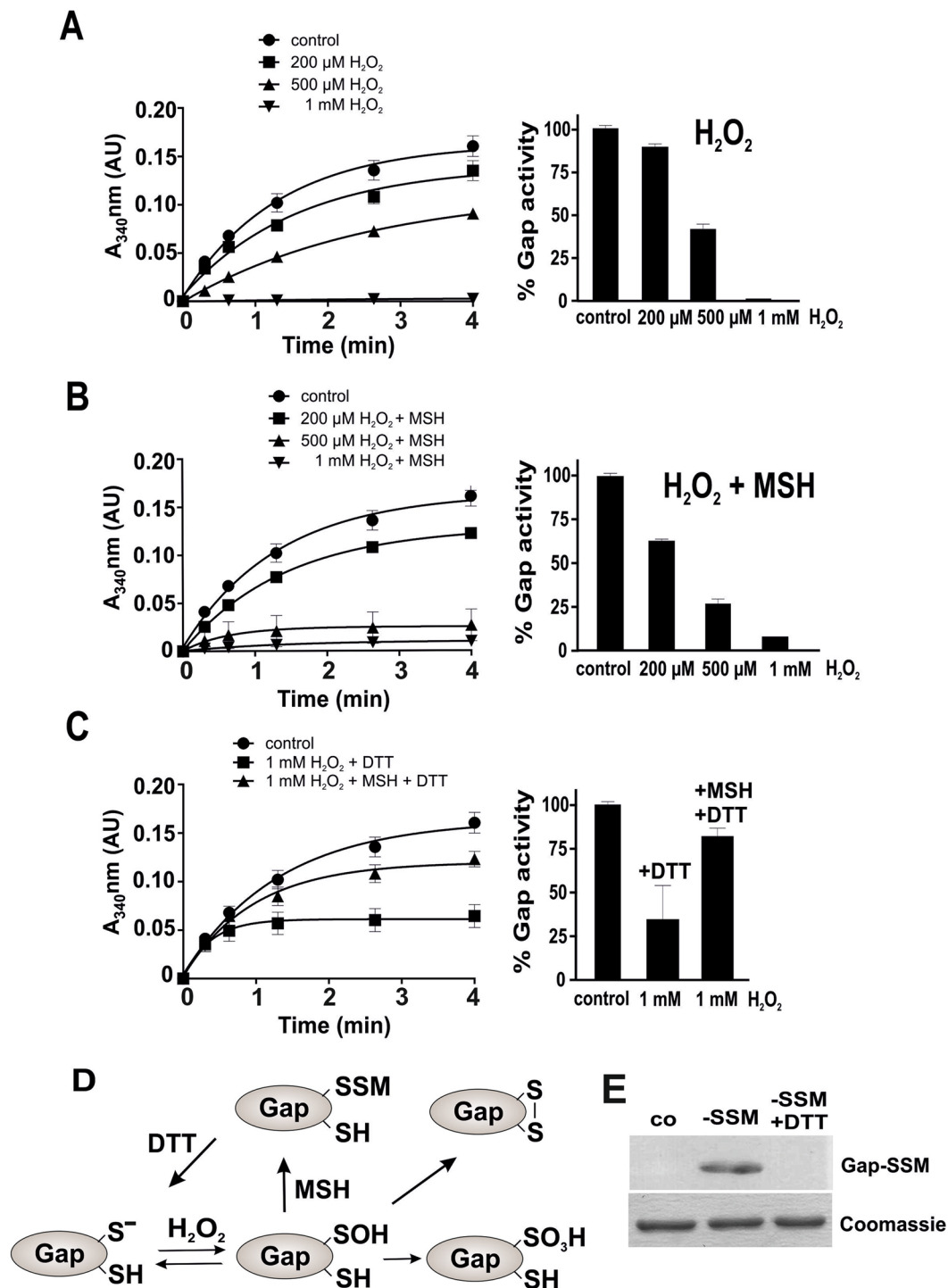


Figure 4. S-mycothiolation protects GapDH against overoxidation under H_2O_2 stress *in vitro*. (A,B) The NAD^+ -dependent GapDH activity was determined in a spectrophotometric assay by monitoring NADH generation during G3P oxidation at 340 nm. Inactivation of GapDH activity was performed using 200 μM , 500 μM and 1 mM H_2O_2 (A) in the absence and (B) in the presence of 1 mM MSH. (A,C) GapDH is 65% irreversibly inactivated with 1 mM H_2O_2 alone due to overoxidation of the active site Cys. (B,C) GapDH activity is reversibly inhibited due to S-mycothiolation with 1 mM H_2O_2 and MSH and could be reactivated by 10 mM DTT. (E) Non-reducing MSH specific Western blot analysis confirmed the S-mycothiolation of GapDH under H_2O_2 and MSH treatment and its reduction by DTT. (D) These results suggest that the GapDH active site Cys forms a sulfenic acid that reacts further to form Cys sulfonic acid and intramolecular disulfides in the presence of 1 mM H_2O_2 alone. GapDH is protected against this irreversible overoxidation by S-mycothiolation of the active site Cys in the presence of MSH and H_2O_2 . All data represent mean values of three independent replicate experiments and the error bars given were calculated as standard error of the mean (SEM).

GapDH inactivation by H_2O_2 and MSH was 80% reversible with 10 mM DTT, which indicates that Cys153 is S-mycothiolated in the presence of MSH and H_2O_2 . The S-mycothiolated Cys153 peptide could be verified by mass spectrometry and by non-reducing MSH-specific Western blot analysis (Figs 4E, S3B and S4A). In addition, the intramolecular Cys153-SS-Cys157 disulfide peptide was also detected by mass spectrometry (Figure S3B). These results provide evidence for the high reactivity of the nucleophilic active site Cys153 towards H_2O_2 , its vulnerability to overoxidation and the protection from overoxidation by S-mycothiolation (Fig. 4E). Moreover, our results support that GapDH inactivation by S-mycothiolation occurs faster compared to overoxidation by H_2O_2 alone which was observed in the activity assays with 200 and 500 μM H_2O_2 (Fig. 4A,B). Thus, S-mycothiolation can efficiently prevent the overoxidation of the GapDH active site.

However, S-mycothiolation of the GapDH active site Cys153 was observed *in vivo* under conditions of NaOCl stress. Thus, we analyzed GapDH inactivation with different NaOCl concentrations in the absence or presence of MSH. The incubation of GapDH with 100 μM NaOCl did not affect its activity and concentrations of 200–500 μM led to a 40% activity decrease (Fig. 5A). GapDH was fully inactivated with 1 mM NaOCl. Interestingly, the treatment of GapDH with 1 mM NaOCl was also partly (30%) reversible with 10 mM DTT (Figure 5C). This suggests that GapDH inactivation must be caused by both, irreversible overoxidation of Cys153 and reversible Cys153-SS-Cys157 intramolecular disulfide bond formation under NaOCl stress (Fig. 5D). Using Orbitrap mass spectrometry, we could confirm the overoxidation of GapDH as main modification which occurred in this case at Cys153 and Cys157. The intramolecular disulfide between Cys153 and Cys157 was also detected under NaOCl stress, but at lower abundance (Figure S3C). In conclusion, GapDH is subject to overoxidation and intramolecular disulfide formation under both, H_2O_2 and NaOCl treatment *in vitro*.

To investigate whether S-mycothiolation can prevent the overoxidation of the active site by NaOCl, we repeated the GapDH activity assays above and pretreated the enzyme with 10-fold molar excess of MSH prior to NaOCl exposure. Exposure of GapDH to 100 μM NaOCl resulted in 35% activity decrease while 200–500 μM NaOCl caused 50% enzyme inactivation (Fig. 5B). Treatment with 1 mM NaOCl in the presence of MSH led to 90% inactivation. Thus, it appears that GapDH inactivation with 100–500 μM NaOCl and MSH is faster compared to inactivation with NaOCl alone. GapDH inactivation by 1 mM NaOCl and MSH was almost completely reversible, since about 75% GapDH activity could be recovered with DTT. These results indicate that the GapDH active site should be protected against overoxidation by S-mycothiolation under NaOCl treatment in the presence of MSH. The S-mycothiolation of GapDH after NaOCl treatment was verified by MSH-specific Western blots and both S-mycothiolated Cys153 and Cys157 peptides were identified by mass spectrometry (Figures S3D and S4B). Apart from S-mycothiolation, we identified less abundant Cys153-SS-Cys157 intramolecular disulfides under NaOCl stress in the presence of MSH. In conclusion, our activity assays provide evidence that the S-mycothiolation pathway occurs faster compared to the overoxidation under both, H_2O_2 and NaOCl treatment *in vitro*. Thus, S-mycothiolation can efficiently protect the active site against overoxidation and irreversible inactivation under H_2O_2 and NaOCl stress *in vitro* (Figs 4D and 5D). In addition, intramolecular disulfides were detected under both, H_2O_2 and NaOCl treatment in the presence and absence of MSH as an additional redox-regulatory mechanism of GapDH.

Reactivation of S-mycothiolated GapDH requires the Mrx1/MSH/Mtr and Trx/TrxR electron transfer pathways.

Previous studies have demonstrated that both, the Mrx1 and Trx electron transfer pathways can function in reduction of the S-mycothiolated peroxidase Mpx *in vitro*^{13,34}. Moreover, de-mycothiolation by Mrx1 was shown to operate faster via a monothiol reaction mechanism compared to the reduction via Trx using a dithiol mechanism. Thus, we were interested to see if the Mrx1 and/or Trx electron transfer pathways could function in the reduction of S-mycothiolated GapDH resulting in recovery of its glycolytic activity *in vitro*. Regeneration of GapDH activity using Mrx1 and/or Trx should work only with the S-mycothiolated protein, but not with the overoxidized GapDH protein. Thus, the GapDH activity assay was performed after treatment of S-mycothiolated and overoxidized GapDH with the Mrx1 and Trx pathways (Fig. 6A,B). The regeneration of GapDH activity after Mrx1 and Trx reduction was followed by monitoring the NADH production at 340 nm. The results showed that both, Mrx1 and Trx can catalyze the reduction of S-mycothiolated GAPDH to regenerate GapDH activity *in vitro* (Fig. 6A,B). In contrast, Mrx1 and Trx could not restore the activity of overoxidized GapDH that was irreversibly inactivated using 10 mM H_2O_2 alone (Fig. 6A,B). To verify the de-mycothiolation of S-mycothiolated GapDH by Mrx1 and Trx, we performed a MSH-specific Western blot analysis (Fig. 6D). The results showed that Mrx1 and the Mrx1 resolving Cys mutant (Mrx1C15S) could reduce the GapDH MSH-mixed disulfide in this de-mycothiolation assay as shown by a decreased intensity of the S-mycothiolated GapDH band. Similarly, the reduction of GapDH-SSM by Trx and the Trx resolving Cys mutant (TrxC35S) are shown using the MSH-specific Western blot analysis. Here, the transfer of MSH to the Trx active site was clearly visible (Fig. 6D).

Next, we analyzed whether there is a catalytically relevant reduction mechanism of GapDH by the Mrx1 and Trx electron pathways which can be monitored by NADPH consumption. The Mrx1/MSH/Mtr/NADPH and Trx/TrxR/NADPH pathways were reconstituted *in vitro* using S-mycothiolated GapDH as substrate and NADPH consumption was followed over time in progress curves. First, we analyzed reduction of S-mycothiolated GapDH with the Mrx1/MSH/Mtr pathway at 340 nm. However, we failed to see any higher NADPH consumption rate using the Mrx1 electron transfer pathway. We concluded that reduction of S-mycothiolated GapDH with the Mrx1 pathway might be too fast and already finished before we started the measurement. Therefore, we decided to shift to a stopped flow device with a 2 ms mixing time. Under the same conditions, we found that most NADPH was already consumed within 5 seconds (Fig. 6E). In contrast, de-mycothiolation of S-mycothiolated GapDH could be measured in the Trx-coupled assay using a spectrophotometer. Here, NADPH is much slower consumed within 100 to 400 seconds. The NADPH consumption rate using Trx was higher for S-mycothiolated GapDH compared to the reduced GapDH control, indicating that Trx is able to reduce S-mycothiolated GapDH (Fig. 6F). In conclusion, our results demonstrate that both Mrx1 and Trx can provide electrons for GapDH

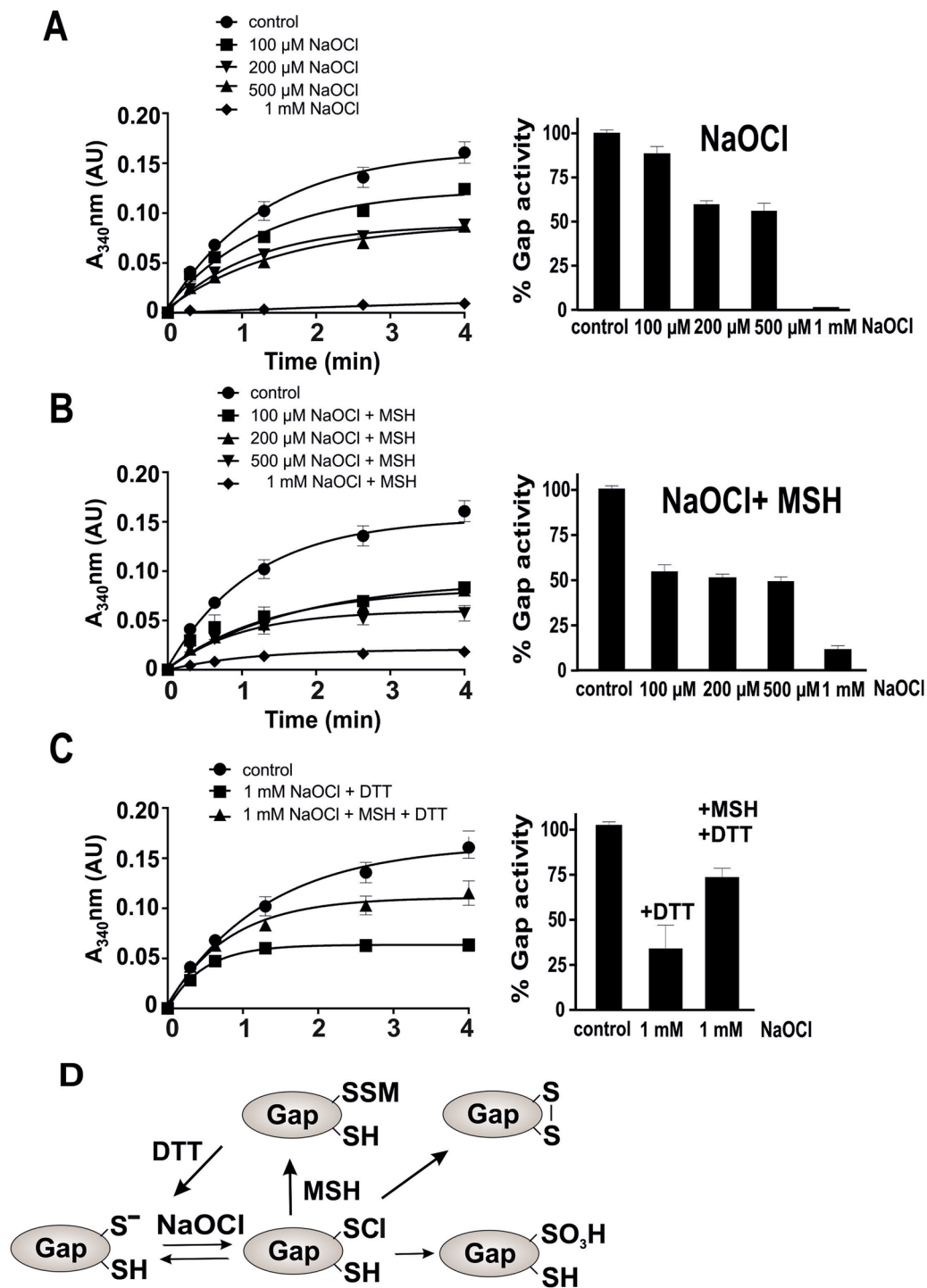


Figure 5. S-mycothiolation protects GapDH against overoxidation under NaOCl stress *in vitro*. (A,B) The NAD⁺-dependent GapDH activity was determined in a spectrophotometric assay by monitoring NADH generation during G3P oxidation at 340 nm. Inactivation of the GapDH activity was performed with 100, 200, 500 μ M and 1 mM NaOCl (A) without or (B) with MSH pre-treatment. (A,C) GapDH inactivation with 1 mM NaOCl alone is mostly irreversible due to the overoxidation of the active site to Cys sulfonic acid. (B,C) GapDH activity is reversibly inhibited due to S-mycothiolation with 1 mM NaOCl and MSH and could be reactivated by 10 mM DTT. The S-mycothiolation of Gap was confirmed by MSH-specific Western blots (Figure S4). (D) These results suggest that the GapDH active site Cys is chlorinated by NaOCl alone to form Cys-sulphenylchloride (-S-Cl) that reacts further to form Cys sulfonic acid and intramolecular disulfides in the absence of MSH. GapDH is protected against overoxidation by S-mycothiolation of the active site Cys in the presence of MSH. All data represent mean values of three independent replicate experiments and the error bars given were calculated as standard error of the mean (SEM).

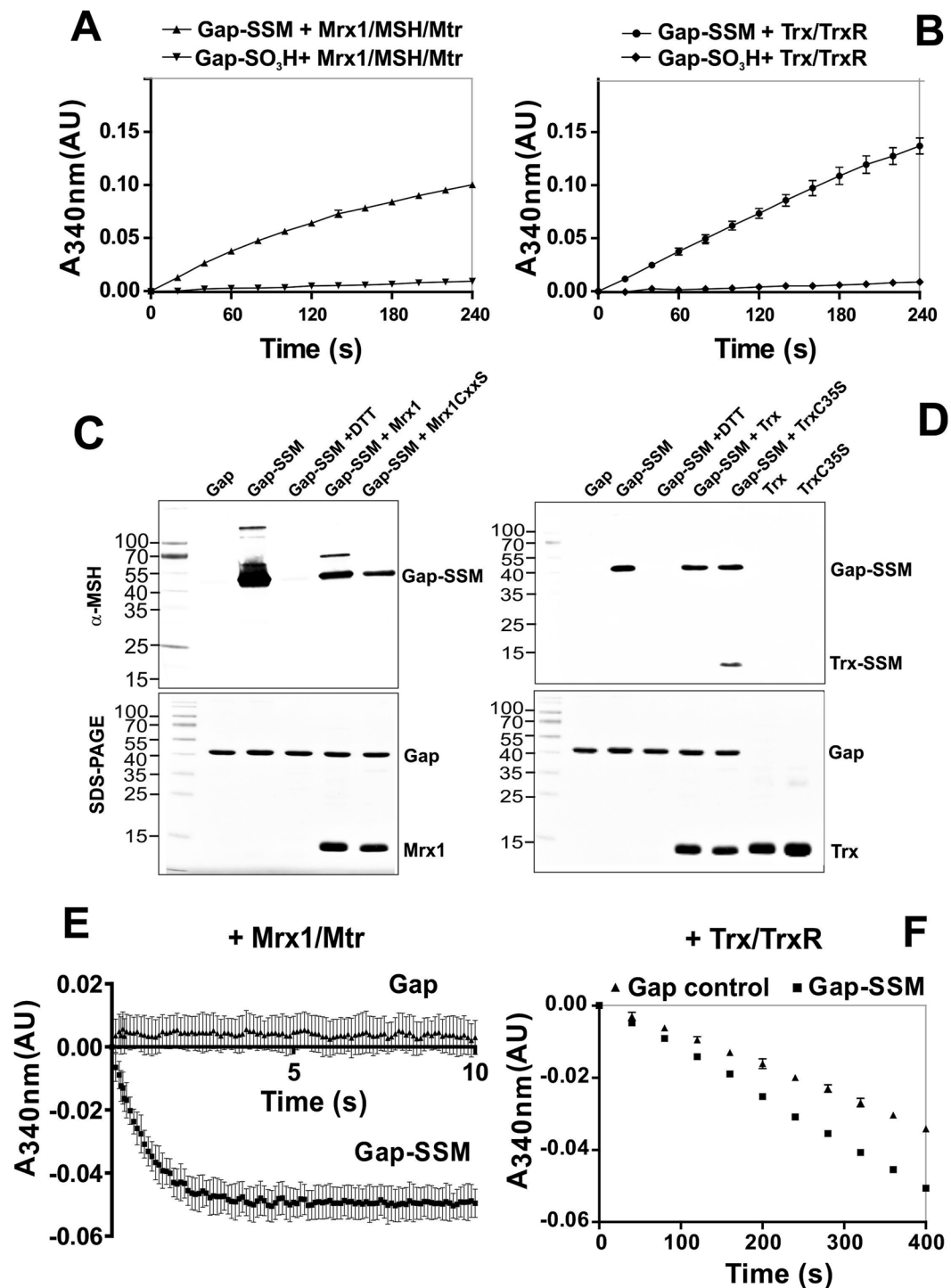


Figure 6. Re-activation of S-mycothiolated GapDH by the Trx/TrxR and Mrx/MSH/Mtr electron transfer pathways. (A,B) GapDH activity could be restored after demycothiolation of S-mycothiolated GapDH with Mrx1 and Trx as shown by NADH production in the G3P oxidation assay. In contrast, overoxidized GapDH that was treated with 10 mM H₂O₂ alone could not be reactivated by the Mrx1 and Trx pathways. (C,D) MSH-specific non-reducing Western blot analysis confirmed the S-mycothiolation of GapDH *in vitro* and its demycothiolation by the Mrx1 and Trx pathways. The transfer of MSH to the Trx resolving Cys mutant TrxC35S is shown. (E,F) The Mrx1/MSH/Mtr and Trx/TrxR electron transfer pathways both reduce S-mycothiolated GapDH with different reaction rates as revealed by progress curves of NADPH consumption. The demycothiolation of GapDH by the Mrx1-pathway was faster compared to the Trx-pathway. All data represent mean values of three independent replicate experiments and the error bars given were calculated as standard error of the mean (SEM).

de-mycothioloation. However, Mrx1 reduces the MSH mixed disulfide of GapDH much faster compared to Trx. Thus, our results show that S-mycothioloation of GapDH can efficiently function in protection of the active site against overoxidation and can be reversed using both, the Mrx1 and Trx pathways *in vitro*.

Discussion

Protein S-mycothioloation is a widespread and emerging redox modification in Actinomycetes and functions in redox regulation and thiol-protection against overoxidation to Cys sulfonic acids under conditions of NaOCl stress^{9, 10}. Hypochlorous acid (HOCl) is encountered by the pathogens *C. diphtheriae* and *M. tuberculosis* particularly during infections. HOCl is generated in neutrophils by the enzyme myeloperoxidase (MPO) with the aim to kill pathogenic bacteria^{35, 36}. HOCl is a strong thiol-oxidant and chlorinating agent that reacts with Cys residues to sulfenylchlorides (-S-Cl) and further to protein disulfides^{37, 38}, such as S-thioloations as we observed in Gram-positive bacteria⁴.

We identified 25 S-mycothioloated proteins in *C. glutamicum*¹⁰ and 26 proteins in *C. diphtheriae* while protein S-mycothioloation was more abundant in *M. smegmatis*⁹ with 58 identified proteins under NaOCl stress. The different numbers of S-mycothioloated proteins might be related to the different MSH contents between corynebacteria and mycobacteria³⁹. Mycobacteria produce high levels of up-to 20 mM MSH⁵ and we recently estimated 6 $\mu\text{mol/g}$ rdw MSH in *M. smegmatis*⁹. However, the MSH-levels determined in *C. diphtheriae* are 20-fold lower with 0.3 $\mu\text{mol/g}$ rdw according to this work and previous studies⁵. Due to the low MSH-content, the number of S-mycothioloated proteins might be lower in *C. diphtheriae* and *C. glutamicum* compared to mycobacteria. This indicates that in addition to MSH, unknown alternative LMW thiols might function in corynebacteria to maintain the thiol-redox homeostasis and to protect proteins by alternative S-thioloations. Recent studies further suggest that overexpression of the mycothiol disulfide reductase (Mtr) under oxidative stress conditions could play an important role in the maintenance of the redox homeostasis by increasing the levels of reduced MSH⁴⁰. In *M. tuberculosis*, MSH and the alternative LMW thiol ergothioneine (EGT) have been shown to be critical for redox homeostasis, energy metabolism and virulence and mutants deficient in MSH or EGT biosynthesis showed overlapping responses in the transcriptome^{41, 42}. The EGT levels were also elevated in a *M. smegmatis* *mshA* mutant⁴³. Thus, it remains to be elucidated whether EGT plays also a role as alternative LMW thiol in corynebacteria. In addition, it is also possible that the lower intracellular MSH level and the lower level of protein S-mycothioloation in corynebacteria is related to their 2–3-fold smaller genome size compared to mycobacteria.

The comparison of the functions and conservation of all identified S-mycothioloated proteins across Actinomycetes indicates that these are involved in a variety of cellular pathways. S-mycothioloated proteins participate in energy metabolism, fatty acid and mycolic acid biosynthesis, nucleotide, cofactor, mycothiol and amino acid biosynthesis, redox regulation, detoxification, transcription and translation. Some S-mycothioloated proteins are conserved and essential targets for S-thioloation across Gram-positive bacteria, such as thiol-peroxidases and peroxiredoxins (Tpx, AhpC), ribosomal proteins (RpsM, RplC), the IMP dehydrogenase (GuaB), the myo-inositol-1-phosphate synthase (Ino1), the methionine synthase (MetE), and the conserved glycolytic GapDH.

These conserved targets for S-mycothioloations overlap also with conserved S-bacillithioloated proteins in *Firmicutes*, such as *Bacillus* and *Staphylococcus* species^{11, 44}. Of note, the methionine synthase MetE is the most abundant S-bacillithioloated metabolic enzyme in *B. subtilis*, while GapDH represents the major S-bacillithioloated protein in *S. aureus*^{21, 33}. GapDH of *S. aureus* contributes with 4% Cys abundance to the total Cys proteome and is the most abundant Cys protein in the proteome. In *C. diphtheriae*, GapDH represents also the most abundant S-mycothioloated protein, but contributes only with 0.75% Cys abundance to the total Cys proteome. In *C. glutamicum*, the major targets for S-mycothioloation are the maltodextrin phosphorylase MalP and the thiol-peroxidase Tpx and it was shown that S-mycothioloation inhibited the activities of MalP and Tpx^{10, 15}. Thus, it seems that abundant redox-sensitive metabolic enzymes are the main targets for inactivation by S-thioloations in different bacteria. The different abundances of the S-mycothioloated MetE, MalP and GapDH in corynebacteria most likely depend on the different minimal growth media used for bacterial cultivations.

In addition, we found that many S-mycothioloated proteins of *C. diphtheriae* contain a high number of Cys residues explaining their susceptibility to oxidative inactivation. The glycolytic GapDH was S-mycothioloated at its active Cys153 residue that is known to be highly susceptible to oxidation by H₂O₂^{45–48}. GapDH is a well-known and conserved target for redox-regulation and S-glutathionylation in response to oxidative stress in several prokaryotic and eukaryotic organisms, including bacteria, malaria parasites, yeast, plants and human cell^{19, 20, 49}. GapDH inactivation in response to oxidative stress has been shown to reprogram central carbon metabolism and to re-direct the glycolytic flux into the pentose phosphate pathway (PPP) to increase NADPH production under conditions of high demands for reducing equivalents^{50, 51}. Thus, the goal of the GapDH inactivation by S-thioloation could be metabolic adaptation to provide more NADPH as reducing power in the cell under oxidative stress. In fact, a change of the global carbon flux was shown in *E. coli* under superoxide and H₂O₂ stress leading to an increased NADPH/NADH ratio^{52, 53}. Post-translational thiol-modifications play a key role in this metabolic adaptation to oxidative stress in different organisms and can change enzyme functions to re-configure central carbon metabolism which confers high metabolic plasticity^{50, 51}.

In this study, we have asked the question whether S-mycothioloation can function in thiol-protection and redox-regulation of GapDH activity in *C. diphtheriae* under H₂O₂- and NaOCl stress. To address this question, GapDH was inactivated with H₂O₂ and NaOCl in the absence and presence of MSH to analyze the kinetics of the irreversible overoxidation and S-mycothioloation pathways *in vitro*. The kinetic curves of H₂O₂ and NaOCl-dependent GapDH inactivation showed that the majority (65%) of the glycolytic activity is rapidly irreversibly inhibited with 1 mM H₂O₂ and NaOCl without pre-exposure to MSH. The mass spectrometry data confirmed the overoxidation of the active site Cys153 with H₂O₂ and NaOCl alone. In addition, 35% of GapDH activity was reversibly inhibited by 1 mM H₂O₂ and NaOCl alone due to an intramolecular Cys153-SS-Cys157 disulfide that was identified using mass spectrometry. In presence of MSH, GapDH inactivation by H₂O₂ and NaOCl was faster due to S-mycothioloation which was fully reversible with DTT and confirmed also by MSH-specific Western blot analysis.

This indicates that the GapDH overoxidation can be prevented by the faster S-mycothiolation. These results are in agreement with kinetic measurements performed for the related GapDH homolog of *S. aureus*²¹. The *S. aureus* GapDH was highly susceptible to overoxidation in the presence of H₂O₂ and NaOCl which could be prevented by S-bacillithiolation²¹. Interestingly, the comparison of the kinetics for the dose-dependent inactivation suggests that the *S. aureus* GapDH enzyme is more sensitive to oxidative inactivation compared to GapDH of *C. diphtheriae* since lower H₂O₂ and NaOCl doses inhibited *S. aureus* GapDH activity. This higher sensitivity of *S. aureus* GapDH may be due to the fact that Cys157 is replaced by a serine in the otherwise highly conserved C₁₅₃TTNC₁₅₇ motif²¹, so there is no possibility of intramolecular disulfide formation to prevent overoxidation (Figure S2). The active site Cys in *Homo sapiens* GapDH was demonstrated to provide a proton relay mechanism that determines H₂O₂-sensitivity of GapDH for oxidation²². On the other hand, *S. aureus* GapDH contains a threonine in position 243 instead of the otherwise conserved valine, which compensates for the disappearance of the oxidation sensitivity in the C157S mutant. This was demonstrated with the *Homo sapiens* GapDH C156S mutant, where an additional V243T mutation restores the oxidation sensitivity²². Our results strongly suggest that the second conserved cysteine might play an important role for oxidation sensitivity of GapDH and prevents overoxidation through intramolecular disulfide formation. Further studies are required to confirm whether Cys157 or other structural features make a difference in the sensitivity of GapDH to overoxidation and S-mycothiolation.

The strong H₂O₂ reactivity of the GapDH active site thiolate was recently shown to depend on a specific H₂O₂ binding pocket, transition state stabilization, and a dedicated proton relay mechanism promoting hydroxyl leaving-group departure^{20,22}. This proton relay also determines the preferred modification by S-glutathionylation in eukaryotic organisms which requires the initial formation of a sulfenic acid at Cys153 followed by reaction with GSH to form the mixed disulfide. This proton relay explains why GapDH of *C. diphtheriae* is a preferred target for S-mycothiolation under H₂O₂ and NaOCl. Our results confirmed the reactivity of the GapDH active site Cys towards H₂O₂- and NaOCl-dependent oxidation and the preference for formation of S-thiolations as observed in other GapDH homologs.

The reduction of S-mycothiolated proteins was previously shown to require both, the Mrx1 and Trx pathways for the regeneration of the activities of Mpx and MsrA *in vitro*^{12,13,16,34,54}. Mpx and MsrA form intramolecular disulfides and S-mycothiolations under H₂O₂ treatment *in vitro* that are reduced by the Trx and Mrx1 pathways. Here, we have shown that reduction and re-activation of S-mycothiolated GapDH also requires both, the Mrx1 and the Trx pathway *in vitro*. We have further shown that Mrx1 is much faster than Trx in reduction of S-mycothiolated GapDH. Thus, Mrx1 can take over the role of Trx, especially when Trx, as a ubiquitous disulfide reductase, is busy with reducing other non-native disulfides upon recovery from oxidative stress. Mrx1 efficiently functions in regeneration of GapDH activity to restore cellular growth and survival. The overlapping roles of Mrx1 and Trx in demycothiolation at different reaction rates were recently shown for Mpx recycling¹³. In agreement with our GapDH results, Mpx de-mycothiolation was also about two orders of magnitude more efficient with the Mrx1 system. De-mycothiolation of Mpx by Mrx1 occurs via a monothiol mechanism, which generates MSSM, and de-mycothiolation by Trx occurs via a dithiol-mechanism, generating oxidized Trx and reduced MSH. Both results suggest Mrx1 is the primary de-mycothiolating enzyme in Actinomycetes, with Trx having only a residual contribution. Under these premises, Trx would only be able to take over the role of Mrx1 if the concentration of reduced MSH is limiting, or if Trx is present at a much higher concentration than Mrx1 inside the cell. In conclusion, de-mycothiolation using the Mrx1 and Trx pathways may be a common mechanism to recover after oxidative stress when the pentose pathway has again produced enough NADPH to ensure the regeneration of oxidized Cys residues.

Similar to our studies, the de-glutathionylating activity of Trx was shown for GapDH isoform 1 (AtGapC1) from *A. thaliana* that could be reactivated by glutaredoxin C and less efficiently by thioredoxin *in vitro*²³. De-glutathionylation using Trx1 and Grx1 was also demonstrated for other GapDH homologs and S-glutathionylated enzymes in the malaria parasite, *Plasmodium falciparum* and in yeast cells^{49,55,56}. In *C. glutamicum*, overexpression of the MSH disulfide reductase Mtr resulted in a higher reduced level of MSH and increased activities of several redox-enzymes, including Mpx, MsrA, Trx, and Mrx1⁴⁰. Thus, future research should be directed to explore the cross-talk of the Mrx1 and Trx systems in regenerating S-mycothiolated proteins and MSH itself to restore the redox balance during the recovery from oxidative stress.

Material and Methods

Bacterial strains and growth conditions. *C. diphtheriae* DSM43989 was grown under vigorous agitation in Heart Infusion broth (HIB) (Difco) at 37°C to an optical density at 580 nm (OD₅₈₀) of 0.75–0.8. For NaOCl stress exposure, the cells were harvested, washed and re-suspended into Belitsky Minimal Medium (BMM) and further cultivated until cells have reached an OD₅₀₀ of ~1. *E. coli* strains used were DH5α and BL21 (DE3)plysS which were cultivated in Luria-Bertani (LB) medium at 37°C in the presence of the appropriate antibiotics, such as ampicillin (100 µg/ml) and chloramphenicol (25 µg/ml). Sodium hypochlorite (NaOCl, 15% stock solution) was purchased from Sigma Aldrich. For stress experiments, *C. diphtheriae* cells were treated with 400 µM NaOCl for 30 min.

Identification of S-mycothiolated peptides using LTQ-Orbitrap Velos mass spectrometry.

N-ethylmaleimide (NEM)-alkylated protein extracts were prepared from *C. diphtheriae* cells exposed to 400 µM NaOCl for 30 min and separated by 15% non-reducing SDS-PAGE followed by tryptic in-gel digestion and LTQ-Orbitrap-Velos mass spectrometry as described¹⁰. Post-translational thiol-modifications of proteins were identified by searching all MS/MS spectra in “dta” format against the *C. diphtheriae* target-decoy protein sequence database extracted from UniprotKB release 12.7 (UniProt Consortium, Nucleic acids research 2007, 35, D193–197) using Sorcerer™-SEQUEST® (Sequest v. 2.7 rev. 11, Thermo Electron including Scaffold 4.0, Proteome Software Inc., Portland, OR). The SEQUEST search parameters and thiol-modifications were used as described¹⁰ using the following parameters: parent ion mass tolerance 10 ppm and fragment ion mass tolerance 1.00 Da. Two tryptic miscleavages were allowed. Methionine oxidation (+15.994915 Da), cysteine alkylation (+125.04767 Da for NEM), S-cysteinylations (+119.004099 Da for C3H7NO2S) and S-mycothiolations

(+484.13627 Da for MSH) were set as variable post-translational modifications in the Sequest search. Sequest identifications required ΔC_n scores of >0.10 and XCorr scores of >2.2 , 3.3 and 3.75 for doubly, triply and quadruply charged peptides. Neutral loss precursor ions characteristic for the loss of myo-inositol (-180 Da) served for verification of the S-mycothiolated peptides. The mass spectrometry (MS) proteomics datasets (MS raw files and Scaffold files) are deposited into the ProteomeXchange database via the PRIDE partner repository with the dataset identifier PXD003321.

Mass spectrometry of the H_2O_2 -treated overoxidized GapDH was performed after in-gel tryptic digestion using nLC-MS/MS by an Orbitrap fusion as described previously⁵⁷.

Monobromobimane-labelling and HPLC-thiol metabolomics analysis. Cells were cultivated in HIB medium and transferred to BMM medium for the NaOCl stress experiments as described above. Thiol-labelling using monobromobimane (mBBr) was performed as described previously¹¹. The mBBr-labelled thiols were separated by reverse phase chromatography and quantified by fluorescence detection using the same HPLC system as described⁵⁸. The following gradient method was applied: 10 min 92% buffer A (10% methanol, 0.25% acetic acid, pH 3,9) supplemented with 8% buffer B (90% methanol, 0.25% acetic acid, pH 3,9), linear increase to 40% buffer B in 10 min, constant flow of 40% buffer B for 5 min, linear increase to 90% buffer B in 5 min, washing with 100% buffer B for 2 min followed by re-equilibration with 8% buffer B for 8 min. The flow rate was constantly set to 1.5 ml min^{-1} .

Expression, cloning and purification of recombinant His₆-tagged GapDH protein. The DIP1310 gene encoding GapDH was amplified by PCR using the primer pairs *Gap*-for (5'-GGAATTCCATATGGTGACGATTCGCGTAGGTATCA-3') and *Gap*-rev (5'-CTAGCTAGCTTAGTGATGGTGATGGTGATGGAGACCCTCACCGACGTATTC-3') with *C. diphtheriae* DSM43989 chromosomal DNA as template. The PCR product was digested with *Nhe*I and *Nde*I restriction enzymes and cloned into a similarly digested pET11b expression vector resulting in pET11b-*gapDH* that was transformed into *E. coli* BL21(DE3)*plysS*. The *gapDH* sequence was confirmed by DNA sequencing. For GapDH overproduction, the *E. coli* BL21(DE3)*plysS* strain with plasmid pET11b-*gap* was cultured in LB broth medium to an OD_{600} of 0.5 to 0.7 at 37 °C. Protein expression was induced with 1 mM IPTG (Isopropyl- β -D-1-thiogalactopyranoside) and cultivation was continued for 4 hours. Recombinant His₆-tagged GapDH was purified by affinity chromatography using His Trap™ HP Ni-NTA columns (5 ml; GE Healthcare, Chalfont St Giles, UK) and the ÄKTA purifier liquid chromatography system (GE Healthcare) according to the instructions of the manufacturers. Purified GapDH was dialyzed against 20 mM Tris-HCl, pH 8.0 and concentrated to 20 mg/ml using Vivaspin Ultra concentrators (Sartorius, Göttingen, Germany). The cloning and purifications of recombinant His₆-tagged proteins Mrx1, Mtr, Trx and TrxR were performed as described previously⁵⁹.

Production and purification of mycothiol. MSH was purified from *M. smegmatis* mc²155 that was grown to the late exponential phase in Middlebrook 7H9 broth with 0.05% Tween 80 and 10% oleic albumin dextrose catalase (OADC) at 37 °C as described¹³. The cells were harvested by centrifugation and disrupted using a French press (Constant Systems). The purified MSH was reduced with TCEP following several additional chromatographic steps. The concentration of MSH was determined by HPLC by correlating the MSH mBBr conjugate elution peak of an ACE 5 C18 column (Achrom) with a known standard. The sample purity was checked with Proton Nuclear Magnetic Resonance (¹H NMR).

Non-reducing Western blot analysis. MSH-specific Western blot analysis of the GapDH MSH-mixed disulfides were carried out using rabbit anti-MSH specific antiserum (1:1000-dilution) as described previously¹³.

Glycolytic GapDH activity assay. GapDH was reduced before the activity assays with 10 mM DTT for 30 minutes at room temperature. Excess of DTT was removed by desalting with Micro Biospin 6 columns (Biorad). Glycolytic GapDH activity was monitored spectrophotometric at 340 nm and 25 °C by the production of NADH. The oxidation of G3P to 1,3-bisphosphoglycerate (1,3 BPG) was measured in an assay mixture containing 1.25 mM NAD⁺ and 0.25 μ M GapDH in argon-flushed 20 mM Tris/HCl with 1.25 mM EDTA and 15 mM sodium arsenate as described previously²². After pre-incubation, the reaction was started by addition of 0.25 mM D,L-G3P. Sodium arsenate was used as a co-substrate to form unstable 1-arseno,3-phosphoglycerate. Degradation of the product allows a favorable equilibrium for measuring the rate of GapDH activity in the glycolytic forward reaction.

Inactivation of GapDH by H₂O₂ and NaOCl treatment. Pre-reduced GapDH (25 μ M) was incubated with different concentrations of H₂O₂ and NaOCl (100, 200, 500 μ M, 1 mM) in the absence or presence of 1 mM MSH for 5 min at 37 °C in an assay mixture containing 1.25 mM NAD⁺ and 0.25 μ M GapDH in argon-flushed 20 mM Tris-HCl with 1.25 mM EDTA and 15 mM sodium arsenate. After the removal of excess H₂O₂ and MSH, 0.25 mM D,L-G3P was added as substrate, GapDH activity was measured spectrophotometric by the production of NADH. The reversibility of the reaction was analyzed by measuring the GapDH activity after reduction with 10 mM DTT for 30 min.

De-mycothiolation of GapDH by the Mrx1/MSH/Mtr and Trx/TrxR pathways. GapDH, Mrx1 and Trx were reduced before the assays with 10 mM DTT for 30 minutes at room temperature. Excess of DTT was removed by desalting with Micro Biospin 6 columns. Pre-reduced GapDH (25 μ M) was pre-incubated with 10-molar excess of MSH at 37 °C for 5 min, then 100-fold molar excess of H₂O₂ was added and the mixture was incubated at 37 °C for 5 min. Excess of H₂O₂ and MSH were removed on a PD-10 desalting column (GE

Healthcare). The NADPH consumption during the de-mycothiolation reactions was monitored spectrophotometrically at 340 nm and 37 °C, using argon-flushed 50 mM Hepes/NaOH, pH 8, 500 mM NaCl, 1 mM EDTA. For the reduction of S-mycothiolated GapDH by the Trx pathway, we used 2 μ M Trx, 5 μ M Trx-reductase and 250 μ M NADPH in a Spectramax 340PC plate reader (Molecular Devices). For the reduction of S-mycothiolated GapDH by the Mrx1 pathway, we used 20 nM Mrx1, 5 μ M MSH, 5 μ M MSSM reductase and 250 μ M NADPH in SX-20 stopped flow (Applied PhotoPhysics). After 5 min pre-incubation of this mixture at 37 °C, 60 μ M mycothiolated GapDH was added to initiate the reaction. Three technical and experimental replicates were performed.

References

- Antelmann, H. & Hellmann, J. D. Thiol-based redox switches and gene regulation. *Antioxid Redox Signal* **14**, 1049–63 (2011).
- Fahey, R. C. Glutathione analogs in prokaryotes. *Biochim Biophys Acta* **1830**, 3182–98 (2013).
- Van Laer, K., Hamilton, C. J. & Messens, J. Low-molecular-weight thiols in thiol-disulfide exchange. *Antioxid Redox Signal* **18**, 1642–53 (2013).
- Loi, V. V., Rossius, M. & Antelmann, H. Redox regulation by reversible protein S-thiolation in bacteria. *Front Microbiol* **6**, 187 (2015).
- Newton, G. L. *et al.* Distribution of thiols in microorganisms: mycothiol is a major thiol in most actinomycetes. *J Bacteriol* **178**, 1990–5 (1996).
- Liu, Y. B. *et al.* Physiological roles of mycothiol in detoxification and tolerance to multiple poisonous chemicals in *Corynebacterium glutamicum*. *Arch Microbiol* **195**, 419–29 (2013).
- Newton, G. L., Buchmeier, N. & Fahey, R. C. Biosynthesis and functions of mycothiol, the unique protective thiol of Actinobacteria. *Microbiol Mol Biol Rev* **72**, 471–94 (2008).
- Rawat, M. *et al.* Mycothiol-deficient *Mycobacterium smegmatis* mutants are hypersensitive to alkylating agents, free radicals, and antibiotics. *Antimicrobial Agents and Chemotherapy* **46**, 3348–3355 (2002).
- Hillion, M. *et al.* Monitoring global protein thiol-oxidation and protein S-mycothiolation in *Mycobacterium smegmatis* under hypochlorite stress. *Sci Rep* **7**, 1195 (2017).
- Chi, B. K. *et al.* Protein S-mycothiolation functions as redox-switch and thiol protection mechanism in *Corynebacterium glutamicum* under hypochlorite stress. *Antioxid Redox Signal* **20**, 589–605 (2014).
- Chi, B. K. *et al.* S-bacillithiolation protects conserved and essential proteins against hypochlorite stress in firmicutes bacteria. *Antioxid Redox Signal* **18**, 1273–95 (2013).
- Tossounian, M. A. *et al.* *Corynebacterium diphtheriae* methionine sulfoxide reductase A exploits a unique mycothiol redox relay mechanism. *J Biol Chem* **290**, 11365–11375 (2015).
- Pedre, B. *et al.* The *Corynebacterium glutamicum* mycothiol peroxidase is a reactive oxygen species-scavenging enzyme that shows promiscuity in thiol redox control. *Mol Microbiol* **96**, 1176–1191 (2015).
- Hugo, M. *et al.* Mycothiol/mycoredoxin 1-dependent reduction of the peroxiredoxin AhpE from *Mycobacterium tuberculosis*. *J Biol Chem* **289**, 5228–39 (2014).
- Si, M. *et al.* Graded response of the multifunctional 2-Cysteine peroxiredoxin, CgPrx, to increasing levels of hydrogen peroxide in *Corynebacterium glutamicum*. *Antioxid Redox Signal* **26**, 1–14 (2017).
- Si, M. R. *et al.* *Corynebacterium glutamicum* methionine sulfoxide reductase A uses both mycoredoxin and thioredoxin for regeneration and oxidative stress resistance. *Appl Environ Microbiol* **81**, 2781–2796 (2015).
- Si, M. R. *et al.* Functional characterization of a mycothiol peroxidase in *Corynebacterium glutamicum* that uses both mycoredoxin and thioredoxin reducing systems in the response to oxidative stress. *Biochem J* **469**, 45–57 (2015).
- Liu, Y. *et al.* Mycothiol protects *Corynebacterium glutamicum* against acid stress via maintaining intracellular pH homeostasis, scavenging ROS, and S-mycothiolating MetE. *J Gen Appl Microbiol* **62**, 144–53 (2016).
- Brandes, N., Schmitt, S. & Jakob, U. Thiol-based redox switches in eukaryotic proteins. *Antioxid Redox Signal* **11**, 997–1014 (2009).
- Hildebrandt, T., Knesting, J., Berndt, C., Morgan, B. & Scheibe, R. Cytosolic thiol switches regulating basic cellular functions: GAPDH as an information hub? *Biol Chem* **396**, 523–537 (2015).
- Imber, M. *et al.* Protein S-bacillithiolation functions in thiol protection and redox regulation of the glyceraldehyde-3-phosphate dehydrogenase Gap in *Staphylococcus aureus* under hypochlorite stress. *Antioxid Redox Signal* (2017).
- Peralta, D. *et al.* A proton relay enhances H₂O₂ sensitivity of GAPDH to facilitate metabolic adaptation. *Nat Chem Biol* **11**, 156–63 (2015).
- Bedhomme, M. *et al.* Glutathionylation of cytosolic glyceraldehyde-3-phosphate dehydrogenase from the model plant *Arabidopsis thaliana* is reversed by both glutaredoxins and thioredoxins *in vitro*. *Biochem J* **445**, 337–47 (2012).
- Zaffagnini, M. *et al.* Glutathionylation in the Photosynthetic Model Organism *Chlamydomonas reinhardtii*: A Proteomic Survey. *Mol Cell Proteomics* **11**, 15 (2012).
- Faria, J. *et al.* Disclosing the essentiality of ribose-5-phosphate isomerase B in *Trypanosomatids*. *Sci Rep* **6**, 26937 (2016).
- Tullius, M. V., Harth, G. & Horwitz, M. A. Glutamine synthetase GlnA1 is essential for growth of *Mycobacterium tuberculosis* in human THP-1 macrophages and guinea pigs. *Infection and Immunity* **71**, 3927–3936 (2003).
- Shenton, D. & Grant, C. M. Protein S-thiolation targets glycolysis and protein synthesis in response to oxidative stress in the yeast *Saccharomyces cerevisiae*. *Biochem J* **374**, 513–9 (2003).
- Hillion, M. & Antelmann, H. Thiol-based redox switches in prokaryotes. *Biol Chem* **396**, 415–44 (2015).
- Ghezzi, P. Protein glutathionylation in health and disease. *Biochim Biophys Acta* **1830**, 3165–72 (2013).
- Ghezzi, P. Regulation of protein function by glutathionylation. *Free Radic Res* **39**, 573–80 (2005).
- Dalle-Donne, I., Rossi, R., Colombo, G., Giustarini, D. & Milzani, A. Protein S-glutathionylation: a regulatory device from bacteria to humans. *Trends Biochem Sci* **34**, 85–96 (2009).
- Leichert, L. I. *et al.* Quantifying changes in the thiol redox proteome upon oxidative stress *in vivo*. *Proc Natl Acad Sci USA* **105**, 8197–202 (2008).
- Chi, B. K. *et al.* S-bacillithiolation protects against hypochlorite stress in *Bacillus subtilis* as revealed by transcriptomics and redox proteomics. *Mol Cell Proteomics* **10**(M111), 009506 (2011).
- Si, M. *et al.* Functional characterization of a mycothiol peroxidase in *Corynebacterium glutamicum* that uses both mycoredoxin and thioredoxin reducing systems in the response to oxidative stress. *The Biochem J* **469**, 45–57 (2015).
- Winterbourn, C. C. & Kettle, A. J. Redox reactions and microbial killing in the neutrophil phagosome. *Antioxid Redox Signal* **18**, 642–60 (2013).
- Winterbourn, C. C., Kettle, A. J. & Hampton, M. B. Reactive Oxygen Species and Neutrophil Function. *Annu Rev Biochem* **85**, 765–92 (2016).
- Davies, M. J. Myeloperoxidase-derived oxidation: mechanisms of biological damage and its prevention. *J Clin Biochem Nutr* **48**, 8–19 (2011).
- Hawkins, C. L., Pattison, D. I. & Davies, M. J. Hypochlorite-induced oxidation of amino acids, peptides and proteins. *Amino Acids* **25**, 259–74 (2003).

39. Newton, G. L. *et al.* Distribution of thiols in microorganisms: Mycothiol is a major thiol in most actinomycetes. *J Bacteriol* **178**, 1990–1995 (1996).
40. Si, M. *et al.* Overexpression of mycothiol disulfide reductase enhances *Corynebacterium glutamicum* robustness by modulating cellular redox homeostasis and antioxidant proteins under oxidative stress. *Sci Rep* **6**, 29491 (2016).
41. Saini, V. *et al.* Ergothioneine Maintains Redox and Bioenergetic Homeostasis Essential for Drug Susceptibility and Virulence of *Mycobacterium tuberculosis*. *Cell Rep* **14**, 572–85 (2016).
42. Sasseti, C. M. & Rubin, E. J. Genetic requirements for mycobacterial survival during infection. *Proc Natl Acad Sci USA* **100**, 12989–94 (2003).
43. Ta, P., Buchmeier, N., Newton, G. L., Rawat, M. & Fahey, R. C. Organic hydroperoxide resistance protein and ergothioneine compensate for loss of mycothiol in *Mycobacterium smegmatis* mutants. *J Bacteriol* **193**, 1981–90 (2011).
44. Chandransu, P., Loi, V.V., Antelmann, H. & Helmmann, J.D. The role of bacillithiol in Gram-positive *Firmicutes*. *Antioxid Redox Signal* (2017).
45. Little, C. & O'Brien, P. J. Mechanism of peroxide-inactivation of the sulphhydryl enzyme glyceraldehyde-3-phosphate dehydrogenase. *Eur J Biochem* **10**, 533–8 (1969).
46. Zaffagnini, M. *et al.* Tuning cysteine reactivity and sulfenic acid stability by protein microenvironment in glyceraldehyde-3-phosphate dehydrogenases of *Arabidopsis thaliana*. *Antioxid Redox Signal* **24**, 502–17 (2016).
47. Winterbourn, C. C. & Hampton, M. B. Thiol chemistry and specificity in redox signaling. *Free Radic Biol Med* **45**, 549–61 (2008).
48. Baty, J. W., Hampton, M. B. & Winterbourn, C. C. Proteomic detection of hydrogen peroxide-sensitive thiol proteins in Jurkat cells. *Biochem J* **389**, 785–95 (2005).
49. Kehr, S. *et al.* Protein S-glutathionylation in malaria parasites. *Antioxid Redox Signal* **15**, 2855–65 (2011).
50. Ralser, M. *et al.* Dynamic rerouting of the carbohydrate flux is key to counteracting oxidative stress. *J Biol* **6**, 10 (2007).
51. Grant, C. M. Metabolic reconfiguration is a regulated response to oxidative stress. *J Biol* **7**, 1 (2008).
52. Rui, B. *et al.* A systematic investigation of *Escherichia coli* central carbon metabolism in response to superoxide stress. *BMC Systems Biology* **4**, 12 (2010).
53. Brumaghim, J. L., Li, Y., Henle, E. & Linn, S. Effects of hydrogen peroxide upon nicotinamide nucleotide metabolism in *Escherichia coli* - Changes in enzyme levels and nicotinamide nucleotide pools and studies of the oxidation of NAD(P)H by Fe(III). *J Biol Chem* **278**, 42495–42504 (2003).
54. Van Laer, K. *et al.* Mycoredoxin-1 is one of the missing links in the oxidative stress defence mechanism of mycobacteria. *Mol Microbiol* **86**, 787–804 (2012).
55. Greetham, D. *et al.* Thioredoxins function as deglutathionylase enzymes in the yeast *Saccharomyces cerevisiae*. *BMC Biochem* **11**, 3 (2010).
56. Tan, S. X. *et al.* The thioredoxin-thioredoxin reductase system can function *in vivo* as an alternative system to reduce oxidized glutathione in *Saccharomyces cerevisiae*. *J Biol Chem* **285**, 6118–26 (2010).
57. Kublik, A. *et al.* Identification of a multi-protein reductive dehalogenase complex in *Dehalococcoides mccartyi* strain CBDB1 suggests a protein-dependent respiratory electron transport chain obviating quinone involvement. *Environ Microbiol* **18**, 3044–56 (2016).
58. Wirtz, M., Droux, M. & Hell, R. O-acetylserine (thiol) lyase: an enigmatic enzyme of plant cysteine biosynthesis revisited in *Arabidopsis thaliana*. *J Exp Bot* **55**, 1785–98 (2004).
59. Ordóñez, E. *et al.* Arsenate reductase, mycothiol, and mycoredoxin concert thiol/disulfide exchange. *J Biol Chem* **284**, 15107–16 (2009).

Acknowledgements

This work was supported by an ERC Consolidator grant (GA 615585) MYCOTHILOME and the DFG Research Training Group GRK1947, project [C1] to H.A. We further acknowledge support from the DFG priority program SPP1710 on “Thiol-based redox switches”, project AN746/4-1 to H.A. and project WI 3560/2-1 and HE 1848/16-1 to M.W. and R.H. This work was further supported by the following institutions: (i) agentschap voor Innovatie door Wetenschap en Technologie (IWT), (ii) Vlaams Instituut voor Biotechnologie (VIB), (iii) the SPR34 project of the Vrije Universiteit Brussel (VUB), (iv) Research Foundation Flanders (FWO), and (v) Flanders Hercules Foundation (grant number HERC16) for the purification platform to J.M. Mass spectrometry of GapDH was performed at the Centre for Chemical Microscopy (ProVIS) at the Helmholtz Centre for Environmental Research, which is supported by European regional development funds (EFRE-Europe Funds Saxony) and the Helmholtz Association.

Author Contributions

M.H., B.P., M.S., M.I., V.V.L., L.A.R., J.M. and H.A. conceived the ideas and hypotheses, designed and performed the GapDH experiments and analyzed the data. M.H. performed the proteomics experiments, processed and analyzed the data. M.H. and J.B. performed the bioinformatics analysis and treemap constructions. S.M., D.B., L.A. and C.W. performed peptide measurements using mass spectrometry. M.W. and R.H. performed the thiol-metabolomics analysis. H.A., M.H., B.P. and J.M. wrote the manuscript and prepared the figures. All authors reviewed and approved the manuscript.

Additional Information

Supplementary information accompanies this paper at doi:10.1038/s41598-017-05206-2

Competing Interests: The authors declare that they have no competing interests.

Publisher's note: Springer Nature remains neutral with regard to jurisdictional claims in published maps and institutional affiliations.



Open Access This article is licensed under a Creative Commons Attribution 4.0 International License, which permits use, sharing, adaptation, distribution and reproduction in any medium or format, as long as you give appropriate credit to the original author(s) and the source, provide a link to the Creative Commons license, and indicate if changes were made. The images or other third party material in this article are included in the article's Creative Commons license, unless indicated otherwise in a credit line to the material. If material is not included in the article's Creative Commons license and your intended use is not permitted by statutory regulation or exceeds the permitted use, you will need to obtain permission directly from the copyright holder. To view a copy of this license, visit <http://creativecommons.org/licenses/by/4.0/>.

© The Author(s) 2017

Chapter 6

Redox-sensing under hypochlorite stress and infection conditions by the Rrf2-family repressor HypR in *Staphylococcus aureus*

Vu Van Loi¹, Tobias Busche^{1,2}, Karsten Tedin³, Jörg Bernhardt⁴, Jan Wollenhaupt⁵, Nguyen Thi Thu Huyen¹, Christoph Weise⁶, Jörn Kalinowski², Markus Wahl⁵, Marcus Fulde³ and Haike Antelmann^{1#}

¹*Freie Universität Berlin, Institute for Biology-Microbiology, D-14195 Berlin, Germany*

²*Bielefeld University, Center for Biotechnology, D-33594 Bielefeld, Germany*

³*Freie Universität Berlin, Institute of Microbiology and Epizootics, Centre for Infection Medicine, D-14163 Berlin, Germany*

⁴*Ernst-Moritz-Arndt-University of Greifswald, Institute, for Microbiology, D-17487 Greifswald, Germany;*

⁵*Freie Universität Berlin, Laboratory of Structural Biochemistry, D-14195 Berlin, Germany*

⁶*Freie Universität Berlin, Institute of Chemistry and Biochemistry, D-14195 Berlin, Germany*

Published in: Antioxidants & Redox Signaling, in press. (2018)

<https://doi.org/10.1089/ars.2017.7354>

#Corresponding author: haike.antelmann@fu-berlin.de

Authors contributions:

Haike Antelmann and **Vu Van Loi** designed the experiments and analyzed data. **Vu Van Loi** performed cloning and mutant constructions, biochemical experiments and phagocytosis assay of this work. He also critically read and approved the final manuscript. Nguyen Thi Thu Huyen, Tobias Busche, and Jörn Kalinowski performed the RNA-seq transcriptome analysis. Jörg Bernhardt was involved in the bioinformatics analysis and treemap constructions. Karsten Tedin and Marcus Fulde helped in the phagocytosis assays. Christoph Weise contributed to peptide measurements using mass spectrometry (MALDI-TOF). Jan Wollenhaupt and Markus Wahl performed size exclusion chromatography-multi angle light scattering (SEC-MALS) analysis for this study.

ORIGINAL RESEARCH COMMUNICATION

Redox-Sensing Under Hypochlorite Stress and Infection Conditions by the Rrf2-Family Repressor HypR in *Staphylococcus aureus*

Vu Van Loi,¹ Tobias Busche,^{1,2} Karsten Tedin,³ Jörg Bernhardt,⁴ Jan Wollenhaupt,⁵ Nguyen Thi Thu Huyen,¹ Christoph Weise,⁶ Jörn Kalinowski,² Markus C. Wahl,⁵ Marcus Fulde,³ and Haike Antelmann¹

Abstract

Aims: *Staphylococcus aureus* is a major human pathogen and has to cope with reactive oxygen and chlorine species (ROS, RCS) during infections, which requires efficient protection mechanisms to avoid destruction. Here, we have investigated the changes in the RNA-seq transcriptome by the strong oxidant sodium hypochlorite (NaOCl) in *S. aureus* USA300 to identify novel redox-sensing mechanisms that provide protection under infection conditions.

Results: NaOCl stress caused an oxidative stress response in *S. aureus* as indicated by the induction of the PerR, QsrR, HrcA, and SigmaB regulons in the RNA-seq transcriptome. The *hypR-merA* (USA300HOU_0588-87) operon was most strongly upregulated under NaOCl stress, which encodes for the Rrf2-family regulator HypR and the pyridine nucleotide disulfide reductase MerA. We have characterized HypR as a novel redox-sensitive repressor that controls MerA expression and directly senses and responds to NaOCl and diamide stress *via* a thiol-based mechanism in *S. aureus*. Mutational analysis identified Cys33 and the conserved Cys99 as essential for NaOCl sensing, while Cys99 is also important for repressor activity of HypR *in vivo*. The redox-sensing mechanism of HypR involves Cys33-Cys99 intersubunit disulfide formation by NaOCl stress both *in vitro* and *in vivo*. Moreover, the HypR-controlled flavin disulfide reductase MerA was shown to protect *S. aureus* against NaOCl stress and increased survival in J774A.1 macrophage infection assays.

Conclusion and Innovation: Here, we identified a new member of the widespread Rrf2 family as redox sensor of NaOCl stress in *S. aureus* that uses a thiol/disulfide switch to regulate defense mechanisms against the oxidative burst under infections in *S. aureus*. *Antioxid. Redox Signal.* 00, 000–000.

Keywords: *Staphylococcus aureus*, Rrf2, redox-sensing regulator, hypochlorite stress

Introduction

STAPHYLOCOCCUS AUREUS IS not only a common commensal bacterium but also a major pathogen that accounts for 40% of nosocomial infections in humans (31). *S. aureus* can cause local wound infections and also severe life-threatening infections, such as septicemia, endocarditis, necrotizing pneu-

monia, catheter-associated infections, and osteomyelitis (3, 12, 60). A major problem to combat *S. aureus* infections is the increasing prevalence of multiple antibiotic-resistant isolates, such as methicillin-resistant *S. aureus* (MRSA) strains that arise in hospitals as well as in the community (57). *S. aureus* USA300 is a highly virulent community-acquired MRSA strain that encodes many virulence factors,

¹Institute for Biology-Microbiology, Freie Universität Berlin, Berlin, Germany.

²Center for Biotechnology, Bielefeld University, Bielefeld, Germany.

³Centre for Infection Medicine, Institute of Microbiology and Epizootics, Freie Universität Berlin, Berlin, Germany.

⁴Institute for Microbiology, Ernst-Moritz-Arndt-University of Greifswald, Greifswald, Germany.

⁵Laboratory of Structural Biochemistry and ⁶Institute of Chemistry and Biochemistry, Freie Universität Berlin, Berlin, Germany.

Innovation

Staphylococcus aureus is an important human pathogen that has to cope with the oxidative burst of the host innate immune system under infection conditions to ensure survival. Here, we have characterized the novel NaOCl-sensing transcription factor HypR that belongs to the Rrf2-family and controls the flavin disulfide reductase MerA under infection conditions. HypR senses and responds to NaOCl via the formation of Cys33-Cys99 intersubunit disulfides resulting in dissociation from its operator and derepression of *hypR-merA* transcription. The *hypR-merA* operon was required for growth and survival under NaOCl stress and in macrophage infection assays and was identified as an important defense mechanism under hypochlorite stress.

including the pore forming toxin Panton–Valentine leukocidin, the pyrogenic toxin superantigens (Sek and Seq), the plasminogen-activator staphylokinase (Sak), the staphylococcal complement inhibitor, and the chemotaxis inhibitory protein (Chp) contributing to the pathogenicity, immune evasion, and resistance to host defenses (24, 25, 85). The pathogen is classified by the “European Center of Disease Prevention and Control” as ESKAPE pathogen because of its fast ability to escape the bactericidal action of antibiotics (76). Thus, to understand the adaptation of the pathogen to the host defense is of utmost importance to identify new drug targets for the treatment of MRSA infections.

During infections, *S. aureus* has to defend against reactive oxygen and chlorine species (ROS, RCS), such as hydrogen peroxide (H₂O₂) and the strong oxidant hypochlorous acid (HOCl) that are produced as first-line defense by activated macrophages and neutrophils with the aim to kill invading pathogens (8, 43, 96, 97). HOCl is generated in neutrophils from H₂O₂ and chloride by the myeloperoxidase (MPO), which is the main mechanism of bacterial killing (39, 48).

As ROS protection mechanism, *S. aureus* uses the low-molecular-weight (LMW) thiol bacillithiol (BSH) that enhances survival in macrophage infection assays. In addition, various redox-sensing regulators of the SarA/MarR-family, such as MgrA and SarZ and the Staphylococcal accessory regulator (SarA), regulate ROS and antibiotic resistance determinants, as well as virulence factors (13–16, 43). MgrA controls the expression of several efflux pumps, which confer resistance toward fluoroquinolone, tetracycline, vancomycin, and penicillin. SarZ regulates the *ohrA* peroxiredoxin and genes involved in virulence, autolysis, cell wall biosynthesis, antibiotic resistance, and energy metabolism. The OhrA peroxiredoxin reduces organic hydroperoxides that are derived from fatty acid oxidation to their organic alcohols (26). Both SarZ and MgrA use a thiol-based redox-sensing mechanism in response to organic hydroperoxides (78, 88). The single Cys residue of SarZ and MgrA can be regulated by S-thiolation with a synthetic LMW thiol leading to allosteric changes in the DNA-binding domains and derepression of transcription of the target genes (1, 15, 43).

To identify novel sodium hypochlorite (NaOCl)-sensitive proteins, we have recently applied the OxICAT method and studied the quantitative thiol-redox proteome of *S. aureus* USA300 under NaOCl stress (46). The redox state of 228 Cys

residues in *S. aureus* could be quantified and 58 NaOCl-sensitive Cys residues were identified with >10% increased oxidations under NaOCl treatment. Of note, the redox-sensing Cys residues of both MarR/OhrR-family regulators MgrA and SarZ showed increased oxidation levels under NaOCl stress. The NaOCl-sensitive proteins include also many antioxidant proteins, detoxification and metabolic enzymes, ribosomal proteins, several Zn-containing proteins, and virulence factors. Moreover, five S-bacillithiolated proteins were identified under NaOCl stress, including Gap, AldA, GuaB, and RpmJ that showed the highest oxidation increase of >20% in the OxICAT analysis. Gap contributes as most abundant S-bacillithiolated protein in the proteome with 4% to the total Cys proteome of *S. aureus*. We have further shown that S-bacillithiolation of Gap functions in redox control and thiol protection under H₂O₂ and NaOCl stress *in vitro* (46). However, while our redox proteomics studies identified many new targets for redox regulation, no HOCl-specific transcription factor was identified that could be specifically involved in sensing of NaOCl stress.

In this study, we applied RNA-seq transcriptomics to identify new redox-sensing regulators in *S. aureus* USA300 that could specifically sense and respond to NaOCl stress and thereby regulate target genes that confer protection under infection conditions. The *hypR-merA* operon was most strongly upregulated under NaOCl in the transcriptome that encodes for the novel redox-sensing regulator HypR and the pyridine nucleotide disulfide reductase mercuric ion reductase (MerA). HypR belongs to the widespread Rrf2 family of transcriptional regulators that include iron/sulfur (FeS)-cluster redox sensors for nitric oxide (NsrR) (23, 90, 98), the iron/sulfur status of the cell (IscR) (82, 83), iron metabolism (RirA) (40), or other signals (67). Other Rrf2 family regulators do not contain FeS clusters, such as the cysteine metabolism repressor (CymR) (28, 47, 84) and the redox-sensing SaiR repressor of *Bacillus anthracis* that controls *spxA2* under disulfide stress conditions and is a close homologue of HypR (68). Using biochemical and genetic approaches, we have characterized HypR as a novel thiol-based redox sensor that senses HOCl stress by intersubunit disulfide formation and protects *S. aureus* under macrophage infection conditions.

Results

NaOCl stress causes an oxidative stress response in the transcriptome and upregulates most strongly the hypR-merA operon (USA300HOU_0588-87) in S. aureus USA300

We were interested to identify novel redox-sensing regulators in *S. aureus* that could be specifically involved in the hypochlorite defense under infection conditions. Thus, we studied the changes in the RNA-seq transcriptome in *S. aureus* USA300 after exposure to sublethal 150 μ M NaOCl stress compared to untreated control cells. The NaOCl stress experiments were performed in Belitsky minimal medium (BMM) to avoid quenching by rich medium components as described in our previous studies (46, 58). Three biological replicate experiments were performed and the samples for RNA isolation were taken before (control) and 30 min after NaOCl stress and subjected to RNA-seq analysis as described (44). For significant expression changes, the log₂ fold change (m-value) cutoff (log₂-fold change NaOCl vs. control)

of ± 1.98 was chosen (95% confidence, $p \leq 0.05$). In total, 89 transcripts were significantly at least fourfold upregulated and 9 were fourfold downregulated under NaOCl stress in the transcriptome data set (Fig. 1 and Supplementary Table S1; Supplementary Data are available online at www.liebertpub.com/ars). In addition, 1442 genes are differentially transcribed below the m-value cutoff under NaOCl stress in the RNA-seq transcriptome of *S. aureus* USA300. All induced and repressed genes above and below the m-value cutoff were sorted into regulons, and a subset of the most interesting upregulated regulons is displayed in Voronoi treemaps (Fig. 2 and Supplementary Table S2).

Previous transcriptome analysis in *Bacillus subtilis* showed that NaOCl stress induces an oxidative stress response as revealed by the induction of the oxidative stress-specific PerR, OhrR, and Spx regulons, as well as by the CtsR regulon indicative of oxidative protein unfolding (20). Furthermore, NaOCl stress resulted in increased expression of the YodB, CatR, HypR, and HxlR regulons in *B. subtilis* that sense reactive electrophilic species (RES), such as quinones and aldehydes (18, 20, 21, 52, 73). In *S. aureus*, we could confirm a similar expression profile under NaOCl stress as revealed by the strong upregulation of the PerR, HrcA, and QsrR (YodB) regulons indicating ROS and RES responses in *S. aureus*. In addition, we noticed the weak two- to threefold induction of few members of the Fur and Zur regulons. Fur and Zur oxidation in their Zn-redox switch motifs was observed under NaOCl stress in our recent OxICAT analyses in *S. aureus* (46) and *Mycobacterium smegmatis* (44). Similarly, the Fur family protein PerR was oxidized to an intramolecular disulfide in *B. subtilis* under NaOCl stress (20). Since Zn-redox switch

motifs are known sensors for HOCl stress also in *E. coli* (45, 95), redox regulation of PerR, Fur, and Zur could involve also thiol oxidation in their Zn-motifs.

The SigmaB regulon was also induced under NaOCl stress in *S. aureus* and *B. subtilis*, which might be indicative for an acid stress response and contributes to virulence (20) (Fig. 2). The induction of the SigmaB regulon was previously shown after internalization of *S. aureus* in human epithelial cells and SigmaB was essential for intracellular growth (77). Of note is further induction of GraRS cell wall stress regulon under NaOCl stress in *S. aureus*. GraRS controls resistance to antimicrobial peptides and cell wall-active antibiotics, such as vancomycin, but contributes also to the oxidative stress resistance of *S. aureus* explaining its upregulation under NaOCl stress (29). The oxidative stress response is further indicated by induction of genes that encode for BSH biosynthesis enzymes and bacilliredoxins, such as *bshA*, *bshB*, *bshC*, and *brxB* in *S. aureus*. The BSH biosynthesis genes are under control of Spx in *B. subtilis* (33) and perhaps also in *S. aureus*.

Apart from the stress regulons, the SaeRS regulon was most strongly induced under NaOCl stress in *S. aureus*. The SaeRS two-component system controls many important toxins, such as α -, β -, and γ -hemolysins, leukocidins, superantigens, surface proteins, proteases, nuclease, coagulase, and immune evasion proteins (7, 38, 56) that exhibit the highest fold change between 20- and 160-fold under NaOCl stress (Supplementary Tables S1 and S2, Figs. 1 and 2). Previous studies established important roles of SaeRS in pathogenicity and biofilm formation in a variety of disease models of infections (56). The SaeRS regulon was most strongly upregulated by neutrophil stress in *S. aureus* as shown in previous microarrays (91). The

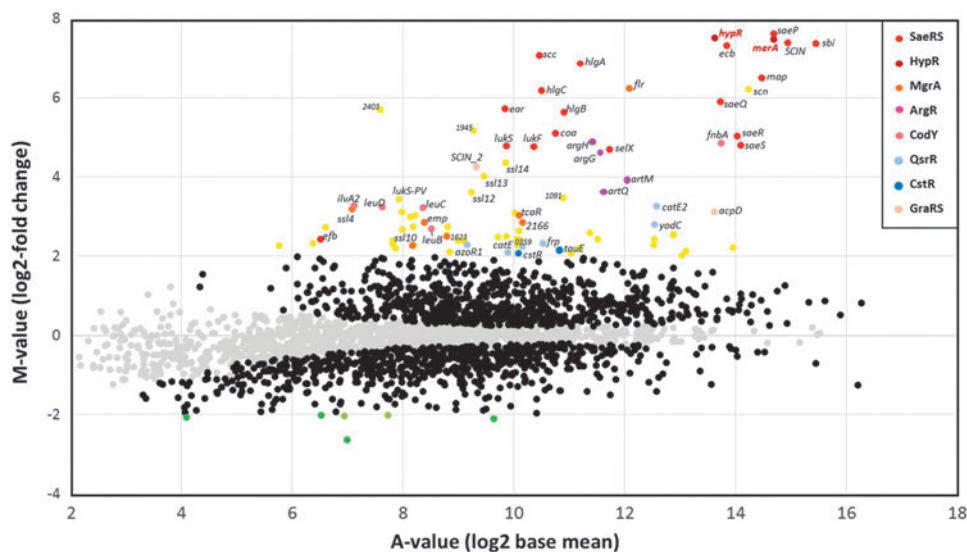


FIG. 1. RNA-seq transcriptomics of *Staphylococcus aureus* USA300 after 30 min of NaOCl stress. For RNA-seq transcriptome profiling, *S. aureus* USA300 was grown in BMM and treated with 150 μ M NaOCl stress for 30 min. The gene expression profile under NaOCl stress is shown as ratio/intensity scatter plot (M/A-plot), which is based on the differential gene expression analysis using DeSeq2. Colored symbols indicate significantly induced (red, magenta, yellow) or repressed (green) transcripts ($M\text{-value} \geq 1.98$ or ≤ -1.98 ; $p\text{-value} \leq 0.05$). Black symbols indicate differential transcribed genes below the M-value cutoff of $1.98 > M > -1.98$ ($p \leq 0.05$). Gray symbols denote transcripts with no fold changes after NaOCl stress ($p > 0.05$). The SaeRS, HypR, MgrA, ArgR, CodY, and QsrR regulons are most strongly upregulated under NaOCl stress. The transcriptome analysis was performed from three biological replicates. The RNA-seq expression data of all genes after NaOCl stress and their regulon classifications are listed in Supplementary Tables S1 and S2. BMM, Belitsky minimal medium; NaOCl, sodium hypochlorite.

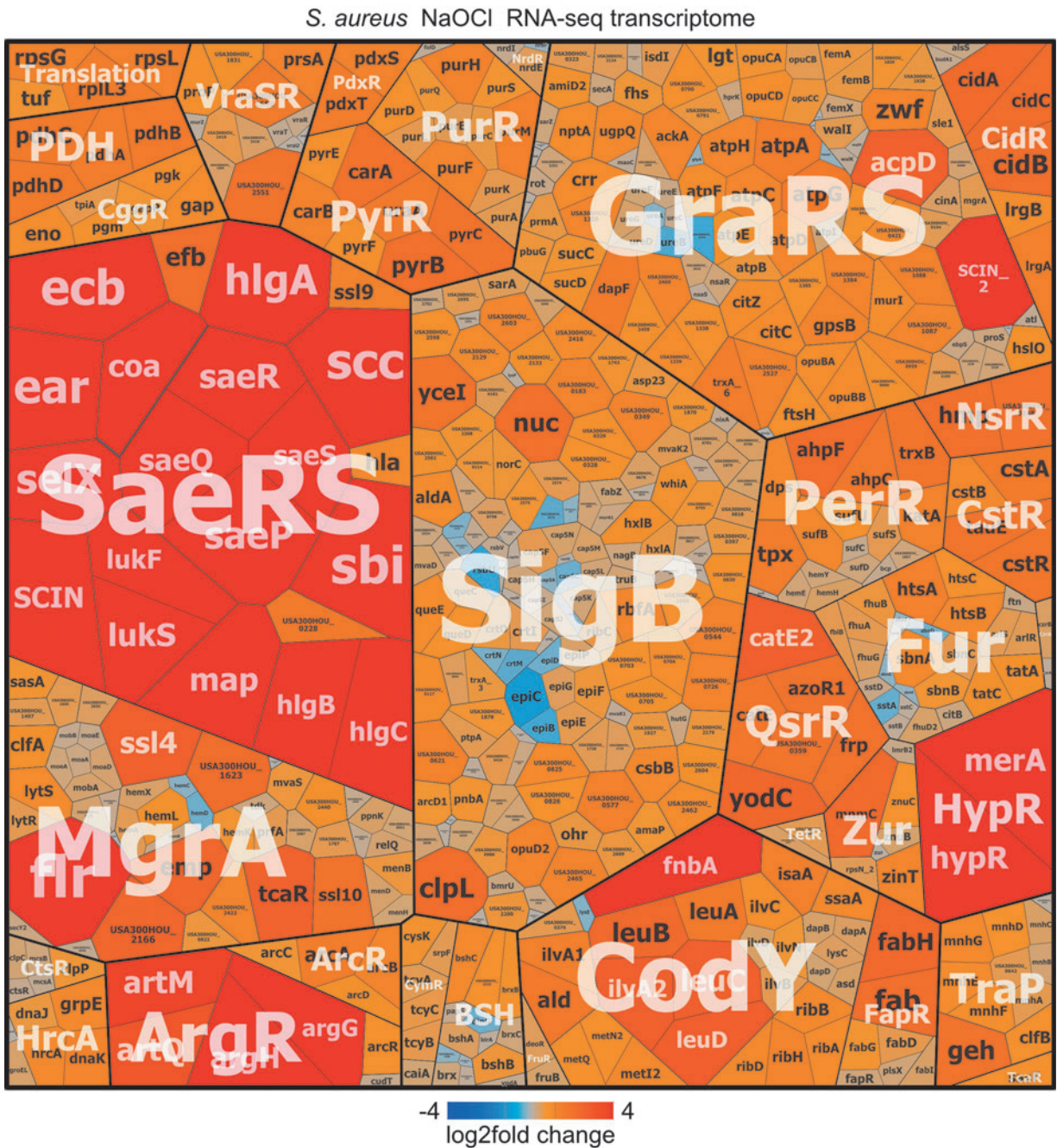


FIG. 2. The transcriptome treemap of *S. aureus* USA300 under NaOCl stress indicates an oxidative stress response and the strong upregulation of the HypR and SaeRS regulons. The transcriptome treemap shows the differential gene expression of *S. aureus* after exposure to 150 μ M NaOCl stress as log₂ fold changes (m-values). The genes are classified into operons and regulons based on the RegPrecise database (<http://regprecise.lbl.gov/RegPrecise/index.jsp>) and previous publications (61). Differential gene expression is visualized using a red-blue color code where red indicates log₂ fold induction and blue repression of transcription under NaOCl stress. The HypR and SaeRS regulons are most strongly upregulated under NaOCl stress in *S. aureus* USA300. The induction of the PerR, HrcA, SigmaB, and QsrR regulons reveals an oxidative stress response in *S. aureus*. The RNA-seq expression data of the selected highly transcribed genes after NaOCl stress and their regulon classifications are listed in Supplementary Table S2.

SaeRS-controlled virulence factors are essential for innate immune evasion since the survival of the *saeRS* mutant was impaired in neutrophil phagocytosis assays (92). Reduction of ROS production by SaeRS-regulated virulence factors inside neutrophils was recently shown as mechanism to avoid pathogen killing (37). Thus, the strong induction of the SaeRS

virulence regulon under NaOCl stress in our transcriptome is reflecting adaptation to infection conditions, such as neutrophil stress.

Among the genes involved in energy metabolism, the expression of the glycolytic *cggR-gap-pgk-tpiA-pgm-eno*-operon and the pyruvate dehydrogenase *pdhABCD* operon was two- to

fourfold elevated. Since the glycolytic Gap is the main thiol switch that is redox controlled and inhibited under NaOCl stress by *S*-bacillithiolation (46), the lack of energy production due to inhibited glycolysis could result in upregulation of the glycolysis enzymes. Furthermore, the two- to threefold induction of the ATP synthase *atpCDGAHFEB* operon under NaOCl stress may indicate ATP depletion. Of note is the further enhanced expression of the CodY regulon under NaOCl that includes the *ilv-leu* and *lysC-asd-dapABD* operons involved in leucine, isoleucine, and lysine biosynthesis, as well as the riboflavin biosynthesis *ribHBAED* operon. Increased demand of riboflavin might be caused by the requirement of flavin cofactors for thiol/disulfide reductases. Moreover, the ArgR regulon genes for biosynthesis of arginine and the ArcR-controlled arginine deiminase operon are strongly induced under NaOCl, which could indicate increased ammonium production to compensate for an acid stress response caused by NaOCl stress.

Most interesting was the 180-fold induction of the USA300HOU_0588-0587 operon under NaOCl treatment (Figs. 2 and 3). USA300HOU_0588 encodes for an uncharacterized Rrf2 family regulator, termed as HypR, and USA300HOU_0587 encodes for the flavin disulfide reductase (FDR) MerA. The strong expression of the *hypR-merA* operon was previously observed in *S. aureus* isolates during phagocytosis with polymorphonuclear leukocytes (PMNs or neutrophils) (91). Thus, our expression profile under NaOCl stress highly resembles that of infection conditions due to the production of ROS and RCS in activated neutrophils. Accordingly, HypR could specify a novel NaOCl-specific transcription factor and defense mechanism of *S. aureus* to avoid destruction by neutrophils. Thus, we studied the redox-sensing regulatory mechanism of HypR and the function of MerA in more detail under NaOCl stress conditions. For the detailed HypR functional analysis, we have

chosen *S. aureus* COL, which is our model strain for functional genomics, and protocols for genetic manipulation are best established in our laboratory for COL, which has less resistance determinants compared to USA300.

Northern blot analysis revealed the specific induction of the hypR-merA operon under NaOCl and diamide stress and its negative regulation by the Rrf2 family repressor HypR

We used Northern blot analysis to study the expression of the *hypR-merA* operon under different thiol-specific stress conditions in *S. aureus* COL, including 1 mM NaOCl, 2 mM diamide, 10 mM H₂O₂, 0.75 mM formaldehyde, and 0.5 mM methylglyoxal (Fig. 4A). These experiments were performed in RPMI medium, which resembles infection conditions and allows faster growth of *S. aureus*, but requires higher sublethal doses of 1 mM NaOCl. The strong upregulation of the *hypR-merA*-specific 1.8 kb mRNA under 1 mM NaOCl and 2 mM diamide stress was confirmed, but no significant increased transcription was found with 10 mM H₂O₂ and aldehyde stress. This indicates that the *hypR-merA* operon responds specifically to disulfide stress, but not to H₂O₂ and aldehydes in *S. aureus*.

Next, we studied the role of HypR in transcriptional regulation of the *hypR-merA* operon in *S. aureus* COL. Using the temperature-sensitive plasmid pMAD, a clean *hypR* deletion mutant was constructed lacking 364 bp of the *hypR* open reading frame. The truncated *hypR-merA* transcript of 1.5 kb (denoted as *TR-merA*) was constitutively expressed in the *hypR* deletion mutant under nonstress conditions, indicating full derepression of *hypR-merA* transcription (Fig. 4B). These results identify HypR as transcriptional repressor of the *hypR-merA* operon that is inactivated under disulfide stress conditions in *S. aureus*.

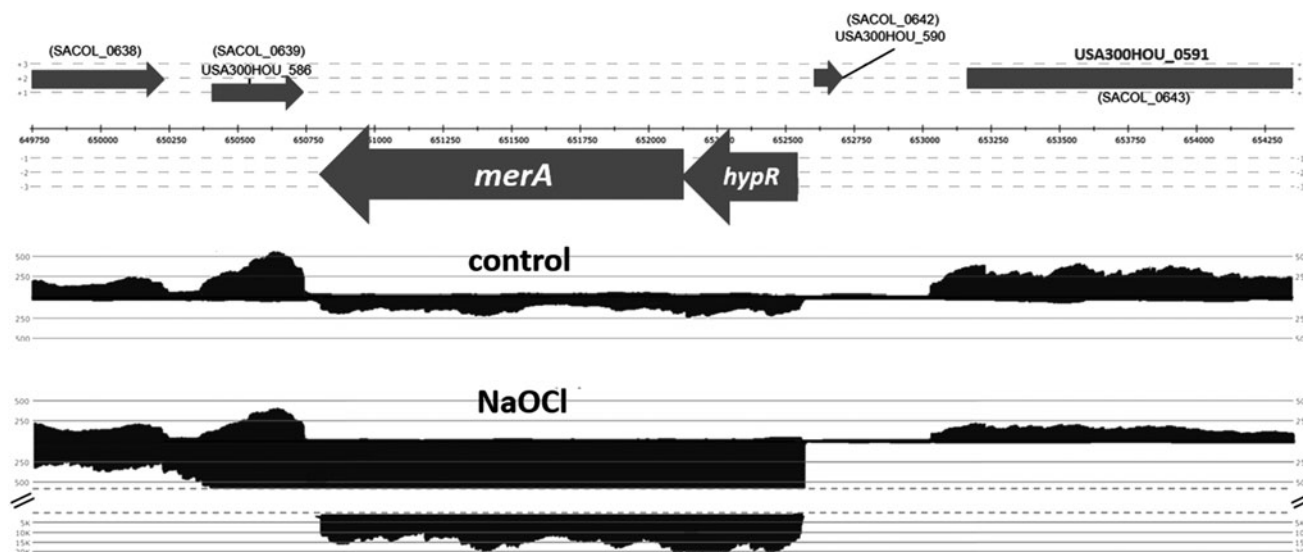


FIG. 3. The *hypR-merA*-operon is most strongly upregulated in the RNA-seq transcriptome of *S. aureus* USA300 under NaOCl stress. The mapped reads for the gene expression profile of the *hypR-merA* locus under control and NaOCl stress are shown as displayed using the Read-Explorer software. Transcription of the *hypR-merA*-operon is 180-fold induced under NaOCl stress in *S. aureus* USA300. The *hypR* gene encodes for an Rrf2 transcriptional regulator and *merA* encodes for a pyridine nucleotide disulfide reductase.

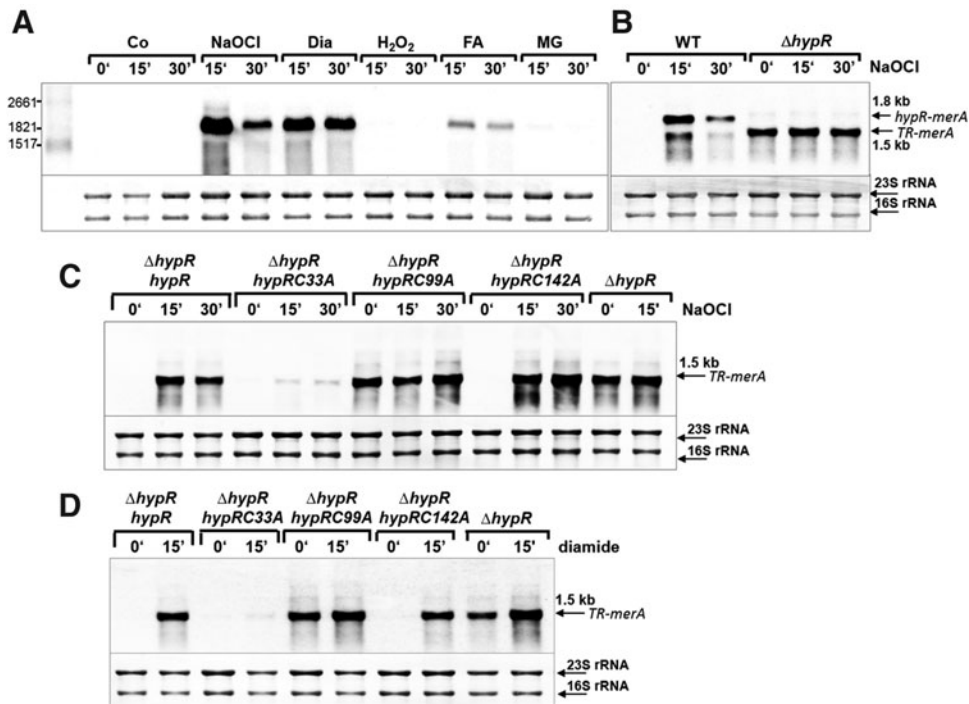


FIG. 4. Northern blot analysis of *hypR-merA* transcription in *S. aureus* COL under NaOCl, diamide, H₂O₂, and aldehyde stress and in *hypR* Cys-Ala mutants. (A) Northern blot analysis was performed using RNA isolated from *S. aureus* COL wild type before (co) and 15 and 30 min after exposure to 1 mM NaOCl, 2 mM diamide, 10 mM H₂O₂, 0.75 mM formaldehyde, and 0.5 mM methylglyoxal stress. (B) Transcription of the *hypR-merA* operon was analyzed in the COL wild-type and in the Δ *hypR* mutant under 1 mM NaOCl stress indicating strong derepression of *hypR-merA* transcription under control conditions in the absence of HypR. (C, D) Northern blot analysis of *hypR-merA* operon transcription in the Δ *hypR* deletion mutant and in Δ *hypR* mutants complemented with *hypR*, *hypRC33A*, *hypRC99A*, and *hypRC142A* before and 15 and 30 min after exposure to 1 mM NaOCl (C) or 2 mM diamide stress (D). The results indicate that Cys33 is required for redox sensing of HypR *in vivo*. For stress experiments, *S. aureus* cells were grown in RPMI medium and treated with thiol-reactive compounds at an OD₅₀₀ of 0.5. The arrows point toward the *hypR-merA* bicistronic mRNA (1.8 kb) in the wild type or the truncated *hypR-merA* transcript (*TR-merA*) (1.5 kb) in the *hypR* mutant. The methylene blue stain is the RNA loading control indicating the 16S and 23S rRNAs. OD₅₀₀, optical density at 500 nms.

Cys99 is required for HypR repressor activity and Cys33 and Cys99 are the NaOCl-sensing Cys residues in vivo

The HypR repressor belongs to the Rrf2 family that includes FeS cluster containing redox sensors for nitric oxide (NsrR) (23, 90, 98), and also SaiR of *B. anthracis* as the closest HypR homologue that does not contain an FeS cluster (68) (Fig. 5A). Three conserved Cys residues (Cys93, Cys99, and Cys105) and Asp8 are essential for FeS cluster coordination in NsrR (90), but only Cys99 is conserved in HypR and SaiR. Instead, HypR has two other Cys residues at the non-conserved positions 33 and 142. The crystal structure of the HypR and SaiR homologue YwnA of *B. subtilis* is available (PDB code 1xd7), which showed 23.5% sequence identity to HypR and shares also the conserved Cys97 (Fig. 5B). Based on the structure of YwnA as template, the HypR and SaiR structures were modeled with SWISS-MODEL (<https://swissmodel.expasy.org>) (10). The HypR structural model indicates that Cys33 is located in the turn between the α 2 and α 3 DNA recognition helices, while Cys99 is at the N-terminus of the long α 6 helix that forms the dimer interface (Fig. 5B). The position of Cys142 could not be modeled since the C-terminal α 8 helix is not present in the YwnA structure that was used as template.

To study the role of the three Cys residues for HypR repressor activity and redox sensing, we analyzed transcription of the *hypR-merA* operon in *hypRC33A*, *hypRC99A*, and *hypRC142A* mutants *in vivo*. The successful complementation of the *hypR* mutant using the pRB473-based expression of *hypR*, *hypRC33A*, *hypRC99A*, and *hypRC142A* under control, NaOCl and diamide stress was confirmed using Northern blots with a *hypR*-specific mRNA probe (Supplementary Fig. S1A, B). Additional Western blot analysis confirmed that the complemented strains expressed HypR, Cys33A, Cys99A, and Cys142A mutant proteins at the same protein levels (Supplementary Fig. S6A, B). Transcriptional analysis of *hypR-merA* expression revealed that the *hypRC33A* mutation did not affect the DNA binding activity of HypR, but impaired its redox sensing since transcription was abolished under NaOCl and diamide stress (Fig. 4C, D). In contrast, the *hypRC99A* mutant was impaired in DNA binding as shown by full derepression of the *hypR-merA* operon under control conditions. The *hypRC142A* mutant behaved similar as the wild type and was not impaired in DNA binding and redox sensing under NaOCl and diamide stress. In conclusion, our Northern blot results revealed that Cys33 is important for redox sensing under NaOCl and diamide stress and Cys99 is required for HypR repressor activity *in vivo*.

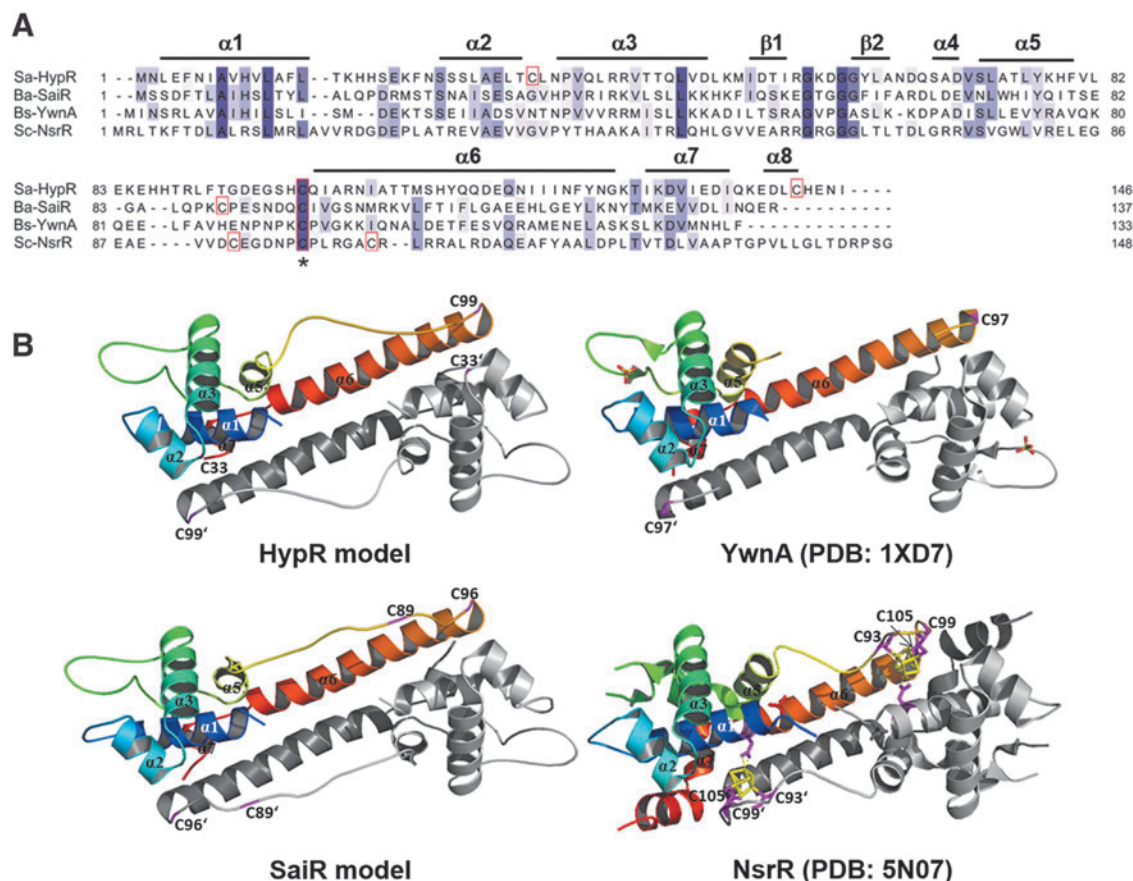


FIG. 5. Multiple protein sequence alignments of the Rrf2 regulators HypR, SaiR, YwnA, and NsrR (A) and structural modeling of HypR and SaiR in comparison to YwnA and NsrR (B). (A) The protein sequence alignment was performed with Clustal Ω 2 and is presented in Jalview. The following protein sequences were aligned and the % identity to HypR is given in parenthesis: HypR (SACOL0641) of *S. aureus* COL, SaiR (BAS3200) of *Bacillus anthracis* (20.4%), YwnA (P71036) of *Bacillus subtilis* (23.48%), and NsrR (Q9L132) of *Streptomyces coelicolor* (17.86%). Intensity of the blue color gradient is based on 50% sequence identity. The conserved Cys99 in HypR is labeled in red with an asterisk (*). (B) The structural models of HypR and SaiR were generated using SWISS-MODEL (<https://swissmodel.expasy.org/>) (10) and visualized with PyMOL using the template of *Bacillus subtilis* YwnA (1xd7) that showed 23.5% and 25.78% sequence identity to HypR and SaiR, respectively. For comparison, we show the structures of YwnA (1xd7) and NsrR (5no7) with labels for the conserved Cys97 in YwnA and the 3 FeS cluster coordinating Cys residues (Cys93, Cys99, and Cys105) in NsrR. The FeS cluster of NsrR is displayed in yellow. FeS, iron/sulfur.

HypR binds specifically to the hypR-merA operator and DNA binding is reversibly inhibited under NaOCl and diamide stress in vitro

The results above suggested that HypR binds directly to the *hypR-merA* promoter region and that Cys33 is the redox-sensing Cys residue that is oxidized under NaOCl and diamide stress. Rrf2 regulators are known to bind as homodimers to operator sequences with dyad symmetry (84). Based on the RNA-seq data, we used the MEME software to identify the putative promoter sequence and a conserved inverted repeat in the upstream region of the *hypR-merA* operon (Fig. 6A). The 12-3-12 bp inverted repeat sequence TAATTGTAACATA-N₃-CAGTTACAATTA was detected in the *hypR-merA* upstream region as possible HypR binding site that overlapped with the putative -10 region. Similar inverted repeats are characteristic as full-length binding sites for other Rrf2 regulators, such as SaiR, CymR, IscrR, and RsrR (67, 68, 82, 84). We searched for the conservation of the putative HypR operator sequence up-

stream of homologous *hypR-merA* operons in the genomes of other *Staphylococcus* species. The multiple-sequence alignment showed that the 12-3-12 bp inverted repeat sequence is highly conserved in the *hypR-merA* upstream promoter regions across *Staphylococci* (Fig. 6B).

To investigate whether HypR binds directly and specifically to the HypR operator sequence under reduced conditions with dithiothreitol (DTT), we used electrophoretic mobility shift assays (EMSA). The gel shift results revealed that purified reduced HypR protein binds with high affinity to the *hypR-merA* upstream region *in vitro* (Fig. 7A). To analyze the specific binding of HypR to the 12-3-12 inverted repeat sequence, we exchanged two nucleotides in each half of the inverted repeat by G-T and A-C (IR-m1 probe) or T-G and C-A (IR-m2 probe) and analyzed the DNA-binding activity of HypR to these mutated DNA probes (Supplementary Fig. S2). HypR was unable to bind to the mutated inverted repeats IR-m1 and IR-m2 *in vitro* supporting the specific binding of HypR to the identified operator sequence. Furthermore, HypR was also

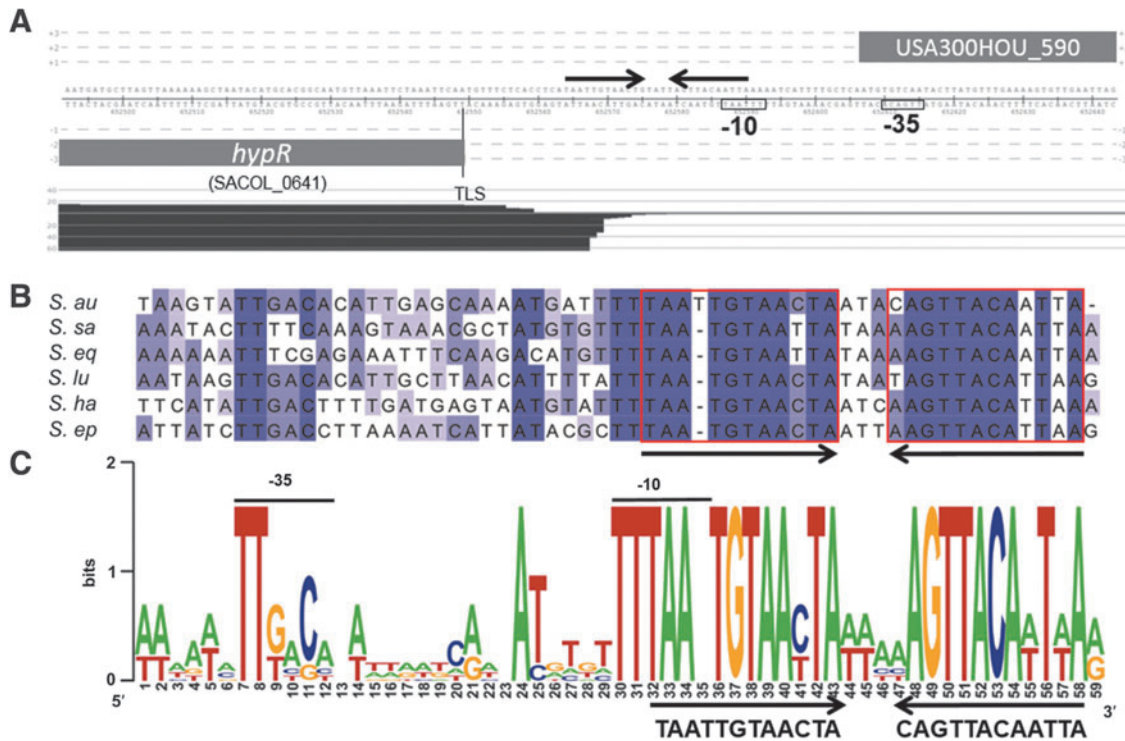


FIG. 6. Alignment of the *hypR-merA* upstream promoter regions with the 12-3-12 bp inverted repeat in *Staphylococcus* species. The upstream promoter region of the *hypR-merA* operon includes a 12-3-12 bp inverted repeat sequence that is highly conserved upstream of other *hypR-merA* homologues across *Staphylococci*, including *S. aureus* (SACOL0641), *Staphylococcus saprophyticus* (SSP2349), *Staphylococcus equorum* (SE1039_01590), *Staphylococcus lugdunensis* (SLGD_02231), *Staphylococcus haemolyticus* (SH2331), and *Staphylococcus epidermidis* (SE0366). (A) Upper panel shows the reads mapped for the *hypR-merA* transcript as visualized using ReadExplorer. The putative -10 and -35 promoter sequences are labeled and the 12-3-12 bp conserved inverted repeat is boxed and indicated by arrows. (B) All upstream promoter sequences of *hypR-merA* homologues were aligned using ClustalΩ2 and presented in Jalview. Intensity of the blue color gradient is based on 50% nucleotide sequence identity. (C) Bottom panel represents the 12-3-12 bp conserved inverted repeat created with WebLogo as HypR operator sequence.

unable to bind to nonspecific DNA probes (*trxA* and *RNAIII* genes) (Supplementary Fig. S2B).

Next, the effects of Cys-Ala mutations in Cys33, Cys99, and Cys142 on the DNA-binding activity of HypR were investigated using gel shift experiments. The reduced HypR-C33A and HypRC142A mutant proteins showed similar DNA-binding affinities compared with the HypR wild-type protein (Fig. 7A). However, the reduced HypRC99A and HypRC99S mutant proteins were unable to bind to the *hypR-merA* promoter, which confirms our *in vivo* results. Next, we analyzed the effect of thiol oxidation of the HypR, HypR-C33A, and HypRC142A proteins on DNA-binding activity *in vitro*. Treatment of HypR, HypRC33A, and HypRC142A mutant proteins with 1–20 μM NaOCl or 10–20 μM diamide resulted in their fast dissociation from the *hypR* operator DNA (Fig. 7B, C). This indicates that HypR as well as the HypRC33A and HypRC142A mutant proteins respond similar to NaOCl and diamide stress *in vitro*. The reduction of the oxidized HypR proteins with DTT restored the DNA-binding ability indicating that HypR responds to NaOCl stress by reversible thiol oxidation. The responsiveness of the HypR-C33A mutant to NaOCl stress *in vitro* is in contrast to lack of NaOCl response and *hypR-merA* transcription in the *hypR-C33A* mutant *in vivo*. Cys33 was identified as redox-sensing

Cys *in vivo*, but the C33A mutant was not impaired in redox sensing under NaOCl and diamide *in vitro*. It might be possible that the purified C33A mutant protein is oxidized to the “wrong” disulfides under disulfide stress *in vitro*, which are not stabilized inside *S. aureus*. In summary, our results show that HypR is a redox-sensing regulator that controls expression of the *hypR-merA* operon and is inactivated due to reversible thiol oxidation under NaOCl and diamide stress leading to release from the promoter DNA.

HypR responds to NaOCl and diamide stress by intermolecular disulfide formation that involves the redox-sensing Cys33 and Cys99

The EMSA results and Northern blots revealed that the DNA-binding activity of HypR is redox regulated by reversible thiol oxidation under NaOCl and diamide stress. Thus, we were interested to elucidate the thiol switch mechanism leading to release of HypR from the target DNA. HypR can be classified as 2-Cys-type redox regulator, such as OhrR from *Xanthomonas campestris* and YodB from *B. subtilis* that sense different thiol reactive compounds by intermolecular disulfide formation between the opposing subunits in the homodimer (2, 27, 43, 74). Thus, HypR most likely also senses and responds

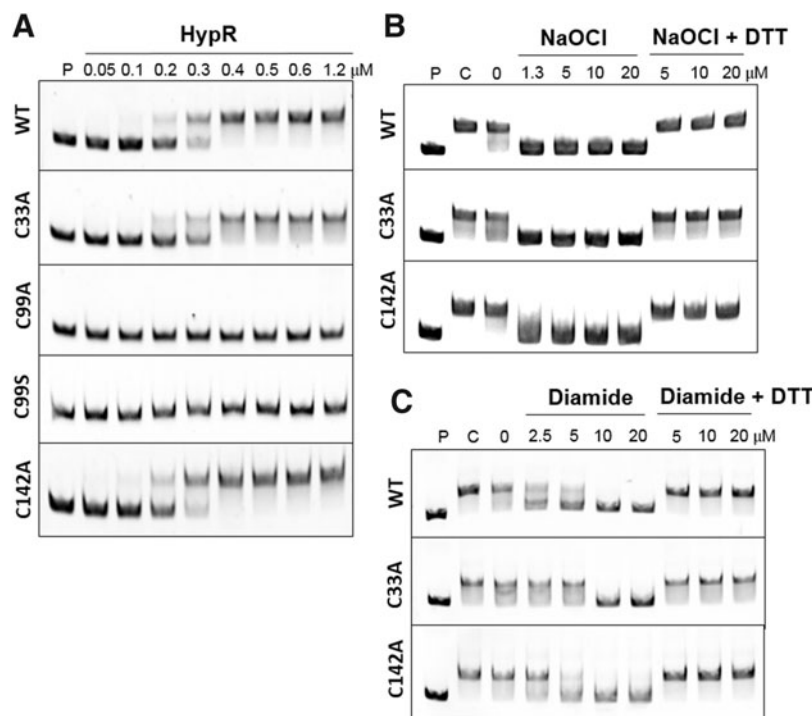


FIG. 7. DNA binding of HypR is inhibited by reversible thiol oxidation under NaOCl and diamide stress *in vitro* and the effect of HypR Cys mutations on DNA binding and redox sensing. (A) EMSAs were used to analyze the DNA-binding activity of purified HypR, HypRC33A, HypRC99A, and HypRC142A proteins to the *hypR-merA* upstream promoter region *in vitro*. Increasing concentrations (0.05–1.25 μM) of HypR were used in the DNA-binding reactions with 0.75 ng of template DNA ranging from –128 to +70 relative to the transcription start site of the *hypR-merA* operon. (B, C) DNA-binding activity of HypR, HypRC33A, and HypRC142A proteins was inhibited by 1.3–20 μM NaOCl (B) or 10–20 μM diamide (C) and could be restored with 1 mM DTT. This indicates that HypR resembles a redox-sensing regulator that is inactivated due to reversible thiol oxidation. The HypRC99A and HypRC99S mutants were unable to bind to the *hypR-merA* target promoter. “P” indicates the free probe, “C” is the HypR-DNA complex in the presence of DTT, and “0” indicates the control of HypR-DNA complex after DTT removal before exposure to NaOCl. DTT, dithiothreitol; EMSA, electrophoretic mobility shift assay.

to NaOCl *via* intersubunit disulfide bonds. Indeed, when we exposed purified HypR to NaOCl or diamide stress, it was quickly oxidized to the disulfide-linked dimer that migrates at the size of 35 kDa in the nonreducing SDS-PAGE (Fig. 8A and Supplementary Fig. S4A). The oxidation of HypR to the intersubunit disulfide was reversible with DTT as shown in the reducing SDS-PAGE (Supplementary Figs. S3A and S4C). Of note, two bands migrated closely together at the size of the HypR disulfide-linked dimer, labeled as 1 and 2 (Fig. 8A). We hypothesized that these two dimers harbor either one or two disulfide bonds between the opposing HypR subunits. The reversible oxidation to the intermolecular disulfide was also observed for the HypRC33A and HypRC142A mutant proteins under NaOCl and diamide stress, but not for the HypRC99A mutant (Fig. 8A, B, Supplementary Figs. S3 and S4). These results are in agreement with the *in vitro* DNA binding assays where the HypRC33A and HypRC142A mutants still responded to NaOCl and diamide stress leading to the relief of repression, while the HypRC99A mutant was impaired in DNA binding. However, the Cys33A mutant was less oxidized to intermolecular disulfides under diamide stress compared to NaOCl, supporting that Cys33 is required for disulfide formation. In conclusion, our results show that HypR is oxidized to intermolecular disulfides under NaOCl and diamide stress,

most likely involving Cys33 and Cys99 as the redox-sensing Cys residues *in vitro*.

We were interested to identify the Cys residues oxidized to the intermolecular disulfide in wild-type HypR under disulfide stress. The bands 1 and 2 of both oxidized HypR disulfides (Fig. 8A) were tryptic digested and subjected to matrix-assisted laser desorption ionization-time of flight mass spectrometry (MALDI-TOF-MS) (Fig. 9). In the overview MS1 scan, a peptide was identified with the size of 3522.74 Da corresponding to the size of the Cys33-SS-Cys99 intermolecular disulfide peptide (Fig. 9A). During fragmentation of this Cys33-SS-Cys99 peptide, the parent ion immediately disappeared and the disulfide bond fragmented into both single Cys33 and Cys99 peptides with the sizes of 1534.72 and 1992.90 Da (Fig. 9B). Moreover, fragment ions of both Cys peptides were observed without the sulfur and with the second sulfur atom that was engaged in the disulfide linkage in the parent ion. Thus, the fragmentation spectrum of this 3522.74 Da peptide is characteristic for the disulfide bond between the Cys33 and Cys99 peptides in oxidized wild-type HypR. Of note, the two oxidized HypR bands 1 and 2 in Figure 8A exhibited the same MS1 spectrum, supporting the idea of either one or two disulfide bonds between the HypR subunits (data not shown).

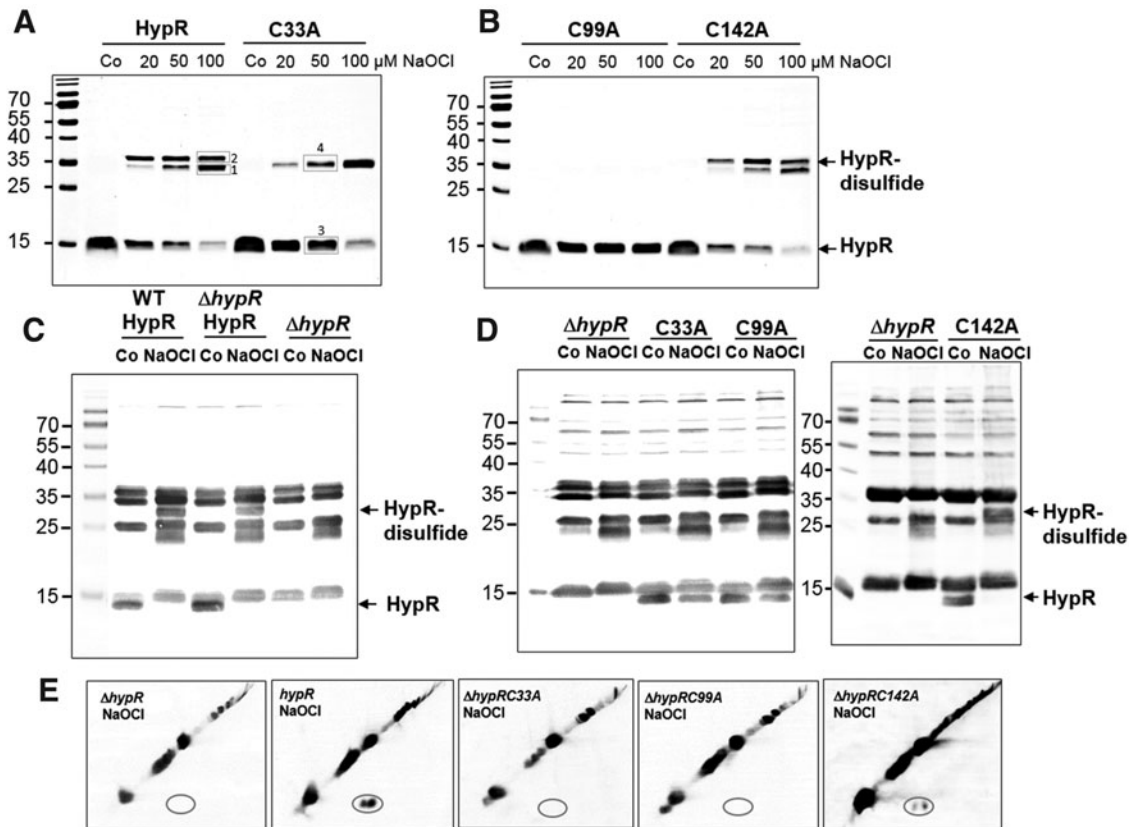


FIG. 8. HypR senses NaOCl stress by intermolecular disulfides, which requires Cys33 and Cys99 *in vitro* and *in vivo*. (A, B) The purified HypR wild-type and Cys mutant proteins were treated with increasing NaOCl concentrations *in vitro* and subjected to nonreducing SDS-PAGE analysis. The reduction of the HypR disulfides after DTT treatment is shown in the reducing SDS-PAGE analysis in Supplementary Figure S3. The HypR intermolecular disulfides (bands 1 and 2) were cut, tryptic digested, and subjected to MALDI-TOF MS/MS analysis as shown in Figure 9 to verify the Cys33-Cys99 disulfide. The bands of the C33A mutant protein that were used for tryptic digestion and MS are boxed and labeled with 3 and 4. The MALDI-TOF results of the C33A mutant tryptic peptides are shown in Supplementary Figure S5B. C. (C, D) For the analysis of HypR disulfides *in vivo*, we used *S. aureus* COL with plasmid pRB473-*hypR*, the Δ *hypR* deletion mutant and Δ *hypR* mutant strains complemented with *hypR*, *hypRC33A*, *hypRC99A*, and *hypRC142A*. *S. aureus* strains were exposed to NaOCl stress, alkylated with NEM, and protein extracts were subjected to nonreducing Western blot analysis using polyclonal rabbit anti-HypR antibodies. The reducing Western blot analysis of the HypR disulfides and loading controls is shown in Supplementary Figure S6. (E) Nonreducing/reducing diagonal SDS-PAGE and HypR-specific Western blot analysis of alkylated protein extracts were performed to verify the intersubunit disulfides for HypR and the HypR-C142A mutant protein under NaOCl stress *in vivo*, but not in the HypRC33A and HypRC99A mutants. Additional diagonal assays using the HypR immunoprecipitates are shown in Supplementary Figure S7. MALDI-TOF-MS, matrix-assisted laser desorption ionization-time of flight mass spectrometry.

In addition, we aimed to identify the disulfide crosslinked Cys residues in the Cys33A mutant that formed under NaOCl stress *in vitro* (Fig. 8A). MALDI-TOF-MS analysis revealed that Cys99 is fully reduced in the oxidized Cys33A mutant protein as shown by the iodoacetamide (IAM)-alkylated Cys99 peptide that was not detected in the oxidized HypR protein (Supplementary Fig. S5C, D). However, Cys142 could not be detected in the Cys33A mutant protein sample. These results suggest that HypR could be oxidized to the wrong Cys142-Cys142 disulfide that may crosslink two HypR dimers *in vitro*. The large peptide size of this putative Cys142-Cys142 disulfide peptide excludes detection by MS.

Next, we used nonreducing Western blot analysis with polyclonal HypR antibodies to confirm the intermolecular disulfides between Cys33 and Cys99 in HypR under NaOCl stress *in vivo*. Protein extracts were prepared from the *S.*

aureus COL wild type, the Δ *hypR* mutant, and the *hypR*, *hypRC33A*, *hypRC99A*, and *hypRC142A* complemented strains under control and NaOCl stress, and the redox state of HypR was analyzed using nonreducing Western blots (Fig. 8C, D). Unfortunately, the HypR polyclonal antibodies showed cross-reactivity with other proteins of *S. aureus* which could not be eliminated after preincubation of the antiserum with Western blots of the *hypR* mutant. However, the HypR specific bands could be clearly distinguished by using protein extracts from *hypR* mutant cells (Fig. 8C). The HypR protein was reduced in all controls of the *hypR*, *hypRC33A*, *hypRC99A*, and *hypRC142A* complemented strains (Fig. 8C, D). Under NaOCl stress, the oxidized HypR and HypRC142A mutant proteins migrated at the size of the intermolecular disulfide at 30 kDa, which was reversible with DTT as shown in the reducing SDS-PAGE (Supplementary

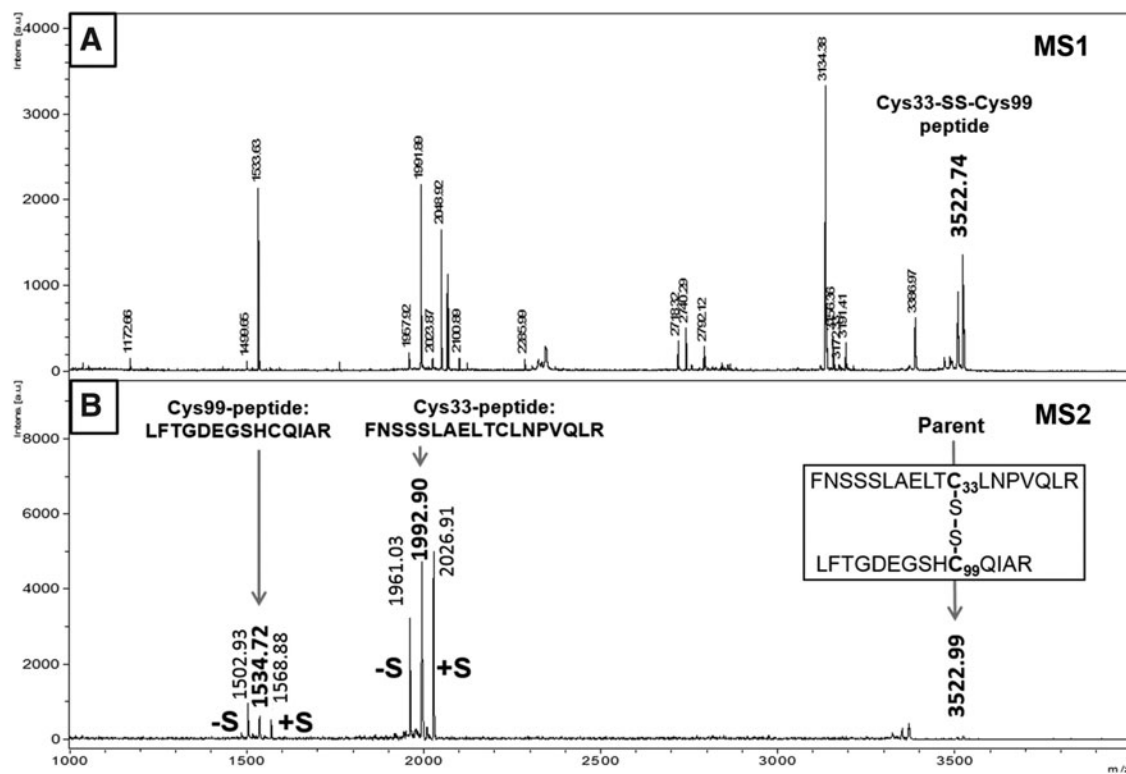


FIG. 9. HypR is oxidized to C33-C99' intermolecular disulfides *in vitro* as revealed by MALDI-TOF-TOF MS. The intermolecular disulfide band of the oxidized HypR wild-type protein of the SDS-PAGE in Figure 8A (band 1) was tryptic digested. The HypR peptides were measured by MALDI-TOF-TOF MS. (A) The *upper panel* indicates the MS1 overview scan of all peptides and (B) the *lower panel* shows the fragmentation of the C33-C99 disulfide peptide (3522.74 Da peak) into the Cys33 (1992.90 Da) and Cys99 peptides (1534.72 Da) in the MS2 scan. The parent ion of the disulfide peptide disappeared in the MS2 scan.

Fig. S6A, B). However, both Cys33A and Cys99A mutants did not form intermolecular disulfides under NaOCl exposure and failed to respond to NaOCl stress *in vivo* (Fig. 8D). These results are in agreement with the transcriptional data of *hypR-merA* expression and indicate that HypR responds to NaOCl stress by the formation of intersubunit disulfides between Cys33 and Cys99 *in vivo* and *in vitro*. To confirm the formation of the intermolecular disulfide in HypR and the involvement of Cys33 and Cys99 in the disulfide crosslink *in vivo*, diagonal nonreducing/reducing SDS-PAGE analyses were performed using the crude protein extracts and immunoprecipitated HypR. The diagonal assays clearly showed that HypR and the HypRC142A mutant protein migrate at the right side of the diagonal in NaOCl-treated cells indicating intermolecular disulfide formation *in vivo* (Fig. 8E). In contrast, no HypR intermolecular disulfide was detected in the HypRC33A and HypRC99A mutant proteins in the diagonal assays (Fig. 8E and Supplementary Fig. S7). These data reveal that Cys33 and Cys99 are the redox-sensing Cys residues of HypR, required for disulfide bond formation both *in vitro* and *in vivo*.

Analysis of the oligomerization states by size exclusion multiangle light scattering and circular dichroism spectroscopy of HypR and HypR Cys mutant proteins

Cys99 is located at the end of the long $\alpha 6$ helix that forms the dimer interface in the HypR structure (Fig. 5B). The

differences in the DNA-binding properties between HypR and the HypRC99A mutant protein raised the question whether the Cys99A mutation affects dimerization of HypR. Thus, we analyzed the oligomerization states of reduced HypR and HypR Cys-Ala mutant proteins using size exclusion chromatography/multiangle light scattering (SEC-MALS) (Supplementary Fig. S8). The results showed that all reduced proteins eluted mostly as dimers with a molecular weight of $\sim 32\text{--}34 \pm 2$ kDa. Due to the redox sensitivity of Cys33 and Cys99, we observed higher molecular weight oligomeric species with molecular masses ranging from 67 to 78 kDa. The oligomer amounts differed between each Cys mutant (15–17%) and might be related to disulfide crosslinks of two HypR dimers due to incomplete reduction of the proteins. Overall, the SEC-MALS results indicate that HypR and the three Cys-Ala mutant proteins are mostly present as dimers in solution.

Next, we used circular dichroism (CD) spectroscopy to compare the secondary structures between reduced HypR and the three Cys-Ala mutants to see whether the Cys99A mutation causes a conformational change. The far UV-CD spectra of HypR and the three Cys-Ala mutants revealed a significant α -helical content in all proteins (Supplementary Fig. S9). The calculation of secondary structure elements using the program DichroWeb (<http://dichroweb.cryst.bbk.ac.uk>) (86, 94) showed that reduced HypR and all three Cys-Ala mutants contain similar contents of α -helices (34–37%), β -sheets (11–13%), and β -turns (18–19%), confirming our

structural model (Fig. 5B). Thus, under reduced conditions, the dimerization and secondary structure elements of HypR are retained in all three HypR Cys-Ala mutant proteins.

HypR and MerA play important roles in the defense of S. aureus against NaOCl stress

Next, we analyzed the role of MerA in protection under NaOCl stress in *S. aureus* COL. MerA is annotated as nicotinamide adenine dinucleotide phosphate (NADPH)-dependent FDR, which contains an active site Cys43 in a highly conserved C₄₃XXXXC₄₈ motif (Supplementary Fig. S10) (4). The active site Cys43 of MerA was also predicted in the THIOREDOXOME database (30). We hypothesized that MerA could be involved in reduction of cellular disulfides formed under oxidative stress and infection conditions. Thus, we analyzed the growth and survival of the *S. aureus merA* and *hypR* mutants and the complemented strains under NaOCl stress. The growth of the *merA* mutant was significantly impaired under sublethal 1.5 mM NaOCl treatment in RPMI medium indicating that the *merA* mutant is more sensitive compared with the wild type (Fig. 10A). The NaOCl-sensitive growth defect of the *merA* mutant could be restored after complementation with *merA* expressed from plasmid pRB473 (Fig. 10B), but not when the active site Cys43 of MerA was replaced by a serine. This indicates that MerA confers resistance to NaOCl and likely functions as defense mechanism under infection conditions in *S. aureus*. However, the *hypR* mutant was also slightly more sensitive to 1.75 mM NaOCl

stress compared with the wild type suggesting that constitutive MerA expression does not confer a resistance phenotype (Fig. 10C, D).

We further studied the survival of the *merA* and *hypR* mutants and their complemented strains under NaOCl stress. Both *merA* and *hypR* mutants were impaired in their survival after exposure to lethal concentrations of 3.5 mM NaOCl (Fig. 11). The survival defect of the *merA* and *hypR* mutants could be restored back to wild-type level after complementation with *merA* and *hypR*, respectively. In agreement with the growth curves, Cys43 of MerA was important for the function of MerA in the NaOCl stress defense in the survival assay. Moreover, the role of Cys33 for redox sensing of HypR was confirmed also in our survival phenotype assays.

MerA and HypR are important for the survival of S. aureus in macrophage infection assays

Since the *hypR-merA* operon was most strongly induced in infection assays (91), we determined the survival of *merA* and *hypR* mutants inside murine macrophages in phagocytosis assays using the cell line J-774A.1. The macrophages were infected with *S. aureus* wild-type and mutant strains and the uptake of bacteria was stopped after 1 h with gentamycin to kill extracellular bacteria. The colony forming units (CFUs) of intracellular *S. aureus* were determined after 2, 4, and 24 h postinfection by plating serial dilutions of the host cell lysates.

After 4 h of infection, the CFUs of intracellular *S. aureus* cells were determined as approximately 10⁶ cells for the wild-

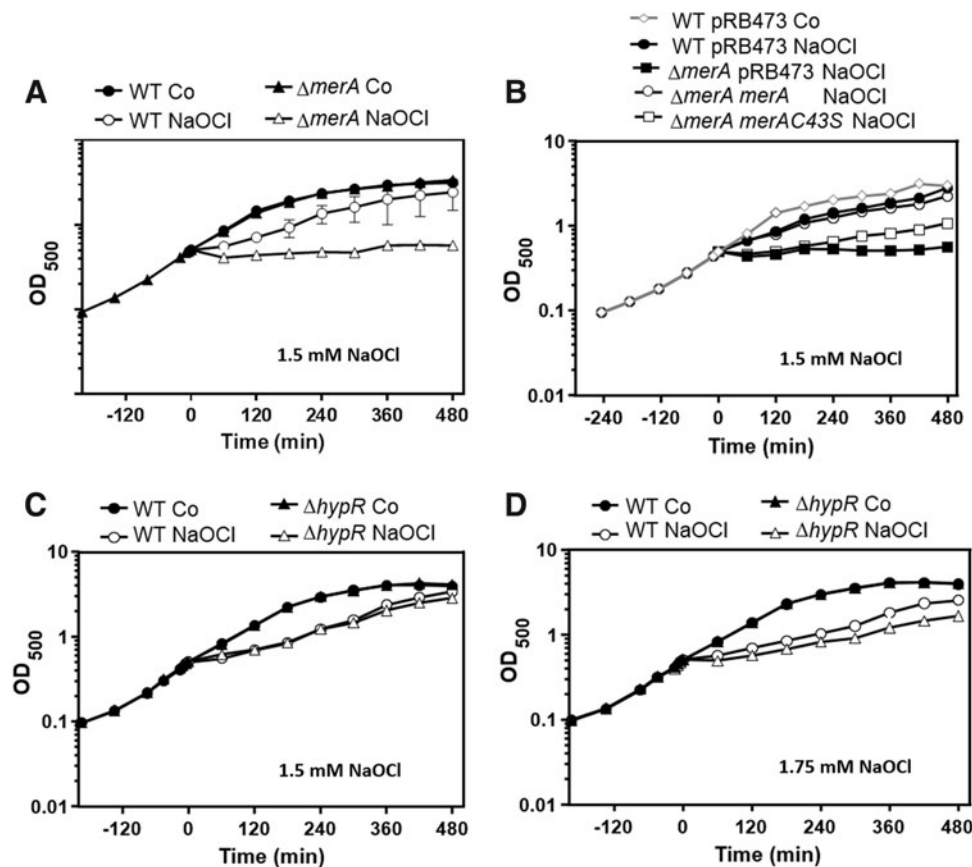


FIG. 10. The flavin disulfide reductase MerA is involved in the defense of *S. aureus* against hypochlorite stress. Growth phenotype analyses of the *S. aureus* wild-type (WT), the $\Delta merA$ mutant (A), the *merA* and *merAC43S* complemented $\Delta merA$ mutant strains (B) and the *hypR* mutant (C, D) before and after exposure to sublethal concentrations of 1.5 and 1.75 mM NaOCl stress at an OD₅₀₀ of 0.5. The NaOCl-sensitive growth phenotype of the *merA* mutant could be restored by complementation with plasmid-encoded *merA* and requires Cys43 in the MerA-active site. The results are from four biological replicate experiments. MerA, mercuric ion reductase.

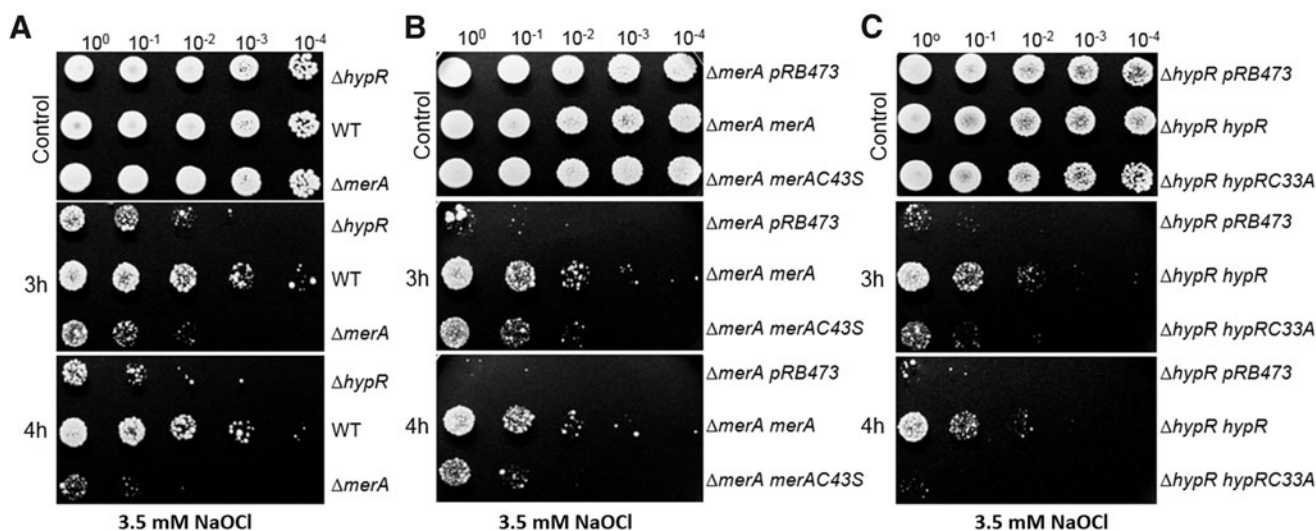


FIG. 11. MerA and HypR are both required for NaOCl stress survival in *S. aureus*. *S. aureus* COL wild-type (WT), $\Delta hypR$ and $\Delta merA$ mutants (A), and their complemented strains and Cys mutants ($\Delta merA merA$, $\Delta merA merAC43S$, $\Delta hypR hypR$, $\Delta hypR hypRC33A$) (B, C) were grown in RPMI until an OD₅₀₀ of 0.5 and treated with 3.5 mM NaOCl. Survival assays were performed by spotting 10 μ l of serial dilutions after 3 and 4 h of NaOCl exposure onto LB agar plates. The active site Cys43 of MerA and the redox-sensing Cys33 of HypR are important for NaOCl stress survival.

type, *hypR*, and *merA* mutants. However, 24 h after phagocytosis, the viable counts of intracellular *S. aureus* cells were decreased to 22.8% for the wild-type mutant and to 11.2% and 13.4% for the *hypR* and *merA* mutants, respectively (Fig. 12A). This indicates that *merA* and *hypR* mutants showed 40% and 50% decreased survival inside macrophages compared with the wild type after 24 h postinfection (Fig. 12C). This survival phenotype could be restored to 75–86% of wild-type level in both mutants after complementation with plasmid-encoded *hypR* and *merA*, respectively (Fig. 12B). These observations strongly indicate that MerA is required for the protection of *S. aureus* against the host innate immune defense under infection conditions. However, our results also show that constitutive expression of MerA in the *hypR* mutant does not increase intramacrophage survival. In conclusion, our *in vitro* growth and survival assays under NaOCl stress and the macrophage infection assays support that MerA is a major NaOCl defense mechanism enhancing survival of *S. aureus* in infection assays.

Discussion

During infections, *S. aureus* has to cope with the oxidative burst of activated macrophages and neutrophils, requiring a complex regulatory network of virulence and antibiotic regulators, for example, of the SarA/MarR family that senses ROS, RES, and RCS (8, 17, 43). However, the redox-sensing mechanisms of *S. aureus* in response to strong bactericidal oxidants, such as hypochloric acid, are largely unknown. It is of utmost importance to understand the mechanisms of intracellular survival of *S. aureus* inside macrophages and neutrophils and the escape from destruction by oxidants to discover new drug targets to combat emerging drug-resistant *S. aureus* infections.

In this work, we have characterized the novel NaOCl-sensing transcription regulator HypR that belongs to the widely distributed Rrf2 family and controls the NADPH-

dependent FDR MerA in *S. aureus*. The *hypR-merA* operon was previously highly induced during phagocytosis with neutrophils (91). In this work, we have used a global RNA-seq analysis and identified the *hypR-merA* operon as most strongly upregulated under NaOCl stress. Detailed Northern blot analysis revealed that NaOCl and diamide stress specifically upregulates the *hypR-merA* operon, while sublethal concentrations of H₂O₂ and aldehydes do not lead to significant induction. Thus, HypR responds strongly to disulfide stress, but not to H₂O₂ and RES *via* intermolecular disulfide formation between Cys33 and Cys99. The sensitivity of *S. aureus* HypR to disulfide stress resembles the redox-sensing mechanisms of the MarR family regulators HypR and OhrR characterized in *B. subtilis* (20, 32, 73) and of the TetR family regulator NemR from *Escherichia coli* (35, 36). These thiol-based regulators sense HOCl, diamide, organic hydroperoxides, or electrophiles, such as N-ethylmaleimide (NEM) and methylglyoxal, and provide protection under HOCl stress. Since diamide is a very unspecific oxidant (49) that is not physiological relevant for *S. aureus*, we regard the Rrf2 regulator HypR as the most specific hypochlorite defense mechanism for *S. aureus*.

Some Rrf2 family transcriptional regulators contain FeS clusters, such as NsrR (23, 90, 98) and IcsR (82, 83), while others do not, such as CymR (28, 47, 84) and the HypR homolog SaiR of *B. anthracis* (68). NsrR and IcsR coordinate [4Fe-4S] clusters with three conserved Cys residues (Cys93, Cys99, and Cys106 in Sc-NsrR) present in the C-terminal domain (Fig. 5A, B) (90). However, only Cys99 in this C-terminal domain is conserved in HypR, while two other Cys residues are located in nonconserved positions at Cys33 and Cys142 (Fig. 5A). Our results support a model that HypR senses and responds to NaOCl stress by intersubunit disulfide bond formation between Cys33 and Cys99 of the opposing subunits of the HypR dimer *in vivo* (Fig. 13). HypR oxidation leads to inactivation of its repressor function and upregulation of the FDR MerA. Thus, the *S. aureus* HypR repressor

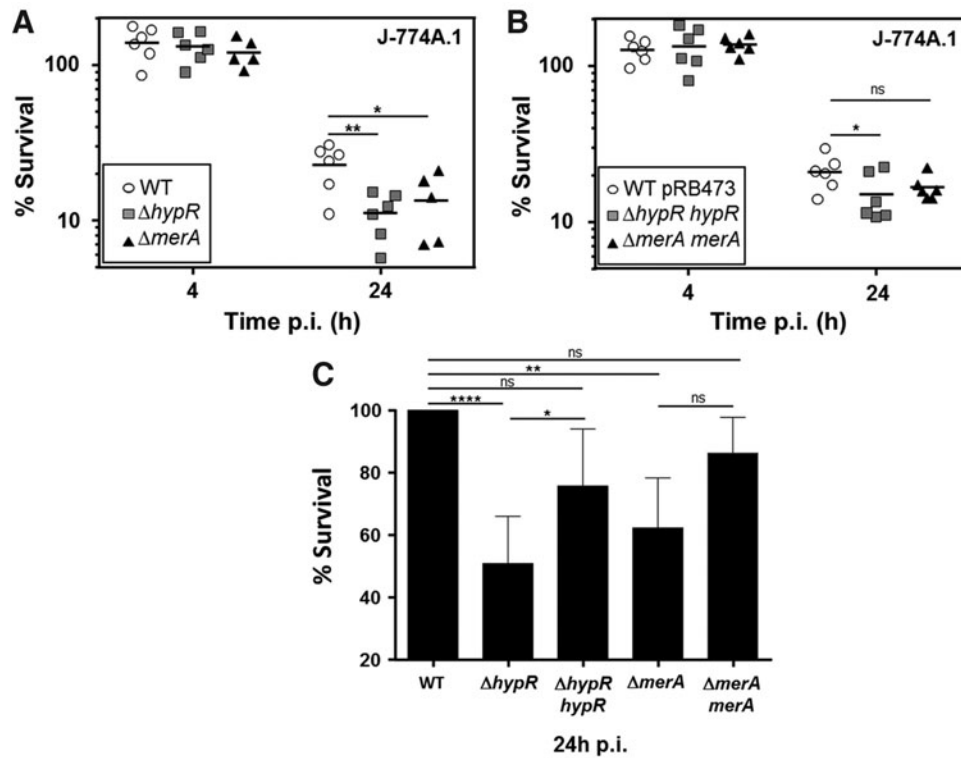


FIG. 12. MerA and HypR are required for survival of *S. aureus* COL in murine macrophages. The survival of *S. aureus* strains was analyzed 2, 4, and 24 h postinfection (p.i.) of the murine macrophage cell line J-774A.1 and the CFUs were determined. (A, B) The percentages in survival of the $\Delta hypR$ and $\Delta merA$ mutants and complemented strains were calculated in 5–6 biological replicate experiments and the survival at the 2-h time point was set to 100%. (C) The average percentage in survival was calculated for each mutant and complemented strain in relation to the wild type (WT), which was set to 100%. Results of 5–6 biological replicates are presented as scatter dots in (A, B) and mean values of percentage survival in comparison to the wild type (C). Error bars represent the SEM and the statistics was calculated using one-way ANOVA and Tukey's multiple comparisons *post hoc* test using the GraphPad Prism software. The *p*-values were determined as follows for the scatter dots (A, B): $p=0.0078$ for WT/ $\Delta hypR$; $p=0.0303$ for WT/ $\Delta merA$; $p=0.0461$ for WTpRB473/ $\Delta hypR hypR$; and $p=0.1234$ for WTpRB473/ $\Delta merA merA$. For the percentage survival (C), the *p*-values were determined as follows: $p<0.0001$ for WT/ $\Delta hypR$, $p=0.0012$ for WT/ $\Delta merA$, $p=0.0511$ for WTpRB473/ $\Delta hypR hypR$, $p=0.4684$ for WTpRB473/ $\Delta merA merA$, $p=0.0459$ for $\Delta hypR/\Delta hypR hypR$, and $p=0.0725$ for $\Delta merA/\Delta merA merA$. Symbols are defined as follows: $^{ns}p>0.05$; $^{*}p\leq 0.05$; $^{**}p\leq 0.01$; and $^{****}p\leq 0.0001$. CFU, colony-forming unit.

can be classified as typical two-Cys-type regulator since its mechanism of repressor inactivation resembles that of the two-Cys-type MarR/DUF24 family repressors HypR and YodB of *B. subtilis* that are redox sensors of NaOCl, diamide, and quinones and inactivated *via* intersubunit disulfide formation (18, 73). The NemR repressor of *E. coli* was shown to sense HOCl and electrophiles, such as NEM and methylglyoxal, by intermolecular disulfide as well as sulfenamide formation (34, 36, 50, 72). Thiol oxidation of these repressors leads to conformational changes and dissociation of the repressors from their operator sites leading to derepression of their target genes.

The structural changes on oxidation have been first studied for the 2-Cys-type MarR/OhrR repressor of *Xanthomonas campestris* that senses organic hydroperoxides by Cys22-Cys127 intersubunit disulfide formation (51). OhrR oxidation breaks a conserved Cys22 hydrogen-bonding network and causes large structural rearrangements in the dimer interface and rigid body rotation of the DNA-binding domains causing dissociation from the DNA (51). Using mutational analysis, we showed that Cys33 and Cys99 of the

S. aureus HypR repressor are important for redox sensing of NaOCl and diamide stress *in vivo*, while Cys99 is required for repressor activity of HypR. Both Cys33 and Cys99 mutants did not form intermolecular disulfides *in vivo* as shown by nonreducing SDS-PAGE analysis. These results clearly support the two-Cys-type oxidation model of HypR for Cys33-Cys99 intermolecular disulfide bond formation. Thus, both Cys33 and Cys99 are required for redox sensing of NaOCl and are oxidized to the intersubunit disulfide *in vitro* and *in vivo*.

In comparison to other Rrf2 transcription factors, HypR shows the highest sequence identity to SaiR of *B. anthracis* (20.4%) and YwnA of *B. subtilis* (23.5%) (Fig. 5A). Moreover, HypR and SaiR show common responses to disulfide stress (diamide, NaOCl) and in infection assays inside macrophages in *B. anthracis* and *S. aureus* (9, 68). YwnA also responds to diamide stress (71) and probably controls the adjacent *ywnB* gene encoding for an NADPH-binding reductase. SaiR of *B. anthracis* may play a related role like HypR of *S. aureus* in the protection against oxidative burst of activated macrophages and neutrophils under infection

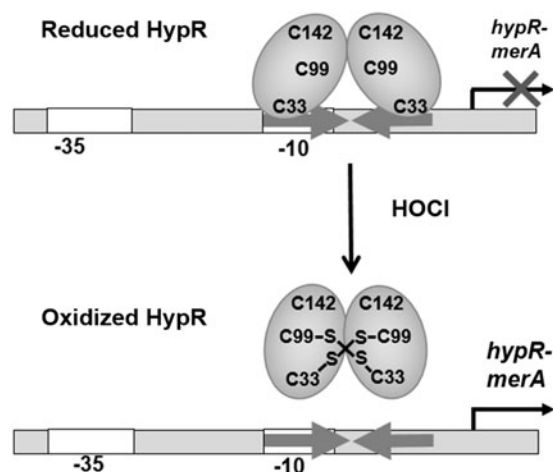


FIG. 13. Redox-sensing mechanism of HypR under hypochlorite stress during infection conditions in *S. aureus*. HypR controls the flavin disulfide reductase MerA, essential for growth and survival under hypochlorite stress and in macrophage infection assays in *S. aureus*. Cys33 and Cys99 of HypR are required for redox sensing *in vivo*. Under NaOCl stress, HypR is oxidized to Cys33-Cys99 intersubunit disulfides leading to derepression of *hypR-merA* transcription.

conditions. SaiR controls a five-gene operon that includes *spxA2*, *saiR*, and 3 unknown function genes (68). SpxA2 is a member of the ArsC (arsenate reductase) family that responds to NaOCl and diamide stress by thiol oxidation and interacts with the α -C-terminal domain of the RNA polymerase to activate transcription of a large disulfide stress regulon (69, 70, 99). SpxA2 together with its paralogue SpxA1 was shown to be required for diamide resistance and the *saiR* mutant conferred a peroxide-resistant phenotype (6, 68). Thus, SaiR of *B. anthracis* and HypR of *S. aureus* both confer protection under oxidative stress conditions in these pathogens *via* control of SpxA2 and MerA, respectively.

SaiR and HypR both share the conserved Cys96 and Cys99, respectively, which is required for repressor activity *in vitro* and *in vivo* as well as for redox sensing *in vitro* (68). To explain, why Cys99 is required for DNA binding, the HypR structure was modeled based on the template of *B. subtilis* YwnA (1xd7) (Fig. 5A, B). The structural model suggests that Cys33 is located in the turn between the DNA recognition $\alpha 2$ and $\alpha 3$ helices, while the conserved Cys99 is at the N-terminus of the long $\alpha 6$ helix that forms the highly hydrophobic dimer interface required for the elongated fold of Rrf2 family regulators (Fig. 5B). Recently, the structure of *Streptomyces coelicolor* NsrR was resolved with its [4Fe-4S] cluster in comparison to the three-Cys-Ala (3CA) mutant (90). Interestingly, the FeS cluster ligand Cys99 is in close proximity to Gly37 of the $\alpha 3$ DNA recognition helix of the opposing subunit. In holo-NsrR, Gly37 forms a hydrogen bond with Asn97, which is interrupted in the 3CA mutant resulting in a shift of the $\alpha 3$ DNA binding helix (90). Gly37 of NsrR is the counterpart of Cys33 in HypR, suggesting that the Cys99A mutant also could break hydrogen bonds of Cys33 leading to structural changes in the DNA-binding helices. This is supported by our mutational results since the C99A and Cys99S mutants are unable to bind DNA both *in vitro* and *in vivo*. The possible proximity of Cys33 and Cys99 in the structural model (based

on the YwnA template) (Fig. 5B) further explains that both are involved in redox sensing of NaOCl and well positioned to form intersubunit disulfides as we confirmed by MS.

Our CD results further showed that HypR contains the predicted high α -helical content. However, we could not show major structural changes in the secondary structure elements between HypR and the three Cys-Ala mutants. It will be interesting to further investigate the crystal structures of reduced and oxidized HypR proteins and the structural changes of the DNA-binding helices on oxidation.

Our gel shift assays and nonreducing SDS-PAGE and Western blot results further revealed that the Cys33 mutant was impaired in redox sensing *in vivo*, but still responsive to NaOCl and diamide stress *in vitro*. However, compared to the wild type HypR protein, the Cys33A mutant showed a lower oxidation under diamide stress in the nonreducing SDS-PAGE *in vitro*. Since we could only detect reduced (alkylated) Cys99 and not the Cys142 peptide in the mass spectrum of the intersubunit disulfide of the Cys33A mutant, the Cys33 mutant protein should be oxidized to the “wrong” “Cys142-Cys142” intersubunit disulfides, crosslinking two HypR dimers *in vitro* that also lead to HypR inactivation. However, this alternative oxidation was not observed *in vivo*, and thus, Cys33-Cys99 intersubunit disulfide formation is the physiologically relevant HOCl-sensing mechanism of HypR. Exposure of the purified Cys33 mutant protein to low doses of NaOCl stress might have much stronger effects *in vitro* and this wrong disulfide might be not stabilized *in vivo*.

Another unanswered question is why *merA* and *hypR* mutants display both sensitivity to NaOCl stress and macrophage infections, significant phenotypes that could be restored by complementation with MerA and HypR. Our unpublished RNA-seq data of the wild-type and the *hypR* mutant identified only the *hypR-merA* operon as upregulated in the *hypR* mutant. Thus, the deficiency of MerA impaired the growth and survival under infections, and also its constitutive overproduction did not confer resistance. It might be possible that overproduction of MerA causes deficiency in the NADPH level, causing in turn a redox poise. The transcriptional results revealed a very low basal level of *hypR-merA* expression indicating that MerA expression is tightly regulated and its constitutive overexpression perhaps toxic for *S. aureus* explaining the NaOCl-sensitive phenotype of the *hypR* mutant.

However, our results clearly identify the NADPH-dependent disulfide reductase MerA as the major HOCl-defense mechanism of *S. aureus*. MerA also enhances the survival of *S. aureus* in J774A.1 murine macrophages during infection assays. The J774A.1 cell line was shown to produce NADPH oxidase and MPO during infections and on activation by drug treatment *in vitro* (55, 65). Increased ROS levels significantly contributed to the antimicrobial activity and killing of intracellular pathogens by the J774A.1 macrophage cell line (54). Thus, MerA could be involved in the defense of *S. aureus* against ROS and HOCl also during macrophage infections. Of note, there is a striking 49.2% sequence identity between MerA of *S. aureus* and the FDR RclA of *E. coli* that is controlled by the RCS-specific transcriptional activator RclR (75) (Supplementary Fig. S10). These conserved flavoenzymes may function as major defense mechanisms under hypochlorite stress in bacteria and are controlled by different redox regulators, the Rrf2 repressor HypR in *S. aureus* and the AraC activator RclR in *E. coli* (75).

MerA is annotated as mercuric reductase, but it lacks the auxiliary C-terminal Cys residues that are important for Hg(II) reduction to elemental Hg⁰ in mercuric ion reductases (4, 63, 64). Instead, MerA belongs to group-I FDR that uses a redox-active disulfide in the highly conserved C₄₃XXXXC₄₈ motif to transfer electrons from NADPH via an FAD cofactor to an unknown disulfide substrate (4). Our results have shown that the MerA-active site Cys43 is important for NaOCl survival since the *merAC43S* mutant was unable to complement the NaOCl-sensitive phenotype of the *merA* mutant. The group-I FDR enzymes with known structures include glutathione disulfide reductase (Gor), thioredoxin reductase (TrxR), and mycothiol disulfide reductase (Mtr). We speculate that MerA could be involved in reduction of cellular LMW thiol/disulfides, such as oxidized bacillithiol disulfide (BSSB) or oxidized coenzymeA disulfide (CoAS2), that are increased under NaOCl stress. Our previous results showed an increased BSH redox potential using the genetically encoded Bacilliredoxin-redox-sensitive green fluorescent protein biosensor (58) and increased protein thiol oxidation under NaOCl stress in *S. aureus* indicating an increased BSSB level (46). Thus, it could be possible that MerA helps to reduce BSSB and CoAS2 to restore the redox balance. On the contrary, expression of MerA and HypR is coregulated, suggesting that both could constitute a redox couple and MerA could be involved in HypR reduction to regenerate the DNA-binding activity of HypR during recovery from HOCl stress. Our future studies are directed to identify the physiological disulfide substrate of MerA to understand the important role of this flavoenzyme in the defense against oxidative burst under macrophage and neutrophil infections.

Experimental procedures

Bacterial strains, growth, and survival assays. Bacterial strains, plasmids, and primers are listed in Supplementary Tables S3–S5. For cloning and genetic manipulation, *E. coli* was cultivated in Luria Bertani (LB) medium. For stress experiments, *S. aureus* USA300 and COL strains were cultivated in LB, RPMI, or BMM as described previously (58). Depending on the growth medium, different concentrations of NaOCl were applied due to the quenching effect of rich medium components, which affected the effective sublethal NaOCl doses. Thus, we applied sublethal 150 μ M NaOCl in BMM as described before (58) for RNA-seq analysis and 1–1.75 mM sublethal NaOCl in rich RPMI medium to analyze the expression and growth phenotype. For survival phenotype assays, *S. aureus* was grown in RPMI medium until an optical density at 500 nm (OD₅₀₀) of 0.5, exposed to a lethal dose of 3.5 mM NaOCl for 2–4 h, and 10 μ l of serial dilutions were spotted onto LB agar plates for 24 h. Complemented mutants that carried the pRB473 plasmid were grown in the presence of 1% xylose and 10 μ g/ml chloramphenicol. Sodium hypochlorite, diamide, DTT, Tris(2-carboxyethyl)phosphine (TCEP), H₂O₂ (35% w/v), formaldehyde, and methylglyoxal were purchased from Sigma Aldrich.

RNA isolation, library preparation, and next-generation cDNA sequencing. *S. aureus* USA300 was cultivated in BMM and treated with 150 μ M NaOCl stress as described previously (58). *S. aureus* cells were harvested before (as untreated

control) and 30 min after exposure to 150 μ M NaOCl and disrupted in 3 mM ethylenediaminetetraacetic acid (EDTA)/200 mM NaCl lysis buffer with a Precellys24 ribolyzer. RNA isolation was performed using the acid phenol extraction protocol as described (19). The RNA quality was checked by Trinean Xpose (Gentbrugge, Belgium) and the Agilent RNA Nano 6000 kit using an Agilent 2100 Bioanalyzer (Agilent Technologies, Böblingen, Germany). Ribo-Zero rRNA Removal Kit (Bacteria) from Illumina (San Diego, CA) was used to remove the rRNA. TruSeq Stranded mRNA Library Prep Kit from Illumina was applied to prepare the cDNA libraries. The cDNAs were sequenced paired end on an Illumina HiSeq 1500 and MiSeq system (San Diego, CA) using 50 and 70 bp read length. The transcriptome sequencing raw data files are available in the ArrayExpress database (www.ebi.ac.uk/arrayexpress) under accession number: E-MTAB-5666.

Bioinformatics data analysis, read mapping, data visualization, and analysis of differential gene expression. Trimmed reads (26 nt) were mapped to the *S. aureus* USA300_TCH1516 genome sequence (accession number CP000730) (41) using SARUMAN (11), allowing one error per read. The forward and reverse reads, if both present and with a maximum distance of 1 kb, were combined to one read containing the reference sequence as insert. Paired mappings with a distance >1 kb were discarded, and paired reads with either only the forward or the reverse read mapping were retained as single mapping reads. For the visualization and counting of short read alignments, ReadXplorer v2.2 (42) was used.

Differential gene expression analysis, including normalization, was performed using Bioconductor package DESeq2 (59) included in the ReadXplorer v2.2 software (42). The signal intensity value (*a*-value) was calculated by log₂ mean of normalized read counts and the signal intensity ratio (*m*-value) by log₂ fold change. The evaluation of the differential RNA-seq data was performed using an adjusted *p*-value cutoff of $p \leq 0.05$ and a signal intensity ratio (*m*-value) cutoff of ≥ 1.98 or ≤ -1.98 . The latter was determined by applying a significance level of 5% to the experiment with the assumption that the majority of genes are not differentially transcribed. Thus, 95% of all *m*-values should fall in this range. Therefore, the standard deviation (STDEV) for all *m*-values was calculated and the cutoff was set to $m = 1.96 * STDEV$. Genes with an *m*-value outside this range and $p \leq 0.05$ were considered as differentially transcribed.

Construction of Voronoi treemaps. The software Paver (DECODON GmbH, Greifswald, Germany) was used to generate the regulon treemap showing log₂ fold changes (*m*-values) of selective genes sorted into operons and regulons that are upregulated under NaOCl stress compared to the untreated control. The treemap construction is based on a model of competing particle swarms for the layout optimization as described (62). The hierarchical structure of the treemap is defined by the regulons (on the first level—bold white labels), genes, and operons (second level—small contrast optimized labels). Cell sizes are defined as absolute log₂ fold changes of expression levels after NaOCl stress divided by the untreated control. Colors are defined by a symmetric divergent color gradient (negative values—blue and positive values orange—red) of NaOCl versus control log₂ fold ratios.

Cloning, expression, and purification of His-tagged HypR and HypR Cys mutant proteins in *E. coli*. The *hypR* gene (SACOL0641) was amplified from chromosomal DNA of *S. aureus* COL by PCR using primers 0641-pET-for-NheI and 0641-pET-rev-BamHI (Supplementary Table S5), digested with *NheI* and *BamHI* and inserted into plasmid pET11b (Novagen) that was digested using the same restriction enzymes to generate plasmid pET11b-*hypR*.

For construction of HypR Cys-to-Ala and Cys-to-Ser variants, the Cys residues of HypR were replaced by alanine or serine, respectively, using PCR mutagenesis. For the *hypR-C33A* mutant, two first-round PCRs were performed using primers 0641-pET-for-NheI and 0641-pET-C33A-Rev and primers 0641-pET-C33A-for and 0641-pET-rev-BamHI (Supplementary Table S5). For the *hypRC99A* mutant, two first-round PCRs were performed using primers 0641-pET-for-NheI and 0641-pET-C99A-rev and primers 0641-pET-C99A-for and 0641-pET-rev-BamHI. For the *hypRC99S* mutant, two first-round PCRs were performed using primers 0641-pET-for-NheI and 0641-pET-C99S-rev and primers 0641-pET-C99S-for and 0641-pET-rev-BamHI. The two PCR products of each first-round PCR were hybridized and subsequently amplified by a second round of PCRs using primers 0641-pET-for-NheI and 0641-pET-rev-BamHI. The PCR products from the second-round PCRs were digested with *NheI* and *BamHI* and inserted into plasmid pET11b digested with the same enzymes to generate plasmids pET11b-*hypR-C33A*, pET11b-*hypRC99A*, and pET11b-*hypRC99S*. The *hypRC142A* gene was amplified from chromosomal DNA of *S. aureus* COL by PCR using primers 0641-pET-for-NheI and 0641-pET-C142A-rev-BamHI, digested with *NheI* and *BamHI* and inserted into plasmid pET11b that was digested using the same restriction enzymes to generate plasmid pET11b-*hypR-C142A*. The correct sequences of all inserts were confirmed by PCR and DNA sequencing.

For expression and purification of His₆-tagged HypR wild-type and Cys mutant proteins, *E. coli* BL21(DE3) *plyS* was used that contains the plasmids pET11b-*hypR*, pET11b-*hypRC33A*, pET11b-*hypRC99A*, pET11b-*hypRC99S*, and pET11b-*hypRC142A*. These *E. coli* expression strains were cultivated in 1 l LB medium until the exponential growth phase at OD₆₀₀ of 0.8 followed by addition of 1 mM isopropyl- β -D-thiogalactopyranoside for 3.5 h at 37°C. *E. coli* strains expressing recombinant His₆-tagged HypR and the HypR Cys mutant proteins were disrupted by sonication in binding buffer (20 mM NaH₂PO₄, 500 mM NaCl, 20 mM imidazole, pH 7.4). Lysates were cleared from cell debris by repeated centrifugation, and purification of the His-tagged proteins was performed using His Trap™ HP Ni-NTA columns (5 ml; GE Healthcare, Chalfont St Giles, United Kingdom) and the ÄKTA purifier liquid chromatography system (GE Healthcare) according to the instructions of the manufacturer. Supplementary Figure S11 shows the HypR purification profile in the Äkta chromatography. A gradient from 0 to 500 mM imidazole was applied in elution buffer (20 mM NaH₂PO₄, 500 mM NaCl, 500 mM imidazole, pH 7.4) and HypR eluted at ~240 mM imidazole. The purity of eluted and pooled fractions was analyzed by reducing SDS-PAGE (Supplementary Fig. S11, inset). The purified proteins were extensively dialyzed against 10 mM Tris-HCl (pH 8.0), 100 mM NaCl, and 30% glycerol and stored at -80°C. The HypR protein concentrations were determined by UV absorbance using a

Thermo Nanodrop 2000c spectrophotometer (Thermo Scientific, Germany). The final HypR protein concentration after dialysis was 2.8 mg/ml (158.7 μ M) with a threefold enrichment after dialysis. Before further usage, HypR proteins were freshly reduced with 10 mM DTT or 10 mM TCEP or as otherwise stated in the methods and figure legends.

Construction of *S. aureus* COL *hypR* and *merA* deletion mutants and complemented Cys-Ala mutant strains. *S. aureus* COL mutants with clean deletions of *hypR* (SACOL0641) and *merA* (SACOL0640) were constructed by allelic replacement *via* the temperature-sensitive shuttle vector pMAD as described previously (5). Briefly, for construction of the plasmids, pMAD- Δ *hypR* and pMAD- Δ *merA*, the flanking gene regions, including 500 bp upstream and downstream of *hypR* and *merA* of *S. aureus* COL, were amplified using the primers SACOL0641-pMAD and SACOL0640-pMAD (Supplementary Table S5). The up- and downstream flanking regions of *hypR* and *merA* were each fused by overlap extension PCR and ligated into the *Bg*III and *Sal*I sites of plasmid pMAD. The pMAD constructs were electroporated into the restriction-negative and methylation-positive intermediate *S. aureus* RN4220 strain and further transferred to *S. aureus* COL by phage transduction using phage 80 (81). Transductants were streaked out on LB agar with 10 μ g/ml erythromycin and 40 μ g/ml 5-bromo-4-chloro-3-indolyl- β -D-galactopyranoside (X-gal) at 30°C. Blue transductants with pMAD integrations were used for plasmid excision by a heat shock and screened for erythromycin-sensitive white colonies on X-gal plates as described (66). The clean deletions of internal gene regions of *hypR* or *merA* were confirmed by PCR and sequencing.

The complemented *hypR* and *merA* deletion mutants and Cys mutant strains were constructed using the pRB473-XylR plasmid as described previously (58). Briefly, *hypR*, *hypR-C33A*, *hypRC99A*, *hypRC142A*, *merA*, and *merAC43S* sequences were amplified from the *E. coli* expression plasmids pET11b-*hypR*, pET11b-*hypRC33A*, pET11b-*hypRC99A*, pET11b-*hypRC142A*, pET11b-*merA*, and pET11b-*merAC43S* using the following primers. Primers 0641-pRB-for-BamHI and 0641-pRB-REV-KpnI were used to construct plasmids pRB473-XylR-*hypR*, pRB473-XylR-*hypRC33A*, and pRB473-XylR-*hypRC99A*. Primers 0641-pRB-for-BamHI and 0641-pRB-REV-KpnI-C2-3A were used to construct pRB473-XylR-*hypRC142A*. Primers 0640-pRB-for-BamHI and 0640-pRB-rev-KpnI were used to construct pRB473-XylR-*merA* and pRB473-XylR-*merAC43S*. Each forward primer also includes the shine-dalgarno sequence of *hypR* or *merA*, respectively. The PCR product was digested with *Bam*HI and *Kpn*I and inserted into the pRB473-XylR shuttle vector that was digested using the same enzymes. The recombinant plasmids were introduced into the Δ *hypR* or Δ *merA* deletion mutants *via* phage transduction as described previously (58).

Northern blot experiments. Northern blot analyses were performed as described previously (93) using RNA isolated from the *S. aureus* COL strains that were exposed to 1 mM NaOCl, 2 mM diamide, 10 mM H₂O₂, 0.75 mM formaldehyde, and 0.5 mM methylglyoxal (MG) for 15 and 30 min as indicated. Hybridizations were performed with the digoxigenin-labeled *hypR*- and *merA*-specific antisense RNA

probes synthesized *in vitro* using T7 RNA polymerase as described previously (89). The primer pairs SACOL0641-for and SACOL0641-rev or SACOL0640-for and SACOL0640-rev were each used for generation of the digoxigenin-labeled *hypR* and *merA* antisense RNA probes, respectively.

EMSAs of HypR. For EMSAs, we amplified a DNA fragment containing the *hypR-merA* upstream region that covered the region from -128 to +70 relative to the transcriptional start site using PCR with the primer set emsa0641-for and emsa0641-rev (Supplementary Table S5). Approximately 0.75 ng of purified PCR products was incubated with different amounts of purified His-HypR and His-HypR Cys mutant proteins for 45 min at room temperature in EMSA binding buffer (10 mM Tris-HCl [pH 7.5], 100 mM KCl, 5% glycerol, 50 μ g/ml bovine serum albumin (BSA), and 5 μ g/ml salmon sperm DNA) in the presence of 10 mM DTT. To study the effect of NaOCl and diamide on the DNA-binding activity *in vitro*, the purified proteins were reduced with 10 mM DTT for 20 min, desalted with Micro-Bio spin columns (Biorad), and diluted to 0.6 μ M in 10 mM Tris-HCl, pH 7.5. Reduced HypR and Cys mutant proteins were oxidized with 1.25–20 μ M NaOCl or 2.5–20 μ M diamide for 10 min at room temperature and incubated with the DNA fragment (0.75 ng) containing the *hypR-merA* promoter. DNA-binding reactions were separated by 4% native polyacrylamide gel electrophoresis in 10 mM Tris, 1 mM EDTA buffer, pH 8, containing 2.5% glycerol at room temperature and constant voltage (180 V) for 30 min. Gels were stained with SYBR green (Thermo Fisher Scientific) for 30 min in the dark and fluorescence was visualized using a Typhoon scanner (Typhoon FLA 9500; GE Healthcare Life Sciences).

CD spectroscopy. CD spectra of DTT-reduced HypR and HypR Cys mutant proteins were obtained using a Jasco J-810 spectropolarimeter with a HAAKE WKL recirculating chiller (D-76227, Karlsruhe). The DTT-reduced proteins were measured at 10 μ M in 20 mM potassium phosphate buffer, pH 7.5, with 1 mM DTT. The quartz cuvettes (2 mm path length, Suprasil Hellma) were set at a constant temperature of 25°C with a Jasco PTC-423S Peltier-type thermocouple. Secondary structure elements were calculated using the program DichroWeb (<http://dichroweb.cryst.bbk.ac.uk>) (86, 94).

SEC-MALS analysis. HypR proteins were diluted in SEC buffer (10 mM HEPES, 500 mM NaCl, pH 7.4, 1 mM TCEP) and reduced with 10 mM TCEP at 25°C for 1 h. The molecular weights and oligomerization states of HypR and the HypR Cys mutants were determined using SEC-MALS analysis at 20°C running in SEC buffer. The reduced HypR protein samples (170 μ M each) were passed over a Superdex 75 10/300 size-exclusion column (GE Healthcare) coupled to a miniDAWN TREOS three-angle light scattering detector (Wyatt Technology) and a RefractoMax520 refractive index detector (ERC). Detectors were aligned, corrected for band broadening, and the photodiodes of the miniDAWN TREOS were normalized with BSA as a reference. Data were analyzed with ASTRA 6.1.4.25 (Wyatt Technology). For calculation of the molecular masses, protein concentrations were determined from the differential refractive index with a specific refractive index increment (dn/dc) of 0.185 ml/g.

Nonreducing/reducing diagonal SDS-PAGE analysis. *S. aureus* COL strains were cultivated in BMM, treated with 150 μ M NaOCl for 30 min as described (58), harvested, and washed in TE-buffer (10 mM Tris-HCl, pH 8; 1 mM EDTA) with 50 mM NEM to alkylate reduced thiols. Cells were disrupted using the ribolyzer, and the protein extracts were obtained after repeated centrifugation. Immunoprecipitation of HypR proteins was performed using HypR-polyclonal antibodies and *S. aureus* protein extracts with Dynabeads protein A (Invitrogen) according to the instructions of the manufacturer. The precipitated HypR proteins were eluted in nonreducing SDS sample buffer (2% SDS, 62.5 mM Tris-HCl [pH 8.0]). The protein extracts and immunoprecipitated HypR proteins were separated by 15% nonreducing/reducing SDS-PAGE as described previously (53). In the first SDS-PAGE, proteins were separated in nonreducing SDS-PAGE sample buffer. The lanes were cut and incubated in reducing SDS sample buffer (with 50 mM DTT) followed by thiol alkylation with 50 mM iodoacetamide (IAM) for each 15 min. The bands were positioned horizontally on an SDS-PAGE gel, separated using reducing SDS-PAGE, and subjected to HypR-specific Western blot analysis as described previously (22). HypR forms intermolecular disulfides between two subunits that run at the right side of the diagonal.

Western blot analysis. *S. aureus* COL cells were harvested, washed in TE buffer (pH 8.0) with 50 mM NEM, disrupted using the ribolyzer, and the protein extract was cleared from cell debris by repeated centrifugation as described above. Protein amounts of 25 μ g were diluted in nonreducing or reducing SDS sample buffer (as above), separated using 15% SDS-PAGE, and the Western blot analysis was performed as described previously (22). Anti-HypR polyclonal rabbit anti-serum was generated using purified His-HypR protein and used at a dilution of 1:500 for Western blot analyses.

MALDI-TOF-MS of *in vitro* oxidized HypR protein. The purified HypR and HypRC33A proteins were oxidized with NaOCl and all reduced thiols were blocked with 50 mM IAM resulting in the mass increase of 57 Da at Cys residues. The oxidized HypR and HypRC33A intermolecular disulfides were separated by nonreducing SDS-PAGE, followed by tryptic digestion of the HypR and HypRC33A disulfide bands as described (21). The peptides were measured using a MALDI-TOF-MS using an Ultraflex-II TOF/TOF instrument (Bruker Daltonics, Bremen, Germany) equipped with a 200 Hz solid-state Smart beam™ laser. The mass spectrometer was operated in the positive reflector mode. Mass spectra were acquired over an m/z range of 600–4000. MS/MS spectra of selected peptides were acquired in the LIFT mode as described previously (87).

Infection assays with murine macrophage cell line J-774A.1. Murine macrophage cell line J-774A.1 (80) was cultivated in Iscove's modified Dulbecco's medium (Biocrom) with 10% heat-inactivated fetal bovine serum (FBS) and seeded in cell culture dishes for 2 days under 5% CO₂ at 37°C as described (79). Before the infection assay, *S. aureus* COL strains were plated overnight on LB agar and re-suspended in eukaryotic growth medium. Macrophages were infected with *S. aureus* cells at a multiplicity of infection (MOI) of 1:25. One hour after infection, the cell culture medium was replaced and 150 μ g/ml gentamycin was added

for 1 h to kill extracellular bacteria and to stop the uptake of *S. aureus*. The intracellular survival was determined at 2, 4, and 24 h after phagocytosis. Infected macrophages were lysed with 0.1% Triton X-100 and the supernatant with internalized intracellular bacteria was plated on agar plates for CFUs.

Acknowledgments

We are grateful to Dorian Jamal Mikolajczak and Prof. Beate Kocsch (Organic chemistry, FU Berlin) for support with CD spectrometry. This work was supported by an ERC Consolidator grant (GA 615585) MYCOTHILOME and grants from the Deutsche Forschungsgemeinschaft (AN746/4-1 and AN746/4-2) within the SPP1710 on “Thiol-based Redox switches” as well as by the SFB973 project C08 to H.A.

Author Disclosure Statement

No competing financial interests exist.

References

- Abomoelak B, Hoye EA, Chi J, Marcus SA, Laval F, Bannantine JP, Ward SK, Daffe M, Liu HD, and Talaat AM. *mosR*, a novel transcriptional regulator of hypoxia and virulence in *Mycobacterium tuberculosis*. *J Bacteriol* 191: 5941–5952, 2009.
- Antelmann H and Helmann JD. Thiol-based redox switches and gene regulation. *Antioxid Redox Signal* 14: 1049–1063, 2011.
- Archer GL. *Staphylococcus aureus*: a well-armed pathogen. *Clin Infect Dis* 26: 1179–1181, 1998.
- Argyrou A and Blanchard JS. Flavoprotein disulfide reductases: advances in chemistry and function. *Prog Nucleic Acid Res Mol Biol* 78: 89–142, 2004.
- Arnaud M, Chastanet A, and Debarbouille M. New vector for efficient allelic replacement in naturally nontransformable, low-GC-content, gram-positive bacteria. *Appl Environ Microbiol* 70: 6887–6891, 2004.
- Barendt S, Lee H, Birch C, Nakano MM, Jones M, and Zuber P. Transcriptomic and phenotypic analysis of paralogous *spx* gene function in *Bacillus anthracis* *sterne*. *Microbiologyopen* 2: 695–714, 2013.
- Baroja ML, Herfst CA, Kasper KJ, Xu SX, Gillett DA, Li J, Reid G, and McCormick JK. The *SaeRS* two-component system is a direct and dominant transcriptional activator of toxic shock syndrome toxin 1 in *Staphylococcus aureus*. *J Bacteriol* 198: 2732–2742, 2016.
- Beavers WN and Skaar EP. Neutrophil-generated oxidative stress and protein damage in *Staphylococcus aureus*. *Pathog Dis* 74: pii: ftw060, 2016.
- Bergman NH, Anderson EC, Swenson EE, Janes BK, Fisher N, Niemeyer MM, Miyoshi AD, and Hanna PC. Transcriptional profiling of *Bacillus anthracis* during infection of host macrophages. *Infect Immun* 75: 3434–3444, 2007.
- Biasini M, Bienert S, Waterhouse A, Arnold K, Studer G, Schmidt T, Kiefer F, Gallo Cassarino T, Bertoni M, Bordoli L, and Schwede T. SWISS-MODEL: modelling protein tertiary and quaternary structure using evolutionary information. *Nucleic Acids Res* 42: W252–W258, 2014.
- Blom J, Jakobi T, Doppmeier D, Jaenicke S, Kalinowski J, Stoye J, and Goesmann A. Exact and complete short-read alignment to microbial genomes using graphics processing unit programming. *Bioinformatics* 27: 1351–1358, 2011.
- Boucher HW and Corey GR. Epidemiology of methicillin-resistant *Staphylococcus aureus*. *Clin Infect Dis* 46 Suppl 5: S344–S349, 2008.
- Chandrangu P, Loi VV, Antelmann H, and Helmann JD. The role of bacillithiol in gram-positive firmicutes. *Antioxid Redox Signal* 2017 [Epub ahead of print]; DOI: 10.1089/ars.2017.7057.
- Chen PR, Bae T, Williams WA, Duguid EM, Rice PA, Schneewind O, and He C. An oxidation-sensing mechanism is used by the global regulator MgrA in *Staphylococcus aureus*. *Nat Chem Biol* 2: 591–595, 2006.
- Chen PR, Brugarolas P, and He C. Redox signaling in human pathogens. *Antioxid Redox Signal* 14: 1107–1118, 2011.
- Chen PR, Nishida S, Poor CB, Cheng A, Bae T, Kuchenmeister L, Dunman PM, Missiakas D, and He C. A new oxidative sensing and regulation pathway mediated by the MgrA homologue SarZ in *Staphylococcus aureus*. *Mol Microbiol* 71: 198–211, 2009.
- Cheung AL, Nishina KA, Trottonda MP, and Tamber S. The SarA protein family of *Staphylococcus aureus*. *Int J Biochem Cell Biol* 40: 355–361, 2008.
- Chi BK, Albrecht D, Gronau K, Becher D, Hecker M, and Antelmann H. The redox-sensing regulator YodB senses quinones and diamide via a thiol-disulfide switch in *Bacillus subtilis*. *Proteomics* 10: 3155–3164, 2010.
- Chi BK, Busche T, Van Laer K, Bäsell K, Becher D, Clermont L, Seibold GM, Persicke M, Kalinowski J, Messens J, and Antelmann H. Protein S-mycothiolation functions as redox-switch and thiol protection mechanism in *Corynebacterium glutamicum* under hypochlorite stress. *Antioxid Redox Signal* 20: 589–605, 2014.
- Chi BK, Gronau K, Mader U, Hessling B, Becher D, and Antelmann H. S-bacillithiolation protects against hypochlorite stress in *Bacillus subtilis* as revealed by transcriptomics and redox proteomics. *Mol Cell Proteomics* 10: M111 009506, 2011.
- Chi BK, Kobayashi K, Albrecht D, Hecker M, and Antelmann H. The paralogous MarR/DUF24-family repressors YodB and CatR control expression of the catechol dioxygenase CatE in *Bacillus subtilis*. *J Bacteriol* 192: 4571–4581, 2010.
- Chi BK, Roberts AA, Huyen TT, Bäsell K, Becher D, Albrecht D, Hamilton CJ, and Antelmann H. S-bacillithiolation protects conserved and essential proteins against hypochlorite stress in firmicutes bacteria. *Antioxid Redox Signal* 18: 1273–1295, 2013.
- Crack JC, Munnoch J, Dodd EL, Knowles F, Al Bassam MM, Kamali S, Holland AA, Cramer SP, Hamilton CJ, Johnson MK, Thomson AJ, Hutchings MI, and Le Brun NE. NsrR from *Streptomyces coelicolor* is a nitric oxide-sensing [4Fe-4S] cluster protein with a specialized regulatory function. *J Biol Chem* 290: 12689–12704, 2015.
- Dal Peraro M and van der Goot FG. Pore-forming toxins: ancient, but never really out of fashion. *Nat Rev Microbiol* 14: 77–92, 2016.
- Diep BA, Gill SR, Chang RF, Phan TH, Chen JH, Davidson MG, Lin F, Lin J, Carleton HA, Mongodin EF, Sensabaugh GF, and Perdreaux-Remington F. Complete genome sequence of USA300, an epidemic clone of community-acquired methicillin-resistant *Staphylococcus aureus*. *Lancet* 367: 731–739, 2006.
- Dubbs JM and Mongkolsuk S. Peroxiredoxins in bacterial antioxidant defense. *Subcell Biochem* 44: 143–193, 2007.

27. Dubbs JM and Mongkolsuk S. Peroxide-sensing transcriptional regulators in bacteria. *J Bacteriol* 194: 5495–5503, 2012.
28. Even S, Burguiere P, Auger S, Soutourina O, Danchin A, and Martin-Verstraete I. Global control of cysteine metabolism by CymR in *Bacillus subtilis*. *J Bacteriol* 188: 2184–2197, 2006.
29. Falord M, Mader U, Hiron A, Debarbouille M, and Msadek T. Investigation of the *Staphylococcus aureus* GraSR regulon reveals novel links to virulence, stress response and cell wall signal transduction pathways. *PLoS One* 6: e21323, 2011.
30. Fomenko DE and Gladyshev VN. Comparative genomics of thiol oxidoreductases reveals widespread and essential functions of thiol-based redox control of cellular processes. *Antioxid Redox Signal* 16: 193–201, 2012.
31. Foster TJ. The *Staphylococcus aureus* “superbug”. *J Clin Invest* 114: 1693–1696, 2004.
32. Fuangthong M, Atichartpongkul S, Mongkolsuk S, and Helmann JD. OhrR is a repressor of ohrA, a key organic hydroperoxide resistance determinant in *Bacillus subtilis*. *J Bacteriol* 183: 4134–4141, 2001.
33. Gaballa A, Antelmann H, Hamilton CJ, and Helmann JD. Regulation of *Bacillus subtilis* bacillithiol biosynthesis operons by Spx. *Microbiology* 159: 2025–2035, 2013.
34. Gray MJ, Li Y, Leichert LI, Xu Z, and Jakob U. Does the transcription factor NemR use a regulatory sulfenamide bond to sense bleach? *Antioxid Redox Signal* 23: 747–754, 2015.
35. Gray MJ, Wholey WY, and Jakob U. Bacterial responses to reactive chlorine species. *Annu Rev Microbiol* 67: 141–160, 2013.
36. Gray MJ, Wholey WY, Parker BW, Kim M, and Jakob U. NemR is a bleach-sensing transcription factor. *J Biol Chem* 288: 13789–13798, 2013.
37. Guerra FE, Addison CB, de Jong NW, Azzolino J, Pallister KB, van Strijp JA, and Voyich JM. *Staphylococcus aureus* SaeR/S-regulated factors reduce human neutrophil reactive oxygen species production. *J Leukoc Biol* 100: 1005–1010, 2016.
38. Guo H, Hall JW, Yang J, and Ji Y. The SaeRS two-component system controls survival of *Staphylococcus aureus* in human blood through regulation of coagulase. *Front Cell Infect Microbiol* 7: 204, 2017.
39. Hampton MB, Kettle AJ, and Winterbourn CC. Involvement of superoxide and myeloperoxidase in oxygen-dependent killing of *Staphylococcus aureus* by neutrophils. *Infect Immun* 64: 3512–3517, 1996.
40. Hibbing ME and Fuqua C. Antiparallel and interlinked control of cellular iron levels by the Irr and RirA regulators of *Agrobacterium tumefaciens*. *J Bacteriol* 193: 3461–3472, 2011.
41. Highlander SK, Hulten KG, Qin X, Jiang H, Yerrapragada S, Mason EO, Jr., Shang Y, Williams TM, Fortunov RM, Liu Y, Igboeli O, Petrosino J, Tirumalai M, Uzman A, Fox GE, Cardenas AM, Muzny DM, Hemphill L, Ding Y, Dugan S, Blyth PR, Buhay CJ, Dinh HH, Hawes AC, Holder M, Kovar CL, Lee SL, Liu W, Nazareth LV, Wang Q, Zhou J, Kaplan SL, and Weinstock GM. Subtle genetic changes enhance virulence of methicillin resistant and sensitive *Staphylococcus aureus*. *BMC Microbiol* 7: 99, 2007.
42. Hilker R, Stadermann KB, Doppmeier D, Kalinowski J, Stoye J, Straube J, Winneballd J, and Goesmann A. ReadXplorer—visualization and analysis of mapped sequences. *Bioinformatics* 30: 2247–2254, 2014.
43. Hillion M and Antelmann H. Thiol-based redox switches in prokaryotes. *Biol Chem* 396: 415–444, 2015.
44. Hillion M, Bernhardt J, Busche T, Rossius M, Maass S, Becher D, Rawat M, Wirtz M, Hell R, Ruckert C, Kalinowski J, and Antelmann H. Monitoring global protein thiol-oxidation and protein S-mycothiolation in *Mycobacterium smegmatis* under hypochlorite stress. *Sci Rep* 7: 1195, 2017.
45. Ilbert M, Graf PC, and Jakob U. Zinc center as redox switch—new function for an old motif. *Antioxid Redox Signal* 8: 835–846, 2006.
46. Imber M, Huyen NTT, Pietrzyk-Brzezinska AJ, Loi VV, Hillion M, Bernhardt J, Thärichen L, Kolsek K, Saleh M, Hamilton CJ, Adrian L, Gräter F, Wahl MC, and Antelmann H. Protein S-bacillithiolation functions in thiol protection and redox regulation of the glyceraldehyde-3-phosphate dehydrogenase gap in *Staphylococcus aureus* under hypochlorite stress. *Antioxid Redox Signal* 2017 [Epub ahead of print]; DOI: 10.1089/ars.2016.6897.
47. Ji Q, Zhang L, Sun F, Deng X, Liang H, Bae T, and He C. *Staphylococcus aureus* CymR is a new thiol-based oxidation-sensing regulator of stress resistance and oxidative response. *J Biol Chem* 287: 21102–21109, 2012.
48. Klebanoff SJ, Kettle AJ, Rosen H, Winterbourn CC, and Nauseef WM. Myeloperoxidase: a front-line defender against phagocytosed microorganisms. *J Leukoc Biol* 93: 185–198, 2013.
49. Kosower NS and Kosower EM. Diamide: an oxidant probe for thiols. *Methods Enzymol* 251: 123–133, 1995.
50. Lee C, Shin J, and Park C. Novel regulatory system nemRA-gloA for electrophile reduction in *Escherichia coli* K-12. *Mol Microbiol* 88: 395–412, 2013.
51. Lee JW, Soonsanga S, and Helmann JD. A complex thiolate switch regulates the *Bacillus subtilis* organic peroxide sensor OhrR. *Proc Natl Acad Sci U S A* 104: 8743–8748, 2007.
52. Leelakriangsak M, Huyen NT, Töwe S, van Duy N, Becher D, Hecker M, Antelmann H, and Zuber P. Regulation of quinone detoxification by the thiol stress sensing DUF24/MarR-like repressor, YodB in *Bacillus subtilis*. *Mol Microbiol* 67: 1108–1124, 2008.
53. Leichert LI and Jakob U. Global methods to monitor the thiol-disulfide state of proteins in vivo. *Antioxid Redox Signal* 8: 763–772, 2006.
54. Li S, Li P, Zhang L, Hu W, Wang M, Liu Y, Tang G, Wang D, Zhou B, and Yan J. The role of reactive oxygen intermediates in the intracellular fate of *Leptospira interrogans* in the macrophages of different hosts. *PLoS One* 12: e0178618, 2017.
55. Liu P, Wu X, Liao C, Liu X, Du J, Shi H, Wang X, Bai X, Peng P, Yu L, Wang F, Zhao Y, and Liu M. *Escherichia coli* and *Candida albicans* induced macrophage extracellular trap-like structures with limited microbicidal activity. *PLoS One* 9: e90042, 2014.
56. Liu Q, Yeo WS, and Bae T. The SaeRS two-component system of *Staphylococcus aureus*. *Genes (Basel)* 7: 81, 2016.
57. Livermore DM. Antibiotic resistance in staphylococci. *Int J Antimicrob Agents* 16 Suppl 1: S3–S10, 2000.
58. Loi VV, Harms M, Müller M, Huyen NTT, Hamilton CJ, Hochgräfe F, Pane-Farre J, and Antelmann H. Real-time imaging of the bacillithiol redox potential in the human pathogen *Staphylococcus aureus* using a genetically

- encoded bacilliredoxin-fused redox biosensor. *Antioxid Redox Signal* 26: 835–848, 2017.
59. Love MI, Huber W, and Anders S. Moderated estimation of fold change and dispersion for RNA-seq data with DESeq2. *Genome Biol* 15: 550, 2014.
 60. Lowy FD. *Staphylococcus aureus* infections. *N Engl J Med* 339: 520–532, 1998.
 61. Mäder U, Nicolas P, Depke M, Pane-Farre J, Debarbouille M, van der Kooi-Pol MM, Guerin C, Derozier S, Hiron A, Jarmer H, Leduc A, Michalik S, Reilman E, Schaffer M, Schmidt F, Bessieres P, Noirot P, Hecker M, Msadek T, Volker U, and van Dijl JM. *Staphylococcus aureus* transcriptome architecture: from laboratory to infection-mimicking conditions. *PLoS Genet* 12: e1005962, 2016.
 62. Mehlan H, Schmidt F, Weiss S, Schüler J, Fuchs S, Riedel K, and Bernhardt J. Data visualization in environmental proteomics. *Proteomics* 13: 2805–2821, 2013.
 63. Moore MJ, Miller SM, and Walsh CT. C-terminal cysteines of Tn501 mercuric ion reductase. *Biochemistry* 31: 1677–1685, 1992.
 64. Moore MJ and Walsh CT. Mutagenesis of the N- and C-terminal cysteine pairs of Tn501 mercuric ion reductase: consequences for bacterial detoxification of mercurials. *Biochemistry* 28: 1183–1194, 1989.
 65. More P and Pai K. In vitro NADH-oxidase, NADPH-oxidase and myeloperoxidase activity of macrophages after *Tinospora cordifolia* (guduchi) treatment. *Immunopharmacol Immunotoxicol* 34: 368–372, 2012.
 66. Müller M, Reiss S, Schlüter R, Mader U, Beyer A, Reiss W, Marles-Wright J, Lewis RJ, Pfortner H, Völker U, Riedel K, Hecker M, Engelmann S, and Pane-Farre J. Deletion of membrane-associated Asp23 leads to upregulation of cell wall stress genes in *Staphylococcus aureus*. *Mol Microbiol* 93: 1259–1268, 2014.
 67. Munnoch JT, Martinez MT, Svistunenko DA, Crack JC, Le Brun NE, and Hutchings MI. Characterization of a putative NsrR homologue in *Streptomyces venezuelae* reveals a new member of the Rrf2 superfamily. *Sci Rep* 6: 31597, 2016.
 68. Nakano MM, Kominos-Marvell W, Sane B, Nader YM, Barendt SM, Jones MB, and Zuber P. spxA2, encoding a regulator of stress resistance in *Bacillus anthracis*, is controlled by SaiR, a new member of the Rrf2 protein family. *Mol Microbiol* 94: 815–827, 2014.
 69. Nakano S, Kuster-Schock E, Grossman AD, and Zuber P. Spx-dependent global transcriptional control is induced by thiol-specific oxidative stress in *Bacillus subtilis*. *Proc Natl Acad Sci U S A* 100: 13603–13608, 2003.
 70. Newberry KJ, Nakano S, Zuber P, and Brennan RG. Crystal structure of the *Bacillus subtilis* anti-alpha, global transcriptional regulator, Spx, in complex with the alpha C-terminal domain of RNA polymerase. *Proc Natl Acad Sci U S A* 102: 15839–15844, 2005.
 71. Nicolas P, Mäder U, Dervyn E, Rochat T, Leduc A, Pigeonneau N, Bidnenko E, Marchadier E, Hoebeke M, Aymerich S, Becher D, Bisicchia P, Botella E, Delumeau O, Doherty G, Denham EL, Fogg MJ, Fromion V, Goelzer A, Hansen A, Hartig E, Harwood CR, Homuth G, Jarmer H, Jules M, Klipp E, Le Chat L, Lecointe F, Lewis P, Liebermeister W, March A, Mars RA, Nannapaneni P, Noone D, Pohl S, Rinn B, Rugheimer F, Sappa PK, Samson F, Schaffer M, Schwikowski B, Steil L, Stülke J, Wiegert T, Devine KM, Wilkinson AJ, van Dijl JM, Hecker M, Völker U, Bessieres P, and Noirot P. Condition-dependent transcriptome reveals high-level regulatory architecture in *Bacillus subtilis*. *Science* 335: 1103–1106, 2012.
 72. Ozyamak E, de Almeida C, de Moura AP, Miller S, and Booth IR. Integrated stress response of *Escherichia coli* to methylglyoxal: transcriptional readthrough from the nemRA operon enhances protection through increased expression of glyoxalase I. *Mol Microbiol* 88: 936–950, 2013.
 73. Palm GJ, Khanh Chi B, Waack P, Gronau K, Becher D, Albrecht D, Hinrichs W, Read RJ, and Antelmann H. Structural insights into the redox-switch mechanism of the MarR/DUF24-type regulator HypR. *Nucleic Acids Res* 40: 4178–4192, 2012.
 74. Panmanee W, Vattanaviboon P, Eiamphungporn W, Whangsuk W, Sallabhan R, and Mongkolsuk S. OhrR, a transcription repressor that senses and responds to changes in organic peroxide levels in *Xanthomonas campestris* pv. phaseoli. *Mol Microbiol* 45: 1647–1654, 2002.
 75. Parker BW, Schwessinger EA, Jakob U, and Gray MJ. The RclR protein is a reactive chlorine-specific transcription factor in *Escherichia coli*. *J Biol Chem* 288: 32574–32584, 2013.
 76. Pendleton JN, Gorman SP, and Gilmore BF. Clinical relevance of the ESKAPE pathogens. *Expert Rev Anti Infect Ther* 11: 297–308, 2013.
 77. Pfortner H, Burian MS, Michalik S, Depke M, Hildebrandt P, Dhople VM, Pane-Farre J, Hecker M, Schmidt F, and Völker U. Activation of the alternative sigma factor SigB of *Staphylococcus aureus* following internalization by epithelial cells - an in vivo proteomics perspective. *Int J Med Microbiol* 304: 177–187, 2014.
 78. Poor CB, Chen PR, Duguid E, Rice PA, and He C. Crystal structures of the reduced, sulfenic acid, and mixed disulfide forms of SarZ, a redox active global regulator in *Staphylococcus aureus*. *J Biol Chem* 284: 23517–23524, 2009.
 79. Pöther DC, Gierok P, Harms M, Mostertz J, Hochgräfe F, Antelmann H, Hamilton CJ, Borovok I, Lalk M, Aharonowitz Y, and Hecker M. Distribution and infection-related functions of bacillithiol in *Staphylococcus aureus*. *Int J Med Microbiol* 303: 114–123, 2013.
 80. Ralph P, Moore MA, and Nilsson K. Lysozyme synthesis by established human and murine histiocytic lymphoma cell lines. *J Exp Med* 143: 1528–1533, 1976.
 81. Rosenblum ED and Tyrone S. Serology, density, and morphology of *Staphylococcal phages*. *J Bacteriol* 88: 1737–1742, 1964.
 82. Santos JA, Pereira PJ, and Macedo-Ribeiro S. What a difference a cluster makes: the multifaceted roles of IscR in gene regulation and DNA recognition. *Biochim Biophys Acta* 1854: 1101–1112, 2015.
 83. Schwartz CJ, Giel JL, Patschkowski T, Luther C, Ruzicka FJ, Beinert H, and Kiley PJ. IscR, an Fe-S cluster-containing transcription factor, represses expression of *Escherichia coli* genes encoding Fe-S cluster assembly proteins. *Proc Natl Acad Sci U S A* 98: 14895–14900, 2001.
 84. Shepard W, Soutourina O, Courtois E, England P, Haouz A, and Martin-Verstraete I. Insights into the Rrf2 repressor family—the structure of CymR, the global cysteine regulator of *Bacillus subtilis*. *FEBS J* 278: 2689–2701, 2011.
 85. Spaan AN, van Strijp JAG, and Torres VJ. Leukocidins: staphylococcal bi-component pore-forming toxins find their receptors. *Nat Rev Microbiol* 15: 435–447, 2017.

86. Sreerama N and Woody RW. Estimation of protein secondary structure from circular dichroism spectra: comparison of CONTIN, SELCON, and CDSSTR methods with an expanded reference set. *Anal Biochem* 287: 252–260, 2000.
87. Suckau D, Resemann A, Schuerenberg M, Hufnagel P, Franzen J, and Holle A. A novel MALDI LIFT-TOF/TOF mass spectrometer for proteomics. *Anal Bioanal Chem* 376: 952–965, 2003.
88. Sun F, Ding Y, Ji Q, Liang Z, Deng X, Wong CC, Yi C, Zhang L, Xie S, Alvarez S, Hicks LM, Luo C, Jiang H, Lan L, and He C. Protein cysteine phosphorylation of SarA/MgrA family transcriptional regulators mediates bacterial virulence and antibiotic resistance. *Proc Natl Acad Sci U S A* 109: 15461–15466, 2012.
89. Tam le T, Eymann C, Albrecht D, Sietmann R, Schauer F, Hecker M, and Antelmann H. Differential gene expression in response to phenol and catechol reveals different metabolic activities for the degradation of aromatic compounds in *Bacillus subtilis*. *Environ Microbiol* 8: 1408–1427, 2006.
90. Volbeda A, Dodd EL, Darnault C, Crack JC, Renoux O, Hutchings MI, Le Brun NE, and Fontecilla-Camps JC. Crystal structures of the NO sensor NsrR reveal how its iron-sulfur cluster modulates DNA binding. *Nat Commun* 8: 15052, 2017.
91. Voyich JM, Braughton KR, Sturdevant DE, Whitney AR, Said-Salim B, Porcella SF, Long RD, Dorward DW, Gardner DJ, Kreiswirth BN, Musser JM, and DeLeo FR. Insights into mechanisms used by *Staphylococcus aureus* to avoid destruction by human neutrophils. *J Immunol* 175: 3907–3919, 2005.
92. Voyich JM, Vuong C, DeWald M, Nygaard TK, Kocianova S, Griffith S, Jones J, Iverson C, Sturdevant DE, Braughton KR, Whitney AR, Otto M, and DeLeo FR. The SaeR/S gene regulatory system is essential for innate immune evasion by *Staphylococcus aureus*. *J Infect Dis* 199: 1698–1706, 2009.
93. Wetzstein M, Völker U, Dedio J, Lobau S, Zuber U, Schiesswohl M, Herget C, Hecker M, and Schumann W. Cloning, sequencing, and molecular analysis of the dnaK locus from *Bacillus subtilis*. *J Bacteriol* 174: 3300–3310, 1992.
94. Whitmore L and Wallace BA. Protein secondary structure analyses from circular dichroism spectroscopy: methods and reference databases. *Biopolymers* 89: 392–400, 2008.
95. Winter J, Ilbert M, Graf PC, Ozcelik D, and Jakob U. Bleach activates a redox-regulated chaperone by oxidative protein unfolding. *Cell* 135: 691–701, 2008.
96. Winterbourn CC and Kettle AJ. Redox reactions and microbial killing in the neutrophil phagosome. *Antioxid Redox Signal* 18: 642–660, 2013.
97. Winterbourn CC, Kettle AJ, and Hampton MB. Reactive oxygen species and neutrophil function. *Annu Rev Biochem* 85: 765–792, 2016.
98. Yuki ET, Elbaz MA, Nakano MM, and Moenne-Loccoz P. Transcription factor NsrR from *Bacillus subtilis* senses nitric oxide with a 4Fe-4S cluster (dagger). *Biochemistry* 47: 13084–13092, 2008.
99. Zuber P. Spx-RNA polymerase interaction and global transcriptional control during oxidative stress. *J Bacteriol* 186: 1911–1918, 2004.

Address correspondence to:
 Prof. Haike Antelmann
 Institute for Biology-Microbiology
 Freie Universität Berlin
 Königin-Luise-Strasse 12-16
 Berlin D-14195
 Germany

E-mail: haike.antelmann@fu-berlin.de

Date of first submission to ARS Central, September 4, 2017;
 date of final revised submission, November 21, 2017; date of
 acceptance, December 9, 2017.

Abbreviations Used

BMM	= belitsky minimal medium
BSA	= bovin serum albumin
BSH	= bacillithiol
BSSB	= oxidized bacillithiol disulfide
CD	= circular dichroism
CFU	= colony-forming unit
Chp	= chemotaxis-inhibitory protein
CoAS2	= oxidized coenzyme A disulfide
CoASH	= coenzyme A
CymR	= cysteine metabolism repressor
DTT	= dithiothreitol
EDTA	= ethylenediaminetetraacetic acid
EMSA	= electrophoretic mobility shift assay
FDR	= flavin disulfide reductase
FeS	= iron/sulfur
H ₂ O ₂	= hydrogen peroxide
HOCl	= hypochloric acid
IAM	= iodoacetamide
IscR	= iron/sulfur status of the cell
LB	= Luria Bertani
LMW	= thiol low-molecular-weight thiol
MALDI-TOF-MS	= matrix-assisted laser desorption ionization-time of flight mass spectrometry
MerA	= mercuric ion reductase
MPO	= myeloperoxidase
MRSA	= methicillin-resistant <i>Staphylococcus aureus</i>
M-value	= log ₂ fold change
NADPH	= nicotinamide adenine dinucleotide phosphate
NaOCl	= sodium hypochlorite
NEM	= N-ethylmaleimide
NsrR	= redox sensors for nitric oxide
OD ₅₀₀	= optical density at 500 nm
RCS	= reactive chlorine species
RES	= reactive electrophilic species
ROS	= reactive oxygen species
SEC-MALS	= size-exclusion chromatography/multiangle light scattering
STDEV	= standard deviation
TCEP	= tris(2-carboxyethyl)phosphine
X-gal	= bromo-4-chloro-3-indolyl-β-D-galactopyranoside

Chapter 7

Real-time imaging of the bacillithiol redox potential in the human pathogen *Staphylococcus aureus* using a genetically encoded bacilliredoxin-fused redox biosensor

Vu Van Loi¹, Manuela Harms², Marret Müller³, Nguyen Thi Thu Huyen¹, Chris J. Hamilton⁴, Falko Hochgräfe², Jan Pané-Farré³ and Haike Antelmann^{1#}

¹*Institute for Biology-Microbiology, Freie Universität Berlin, D-14195 Berlin, Germany*

²*Junior Research Group Pathoproteomics and* ³*Institute for Microbiology,*

³*Ernst-Moritz-Arndt-University of Greifswald, D-17487 Greifswald, Germany*

⁴*School of Pharmacy, University of East Anglia, Norwich Research Park, Norwich, NR4 7TJ, UK*

Published in: Antioxidants & Redox Signaling. 26: 835-848. (2017)

<https://doi.org/10.1089/ars.2016.6733>

#Corresponding author: haike.antelmann@fu-berlin.de

Authors contributions

Haike Antelmann and **Vu Van Loi** designed the experiments, analyzed data and wrote the paper. **Vu Van Loi** performed cloning and mutant constructions, imaging, and biosensor measurements of this work. Manuela Harms and Falko Hochgräfe carried out infection assay. Marret Müller and Jan Pané-Farré helped in imaging. Nguyen Thi Thu Huyen was involved in survival assays. Chris J. Hamilton provided bacillithiol for this study.



ORIGINAL RESEARCH COMMUNICATION

Real-Time Imaging of the Bacillithiol Redox Potential in the Human Pathogen *Staphylococcus aureus* Using a Genetically Encoded Bacilliredoxin-Fused Redox Biosensor

Vu Van Loi,¹ Manuela Harms,² Marret Müller,³ Nguyen Thi Thu Huyen,¹ Chris J. Hamilton,⁴ Falko Hochgräfe,² Jan Pané-Farré,³ and Haike Antelmann¹

Abstract

Aims: Bacillithiol (BSH) is utilized as a major thiol-redox buffer in the human pathogen *Staphylococcus aureus*. Under oxidative stress, BSH forms mixed disulfides with proteins, termed as *S*-bacillithiolation, which can be reversed by bacilliredoxins (Brx). In eukaryotes, glutaredoxin-fused roGFP2 biosensors have been applied for dynamic live imaging of the glutathione redox potential. Here, we have constructed a genetically encoded bacilliredoxin-fused redox biosensor (Brx-roGFP2) to monitor dynamic changes in the BSH redox potential in *S. aureus*.

Results: The Brx-roGFP2 biosensor showed a specific and rapid response to low levels of bacillithiol disulfide (BSSB) *in vitro* that required the active-site Cys of Brx. Dynamic live imaging in two methicillin-resistant *S. aureus* (MRSA) USA300 and COL strains revealed fast and dynamic responses of the Brx-roGFP2 biosensor under hypochlorite and hydrogen peroxide (H₂O₂) stress and constitutive oxidation of the probe in different BSH-deficient mutants. Furthermore, we found that the Brx-roGFP2 expression level and the dynamic range are higher in *S. aureus* COL compared with the USA300 strain. In phagocytosis assays with THP-1 macrophages, the biosensor was 87% oxidized in *S. aureus* COL. However, no changes in the BSH redox potential were measured after treatment with different antibiotics classes, indicating that antibiotics do not cause oxidative stress in *S. aureus*.

Conclusion and Innovation: This Brx-roGFP2 biosensor catalyzes specific equilibration between the BSH and roGFP2 redox couples and can be applied for dynamic live imaging of redox changes in *S. aureus* and other BSH-producing Firmicutes. *Antioxid. Redox Signal.* 26, 835–848.

Keywords: *Staphylococcus aureus*, bacillithiol, bacilliredoxin, redox biosensor, roGFP, oxidative stress

Introduction

STAPHYLOCOCCUS AUREUS is an opportunistic human pathogen causing not only local skin infections but also life-threatening diseases such as septicemia, endocarditis, and necrotizing pneumoniae (1, 3, 21). The success of the pathogen is mediated by virulence factors and the development of multiple antibiotic-resistant *S. aureus* strains, such as methicillin-resistant isolates (MRSA) (19). *S. aureus* has to cope with oxidative stress by reactive oxygen species (ROS),

such as hydrogen peroxide (H₂O₂) and the strong oxidant hypochloric acid by the oxidative burst of macrophages and neutrophils under infection conditions (41).

As defense mechanisms, *S. aureus* uses various redox-sensing virulence regulators and the thiol-redox buffer bacillithiol (BSH) (5, 13, 20, 28, 30, 32–34). BSH functions in detoxification of ROS, hypochlorite, diamide, methylglyoxal, electrophiles, and antibiotics, such as rifampicin and fosfomycin or heavy metal ions, and protects *S. aureus* against the oxidative burst by activated macrophages in phagocytosis

¹Institute for Biology-Microbiology, Freie Universität Berlin, Berlin, Germany.

²Junior Research Group Pathoproteomics, Ernst-Moritz-Arndt-University of Greifswald, Greifswald, Germany.

³Institute for Microbiology, Ernst-Moritz-Arndt-University of Greifswald, Greifswald, Germany.

⁴School of Pharmacy, University of East Anglia, Norwich Research Park, Norwich, United Kingdom.

Innovation

In eukaryotes, glutaredoxin-fused roGFP2 biosensors have been successfully applied for dynamic live imaging of the glutathione redox potential. Here, we have constructed the first genetically encoded bacilliredoxin-fused redox biosensor (Brx-roGFP2) that is specific to measure dynamic changes in the bacillithiol redox potential in the human pathogen *Staphylococcus aureus* under oxidative stress and infection conditions *in vivo*. Using this biosensor, we could confirm that different antibiotics do not cause oxidative stress in *S. aureus*. This Brx-roGFP2 biosensor can be applied to measure redox potential changes across clinical *S. aureus* isolates and to screen for new redox-active antibiotics to treat methicillin-resistant *S. aureus* infections.

assays (10, 20, 32, 33). Under hypochlorite stress, BSH forms mixed disulfides with proteins (*S*-bacillithiolations) as a widespread thiol protection and a redox-switch mechanism that is analogous to *S*-glutathionylation in eukaryotes (6, 7, 17, 20).

In *Bacillus subtilis*, two glutaredoxin-like enzymes YphP (BrxA) and YqiW (BrxB) with unusual CGC motifs were characterized as bacilliredoxins (Fig. 1A and Supplementary Fig. S1; Supplementary Data are available online at www.liebertpub.com/ars) that catalyze the reduction of *S*-bacillithiolated proteins, leading to formation of bacillithiolated Brx (Brx-SSB) as an intermediate of this bacilliredoxin electron pathway (9). Reduction of Brx-SSB requires BSH, resulting in bacillithiol disulfide (BSSB) formation that could be recycled by the putative BSSB reductase YpdA at the expense of nicotinamide adenine dinucleotide phosphate (NADPH) (Fig. 1B) (9, 10, 12, 20).

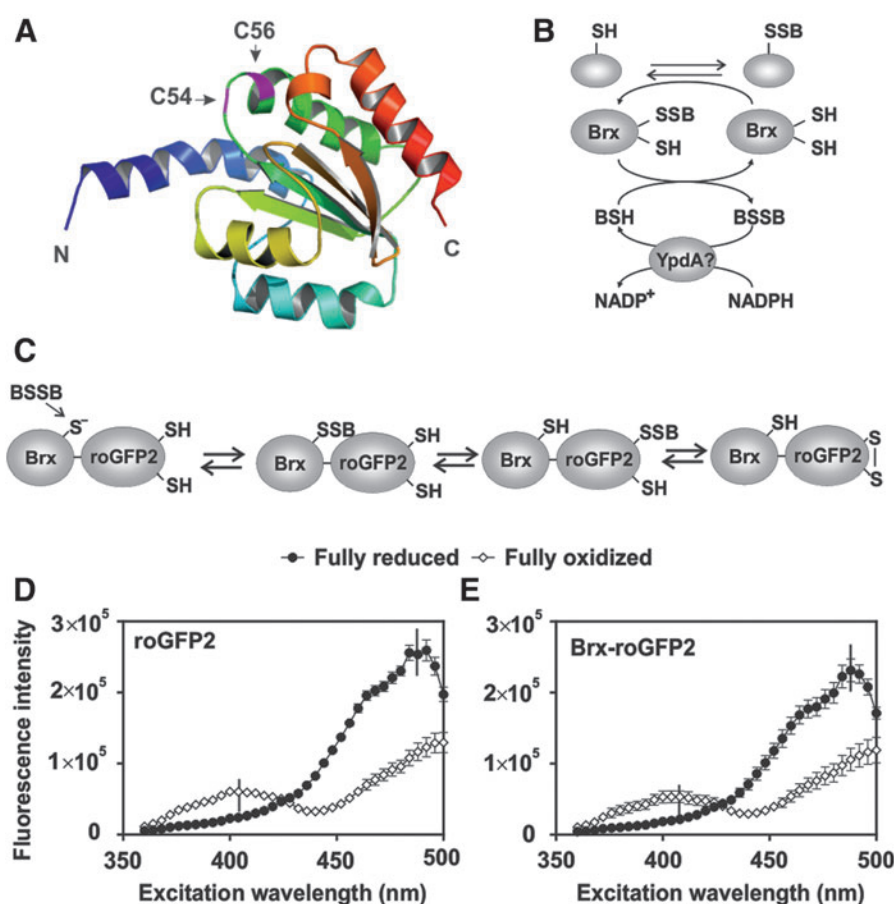


FIG. 1. Structure of the bacilliredoxin (Brx) SAUSA300_1321, Brx electron pathway, principle of the Brx-roGFP2 redox pathway, and excitation spectra of Brx-roGFP2 and roGFP2. (A) Bacilliredoxins are Trx-fold proteins of the UPF0403 family with an unusual CGC active-site motif. The structure of Brx (SAUSA300_1321) was generated using the software Phyre2 and PyMol. (B) The *S*-bacillithiolated proteins are reduced by bacilliredoxins (Brx), leading to Brx-SSB formation. Regeneration of Brx requires BSH and the putative NADPH-dependent BSSB reductase YpdA. (C) In the Brx-roGFP2 fusion, Brx reacts with BSSB, leading to Brx-SSB formation, subsequent transfer of the BSH moiety to the coupled roGFP2, and re-arrangement to the roGFP2 disulfide. The roGFP2 disulfide causes a change of the 405/488 nm excitation ratio. (D, E) Purified roGFP2 and Brx-roGFP2 were fully oxidized and reduced with 5 mM diamide and 10 mM DTT, respectively, and the fluorescence excitation spectra were monitored using the microplate reader ($n=7-9$, $p<0.0001$ in all samples). In all graphs, mean values are shown, error bars represent the SEM, and p -values are calculated using a Student's unpaired two-tailed t -test by the graph prism software. BSH, bacillithiol; BSSB, bacillithiol disulfide; DTT, dithiothreitol; NADPH, nicotinamide adenine dinucleotide phosphate; SEM, standard error of the mean; Trx, thioredoxin. To see this illustration in color, the reader is referred to the web version of this article at www.liebertpub.com/ars

The standard thiol-redox potential of BSH was calculated as $E^{0'}(\text{BSSB}/\text{BSH}) = -221 \text{ mV}$, which is higher than the glutathione redox potential [$E^{0'}(\text{GSSG}/\text{GSH}) = -240 \text{ mV}$] (30, 36). To date, all previous studies have used fluorescent bimane labeling of thiols for quantification of BSH and BSSB levels by high-pressure liquid chromatography under control and stress conditions as an indicator of the changes in the BSH redox potential. According to this method, the BSH/BSSB ratios range from 100:1 to 400:1 in *B. subtilis*, suggesting that BSH is mostly present in its reduced form (36). Under conditions of *S*-bacillithiolation provoked by sodium hypochlorite (NaOCl) stress, the level of BSSB increases, indicating a more oxidized BSH redox potential (7). However, the applied methods require disruption of cells and do not allow dynamic measurements of the changes in the BSH redox potential (25, 35).

Thus, recent advances in the design of genetically encoded redox biosensors, such as redox-sensitive green fluorescent proteins (roGFPs), have facilitated the real-time imaging of the cellular redox potential without cell disruption and at high sensitivity under *in vivo* conditions (11, 24, 35). These roGFP biosensors allow the ratiometric measurements based on two excitation maxima at 405 and 488 nm that change on oxidation (24, 25). RoGFP2 was fused to human glutaredoxin to construct the Grx-roGFP2 biosensor for real-time measurements of dynamic changes in the GSH redox potential (E_{GSH}) in different compartments and different eukaryotic organisms. Grx-roGFP2 detects nanomolar concentrations of GSSG against a backdrop of millimolar GSH within seconds (11, 24).

Recently, roGFP-based biosensors were applied in pathogenic organisms to study E_{GSH} changes under infection conditions and antibiotic treatment, including the malaria parasite *Plasmodium falciparum* (15) and the Gram-negative bacterium *Salmonella* Typhimurium (38, 39). In malaria parasites, several antimalarial drugs affected the cellular redox metabolism and showed differential responses of the Grx-roGFP2 biosensor under short- and long-term measurements *in vivo* (15). In *Mycobacterium tuberculosis*, an analogous Mrx1-roGFP2 biosensor was developed for dynamic measurements of the mycothiol redox potential (E_{MSH}) in drug-resistant isolates and inside macrophages (2, 24). The Mrx1-roGFP2 biosensor was applied to screen for new ROS-generating anti-TB drugs that affected E_{MSH} (37).

In this study, we have constructed the first bacilliredoxin-fused roGFP biosensor that is highly specific to measure changes of the BSH redox potential in MRSA strains USA300 and COL under oxidative stress and after infection of THP-1 human macrophage-like cells.

Results

Construction of a Brx-roGFP2 biosensor that is highly specific for BSSB

The thioredoxin-fold proteins of the UPF0403 family YphP and YqiW were characterized as bacilliredoxins (BrxA and BrxB) in *B. subtilis* that function in reduction of *S*-bacillithiolated proteins and share an unusual CGC active-site motif (Fig. 1A) (9). Both Brx were *S*-bacillithiolated at their active-site Cys *in vivo* and *in vitro* to form Brx-SSB during their catalytic cycle (9). Blast searches identified two bacilliredoxin homologs in *S. aureus* USA300 (SAUSA300_1321 and SAU-

SA300_1463). SAUSA300_1321 showed 54% sequence identity with YphP, whereas SAUSA300_1463 shared a stronger sequence identity (68%) with YqiW of *B. subtilis* (Supplementary Fig. S1). We selected the YphP-homolog SAUSA300_1321 (renamed Brx) for construction of a Brx-roGFP2 fusion protein. *S. aureus* Brx and Brx Cys-Ala mutant proteins (BrxA₅₄GC₅₆, BrxC₅₄GA₅₆, and BrxA₅₄GA₅₆) were each fused *via* the 30aa glycine-serine linker (11) to the N-terminus of roGFP2 to construct the Brx-roGFP2 biosensor variants. Analogous to the reaction of Grx1-roGFP2 and Mrx1-roGFP2 with GSSG or mycothiol disulfide (MSSM) (2, 24), oxidation of the Brx-roGFP2 biosensor should occur specifically by BSSB that targets the active-site Cys54 of Brx to form Brx-SSB. This leads to the transfer of the BSH moiety to the coupled roGFP2, forming *S*-bacillithiolated roGFP2, which re-arranges to the roGFP2 disulfide and results in ratiometric changes of the excitation maxima at 405 and 488 nm (Fig. 1C).

The His-tagged Brx-roGFP2 protein was expressed in *Escherichia coli*, purified, and compared with roGFP2 for its ratiometric changes in the fully reduced and oxidized forms using the microplate reader. The thiol-reactive oxidant diamide was used for complete oxidation, and the thiol-reducing compound dithiothreitol (DTT) was applied for complete reduction of the biosensor. Similar to roGFP2, Brx-roGFP2 exhibits two excitation maxima at 405 and 488 nm and responds in a ratiometric manner to 5 mM diamide and 10 mM DTT (2, 24) (Fig. 1D, E). The degree of oxidation (OxD) was calculated according to the fluorescence excitation intensities at 405 and 488 nm of fully oxidized and reduced Brx-roGFP2 probes as previously described (11). For all following measurements, the OxD values of fully reduced and oxidized probes were calibrated as 0 and 1 and the OxD values of the actual measurements were related to these controls.

Furthermore, it was analyzed whether the Brx-roGFP2 response is sensitive to pH changes that could occur during infections. The Brx-roGFP2 probe was diluted into phosphate buffer solutions at different pH values ranging from 5.8 to 8.0 and treated with diamide and DTT (Supplementary Fig. S2). The 405/488 nm excitations ratios were not affected by different pH values, indicating that the probe is insensitive to pH changes.

Purified Brx-roGFP2 showed a very fast and specific response to physiological BSSB levels (10–100 μM), but not to other thiol disulfides (GSSG, MSSM, cystine, and CoAS disulfide) (Fig. 2A, B). In contrast, roGFP2 did not respond to 10–100 μM BSSB, confirming that Brx-roGFP2 is specific to detect E_{BSH} changes (Fig. 2C). Furthermore, Grx-roGFP2 was oxidized specifically by 100 μM GSSG, but it was unresponsive to BSSB, indicating that Grx is not specific for the BSH/BSSB redox couple (11) (Fig. 2D).

The specificity of Brx for BSSB should be determined by the C₅₄GC₅₆ active-site motif. Hence, the response of Brx-roGFP2 was compared with that of Brx Cys mutant roGFP2 fusions, where the active-site Cys54 and the resolving Cys56 of Brx are each replaced by an alanine (BrxAGC, BrxCGA, and BrxAGA). Brx-roGFP2 and the resolving Brx Cys56 mutant (BrxCGA-roGFP2) showed very fast oxidation by 10–100 μM BSSB, whereas the BrxAGC-roGFP2 and BrxAGA-roGFP2 active-site mutant proteins failed to respond to 10 μM BSSB and showed weaker responses to

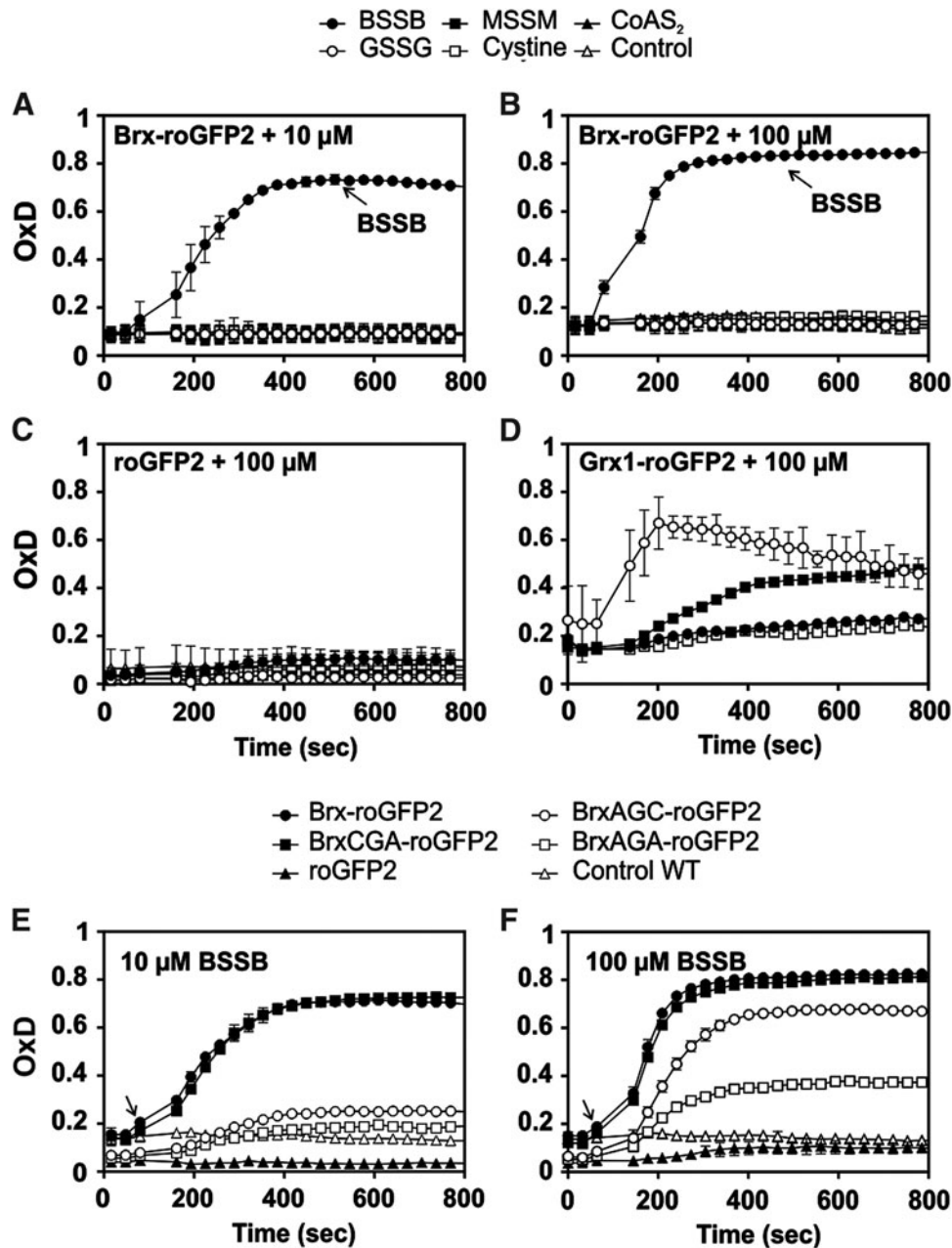


FIG. 2. Responses of purified Brx-roGFP2, Grx1-roGFP2, and roGFP2 *in vitro* to BSSB, GSSG, MSSM, cystine, and CoAS-disulfide. (A, B) Brx-roGFP2 responds specifically to 10 and 100 μ M BSSB *in vitro* but is nonresponsive to GSSG, MSSM, cystine, and CoAS disulfide ($n=3$; $p<0.0045$ for 10 μ M and $p<0.01$ for 100 μ M in all samples). (C) The roGFP2 probe does not respond to 100 μ M thiol disulfides ($n=3$; $p<0.0001$ for BSSB, GSSG, and MSSM; $p=0.93$ for cystine). (D) The Grx1-roGFP2 fusion shows a specific response to 100 μ M GSSG, but not to other thiol disulfides ($n=3$; $p<0.0033$ for all samples). (E, F) The response of Brx-roGFP2 to 10 μ M BSSB (E) and 100 μ M BSSB (F) was compared with the Brx-Cys mutant proteins BrxAGC-roGFP2, BrxCGA-roGFP2, BrxAGA-roGFP2, and roGFP2 ($n=3$; $p=0.27$ for 10 μ M BSSB BrxAGA; $p<0.0001$ for all others). Arrows denote the time point of oxidant exposure. The results showed that the Brx-roGFP2 response depends on the active-site Cys54 of Brx. The thiol disulfides were injected into the microplate wells 90 s after the start of measurements, and the biosensor response and OxD were analyzed using the CLARIOstar microplate reader. In all graphs, mean values are shown, error bars represent the SEM, and p -values are calculated using a Student's unpaired two-tailed t -test by the graph prism software. GSSG, oxidized glutathione disulfide; MSSM, mycothiol disulfide; OxD, oxidation degree.

100 μ M BSSB (Fig. 2E, F). In previous studies, the BSH content was determined as 0.5–1.6 μ mol/g raw dry weight in BSH-producing *S. aureus* strains (36). This equates to 0.5–1.6 mM intracellular BSH, assuming a 50% water content of the cellular biomass as determined for related bacteria (4).

The BSH/BSSB ratio was estimated as 1:20–1:40 (28, 32), indicating that the physiological BSSB content should be below 100 μ M in *S. aureus*. Thus, the Brx-roGFP2 biosensor is highly specific to detect physiological levels of 10–100 μ M BSSB *in vitro*.

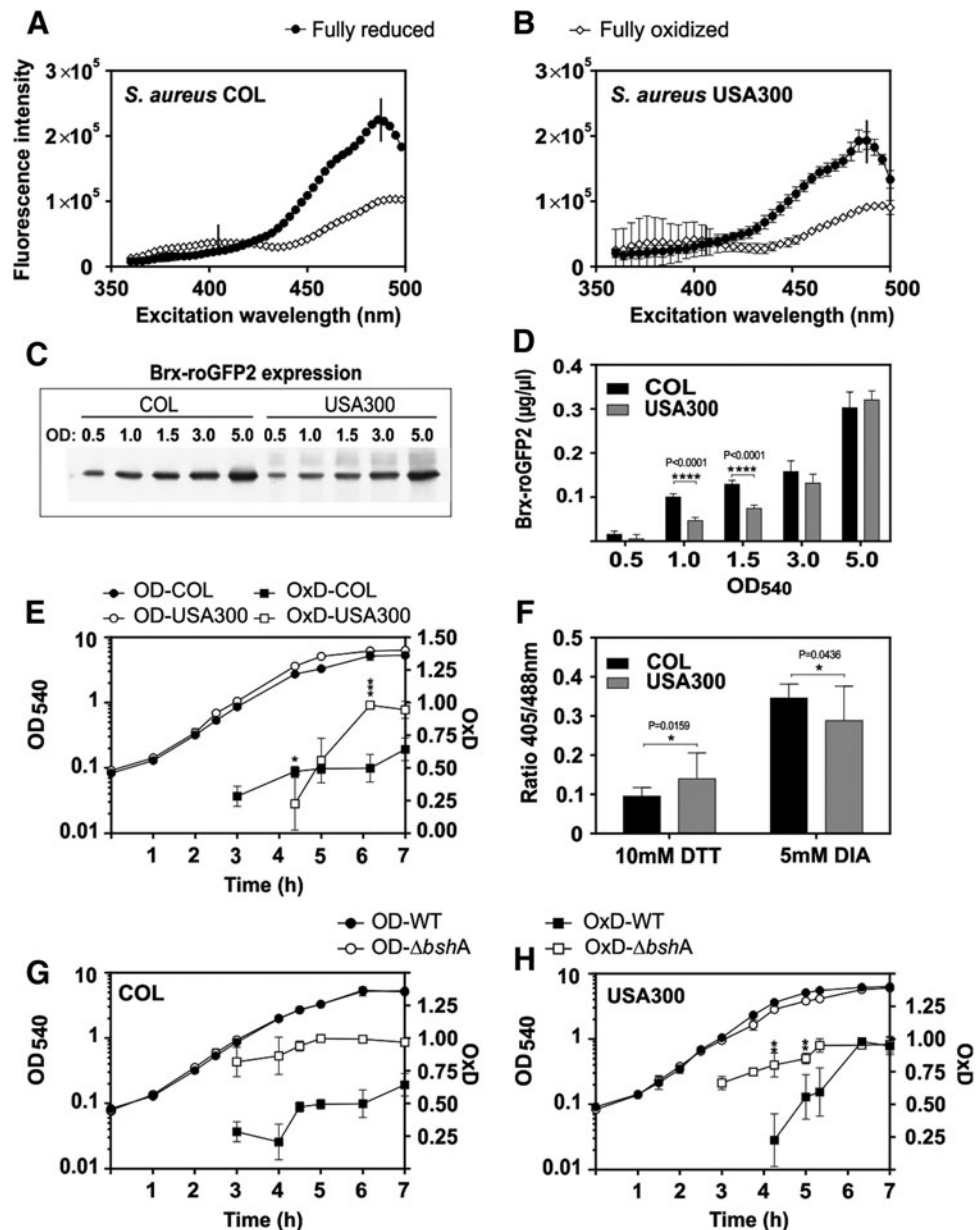


FIG. 3. Comparison of the Brx-roGFP2 response and expression in *S. aureus* COL and USA300 wild type and *bshA* mutants during the growth. (A, B) Ratiometric response of Brx-roGFP2 in *S. aureus* COL and USA300 after oxidation of cells by 5 mM diamide and reduction by 10 mM DTT ($n=7-8$; $p<0.0001$ in all samples). (C, D) Expression of Brx-roGFP2 is higher in *S. aureus* COL compared with USA300 during the log phase ($n=3$; $p<0.0001$ at OD1–1.5), and (E) the OxD is the most strongly increased during the stationary phase in USA300 ($n=3$; $p=0.0009$ at 6 h). (F) The dynamic range of Brx-roGFP2 is higher in *S. aureus* COL compared with USA300 ($n=3$; $p=0.0159$ DTT; $p=0.0436$ diamide). (G, H) The Brx-roGFP2 biosensor is constitutively oxidized in the *S. aureus* COL and USA300 *bshA* mutants in comparison to the wild-type strains ($n=3$; $p<0.0001$ in COL at all time points; $p<0.01$ in USA300 at 4–5.5 h). Symbols are defined as follows: ^{ns} $p>0.05$; * $p\leq 0.05$; ** $p\leq 0.01$; *** $p\leq 0.001$; and **** $p\leq 0.0001$. The OxD was calculated based on 405/488 nm excitation ratios with emission at 510 nm and related to the fully oxidized and reduced controls as described in the Materials and Methods section. In all graphs, mean values are shown, error bars represent the SEM, and p -values are calculated using a Student's unpaired two-tailed t -test by the graph prism software.

Response of Brx-roGFP2 in *S. aureus* MRSA strains COL and USA300 along the growth curve and effect of BSH deficiency on the biosensor response

To monitor the changes in E_{BSH} inside *S. aureus*, Brx-roGFP2 was expressed ectopically from plasmid pRB473

under control of a xylose-inducible promoter in two MRSA isolates COL and USA300. The *S. aureus* wild-type strains were grown in Luria Bertani (LB) medium overnight with xylose, and the strong roGFP2 fluorescence could be monitored using the microplate reader and fluorescence microscopy. First, we confirmed the ratiometric response of the Brx-roGFP2

biosensor inside *S. aureus* cells in the fully oxidized and reduced state after treatment with 5 mM diamide and 10 mM DTT, respectively, and monitored the changes at the 405 and 488 nm excitation maxima (Fig. 3A, B). Western blot analyses confirmed that Brx-roGFP2 is expressed as a full-length protein and is not degraded during the growth in *S. aureus* (Supplementary Fig. S3).

Next, the changes of the BSH redox potential were monitored during different stages of growth in LB medium in *S. aureus* (Fig. 3C–E). In fact, the expression and fluorescence intensity of Brx-roGFP2 varied between the *S. aureus* COL and USA300 wild-type strains along the growth. Although a significant Brx-roGFP2 fluorescence signal was detected in *S. aureus* COL already during the exponential growth, the expression and fluorescence of Brx-roGFP2 were much weaker in *S. aureus* USA300 during the log phase (Fig. 3C, D and Supplementary Fig. S4A, B). In both strains, the OxD of the Brx-roGFP2 increased during the stationary phase, reflecting growth-dependent redox changes (Fig. 3E). Furthermore, we observed that the dynamic range of the 405/488 nm ratios of fully reduced and oxidized Brx-roGFP2 was higher in COL (3.77 ± 0.65) compared with USA300 (2.37 ± 0.98) (Fig. 3F).

However, we confirmed that the level of Brx-roGFP2 did not affect the OxD, since serial dilutions of *S. aureus* cells that were harvested at an optical density (OD) of 4.0 showed the same OxD level (Supplementary Fig. S4C, D). Based on the OxD of the biosensor, the intracellular BSH redox potential was calculated using the Nernst' equation, ranging from -300 to -270 mV in COL and from -300 to -235 mV in USA300 during exponential growth until transition into the stationary phase (Supplementary Table S5).

We further compared biosensor oxidations between COL and USA300 wild types and isogenic BSH-deficient mutants. The biosensor was fully oxidized in the COL and USA300 *bshA* mutants, indicating an impaired redox balance and increased oxidative stress in the *bshA* mutant (Fig. 3G, H). This constitutive biosensor oxidation was also observed in strain RN4220, which is a natural *bshC* mutant of the *S. aureus* NCTC8325 lineage (27, 32, 33) (Supplementary Fig. S5). Western blot analyses confirmed that the biosensor is similarly expressed in the COL wild type and *bshA* mutant (Supplementary Fig. S6).

Response of Brx-roGFP2 in *S. aureus* COL to oxidative stress

The changes in E_{BSH} were further investigated in *S. aureus* COL wild type in response to oxidative stress, provoked by H_2O_2 and NaOCl. Previous studies have shown that NaOCl stress leads to *S*-bacillithiolation of proteins and a decreased BSH/BSSB redox ratio (7). Since *S. aureus* is extremely resistant to H_2O_2 (14, 40), the physiological sub-lethal concentrations of oxidants were determined (Fig. 4A, B). In addition, the role of BSH in the resistance to NaOCl and H_2O_2 was analyzed in survival assays. The *bshA* mutant was more sensitive than the wild type to 150 μ M NaOCl and 300 mM H_2O_2 , indicating that BSH contributes to oxidative stress resistance.

The change in E_{BSH} after exposure to 1–100 mM H_2O_2 and 10–100 μ M NaOCl and the time for detoxification of oxidants and recovery of the reduced state were investigated. The biosensor was rapidly and reversibly oxidized by 10–50 mM H_2O_2 , and cells approached a more reduced state within

70 min (Fig. 4C). Remarkably, 100 mM H_2O_2 did not result in complete oxidation of the biosensor (*e.g.*, OxD = 1), although *S. aureus* cells were unable to restore their reduced state. Treatment of cells with low doses of 10–20 μ M NaOCl resulted in reversible biosensor oxidation and required 200 min for regeneration of the reduced state. The biosensor was fully oxidized by 100 μ M NaOCl, but cells were unable to recover (Fig. 4D). Using nonreducing BSH-specific Western blot analysis, we further confirmed that 100 μ M NaOCl stress leads to the same increase of *S*-bacillithiolated proteins in *S. aureus* COL and COL Brx-roGFP2 strains, indicating that Brx-roGFP2 expression did not affect the *S*-bacillithiolation pattern (Supplementary Fig. S7).

To analyze the impact of Brx in the biosensor response to the oxidants *in vivo*, attempts were made to express unfused roGFP2 in *S. aureus* COL. However, in contrast to the Brx-roGFP2 fusion, expression of unfused roGFP2 failed in *S. aureus* COL containing the pRB473-roGFP2 plasmid. Thus, we compared the biosensor responses of the various Brx Cys mutant fusions (BrxAGC, BrxCGA, and BrxAGA) with the different oxidants *in vivo*. The response of Brx-roGFP2 and BrxCGA-roGFP2 to 50 mM H_2O_2 was fast and reversible, with recovery of the reduced state after 120 min. In contrast, oxidation of the Brx active-site Cys mutant fusions (BrxAGC and BrxAGA) by H_2O_2 was slower and not fully reversible (Fig. 4E). We further analyzed the responses of the BrxAGC, BrxCGA, and BrxAGA Cys mutant fusions to 20 μ M NaOCl. All Brx Cys mutants responded similarly to NaOCl, whereas the BrxAGA double-Cys mutant was unable to recover after 120 min (Fig. 4F). This indicates that a direct response of Brx-roGFP2 to high doses of 50 mM H_2O_2 and to the strong oxidant NaOCl could, in part, account for the oxidant responses in the absence of the CGC motif of Brx.

To monitor the direct biosensor response to the oxidants, both purified roGFP2 and Brx-roGFP2 proteins were treated with different concentrations of H_2O_2 and NaOCl (Supplementary Fig. S8). The results showed that both roGFP2 and Brx-roGFP2 respond strongly to 1–10 mM H_2O_2 and 50–100 μ M NaOCl, leading to complete biosensor oxidation. This confirms that the Brx-roGFP2 biosensor could also directly respond to high H_2O_2 doses and the strong oxidant NaOCl *in vivo* in the absence of the Brx CGC motif. Another possibility could be that the third conserved Cys of Brx at the C-terminus (Cys144) is *S*-bacillithiolated by BSSB *in vivo* in the absence of the CGC motif, leading to subsequent biosensor oxidation.

Confocal laser scanning microscopy of Brx-roGFP2 fluorescence in *S. aureus* COL wild type and Δ bshA mutant cells

The redox-dependent changes of Brx-roGFP2 fluorescence in *S. aureus* COL wild type and *bshA* mutant cells were analyzed using confocal laser scanning microscopy (CLSM) both before and after NaOCl stress. The biosensor fluorescence intensities were measured after excitation at 405 and 488 nm and false-colored in red and green, respectively (Fig. 5). The oxidation state of the biosensor is visualized by an overlay of both red and green images. Confocal imaging showed that Brx-roGFP2 is reduced in nontreated wild-type cells and resembles that of DTT-treated reduced cells with bright fluorescence at the 488 nm excitation wavelength

FIG. 4. Effect of NaOCl and H₂O₂ on the survival of *S. aureus* wild type and *bshA* mutants and oxidative stress responses of Brx-roGFP2 and Brx Cys-mutant fusions in *S. aureus* COL. (A, B) The *S. aureus* COL and USA300 *bshA* mutants are more sensitive to NaOCl and H₂O₂ stress compared with the wild type as revealed by survival assays (n=3; p=0.07 at 450 mM H₂O₂; p=0.0126 at 150 μM NaOCl). (C, D) The Brx-roGFP2 biosensor in *S. aureus* COL is rapidly and reversibly oxidized by sub-lethal concentrations of 1–50 mM H₂O₂ and 10–20 μM NaOCl, whereas higher doses result in constitutive biosensor oxidation (n=4; p=0.3186 at 1 mM H₂O₂; p<0.0001 in all other samples). (E, F) The response of Brx-roGFP2 and BrxCGA-roGFP2 to H₂O₂ and NaOCl is reversible compared with the active Cys Brx mutant fusions in *S. aureus* COL, which is not reversible (n=5; p<0.0001 in all samples). Arrows denote the time point of oxidant exposure. In all graphs, mean values are shown, error bars represent the SEM, and p-values are calculated using a Student's unpaired two-tailed t-test by the graph prism software. H₂O₂, hydrogen peroxide; NaOCl, sodium hypochlorite.

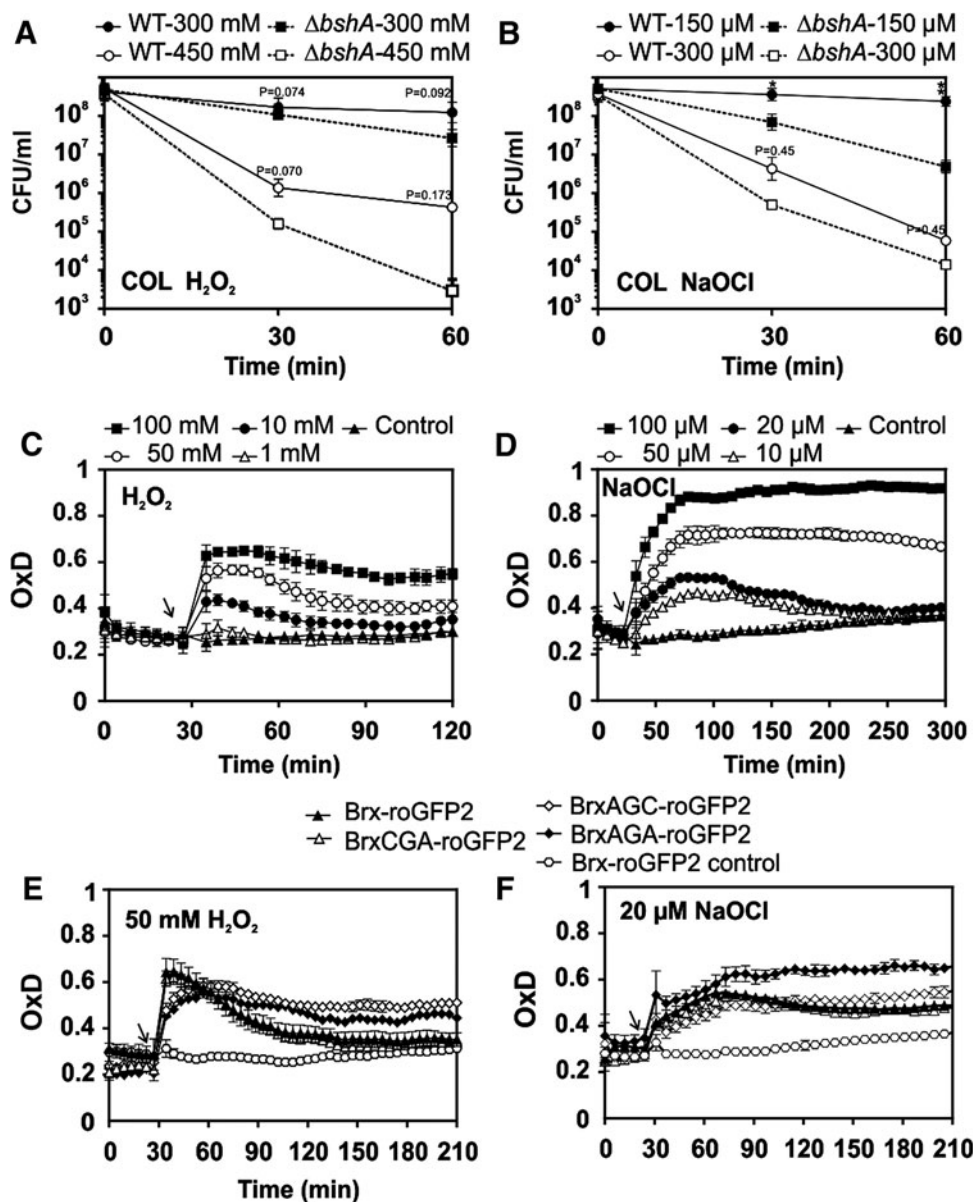


(Fig. 5). NaOCl stress leads to a decreased fluorescence intensity at the 488 nm excitation maximum and a strongly increased fluorescence at the 405 nm excitation maximum, as shown in the histograms. Thus, NaOCl-treated wild-type cells are visualized as red cells in the overlay images similar to the fully oxidized wild-type control. In the *S. aureus* COL *bshA* mutant, the Brx-roGFP2 biosensor was fully oxidized under control conditions as shown by the strong fluorescence in the 405 nm (red) channel that resembles the NaOCl-treated sample. The redox states of wild type and *bshA* mutant cells were calculated from five representative single cells and also using measurements in the microplate reader for comparison (Fig. 5C, D).

Response of Brx-roGFP2 in *S. aureus* after internalization by THP-1 macrophages

Next, we measured the changes in *E_{BSH}* of *S. aureus* under infection-like conditions during phagocytosis

assays with activated THP-1 macrophages. Infection assays were performed with *S. aureus* COL cells at a multiplicity of infection (MOI) of 25, and fluorescence excitation intensities were monitored at 405 and 488 nm. After 1 h of infection with *S. aureus* COL, about 70–80% of THP-1 cells showed a green fluorescence. As fully oxidized and reduced controls, infected macrophages were treated with 150 μM NaOCl and 20 mM DTT, respectively, and the mean fluorescence intensity (MFI) at 405 and 488 nm was analyzed using flow cytometry (Supplementary Table S7). The 405/488 nm ratio of the MFI of fully reduced and oxidized THP-1 controls was calibrated to 0% and 100% oxidation and related to the 405/488 nm ratio of the MFI of infected macrophages. In comparison to these fully reduced and oxidized THP-1 controls, the biosensor was 87% oxidized in *S. aureus* COL during infection after uptake by macrophage-like cells (Supplementary Table S7).

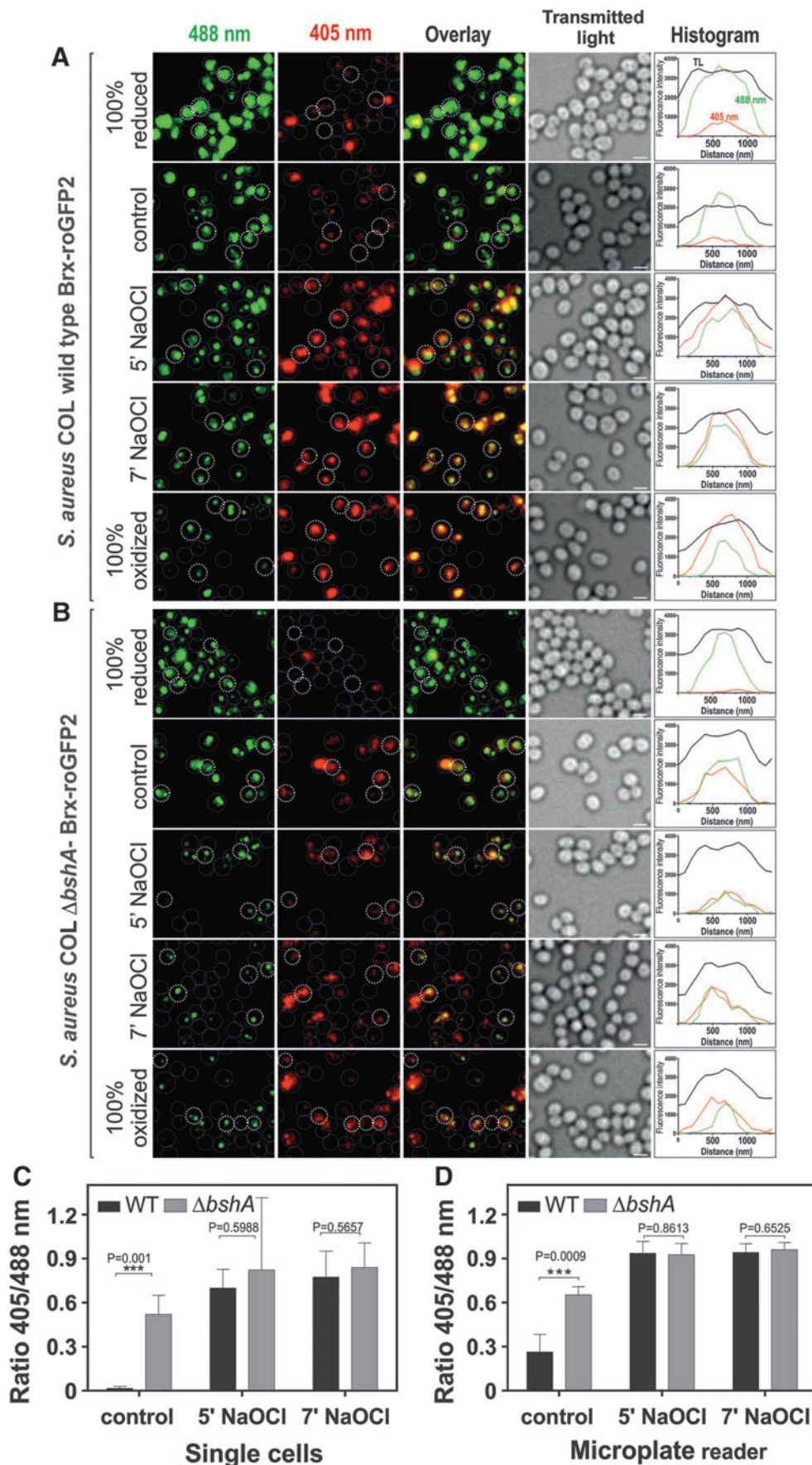


FIG. 5. Live-imaging of *S. aureus* COL Brx-roGFP2 in the wild type and the *bshA* mutant during NaOCl stress. (A, B) *S. aureus* COL Brx-roGFP2 wild type and *bshA* mutant strains were exposed to 150 μ M NaOCl, blocked with NEM, and analyzed using CLSM. Cells treated with 10 mM DTT and 5 mM diamide were used as fully reduced and oxidized controls, respectively. Fluorescence emission was measured at 505–550 nm after excitation at 405 and 488 nm. Fluorescence intensities at the 488 and 405 nm excitation maxima are false-colored in green and red, respectively, and are shown in the overlay images and histograms for single cells. The NaOCl-induced oxidation in the wild type and constitutive oxidation of the biosensor in the $\Delta bshA$ mutant are visualized by the overlay images, and the cells are encircled based on the transmitted light image. The histograms show average fluorescence intensities at 405 and 488 nm calculated from five representative single cells. (C) The average 405/488 nm ratios of the wild type and *bshA* mutant samples were calculated from five representative single cells each for the wild type and *bshA* mutant that are marked with bold circles ($n=5$; $p=0.001$ for control WT/*bshA*). (D) For comparison, the 405/488 nm ratios were also calculated from the same *S. aureus* samples using the microplate reader ($n=3$; $p=0.0009$ for control WT/*bshA*). Symbols are defined as follows: *** $p < 0.001$. In all graphs, mean values are shown, error bars represent the SEM, and p -values are calculated using a Student's unpaired two-tailed t -test by the graph prism software. CLSM, confocal laser scanning microscopy; NEM, *N*-ethylmaleimide. To see this illustration in color, the reader is referred to the web version of this article at www.liebertpub.com/ars

Effects of antibiotics on the Brx-roGFP2 biosensor response in *S. aureus* COL

We were interested in the changes of the BSH redox potential in response to sub-lethal antibiotics that are commonly used to treat MRSA infections. The aim was to clarify a long debate about the involvement of oxidative stress in the killing mode of antibiotics (16, 18). We have chosen antibiotics with different cellular target sites, including RNA polymerase inhibitors (rifampicin), cell-wall biosynthesis inhibitors (fosfomycin, ampicillin, oxacillin, and vancomycin), aminoglycosides as protein biosynthesis inhibitors that target the ribosome (gentamycin, lincomycin, erythromycin, and linezolid), and fluoroquinolones (ciprofloxacin) that inhibit the DNA gyrase and topoisomerase IV to block DNA replication.

S. aureus COL with Brx-roGFP2 was treated with sub-lethal concentrations of antibiotics and analyzed for its biosensor response. The sub-lethal antibiotics doses that caused a reduced growth rate were determined as 0.1 μ M erythromycin, 0.1 μ M rifampicin, 5 μ M vancomycin, 30 μ M ciprofloxacin, 0.5 μ g/ml gentamicin, 10 μ M ampicillin, 50 mM fosfomycin, 5 μ M lincomycin, 2 μ g/ml linezolid, and 2 mM oxacillin. The measurement of the Brx-roGFP2 response revealed no increased biosensor oxidation by any of these antibiotics compared with the untreated control (Fig. 6 and Supplementary Table S6). These results document that sub-lethal antibiotics do not cause changes in the BSH redox potential in *S. aureus*.

Discussion

Redox-sensitive GFPs have been recently fused to glutaredoxin and mycoredoxin for dynamic measurements of the intracellular redox potential in eukaryotes and mycobacteria in real time and at high sensitivity and spatiotemporal resolution (35). Here, we coupled the bacilliredoxin (Brx) to roGFP2 to measure the intracellular BSH redox potential in *S. aureus* cells under infection conditions, ROS, and antibiotics treatments. This Brx-roGFP2 biosensor is highly sensitive and specific for physiological levels of BSSB, whereas unfused roGFP2 and the BrxAGC active-site mutant roGFP2 fusion are much lower responsive to BSSB *in vitro*.

The role of the active-site Cys of Brx for reduction of *S. bacillithiolated* OhrR and MetE has been previously shown for *B. subtilis* BrxA and BrxB (9). The specific reaction of the active site Cys54 with BSSB was verified here for the *S. aureus* Brx homolog SAUSA300_1321 in the Brx-roGFP2 fusion. Thus, coupling of roGFP2 with the Brx facilitates rapid equilibration of the biosensor with the BSH/BSSB redox pair to selectively measure changes in the BSH redox potential. However, weaker responses of the BrxAGC and BrxAGA active site and double mutants were observed by 100 μ M BSSB, which could depend on the third C-terminal Cys144 residue that is also conserved across the UPF0403 family of Brx-homologs (Supplementary Fig. S1).

The Brx-roGFP2 biosensor was applied to monitor the changes in the BSH redox potential inside the archaic hospital-acquired MRSA isolate COL and the community-acquired MRSA strain USA300. In both MRSA strains, BSH is required for survival under oxidative stress and infection-related conditions during phagocytosis with macrophages (32, 33). Here, we confirmed that BSH-deficient mutants of *S. aureus* COL and USA300 are more sensitive to H₂O₂ and

NaOCl compared with the wild types. We further monitored the perturbations in the BSH redox potential during growth, oxidative challenge, and infection assays with THP-1 macrophages. Increases in E_{BSH} were observed in *S. aureus* COL and USA300 strains during the stationary phase in LB medium compared with the log phase. However, we confirmed that the expression level of Brx-roGFP2 did not affect the OxD (Supplementary Fig. S4C, D).

The dynamic range of Brx-roGFP2 was lower in USA300 compared with COL, which could depend on the 1.6-fold higher BSH levels in USA300 (32). Differences in the basal level oxidation and dynamic range were also observed between drug-sensitive (3D7) and -resistant (Dd2) *P. falciparum* parasites (15). In *P. falciparum* 3D7, the lower basal OxD of the biosensor could be explained by the higher GSH levels. Thus, the higher BSH levels in USA300 could result in a higher reducing capacity and a lower biosensor response to diamide.

We further showed that the Brx-roGFP2 biosensor in *S. aureus* COL responds rapidly to ROS, such as H₂O₂ and NaOCl. However, *S. aureus* is resistant to high levels of 300 mM H₂O₂ (40). Thus, treatment of *S. aureus* with 1–10 mM H₂O₂ resulted in only a slightly increased biosensor oxidation with rapid regeneration of the reduced state. Exposure to 50–100 μ M NaOCl stress caused the complete and constitutive oxidation of the biosensor and correlates with the observed *S*-bacillithiolation of proteins and increased levels of BSSB under NaOCl stress in *S. aureus* (7). The comparison of the biosensor response of Brx-roGFP2 with that of the Brx Cys mutant fusion revealed a similar response but changes in the recovery after H₂O₂ and NaOCl stress, which was impaired in the Brx active-site mutants. Thus, the biosensor could also directly respond to the high H₂O₂ levels and the strong oxidant NaOCl *in vivo*.

The changes in BSH redox potential were also measured inside *S. aureus* COL during phagocytosis assays in THP-1 macrophage cell lines. The flow cytometric data showed that the Brx-roGFP2 biosensor was 87% oxidized in *S. aureus* COL under infection conditions.

The comparison of the biosensor response in *S. aureus* COL and USA300 wild types and the isogenic *bshA* mutants as well as in the natural *bshC*-deficient strain RN4220 revealed a constitutive oxidation of the probe in the absence of BSH. This high biosensor oxidation in BSH-deficient strains is also visualized by confocal imaging at the cellular level. These results are in agreement with the constitutive oxidation of the Grx-roGFP2 biosensor on GSH depletion in *Arabidopsis thaliana* seeds (23). Thus, our data clearly document the impaired redox balance in the absence of BSH and the major role of BSH in keeping the reduced state of the cytoplasm in *S. aureus* cells. In addition to BSH depletion, much lower NADPH levels were previously measured in the Δ *bshA* mutant, which could contribute to the impaired thiol-redox balance (32).

In *S. aureus*, coenzyme A and Cys were suggested to function as alternative thiol-redox buffers and *S. aureus* also encodes a CoAS disulfide reductase to keep CoASH in the reduced state (22). However, based on the microscopic and macroscopic pK_a values of BSH, the level of the reactive thiolate anion is much higher in BSH compared with CoASH and Cys at physiological pH values (36). Thus, BSH is the only available nucleophilic thiol that reacts with protein

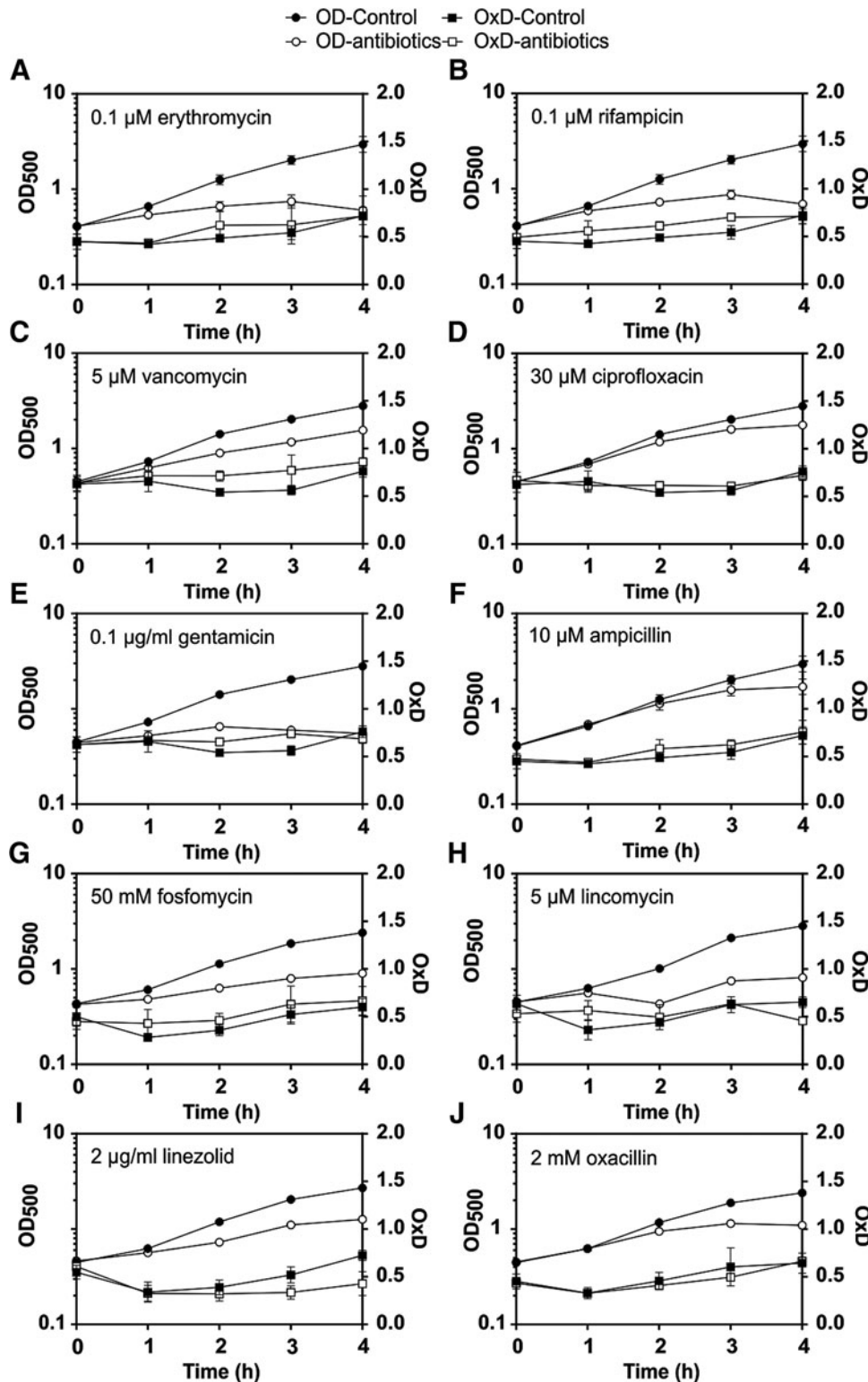


FIG. 6. Growth curves and OxD of *S. aureus* COL Brx-roGFP2 after exposure to sub-lethal concentrations of antibiotics that decreased the growth rate. *S. aureus* was exposed to sub-lethal concentrations of antibiotics at an OD₅₀₀ of 0.5, and the OxD of Brx-roGFP2 was monitored in treated and untreated cells ($n=4$; $p>0.05$ for OxD control/antibiotics treatment in all samples). The following sub-lethal antibiotics were used: (A) 0.1 μ M erythromycin, (B) 0.1 μ M rifampicin, (C) 5 μ M vancomycin, (D) 30 μ M ciprofloxacin, (E) 0.1 μ M gentamicin, (F) 10 μ M ampicillin, (G) 50 mM fosfomycin, (H) 5 μ M lincomycin, (I) 2 μ g/ml linezolid, and (J) 2 mM oxacillin. There was no increased oxidation by antibiotics in *S. aureus*. In all graphs, mean values are shown, error bars represent the SEM, and p -values are calculated using a Student's unpaired two-tailed t -test by the graph prism software.

disulfides that are formed under oxidative stress in *S. aureus* (29, 30, 36). Consistent with this notion, neither cystine nor CoAS disulfide were recognized by Brx at physiological concentrations to oxidize the biosensor *in vitro*.

Previous studies identified the OhrR repressor as redox controlled under organic peroxide and NaOCl stress by *S*-cysteinylation and *S*-bacillithiolation (6, 17). BrxA and BrxB

were specific for reduction and reactivation of *S*-bacillithiolated OhrR, but they could not regenerate *S*-cysteinylated OhrR (9). These results further support our findings about the specificity of Brx of *S. aureus* for BSSB.

Finally, we studied the changes in the BSH redox potential in *S. aureus* after treatment with sub-lethal doses of different antibiotics to clarify the role of oxidative stress as a killing

mode for antibiotics, a controversial debate among microbiologists (16, 18). However, we could not detect changes in the BSH redox potential after treatment with rifampicin, fosfomycin, ampicillin, oxacillin, vancomycin, aminoglycosides, and fluoroquinolones. Similar to our results, no roGFP2 response was detected by any of these antibiotics in *Salmonella* (39). However, *S. aureus* is resistant to 100 mM H₂O₂ without the killing effect. Thus, *S. aureus* might be resistant to ROS produced under antibiotics treatment.

In conclusion, we have constructed a novel Brx-roGFP2 biosensor that is highly specific to sense the reduced pool of BSH inside *S. aureus* cells and that responds to oxidative stress under infection-like conditions inside macrophages. Using this novel tool, we could demonstrate that commonly used antibiotics do not cause oxidative stress when applied to *S. aureus* and that BSH-deficient mutants have an impaired redox balance and reduced virulence. *S. aureus* is an important human pathogen with new MRSA strains and other multiple antibiotic-resistant isolates emerging quickly. This novel probe can be applied in drug research to screen for new redox-active antibiotics that affect the BSH redox potential in *S. aureus*. In addition, the difference in the ROS detoxification capacity and resistance to host defenses can be monitored across emerging MRSA isolates to understand the connection between virulence factor expression, antibiotics resistance, and the BSH redox potential in *S. aureus*.

Materials and Methods

Bacterial strains, growth conditions, stress, and antibiotics treatments

Bacterial strains, plasmids, and primers are listed in Supplementary Tables S1–S3. For cloning and genetic manipulation, *E. coli* was cultivated in LB medium. *S. aureus* strains with the pRB473-XylR-Brx-roGFP2 plasmids were cultivated in LB medium with 1% xylose to ensure constitutive expression of the biosensor. For stress experiments, *S. aureus* cells were grown in LB until an optical density at 540 nm (OD₅₄₀) of 1.0 and were transferred to Belitsky minimal medium (BMM) with 1% xylose. The fully reduced control cells were treated with 10 mM DTT and the fully oxidized control was treated with 5 mM diamide for 20 min each, harvested with 10 mM *N*-ethylmaleimide (NEM) to block the biosensor redox state, and transferred to the microplate wells. The samples for stress exposure were transferred to the microplates, and different oxidants were injected into the wells of microplates. The Brx-roGFP2 biosensor fluorescence emission was measured at 510 nm after excitation at 405 and 488 nm using the CLARIOstar microplate reader (BMG Labtech) as described next for the *in vitro* measurements. Three biological tests were performed for each stress experiment.

For the survival assays, *S. aureus* COL wild type and the *bshA* mutant were treated with NaOCl and H₂O₂ at an OD₅₀₀ of 1.0 in BMM and serial dilutions were plated on LB agar plates and counted for colony-forming units. The survival assays were performed in three biological replicates for each strain.

For the determination of the growth-inhibitory and sub-lethal antibiotics concentrations, *S. aureus* was cultivated in RPMI medium and the antibiotics erythromycin, rifampicin, vancomycin, ciprofloxacin, gentamicin, ampicillin, fosfomycin, lincomycin, linezolid, or oxacillin were added at an

OD₅₀₀ of 0.5 to monitor the reduction in growth as previously described (8). The measurements of the biosensor responses after antibiotics treatment were performed in *S. aureus* Brx-roGFP2 cells that were grown in RPMI medium and treated with sub-lethal antibiotics doses that reduced the growth rate. Cells were harvested after different times of antibiotics treatment, washed with phosphate-buffered saline (PBS), and blocked with NEM before the microplate reader measurements. Four biological replicates were performed for each antibiotics stress experiment. Sodium hypochlorite, diamide, DTT, H₂O₂ (35% w/v), and antibiotics (erythromycin, rifampicin, vancomycin, ciprofloxacin, gentamicin, ampicillin, fosfomycin, lincomycin, linezolid, and oxacillin) were purchased from Sigma-Aldrich.

Construction, expression, and purification of Brx-roGFP2 in E. coli

The Grx-roGFP2 containing plasmid pQE60-Grx1-roGFP2 was obtained from Tobias Dick and colleagues (11) and used as a template for construction of the Brx-roGFP2 fusion. The *brx* gene (SAUSA300_1321) was amplified from chromosomal DNA of *S. aureus* USA300 by polymerase chain reaction (PCR) using primers SAUSA300-1321yphP-FOR-BamHI-NcoI and SAUSA300-1321yphP-REV-SpeI (Supplementary Table S3), digested with *Bam*HI and *Spe*I, and inserted into plasmid pQE60-Grx1-roGFP2 that was digested using the same restriction enzymes to generate plasmid pQE60-Brx-roGFP2. The *brx-roGFP2* sequence was amplified from plasmid pQE60-Brx-roGFP2 by PCR using primers 1321-roGFP2-FOR-NheI and roGFP2-REV-BamHI, digested with *Nhe*I and *Bam*HI, and sub-cloned into pET11b (Novagen) after digestion by the same enzymes to generate plasmid pET11b-Brx-roGFP2.

For construction of the roGFP2 fusions with the Brx-Cys-to-Ala variants, the Cys residues of the C₅₄GC₅₆ active site were replaced by alanine using PCR mutagenesis. For the *brxC54A* mutant, two first-round PCR reactions were performed using primers SAUSA300-1321yphP-FOR-BamHI-NcoI and SAUSA300-1321-yphP-C56A-REV and primers SAUSA300-1321-yphP-C54A-FOR and SAUSA300-1321yphP-REV-SpeI. For the *brxC56A* mutant, two first-round PCR reactions were performed using primers SAUSA300-1321yphP-FOR-BamHI-NcoI and SAUSA300-1321-yphP-C56A-REV and primers SAUSA300-1321-yphP-C56A-FOR and SAUSA300-1321yphP-REV-SpeI. The two PCR products of each first-round PCR reaction were hybridized and, subsequently, amplified by a second-round PCR reaction using primers SAUSA300-1321yphP-FOR-BamHI-NcoI and SAUSA300-1321yphP-REV-SpeI. The PCR products from the second-round PCRs were then digested with *Bam*HI and *Spe*I and inserted into plasmid pQE60-Grx1-roGFP2 that was digested with the same enzymes. Sub-cloning of the Brx-Cys-to-Ala mutant roGFP2 fusions into pET11b was performed as described earlier.

To construct the *brxC54A-C56A* double mutant, first-round PCR was performed using primers 1321-roGFP2-FOR-NheI and 1321-brx-C54A56A-REV and primers 1321-brx-C54A56A-FOR and SAUSA300-1321yphP-REV-SpeI. Then, the PCR products from first-round PCR reactions were fused by PCR using primers 1321-roGFP2-FOR-NheI and SAUSA300-1321yphP-REV-SpeI. The PCR product from the second-round

PCR was then digested with *NheI* and *SpeI* and inserted into plasmid pET11b-Brx-roGFP2 that was digested with the same enzymes.

To construct plasmid pET11b-roGFP2, primers roGFP2-FOR-*NheI* and roGFP2-REV-*BamHI* were used to amplify *roGFP2* from plasmid pQE60-Grx1-roGFP2. The PCR product was digested with *NheI* and *BamHI* and inserted into plasmid pET11b that was digested with the same enzymes. The correct sequences of all plasmid inserts were confirmed by PCR amplification and sequencing.

For Brx-roGFP2 expression, *E. coli* BL21(DE3) *plysS* containing the pET11-Brx-roGFP2 plasmids was grown in 1 L LB medium and 1 mM IPTG (isopropyl- β -D-thiogalactopyranoside) was added at the exponential phase (OD₆₀₀ of 0.8) for 16 h at 25°C. Recombinant His-Brx-roGFP2 and the Brx-Cys-to-Ala mutant roGFP2 fusion proteins were purified using PrepEase His-tagged high-yield purification resin (USB) under native conditions according to the manufacturer's instructions (USB). The purified proteins were extensively dialyzed against 10 mM Tris-HCl (pH 8.0), 100 mM NaCl, and 50% glycerol and stored at -80°C.

Microplate reader measurements of Brx-roGFP2 and calculation of OxD and E_{B_{SH}}

To study the Brx-roGFP2 response *in vitro*, the purified proteins were reduced with 10 mM DTT for 20 min, desalted with Micro-Bio spin columns (Bio-Rad), and diluted to 1 μ M in 100 mM potassium phosphate buffer, pH 7.0. Fluorescence excitation spectra of Brx-roGFP2 were analyzed both before and after exposure to the oxidants using the CLARIOstar microplate reader (BMG Labtech) with the Control software version 5.20 R5. Fluorescence excitation spectra were scanned from 360 to 500 nm with a bandwidth of 10 nm, and emission was measured at 510 nm. Gain setting was adjusted for each excitation maximum. The data were analyzed using the MARS software version 3.10 and exported to Excel. Each *in vitro* measurement was performed in triplicate, as indicated in the figure legend. The OxD of the biosensor was calculated using Equation (1), as previously described (24, 25).

$$\text{OxD} = \frac{1405 \times 1488_{\text{red}} - 1405_{\text{red}} \times 1488}{1405 \times 1488_{\text{red}} - 1405 \times 1488_{\text{ox}} + 1405_{\text{ox}} \times 1488 - 1405_{\text{red}} \times 1488} \quad (1)$$

The values I405 and I488 are the observed fluorescence excitation intensities at 405 and 488 nm, respectively. The values I405_{red}, I488_{red}, I405_{ox}, and I488_{ox} are the fluorescence excitation intensities at 405 and 488 nm of fully reduced and oxidized probes, respectively.

The biosensor redox potential E_{roGFP2} was calculated according to the Nernst Equation (2), as previously described (25).

$$E_{\text{roGFP2}} = E_{\text{roGFP2}}^{\circ} - \left(\frac{RT}{2F} \right) * \ln \left(\frac{1 - \text{OxD}_{\text{roGFP2}}}{\text{OxD}_{\text{roGFP2}}} \right) \quad (2)$$

Because the biosensor equilibrates with the BSH/BSSB redox couple, $E_{\text{BSH}} = E_{\text{roGFP2}}$.

Construction of Brx-roGFP2 fusions in *S. aureus*

The *brx-roGFP2* sequence was amplified with primers SAUSA300-1321-FOR-*BamHI*-2 and roGFP2-REV-*KpnI*-3, and the forward primer also includes the Shine-Dalgarno sequence of the *brx* gene. The PCR product was digested with *BamHI* and *KpnI* and inserted into the pRB473-*XylR* shuttle vector that was digested using the same enzymes to generate pRB473-*XylR*-Brx-roGFP2. The plasmids were cloned in *E. coli* DH5 α and electroporated into competent cells of *S. aureus* RN4220. The plasmids were transferred into the *S. aureus* target strains COL and USA300 by phage transduction using bacteriophage 80 as previously described (26). *S. aureus* transductants were selected on LB agar with chloramphenicol. The plasmids were isolated and confirmed by PCR and sequencing of the *brx-roGFP2* fusion.

Western blot analyses for Brx-roGFP2 expression and BSH-mixed disulfides in *S. aureus*

S. aureus strains with Brx-roGFP2 were grown in LB with 1% xylose and harvested at different times during the growth. Cells were washed in Tris-buffer (pH 8.0) with 10 mM NEM, disrupted using the ribolyzer and the protein extract was cleared from cell debris by repeated centrifugation. Protein amounts of 25 μ g were analyzed by Western blot analysis using mouse-anti-GFP monoclonal antibodies (Cat. No. 12616810949; Tebu Biosciences) as previously described (11). Quantification was performed using the ImageJ software (ver. 1.48, <http://imagej.nih.gov>) based on a standard curve with purified Brx-roGFP2. The BSH-mixed disulfides were analyzed after exposure of *S. aureus* cells to 100 μ M NaOCl using nonreducing SDS-PAGE and BSH-specific Western blot analysis with polyclonal rabbit BSH-antibodies as previously described (7).

CLSM of *S. aureus* Brx-roGFP2 strains

S. aureus strains with Brx-roGFP2 were exposed to 150 μ M NaOCl, harvested both before and after the stress, blocked with NEM, and analyzed by CLSM using a ZEISS LSM510meta. The microscope was equipped with a 100 \times 1.3 M27 EC plan-neofluar oil objective. Fluorescence excitation was performed at 405 and 488 nm, and emission was measured using the 505–550 nm band pass filter. Cells treated with 10 mM DTT and 5 mM diamide were used as fully reduced and oxidized controls, respectively. The argon/2 and 405 nm laser power were set to 20% and 8%, respectively. The smart gain was 948 V. All setting parameters for the CLSM are listed in Supplementary Table S4. The microscope was calibrated with fully oxidized and reduced *S. aureus* Brx-roGFP2 controls. Quantification of the OxD values was performed from five cells each from each sample, and the experiments were performed in two biological replicates.

Flow cytometry of *S. aureus* Brx-roGFP2 strains during infection of THP-1 macrophage cell lines

For the infection assays, we used the human monocytic leukemia cell line THP-1, which was purchased from the DSMZ strain collection in Heidelberg (DSMZ-No. ACC-16). The cell line was authenticated by multiplex PCR of mini-satellite markers, which revealed a unique DNA profile, and the expression of fusion gene MLL-MLLT3 (MLL-AF9) was confirmed by real-time PCR. Cell cultures were checked for

absence of mycoplasma contaminations by PCR on a regular basis. This cell line is not included in the database of commonly misidentified cell lines as maintained by ICLAC. THP-1 cells were cultivated in RPMI-1640 medium with 10% heat-inactivated fetal bovine serum (FBS) and seeded in 60 mm cell culture dishes at a density of 4.5×10^6 cells. Differentiation was induced by 100 nM phorbol 12-myristate 13-acetate (PMA) for 24 h, followed by washing of cells with Hanks' balanced salts solution and the addition of fresh medium without PMA.

After 24 h of incubation, infection assays of THP-1 macrophages with *S. aureus* were performed as follows. First, *S. aureus* COL cells expressing Brx-roGFP2 were grown in LB with 1% xylose until OD₅₄₀ of 0.5 was reached. Bacterial cells were harvested, washed twice, and incubated in RPMI-1640 medium. Infection of THP-1 cells with *S. aureus* Brx-roGFP2 was performed at an MOI of 25 for 1 h. The infected THP-1 cells were washed twice in PBS buffer, detached with 0.05% trypsin and 0.02% EDTA, centrifuged, and resuspended in PBS buffer with 1% FBS.

Measurement by flow cytometry was performed on an Attune Acoustic Focusing Cytometer (Life Technologies) with excitation at 405 and 488 nm and emission at 515–545 nm. Ten thousand events were gated, and the MFI was determined with Attune software V2.1.0 or FlowJo V10.07 (Tree Star). For reduced and oxidized controls, infected THP-1 cells were treated with 20 mM DTT and 150 μ M NaOCl, respectively. Infection experiments were performed in three biological replicates.

Acknowledgments

This work was supported by a grant from the Deutsche Forschungsgemeinschaft (AN746/4-1) within the SPP1710 on “Thiol-based Redox switches” and by the DFG grants AN746/3-1 and project C1 of the research training group GRK1947 to H.A. The support from the SFB-TR34 (project A8) to M.M. and J.P.-F. is further acknowledged. The authors are grateful to Tobias Dick for providing the plasmid pQE60 with the Grx-roGFP2 fusion and to Ambrose Cheung for the kind gift of the *S. aureus* *bshA* mutants in the COL and USA300 backgrounds. They would also like to thank all members of the SPP1710 consortium for stimulating discussions about their Brx-roGFP2 biosensor results.

Author Disclosure Statement

No competing financial interests exist.

References

1. Archer GL. *Staphylococcus aureus*: a well-armed pathogen. *Clin Infect Dis* 26: 1179–1181, 1998.
2. Bhaskar A, Chawla M, Mehta M, Parikh P, Chandra P, Bhave D, Kumar D, Carroll KS, and Singh A. Reengineering redox sensitive GFP to measure mycothiol redox potential of *Mycobacterium tuberculosis* during infection. *PLoS Pathog* 10: e1003902, 2014.
3. Boucher HW and Corey GR. Epidemiology of methicillin-resistant *Staphylococcus aureus*. *Clin Infect Dis* 46(Suppl 5): S344–S349, 2008.
4. Bratbak G and Dundas I. Bacterial dry matter content and bio-mass estimations. *Appl Environ Microbiol* 48: 755–757, 1984.
5. Chen PR, Brugarolas P, and He C. Redox signaling in human pathogens. *Antioxid Redox Signal* 14: 1107–1118, 2011.
6. Chi BK, Gronau K, Mäder U, Hessling B, Becher D, and Antelmann H. S-bacillithiolation protects against hypochlorite stress in *Bacillus subtilis* as revealed by transcriptomics and redox proteomics. *Mol Cell Proteomics* 10: M111.009506, 2011.
7. Chi BK, Roberts AA, Huyen TT, Bäsell K, Becher D, Albrecht D, Hamilton CJ, and Antelmann H. S-bacillithiolation protects conserved and essential proteins against hypochlorite stress in firmicutes bacteria. *Antioxid Redox Signal* 18: 1273–1295, 2013.
8. Dörries K, Schlueter R, and Lalk M. Impact of antibiotics with various target sites on the metabolome of *Staphylococcus aureus*. *Antimicrob Agents Chemother* 58: 7151–7163, 2014.
9. Gaballa A, Chi BK, Roberts AA, Becher D, Hamilton CJ, Antelmann H, and Helmann JD. Redox regulation in *Bacillus subtilis*: the bacilliredoxins BrxA(YphP) and BrxB(YqiW) function in de-bacillithiolation of S-bacillithiolated OhrR and MetE. *Antioxid Redox Signal* 21: 357–367, 2014.
10. Gaballa A, Newton GL, Antelmann H, Parsonage D, Upton H, Rawat M, Claiborne A, Fahey RC, and Helmann JD. Biosynthesis and functions of bacillithiol, a major low-molecular-weight thiol in Bacilli. *Proc Natl Acad Sci U S A* 107: 6482–6486, 2010.
11. Gutscher M, Pauleau AL, Marty L, Brach T, Wabnitz GH, Samstag Y, Meyer AJ, and Dick TP. Real-time imaging of the intracellular glutathione redox potential. *Nat Methods* 5: 553–559, 2008.
12. Helmann JD. Bacillithiol, a new player in bacterial redox homeostasis. *Antioxid Redox Signal* 15: 123–133, 2011.
13. Hillion M and Antelmann H. Thiol-based redox switches in prokaryotes. *Biol Chem* 396: 415–444, 2015.
14. Horsburgh MJ, Clements MO, Crossley H, Ingham E, and Foster SJ. PerR controls oxidative stress resistance and iron storage proteins and is required for virulence in *Staphylococcus aureus*. *Infect Immun* 69: 3744–3754, 2001.
15. Kasozi D, Mohring F, Rahlfs S, Meyer AJ, and Becker K. Real-time imaging of the intracellular glutathione redox potential in the malaria parasite *Plasmodium falciparum*. *PLoS Pathog* 9: e1003782, 2013.
16. Kohanski MA, Dwyer DJ, Hayete B, Lawrence CA, and Collins JJ. A common mechanism of cellular death induced by bactericidal antibiotics. *Cell* 130: 797–810, 2007.
17. Lee JW, Soonsanga S, and Helmann JD. A complex thiolate switch regulates the *Bacillus subtilis* organic peroxide sensor OhrR. *Proc Natl Acad Sci U S A* 104: 8743–8748, 2007.
18. Liu Y and Imlay JA. Cell death from antibiotics without the involvement of reactive oxygen species. *Science* 339: 1210–1213, 2013.
19. Livermore DM. Antibiotic resistance in staphylococci. *Int J Antimicrob Agents* 16(Suppl 1): S3–S10, 2000.
20. Loi VV, Rossius M, and Antelmann H. Redox regulation by reversible protein S-thiolation in bacteria. *Front Microbiol* 6: 187, 2015.
21. Lowy FD. *Staphylococcus aureus* infections. *N Engl J Med* 339: 520–532, 1998.
22. Mallett TC, Wallen JR, Karplus PA, Sakai H, Tsukihara T, and Claiborne A. Structure of coenzyme A-disulfide reductase from *Staphylococcus aureus* at 1.54 Å resolution. *Biochemistry* 45: 11278–11289, 2006.
23. Meyer AJ, Brach T, Marty L, Kreye S, Rouhier N, Jacquot JP, and Hell R. Redox-sensitive GFP in *Arabidopsis thaliana*

- is a quantitative biosensor for the redox potential of the cellular glutathione redox buffer. *Plant J* 52: 973–986, 2007.
24. Meyer AJ and Dick TP. Fluorescent protein-based redox probes. *Antioxid Redox Signal* 13: 621–650, 2010.
 25. Morgan B, Sobotta MC, and Dick TP. Measuring E(GSH) and H₂O₂ with roGFP2-based redox probes. *Free Radic Biol Med* 51: 1943–1951, 2011.
 26. Müller M, Reiss S, Schlüter R, Mäder U, Beyer A, Reiss W, Marles-Wright J, Lewis RJ, Pfortner H, Völker U, Riedel K, Hecker M, Engelmann S, and Pane-Farre J. Deletion of membrane-associated Asp23 leads to upregulation of cell wall stress genes in *Staphylococcus aureus*. *Mol Microbiol* 93: 1259–1268, 2014.
 27. Newton GL, Fahey RC, and Rawat M. Detoxification of toxins by bacillithiol in *Staphylococcus aureus*. *Microbiology* 158: 1117–1126, 2012.
 28. Newton GL, Rawat M, La Clair JJ, Jothivasan VK, Budiarto T, Hamilton CJ, Claiborne A, Helmann JD, and Fahey RC. Bacillithiol is an antioxidant thiol produced in *Bacilli*. *Nat Chem Biol* 5: 625–627, 2009.
 29. Perera VR, Newton GL, Pamell JM, Komives EA, and Pogliano K. Purification and characterization of the *Staphylococcus aureus* bacillithiol transferase BstA. *Biochim Biophys Acta* 1840: 2851–2861, 2014.
 30. Perera VR, Newton GL, and Pogliano K. Bacillithiol: a key protective thiol in *Staphylococcus aureus*. *Expert Rev Anti Infect Ther* 13: 1089–1107, 2015.
 31. This reference has been deleted.
 32. Posada AC, Kolar SL, Dusi RG, Francois P, Roberts AA, Hamilton CJ, Liu GY, and Cheung A. Importance of bacillithiol in the oxidative stress response of *Staphylococcus aureus*. *Infect Immun* 82: 316–332, 2014.
 33. Pöther DC, Gierok P, Harms M, Mostertz J, Hochgräfe F, Antelmann H, Hamilton CJ, Borovok I, Lalk M, Aharonowitz Y, and Hecker M. Distribution and infection-related functions of bacillithiol in *Staphylococcus aureus*. *Int J Med Microbiol* 303: 114–123, 2013.
 34. Rajkarnikar A, Strankman A, Duran S, Vargas D, Roberts AA, Barretto K, Upton H, Hamilton CJ, and Rawat M. Analysis of mutants disrupted in bacillithiol metabolism in *Staphylococcus aureus*. *Biochem Biophys Res Commun* 436: 128–133, 2013.
 35. Schwarzländer M, Dick TP, Meye AJ, and Morgan B. Dissecting redox biology using fluorescent protein sensors. *Antioxid Redox Signal* 24: 680–712, 2016.
 36. Sharma SV, Arbach M, Roberts AA, Macdonald CJ, Groom M, and Hamilton CJ. Biophysical features of bacillithiol, the glutathione surrogate of *Bacillus subtilis* and other firmicutes. *Chembiochem* 14: 2160–2168, 2013.
 37. Tyagi P, Dharmaraja AT, Bhaskar A, Chakrapani H, and Singh A. *Mycobacterium tuberculosis* has diminished capacity to counteract redox stress induced by elevated levels of endogenous superoxide. *Free Radic Biol Med* 84: 344–354, 2015.
 38. van der Heijden J, Bosman ES, Reynolds LA, and Finlay BB. Direct measurement of oxidative and nitrosative stress dynamics in *Salmonella* inside macrophages. *Proc Natl Acad Sci U S A* 112: 560–565, 2015.
 39. van der Heijden J, Vogt SL, Reynolds LA, Pena-Diaz J, Tupin A, Aussel L, and Finlay BB. Exploring the redox balance inside gram-negative bacteria with redox-sensitive GFP. *Free Radic Biol Med* 91: 34–44, 2015.
 40. Weber H, Engelmann S, Becher D, and Hecker M. Oxidative stress triggers thiol oxidation in the glyceraldehyde-3-phosphate dehydrogenase of *Staphylococcus aureus*. *Mol Microbiol* 52: 133–140, 2004.
 41. Winterbourn CC and Kettle AJ. Redox reactions and microbial killing in the neutrophil phagosome. *Antioxid Redox Signal* 18: 642–660, 2013.

Address correspondence to:

Prof. Haike Antelmann
 Institute for Biology-Microbiology
 Freie Universität Berlin
 Königin-Luise-Strasse 12-16
 Berlin D-14195
 Germany

E-mail: haike.antelmann@fu-berlin.de

Date of first submission to ARS Central, April 26, 2016; date of final revised submission, July 1, 2016; date of acceptance, July 5, 2016.

Abbreviations Used

BMM	= Belitsky minimal medium
Brx	= bacilliredoxin
BSH	= bacillithiol
BSSB	= bacillithiol disulfide
CLSM	= confocal laser scanning microscopy
CoASH	= coenzyme A
DTT	= dithiothreitol
EDTA	= ethylenediaminetetraacetic acid
FBS	= fetal bovine serum
Grx	= glutaredoxin
GSH	= glutathione
GSSG	= oxidized glutathione disulfide
H ₂ O ₂	= hydrogen peroxide
IPTG	= isopropyl-β-D-thiogalactopyranoside
LB	= Luria Bertani
MFI	= mean fluorescence intensity
MOI	= multiplicity of infection
Mrx1	= mycoredoxin1
MSH	= mycothiol
MSSM	= mycothione or mycothiol disulfide
NADPH	= nicotinamide adenine dinucleotide phosphate
NaOCl	= sodium hypochlorite
NEM	= N-ethylmaleimide
OD ₅₀₀	= optical density at 500nm
OxD	= oxidation degree
PBS	= phosphate-buffered saline
PCR	= polymerase chain reaction
PMA	= phorbol 12-myristate 13-acetate
roGFP	= redox-sensitive green fluorescent protein
ROS	= reactive oxygen species
SDS-PAGE	= sodium dodecyl sulfate–polyacrylamide gel electrophoresis
SEM	= standard error of the mean
Trx	= thioredoxin

Chapter 8

Application of genetically encoded redox biosensors to measure dynamic changes in the glutathione, bacillithiol and mycothiol redox potentials in pathogenic bacteria

Quach Ngoc Tung¹, Nico Linzner¹, Vu Van Loi¹, and Haike Antelmann^{1*}

¹*Institute for Biology-Microbiology, Freie Universität Berlin, D-14195 Berlin, Germany*

Published in: Free Radical Biology & Medicine. in press. (2018)

<https://doi.org/10.1016/j.freeradbiomed.2018.02.018>

#Corresponding author: haike.antelmann@fu-berlin.de

Authors contributions

Haike Antelmann and Quach Ngoc Tung wrote the main part of the review and prepared most of the figures. Vu Van Loi and Nico Linzner wrote the Brx-roGFP2 and Grx-roGFP2 biosensor part, respectively.



Contents lists available at ScienceDirect

Free Radical Biology and Medicine

journal homepage: www.elsevier.com/locate/freeradbiomed

Review Article

Application of genetically encoded redox biosensors to measure dynamic changes in the glutathione, bacillithiol and mycothiol redox potentials in pathogenic bacteria

Quach Ngoc Tung, Nico Linzner, Vu Van Loi, Haike Antelmann*

Freie Universität Berlin, Institute for Biology-Microbiology, Königin-Luise-Strasse 12-16, D-14195 Berlin, Germany

ARTICLE INFO

Keywords:

Listeria monocytogenes
Salmonella Typhimurium
Staphylococcus aureus
Mycobacterium tuberculosis
 Glutathione
 Bacillithiol
 Mycothiol
 roGFP2/redox biosensors

ABSTRACT

Gram-negative bacteria utilize glutathione (GSH) as their major LMW thiol. However, most Gram-positive bacteria do not encode enzymes for GSH biosynthesis and produce instead alternative LMW thiols, such as bacillithiol (BSH) and mycothiol (MSH). BSH is utilized by *Firmicutes* and MSH is the major LMW thiol of *Actinomycetes*. LMW thiols are required to maintain the reduced state of the cytoplasm, but are also involved in virulence mechanisms in human pathogens, such as *Staphylococcus aureus*, *Mycobacterium tuberculosis*, *Streptococcus pneumoniae*, *Salmonella enterica* subsp. *Typhimurium* and *Listeria monocytogenes*. Infection conditions often cause perturbations of the intrabacterial redox balance in pathogens, which is further affected under antibiotics treatments. During the last years, novel glutaredoxin-fused roGFP2 biosensors have been engineered in many eukaryotic organisms, including parasites, yeast, plants and human cells for dynamic live-imaging of the GSH redox potential in different compartments. Likewise bacterial roGFP2-based biosensors are now available to measure the dynamic changes in the GSH, BSH and MSH redox potentials in model and pathogenic Gram-negative and Gram-positive bacteria.

In this review, we present an overview of novel functions of the bacterial LMW thiols GSH, MSH and BSH in pathogenic bacteria in virulence regulation. Moreover, recent results about the application of genetically encoded redox biosensors are summarized to study the mechanisms of host-pathogen interactions, persistence and antibiotics resistance. In particular, we highlight recent biosensor results on the redox changes in the intracellular food-borne pathogen *Salmonella Typhimurium* as well as in the Gram-positive pathogens *S. aureus* and *M. tuberculosis* during infection conditions and under antibiotics treatments. These studies established a link between ROS and antibiotics resistance with the intracellular LMW thiol-redox potential. Future applications should be directed to compare the redox potentials among different clinical isolates of these pathogens in relation to their antibiotics resistance and to screen for new ROS-producing drugs as promising strategy to combat antimicrobial resistance.

1. Functions of low molecular weight thiols in pathogenic bacteria

1.1. Functions of glutathione in virulence and protein S-glutathionylation in pathogenic bacteria

Low molecular weight (LMW) thiols play important roles to maintain the reduced state of the cytoplasm in all organisms [1,2]. Glutathione (GSH) functions as major LMW thiol in Gram-negative bacteria and in few Gram-positives, such as *Streptococci*, *Listeria*, *Lactobacilli* and *Clostridia* (Fig. 1). However, some Gram-positive pathogens also use ABC transporters to import GSH either from host cells or from the growth medium, as shown for *Streptococcus pneumoniae* and *Listeria*

monocytogenes [3,4]. The biosynthesis and functions of GSH have been widely studied in *Escherichia coli*, which produces millimolar concentrations of GSH [2,5]. GSH maintains protein thiols in its reduced state, functions as a storage form of cysteine and is resistant to metal-catalyzed autooxidation [2]. GSH undergoes autooxidation 7 times slower compared to free Cys. Under oxidative stress, GSH is oxidized to glutathione disulfide (GSSG) which is reduced by the glutathione reductase (Gor) on expense of NADPH (Fig. 2). The GSH/GSSG ratio ranges from 30:1 to 100:1 and the standard thiol-disulfide redox potential of GSH was determined as $E^0(\text{GSSG}/\text{GSH}) = -240 \text{ mV}$ at physiological pH values in the cytoplasm of *E. coli* [1,6]. Many detoxification functions of GSH have been studied in *E. coli*. GSH is important

* Corresponding author.

E-mail address: haike.antelmann@fu-berlin.de (H. Antelmann).<https://doi.org/10.1016/j.freeradbiomed.2018.02.018>

Received 24 December 2017; Received in revised form 8 February 2018; Accepted 13 February 2018

0891-5849/© 2018 The Author(s). Published by Elsevier Inc. This is an open access article under the CC BY-NC-ND license (<http://creativecommons.org/licenses/by-nc-nd/4.0/>).

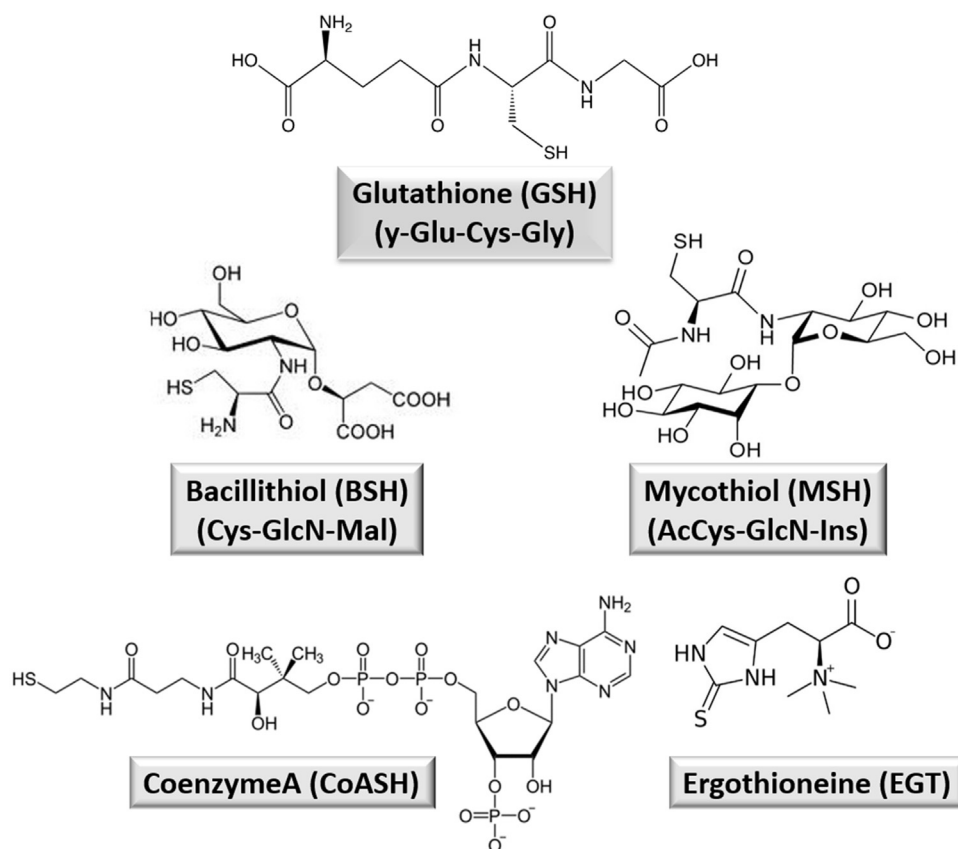


Fig. 1. Structures of major bacterial low molecular weight (LMW) thiols. The major LMW thiols are glutathione (GSH) present in Gram-negative bacteria and few Gram-positive bacteria. Bacillithiol (BSH) is the major LMW thiol in *Firmicutes*, such as *Bacillus* and *Staphylococcus* species. Mycothiol (MSH) is utilized in all *Actinomycetes*, including mycobacteria, corynebacteria and streptomycetes. Coenzyme A (CoASH) also serves as alternative LMW thiol-redox buffer in *S. aureus* and *B. anthracis*. Ergothioneine (EGT) is a histidine-derived alternative LMW thiol in mycobacteria.

for the defense against redox active compounds, xenobiotics, antibiotics, toxic metals and metalloids as reviewed previously [5]. Of note, GSH is an important cofactor of glyoxalases involved in detoxification of the toxic electrophile methylglyoxal as natural byproduct of the glycolysis in *E. coli* [7–10].

Apart from its well-studied detoxification functions, GSH contributes to the virulence of important human pathogens. The involvement of GSH in virulence has been studied in the extracellular facultative anaerobic pathogen *S. pneumoniae* as well as for the intracellular food-borne pathogens *L. monocytogenes* and *Salmonella enterica* subsp. *Typhimurium* (*S. Typhimurium*) [3,4,11–14]. The glutathione reductase Gor and the GSH-uptake system GshT protect *S. pneumoniae* against oxidative stress and toxic metal ions and are required for colonization and invasion in a mice model of infection [3]. *L. monocytogenes* is a facultative intracellular pathogen that has a saprophytic lifestyle in the soil and a parasitic in the host [15]. Specific evasion strategies enable to escape the phagolysosome and to proliferate inside the host cell cytosol. *L. monocytogenes* utilizes host-derived GSH, but can also synthesize bacterial GSH via the GshF fusion protein [14]. Bacterial and host-derived GSH are both important for virulence and expression of virulence factors in *L. monocytogenes*. The virulence mechanism involves activation of the positive regulatory factor A (PrfA) by allosteric binding of GSH as cofactor to PrfA [13,14] (Fig. 3). PrfA is a member of the CRP/FNR family and the master regulator for many virulence factors including the actin assembly factor ActA. ActA mediates actin polymerization and is essential for intracellular spread of the pathogen across host cells [15]. The structure of the PrfA-GSH complex has been recently determined to investigate the mechanisms for activation of PrfA upon GSH binding. GSH binding to a specific tunnel site of PrfA induces conformational changes in the tunnel site of PrfA that stabilizes the helix-turn-helix (HTH) motifs and primes PrfA for binding to the operator DNA [13]. Another structural study of the PrfA-GSH complex suggested that GSH

binding induces local conformational changes in PrfA, allowing DNA binding and activation of gene transcription [16]. The GSH level and the reduced cytosol of the host cells further influence the virulence of *L. monocytogenes* [17]. Bacteria cultivated under reducing growth conditions in minimal medium with GSH had a higher PrfA activation state and virulence factor expression resulting in higher virulence in a murine infection model [17]. PrfA controls also listeriolysin O (LLO) as cholesterol-dependent cytolysin (CDC) required for host-cell lysis [15]. Interestingly, LLO was shown to be regulated by S-glutathionylation at a conserved Cys residue by host and bacterial derived GSH which inhibits its hemolytic activity to lyse red blood cells [18]. These two examples of PrfA and LLO highlight the important roles of GSH in activation of virulence factors expression and redox regulation in an important intracellular pathogen.

The intracellular pathogen *S. Typhimurium*, which causes gastroenteritis, resides inside a *Salmonella*-containing vacuole (SCV) and injects *Salmonella* pathogenicity island 2 effectors (SP-2) via a type-III-secretion system (T3SS) directly into the host cell. *S. Typhimurium* encounters oxidative stress by the phagocyte NADPH oxidase (Nox) that produces Reactive Oxygen Species (ROS) as oxidative burst. Reactive Nitrogen Species (RNS) are generated by the inducible NO synthase (iNOS) inside macrophages and neutrophils (Fig. 3). In *S. Typhimurium*, GSH-deficient mutants displayed an increased sensitivity to ROS and RNS and were attenuated in an acute model of salmonellosis in NRAMP^R mice that produces a high NO level [11]. Thus, GSH is important for the defense against ROS and RNS produced by Nox and iNOS as shown in the model of salmonellosis [11]. In addition, GSH was shown to be required for efficient transcription of the Spi-2 targets under NO stress. The Spi-2 system interferes with lysosomal trafficking and promotes intracellular replication inside the SCV [19,20]. Spi-2 reduces the contact between *Salmonella*-containing vacuoles (SCV) and NADPH phagocyte oxidase vesicles. Thus, Spi-2 protects *S. Typhimurium* against the oxidative burst inside macrophages by maintaining

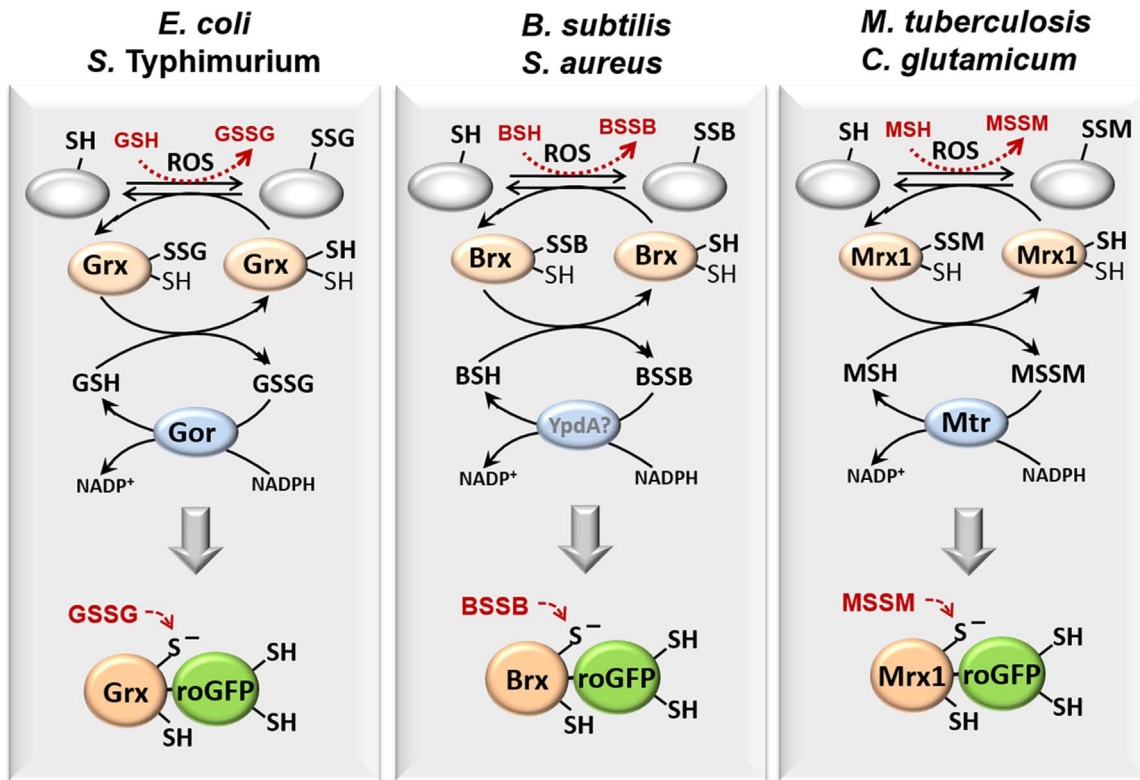


Fig. 2. Reduction of S-glutathionylations, S-bacillithiolations and S-mycothiolations by glutaredoxin, bacilliredoxin and mycoredoxin pathways and design of genetically encoded Grx1-roGFP2, Brx-roGFP2 and Mrx1-roGFP2 biosensors. The S-glutathionylated proteins are reduced by glutaredoxins (Grx) leading to a Grx-SSG intermediate that is reduced by GSH and the NADPH-dependent GSSG reductase (Gor). These pathways for reduction of S-glutathionylated proteins are present in *E. coli*, *S. Typhimurium* and other Gram-negative bacteria. Analogous bacilliredoxin and mycoredoxin pathways are present in BSH- and MSH-producing Gram-positive bacteria, such as *S. aureus* and *B. subtilis* as BSH producer and *M. tuberculosis* and *C. glutamicum* that utilize MSH. The S-bacillithiolated proteins are reduced by bacilliredoxins (Brx) leading to Brx-SSB formation. The regeneration of Brx-SSB could require BSH and perhaps the NADPH-dependent pyridine nucleotide oxidoreductase YpdA. In *Actinomycetes*, mycoredoxin1 (Mrx1) catalyzes reduction of S-mycothiolated proteins leading to Mrx1-SSM generation that is recycled by MSH and the NADPH-dependent MSSM reductase Mtr. The genetically-encoded biosensors were used to measure the dynamic changes of the intracellular redox potentials in eukaryotes and Gram-negative bacteria, such as *E. coli* and *S. Typhimurium* (Grx1-roGFP2) as well as in the Gram-positive bacteria *S. aureus* (Brx-roGFP2) and *M. tuberculosis* (Mrx1-roGFP2), respectively.

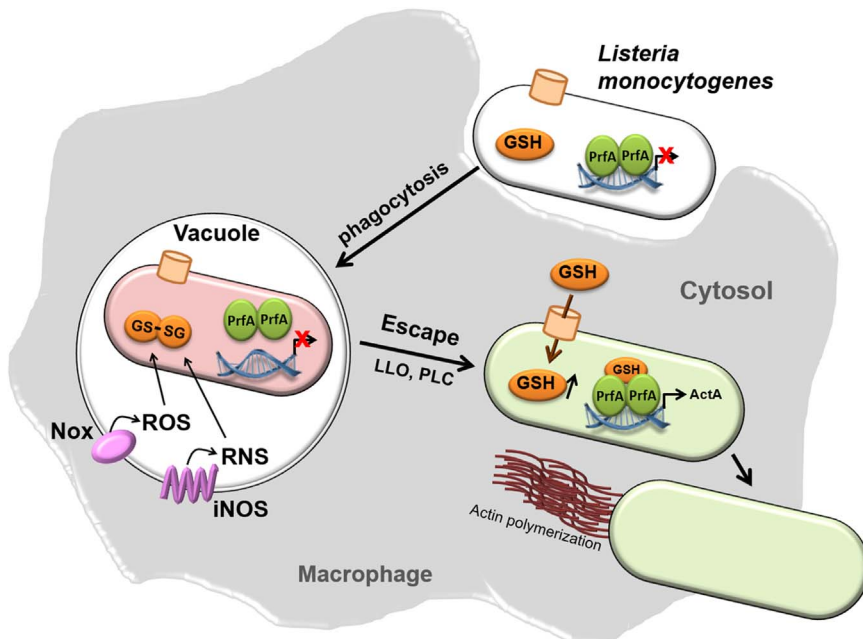


Fig. 3. Functions of GSH in PrfA activation for virulence factor expression in the intracellular pathogen *Listeria monocytogenes*. After phagocytosis by macrophages, the intracellular pathogen *L. monocytogenes* resides in an oxidizing vacuole (red), containing ROS and RNS that are produced by Nox and iNOS. *L. monocytogenes* has the ability to synthesize GSH, but can utilize GSH from host cells. In the oxidizing vacuole, GSH produced by *L. monocytogenes* is oxidized to GSSG, which does not bind the PrfA transcription factor [14]. *L. monocytogenes* escapes into the reducing host cell cytosol, leading to GSH regeneration and uptake of GSH from host cells. PrfA binds GSH and activates transcription of PrfA regulon genes, such as *actA*. ActA expression leads to Actin polymerization that allows movement of *L. monocytogenes* through host cells. This figure is adapted from Ref. [14].

the intracellular thiol-redox balance [12,21]. The importance of this T3SS Spi-2 for ROS evasion was demonstrated using the roGFP2 biosensor as outlined in the biosensor section [12].

In *Yersinia pestis*, host-derived GSH functions in S-glutathionylation of the T3SS effector protein LcrV. *Y. pestis* causes bubonic plaques as extraordinary virulence mechanism and employs a T3SS for secretion of Yop effectors directly into the host cell cytoplasm [22]. These effectors function in pathogen evasion and neutralization of the host immune defense. The T3SS first secretes the LcrV protein, a plaque-protecting antigen that forms the needle cap protein of the T3SS and is essential for plaque pathogenesis [23,24]. LcrV is S-glutathionylated at Cys273 by host-derived GSH after its translocation and S-glutathionylation of LcrV is important for virulence of *Y. pestis* [25]. S-glutathionylated LcrV binds to host ribosomal protein S3 (RPS3), promotes effector secretion and macrophage killing. In addition, S-glutathionylation of LcrV contributes to bubonic plague pathogenesis in mice and rat models of infections [25]. In conclusion, GSH was shown to control expression and modification of virulence factors that are secreted by the T3SS in bacterial pathogens. Moreover, GSH is essential for survival under infection conditions in different pathogens, such as *S. pneumoniae*, *L. monocytogenes* and *S. Typhimurium*.

1.2. Functions of bacillithiol in the virulence and protein S-bacillithiolation in Gram-positive Firmicutes

The Gram-positive Firmicutes bacteria, such as *Bacillus* and *Staphylococcus* species utilize bacillithiol (BSH, Cys-GlcN-malate) as their major LMW thiol (Fig. 1) [26,27]. In *B. subtilis* and *S. aureus*, BSH is important for detoxification of many redox-active compounds. BSH-deficient mutants showed growth and survival defects after treatment with ROS, electrophiles, HOCl, toxins, alkylating agents, heavy metals and redox-active antibiotics, such as fosfomicin and rifampicin [28–30]. BSH functions as cofactor for thiol-dependent detoxification enzymes, such as thiol-S-transferases (FosB) and glyoxalases (GlxA/B). These thiol-dependent enzymes conjugate BSH to toxic electrophiles, fosfomicin and methylglyoxal for its detoxification [28,31]. BSH has also an impact on metal homeostasis and functions in Zn²⁺-storage, FeS cluster assembly and copper buffering [32–35]. The standard thiol-redox potential of BSH was calculated as $E^0(\text{BSSB}/\text{BSH}) = -221 \text{ mV}$ and the BSH/BSSB ratios were determined as 100:1–400:1 under control conditions in *B. subtilis* cells [35–37]. Under NaOCl stress, the BSSB level is increased indicating a more oxidized BSH redox potential [38]. The NADPH-dependent pyridine nucleotide disulfide reductase YpdA is supposed to function as BSSB reductase (Fig. 2), but its role in regeneration of BSH has not been demonstrated.

Of note, BSH has an important role for virulence in the major pathogen *S. aureus*. BSH protects *S. aureus* under infection-like conditions in phagocytosis assays using human and murine macrophages [29,30]. The survival of BSH-minus clinical MRSA strains was strongly impaired in human whole-blood survival assays [29]. The exact protective role of BSH inside the host is unknown, but the yellow antioxidant pigment staphyloxanthin was present at lower amounts in the absence of BSH [29]. *S. aureus* isolates carry many mobile genetic elements, such as prophages, pathogenicity islands, transposons and plasmids explaining their high genome diversity. Due to a former transposon or other insertion element, *S. aureus* NCTC8325 derivatives (e.g. SH1000) are *bshC* mutants and do not produce BSH [29,30,39]. Thus, also *S. aureus* SH1000 was impaired in survival inside murine macrophages and human epithelial cells and the phenotype could be restored by complementation with plasmid-encoded *bshC* [29,30]. Thus, BSH functions as virulence mechanism in the defense against the host immune system in *S. aureus* clinical isolates. Macrophages and neutrophils produce large quantities of ROS and HOCl as well as bactericidal ammonium chloramines during the oxidative burst [40–42]. Thus, the defense mechanism of BSH could involve regulatory mechanisms by formation of BSH mixed protein disulfides (S-bacillithiolations) in *S. aureus* inside

neutrophils and macrophages.

To get insights into the targets for S-bacillithiolations in *S. aureus* under infection-like conditions, we have studied the quantitative thiol-redox proteome of *S. aureus* USA300 under NaOCl stress using the OxICAT approach [43]. In total, 58 Cys residues with > 10% increased thiol-oxidation could be quantified under NaOCl stress. In addition, five S-bacillithiolated were identified in *S. aureus* under NaOCl stress by shotgun proteomics. These S-bacillithiolated proteins showed the highest oxidation increase of > 29% in the OxICAT analysis. The glyceraldehyde-3-phosphate dehydrogenase Gap was identified as most abundant S-bacillithiolated protein representing 4% of the total Cys abundance in the proteome. Protein S-bacillithiolation functions in redox regulation and protects the active site Cys151 of *S. aureus* Gap under H₂O₂ and NaOCl stress against overoxidation *in vitro* [43]. Future studies should reveal whether S-bacillithiolation of Gap or other proteins could provide protection of *S. aureus* under infection conditions inside macrophages and neutrophils. This adaptation to infection conditions in *S. aureus* could involve the metabolic re-configuration of central carbon metabolism as shown in eukaryotic organisms [44,45]. In yeast cells, Gap oxidation has been linked to the re-direction of the glycolytic flux into the pentose phosphate pathway (PPP) to increase NADPH levels. NADPH is used as electron donor for thioredoxin and glutathione reductases to recover from oxidative stress [44,45]. Similar mechanisms could be relevant also for *S. aureus* to enhance survival under infection conditions.

Apart from BSH, *S. aureus* produces also coenzymeA (CoASH) as abundant alternative LMW thiols and essential cofactor in cellular metabolism. Moreover, a CoASH disulfide oxidoreductase (Cdr) is encoded in the genome of *S. aureus* that could be involved in reduction of CoAS disulfides [27]. However, the functions of CoASH and Cdr for the redox regulation of proteins by CoA-thiolations are unknown in *S. aureus*. Recently, CoA-thiolation was shown in mammalian cells as a widespread post-translational redox modification under oxidative stress [46]. Numerous Cys peptides with CoA-thiolation sites were detected in H₂O₂-treated heart cells and in the mitochondria of liver cells from starved rats [46]. The authors developed a monoclonal antibody for enrichment of CoA-thiolated proteins and identified 80 CoA mixed disulfides (58 proteins) in heart cells and 43 CoA-thiolated Cys peptides (33 proteins) in liver cells using mass spectrometry. Many CoA-thiolated proteins function in main metabolic pathways, like the TCA cycle and the beta-oxidation pathway of fatty acids. These pathways involve activated CoA-derivatives, such as acetyl-CoA indicating that CoA metabolism and CoA-thiolation are functionally connected. It was also demonstrated that CoA-thiolation can inactivate enzymes and function in redox regulation of the glycolytic GapDH, the isocitrate dehydrogenase IDH and other metabolic enzymes [46]. Thus, it will be interesting to reveal if GapDH and other S-bacillithiolated proteins are also targets for CoA-thiolation in *S. aureus* under NaOCl stress.

The reduction of S-bacillithiolated proteins is catalyzed by bacilliredoxins (BrxA and BrxB) that belong to DUF1094 family. Brx proteins possess an unusual CGC motif, but function similar like glutaredoxins in *B. subtilis* and *S. aureus* (Fig. 2) [43,47]. Thus, Brx of *S. aureus* has been used to construct the first Brx-roGFP2-fused biosensor to measure changes in the BSH redox potential in *S. aureus* under oxidative stress and infection conditions inside human macrophages as outlined in the biosensor section.

1.3. Functions of mycothiol in the virulence and protein S-mycothiotionation in Actinomycetes

Mycothiotion (MSH; NAc-Cys-GlcNAc-myoinositol) is the major LMW thiol in high-GC Gram-positive Actinomycetes, including *Streptomyces*, *Mycobacterium* and *Corynebacterium* species (Fig. 1) [48,49]. Under oxidative stress, MSH is oxidized to MSH disulfide (MSSM) and maintained in a reduced state by the mycothiol disulfide reductase Mtr. MSH is involved in detoxification of numerous compounds, such as ROS,

RES, alkylating agents, toxins, antibiotics (erythromycin, vancomycin, rifampin, azithromycin), heavy metals and toxic metalloids, aromatic compounds, ethanol and glyphosates as studied in different *Actinomyces* [48,50–53]. In *Streptomyces lincolnensis*, MSH participates in the biosynthesis of the sulfur-containing antibiotics lincomycin [54]. For more details of these many detoxification functions of MSH and MSH-dependent enzymes, the reader is referred to previous and recent reviews [28,55].

Under hypochlorite stress, MSH was shown to form mixed disulfides with protein thiols, termed as protein S-mycothiolation [56–58]. Protein S-mycothiolation protects protein thiols against the formation of sulfinic and sulfonic acids and regulates protein activities, as demonstrated in *Corynebacterium glutamicum*, *Corynebacterium diphtheriae* and *Mycobacterium smegmatis*. About 25 S-mycothiolated proteins were identified in *C. glutamicum* [56], 26 proteins in *C. diphtheriae* [58] and 58 in *M. smegmatis* under NaOCl stress [57]. Among the S-mycothiolated proteins, several are conserved S-thiolated at their active sites Cys residues in different Gram-positive bacteria, including thiol-peroxidases/peroxiredoxins (Tpx, AhpC), ribosomal proteins (RpsM, RplC), the IMP dehydrogenase (GuaB), the myo-inositol-1-phosphate synthase (Ino1), the methionine synthase (MetE) and the glycolytic GapDH [38,56]. The extent of protein S-mycothiolation correlates with the different MSH levels in corynebacteria and mycobacteria [59]. While *M. smegmatis* contains 6 $\mu\text{mol/g}$ raw dry weight (rdw) MSH [57], only 0.3 $\mu\text{mol/g}$ rdw were determined in *C. diphtheriae* [58]. Thus, corynebacteria most likely utilize also alternative LMW thiols which remains to be investigated.

Mycobacteria utilize the histidine-derivative ergothioneine (EGT) as another alternative LMW thiol. MSH and EGT are both required for full virulence and redox homeostasis of *Mycobacterium tuberculosis* (*Mtb*) [60,61]. Both LMW thiols contribute also to full peroxide resistance of *M. smegmatis* [62]. EGT levels are even increased in the *mshA* mutant confirming that EGT can compensate for the absence of MSH [63]. Our redox proteomics studies revealed an increased thiol-oxidation level in the *M. smegmatis mshC* mutant which could involve alternative S-ergothionylation which remains to be elucidated [57]. However, in contrast to MSH, EGT is actively secreted into the supernatant [62]. Future studies should be directed to study the role of EGT secretion in regulation of EGT levels, modulation of host ROS levels and S-thiolation of bacterial and host proteins during infections.

Protein S-mycothiolation is redox-regulated by both, the mycothiolation and thioredoxin pathways as demonstrated for thiol peroxidases (Tpx, Mpx, AhpE), the methionine sulfoxide reductase (MsrA) and the glycolytic GapDH *in vitro* [56,58,64–66]. Reduction of S-mycothiolated GapDH occurred much faster by Mrx1 compared to Trx *in vitro* indicating that Mrx1 is probably the main de-mycothiolating enzyme *in vivo* [58]. In addition, S-mycothiolation of GapDH is faster compared to its overoxidation *in vitro*. The methionine synthase MetE was further protected by S-mycothiolation under acid stress conditions in *C. glutamicum* [67]. These results indicate that S-mycothiolation can efficiently protect the active site Cys residues against overoxidation to sulfinic or sulfonic acids and can be reversed by both, the Mrx1 and Trx pathways. Mrx1 was used to construct the first MSH specific genetically encoded biosensor Mrx1-roGFP2 to measure changes in the MSH redox potential.

Apart from S-mycothiolation, MSH plays also an important role for growth, survival and antibiotics resistance under infection conditions in the major pathogen *Mtb* [61,68]. *Mtb* is the etiologic agent of tuberculosis (TB) disease resulting in about 2 million human death each year [69]. Due to the slow intracellular growth of *Mtb* inside the phagosomes of macrophages, TB patients have to be treated with antibiotics for several months, resulting in multiple and extreme drug resistant *Mtb* isolates (MDR/XDR) as a major health burden. MSH is involved in the activation of the first-line anti-TB drug isoniazid (INH) in *Mtb* [70]. INH is a pro-drug that is activated by the catalase KatG and MSH resulting in a NAD-INH adduct that finally inhibits InhA of the

mycolic acid biosynthesis pathway [71]. Thus, the evolved INH resistant *Mtb* isolates often carry spontaneous mutations in *katG*, *mshA* and in the target gene *inhA* [51]. This requires alternative drug developments to treat emerging resistant *Mtb* isolates. Since MSH is important for virulence of *Mtb*, inhibitors of MSH biosynthesis and recycling have been successfully applied in combination therapies that target MshB, MshC, Mtr and the MSH-S-conjugate amidase Mca as new anti-TB drugs [72]. Moreover, ROS-producing compounds have been designed and may have a great potential to tackle anti-tuberculosis drug resistance. In the later sections, we will highlight recent work in drug research showing the power of the genetically encoded Mrx1-roGFP2 biosensor to study the role of MSH in antibiotics resistance, to reveal the involvement of ROS in the killing mode of antibiotics under infection conditions and to develop new combination therapies involving ROS-producing compounds.

2. Dynamic redox potential measurements using roGFP2-based biosensors in pathogens

The development of redox-sensitive green fluorescent proteins (roGFPs) has enabled the ratiometric measurement of the cellular redox potential at high sensitivity and spatiotemporal resolution using live-imaging approaches [73–76]. For construction of roGFPs, two redox-active Cys residues (Cys147 and Cys204) were introduced in the GFP molecule that form a disulfide bond upon oxidation resulting in conformational changes of the chromophore and fluorescence changes [76]. The roGFP2 biosensor has two excitation maxima at 405 and 488 nm, which change upon oxidation resulting in a ratiometric biosensor response [74,77]. The Cys pair in roGFPs has been shown to equilibrate with the GSH/GSSG redox couple and the probes are widely used to measure the changes in the GSH redox potential in living eukaryotic cells [76]. However, the equilibration of endogenously expressed roGFPs with the GSH/GSSG pair is too slow and limited by the Grx expression levels. The Grx levels vary also in different compartments and are rate-limiting factors in the thiol-disulfide exchange reactions between the probe and the GSH pool.

To facilitate the specific response of roGFP2 with the GSH/GSSG redox couple, human glutaredoxin was fused to roGFP2 to construct the Grx1-roGFP2 biosensor for real-time measurements of the dynamic changes in the GSH redox potential (E_{GSH}) in eukaryotic organisms [75]. The Grx1-roGFP2 biosensor responds much faster within seconds to nanomolar concentrations of GSSG compared to unfused roGFP2 [74,75]. Thus, the Grx1-roGFP2 probe is highly specific and detects small changes in the GSH redox potential in living eukaryotic cells. To date, roGFP2 and Grx1-roGFP2 biosensors have been applied in many eukaryotic organisms and pathogens to study intracellular redox changes in *Arabidopsis thaliana*, *Caenorhabditis elegans* [75,78,79], yeast cells and the malaria parasite *Plasmodium falciparum* [80]. In particular, pathogens are well suited to analyze the effect of drugs on the cellular redox metabolism and hence, the biosensors can help to screen for novel ROS-producing drugs. In this part of the review, we will present an overview about the application of roGFP2 biosensors in major human pathogens, including the foodborne intracellular pathogen *S. Typhimurium*, the extracellular Gram-positive pathogen *S. aureus* and in the intracellular major pathogen *M. tuberculosis*. Altogether, the biosensor results have advanced our understanding of the mechanisms of survival and intracellular replication, ROS evasion and persistence as well as antibiotics resistance in many important human pathogens.

2.1. Dynamic roGFP2-based biosensors to measure redox changes in Gram-negative bacteria

The roGFP2 biosensors were first applied in Gram-negative bacteria to measure the redox changes during growth, under oxidant and antibiotics treatment as well as infection conditions. In *E. coli*, plasmid-

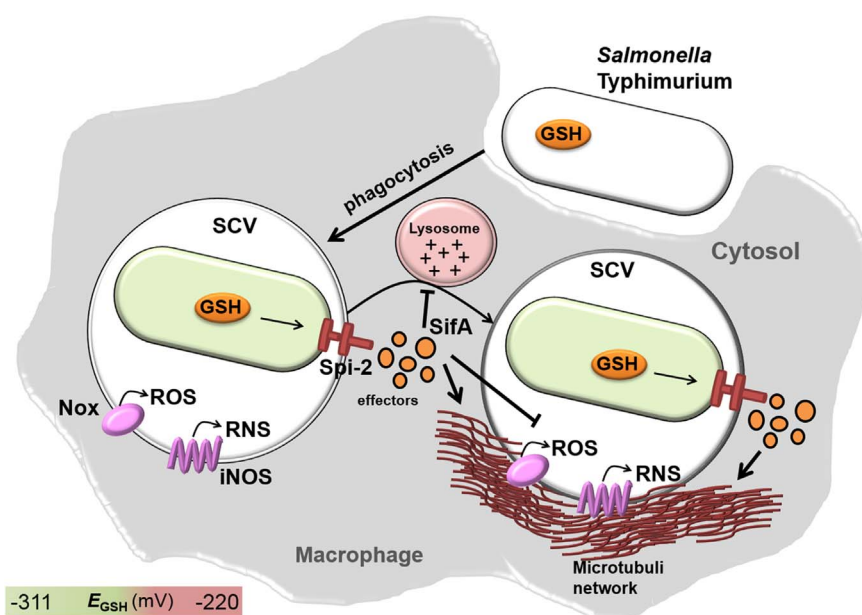


Fig. 4. Mechanisms of ROS evasion allowing intracellular replication of *Salmonella Typhimurium* inside the SCV to escape the host immune defense as revealed by the roGFP2 biosensor. The intracellular pathogen *S. Typhimurium* produces GSH and replicates inside macrophages in a *Salmonella*-containing vacuole (SCV). *S. Typhimurium* escapes ROS in the SCV by the type-III-secretion system Spi-2 that injects effectors directly into the host cell cytoplasm. GSH is required for transcription of the Spi-2 targets under NO stress. *S. Typhimurium* cells are highly reduced (green) inside in the SCV, while those that escape into host cells cytoplasm are oxidized [12]. The Spi-2 effector SifA affects co-localization of SCV and Nox vesicles, which contributes to ROS evasion [12]. The Spi-2 effectors also interfere with lysosomal trafficking, promoting intracellular replication inside the SCV [19,20]. Thus, the Spi-2 system via its effector SifA functions in ROS evasion, controls vacuole integrity and maintains the intracellular redox balance of *S. Typhimurium* inside the SCV to allow intracellular replication [12].

encoded roGFP2 was used to observe cellular oxidation in response to different oxidants, toxic heavy metals and metalloids [81,82]. Toxic biocides, pollutants and metalloids are often found as environmental contaminants and originate from anthropogenic and natural sources. Thus, roGFP2 served as diagnostic tool to measure oxidative stress in *E. coli* by toxic environmental contaminants. Low levels of 0.1–1 mM H_2O_2 resulted in a rapid roGFP2 biosensor response. The roGFP2 biosensor showed also a fast response to heavy metals, such as Cd^{2+} , Zn^{2+} , Cu^{2+} , Pb^{2+} , arsenite and selenite as well as biocides and redox-cycling agents (menadione, naphthalene). However, quantification of the biosensor response using the microplate reader was not possible after exposure to toxic heavy metals or metalloids due to instability of the roGFP2 biosensor [81]. To increase roGFP2 stability, *E. coli* cells expressing the roGFP2 biosensor were immobilized in a transparent *k*-carrageenan (KC) matrix for further toxicity measurements [83]. The detection limit to measure a biosensor response was defined as 0.2 $\mu g/l$ for arsenite and 5.8 ng/l for selenite. These immobilized roGFP2 expressing *E. coli* cells were applied to screen for bioavailability and toxic effects of pollutants [83].

2.1.1. The T3SS Spi-2 contributes to ROS evasion in *S. Typhimurium*

The first physiological studies in pathogenic Gram-negative bacteria using roGFP2 biosensors were performed in the intracellular pathogen *S. Typhimurium* that replicates inside the SCV [12]. *S. Typhimurium* escapes ROS by the T3SS Spi-2 that injects effectors directly into the host cell cytoplasm (Fig. 4). Thus, the biosensor was used to elucidate whether the T3SS Spi-2 contributes to evasion from the host innate immune defense to escape ROS and RNS. The intrabacterial redox changes were measured in *S. Typhimurium* after infection of HeLa cells and THP-1 cells that produce different ROS levels. In addition, the influences of the Spi-2 system and its effector SifA on ROS evasion strategies were investigated using *ssaR* and *sifA* mutants which are reviewed in this part.

S. Typhimurium encounters an acidic environment inside macrophages. Thus, it was first confirmed that the purified roGFP2 probe is not pH-sensitive *in vitro*. Next, the biosensor response inside *S. Typhimurium* cells was measured after treatment with H_2O_2 and the NO donor SpermineNONOate since *S. Typhimurium* has to cope with ROS and RNS that are produced by Nox and iNOS after phagocytosis. The roGFP2 biosensor responds very fast and reversible to 50–500 μM H_2O_2 , but only high concentrations of 25 mM H_2O_2 lead to full oxidation of the probe inside *S. Typhimurium*. However, due to the

detoxification by catalases and peroxidases, cells could quickly regenerate the reduced state even after treatment with high H_2O_2 levels. In contrast, exposure to 5–20 mM of the NO-donor resulted in a strongly increased biosensor oxidation with no recovery of the reduced state. These experiments verified that the probe detects intrabacterial redox changes under physiological micromolar ROS and RNS challenge.

To analyze the redox changes in *S. Typhimurium* after infection of host cells, epithelium-like HeLa cells and macrophages-like THP-1 cells were used. Interestingly, *S. Typhimurium* replicating inside THP-1 cells experienced higher levels of redox stress compared to bacteria infected in HeLa cells. The THP-1 cell line is known to produce higher ROS levels and is able to kill the majority of *S. Typhimurium* cells [12]. Moreover, redox stress heterogeneity was observed between different *S. Typhimurium* cells that maybe important to understand persistence and antibiotic resistance mechanisms.

In human and murine macrophages it was further shown that *S. Typhimurium* cells experience more redox stress in the cytosol compared to that residing in the SCV indicating that replication inside the vacuole contributes to ROS evasion. Thus, the role of the T3SS Spi-2 as ROS evasion strategy inside the SCV was investigated in the *ssaR* mutant that lacks the functional Spi-2 system (Fig. 4) [12]. The *ssaR* mutant displayed a higher oxidation level in THP-1 cells compared to the wild type indicating that the Spi-2 system contributes to ROS evasion. Previous studies revealed that Spi-2 effectors affect co-localization of SCV and phagocyte Nox vesicles, which contributes to ROS evasion [12,21]. Among the Spi-2 effectors, SifA was shown to control vacuole integrity as ROS evasion strategy. The biosensor measurements revealed that ROS evasion by the Spi-2 system requires an intact SCV since the *sifA* mutant experienced a higher redox stress [12]. Thus, the Spi-2 system functions via its effector SifA in ROS evasion to maintain the reduced state of the cytoplasm and to allow intracellular survival of *S. Typhimurium* [12].

2.1.2. Regulation of H_2O_2 detoxification and ROS-generation by antibiotics and toxic metals

Bacteria have evolved different antioxidant enzymes for ROS detoxification, such as catalases, thiol-dependent peroxidases, peroxiredoxins and superoxide dismutase [84]. The role of many H_2O_2 scavenging enzymes is often unknown in bacteria [85] and hence roGFP2 biosensors can contribute to study the dynamics and activity of ROS-degradation by the different bacterial enzymes. Thus, the roGFP2 biosensor was applied to measure redox changes and the ROS

detoxification capacity after treatment with H_2O_2 , toxic heavy metals and antibiotics across different Gram-negative bacteria, including non-pathogenic and pathogenic *E. coli*, *Citrobacter rodentium*, *Yersinia pseudotuberculosis*, *Salmonella enterica* serovar Typhi and *S. Typhimurium* [86]. Using specific mutants in catalases and peroxidases, the kinetics of H_2O_2 detoxification was monitored for each antioxidant enzyme in different bacteria. Although the bacterial species were evolutionary related, the activities of their H_2O_2 detoxification enzymes showed strong variations. This enabled also to measure the ROS detoxification capacity of *S. Typhimurium* during priming with sub-lethal doses of $500 \mu M H_2O_2$ and subsequent challenge with higher doses of $1 mM H_2O_2$ compared to naïve cells. The primed bacteria could faster detoxify $1 mM H_2O_2$ and recover to the reduced state compared to naïve bacteria [86].

In *S. Typhimurium*, the biosensor further allowed to measure endogenous ROS production in a catalase/peroxidase-negative *hpxf* mutant during different growth phases, media and temperatures. The endogenous ROS levels were highest during the later exponential growth at $37^\circ C$ in rich media compared to minimal medium. Thus, optimal growth conditions that allow a maximum growth rate correlate with high oxygen consumption and increased ROS generation. Similar as in the first *E. coli* roGFP2 approach [83], the toxicity of metals was assessed due to ROS production using the biosensor in *S. Typhimurium* [86]. While certain metal ions are required for H_2O_2 detoxification, exposure of *S. Typhimurium* to zinc and nickel contributed to ROS generation by inhibition of ROS detoxification enzymes (zinc) or spontaneous thiol-oxidation (nickel).

Next, biosensor measurements were performed under antibiotics treatment to validate whether ROS are involved in the killing mode of antibiotics, a continuous and controversial debate among microbiologists [87–89]. The oxidation-sensitive *S. Typhimurium hpxf* mutant was exposed to different antibiotics classes, including aminoglycosides, quinolones, cephalosporine and β -lactam antibiotics, but no increased biosensor oxidation could be monitored. This indicates that these antibiotics classes do not enhance endogenous ROS as killing mode in the *S. Typhimurium hpxf* mutant [86]. In contrast, Shukla and coworkers [90] showed that exposure to ampicillin, amikacin and ciprofloxacin leads to an impaired redox balance and increased biosensor oxidation in *E. coli*. Moreover, hydrogen persulfide (H_2S) was shown to protect *E. coli* against oxidative stress triggered by bactericidal antibiotics which is controlled by two mechanisms. H_2S mediated antibiotic tolerance involves rerouting of the electron flow from the energy-efficient cytochrome bo oxidase (Cyo) to the less-energy efficient cytochrome bd oxidase (CydBD) to maintain the respiratory flux and the redox balance. In addition, H_2S enhances the activities of the antioxidant enzymes catalase and superoxide dismutase which contributes to ROS detoxification under antibiotics treatments [90].

In *S. Typhimurium*, the roGFP2 biosensor was further applied to determine the real-time H_2O_2 -influx [91]. The H_2O_2 -influx was calculated by multiplication of the membrane permeability coefficient (P), the membrane surface area (A) and the difference between the inner and outer H_2O_2 concentrations (ΔC) as revealed by the degree of biosensor oxidation. The results showed that H_2O_2 first enters the cells by passive diffusion which is suddenly stopped, also termed as “switching point”. This stop in the H_2O_2 influx was caused by changes in the outer membrane permeability, as verified by spheroplasts lacking an outer membrane. The spheroplasts exhibited a significantly faster H_2O_2 -influx without the “switching point”. The outer membrane proteins OmpA and OmpC were shown to regulate the H_2O_2 influx by opening and closing of their beta barrel structures [91].

Altogether, the roGFP2 biosensor has been widely used to measure the intrabacterial redox changes in several Gram-negative bacteria during the growth and under treatment with ROS and redox-active compounds, such as toxic metals and antibiotics as well as during infection and intracellular replication. The results revealed surprising differences in the H_2O_2 detoxification kinetics by antioxidant enzymes,

such as catalases and peroxidases across closely related bacteria. Different antibiotics did not caused increased ROS-formation in a *S. Typhimurium* ROS-sensitive mutant [86], while Shukla and coworkers [90] revealed enhanced roGFP2 oxidation by antibiotics in *E. coli* cells. These different studies using the same roGFP2 biosensors further contribute to the controversial debate about the involvement of ROS in the killing mode of antibiotics. Moreover, roGFP2 biosensor measurements revealed that H_2O_2 -influx is regulated by switching point due to OMPs that can open and close their beta-barrel. Of particular importance are further the roGFP2 biosensor measurements of *S. Typhimurium* inside the SCV. It was shown that the type-III-secretion system Spi-2 is required for ROS evasion and this depends on an intact vacuole. The bacteria were protected against ROS inside the SCV while bacteria that escaped into the host cell cytoplasm were more oxidized by ROS.

However, as critical remark, it has to be mentioned that the authors used only uncoupled roGFP2 for all measurements of the intrabacterial redox potential in *S. Typhimurium*. The unfused roGFP2 biosensor suffers from its low specificity for the GSH/GSSG redox couple and the limited availability of endogenous Grx. Thus, whether the roGFP2 probe specifically responds to GSH redox potential changes or other redox signals is not known. Future studies should be performed using the Grx1-roGFP2 biosensor which is highly specific to measure ratio-metric changes in the GSH redox potential [75]. It will be also interesting to apply the Grx1-roGFP2 biosensor to study the mechanisms of ROS evasion in other GSH-utilizing intracellular pathogens, such as *L. monocytogenes* and *Legionella pneumophila*.

2.2. Dynamic measurement of the BSH redox potential (E_{BSH}) using the Brx-roGFP2 biosensor in the human pathogen *S. aureus*

We have recently fused bacilliredoxin (Brx) of *S. aureus* to roGFP2 to construct the first genetically encoded Brx-roGFP2 biosensor for dynamic measurement of the intracellular BSH redox potential (E_{BSH}) in *S. aureus* [92]. The BSH redox potential changes were determined during the growth, under ROS and NaOCl stress, during infection inside THP-1 macrophages and antibiotics treatments in two clinical MRSA isolates COL and USA300. In both MRSA strains, BSH enhances the survival during phagocytosis with human and murine macrophage-like cell lines [29,30]. Brx-roGFP2 is highly specific for physiological levels of $10\text{--}100 \mu M BSSB$ which depends on the Brx active site Cys *in vitro*. Thus, Brx-roGFP2 facilitates rapid equilibration of the biosensor with the BSH/BSSB couple to determine the changes in the BSH redox potential inside *S. aureus*.

First, an increased biosensor oxidation was measured in *S. aureus* COL and USA300 in rich medium during the stationary phase compared to the log phase. The dynamic range of Brx-roGFP2 was higher in COL compared to USA300, which may depends on their different BSH levels [29]. USA300 is a highly virulent CA-MRSA strain, which produces many unique virulence factors encoded on prophages, pathogenicity islands and other mobile genetic elements [93]. In addition, USA300 has a higher level of BSH compared to COL. Thus, the biosensor response of USA300 could be lower under diamide stress resulting in a lower dynamic range of fully reduced versus oxidized probes. In addition, strain USA300 could be less permeable or more resistant to diamide compared to COL, leading only to partial biosensor oxidation. Future studies should involve other strong oxidants, such as cumene hydroperoxide or redox cycling agents for full oxidation of the biosensor to increase the dynamic range in USA300.

Treatment of *S. aureus* COL with different oxidants resulted in a fast biosensor response, but at different oxidation degrees. While doses of $50\text{--}100 \mu M NaOCl$ stress lead to the fully oxidation of the biosensor, exposure of *S. aureus* to $1\text{--}10 mM H_2O_2$ revealed only a slightly increased oxidation degree with rapid regeneration of the reduced state. This lower biosensor response under H_2O_2 stress might be due to the high H_2O_2 resistance of *S. aureus* which is able to survive up to $300 mM H_2O_2$ [94]. We further measured the changes in BSH redox potential

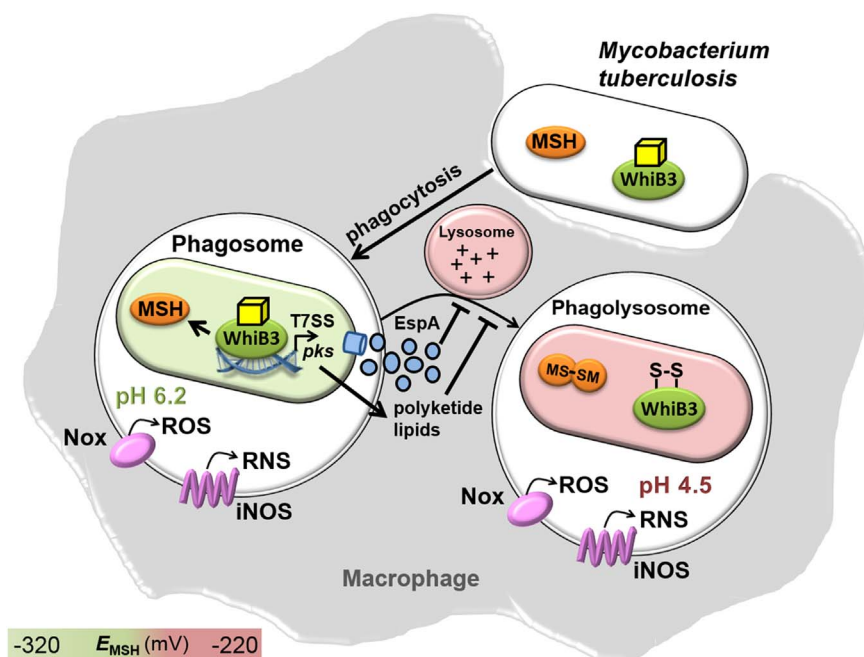


Fig. 5. The role of E_{MSH} and the WhiB3 transcription factor in *M. tuberculosis* persistence under acidic conditions during infection of macrophages as shown by the Mrx1-roGFP2 biosensor. *M. tuberculosis* is an intracellular pathogen that replicates inside the acidic phagosome of macrophages (pH ~ 6.2) preventing phagosomal maturation to phagolysosomes as survival mechanism. During immune activation of macrophages, phagosomes are fused with lysosomes resulting in further pH decrease to pH 4.5. The mild acidification in phagosomes causes a highly reduced E_{MSH} inside *M. tuberculosis*, while strong acidification leads to oxidized E_{MSH} as measured in phagolysosomes [96]. The WhiB3 transcription factor senses acidic conditions in the phagosome and activates transcription of WhiB3 regulon genes, such as type-VII-secretion system effectors (EspA) and polyketide lipids that inhibit phagosomal maturation. WhiB3 causes up-regulation of antioxidant systems (MSH, Trx) to restore the redox balance and to promote survival and persistence of *M. tuberculosis* inside the phagosome.

This figure is adapted from Ref. [96].

inside *S. aureus* COL after infection of THP-1 macrophages using flow cytometry. The Brx-roGFP2 biosensor was 87% oxidized in *S. aureus* COL inside macrophages indicating that *S. aureus* experiences oxidative stress after internalization. In future studies, the redox dynamics of persister cells inside macrophages should be investigated to reveal the BSH redox dynamics during internalization, which is often the cause of chronic *S. aureus* infections.

The biosensor response was also measured in *S. aureus* COL and USA300 *bshA* mutants and in RN4220, which is a natural *bshC* mutant of the NCTC8325-4 lineage. Brx-roGFP2 was fully oxidized in the BSH-deficient mutants indicating an impaired redox balance in the absence of BSH. In previous studies, a lower NADPH level was found in the *bshA* mutant perhaps explaining its impaired redox balance [29]. To clarify whether ROS generation contributes to the killing mode of antibiotics, *S. aureus* was exposed to sub-lethal doses of different antibiotics classes, including rifampicin, fosfomicin, ampicillin, oxacillin, vancomycin, aminoglycosides and fluoroquinolones. However, no increased oxidation degree of the Brx-roGFP2 biosensor was measured under antibiotics treatment, which confirms the findings in *S. Typhimurium* [86]. However, the biosensor responds fast to oxidants and could be a valuable tool in drug-research to screen for new ROS-generating antibiotics that affect the BSH redox potential in *S. aureus*. Future studies should be directed to measure the ROS detoxification capacity in mutants lacking antioxidant systems and in MRSA-isolates of various genetic lineages to unravel the link between ROS resistance and the BSH redox potential in *S. aureus*.

2.3. Dynamic measurements of the MSH redox potential (E_{MSH}) in *Mycobacterium tuberculosis* using the Mrx1-roGFP2 biosensor

In *Mtb*, an analogous Mrx1-roGFP2 biosensor was developed for dynamic measurements of the MSH redox potential (E_{MSH}) in drug-resistant isolates and inside the acidic phagosomes of macrophages [74,95,96]. The increasing prevalence of persistent and chronic relapsing *Mtb* infections as well as multiple and extreme drug-resistant (MDR/XDR) *Mtb* isolates are a major health burden. Thus, the development of new drugs against severe tuberculosis infections is an urgent need. The new biosensor was successfully applied to screen for ROS-generating anti-TB drugs and combination therapies (e.g. augmentin or isoniazid combinations) that affected E_{MSH} to study drug actions linked

to the E_{MSH} to combat life-threatening TB infections [95,97–99]. It was revealed that the E_{MSH} inside infected macrophages is heterogeneous with sub-populations that have reduced, oxidized and basal levels of E_{MSH} . This redox heterogeneity depends on sub-vacuolar compartments inside macrophages and the cytoplasmic acidification that requires WhiB3 as central redox regulator [95,96]. These results using the Mrx1-roGFP2 biosensor have advanced the understanding how this major pathogen copes with anti-TB drug and persists inside macrophages. The major results obtained with Mrx1-roGFP2 are summarized in this part of the review.

After construction of the Mrx1-roGFP2 biosensor, it was demonstrated that the Mrx1-roGFP2 fusion is specific to measure MSSM, but does not respond to other LMW thiol-disulfides [95]. It was further controlled that overexpression of Mrx1-roGFP2 does not affect cellular metabolism, stress resistance and the basal level of E_{MSH} in *Mtb* [95]. Importantly, differences were observed in the biosensor response between slow growing *Mtb* strains and fast growing *M. smegmatis* resulting in a delayed response to H_2O_2 in *Mtb* and a rapid H_2O_2 response in *M. smegmatis* [95]. However, there was only little variation between the basal E_{MSH} in various drug-resistant (MDR/XDR) and drug-sensitive clinical *Mtb* isolates during laboratory growth, where the intracellular E_{MSH} was calculated as highly reduced with values of -273 mV to -280 mV [95]. However, in slow growing *Mtb* strains the E_{MSH} is more oxidizing compared to fast growing *M. smegmatis*. In *M. smegmatis*, a basal E_{MSH} of -300 mV was calculated which is consistent with the higher MSH/MSSM ratio (200:1) in *M. smegmatis* compared to that in *Mtb* (50:1) [100].

2.3.1. E_{MSH} redox heterogeneity in *Mtb* sub-populations depends on specific vacuole compartments

In general, different *Mtb* strains did not show strong variations in their intracellular E_{MSH} when grown under *in vitro* conditions in growth media. However, this was completely different under *in vivo* infection conditions. Different *Mtb* sub-populations with reduced (-300 mV), oxidized (-240 mV) and basal E_{MSH} (-270 mV) could be observed and quantified by flow cytometry under infection conditions inside THP-1 macrophages [95]. It was further shown that the reduced E_{MSH} sub-population is decreased and the oxidized E_{MSH} sub-population is increased at later time points of macrophage infections which correlates with a decreased MSH/MSSM ratio [95]. Thus, the intramacrophage

environment induces redox heterogeneity with different E_{MSH} sub-populations in *Mtb*. Of note, the sub-populations with reduced, oxidized and basal E_{MSH} were different during the time course of infections and also between various MDR/XDR *Mtb* isolates indicating a strongly varying redox balance between *Mtb* isolates. Immune activation further leads to an oxidative shift of *Mtb* sub-populations, which resulted from NO stress as part of host innate immune defense [95].

Mtb is an intracellular pathogen, that is engulfed by macrophages and trapped in an organelle, called the phagosome (Fig. 5). Phagosomal maturation occurs by the interaction of phagosomes with endosomes and fusion with lysosomes to phagolysosomes, a highly acidic and microbicidal compartment that finally degrades invading bacteria [101]. However, *Mtb* successfully restricts phagosomal maturation by preventing fusion of phagosomes with lysosomes. This enables *Mtb* to persist and replicate inside the phagosome to cause chronic and relapsing *Mtb* infections [102,103]. It was suggested, that the different sub-vacuolar compartments might induce this E_{MSH} redox heterogeneity in *Mtb* [95]. The *Mtb* sub-populations were investigated in different vacuolar compartments including early endosomes, autophagosomes and lysosomes. Interestingly, the *Mtb* sub-population located in autophagosome showed almost oxidized E_{MSH} , while those residing in lysosomes were 58% oxidized and the sub-population in early endosomes showed mostly (54%) reduced E_{MSH} . Thus, the biosensor identified the sources of redox heterogeneity as the specific compartments in which *Mtb* resides inside macrophages.

2.3.2. Mechanisms of antibiotics-mediated ROS generation as strategy to combat drug resistance in *Mtb*

Due to the controversial debate about the role of ROS in antibiotic-mediated bacterial killing, the changes in intramycobacterial E_{MSH} were investigated after exposure to anti-TB drugs. In agreement with the biosensor responses under antibiotics stress in *S. Typhimurium* and *S. aureus* [86,92], no oxidative shift in E_{MSH} was reported in shake-flask experiments with *Mtb* populations that were exposed to sub-lethal anti-TB-drugs, e.g. isoniazide, ethambutol and rifampicin [95]. The only exception was the redox-cycling drug clofazimine, which caused an oxidative shift in E_{MSH} in *Mtb* shake-flask cultures. However, under macrophage infections, different antibiotics classes caused oxidative stress as shown by an oxidative shift in the E_{MSH} sub-populations, which was accompanied by increased killing of bacteria. Moreover, the redox heterogeneous sub-populations vary in their susceptibilities to antibiotics. The more oxidized population in autophagosomes and lysosomes was more susceptible to antibiotics killing, while the reduced population in endosomes displayed resistance to anti-TB drugs. Thus, immune activation inside macrophages potentiates drug killing while populations with reduced E_{MSH} promote antibiotics tolerance. Together these results showed important novel insights into the redox heterogeneity of *Mtb* sub-populations in different macrophage compartments, their susceptibility to antibiotics and the mechanisms of persistence [95].

In subsequent studies, several efforts were undertaken to understand the mechanisms of drug resistance and to develop new ROS-producing anti-TB drugs. These ROS-generating drug were used alone and in combination therapies as promising strategy to counteract the increasing problem of antimicrobial resistance and to combat XDR/MDR *Mtb* isolates [97–99]. First, hydroquinone-based antibiotics were synthesized, including ATD-3169 which was shown to cause superoxide production in *Mtb* isolates and increases the irreversible oxidized *Mtb* sub-population [99]. Next, combination therapies of isoniazid (INH) and inhibitors of antioxidant responses were found as promising strategy to threat drug resistant *Mtb* isolates [98]. Such inhibitors of antioxidant responses were ebselen, vancomycin and phenylarsine oxide that were highly effective in combination with INH to kill drug resistant *Mtb* isolates.

INH is a pro-drug that is activated by the catalase KatG and converted to a NAD-INH-adduct, that subsequently inhibits the enoyl-ACP

reductase (InhA) in the mycolic acid biosynthesis pathway [98]. To identify the mechanisms of drug resistant *Mtb* strains, isoniazid resistance was studied in more detail in laboratory evolved INH-resistant *M. smegmatis* strains [98]. Genome sequencing revealed that INH resistant strains carried point mutations in genes for NADH dehydrogenase (*ndh*), catalase (*katG*) or the 3-dehydroquinate synthase (*aroB*). Transcriptomics identified antioxidant responses as dominating in the differentially transcribed genes in the INH resistant *M. smegmatis* strains. Moreover, the INH resistant strain was more sensitive to compounds that block antioxidant responses and disturb E_{MSH} . In agreement with this finding, the Mrx1-roGFP2 biosensor measurements revealed an oxidized shift in basal E_{MSH} and a higher sensitivity to oxidative stress by H_2O_2 in the INH-resistant *M. smegmatis* strain [98]. This higher ROS-sensitivity was not only observed in the INH-resistant *M. smegmatis* strain, but also in clinical MDR and XDR *Mtb* patient isolates. Thus, the evolution of drug resistance is associated with changes in the basal E_{MSH} and shifted to the oxidized redox state in multiple resistant *Mtb* isolates. Finally, it was shown that antibiotics that produce ROS or block antioxidant responses are in combination with INH more potent to induce oxidative shift in E_{MSH} during infections. These drugs should be promising strategies to tackle tuberculosis disease and to combat drug resistant isolates [98].

2.3.3. E_{MSH} regulates the redox state of *WhiB4* mediating augmentin resistance and tolerance

In another study, the mode of action for combination therapy of β -lactam antibiotics (amoxicillin) with β -lactamase inhibitors (clavulanate), termed as augmentin, has been studied. The Mrx1-roGFP2 biosensor revealed a role of E_{MSH} and the *WhiB4* redox sensor in augmentin resistance (Fig. 6) [97]. To study the mode of action of augmentin, a transcriptomics approach was used and identified cell wall and oxidative stress responses, respiration and carbon metabolism induced under augmentin treatment. Using biosensor measurements, an increase in the oxidized E_{MSH} sub-population was observed by augmentin over time during *Mtb* infections inside macrophages. Thus, augmentin effects the redox balance in *Mtb*, which potentiates its mycobactericidal effect and contributes to augmentin killing [97]. Furthermore, MSH was shown to protect *Mtb* from toxicity under augmentin treatment in survival assays. In further analysis, the FeS-cluster redox sensor *WhiB4* was identified which regulates the shift to the oxidized E_{MSH} sub-population after augmentin treatment. Moreover, this oxidized shift modulates expression of the β -lactamase *BlaC*, which is regulated by *WhiB4* in a redox-dependent manner. Specifically, *BlaC* is overexpressed in the *whiB4* mutant which increases resistance to β -lactam antibiotics (Fig. 6). In contrast, overexpression of oxidized *WhiB4* under augmentin treatment resulted in strong *blaC* repression and increased killing by β -lactams potentiating drug action. Thus, *WhiB4* was identified as central regulator of β -lactam antibiotics resistance and the oxidative shift in E_{MSH} after augmentin combination therapy [97].

2.3.4. E_{MSH} regulates the redox state of *WhiB3* mediating acid resistance and inhibition of phagosomal maturation

WhiB3 is another FeS cluster redox sensor that is also regulated by E_{MSH} and is essential for acid resistance of *Mtb* which allows survival of *Mtb* inside the acidic phagosome upon immune-stimulation [60,104,105]. *WhiB3* was shown to play a protective role together with MSH under acidic stress conditions inside the phagosome of activated macrophages (Fig. 5) [96]. *WhiB3* mediates acid resistance and inhibits phagosomal maturation, which is linked to changes in E_{MSH} under infection conditions. *WhiB3* controls genes for lipid biosynthesis, secretion of the type-VII-secretion effectors as well as MSH biosynthesis and recycling under acidic stress. The limited decreased pH upon acidification of the phagosome (pH \sim 6.2) results in a reductive shift of E_{MSH} sub-populations and *WhiB3* as well as MSH were found as key regulators for this reductive shift in E_{MSH} . *WhiB3* was further required

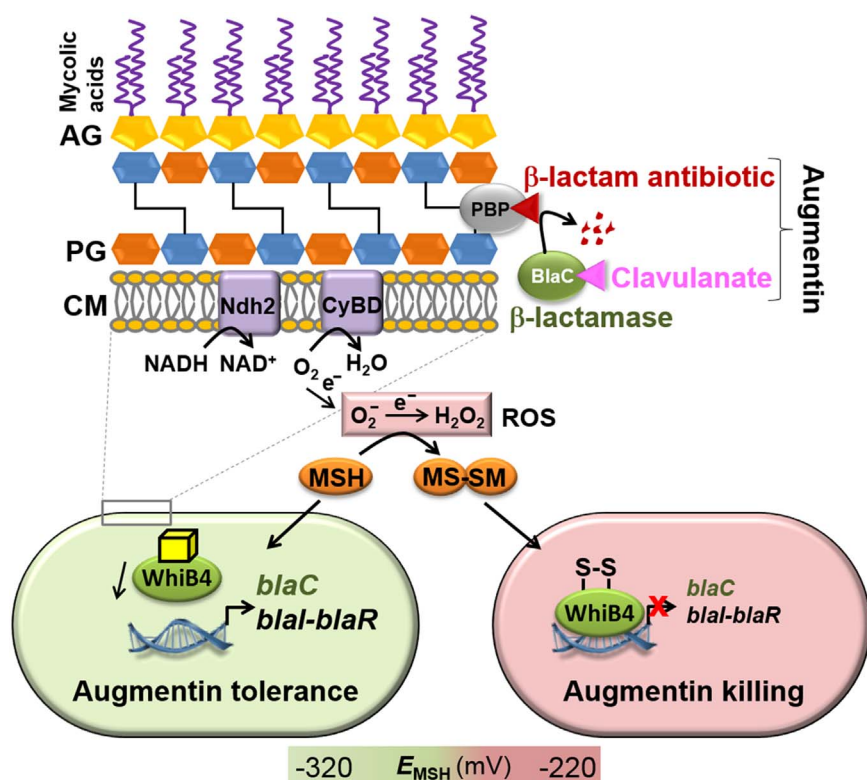


Fig. 6. The augmentin combination therapy of β -lactam antibiotics and β -lactamase inhibitor (clavulanate) causes ROS formation and changes in E_{MSH} in *Mtb* that affect WhiB4-mediated expression of β -lactamase expression. β -lactam antibiotics inhibit penicillin-binding proteins that cross-link the peptide side chains of the peptidoglycan (PG). Clavulanate inhibits the β -lactamase BlaC in *Mtb* that is controlled by the BlaI repressor and WhiB4. The combination therapy of β -lactam and Clavulanate (Augmentin) causes cell wall stress and ROS production in *Mtb* due to the re-direction of aerobic respiration via the Ndh2 and CyBD routes [97]. Increased ROS leads to the oxidative shift of E_{MSH} and oxidation of WhiB4 that represses transcription of *blaC* and the *blaI-blaR* operon resulting in down-regulation of the β -lactamase BlaC and killing by augmentin [97]. Tolerance to augmentin is induced by down-regulation or reduction of WhiB4 presumable in the reduced E_{MSH} sub-population resulting in derepression of the β -lactamase-encoding *blaC* gene directly or indirectly via derepression of the *blaI* operon and proteolytic degradation of the BlaI repressor by the protease BlaR. This figure is adapted from Ref. [97]. Abbreviations: CM: cytoplasmic membrane, PG: peptidoglycan, Ndh2: NADH dehydrogenase 2, CyBD: cytochrome BD oxidase, PBP: penicillin-binding protein.

for survival under acidic conditions and protects *Mtb* from acid stress by controlling genes that restrict phagosomal maturation to subvert acidification and by down-regulation of the innate immune response. The *whiB3* mutant was also attenuated in the lung of guinea pigs. These results revealed a link between phagosome acidification, the reductive shift in E_{MSH} and virulence of *Mtb* that is controlled by WhiB3 mediating acid resistance and inhibiting phagosomal maturation as mechanism of persistent and chronic *Mtb* infections [96].

2.3.5. E_{MSH} is controlled by the sulfur assimilation pathway, the membrane SodA/DoxX/SseA complex and macrophage GSH production that are required for survival of *Mtb*

For the treatment of persistent *Mtb* infections, the sulfur assimilation pathway was selected as promising target that is required for biosynthesis of sulfur-containing amino acids and thiol-cofactors, such as cysteine and MSH [106]. The sulfur assimilation pathway, including the enzyme 5' adenosine phosphosulfate (APS) reductase (CysH), was especially important for virulence and survival of *Mtb* during chronic and persistent infections in mice and macrophage models [107,108]. Thus, a high-throughput drug screening approach was used to identify three inhibitors of the APS reductase as potent anti-TB compounds that decreased the levels of sulfur-containing metabolites, including MSH [106]. Using the Mrx1-roGFP2 biosensor, an oxidative shift in E_{MSH} was measured in response to these APS reductase inhibitors indicating the link between persistence, antibiotic tolerance and the sulfate assimilation pathway in *Mtb*.

In another study, the Mrx1-roGFP2 biosensor was used to identify the link between a novel membrane-associated oxidoreductase complex (MRC) and the MSH redox potential [109]. Using a Tn-seq approach, the authors screened for interactions of pathways required in *Mtb* for detoxification of radicals from the phagocyte oxidative burst. The superoxide dismutase (SodA), an integral membrane protein (DoxX) and the conserved thiol oxidoreductase SseA were identified as functionally linked MRC and the electron transfer was verified *in vivo*. Single mutants in each MRC component are similar sensitive to radical stress and exhibited an oxidized E_{MSH} as revealed by Mrx1-roGFP2 biosensor

measurements. This study established a link between a novel oxidative stress resistance network with the E_{MSH} in *Mtb* to overcome the oxidative burst during infections [109].

An interaction between macrophage-derived GSH and E_{MSH} during *Mtb* infection has been revealed using the Mrx1-roGFP2 biosensor in a mice model of tuberculosis [110]. The GSH pool of macrophages depends on the xCT cystine-glutamate transporter, which is induced during *Mtb* infection. The deletion of xCT resulted in protection against TB and decreased pulmonary pathology in the mice lung. Mrx1-roGFP2 biosensor measurement revealed an oxidized E_{MSH} of *Mtb* in the infected mice xCT mutant. The increased E_{MSH} is caused by a decreased GSH production in the macrophages indicating a link between host GSH and bacterial MSH redox homeostasis. This study has further identified inhibitors of the xCT transporter as host-directed drugs for TB treatment [110].

Finally, the Mrx1-roGFP2 biosensor was applied in a mycobacterial biofilms under hypoxic conditions [111]. In the absence of oxygen as terminal electron acceptor, novel polyketide quinones were produced as alternative electron carriers in the respiratory chain to maintain bioenergetics and the membrane potential. About 70% of mycobacterial cells showed alterations in E_{MSH} under hypoxic biofilm conditions compared to planktonic cells, including 53% of cells with more reduced E_{MSH} and 16% with oxidative shift in E_{MSH} . Thus, the different oxygen levels across the biofilm affect the membrane potential and the MSH redox balance [111].

In summary, the Mrx1-roGFP2 biosensor was approved as valuable tool to study the mechanisms of redox heterogeneity, persistence and survival of *Mtb* under acidic conditions inside macrophage vacuolar compartments and the evolution and changes in E_{MSH} in drug resistant *Mtb* isolates. The biosensor has further contributed to elucidate novel ROS defense mechanisms in *Mtb*, such as the radical scavenging membrane MRC complex and the role of host GSH to regulate the MSH redox balance of *Mtb* inside macrophages. In drug research, the biosensor was used to study the regulation and mode of action of combination therapies (INH and augmentin) involving ROS-generating antibiotics as well as novel inhibitors of the sulfate-assimilation pathway as

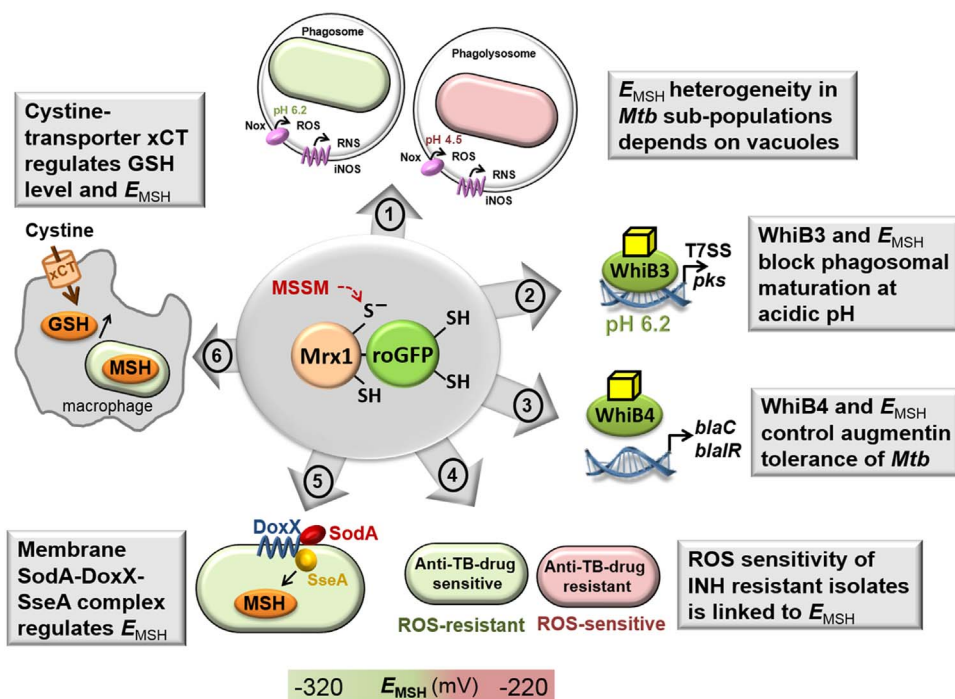


Fig. 7. Summary of the E_{MSH} changes in *Mtb* as measured using the Mrx1-roGFP2 biosensor. The genetically encoded Mrx1-roGFP2 biosensor contributed to a deeper understanding of pathogenicity, survival and anti-tuberculosis drug resistance mechanisms as follows: (1) E_{MSH} redox heterogeneity was shown in *Mtb* sub-populations that depends on the location in specific vacuole compartments [95]. (2) The WhiB3 sensor and E_{MSH} control induction of type-VII secretion systems and polyketide lipids under acid conditions in the phagosome to inhibit phagosomal maturation [96]. (3) The WhiB4 redox sensor and E_{MSH} control expression of β -lactamase to induce augmentin tolerance in the reduced *Mtb* population and augmentin killing in the oxidized *Mtb* population [97]. (4) Isoniazid (INH) resistant *Mtb* isolates have an oxidative E_{MSH} and are highly ROS-sensitive, while INH-sensitive strains are more resistant to ROS due to a more reduced E_{MSH} [98]. (5) The membrane-associated oxidoreductase complex (SodA-DoxX-SseA) regulates radical detoxification and MSH redox balance under infection conditions [109]. (6) The cystine-glutamate transporter xCT regulates cystine import into macrophages, resulting in increased host-GSH biosynthesis and a reduced E_{MSH} which contributes to TB disease in a mice infection model [110].

promising future anti-TB drugs to treat MDR/XDR, persistent and chronic *Mtb* infections. These main results revealed thus far using Mrx1-roGFP2 biosensor measurements in *Mtb* are summarized in the schematics of Fig. 7. Similar mechanisms might be relevant for other intracellular pathogens and persistent bacterial infections. As revealed in *Mtb* using the Mrx1-roGFP2 biosensor, redox heterogeneity of the intracellular pathogen *S. Typhimurium* could be also dependent on sub-vacuolar compartments. Inside the SCV, *S. Typhimurium* could be more tolerant to antibiotics due to a more reduced intrabacterial redox potential, which facilitates the persistent state. In contrast, cytosolic bacteria should have a more oxidized redox state and should be susceptible to clinical relevant antibiotics. The mechanisms of persistence and antibiotics resistance as result of redox heterogeneity remain interesting subject for future studies in redox infection biology.

Acknowledgements

This work was supported by grants from the Deutsche Forschungsgemeinschaft (AN746/4-1 and AN746/4-2) within the SPP1710 on “Thiol-based Redox switches” and by the DFG Project C08 within the SFB973 to H.A. Further funding was provided by the DFG Research Training Group GRK1947, project (C1) and by an ERC Consolidator Grant (GA 615585) MYCOTHILOME to H.A.

Author disclosure statement

No competing financial interests exist.

References

- [1] K. Van Laer, C.J. Hamilton, J. Messens, Low-molecular-weight thiols in thiol-disulfide exchange, *Antioxid. Redox Signal.* 18 (2013) 1642–1653.
- [2] R.C. Fahey, Glutathione analogs in prokaryotes, *Biochim. Biophys. Acta* 1830 (2013) 3182–3198.
- [3] A.J. Potter, C. Trappetti, J.C. Paton, *Streptococcus pneumoniae* uses glutathione to defend against oxidative stress and metal ion toxicity, *J. Bacteriol.* 194 (2012) 6248–6254.
- [4] B. Vergauwen, K. Verstraete, D.B. Senadheera, A. Dansercoer, D.G. Cvitkovitch, E. Guedon, S.N. Savvides, Molecular and structural basis of glutathione import in Gram-positive bacteria via GshT and the cystine ABC importer TcyBC of *Streptococcus mutans*, *Mol. Microbiol.* 89 (2013) 288–303.
- [5] L. Masip, K. Veeravalli, G. Georgiou, The many faces of glutathione in bacteria, *Antioxid. Redox Signal.* 8 (2006) 753–762.
- [6] C. Hwang, H.F. Lodish, A.J. Sinskey, Measurement of glutathione redox state in cytosol and secretory pathway of cultured cells, *Methods Enzymol.* 251 (1995) 212–221.
- [7] I.R. Booth, G.P. Ferguson, S. Miller, C. Li, B. Gunasekera, S. Kinghorn, Bacterial production of methylglyoxal: a survival strategy or death by misadventure? *Biochem. Soc. Trans.* 31 (2003) 1406–1408.
- [8] G.P. Ferguson, I.R. Booth, Importance of glutathione for growth and survival of *Escherichia coli* cells: detoxification of methylglyoxal and maintenance of intracellular K^+ , *J. Bacteriol.* 180 (1998) 4314–4318.
- [9] G.P. Ferguson, S. Totemeyer, M.J. MacLean, I.R. Booth, Methylglyoxal production in bacteria: suicide or survival? *Arch. Microbiol.* 170 (1998) 209–218.
- [10] M.J. MacLean, L.S. Ness, G.P. Ferguson, I.R. Booth, The role of glyoxalase I in the detoxification of methylglyoxal and in the activation of the KefB K^+ efflux system in *Escherichia coli*, *Mol. Microbiol.* 27 (1998) 563–571.
- [11] M. Song, M. Husain, J. Jones-Carson, L. Liu, C.A. Henard, A. Vazquez-Torres, Low-molecular-weight thiol-dependent antioxidant and antinitrosative defences in *Salmonella* pathogenesis, *Mol. Microbiol.* 87 (2013) 609–622.
- [12] J. van der Heijden, E.S. Bosman, L.A. Reynolds, B.B. Finlay, Direct measurement of oxidative and nitrosative stress dynamics in *Salmonella* inside macrophages, *Proc. Natl. Acad. Sci. USA* 112 (2015) 560–565.
- [13] M. Hall, C. Grundstrom, A. Begum, M.J. Lindberg, U.H. Sauer, F. Almqvist, J. Johansson, A.E. Sauer-Eriksson, Structural basis for glutathione-mediated activation of the virulence regulatory protein PrfA in *Listeria*, *Proc. Natl. Acad. Sci. USA* 113 (2016) 14733–14738.
- [14] M.L. Reniere, A.T. Whiteley, K.L. Hamilton, S.M. John, P. Lauer, R.G. Brennan, D.A. Portnoy, Glutathione activates virulence gene expression of an intracellular pathogen, *Nature* 517 (2015) 170–173.
- [15] N.E. Freitag, G.C. Port, M.D. Miner, *Listeria monocytogenes* – from saprophyte to intracellular pathogen, *Nat. Rev. Microbiol.* 7 (2009) 623–628.
- [16] Y. Wang, H. Feng, Y. Zhu, P. Gao, Structural insights into glutathione-mediated activation of the master regulator PrfA in *Listeria monocytogenes*, *Protein Cell* 8 (2017) 308–312.
- [17] J.L. Portman, S.B. Dubensky, B.N. Peterson, A.T. Whiteley, D.A. Portnoy, Activation of the *Listeria monocytogenes* virulence program by a reducing environment, *mBio* 8 (2017) e01595-17.
- [18] J.L. Portman, Q. Huang, M.L. Reniere, A.T. Iavarone, D.A. Portnoy, Activity of the pore-forming virulence factor listeriolysin O is reversibly inhibited by naturally occurring S-glutathionylation, *Infect. Immun.* 85 (2017) e00959-16.
- [19] K. McGourty, T.L. Thurston, S.A. Matthews, L. Pinaud, L.J. Mota, D.W. Holden, *Salmonella* inhibits retrograde trafficking of mannose-6-phosphate receptors and lysosome function, *Science* 338 (2012) 963–967.
- [20] K. Uchiya, M.A. Barbieri, K. Funato, A.H. Shah, P.D. Stahl, E.A. Groisman, A *Salmonella* virulence protein that inhibits cellular trafficking, *EMBO J.* 18 (1999) 3924–3933.
- [21] A. Vazquez-Torres, Y. Xu, J. Jones-Carson, D.W. Holden, S.M. Lucia, M.C. Dinauer, P. Mastroeni, F.C. Fang, *Salmonella* pathogenicity island 2-dependent evasion of the phagocyte NADPH oxidase, *Science* 287 (2000) 1655–1658.
- [22] M.M. Marketon, R.W. DePaolo, K.L. DeBord, B. Jabri, O. Schneewind, Plague bacteria target immune cells during infection, *Science* 309 (2005) 1739–1741.

- [23] C.A. Mueller, P. Broz, S.A. Muller, P. Ringler, F. Erne-Brand, I. Sorg, M. Kuhn, A. Engel, G.R. Cornelis, The V-antigen of *Yersinia* forms a distinct structure at the tip of injectisome needles, *Science* 310 (2005) 674–676.
- [24] V.T. Lee, C. Tam, O. Schneewind, LcrV, a substrate for *Yersinia enterocolitica* type III secretion, is required for toxin targeting into the cytosol of HeLa cells, *J. Biol. Chem.* 275 (2000) 36869–36875.
- [25] A. Mitchell, C. Tam, D. Elli, T. Charlton, P. Osei-Owusu, F. Fazlollahi, K.F. Faull, O. Schneewind, Glutathionylation of *Yersinia pestis* LcrV and its effects on plague pathogenesis, *mBio* 8 (2017).
- [26] A. Gaballa, G.L. Newton, H. Antelmann, D. Parsonage, H. Upton, M. Rawat, A. Claiborne, R.C. Fahey, J.D. Helmann, Biosynthesis and functions of bacillithiol, a major low-molecular-weight thiol in Bacilli, *Proc. Natl. Acad. Sci. USA* 107 (2010) 6482–6486.
- [27] G.L. Newton, M. Rawat, J.J. La Clair, V.K. Jothivasan, T. Budiarto, C.J. Hamilton, A. Claiborne, J.D. Helmann, R.C. Fahey, Bacillithiol is an antioxidant thiol produced in bacilli, *Nat. Chem. Biol.* 5 (2009) 625–627.
- [28] V.V. Loi, M. Rossius, H. Antelmann, Redox regulation by reversible protein S-thiolation in bacteria, *Front. Microbiol.* 6 (2015) 187.
- [29] A.C. Posada, S.L. Kolar, R.G. Dusi, P. Francois, A.A. Roberts, C.J. Hamilton, G.Y. Liu, A. Cheung, Importance of bacillithiol in the oxidative stress response of *Staphylococcus aureus*, *Infect. Immun.* 82 (2014) 316–332.
- [30] D.C. Pöther, P. Gierok, M. Harms, J. Mostertz, F. Hochgräfe, H. Antelmann, C.J. Hamilton, I. Borovok, M. Lalk, Y. Aharonowitz, M. Hecker, Distribution and infection-related functions of bacillithiol in *Staphylococcus aureus*, *Int. J. Med. Microbiol.* 303 (2013) 114–123.
- [31] P. Chandrangu, R. Dusi, C.J. Hamilton, J.D. Helmann, Methylglyoxal resistance in *Bacillus subtilis*: contributions of bacillithiol-dependent and independent pathways, *Mol. Microbiol.* 91 (2014) 706–715.
- [32] Z. Rosario-Cruz, J.M. Boyd, Physiological roles of bacillithiol in intracellular metal processing, *Curr. Genet.* 62 (2016) 59–65.
- [33] Z. Fang, P.C. Dos Santos, Protective role of bacillithiol in superoxide stress and Fe-S metabolism in *Bacillus subtilis*, *MicrobiologyOpen* 4 (2015) 616–631.
- [34] Z. Rosario-Cruz, H.K. Chahal, L.A. Mike, E.P. Skaar, J.M. Boyd, Bacillithiol has a role in Fe-S cluster biogenesis in *Staphylococcus aureus*, *Mol. Microbiol.* 98 (2015) 218–242.
- [35] P. Chandrangu, V.V. Loi, H. Antelmann, J.D. Helmann, The Role of Bacillithiol in Gram-Positive Firmicutes, *Antioxid. Redox Signal.* 28 (2018), 445–462.
- [36] S.V. Sharma, M. Arbach, A.A. Roberts, C.J. Macdonald, M. Groom, C.J. Hamilton, Biophysical features of bacillithiol, the glutathione surrogate of *Bacillus subtilis* and other Firmicutes, *Chembiochem* 14 (2013) 2160–2168.
- [37] V.R. Perera, G.L. Newton, K. Pogliano, Bacillithiol: a key protective thiol in *Staphylococcus aureus*, *Exp. Rev. Anti-Infect. Ther.* 13 (2015) 1089–1107.
- [38] B.K. Chi, A.A. Roberts, T.T. Huyen, K. Bäsell, D. Becher, D. Albrecht, C.J. Hamilton, H. Antelmann, S-bacillithiolation protects conserved and essential proteins against hypochlorite stress in firmicutes bacteria, *Antioxid. Redox Signal.* 18 (2013) 1273–1295.
- [39] G.L. Newton, R.C. Fahey, M. Rawat, Detoxification of toxins by bacillithiol in *Staphylococcus aureus*, *Microbiology* 158 (2012) 1117–1126.
- [40] C.C. Winterbourn, A.J. Kettle, Redox reactions and microbial killing in the neutrophil phagosome, *Antioxid. Redox Signal.* 18 (2013) 642–660.
- [41] C.C. Winterbourn, A.J. Kettle, M.B. Hampton, Reactive oxygen species and neutrophil function, *Annu. Rev. Biochem.* 85 (2016) 765–792.
- [42] J.N. Green, A.L.P. Chapman, C.J. Bishop, C.C. Winterbourn, A.J. Kettle, Neutrophil granule proteins generate bactericidal ammonia chloramine on reaction with hydrogen peroxide, *Free Radic. Biol. Med.* 113 (2017) 363–371.
- [43] M. Imber, N.T.T. Huyen, A.J. Pietrzyk-Brzezinska, V.V. Loi, M. Hillion, J. Bernhardt, L. Thärichen, K. Kolske, M. Saleh, C.J. Hamilton, L. Adrian, F. Gräter, M.C. Wahl, H. Antelmann, Protein S-bacillithiolation functions in thiol protection and redox regulation of the glyceraldehyde-3-phosphate dehydrogenase gap in *Staphylococcus aureus* under hypochlorite stress, *Antioxid. Redox Signal.* 28 (2018), 410–430.
- [44] N. Brandes, S. Schmitt, U. Jakob, Thiol-based redox switches in eukaryotic proteins, *Antioxid. Redox Signal.* 11 (2009) 997–1014.
- [45] M. Ralser, M.M. Wamelink, A. Kowald, B. Gerisch, G. Heeren, E.A. Struys, E. Klipp, C. Jakobs, M. Breitenbach, H. Lehrach, S. Krobitsch, Dynamic rerouting of the carbohydrate flux is key to counteracting oxidative stress, *J. Biol.* 6 (2007) 10.
- [46] Y. Tsuchiya, S.Y. Peak-Chew, C. Newell, S. Miller-Aidoo, S. Mangal, A. Zhyvoloup, J. Bakovic, O. Malanchuk, G.C. Pereira, V. Kotiadis, G. Szabadkai, M.R. Duchon, M. Campbell, S.R. Cuenca, A. Vidal-Puig, A.M. James, M.P. Murphy, V. Filonenko, M. Skehel, I. Gout, Protein CoAlation: a redox-regulated protein modification by coenzyme A in mammalian cells, *Biochem. J.* 474 (2017) 2489–2508.
- [47] A. Gaballa, B.K. Chi, A.A. Roberts, D. Becher, C.J. Hamilton, H. Antelmann, J.D. Helmann, Redox regulation in *Bacillus subtilis*: the bacilliredoxins BhrA(YphP) and BrxB(YqiW) function in de-bacillithiolation of S-bacillithiolated OsrA and MetE, *Antioxid. Redox Signal.* 21 (2014) 357–367.
- [48] G.L. Newton, N. Buchmeier, R.C. Fahey, Biosynthesis and functions of mycothiol, the unique protective thiol of Actinobacteria, *Microbiol. Mol. Biol. Rev.* 72 (2008) 471–494.
- [49] V.K. Jothivasan, C.J. Hamilton, Mycothiol: synthesis, biosynthesis and biological functions of the major low molecular weight thiol in actinomycetes, *Nat. Prod. Rep.* 25 (2008) 1091–1117.
- [50] N.A. Buchmeier, G.L. Newton, R.C. Fahey, A mycothiol synthase mutant of *Mycobacterium tuberculosis* has an altered thiol-disulfide content and limited tolerance to stress, *J. Bacteriol.* 188 (2006) 6245–6252.
- [51] N.A. Buchmeier, G.L. Newton, T. Koledin, R.C. Fahey, Association of mycothiol with protection of *Mycobacterium tuberculosis* from toxic oxidants and antibiotics, *Mol. Microbiol.* 47 (2003) 1723–1732.
- [52] M. Rawat, C. Johnson, V. Cadiz, Y. Av-Gay, Comparative analysis of mutants in the mycothiol biosynthesis pathway in *Mycobacterium smegmatis*, *Biochem. Biophys. Res. Commun.* 363 (2007) 71–76.
- [53] Y.B. Liu, M.X. Long, Y.J. Yin, M.R. Si, L. Zhang, Z.Q. Lu, Y. Wang, X.H. Shen, Physiological roles of mycothiol in detoxification and tolerance to multiple poisonous chemicals in *Corynebacterium glutamicum*, *Arch. Microbiol.* 195 (2013) 419–429.
- [54] Q. Zhao, M. Wang, D. Xu, Q. Zhang, W. Liu, Metabolic coupling of two small-molecule thiols programs the biosynthesis of lincomycin A, *Nature* 518 (2015) 115–119.
- [55] A.M. Reyes, B. Pedre, M.I. De Armas, M.A. Tossounian, R. Radi, J. Messens, M. Trujillo, Chemistry and redox biology of mycothiol, *Antioxid. Redox Signal.* 28 (2018), 487–504.
- [56] B.K. Chi, T. Busche, K. Van Laer, K. Basell, D. Becher, L. Clermont, G.M. Seibold, M. Persicke, J. Kalinowski, J. Messens, H. Antelmann, Protein S-mycothiolation functions as redox-switch and thiol protection mechanism in *Corynebacterium glutamicum* under hypochlorite stress, *Antioxid. Redox Signal.* 20 (2014) 589–605.
- [57] M. Hillion, J. Bernhardt, T. Busche, M. Rossius, S. Maafs, D. Becher, M. Rawat, M. Wirtz, R. Hell, C. Rückert, J. Kalinowski, H. Antelmann, Monitoring global protein thiol-oxidation and S-mycothiolation in *Mycobacterium smegmatis* under hypochlorite stress using Voronoi redox treemaps, *Sci. Rep.* (2017).
- [58] M. Hillion, M. Imber, B. Pedre, J. Bernhardt, M. Saleh, V.V. Loi, S. Maass, D. Becher, L. Astolfi Rosado, L. Adrian, C. Weise, R. Hell, M. Wirtz, J. Messens, H. Antelmann, The glyceraldehyde-3-phosphate dehydrogenase GapDH of *Corynebacterium diphtheriae* is redox-controlled by protein S-mycothiolation under oxidative stress, *Sci. Rep.* 7 (2017) 5020.
- [59] G.L. Newton, K. Arnold, M.S. Price, C. Sherrill, S.B. Delcardayre, Y. Aharonowitz, G. Cohen, J. Davies, R.C. Fahey, C. Davis, Distribution of thiols in microorganisms: mycothiol is a major thiol in most actinomycetes, *J. Bacteriol.* 178 (1996) 1990–1995.
- [60] V. Saini, B.M. Cumming, L. Guidry, D.A. Lamprecht, J.H. Adamson, V.P. Reddy, K.C. Chinta, J.H. Mazorodze, J.N. Glasgow, M. Richard-Greenblatt, A. Gomez-Velasco, H. Bach, Y. Av-Gay, H. Eoh, K. Rhee, A.J.C. Steyn, Ergothioneine maintains redox and bioenergetic homeostasis essential for drug susceptibility and virulence of *Mycobacterium tuberculosis*, *Cell Rep.* 14 (2016) 572–585.
- [61] C.M. Sasseti, E.J. Rubin, Genetic requirements for mycobacterial survival during infection, *Proc. Natl. Acad. Sci. USA* 100 (2003) 12989–12994.
- [62] C. Sao Emani, M.J. Williams, I.J. Wiid, N.F. Hiten, A.J. Viljoen, R.D. Pietersen, P.D. van Helden, B. Baker, Ergothioneine is a secreted antioxidant in *Mycobacterium smegmatis*, *Antimicrob. Agents Chemother.* 57 (2013) 3202–3207.
- [63] P. Ta, N. Buchmeier, G.L. Newton, M. Rawat, R.C. Fahey, Organic hydroperoxide resistance protein and ergothioneine compensate for loss of mycothiol in *Mycobacterium smegmatis* mutants, *J. Bacteriol.* 193 (2011) 1981–1990.
- [64] M.A. Tossounian, B. Pedre, K. Wahni, H. Erdogan, D. Vertommen, I. Van Molle, J. Messens, *Corynebacterium diphtheriae* methionine sulfoxide reductase exploits a unique mycothiol redox relay mechanism, *J. Biol. Chem.* 290 (2015) 11365–11375.
- [65] B. Pedre, I. Van Molle, A.F. Villadangos, K. Wahni, D. Vertommen, L. Turell, H. Erdogan, L.M. Mateos, J. Messens, The *Corynebacterium glutamicum* mycothiol peroxidase is a reactive oxygen species-scavenging enzyme that shows promiscuity in thiol redox control, *Mol. Microbiol.* 96 (2015) 1176–1191.
- [66] M. Hugo, K. Van Laer, A.M. Reyes, D. Vertommen, J. Messens, R. Radi, M. Trujillo, Mycothiol/mycoredoxin 1-dependent reduction of the peroxiredoxin AhpE from *Mycobacterium tuberculosis*, *J. Biol. Chem.* 289 (2014) 5228–5239.
- [67] Y. Liu, X. Yang, Y. Yin, J. Lin, C. Chen, J. Pan, M. Si, X. Shen, Mycothiol protects *Corynebacterium glutamicum* against acid stress via maintaining intracellular pH homeostasis, scavenging ROS, and S-mycothiolating MetE, *J. Gen. Appl. Microbiol.* 62 (2016) 144–153.
- [68] D. Sareen, G.L. Newton, R.C. Fahey, N.A. Buchmeier, Mycothiol is essential for growth of *Mycobacterium tuberculosis* Erdman, *J. Bacteriol.* 185 (2003) 6736–6740.
- [69] Z. Ma, C. Lienhardt, H. McIlleron, A.J. Nunn, X. Wang, Global tuberculosis drug development pipeline: the need and the reality, *Lancet* 375 (2010) 2100–2109.
- [70] M.H. Hazbon, M. Brimacombe, M. Bobadilla del Valle, M. Cavatore, M.I. Guerrero, M. Varma-Basil, H. Billman-Jacobe, C. Lavender, J. Fyfe, L. Garcia-Garcia, C.I. Leon, M. Bose, F. Chaves, M. Murray, K.D. Eisenach, J. Sifuentes-Osornio, M.D. Cave, A. Ponce de Leon, D. Alland, Population genetics study of isoniazid resistance mutations and evolution of multidrug-resistant *Mycobacterium tuberculosis*, *Antimicrob. Agents Chemother.* 50 (2006) 2640–2649.
- [71] R. Rawat, A. Whitty, P.J. Tonge, The isoniazid-NAD adduct is a slow, tight-binding inhibitor of InhA, the *Mycobacterium tuberculosis* enoyl reductase: adduct affinity and drug resistance, *Proc. Natl. Acad. Sci. USA* 100 (2003) 13881–13886.
- [72] S.S. Nilewar, M.K. Kathiravan, Mycothiol: a promising antitubercular target, *Bioorg. Chem.* 52 (2014) 62–68.
- [73] M. Schwarlander, T.P. Dick, A.J. Meyer, B. Morgan, Dissecting redox biology using fluorescent protein sensors, *Antioxid. Redox Signal.* 24 (2016) 680–712.
- [74] A.J. Meyer, T.P. Dick, Fluorescent protein-based redox probes, *Antioxid. Redox Signal.* 13 (2010) 621–650.
- [75] M. Gutschler, A.L. Pauleau, L. Marty, T. Brach, G.H. Wabnitz, Y. Samstag, A.J. Meyer, T.P. Dick, Real-time imaging of the intracellular glutathione redox potential, *Nat. Methods* 5 (2008) 553–559.
- [76] D.S. Bilan, V.V. Belousov, New tools for redox biology: from imaging to manipulation, *Free Radic. Biol. Med.* 109 (2017) 167–188.
- [77] B. Morgan, M.C. Sobotta, T.P. Dick, Measuring E(GSH) and H₂O₂ with roGFP2-based redox probes, *Free Radic. Biol. Med.* 51 (2011) 1943–1951.
- [78] A.J. Meyer, T. Brach, L. Marty, S. Kreye, N. Rouhier, J.P. Jaquot, R. Hell,

- Redox-sensitive GFP in *Arabidopsis thaliana* is a quantitative biosensor for the redox potential of the cellular glutathione redox buffer, *Plant J.* 52 (2007) 973–986.
- [79] P. Back, W.H. De Vos, G.G. Depuydt, F. Matthijssens, J.R. Vanfleteren, B.P. Braeckman, Exploring real-time in vivo redox biology of developing and aging *Caenorhabditis elegans*, *Free Radic. Biol. Med.* 52 (2012) 850–859.
- [80] D. Kasozi, F. Mohring, S. Rahlfs, A.J. Meyer, K. Becker, Real-time imaging of the intracellular glutathione redox potential in the malaria parasite *Plasmodium falciparum*, *PLoS Pathog.* 9 (2013) e1003782.
- [81] C.R. Arias-Barreiro, K. Okazaki, A. Koutsaftis, S.H. Inayat-Hussain, A. Tani, M. Katsuhara, K. Kimbara, I.C. Mori, A bacterial biosensor for oxidative stress using the constitutively expressed redox-sensitive protein roGFP2, *Sensors* 10 (2010) 6290–6306.
- [82] G.T. Hanson, R. Aggeler, D. Oglesbee, M. Cannon, R.A. Capaldi, R.Y. Tsien, S.J. Remington, Investigating mitochondrial redox potential with redox-sensitive green fluorescent protein indicators, *J. Biol. Chem.* 279 (2004) 13044–13053.
- [83] L. Ooi, L.Y. Heng, I.C. Mori, A high-throughput oxidative stress biosensor based on *Escherichia coli* roGFP2 cells immobilized in a κ-carrageenan matrix, *Sensors* 15 (2015) 2354–2368.
- [84] J.A. Imlay, The molecular mechanisms and physiological consequences of oxidative stress: lessons from a model bacterium, *Nat. Rev. Microbiol.* 11 (2013) 443–454.
- [85] S. Mishra, J. Imlay, Why do bacteria use so many enzymes to scavenge hydrogen peroxide? *Arch. Biochem. Biophys.* 525 (2012) 145–160.
- [86] J. van der Heijden, S.L. Vogt, L.A. Reynolds, J. Pena-Diaz, A. Tupin, L. Aussel, B.B. Finlay, Exploring the redox balance inside gram-negative bacteria with redox-sensitive GFP, *Free Radic. Biol. Med.* 91 (2016) 34–44.
- [87] M.A. Kohanski, D.J. Dwyer, B. Hayete, C.A. Lawrence, J.J. Collins, A common mechanism of cellular death induced by bactericidal antibiotics, *Cell* 130 (2007) 797–810.
- [88] Y. Liu, J.A. Imlay, Cell death from antibiotics without the involvement of reactive oxygen species, *Science* 339 (2013) 1210–1213.
- [89] I. Keren, Y. Wu, J. Inocencio, L.R. Mulcahy, K. Lewis, Killing by bactericidal antibiotics does not depend on reactive oxygen species, *Science* 339 (2013) 1213–1216.
- [90] P. Shukla, V.S. Khodade, M. SharathChandra, P. Chauhan, S. Mishra, S. Siddaramappa, B.E. Pradeep, A. Singh, H. Chakrapani, "On demand" redox buffering by H₂S contributes to antibiotic resistance revealed by a bacteria-specific H₂S donor, *Chem. Sci.* 8 (2017) 4967–4972.
- [91] J. van der Heijden, L.A. Reynolds, W. Deng, A. Mills, R. Scholz, K. Imami, L.J. Foster, F. Duong, B.B. Finlay, *Salmonella* rapidly regulates membrane permeability to survive oxidative stress, *mBio* 7 (2016) e01238–01216.
- [92] V.V. Loi, M. Harms, M. Müller, N.T.T. Huyen, C.J. Hamilton, F. Hochgräfe, J. Pane-Farre, H. Antelmann, Real-time imaging of the bacillithiol redox potential in the human pathogen *Staphylococcus aureus* using a genetically encoded bacilliredoxin-fused redox biosensor, *Antioxid. Redox Signal.* 26 (2017) 835–848.
- [93] B.A. Diep, S.R. Gill, R.F. Chang, T.H. Phan, J.H. Chen, M.G. Davidson, F. Lin, J. Lin, H.A. Carleton, E.F. Mongodin, G.F. Sensabaugh, F. Perdreau-Remington, Complete genome sequence of USA300, an epidemic clone of community-acquired methicillin-resistant *Staphylococcus aureus*, *Lancet* 367 (2006) 731–739.
- [94] H. Weber, S. Engelmann, D. Becher, M. Hecker, Oxidative stress triggers thiol oxidation in the glyceraldehyde-3-phosphate dehydrogenase of *Staphylococcus aureus*, *Mol. Microbiol.* 52 (2004) 133–140.
- [95] A. Bhaskar, M. Chawla, M. Mehta, P. Parikh, P. Chandra, D. Bhave, D. Kumar, K.S. Carroll, A. Singh, Reengineering redox sensitive GFP to measure mycothiol redox potential of *Mycobacterium tuberculosis* during infection, *PLoS Pathog.* 10 (2014) e1003902.
- [96] M. Mehta, R.S. Rajmani, A. Singh, *Mycobacterium tuberculosis* WhiB3 responds to vacuolar pH-induced changes in mycothiol redox potential to modulate phagosomal maturation and virulence, *J. Biol. Chem.* 291 (2016) 2888–2903.
- [97] S. Mishra, P. Shukla, A. Bhaskar, K. Anand, P. Baloni, R.K. Jha, A. Mohan, R.S. Rajmani, V. Nagaraja, N. Chandra, A. Singh, Efficacy of beta-lactam/beta-lactamase inhibitor combination is linked to WhiB4-mediated changes in redox physiology of *Mycobacterium tuberculosis*, *Elife* 6 (2017) e25624.
- [98] J. Padiadpu, P. Baloni, K. Anand, M. Munshi, C. Thakur, A. Mohan, A. Singh, N. Chandra, Identifying and tackling emergent vulnerability in drug-resistant mycobacteria, *ACS Infect. Dis.* 2 (2016), pp. 592–607.
- [99] P. Tyagi, A.T. Dharmaraja, A. Bhaskar, H. Chakrapani, A. Singh, *Mycobacterium tuberculosis* has diminished capacity to counteract redox stress induced by elevated levels of endogenous superoxide, *Free Radic. Biol. Med.* 84 (2015) 344–354.
- [100] K.S. Ung, Y. Av-Gay, Mycothiol-dependent mycobacterial response to oxidative stress, *FEBS Lett.* 580 (2006) 2712–2716.
- [101] V. Poirier, Y. Av-Gay, Intracellular growth of bacterial pathogens: the role of secreted effector proteins in the control of phagocytosed microorganisms, *Microbiol. Spectr.* 3 (2015).
- [102] S. Ehrh, D. Schnappinger, Mycobacterial survival strategies in the phagosome: defence against host stresses, *Cell Microbiol.* 11 (2009) 1170–1178.
- [103] D. Schnappinger, S. Ehrh, M.I. Voskuil, Y. Liu, J.A. Mangan, I.M. Monahan, G. Dolganov, B. Efron, P.D. Butcher, C. Nathan, G.K. Schoolnik, Transcriptional adaptation of *Mycobacterium tuberculosis* within macrophages: insights into the phagosomal environment, *J. Exp. Med.* 198 (2003) 693–704.
- [104] G.B. Coulson, B.K. Johnson, H. Zheng, C.J. Colvin, R.J. Fillinger, E.R. Haiderer, N.D. Hammer, R.B. Abramovitch, Targeting *Mycobacterium tuberculosis* sensitivity to thiol stress at acidic pH kills the bacterium and potentiates antibiotics, *Cell Chem. Biol.* 24 (2017) 993–1004 (e1004).
- [105] A. Singh, L. Guidry, K.V. Narasimulu, D. Mai, J. Trombley, K.E. Redding, G.I. Giles, J.R. Lancaster Jr, A.J. Steyn, *Mycobacterium tuberculosis* WhiB3 responds to O₂ and nitric oxide via its [4Fe-4S] cluster and is essential for nutrient starvation survival, *Proc. Natl. Acad. Sci. USA* 104 (2007) 11562–11567.
- [106] P.B. Palde, A. Bhaskar, L.E. Pedro Rosa, F. Madoux, P. Chase, V. Gupta, T. Spicer, L. Scampavia, A. Singh, K.S. Carroll, First-in-class inhibitors of sulfur metabolism with bactericidal activity against non-replicating *M. tuberculosis*, *ACS Chem. Biol.* 11 (2016) 172–184.
- [107] J. Rengarajan, B.R. Bloom, E.J. Rubin, Genome-wide requirements for *Mycobacterium tuberculosis* adaptation and survival in macrophages, *Proc. Natl. Acad. Sci. USA* 102 (2005) 8327–8332.
- [108] R.H. Senaratne, A.D. De Silva, S.J. Williams, J.D. Mougous, J.R. Reader, T. Zhang, S. Chan, B. Sidders, D.H. Lee, J. Chan, C.R. Bertozzi, L.W. Riley, 5'-Adenosinephosphosulphate reductase (CysH) protects *Mycobacterium tuberculosis* against free radicals during chronic infection phase in mice, *Mol. Microbiol.* 59 (2006) 1744–1753.
- [109] S. Nambi, J.E. Long, B.B. Mishra, R. Baker, K.C. Murphy, A.J. Olive, H.P. Nguyen, S.A. Shaffer, C.M. Sasseti, The oxidative stress network of *Mycobacterium tuberculosis* reveals coordination between radical detoxification systems, *Cell Host Microbe* 17 (2015) 829–837.
- [110] Y. Cai, Q. Yang, M. Liao, H. Wang, C. Zhang, S. Nambi, W. Wang, M. Zhang, J. Wu, G. Deng, Q. Deng, H. Liu, B. Zhou, Q. Jin, C.G. Feng, C.M. Sasseti, F. Wang, X. Chen, xCT increases tuberculosis susceptibility by regulating antimicrobial function and inflammation, *Oncotarget* 7 (2016) 31001–31013.
- [111] A. Anand, P. Verma, A.K. Singh, S. Kaushik, R. Pandey, C. Shi, H. Kaur, M. Chawla, C.K. Elechalawar, D. Kumar, Y. Yang, N.S. Bhavesh, R. Banerjee, D. Dash, A. Singh, V.T. Natarajan, A.K. Ojha, C.C. Aldrich, R.S. Gokhale, Polyketide quinones are alternate intermediate electron carriers during mycobacterial respiration in oxygen-deficient niches, *Mol. Cell* 60 (2015) 637–650.

Curriculum vitae

General Information

Name: Vu, Van Loi
Academic title: MSc. Biology
Gender: Male
Nationality: Vietnam
Institute address: Freie Universität Berlin
Institut für Biologie-Mikrobiologie
Königin-Luise-Straße 12-16
14195 Berlin, Germany
Tel. number: 030-838-57130
E-Mail address: vu.v.loi@fu-berlin.de

Academic Education and Qualifications

2004-2008 Engineer of Biotechnology, Hanoi Open University, Hanoi, Vietnam
Thesis project: "Selection of optimum conditions for lignin peroxidase production by *Streptomyces chromofuscus* HX10.7"

06/2008-02/2014 Researcher, Institute of Biotechnology, Vietnam Academy of science and technology, Hanoi, Vietnam

2010-2012 Master of science in Biology, Institute of Ecology and Biological Resources, Vietnam Academy of Science and Technology
Thesis project: "Cloning and expression lignin peroxidase isozyme H8 in *Pichia pastoris*."

03/2014-09/2015 PhD student within the SPP1710, Supervisor: Prof. Dr. Haike Antelmann, Institute for Microbiology, Ernst-Moritz-Arndt-University Greifswald

10/2015- to date PhD student within the SPP1710, Supervisor: Prof. Dr. Haike Antelmann, Freie Universität Berlin, Institut für Biologie-Mikrobiologie
Project: "Redox-sensing mechanisms under hypochlorite stress in *Staphylococcus aureus*"

Certificates and Awards

2010 Third prize for the Young Scientist awarded by Vietnam Academy of Science and Technology

03/2012 Certificate of training course on "Fungal Natural Product Molecular Genetics", organized through the Vietnam-UK Natural Products Research Network, by the Institute of Chemistry and Institute of Biotechnology-VAST, Hanoi, Vietnam

09/2012	Certificate of training course on “Modern Fundamentals and Application of Red Biotechnology”, organized by the University of Greifswald, Germany - in cooperation with the Institute of Biotechnology, Vietnam Academy of Science and Technology
10/2013	Certificate of training course on “First South-East Asia Workshop in Aquatic Microbial Ecology (ASIAME), held in Nha Trang, Vietnam
7/2014	Certificate of training course on “Summer School 2014 of DFG SPP 1710 Dynamics of thiol-based redox switches in cellular physiology”, Justus-Liebig-Universität Gießen, Germany

Publications

- **Loi VV**, Busche T, Bernhardt J, Tedin K, Wollenhaupt J, Huyen NTT, Weise C, Kalinowski J, Wahl M, Fulde M, Antelmann H. Redox-sensing under hypochlorite stress and infection conditions by the Rrf2-family repressor HypR in *Staphylococcus aureus*. *Antioxid Redox Signal*. in press. doi: 10.1089/ars.2017.7354 (2018)
- Imber M*, **Loi VV***, Reznikov S, Fritsch VN, Pietrzyk-Brzezinska AJ, Prehn J, Hamilton CJ, Wahl MC, Bronowska AK, Antelmann H. The aldehyde dehydrogenase AldA contributes to the hypochlorite defense and is redox-controlled by protein S-bacillithiolation in *Staphylococcus aureus*. *Redox Biol*. 15: 557-568. (2018)
- Imber M*, Huyen NT*, Pietrzyk-Brzezinska AJ*, **Loi VV***, Hillion M, Bernhardt J, Thärichen L, Kolšek K, Saleh M, Hamilton CJ, Adrian L, Gräter F, Wahl MC, Antelmann H. Protein S-bacillithiolation functions in thiol protection and redox regulation of the glyceraldehyde-3-phosphate dehydrogenase Gap in *Staphylococcus aureus* under hypochlorite stress. *Antioxid Redox Signal*. 28: 410-430. (2018)
- Chandrangsu P, **Loi VV**, Antelmann H, Helmann JD. The role of bacillithiol in Gram-positive *Firmicutes*. *Antioxid Redox Signal*. 28: 445-462. (2018)
- Tung QN, Linzner N, **Loi VV**, Antelmann H. Application of genetically encoded redox biosensors to measure dynamic changes in the glutathione, bacillithiol and mycothiol redox potentials in pathogenic bacteria. *Free Radic Biol Med*. in press. doi: 10.1016/j.freeradbiomed.2018.02.018 (2018)
- **Loi VV**, Harms M, Müller M, Huyen NT, Hamilton CJ, Hochgräfe F, Pané-Farré J, Antelmann H. Real-time imaging of the bacillithiol redox potential in the human pathogen *Staphylococcus aureus* using a genetically encoded bacilliredoxin-fused redox biosensor. *Antioxid Redox Signal*. 26: 835-848. (2017)
- Hillion M, Imber M, Pedre B, Bernhardt J, Saleh M, **Loi VV**, Maaß S, Becher D, Astolfi Rosado L, Adrian L, Weise C, Hell R, Wirtz M, Messens J, Antelmann H. The glyceraldehyde-3-phosphate dehydrogenase GapDH of *Corynebacterium diphtheriae* is redox-controlled by protein S-mycothiolation under oxidative stress. *Sci Rep* 7: 5020. (2017)
- **Loi VV**, Rossius M, Antelmann H. Redox regulation by reversible protein S-thiolation in bacteria. *Front Microbiol*. 6:187. (2015)

*Shared first authorships.

Presentations at national and international conferences

- **24-27th September 2017:** Molecular basis of life 2017-International fall meeting of the German society for biochemistry and molecular biology (GBM), Ruhr University Bochum, Germany.
Chalk talk “Real-time imaging of the bacillithiol redox potential in the human pathogen *Staphylococcus aureus* using a genetically encoded bacilliredoxin-fused redox biosensor”.
- **17-21st September 2017:** Thiol oxidation in toxicity and signalling Workshop, Sant Feliu de Guixols, Spain.
Poster presentation “Real-time imaging of the bacillithiol redox potential in the human pathogen *Staphylococcus aureus* using a genetically encoded bacilliredoxin-fused redox biosensor”.
- **17-18th July 2017:** Collaborative research center CRC 973-Retreat, Döll, Germany.
Oral presentation “Priming and memory of *Staphylococcus aureus* in response to oxidative and electrophile stress”.
- **11-15th June 2017:** 19th international conference on Bacilli & Gram-positive bacteria.
Oral presentation “Real-time imaging of the bacillithiol redox potential in the human pathogen *Staphylococcus aureus* using a genetically encoded bacilliredoxin-fused redox biosensor”.
- **5-8th March 2017:** Microbiology and infection 2017-5th Joint conference of the DGHM & VAAM, Würzburg, Germany.
Poster presentation “Real-time imaging of the bacillithiol redox potential in the human pathogen *Staphylococcus aureus* using a genetically encoded bacilliredoxin-fused redox biosensor”.
- **19-20th October 2016:** 2nd Conference on post-translational modifications in bacteria, Lyon, France.
Oral presentation “Real-time imaging of the bacillithiol redox potential in the human pathogen *Staphylococcus aureus* using a genetically encoded bacilliredoxin-fused redox biosensor”.
- **15-19th September 2016:** 6th Symposium of the SPP 1710, Kloster Irsee, Irsee, Germany.
Poster presentation “Real-time imaging of the bacillithiol redox potential in the human pathogen *Staphylococcus aureus* using a genetically encoded bacilliredoxin-fused redox biosensor”.
- **13-16th March 2016:** VAAM conference, Jena, Germany.
Oral presentation “Real-time imaging of the bacillithiol redox potential in the human pathogen *Staphylococcus aureus* using a genetically encoded bacilliredoxin-fused redox biosensor”.
- **29th February-1st March 2016:** 5th Symposium of the SPP1710, Rauishholzhausen, Germany.
Oral presentation: “Real-time imaging of the bacillithiol redox potential in the human pathogen *Staphylococcus aureus* using a genetically encoded bacilliredoxin-fused redox biosensor”.
- **12-17th September 2015:** ESF-EMBO Symposium thiol-based redox switches in life sciences, Eden Roc Hotel, Sant Feliu, Spain.
Poster presentation “Real-time imaging of the bacillithiol redox potential in the human pathogen *Staphylococcus aureus* using a genetically encoded bacilliredoxin-fused redox biosensor”.
- **20-21st March 2015:** 3rd Symposium of the SPP1710, Rauschholzhausen, Germany,

Poster presentation “Real-time imaging of the bacillithiol redox potential in the human pathogen *Staphylococcus aureus* using a genetically encoded bacilliredoxin-fused redox biosensor”.

- **1-4th March 2015:** VAAM conference, Marburg, Germany.
Poster presentation “Real-time imaging of the bacillithiol redox potential in the human pathogen *Staphylococcus aureus* using a genetically encoded bacilliredoxin-fused redox biosensor”.
- **22-23rd September 2014:** 2nd Symposium of the SPP1710, Heidelberg, Germany,
Poster presentation “Real-time imaging of the bacillithiol redox potential in the human pathogen *Staphylococcus aureus* using a genetically encoded bacilliredoxin-fused redox biosensor”.

Acknowledgements

I would like to express my gratitude to my supervisor, Prof. Dr. Haike Antelmann for giving me a great opportunity to work on this exciting research project. She introduced me into the regulation of resistance mechanisms in bacteria, particularly redox biology and taught me many interesting techniques to analyze protein modifications, bacterial physiology and cutting-edge technologies such as redox biosensors. She shared with me her exceptional experiences in the redox metabolism of the human pathogen *S. aureus*. She encouraged and gave me the chance to participate plenty of symposiums and international conferences. I am grateful for her guidance and support during the time of my PhD thesis in Greifswald and Berlin, Germany.

I would also like to thank all members of the SPP1710 consortium, especially Prof. Andreas Meyer (University of Bonn, Germany), Prof. Dr. Markus Schwarzländer (Universität Münster), PD. Dr. Tobias Dick (German Cancer Research Center (DKFZ), Universitätsklinikums Heidelberg, Germany), and Junior Prof. Bruce Morgan (Technische Universität Kaiserslautern, Germany) for stimulating discussions and helps with Brx-roGFP2 biosensor measurements.

My special thanks also go to Dr. Kasten Tedin and Prof. Marcus Fulde (Institute of Microbiology and Epizootics, Freie Universität Berlin). Prof. Dr. Markus Wahl (Laboratory of Structural Biochemistry, Freie Universität Berlin,) Dr. Jan Pané-Farré (Universität Greifswald), who provided me an opportunity to join their team for various experiments, and all collaboration partners for their great supports and valuable discussions during my PhD thesis

I want to thank all colleagues at the Institute of Microbiology (Universität Greifswald) and Institut für Biologie-Mikrobiologie (Freie Universität Berlin), for their kindness and friendship, especially Dana Clausen, and Melanie Skibbe for excellent technical assistance.

I would like to thank Dr. Pham Thi Bich Hop and Dr. Phan Thi Hong Thao at the Institute for Biotechnology, Vietnam Academy of Science and Technology for supporting me to complete my PhD work.

I wish to acknowledge the Deutsche Forschungsgemeinschaft within the SPP1710 on "Thiol-based Redox switches", and the SFB973 project C08, and the ERC Consolidator grant MYCOTHIOLOME for the generous financial support.

Last but not least, my deep gratitude goes to my family and friends, especially Do Hien Giang who have given me so much support, encouragement, and strength.

Declaration

I hereby certify that this thesis has not been submitted for a degree or any other qualification at Freie Universität Berlin or any other institution. I declare that I have written this thesis by myself under the guidance and supervision of Prof. Dr. Haike Antelmann, Institut für Biologie-Mikrobiologie, Freie Universität Berlin. Furthermore, I did not take any text sections of a third person without identification.

Berlin,

Vu Van Loi